

**Application of advanced  
multimodal brain imaging  
techniques to amyotrophic  
lateral sclerosis.**

Dr Rebecca Joan Broad  
(Parokkaran)

Student number 14802039

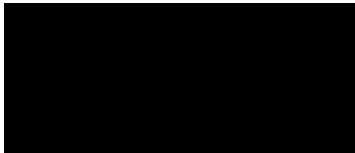
A thesis submitted in partial fulfilment of  
the requirements of the University of  
Brighton for the degree of Doctor of  
Medicine

October 2019

## **Declaration**

I declare that the research contained in this thesis, unless otherwise formally indicated within the text, is the original work of the author. The thesis has not been previously submitted to this or any other university for a degree, and does not incorporate any material already submitted for a degree.

Signed:



Date: 7/10/2019

## **Acknowledgements**

I would firstly like to thank my family for their acceptance in me devoting a lot of my attention to research. In particular my children Gabriel, Evangeline, and Ariella with whom I sacrificed precious time so that I could focus on completing my thesis. Also, my husband Chris and my parents who have been a source of support and stability.

I would like to extend a large amount of gratitude to my supervisors for their patience and expertise. I feel very privileged to have been able to do research under their guidance. Professor Nigel Leigh is an inspiration to me and I would like to thank him for sharing his unlimited wisdom, as well as his belief in my ability to succeed in research. I would also like to thank Professor Mara Cercignani, who provided me with a wealth of knowledge regarding imaging techniques and patiently taught me how to perform analyses using SPM12. I wish to thank Dr Matthew Gabel who provided emotional support during my MD and was also my source of statistical advice. He graciously helped me with my initial imaging processing, and taught me how to use linux, freesurfer, and FSLview. I was also fortunate enough to receive guidance from Dr Nicholas Dowell and Dr Charlotte Rae. I will be eternally grateful to all of these people.

I have been amazed by the altruistic nature of the participants with amyotrophic lateral sclerosis, and their families, without whom my MD research would not have been possible. I would like to dedicate my thesis to two people, both of whom participated in my study. Firstly, Andy Spriggs (29.11.1948 – 28.12.17), a kindred spirit who shared my love of running. Through his participation in marathons he helped raise funds for the MND association. Secondly, Chris Sheridan who works as vice-chair for the West Sussex North Branch of the Motor Neurone Disease Association. As well as organising fundraising events she provides a source of valuable support to those living with MND.

Finally, I want to thank the Motor Neurone Disease Association who kindly funded my research.

*“All we know is still infinitely less than all that still remains unknown”  
- William Harvey 1657*

## ABSTRACT

### Background

Amyotrophic lateral sclerosis (ALS) is a clinically distinct yet pathogenically heterogeneous neurodegenerative disorder. Typified by progressive loss of spinal and cortical motor neurons, ALS contributes significantly to morbidity and mortality worldwide.

Assessing the neurodegeneration associated with ALS in life remains a major challenge. Magnetic Resonance Imaging (MRI), especially Diffusion Tensor Imaging (DTI), has allowed consistent patterns of cerebral white matter (WM) degeneration, associated with ALS, to be characterised. However, DTI measures do not reflect specific histological processes. In addition, DTI does not provide the optimal model of analysis in areas of complex dendritic architecture, such as the grey matter (GM) neuropil.

Advanced imaging techniques are increasing our capacity to scrutinize both structural and functional integrity of neurones. Neurite Orientation Dispersion and Density Imaging (NODDI) assesses the density and organisation of neurites, characterising microstructural features associated with disease. Quantitative magnetisation transfer imaging (qMTi) evaluates changes in molecular integrity and provides assessment of myelin integrity.

In this study I combined NODDI with qMTi, to interrogate the structural and functional alterations occurring in ALS '*in vivo*'. I also incorporated DTI and surface-based morphometry (SBM) to further analyse the NODDI results.

### Aim

To use multimodal brain imaging in a cross-sectional study of ALS to scrutinize the changes occurring within the corticospinal tract (CST) and to test the hypothesis that alterations within the precentral gyrus (PCG) are fundamental to the underlying neurodegenerative process.

### Methods

23 participants with ALS and 23 healthy controls were recruited into this neuroimaging study. ALS participants were clinically assessed for disease distribution and severity. All participants underwent diffusion-weighted and magnetization transfer MRI scans.

The NODDI toolbox was used to produce maps of neurite density index (NDI), orientation dispersion index (ODI), and isotropic component (ISO).

The diffusion tensor was fitted yielding measures of fractional anisotropy (FA) mean diffusivity (MD), axial diffusivity (AD), and radial diffusivity (RD).



The balanced steady-state free precession method was used to provide estimates of fractional size of the restricted pool ( $F$ ), forward magnetization exchange rate ( $k_f$ ), and relaxation time of the free pool ( $T_{2f}$ ).

Voxel-based analysis was performed using SPM12, including age as covariate, to evaluate for statistically significant group differences in NODDI, DTI, and qMTi parameters.

Surface-based morphometry (SBM) was performed, by applying the automated processing stream within Free-Surfer to the high resolution MPRAGE images, to evaluate for significant differences in cortical thickness, surface area, and volumes within regions of interest.

## Results

NDI was significantly reduced throughout extensive regions of the corticospinal tract (CST) of the ALS group, and also within the corpus callosum and PCG ( $P < 0.001$ ). ODI was significantly reduced in the ALS group, within a region of the right corona radiata extending into the right PCG ( $P = 0.014$ ). ISO was significantly increased in the right lateral ventricle ( $P = 0.006$ ).

Alterations in  $F$  and  $T_{2f}$  only became apparent at less stringent statistical thresholds. The parameter reflecting myelin content,  $F$ , was relatively preserved in the ALS group, with only a small area of the caudal medulla showing reduced  $F$  ( $P = 0.001$  uncorrected). While  $T_{2f}$  was increased in frontal cortical regions and the right lateral ventricle ( $P = 0.002$  uncorrected). However,  $k_f$  was significantly reduced within the corona radiata bilaterally and the cingulate gyrus ( $P < 0.001$ ), indicating altered molecular integrity within these axons.

DTI measures of FA, MD, AD, and RD were consistent with previous findings of altered diffusivity within the CST in ALS.

Using SBM significant reduction in cerebral volumes were detected in the PCG ( $P = 0.037$ ), corpus callosum ( $P = 0.021$ ), WM ( $P = 0.037$ ), cortical GM ( $P = 0.034$ ), and brainstem ( $P = 0.027$ ). The total cortical volume was also significantly reduced ( $P = 0.018$ ), while the volume of the ventricles was significantly increased ( $P < 0.001$ ).

## Conclusions

ALS is associated with extensive axonal loss within the CST and corpus callosum, as well as altered dendrite complexity in the PCG. Neurite density and composition changes within the PCG are in keeping with the hypothesis that cortical dendrite alterations are occurring alongside the apparent central axonopathy underlying ALS.

NODDI highlighted CST axonal loss as the main contributing factor to the altered diffusivity profile observed using DTI in ALS. SBM analysis confirmed reduced cerebral WM and GM volumes associated with increased volume of the ventricles, consistent with cerebral atrophy.

Myelin content appears relatively preserved on qMTi, despite the loss of motor axons shown using NODDI, providing evidence against CST demyelination as a core feature of ALS. Altered molecular integrity within the upper CST axons supports axonal dysfunction in this region, occurring alongside the neurodegenerative changes demonstrated using NODDI.

Together the NODDI and qMTi findings are compatible with a central axonopathy underlying ALS with possible secondary myelin damage. The dissociation between myelin and axonal damage within the CST in ALS suggests novel pathological mechanisms, which are not yet fully understood. Insights into abnormal microstructure and altered biological mechanisms occurring '*in vivo*' can be achieved using NODDI and qMT in ALS.

## Table of contents

List of figures . . . . .	xii
List of tables . . . . .	xiv
List of abbreviations . . . . .	xvi

## CHAPTER 1: INTRODUCTION

<b>1.1 Amyotrophic Lateral Sclerosis (ALS)</b> . . . . .	<b>2</b>
1.1.1 ALS Clinical Phenotypes . . . . .	2
1.1.2 ALS and Fronto-Temporal Dementia (FTD) . . . . .	6
1.1.3 Familial ALS and Genetics . . . . .	8
1.1.4 Diagnosis . . . . .	11
1.1.5 Epidemiology . . . . .	13
1.1.6 Clinical assessments in ALS . . . . .	13
1.1.6.1 The revised Amyotrophic Lateral Sclerosis Functional Rating Scale (ALSFRS-R) . . . . .	13
1.1.6.2 The Total Medical Research Council (MRC) Score . . . . .	14
1.1.6.3 The Upper Motor Neurone Score . . . . .	15
1.1.6.4 The Edinburgh Cognitive and Behavioural Screen in Amyotrophic Lateral Sclerosis (ECAS) . . . . .	16
1.1.6.5 Clinical Staging of ALS . . . . .	17
1.1.7 Histopathological features within the motor system . . . . .	19
1.1.8 Molecular Pathogenesis . . . . .	21
1.1.8.1 Protein aggregation . . . . .	21
1.1.8.2 Neurofilament accumulation . . . . .	22
1.1.8.3 Axonal transport . . . . .	22
1.1.8.4 Glutamate excitotoxicity . . . . .	23
1.1.8.5 Oxidative stress . . . . .	24
1.1.8.6 Mitochondrial dysfunction . . . . .	25
1.1.8.7 Inflammation and glial cells . . . . .	25
1.1.8.8 RNA processing . . . . .	26
1.1.9 ALS Onset and Propagation . . . . .	27
1.1.10 Management . . . . .	29
1.1.10.1 Supportive and symptomatic management . . . . .	29
1.1.10.2 Disease modifying treatments . . . . .	30
1.1.11 Prognosis . . . . .	32
<b>1.2 Imaging in Amyotrophic Lateral Sclerosis</b> . . . . .	<b>34</b>
1.2.1 The Basics of Magnetic Resonance Imaging . . . . .	35
1.2.2 MRI in ALS . . . . .	36

1.2.3	Structural MRI . . . . .	37
1.2.4	Diffusion Tensor Imaging . . . . .	38
1.2.4.1	The Principles of Diffusion Tensor Imaging . . . . .	38
1.2.4.2	Diffusion Tensor Imaging in ALS . . . . .	41
1.2.4.3	Diffusion Tensor Imaging Structural Connectivity and Tractography . . . . .	43
1.2.4.4	Fractional Anisotropy as an Imaging Biomarker of Disease Progression in ALS . . . . .	44
1.2.4.5	Limitations of Diffusion Tensor Imaging . . . . .	44
1.2.5	Neurite Orientation Dispersion and Density Imaging (NODDI) . . . . .	45
1.2.5.1	The Principles of NODDI . . . . .	45
1.2.5.2	The NODDI Tissue Model . . . . .	46
1.2.5.3	NODDI segmentation model . . . . .	48
1.2.5.4	Neurological Studies using NODDI . . . . .	49
1.2.5.5	Advantages and limitations of NODDI . . . . .	50
1.2.6	Quantitative Magnetization Transfer Imaging . . . . .	53
1.2.6.1	Magnetization Transfer . . . . .	53
1.2.6.2	The Principles of Quantitative Magnetization Transfer . . . . .	56
1.2.6.3	Neurological Studies using qMT . . . . .	57
<b>1.3</b>	<b>Research Rationale, Objectives, and Study Design . . . . .</b>	<b>58</b>
1.3.1	Research Rational . . . . .	58
1.3.2	Research Objectives . . . . .	59
1.3.2.1	NODDI Hypotheses . . . . .	60
1.3.2.2	qMTi Hypotheses . . . . .	60
1.3.3	Study Design . . . . .	61
1.3.3.1	Sample size calculation . . . . .	61
1.3.3.2	Study approval and funding . . . . .	62
 <b>CHAPTER 2: CLINICAL DATA ACQUISITION AND ANALYSIS</b>		
<b>2.1</b>	<b>Participant Recruitment . . . . .</b>	<b>64</b>
<b>2.2</b>	<b>Participant Consenting and Screening . . . . .</b>	<b>64</b>
<b>2.3</b>	<b>Clinical Data Acquisition . . . . .</b>	<b>65</b>
2.3.1	Clinical Assessments of ALS participants . . . . .	65
2.3.2	The total Medical Research Council (MRC) score . . . . .	65
2.3.3	The upper motor neurone score . . . . .	66
2.3.4	The revised Amyotrophic Lateral Sclerosis Functional Rating Score (ALSFRS-R) . . . . .	66

2.3.5	The rate of change in ALSFRS-R .....	66
2.3.6	The Edinburgh Cognitive and Behavioural Screen in Amyotrophic Lateral Sclerosis (ECAS) .....	66
2.3.7	King's staging allocation .....	67
<b>2.4</b>	<b>Clinical Data Statistical analysis .....</b>	<b>67</b>
2.4.1	Participant demographics and clinical characteristics .....	67
2.4.2	ECAS cognitive scores and behavioural changes .....	68
2.4.3	Clinical Data Correlations .....	68
<b>2.5</b>	<b>Clinical Data Analysis .....</b>	<b>68</b>
2.5.1	Participant Demographics .....	69
2.5.2	Clinical Characteristics of the ALS group .....	69
2.5.3	Cognitive Impairment and Behavioural Changes .....	72
<b>2.6</b>	<b>Clinical Data Correlations .....</b>	<b>76</b>
<b>2.7</b>	<b>Clinical Results Discussion .....</b>	<b>78</b>
 <b>CHAPTER 3: QUANTITATIVE DIFFUSION-WEIGHTED MRI IN ALS</b>		
<b>3.1</b>	<b>Background .....</b>	<b>86</b>
<b>3.2</b>	<b>Hypotheses .....</b>	<b>87</b>
<b>3.3</b>	<b>Diffusion weighted MRI acquisition .....</b>	<b>88</b>
<b>3.4</b>	<b>Quantitative Diffusion Weighted MRI Data Processing .....</b>	<b>89</b>
<b>3.5</b>	<b>Statistical analysis of NODDI and DTI Data .....</b>	<b>90</b>
3.5.1	Whole brain voxel-wise analysis of NODDI and DTI parameters .....	90
3.5.2	Subgroup Analysis using NODDI parameters .....	90
3.5.3	Correlation Analysis of NODDI parameters with clinical measures of ALS .....	91
<b>3.6</b>	<b>NODDI parameters within the precentral gyrus .....</b>	<b>91</b>
<b>3.7</b>	<b>Whole Brain Voxel-Wise analysis comparing ALS and control groups ...</b>	<b>92</b>
3.7.1	NODDI Parameters .....	92
3.7.2	Diffusion tensor imaging parameters .....	92
<b>3.8</b>	<b>Analysis of NODDI parameters within the precentral gyrus .....</b>	<b>95</b>
<b>3.9</b>	<b>Subgroup analysis using the NODDI parameters .....</b>	<b>97</b>
3.9.1	Distribution of ALS .....	97
3.9.2	Kings Stages of ALS .....	99
3.9.2.1	NDI .....	99

3.9.2.2	ODI .....	99
3.9.2.3	ISO .....	103
3.9.3	Cognitive Involvement .....	104
<b>3.10</b>	<b>Correlation of the NODDI parameters with clinical measures of ALS ...</b>	<b>107</b>
<b>3.11</b>	<b>Quantitative diffusion weighted MRI parameters discussion .....</b>	<b>110</b>
3.11.1	NODDI detects cortical and corticospinal tract degeneration in ALS .....	110
3.11.2	NODDI parameter subgroup analysis discussion .....	113
3.11.3	NODDI parameter correlation with clinical measures of ALS discussion .....	117
3.11.4	NODDI in ALS limitations and conclusions .....	119
 <b>CHAPTER 4: QUANTITATIVE MAGNETIZATION TRANSFER IMAGING IN ALS</b>		
<b>4.1</b>	<b>Background .....</b>	<b>122</b>
<b>4.2</b>	<b>Hypotheses .....</b>	<b>123</b>
<b>4.3</b>	<b>Magnetization Transfer Magnetic Resonance Imaging Acquisition .....</b>	<b>124</b>
<b>4.4</b>	<b>Quantitative Magnetization Transfer (qMTi) Processing .....</b>	<b>125</b>
<b>4.5</b>	<b>Statistical Analysis of the qMTi data .....</b>	<b>125</b>
4.5.1	Whole Brain Voxel-Wise Analysis of qMTi Parameters .....	125
4.5.2	Subgroup Analysis using qMTi parameters .....	126
4.5.3	Correlation Analysis of qMTi parameters with clinical measures of ALS .....	126
4.5.4	Correlation of qMTi parameters with NODDI indices .....	127
<b>4.6</b>	<b>QMTi parameter whole brain comparison of ALS and control groups ...</b>	<b>127</b>
<b>4.7</b>	<b>QMTi parameter subgroup analysis results .....</b>	<b>129</b>
4.7.1	Distribution of ALS .....	129
4.7.2	Kings Stages of ALS .....	131
4.7.3	Cognitive involvement .....	132
<b>4.8</b>	<b>Correlation between qMTi data and clinical parameter results .....</b>	<b>132</b>
<b>4.9</b>	<b>Correlation between NODDI and qMTi parameter results .....</b>	<b>134</b>
<b>4.10</b>	<b>QMTi in ALS discussion .....</b>	<b>135</b>
4.10.1	Axonal dysfunction in ALS .....	136
4.10.2	Demyelination in ALS .....	140
4.10.3	Atrophy in ALS .....	143

4.10.4	QMTi in ALS limitations and conclusions	144
--------	---	-----

## **CHAPTER 5: STRUCTURAL MRI IN ALS**

<b>5.1</b>	<b>Background</b>	<b>146</b>
<b>5.2</b>	<b>Hypotheses</b>	<b>147</b>
<b>5.3</b>	<b>Structural imaging data acquisition</b>	<b>149</b>
<b>5.4</b>	<b>Structural imaging data processing</b>	<b>150</b>
<b>5.5</b>	<b>Surface-based morphometry statistical analysis</b>	<b>151</b>
5.5.1	SBM analysis comparing ALS and control groups	151
5.5.2	Subgroup analysis using SBM measures	151
5.5.3	Correlation analysis of SBM metrics with clinical measures of ALS	151
5.5.4	Correlation analysis of NODDI parameters with SBM metrics	151
<b>5.6</b>	<b>SBM results comparing ALS and control groups</b>	<b>152</b>
5.6.1	Cerebral volumes	152
5.6.2	Cortical thickness	157
5.6.3	Surface area	157
<b>5.7</b>	<b>SBM parameter subgroup analysis results</b>	<b>157</b>
5.7.1	Distribution of ALS	157
5.7.1.1	Cerebral volumes	161
5.7.1.2	Cortical thickness	156
5.7.1.3	Surface area	163
5.7.2	Kings Stages of ALS	164
5.7.2.1	Cerebral volumes	164
5.7.2.2	Cortical thickness	170
5.7.2.3	Surface area	172
5.7.3	Cognitive involvement	175
5.7.3.1	Cerebral volumes	175
5.7.3.2	Cortical thickness	178
5.7.3.3	Surface area	179
<b>5.8</b>	<b>Correlation between SBM data and clinical parameter results</b>	<b>181</b>
<b>5.9</b>	<b>Correlation between NODDI and SBM parameter results</b>	<b>183</b>
5.9.1	Correlation between NDI and SBM measures	183
5.9.2	Correlation between ODI and SBM measures	185
5.9.3	Correlation between ISO and SBM measures	190
<b>5.10</b>	<b>SBM in ALS discussion</b>	<b>195</b>

5.10.1	SBM volumes detect widespread atrophy associated with ALS . . . . .	196
5.10.2	SBM demonstrates PCG Atrophy in ALS . . . . .	198
5.10.3	SBM demonstrates GM Atrophy in ALS . . . . .	200
5.10.4	SBM demonstrates WM atrophy in ALS . . . . .	202
5.10.5	SBM measures correlate with NODDI parameters . . . . .	204
5.10.5.1	Correlations with NDI . . . . .	204
5.10.5.2	Correlations with ODI . . . . .	204
5.10.5.3	Correlations with ISO . . . . .	205
5.10.6	SBM in ALS limitations and conclusions . . . . .	206
<b>CHAPTER 6: MULTIMODAL IMAGING ANALYSIS OF NEURO-DEGENERATIVE CHANGES IN ALS</b>		
<b>6.1 Discussion</b> . . . . .		<b>210</b>
6.1.1 Multimodal analysis of WM changes in ALS . . . . .		210
6.1.2 Multimodal analysis of GM changes in ALS . . . . .		212
6.1.3 Multimodal analysis of atrophy in ALS . . . . .		213
<b>6.2 Conclusions</b> . . . . .		<b>214</b>
6.2.1 NODDI conclusions . . . . .		214
6.2.2 qMTi conclusions . . . . .		215
6.2.3 SBM conclusions . . . . .		215
<b>6.3 Study limitations</b> . . . . .		<b>216</b>
<b>6.4 Future Directions</b> . . . . .		<b>217</b>
<b>References</b> . . . . .		<b>219</b>
<b>Appendix</b> . . . . .		<b>259</b>
A1	Revised ALS functional rating scale (ALSFRS-R) . . . . .	259
A2	MRC score . . . . .	261
A3	UMN score . . . . .	263
A4	Edinburgh cognitive and behavioural screen in ALS (ECAS) . . . . .	264
A5	Favourable ethical opinion . . . . .	274
A6	BSMS Sponsorship . . . . .	278
A7	DeNDRoN . . . . .	280
A8	MNDA Funding . . . . .	281
A9	Consent forms . . . . .	283
A10	Screening forms . . . . .	285
A11	MRI safety questionnaire . . . . .	286



## List of Figures

Figure 1.1	Clinical, Genetic, and Pathological Overlap of ALS and FTD . . . . .	6
Figure 1.2	Major genes responsible for familial and sporadic ALS . . . . .	9
Figure 1.3	Genetic Landscape in ALS . . . . .	9
Figure 1.4	Atrophy of the spinal anterior nerve roots in ALS . . . . .	19
Figure 1.5	ALS associated pathological alterations in Betz cells of the motor cortex . . . . .	20
Figure 1.6	Neurodegenerative mechanisms proposed in ALS . . . . .	24
Figure 1.7	Multidisciplinary care in ALS . . . . .	29
Figure 1.8	The effect of magnetic field strength on net magnetization . . . . .	36
Figure 1.9	The Diffusion Tensor Model . . . . .	39
Figure 1.10	Diffusion Tensor Eigenvalues . . . . .	40
Figure 1.11	NODDI Tissue Compartment Model . . . . .	46
Figure 1.12	Watson distribution for a range of OD values . . . . .	47
Figure 1.13	The NODDI Parameters . . . . .	49
Figure 1.14	Transfer of magnetization between free and bound protons . . . . .	54
Figure 1.15	Two-pool model for quantification of MT . . . . .	56
Figure 1.16	The QMT parameters . . . . .	57
Figure 1.17	Sample Size Calculation using statistical software program . . . . .	62
Figure 2.1	Bimodal distribution of $\Delta$ ALSFRS-R . . . . .	72
Figure 2.2	Frequency of abnormal performance in the ALS group within each of the cognitive domains assessed using the ECAS . . . . .	75
Figure 2.3	Frequency of altered behaviour in the six behavioural domains . . . . .	75
Figure 2.4	A figure to show the parameter correlations within the clinical data . . . . .	77
Figure 3.1	Figure demonstrating the areas of significant difference between the ALS and control groups on whole brain analysis of the NODDI parameters . . . . .	93
Figure 3.2	Areas of significant difference between ALS and control groups on whole brain analysis of the DTI parameters . . . . .	95
Figure 3.3	Box plots to show the changes in PCG NODDI parameters in ALS . . . . .	96
Figure 3.4	Whole brain analysis of NODDI parameters comparing bulbar and limb ALS, limb confined ALS, and control subgroups . . . . .	98
Figure 3.5	Regions of difference on whole brain analysis of NDI comparing King's stages of ALS and control subgroups . . . . .	100
Figure 3.6	Regions of difference on whole brain analysis of ODI comparing King's stages of ALS and control subgroups . . . . .	102

Figure 3.7	Regions of difference on whole brain analysis of ISO comparing King's stages of ALS and control subgroups . . . . .	103
Figure 3.8	Whole brain analysis of NODDI parameters comparing normal ECAS, abnormal ECAS, and control subgroups . . . . .	106
Figure 3.9	NODDI parameter correlation with measures of ALS disease severity . . . . .	108
Figure 3.10	Correlation between ISO and age across all participants . . . . .	109
Figure 4.1:	Areas of significant difference between the ALS and control groups on whole brain analysis of $k_f$ . . . . .	128
Figure 4.2	Whole brain analysis showing reduced F and increased $T_{2f}$ in the ALS group at a less stringent statistical threshold . . . . .	129
Figure 4.3	Whole brain analysis demonstrates regions of significantly reduced $k_f$ on subgroup comparison . . . . .	131
Figure 4.4	Correlation between qMTi data and clinical parameters on whole brain analysis of the ALS group . . . . .	133
Figure 4.5	Correlation between qMTi and NODDI in the ALS group at a less stringent statistical threshold . . . . .	135
Figure 5.1	Comparison of the mean cerebral cortex volumes between control and ALS groups . . . . .	154
Figure 5.2	Comparison of the mean cerebral WM volumes between control and ALS groups . . . . .	154
Figure 5.3	Comparison of mean GM volumes between control and ALS groups . . . . .	155
Figure 5.4	Comparison of mean PCG volumes between control and ALS groups . . . . .	155
Figure 5.5	Comparison of mean normalized volumes of the ventricular system, brainstem, and corpus callosum between control and ALS groups. . . . .	156
Figure 5.6	Comparison of mean cortical thickness between control and ALS groups . . . . .	156
Figure 5.7	Comparison of PCG volumes between limb only and bulbar limb ALS subgroups . . . . .	160
Figure 5.8	Comparison of cerebral WM volume between King's stage 2 and King's stage 3 ALS subgroups . . . . .	169
Figure 5.9	Correlation between SBM parameters and clinical measures of ALS . . . . .	181
Figure 5.10	Correlation between NDI and SBM parameters . . . . .	184
Figure 5.11	Correlation between ODI and SBM volume measures . . . . .	187

Figure 5.12	Correlation of ODI with WM and corpus callosum volumes . . . . .	188
Figure 5.13	Correlation of ODI with PCG and ventricle volumes . . . . .	189
Figure 5.14	Correlation between ODI and cortical thickness . . . . .	190
Figure 5.15	Correlation between ISO and SBM volume measures . . . . .	193
Figure 5.16	Correlation between ISO and ventricle volume . . . . .	194
Figure 5.17	Correlation between ISO and temporal lobe SBM measures . . . . .	194

## List of Tables

Table 1.1	The clinical features of MND subtypes . . . . .	4
Table 1.2	Genetics of ALS and ALS-FTD . . . . .	10
Table 1.3	Recent genetic discoveries in ALS . . . . .	11
Table 1.4	Revised El Escorial Criteria with applied awaji-shima consensus . . . . .	12
Table 1.5	ECAS cognitive scoring and assessed behavioural changes . . . . .	16
Table 1.6	Diagnosis of ALS-Frontotemporal Spectrum Disorder using the ECAS .	17
Table 1.7	Comparison of the King’s Clinical Staging with MITOS staging system .	18
Table 1.8	Management of ALS symptoms . . . . .	31
Table 1.9	Factors affecting rate of progression . . . . .	33
Table 1.10	Similarities and differences between NODDI and DTI . . . . .	51
Table 2.1	Inclusion and Exclusion Criteria . . . . .	62
Table 2.2	ECAS cut of scores for detecting cognitive impairments . . . . .	64
Table 2.3	Demographics of ALS and healthy control groups . . . . .	65
Table 2.4	Clinical characteristics of the ALS group . . . . .	67
Table 2.5	Individual participant with sporadic ALS clinical data . . . . .	68
Table 2.6	Phenotypes within the ALS group . . . . .	69
Table 2.7	ECAS scores and behavioural changes in the ALS group . . . . .	71
Table 2.8	Correlations between clinical variables within the ALS group . . . . .	73
Table 3.1	Regions of significant differences in quantitative diffusion imaging parameters between ALS and control groups . . . . .	90
Table 3.2	NODDI parameters within the PCG . . . . .	92
Table 3.3	Regions of significant differences in NODDI parameters comparing ALS subgroups and the control group . . . . .	95
Table 3.4	Regions of significant differences in NODDI parameters comparing King’s Stages of ALS subgroups and the control group . . . . .	97
Table 3.5	Regions of significant differences in NODDI parameters comparing cognitive subgroups of ALS and the control group . . . . .	101
Table 3.6	Regions of significant correlation between NODDI parameters and clinical measures of ALS severity . . . . .	104

Table 4.1	Regions of significant differences in qMT parameter $k_f$ between ALS and control groups . . . . .	124
Table 4.2:	Regions of differences in qMT parameters $F$ and $T_{2f}$ between ALS and control groups at a less stringent statistical threshold . . . . .	126
Table 4.3	Regions of significantly reduced $k_f$ on subgroup comparison using whole brain analysis . . . . .	127
Table 4.4	Regions of significant correlation between qMTi parameters and clinical measures of ALS severity . . . . .	129
Table 4.5	Regions of correlation between qMTi and NODDI parameters on whole brain analysis of the ALS group . . . . .	131
Table 5.1	Region of interest SBM measures comparing control and ALS group .	148
Table 5.2	Subgroup analysis comparing cerebral volumes in regions of interest between control and ALS subgroups based on disease distribution . . . . .	153
Table 5.3	Subgroup analysis comparing cortical thickness in regions of interest between control and ALS subgroups based on disease distribution . . . . .	156
Table 5.4	Subgroup analysis comparing surface area in regions of interest between control and ALS subgroups based on disease distribution . . .	158
Table 5.5	Subgroup analysis comparing region of interest cerebral volumes between control and ALS subgroups based on King's stage of ALS . . . . .	160
Table 5.6	Subgroup analysis comparing region of interest cortical thickness between control and ALS subgroups based on King's stage of ALS . . . . .	165
Table 5.7	Subgroup analysis comparing region of interest surface area between control and ALS subgroups based on King's stage of ALS . . .	168
Table 5.8	Subgroup analysis comparing region of interest volume between control and ALS cognitive subgroups . . . . .	171
Table 5.9	Subgroup analysis comparing region of interest cortical thickness between control and ALS cognitive subgroups . . . . .	173
Table 5.10	Subgroup analysis comparing region of interest cerebral surface area between control and ALS cognitive subgroups . . . . .	175
Table 5.11	Correlation of SBM parameters with clinical measures of ALS . . . . .	177
Table 5.12	Regions of significant correlation between NDI and SBM parameters .	177
Table 5.13	Regions of significant correlation between ODI and SBM parameters .	180
Table 5.14	Regions of significant correlation between ISO and SBM parameters .	186

## Abbreviations

<b>AD</b>	Axial diffusivity
<b>ALS</b>	Amyotrophic lateral sclerosis
<b>ALSbi</b>	ALS with behavioural impairment
<b>ALSci</b>	ALS with cognitive impairment
<b>ALScbi</b>	ALS with cognitive and behavioural impairment
<b>ALSFRS-R</b>	Revised ALS functional rating scale
<b>ΔALSFRS-R</b>	Rate of change in ALSFRS-R
<b>ALSFTD</b>	ALS with frontotemporal dementia
<b>ALSFTSD</b>	ALS frontotemporal spectrum disorder
<b>CISC</b>	Clinical imaging sciences centre
<b>CNS</b>	Central nervous system
<b>C9orf72</b>	Chromosome 9, open reading frame 72
<b>CSF</b>	Cerebrospinal fluid
<b>CST</b>	Corticospinal tract
<b>CT</b>	Cortical thickness
<b>DTI</b>	Diffusion tensor imaging
<b>ECAS</b>	Edinburgh cognitive and behavioural screen
<b>F</b>	Fractional size of the restricted pool
<b>FA</b>	Fractional anisotropy
<b>FTD</b>	Frontotemporal dementia
<b>FUS</b>	Fused in sarcoma
<b>GABA</b>	γ-aminobutyric acid
<b>GM</b>	Grey matter
<b>IBM</b>	International business machines corporation
<b>ISO</b>	Isotropic compartment
<b>k<sub>f</sub></b>	Forward magnetization exchange rate
<b>LMN</b>	Lower motor neurone
<b>MD</b>	Mean diffusivity
<b>MND</b>	Motor neurone Disease
<b>MRI</b>	Magnetic resonance imaging
<b>MTC</b>	Magnetization transfer contrast
<b>MTR</b>	Magnetization transfer ratio
<b>NDI</b>	Neurite density index
<b>NODDI</b>	Neurite orientation dispersion and density imaging
<b>ODI</b>	Orientation dispersion index
<b>PBP</b>	Progressive bulbar palsy
<b>PCG</b>	Precentral gyrus
<b>PLIC</b>	Posterior limb of the internal capsule
<b>PLS</b>	Primary lateral sclerosis
<b>PMA</b>	Progressive muscular atrophy
<b>qMTi</b>	Quantitative magnetization transfer imaging
<b>RD</b>	Radial diffusivity
<b>ROI</b>	Region of interest
<b>RsfMRI</b>	Resting-state functional MRI
<b>SA</b>	Surface area
<b>SBM</b>	Surface-based morphometry
<b>SOD1</b>	Superoxide dismutase 1
<b>SPM12</b>	Statistical parametric mapping, version 12
<b>SPSS</b>	Statistical package for the social sciences
<b>T<sub>2f</sub></b>	Relaxation time of the free pool
<b>TDP-43</b>	Trans-activation response DNA-binding protein 43
<b>UMN</b>	Upper motor neurone
<b>WM</b>	White matter

# **CHAPTER 1: INTRODUCTION**

## CHAPTER 1 INTRODUCTION

The first part of this chapter will provide an overview of amyotrophic lateral sclerosis (ALS), also referred to in the United Kingdom as motor neurone disease (MND). This relentlessly progressive neurodegenerative disease of spinal and cortical motor neurones ultimately renders a sufferer unable to move, speak, and breathe.<sup>1,2</sup> Death typically occurs within 5 years of symptom onset.<sup>1-5</sup> ALS therefore contributes significantly to morbidity and mortality worldwide, but currently no treatment is available for halting progression of the disease.<sup>6,7</sup>

There are major challenges in finding an effective treatment for ALS due to the exquisite complexity of the disease pathogenesis, which is not yet fully understood, along with the heterogeneity of the disease in both phenotype and genotype.<sup>8-15</sup>

Neuroimaging offers a tool for investigating the alterations occurring within the brain in those living with ALS. There is a drive towards finding imaging biomarkers for diagnostic, staging, and deep phenotyping in ALS, in order to stratify patients more appropriately for clinical trials, in the hope that this will lead to better success in finding treatment options.<sup>4,16-20</sup>

In the second part of this chapter I will cover the background of advanced magnetic resonance imaging (MRI) techniques used in ALS and what these have demonstrated so far regarding the pathophysiological basis of ALS. I will then give an overview of two relatively novel advanced imaging techniques which I have used in my research study with the aim of better understanding the structural and functional changes accompanying ALS '*in vivo*'.

### 1.1 Amyotrophic Lateral Sclerosis (ALS)

#### 1.1.1 ALS Clinical Phenotypes

The French physician Jean-Martin Charcot first described the association between the pathological and clinical findings in ALS in 1874, using the term la sclérose latérale amyotrophique.<sup>21-25</sup> To this day amyotrophic lateral sclerosis (ALS) remains a universally applied diagnostic term, in particular when referring to the most common presentation of the disease with clinical features reflecting involvement of both upper and lower motor neurones.<sup>1,3,5,26</sup>

In the UK the term MND is used collectively to encompass all the different ALS-related disorders, see table 1.1. This nomenclature was introduced by Lord Walter Russel Brain,<sup>27</sup> (Brain 1962), who recognized the relationship between the syndromes of ALS, progressive bulbar palsy (PBP), and progressive muscular atrophy (PMA). He observed the variation in upper and lower motor neuron component clinically amongst

these syndromes and the variable distribution in loss of the anterior horn cells pathologically.

Disease onset appears to be random and focal, where symptoms can present in the bulbar muscles (about 25%), limbs muscles (about 70%), and axial or respiratory muscles (about 5%).<sup>3,13,28–32</sup> This is likely to reflect a similarly discrete and random pathological process occurring within the motor neuroaxis, where upper motor neurone (UMN) and lower motor neurone (LMN) networks converge. Motor dysfunction in the region of onset progresses and there is concurrent spread to affect neighbouring muscle groups. This suggests that there is neuro-anatomically contiguous spread of the underlying aetiology within the motor system.<sup>13,33,34</sup> Once the disease process has been triggered, spread is thought to occur by two mechanisms depending on the location of the pathology and the relevant neuroanatomy. Spread of pathology across the spinal cord is possible at the level of the LMN, which can lead to symptoms arising in the contralateral limb.<sup>13,35</sup> UMN symptoms typically spread in an ipsilateral manner, from arm to leg, due to the somatotopic representation of the body within the primary motor cortex. Clinical phenotypes therefore become increasingly complex over time due to independent spread of pathology at the UMN and LMN levels.<sup>13,34,36,37</sup>

The UMN's are comprised of the giant Betz cells or pyramidal neurones, which reside in layer V of the cerebral neocortex histologically.<sup>38</sup> They arise predominantly within the primary motor cortex where they are arranged somatotopically between the sylvian fissure and cingulate gyrus. Their myelinated axons project caudally through the centrum semiovale, corona radiata, (posterior limb) internal capsule, and into the cerebral peduncle, from where they descend through the pons and medullary pyramids before entering the anterior horn of the spinal cord and terminating on the alpha motor neurones. These pathways are known collectively as the pyramidal or cortico-spinal tracts (CST).<sup>39,40</sup> Clinical features of UMN dysfunction are spasticity, loss of fine motor skills, and hyperreflexia.<sup>3,29,32,41</sup>

The spinal alpha motor neurones are the LMNs, the cell bodies of which are located in both the anterior horn (Rexed laminar IX) of the spinal cord and also more rostrally within the cranial nerve motor nuclei of the brainstem. LMNs are also organized somatotopically and project to muscles segmentally.<sup>13,42</sup> LMN dysfunction leads to wasting, fasciculation, weakness, flaccidity, and diminished deep tendon reflexes.<sup>3,29,32,41</sup>

Sporadic ALS is typically characterized by the degeneration of both UMN and LMN groups. However, the clinical phenotypes are extremely heterogeneous and vary in site of onset, extent of UMN and LMN involvement, and rate of progression,<sup>3,28,30,32,41,43</sup> see table 1.1.



**Table 1.1: The clinical features of MND subtypes.**

MND subtype	Clinical Features	References
Charcot-type ALS subtypes: - <ul style="list-style-type: none"> <li>• Spinal onset ALS</li> <li>• Bulbar onset ALS</li> </ul>	The most common phenotype of ALS is a combination of UMN and LMN signs in the limbs (cervical or lumbar disease onset). Rarely thoracic onset occurs, which may present with truncal weakness. Bulbar onset ALS, presents with difficulties in speech and swallowing, with limb involvement later in the course of the disease.	Wijesekera LC & Leigh PN, 2009. <sup>1</sup> Norris F et al., 1993. <sup>30</sup>
Regional variants of ALS <ul style="list-style-type: none"> <li>• Flail arm variant (Brachial amyotrophic diplegia)</li> <li>• Flail leg variant (Leg amyotrophic diplegia)</li> <li>• Progressive bulbar palsy or Isolated bulbar ALS</li> </ul>	In regional variants of ALS, the disease remains localized to a single spinal segment for more than a year. They are usually asymmetrical at onset but become symmetrical over time. The pattern of flail arm onset is typically proximal while flail leg is often distal. These eventually progress into Charcot-type ALS.	Jawdat O et al., 2015. <sup>44</sup> Wijesekera LC & Leigh PN, 2009. <sup>1</sup>
Primary lateral sclerosis (PLS)	Slowly progressive UMN disorder of the limbs and bulbar muscles. Patients lacking LMN involvement after 4 years are unlikely to progress to ALS.	Stratland JM et al., 2015. <sup>50</sup>
Progressive muscular atrophy (PMA)	A rare, sporadic, adult onset, slowly progressive LMN disorder affecting the limbs. UMN features emerge in up to 30% within 5-10 years of onset.	Liewluck T & Saperstein DS, 2015. <sup>54</sup>
Geographical variants of ALS <ul style="list-style-type: none"> <li>• Guam ALS</li> <li>• Madras ALS</li> </ul>	ALS is prevalent among the indigenous Chamorros of Guam and is distinguished by association with a parkinsonism-dementia complex and the Guam retinal pigment epitheliopathy  Young adult onset of asymmetrical slowly progressive limb weakness, facial and bulbar palsy, cranial nerve involvement including sensorineural deafness.	Morris HR et al., 2001. <sup>45</sup> Geser F et al., 2008. <sup>46</sup>  Shankar SK et al., 2000. <sup>47</sup>

A table to show the clinical features of MND subtypes including those originally described by Charcot, regional variants, UMN and LMN subtypes, and geographic variants.

The most frequent phenotype is spinal onset ALS, initially affecting either the arms or legs, relating to cervical and lumbar spine disease onset respectively. Rarely the thoracic spinal segments are the first to be involved leading to symptoms of truncal weakness and often early respiratory compromise.<sup>3,30,32,41,48</sup>

There are two variants of ALS which present with bulbar symptoms of dysarthria or dysphagia. Those with bulbar onset ALS often develop limb symptoms within 1-2 years and this presentation is associated with reduced survival.<sup>1,3,30</sup> However, PBP can be distinguished from bulbar-onset ALS and is associated with a better prognosis of up to 4 years. PBP is typically seen in women of over 65 years and the disease remains localized for longer with predominantly UMN features.<sup>3,48</sup> A better prognosis is also seen in the initially localized “flail arm” and “flail leg” variants, both of which are predominantly lower motor neuron at presentation.<sup>3,41</sup>

There are sporadic variants of ALS which exist at either end of a spectrum and remain largely restricted to either the UMN or the LMNs. These are known as primary lateral sclerosis (PLS) and PMA respectively. The recognition of PLS was by German neurologist Wilhelm Heinrich Erb in the mid-1870s.<sup>49</sup> This is a rare syndrome of purely UMN dysfunction accounting for 1-3% of all MND presentations<sup>50-54</sup>

Despite being functionally debilitating over time the disease course for PLS is more benign, with slower progression than typical ALS. A small proportion of those who present with only UMN involvement initially go on to develop LMN features and electrophysiological LMN changes within the first four years<sup>51,55-57</sup>

PMA is at the other end of the spectrum being characterized by purely LMN involvement, however, like PLS it is sporadic and rare affecting 5–10% of those with MND.<sup>58</sup> A higher proportion (20-30%) of those with PMA develop UMN features within 5–10 years of symptom onset.<sup>59</sup> In addition subclinical evidence of UMN degeneration is evident in a proportion of PMA patients in neurophysiology, radiology, and pathology studies.<sup>58-61</sup>

There are forms of ALS observed in specific geographical locations which appear somewhat distinct from the classical ALS described, for example Guamanian and Madras ALS variants, please see table 1.1.

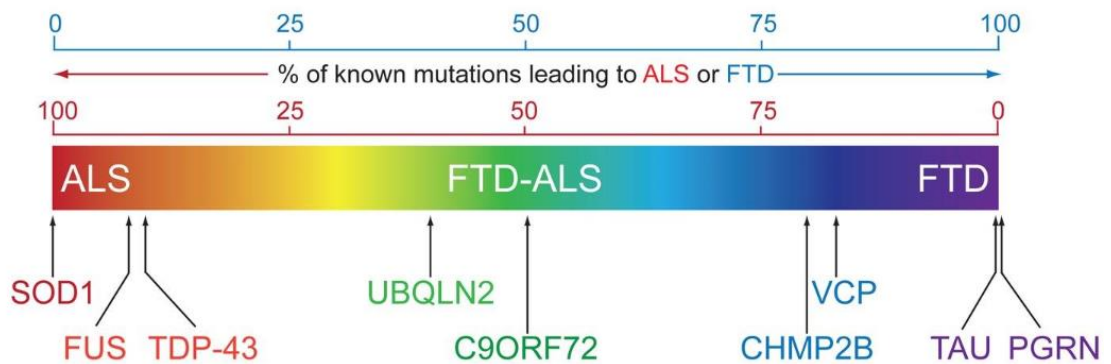
I will be using the term ALS to describe the disorder originally defined by Charcot, where a combination of upper and lower motor neuron involvement is accompanied by a spectrum of clinical phenotypes in terms of site of onset (arm, leg, bulbar) and subsequent spread of signs to cause widespread motor system dysfunction.

### 1.1.2 ALS and Frontotemporal Dementia (FTD)

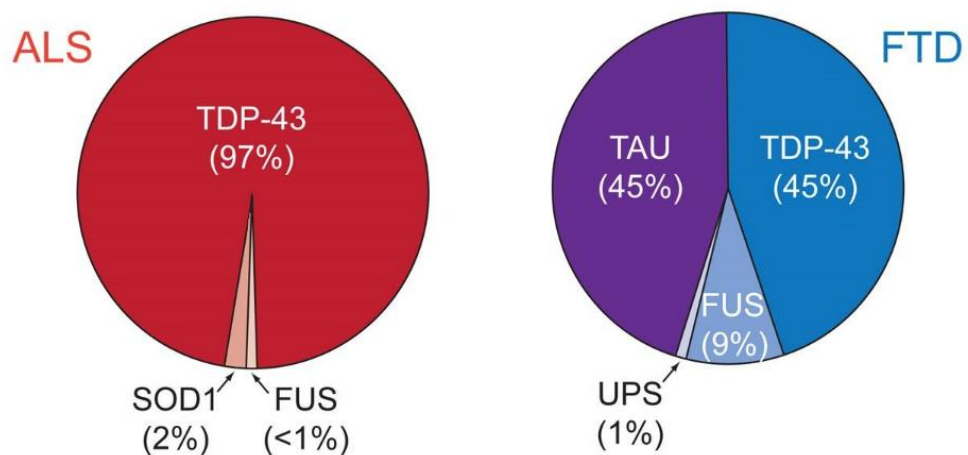
ALS is on a spectrum with frontotemporal dementia (FTD), clinically, genetically and pathologically, see figure 1.1.<sup>62,63</sup> FTD, also known as frontotemporal lobar degeneration, is the second most common dementia following Alzheimer's disease. It is characterised by personality and behavioural changes, as well as deficit in language skills, associated with neuronal degeneration within the frontal and temporal cortices<sup>64-66</sup>

**Figure 1.1: Clinical, genetic, and pathological overlap of ALS and FTD**

#### A. Genetics of ALS and FTD



#### B. Pathological inclusions in ALS and FTD



A figure to show the clinical, genetic, and pathological overlap between ALS and FTD, used with permission from Ling S et al., Neuron 2013.<sup>62</sup> (A) ALS and FTD represent a continuum of a broad neurodegenerative disorder with each presenting the extremes of a spectrum of overlapping clinical symptoms (ALS in red and FTD in purple). Major known genetic causes for ALS and FTD are plotted according to the ratio of known mutations. (B) Pathological protein inclusions in ALS and FTD, according to the major accumulated protein. Inclusions of TDP-43 and FUS in ALS and FTD reflect the pathological overlap of ALS and FTD.

Genetic discoveries, improved understanding of molecular mechanisms, and advances in neuroimaging techniques have all played important roles in the linking of ALS to FTD.<sup>67-70</sup> This concept of a continuum between ALS and FTD, which has become evident

at the clinical, genetic, and pathological levels, emerged particularly during the last decade,<sup>62,63,67</sup> see figure 1.1.

It has been estimated that 15% of patients with FTD present with motor neurone dysfunction sufficient for the diagnostic criteria of ALS, while 15% of patients with ALS exhibit cognitive and behavioural changes meeting the diagnostic criteria for FTD.<sup>71,72</sup> However, in a further 35% of patients with ALS there is evidence of fronto-temporal dysfunction, where milder behavioural and cognitive deficits are present that do not meet the criteria for FTD.<sup>72-75</sup>

The international diagnostic criteria for frontotemporal dysfunction in ALS were developed in 2009.<sup>76</sup> These recognised that ALS could exist as a pure motor syndrome, coexist with FTD, or exhibit neuropsychological deficits insufficient to meet the diagnostic criteria for FTD but nonetheless causing impairment in either cognitive function (ALS with cognitive impairment; ALS<sub>ci</sub>) or in behaviour (ALS behavioural impairment; ALS<sub>bi</sub>). The criteria also acknowledged that a small proportion of ALS patients could develop a dementia not typical of FTD, and instead called ALS-Dementia.

More recently the term ALS frontotemporal spectrum disorder (ALS-FTSD) has been introduced to encompass the range of deficits associated with frontotemporal pathology in ALS.<sup>77</sup> This includes ALS cognitive impairment (ALS<sub>ci</sub>), ALS behavioural impairment (ALS<sub>bi</sub>), and ALS cognitive and behavioural impairment (ALS<sub>cbi</sub>). These are typically identified using the Edinburgh Cognitive and Behavioural Screen (ECAS).

The ECAS was introduced in 2014 as a means of screening for both cognitive and behavioural changes in the clinical setting.<sup>78</sup> This multi-domain assessment designed for use in patients with motor deficits has been validated against extensive neuropsychology,<sup>79</sup> see section 1.1.6.4 on ECAS, appendix A4 for the full ECAS assessment and Table 1.5 for ECAS scoring.

The hallmarks of cognitive dysfunction in ALS are deficits in executive function, verbal fluency, language, and social cognition.<sup>71,73-78,80</sup> The frontal cortex has been identified as associated with the cognitive profile associated with ALS in both structural and functional imaging studies,<sup>81,82</sup> in particular the dorsolateral prefrontal cortex.<sup>83,84</sup> More recently a study using transmission electron microscopy to study synapses in the prefrontal cortex showed a significant decrease in synaptic density in the ALS cohort and increase in the number of degenerating, electron dense, pre-synaptic terminals.<sup>72</sup> Interestingly these synaptic alterations were not accompanied by significant atrophy.

Language deficits and behavioural abnormalities can exist independently or occur alongside executive dysfunction.<sup>85-87</sup> Frontotemporal dysfunction as well as isolated cognitive or behavioural changes are associated with a significantly worse prognosis in ALS and have important management implications as they increase caregiver burden. The reduction in ALS survival associated with executive dysfunction

is independent to other prognostic factors such as age of onset, baseline severity of disease, and respiratory status.<sup>72-74,84-86</sup>

The most common behavioural abnormality in ALS is reported as apathy<sup>74,88</sup> and, when present, is associated with changes in the anterior cingulate gyri on voxel-based morphometry and diffusion tensor imaging.<sup>74,89,90</sup> Additional features include loss of empathy and disinhibition.<sup>74,91</sup> Typical deficits in social cognition observed in ALS are lack of insight and reduced ability to recognize the emotional states of others.<sup>87,92,93</sup>

Memory deficits have also been demonstrated to be associated with ALS, where impaired verbal memory has been shown to correlate with hippocampal atrophy of the grey matter. However, the presence of memory deficit does not appear to affect prognosis in ALS.<sup>74,88,89</sup>

Visuospatial skills appear to be relatively well preserved in ALS and when present are thought to be mediated through language dysfunction.<sup>74,88,89,94</sup>

Occasionally ALS is associated with psychiatric symptoms such as hallucinations and delusions, which may be the initial feature, often followed by cognitive and finally amyotrophic symptoms.<sup>95</sup> This is thought to be a characteristic of ALS-FTD syndrome associated with the C9orf72 gene mutation. In one study, psychotic symptoms predated the onset of either ALS or FTD in 38% of patients found to harbour the C9orf72 mutation.<sup>69,96</sup>

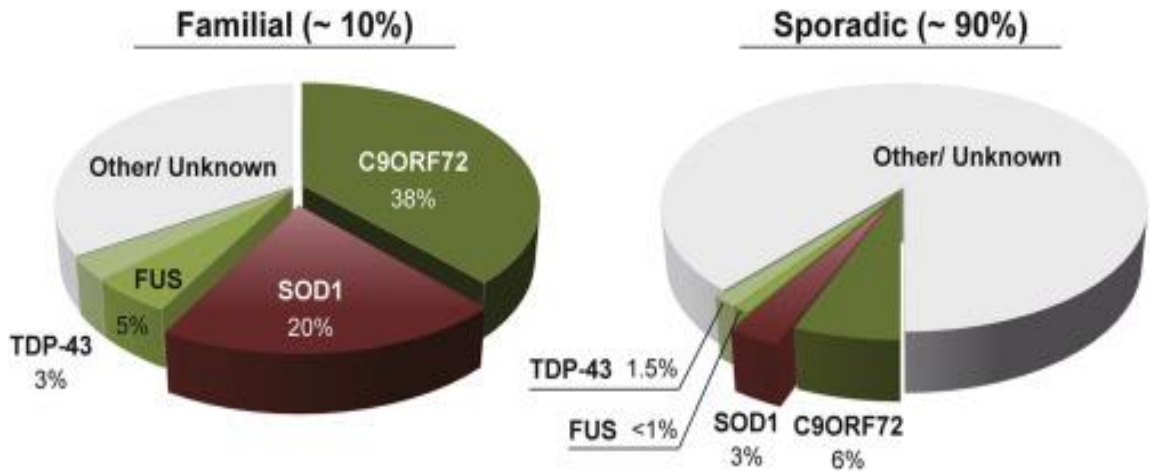
### **1.1.3 Familial ALS and Genetics**

The majority of ALS cases are sporadic 90–95%, with familial ALS accounting for only 5–10% of cases.<sup>1,3,5,26</sup> However, some of the more common genes responsible for familial ALS are also found in a proportion of sporadic ALS cases, see figure 1.2.<sup>97</sup> Familial ALS exhibits predominantly autosomal dominant inheritance, however autosomal recessive and X-linked forms also exist, see table 1.2.<sup>98,99</sup>

It is likely that all cases of sporadic ALS have a heritable component. A recent population-based study looking at heritability of ALS found that those who have a first degree relative with sporadic ALS are at increased risk of developing ALS (1.4% lifetime risk), compared with the general population (0.3% lifetime risk).<sup>100</sup>

The genetic heterogeneity of ALS has become evident through the implementation of whole genome sequencing techniques, which have identified a wide range of DNA variants now recognized as being potentially disease modifying or causative, see table 1.2 and figure 1.3. More than 20 gene mutations are now thought to be linked to ALS, however for a large proportion of patients no gene defect is identified.<sup>101,102</sup>

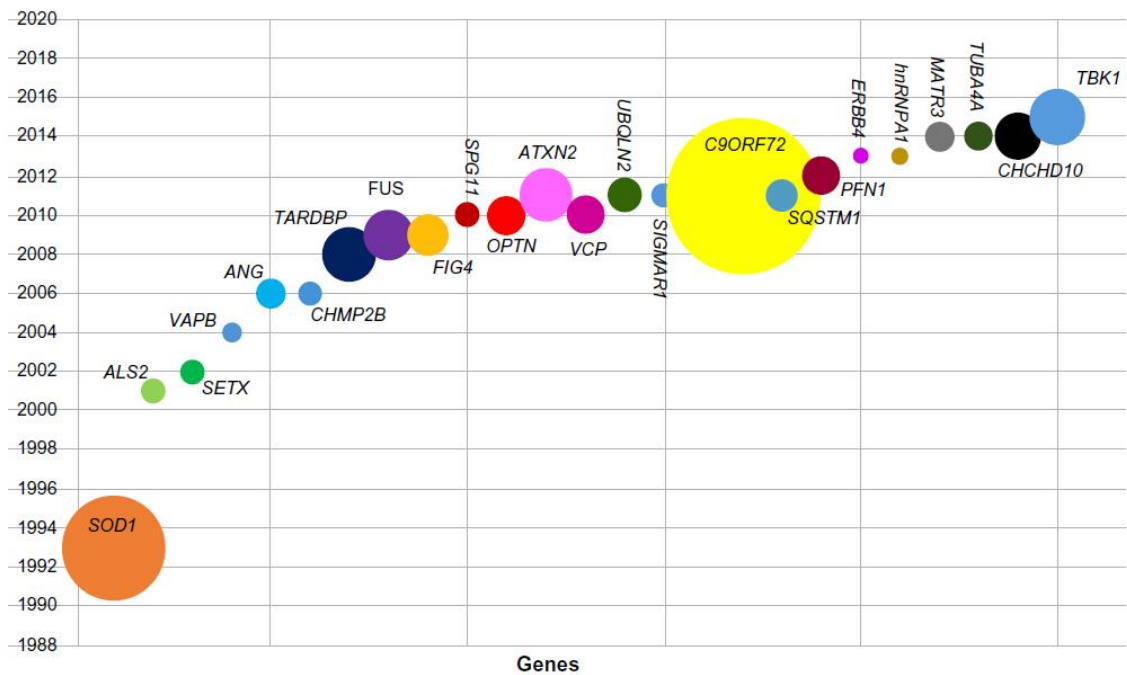
**Figure 1.2: Major genes responsible for familial and sporadic ALS.**



A figure to show the main gene mutations recognized in familial and sporadic ALS, demonstrating the genetic overlap and also the large proportion of unknown genetic factors contributing to sporadic ALS. Taken with permission from Hayashi A et al., 2016.<sup>96</sup>

The most common gene variant in ALS is the abnormal expansion of a hexanucleotide repeat (GGGGCC) in open reading frame 72 of chromosome 9 (C9orf72). This along with superoxide dismutase 1 (SOD1), transactive response DNA-binding protein 43 (TDP-43), and fused in sarcoma (FUS) constitute the genetic component found in over 50% of patients with ALS.<sup>97,98,100,101</sup>

**Figure 1.3: Genetic landscape in ALS**



A figure to demonstrate the expanding number of genes relating to ALS, reproduced with permission from Alsultan A et al., 2016.<sup>100</sup> Genes are plotted against the year they were discovered and the size of the circle reflects the frequency of the mutation.

**Table 1.2: Genetics of ALS and ALS-FTD**

	Gene	C/S	Onset (inheritance)	References
ALS 1	Superoxide dismutase 1 (SOD1)	21q22.1	Adult > juvenile (AD)	Rosen D et al., 1993 <sup>103</sup>
ALS 2	Alsin	2q33.2	Juvenile (AR)	Yang Y et al. 2001 <sup>104</sup>
ALS 3	Unknown (ALS3)	18q21	Adult (AD)	Hand C et al., 2002 <sup>105</sup>
ALS 4	Senataxin (SETX)	9q34	Juvenile > adult (AD)	Chen Y et al., 2004 <sup>106</sup>
ALS 5	Spatacsin (SPG11)	15q21.1	Juvenile > adult (AR)	Orlacchio A et al., 2010 <sup>107</sup>
ALS 6	Fused in sarcoma/ translocated in liposarcoma (FUS/TLS)	16p11.2	Adult > juvenile (AD)	Kwiatkowski T et al., 2009 <sup>108</sup>
ALS 7	Unknown (ALS7)	20q13	Adult (AD)	Sapp P et al., 2003 <sup>109</sup>
ALS 8	Vesicle associated membrane protein (VAPB)	20q13.3	Adult > juvenile (AD)	Nishimura A et al., 2004 <sup>110</sup>
ALS 9	Angiogenin (ANG)	14q11.2	Adult > juvenile (AD)	Greenway M et al., 2006 <sup>111</sup>
ALS 10	TAR DNA binding protein (TDP43)	1p36.22	Adult (AD)	Sreedharan J et al., 2008 <sup>112</sup>
ALS 11	Factor induced gene 4 (FIG4)	6q21	Adult (AD)	Chow C et al., 2009 <sup>113</sup>
ALS 12	Optineurin (OPTN)	10p13	Adult(AD/AR)	Maruyama H et al., 2010 <sup>114</sup>
ALS 13	Ataxin 2 (ATXN2)	12q24	Adult > juvenile (AD)	Elden A et al., 2010 <sup>115</sup>
ALS 14	Vasolin-containing protein (VCP)	9p13	Adult > juvenile (AD)	Johnson J et al., 2010 <sup>116</sup>
ALS 15	Ubiquilin 2 (UBQLN2)	Xp11.21	Adult > juvenile (XD)	Deng H et al., 2011 <sup>117</sup>
ALS 16	Sigma non-opioid intracellular receptor 1 (SIGMAR1)	9q13.3	Juvenile (AD)	Al-Saif A et al., 2011 <sup>118</sup>
ALS 17	Chromatin modifying protein 2B (CHMP2B)	3p12.1	Adult (AD)	Cox L et al., 2010 <sup>119</sup>
ALS 18	Profilin 1 (PFN1)	17p13.2	Adult (AD)	Wu C et al., 2012 <sup>120</sup>
ALS 19	Erb-b2 receptor tyrosine kinase 4 (ERBB4)	2q33.3-q34	Adult (AD)	Takahashi Y et al., 2013 <sup>121</sup>
ALS 20	Heterogeneous nuclear ribonucleoprotein A1 (hnRNPA1)	12q13.1	Adult (AD)	Kim H et al., 2013 <sup>122</sup>
ALS-FTD1	C9ORF72	9q21.2	Adult (AD)	Renton A et al. 2011 <sup>123</sup>

A table to show the genetic subtypes of ALS and FTD, adapted from Alsultan A et al., 2016.<sup>100</sup> C/S, chromosome; AD, autosomal dominant; AR, autosomal recessive; XD, X-linked dominant.

**Table 1.3: Recent genetic discoveries in ALS**

Gene	Chromosome	Description
TBK1	12q14.1	TANK binding kinase 1 interacts with autophagy adapters such as Optineurin and is involved in the removal of defective mitochondria. TBK1 ALS variants are associated with the ALS-FTD spectrum. <sup>124</sup>
CCNF	16p13.3	Cyclin F is a ubiquitously expressed protein involved in degradation of abnormal proteins and co-ordinating the cell cycle. <sup>125</sup>
GLE1	9q34.11	GLE 1 encodes two isoforms involved in nuclear export of mRNA and stress granule function. <sup>126</sup>
TUBA4A	2q35	Tubulin alpha 4A is involved in the structural stability and dynamics of the cytoskeleton microtubules. <sup>127</sup>
MATR3	5q31.3	Matrin-3 is a nuclear matrix protein that binds to RNA and DNA. It also interacts with TDP-43. Johnson JO et al., 2014 (106 LW) <sup>128</sup>
NEK1	4q33	NEK1 is involved in regulating mitochondrial cell death. The family of kinases to which NEK1 belongs is involved in preventing DNA damage induced cell death. <sup>129</sup>
TIA1	2p13.3	T-cell-restricted intracellular antigen-1 (TIA1), is a cytotoxic granule-associated RNA-binding protein <sup>130</sup>
GLT8D1	3p21.1	GLT8D1 encodes a glycosyltransferase enzyme, which is widely expressed but its function is unknown. <sup>131</sup>
ANXA11	10q22.3	Annexin A11 is a vesicular trafficking protein, which belongs to a group of calcium-dependent phospholipid-binding proteins. <sup>132</sup>
KIF5A	12q13.3	KIF5A is involved in axonal transport along the cytoskeleton, and mediates the transport of RNA binding proteins. <sup>133</sup>

A table to show more recently discovered gene mutations associated with ALS, adapted from White M and Sreedharan J. 2016.<sup>134</sup>

The genetic component in susceptibility to developing ALS is evident; however, the relationship between DNA variations and disease pathogenesis is complex. There are likely to be combined effects of multiple genes which ultimately determine an individual's susceptibility to ALS. This along with environmental factors and stochastic accumulation of DNA methylation damage within the genome through life could contribute to the overall likelihood of developing the disease.<sup>135</sup> Molecular genetic studies in ALS have provided crucial advances in the understanding of disease pathogenesis and identified potential therapeutic targets<sup>135–137</sup>

#### 1.1.4 Diagnosis

The diagnosis of ALS remains clinical and is based on detecting the presence of a progressive motor syndrome with evidence of both upper and lower motor neuron



degeneration in the absence of electrophysiological or neuroimaging evidence for an alternative disease process.<sup>1,3,5,31,138</sup>

The El Escorial Criteria were introduced in 1994 by the world federation of neurology and later revised in 1998 with the Airlie house criteria.<sup>139,140</sup> The Awaji consensus provided further recommendations in 2008, in order to recognize the importance of electrophysiological findings in improving diagnostic capacity.<sup>141,142</sup> These criteria categorize the diagnosis of ALS into three levels of certainty; definite, probable, or possible, according to the presence and spread of UMN and LMN signs on clinical and neurophysiological assessment. However, the criteria were originally developed for the purposes of clinical research and are recognized as having limitations in clinical practice as they are not fully encompassing of the heterogeneity in ALS, particularly the restricted phenotypes such as progressive bulbar palsy and flail limb variants, as well as PLA and PMA<sup>143,144</sup>. The World Federation of Neurology therefore published a further revision in 2015 with the principle recommendation of the former criteria for ‘possible ALS’ being sufficient for a diagnosis of ALS to facilitate more timely diagnosis and the opportunity for those with restricted phenotypes to participate in clinical trials.<sup>145</sup> An alternative diagnostic framework incorporating a phenotypic classification and recognizing the cognitive domain would be beneficial in clinical practice.<sup>5</sup>

There is a consistently recognized diagnostic delay of approximately one year from symptom onset, likely due to the insidious onset of initially mild symptomatology.<sup>1,3,4,31,146,147</sup>

**Table 1.4: Revised El Escorial criteria with applied awaji-shima consensus**

Definite ALS	Clinical or electrophysiological evidence of UMN and LMN dysfunction in the bulbar region and at least two spinal regions Or UMN and LMN signs in three spinal regions
Probable ALS	Clinical or electrophysiological evidence of UMN and LMN dysfunction in at least two regions, with some UMN signs rostral to LMN signs
Possible ALS	Clinical or electrophysiological evidence of UMN and LMN dysfunction in one region Or UMN signs alone in at least two regions Or LMN signs rostral to UMN signs

A table to show the combined El Escorial criteria and awaji-shima consensus, adapted from Costa J et al., 2012.<sup>140</sup>

### **1.1.5 Epidemiology**

ALS is a rare disease with an incidence of 1-3/100,000 in Europe and a prevalence of 7-9/100,000.<sup>148,149</sup> The overall lifetime risk for ALS is 1:400 for women and 1:350 for men.<sup>3</sup> The mean life expectancy from symptom onset is 30 months.<sup>26</sup> Peak age of onset is 58-63 years for sporadic ALS and incidence decreases rapidly after the age of 80 years.<sup>3</sup>

The established risk factors for developing ALS are family history, older age, and male gender.<sup>150,151</sup> Environmental factors such as physical activity, body mass index, head trauma, smoking, exposure to pesticides, proximity to blue-green algae, and military service have all been proposed but remain speculative associations.

### **1.1.6 Clinical Assessments in ALS**

#### **1.1.6.1 The revised ALS functional rating Scale (ALSFRS-R)**

The ALSFRS-R is a questionnaire used to assess the functional ability of participants with ALS in carrying out common daily activities.<sup>152</sup> The original ALS functional rating scale (ALSFRS) was developed in 1996 as a feasible tool to evaluate functional capabilities as well as functional decline over time in patients with ALS.<sup>153</sup> It was validated against quantitative muscle testing and global assessment scales and gained popularity as a screening measure for clinical trials in ALS.<sup>154</sup> However, the original ALSFRS did not include assessment of respiratory function, and subsequently the ALSFRS-R was developed in 1999.<sup>152</sup>

In the ALSFRS-R bulbar function, gross motor function, fine motor function, and respiratory function, are each assessed with a series of three questions, which are allocated a score on the scale of 0 – 4. This gives a maximum possible score of 12 for each domain and a total score of 48, see appendix A1. The ALSFRS-R provides a profile of functional loss within these clinically relevant domains, which can be used as a marker of disease severity and propagation. However, studies examining functional validity suggest that, due to being multidimensional, the total ALSFRS-R score is not a valid representation of disease severity.<sup>155–157</sup>

Nonetheless, the ALSFRS-R has become a universally employed rating scale in both research trials and clinical practice. It has also been incorporated into ALS disease progression and survival models.<sup>158–164</sup>

In the individual patient with ALS, the decline in ALSFRS-R is not usually consistent throughout the course of their disease.<sup>165</sup> Plateaus and even small reversals in the ALSFRS-R score have been reported over short periods of time.<sup>166</sup> However, ultimately multiple domain scores will decrease over time as the disease progresses. Within the ALS population there is also heterogeneity in decline in ALSFRS-R, which is influenced by additional factors such as age, body mass index, FVC, and phenotype.<sup>165</sup>

The ALSFRS-R showed higher sensitivity for monitoring disease progression when compared to MRI biomarkers.<sup>167</sup>

In clinical trials the ALSFRS-R is often measured longitudinally at certain time points to monitor decline in ALSFRS-R.<sup>166</sup> However, as this is not always possible in research, the rate of change of ALSFRS-R ( $\Delta$ ALSFRS-R) is used as an alternative measure of rate of disease progression.<sup>168</sup> This is determined by dividing the change in ALSFRS-R score by the disease duration, assuming that the ALSFRS-R was 48 at disease onset.<sup>169,170</sup>

In MRI studies of ALS the ALSFRS-R sub-scores have been shown to correlate with voxel based morphology measures of cortical volume and cortical thickness in relevant areas of the primary motor cortex.<sup>171,172</sup> Rate of progression has been shown to negatively correlate with volume of the left primary motor cortex.<sup>170</sup> A measure of axonal integrity, Fractional Anisotropy (FA), of the corticospinal tract assessed using diffusion tensor imaging (DTI) tract-based spatial statistics also demonstrates correlation with ALS rate of progression.<sup>173</sup>

#### **1.1.6.2 The Total Medical Research Council (MRC) Score**

The Medical Research Council (MRC) first published a scale for muscle power in 1942 (Aids to the Investigation of Peripheral Nerve Injuries, War Memorandum No. 7), during the second world war, when there was a sudden increase in cases of peripheral nerve damage. Over the years this text was revised and reprinted many times, becoming a text valued by practicing clinicians. In 1976 it was republished with a new title 'Aids to the Examination of the Peripheral Nervous System (Memorandum No. 45). Now in its fifth edition, this atlas remains regarded with high esteem by physicians keen to understand how to assess for abnormal function of peripheral nerves.<sup>174</sup>

The MRC muscle scale grades muscle power on a scale of 0 to 5, where 0 represents no muscle contraction, 1 is used for a flicker of contraction, 2 represents movement with gravity eliminated, 3 is used for active movement against gravity, 4 represents active movement against gravity and resistance, and 5 relates to normal power expected for that muscle. When a full neurological examination is performed there are typically twenty two pairs of muscles assessed for power, therefore when added together this gives a possible maximum total score out of 220, please see pages 4-6 of the neurological assessment in appendix A2.

One study comparing the MRC scale to an analogue scale where power was expressed as a percentage of the maximum expected for that muscle suggested that the MRC grade could be more reliable in weaker muscles (grade 0-3) but less accurate in stronger muscles (grade 4-5).<sup>175</sup> Studies reporting a statistically significant correlation between clinical MRC score and imaging markers of disease in ALS are limited, however

one functional MRI (fMRI) study demonstrated correlation between reduced activity in the left primary motor cortex and MRC total score.<sup>170</sup>

Alternative neurophysiological techniques Motor Unit Number Estimation (MUNE) and Motor Unit Number Index (MUNIX), which quantify the number of motor units, have become established in recent years.<sup>176</sup> Nonetheless, the MRC scale provides a practical means to easily assess muscle strength and is often incorporated into the assessments of ALS participants in clinical trials and research studies.<sup>170</sup> Furthermore, good reliability and reproducibility for manual muscle testing have been demonstrated in ALS.<sup>177</sup>

### **1.1.6.3 The Upper Motor Neurone Score**

Upper motor neuron (UMN) dysfunction is a crucial component to detect for the diagnosis of ALS.<sup>1,3,5,8</sup> Clinical identification is by eliciting features such as spasticity, clonus, brisk reflexes, spread of reflexes, and positive Babinski sign. However, detecting signs of UMN dysfunction can be challenging when there is concurrent lower motor neuron (LMN) involvement, particularly in the earlier stages of disease.<sup>178,179</sup> UMN signs are reportedly absent in 7-10% of those initially presenting with ALS.<sup>180</sup> In later stages of ALS, preserved reflexes in a weak and wasted limb can be an indication of simultaneous UMN involvement.<sup>139</sup> However, the extent of UMN degeneration may not be accurately presented by the clinical phenotype as suggested by post-mortem studies, where UMN degeneration is reported identified in 50-75% of patients lacking clinical signs of corticospinal tract involvement.<sup>181</sup> This highlights the requirement for improved biomarkers of UMN pathology in ALS. Timely identification of UMN involvement would reduce diagnostic delay and improve access to clinical trials, where the eligibility criteria are usually stringent. Furthermore, assessment of cortical motor neuron involvement is vital for gaining insight into the pathogenesis of ALS.<sup>182</sup>

Approaches to study UMN function include clinical physiological techniques such as Transcranial Magnetic Stimulation (TMS), and neuroimaging techniques including structural MR and functional MRI, Diffusion Tensor Imaging (DTI), and Positron Emission Tomography (PET).<sup>180,182-184</sup> DTI derived values of FA within the CST have been reported to correlate with UMN scores in studies of ALS.<sup>180</sup>

In this study the UMN burden will be evaluated using the UMN score previously described by Turner MR et al., 2004,<sup>185</sup> see appendix A3. Tendon reflexes at the face, jaw, biceps, supinators, triceps, fingers, knees, and ankles are assessed for pathological briskness, and there is additional assessment for extensor plantar responses (Babinski sign). The total possible score is 16 according to the presence of pathologically brisk reflexes at all sites bilaterally and positive Babinski sign bilaterally.

#### 1.1.6.4 The Edinburgh Cognitive and Behavioural Screen in ALS (ECAS)

The Edinburgh Cognitive and Behavioural Screen in Amyotrophic Lateral Sclerosis (ECAS) is a screening tool designed to detect cognitive and behavioural changes in ALS,<sup>77</sup> see appendix A4 for full ECAS assessment document. The ECAS categorizes components of cognitive function into domains which are either relatively specific to ALS (language, verbal fluency, executive function) or relatively non-specific to ALS (memory and visuospatial), see table 1.5.

It was designed to distinguish between different profiles of cognitive impairments, for example Alzheimer's dementia versus fronto-temporal dementia. It allows for difficulties in verbal communication and weakness of the hands so that most participants with ALS are able to complete the ECAS without being limited by the physical burden of the disease.

**Table 1.5: ECAS cognitive scoring and assessed behavioural changes.**

Cognitive Scores			Behavioural Assessment	
Component	Total score possible	Cut off	Behavioural	Present or absent
Language	28	26	Behavioural disinhibition	Present or absent
Verbal Fluency	24	14	Apathy or inertia	Present or absent
Executive	48	33	Loss of sympathy or empathy	Present or absent
<b>ALS Specific score</b>	<b>100</b>	<b>77</b>		
Memory	24	13	Perseverative, stereotypes, compulsive or ritualistic behaviour	Present or absent
Visuospatial	12	10	Hyper-orality or altered food preferences	Present or absent
<b>ALS non-specific score</b>	<b>36</b>	<b>24</b>		
<b>ECAS total score</b>	<b>136</b>	<b>105</b>	Psychosis	Present or absent

A table to show the cut off scores in the ECAS cognitive domains as well as the behavioural traits that may be observed in ALS.

In addition, there is a behavioural assessment screen for the typical behavioural changes observed in ALS. Scoring of cognitive domains and documentation of behavioural changes are shown in table 1.5. The maximum sensitivity and specificity to detect ALS cognitive impairment is gained by using a combination of deficit in either ALS-specific scores or ECAS total.<sup>78</sup>

Table 1.6 demonstrates how ALS-FTSD can be diagnosed according to the recently revised diagnostic criteria using the ECAS,<sup>76</sup> where the cut off scores are given in table 1.5.

**Table 1.6: Diagnosis of ALS-Frontotemporal Spectrum Disorder using the ECAS**

<b>ALS-FTSD</b>	<b>Deficit</b>
ALSci	Deficit in ether ECAS
	OR ALS-specific scores
ALSbi	Presence of apathy
	OR Two other behavioural symptoms <sup>76,77,490</sup>
ALScbi	Combined deficits meeting the criteria for both ALSci and ALSbi
ALS-FTD	Evidence of progressive deterioration in behaviour and/or cognition AND the presence of at least two behavioural symptoms together with deficit in ALS-specific ECAS scores <sup>490</sup>
	OR the presence of at least two behavioural /cognitive symptoms together with psychotic symptoms and/or loss of insight.
	OR the presence of language impairment meeting the criteria for semantic dementia/ semantic variant primary progressive aphasia (PPA) or non-fluent PPA, which may co-exist with cognitive and behavioural deficits described above
ALS-D	ALS with dementia not typical of FTD

A table to demonstrate the different cognitive and/or behavioural disorders within the frontotemporal spectrum and the associated deficits, adapted from Strong M et al., 2017)<sup>76</sup>

#### **1.1.6.5 Clinical Staging of ALS**

The standard clinical assessments described above can be combined and used to derive stages of ALS. Staging of the disease is of particular importance for the purpose of clinical trials in ALS, as it allows assessment of progression in a typically heterogeneous population and thereby provides more robust analysis of treatment affect. It is also useful

to stratify ALS participants in research studies according to stage of disease and assess whether this has any implications on the findings. As anticipated more advanced stages are often associated with more statistically significant results.<sup>186</sup> The most widely used staging systems used clinically are the King’s Clinical Staging<sup>187</sup> and the MITOS staging systems,<sup>188</sup> see table 1.7.

In the King’s staging system, stages 1–3 are based on the number of body regions affected by ALS (bulbar, upper limb, lower limb involvement), while stage 4 reflects nutritional and/or respiratory failure.

The Milano–Torino staging (MITOS) system is based on the ALSFRS-R, where each stage reflects the loss of independence in that number of functional domains (bulbar, gross motor, fine motor and respiratory). Neither of these staging classifications incorporate cognitive or behavioural features of ALS. In both staging systems stage 0 denotes the pre-symptomatic stage and stage 5 represents death.

**Table 1.7: Comparison of the King’s Clinical Staging with MITOS staging system**

Stage	King’s Clinical Stage	MITOS Stage
0	Pre-symptomatic (disease onset)	Functional involvement (early disease)
1	One clinical region involved	Loss of independence in one functional domain
2	Two clinical regions involved	Loss of independence in two functional domains
3	Three clinical regions involved	Loss of independence in three functional domains
4	Nutritional or respiratory failure	Loss of independence in four functional domains
5	Death	Death

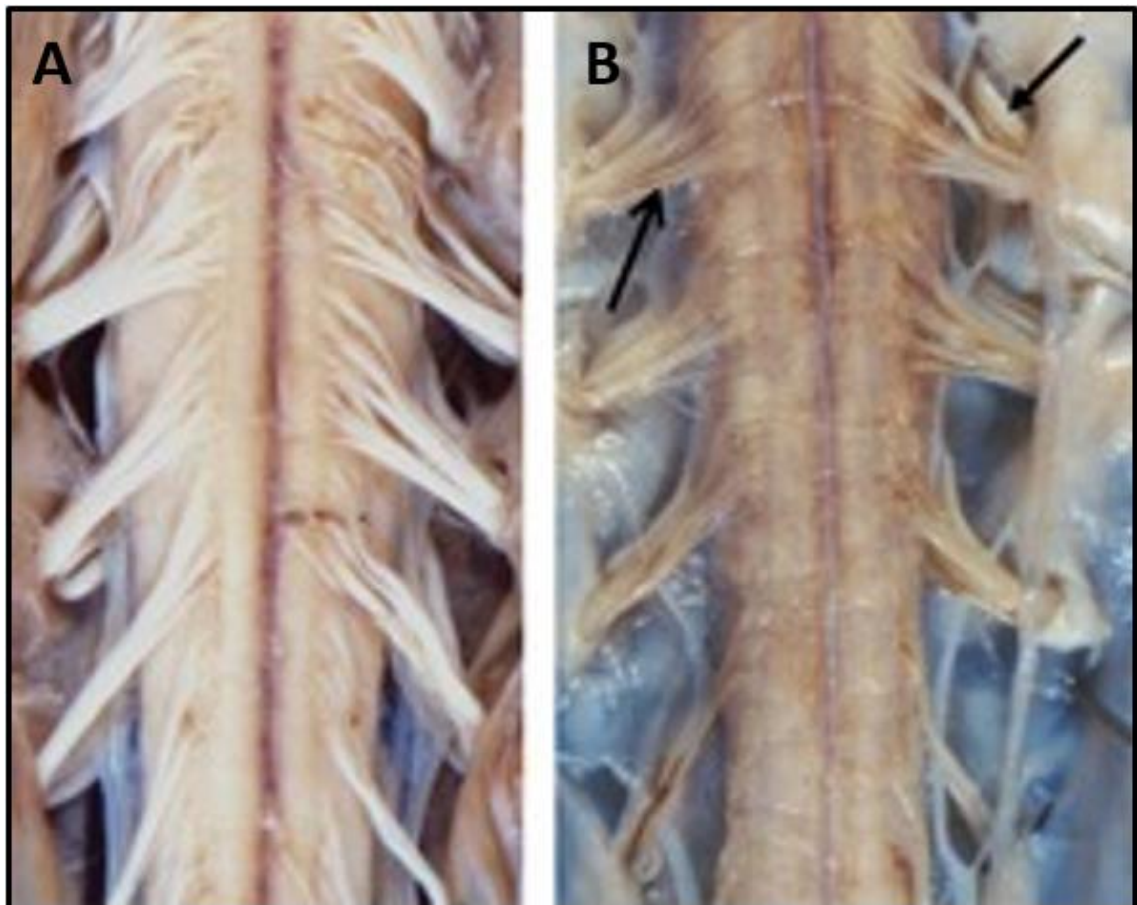
The King’s staging system is reportedly more sensitive to early changes in ALS, while the MITOS staging is more sensitive in the later stages of the disease.<sup>189–191</sup> As a result, further staging systems for ALS have recently been proposed in the literature, such as the ‘Fine Til Nine’ (FT9) staging system, which is also based on the ALSFRS-R scale where the stage is allocated according to the number of ALSFRS-R domains where the score falls below 9.<sup>192</sup>

### 1.1.7 Histopathological features within the motor system

There is ample evidence to suggest that ALS is a multisystem disease process affecting the brain and the spinal cord. However, the motor system is the fundamental target for the pathological insult and this is evident both clinically and pathologically.<sup>1,3,5,8</sup> The cardinal features of ALS on autopsy, which represents the end stage of the disease, are loss of anterior horn cells within the spinal cord, reduced motor cells in the lower cranial nerve motor nuclei, and degeneration of the corticospinal tracts.<sup>193–195</sup>

Macroscopic examination of the post mortem brain in ALS may show no gross abnormality but, in some cases, demonstrates atrophy predominantly of the precentral gyri<sup>196</sup> or generalized atrophy of the cerebral hemispheres.<sup>193</sup> Atrophy of the frontal and temporal cortex is typically seen in patients with ALS-FTD.<sup>195</sup> Flattening of the pyramidal bulbs is also described.<sup>197</sup> A reduction in white matter is often observed predominantly within the corticospinal tracts.<sup>196</sup> The anterior nerve roots and the lateral horns of the spinal cord often appear sclerotic, see figure 1.4. Finally, the skeletal muscles often exhibit striking atrophy, pallor, and fibrosis.<sup>196</sup>

**Figure 1.4: Atrophy of the spinal anterior nerve roots in ALS.**

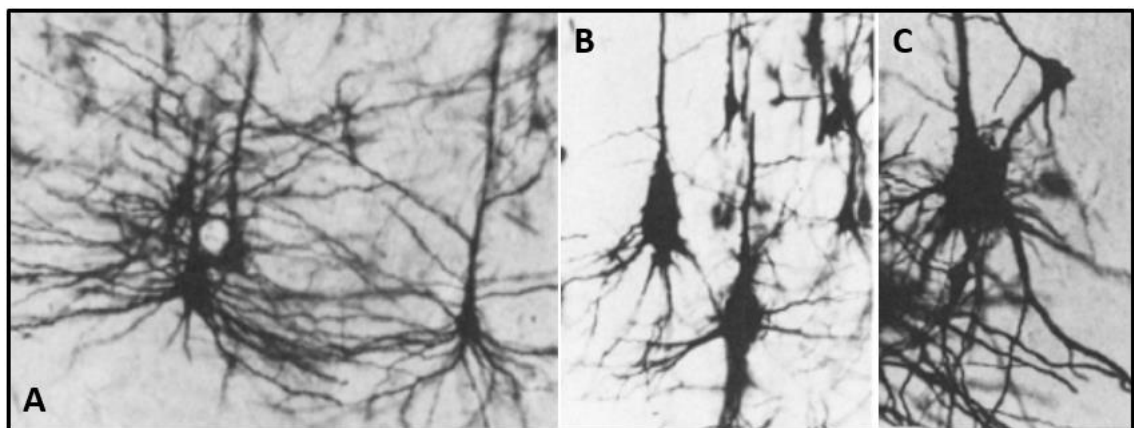


A figure to show anterior nerve root atrophy in the spinal cord of those with ALS at post mortem (B), compared with control (A), adapted from <https://static.cambridge.org>



Microscopic changes are universally evident in ALS and involve all components of the motor system. In the motor cortex loss of the giant pyramidal cells of Betz in lamina 5 of the precentral gyrus (PCG) is a recognized feature of ALS.<sup>194,197</sup> However, there is some controversy as one study failed to detect a reduction in total number of neurones within the primary motor cortex using the rigorous technique of stereological quantification,<sup>198</sup> while others have found loss of both large pyramidal neurones and GABAergic interneurons in the primary motor cortex associated with ALS.<sup>199</sup> The remaining Betz cells may appear shrunken and exhibit pathological alterations such as a decline in dendritic arborization affecting both the apical and basal regions, reduced numbers of dendritic spines, and fragmentation or irregularities of the remaining dendrites, see figure 1.5.<sup>195,200</sup> Dendritic changes in the motor cortex are associated with a reactive astrocytic gliosis of the Betz cell soma, vacuolization, and spongiosis,<sup>195,196</sup> see figure 1.5. Degeneration of the commissural fibers linking the cerebral hemispheres through the corpus callosum have frequently been observed to be involved histopathologically.<sup>192,193,196</sup>

**Figure 1.5: ALS associated pathological alterations in Betz cells of the motor cortex.**



A: Normal Betz cells. B: Moderate denegeneration of Betz cells with reduced dendrites and early gliosis. C: Reactive gliosis of the Betz cell soma, reduced dendrites, and loss of dendritic spines. Adapted from Hammer RP et al., 1979.<sup>195</sup>

Axonal loss associated with myelin pallor and gliosis is observed within the descending CSTs in post mortem studies.<sup>194</sup> Variable degeneration of the corticospinal tracts can be traced from the subcortical WM caudally into the posterior limb of the internal capsule, through the pons and medullary pyramids into the cord.<sup>193,194,201</sup> In 1941 Charles Davison studied 37 autopsy cases of ALS and found that 12 had total CST degeneration from the motor cortex to the spinal cord. In 2 cases CST degeneration was evident from the cerebral peduncles and in a further 19 degeneration extended from the brainstem (7-pons, 12-medullar) to the spinal cord. In the 4 remaining cases degeneration was limited

to the spinal cord.<sup>200</sup> In 45 cases studied by Betty Brownell et al., 1970 less than half had complete pyramidal degeneration and in 10 CST degeneration was undetectable.<sup>193</sup> This is likely to reflect the variability in distribution of degeneration associated with ALS.

In the spinal cord, degeneration of anterior horn cells is a consistent feature, associated with atrophy, loss of dendrites, and gliosis of the remaining large alpha neurones.<sup>195</sup> There is relative sparing of the motor nucleus of Onufrowicz in the second sacral segment (S2) of the spinal cord.<sup>202</sup> The motor neurones within the ventral horn of the brainstem are similarly affected, however there is relative sparing of the oculomotor cranial nerve nuclei.<sup>1</sup>

While predominantly affecting the motor regions, degenerative changes have also been reported in the temporal, parietal, and cingulate gyri.<sup>193</sup> Degenerating fibres associated with reactive gliosis have also been described in the basal ganglia.<sup>195</sup>

### **1.1.8 Molecular Pathogenesis**

The disease mechanisms underlying ALS are not fully understood and are likely to be complex. The motor neurons of the brain and spinal cord are some of the largest cells in the body with a cell body of 0.1mm and axons reaching up to 1 metre in length. This unique structure may explain selective vulnerability of the motor system to the degenerative process occurring in ALS.<sup>37</sup>

Motor neuron degeneration is thought to be the end point for a number of converging pathogenic cellular mechanisms. Many questions remain unanswered such as what is the trigger leading to initiation of degeneration, why are the motor neurones selectively vulnerable, and what are the molecular mechanisms leading to propagation of the pathogenic process.

#### **1.1.8.1 Protein aggregation**

A key histopathological feature associated with degeneration of both the upper and lower motor neurones is the presence of intra-neuronal inclusions within the degenerating neurons and associated glial cells.<sup>1</sup> These abnormal protein aggregates are thought to be pathogenic, however it is difficult to distinguish between cause and consequence.<sup>1,3-5,195,203</sup> Mutated proteins accumulate, oligomerize and aggregate, gaining toxic function.<sup>204,205</sup> Aberrant inclusions containing mutated TDP-43, FUS, and SOD-1 have been found in both sporadic and familial cases of ALS.<sup>1,195,203,204</sup>

TDP-43 protein inclusions are found in most cases of ALS and are also found in some cases of fronto-temporal dementia.<sup>206-210</sup> TDP-43 is a widely expressed and highly conserved RNA-binding protein involved in regulation of RNA metabolism, in particular pre-mRNA splicing, mRNA stability and transport. Preventing DNA damage is an

important role of TDP-43.<sup>211</sup> TDP-43 is normally located in the nucleus but aberrant protein inclusions accumulate in the cytoplasm, possible due to mutations that lead to changes in protein expression, structural conformation, and ability to be shuttled to the nucleus.<sup>212–214</sup> Inclusions containing mutated FUS, another RNA-binding nuclear protein which accumulates in the cytoplasm, and mutated SOD-1 protein are also associated with ALS.<sup>196,215</sup>

Additional components of the protein inclusions in ALS are ubiquitin, neurofilaments, mitochondrial proteins and chaperones. Accumulation of ubiquitinated protein aggregates within the cytoplasm could have a deleterious effect on the function of the proteasome, preventing normal degradation of proteins and facilitating protein accumulation, thereby contributing to motor neuron degeneration.<sup>195</sup> The proteins found within aggregates are intimately linked to vital neuronal cellular processes including oxidative stress, altered RNA processing, mitochondrial dysfunction, inflammation, and excitotoxicity.

RNA binding proteins such as TDP43 and FUS have two potential conformations, the unfolded and the aggregated state. Once the aggregated conformation has been adopted these proteins can sequester further proteins to join the aggregated state and spread accumulation of aggregated proteins in a prion-like manner, providing one potential hypothesis to the spread of pathology in ALS.<sup>216,217</sup>

#### **1.1.8.2 Neurofilament accumulation**

Another pathological hallmark in ALS is the accumulation of aggregated neurofilaments within the proximal axon and cell bodies, often together with peripherin.<sup>218</sup> These intermediate filaments are the most abundant components of myelinated axon cytoskeleton.<sup>205</sup> Mutations in both neurofilament and peripherin genes are associated with familial forms of ALS.<sup>134</sup> Mutations in neurofilament genes leads to abnormal phosphorylation, hindering their transport along the axon and leading to accumulation in the cell body and proximal axon. Accumulation of aberrant neurofilament may hinder the transport of other vital constituents for cellular processes (e.g. mitochondria).<sup>205</sup>

#### **1.1.8.3 Axonal transport**

Impaired axonal transport is one theory behind the erroneous protein aggregates and accumulation of neurofilament within the axons.<sup>219–222</sup> Physiological mechanisms of axonal transport rely on the normal functioning of kinesin for anterograde transport along the axon away from the soma towards the axon terminal and the dynein-dynactin complex for retrograde transport towards the soma. Additionally, neurofilaments, microtubules, and other soluble proteins are required for normal functioning of these

systems. There is constant trafficking of cargo such as mitochondria, secretory vesicles, endosomes, and neurotrophin. The intracellular transport mechanisms are fundamental in maintaining the health of the whole neuronal cell from the nucleus to the distal axon, which can reach up to 1 metre. The intracellular transport mechanisms are therefore fundamental in maintaining the health of the whole cell from the nucleus to the distal axon and synapse. This highlights an inherent vulnerability of the motor neurones, where altered efficiency of transporting cargo has potential to stress the cell and if not resolved may ultimately lead to cell death.<sup>218-221</sup>

Impaired axonal transport is evident in SOD-1 transgenic mice models of ALS.<sup>223,224</sup> Aggregates of TDP-43, SOD-1, and FUS proteins, within the axon potentially contribute to interrupted transport mechanisms.<sup>205,219</sup>

#### **1.1.8.4 Glutamate excitotoxicity**

Dysregulation of glutamate signalling is implicated as a mechanism of motor neuron loss in sporadic ALS. Excess glutamate induces repetitive stimulation of postsynaptic glutamate receptors, potentially leads to massive influx of calcium into the neurons followed by increased nitric oxide resulting in neuronal toxicity and ultimately death.

Studies have shown increased glutamate levels in the CSF of patients with ALS, raising the suspicion of glutamate-mediated mechanisms contributing to neuronal cell death in ALS.<sup>225-227</sup>

The glial glutamate transporter EAAT2 is responsible for clearing synaptic glutamate.<sup>226</sup> One study found a reduction in glutamate transport in ALS, associated with a loss of the EAAT2 protein.<sup>228</sup> A genetic mutation affecting the EAAT2 transporter has been identified in a patient with sporadic ALS, which causes aberrant targeting to the neuronal membrane and subsequent decrease in glutamate uptake.<sup>229</sup> Affected spinal neurons have been shown to have reduced intracellular calcium-binding components (eg; Calbindin), supporting an excitotoxic component to neuronal loss.<sup>230,231</sup>

Alternative potential mechanisms contributing to excitotoxicity are the disruption of cortical inhibitory  $\gamma$ -aminobutyric acid (GABA) circuits, motor neuron ionic channel dysfunction, and astrocytic dysregulation of potassium homeostasis.<sup>232,233</sup>

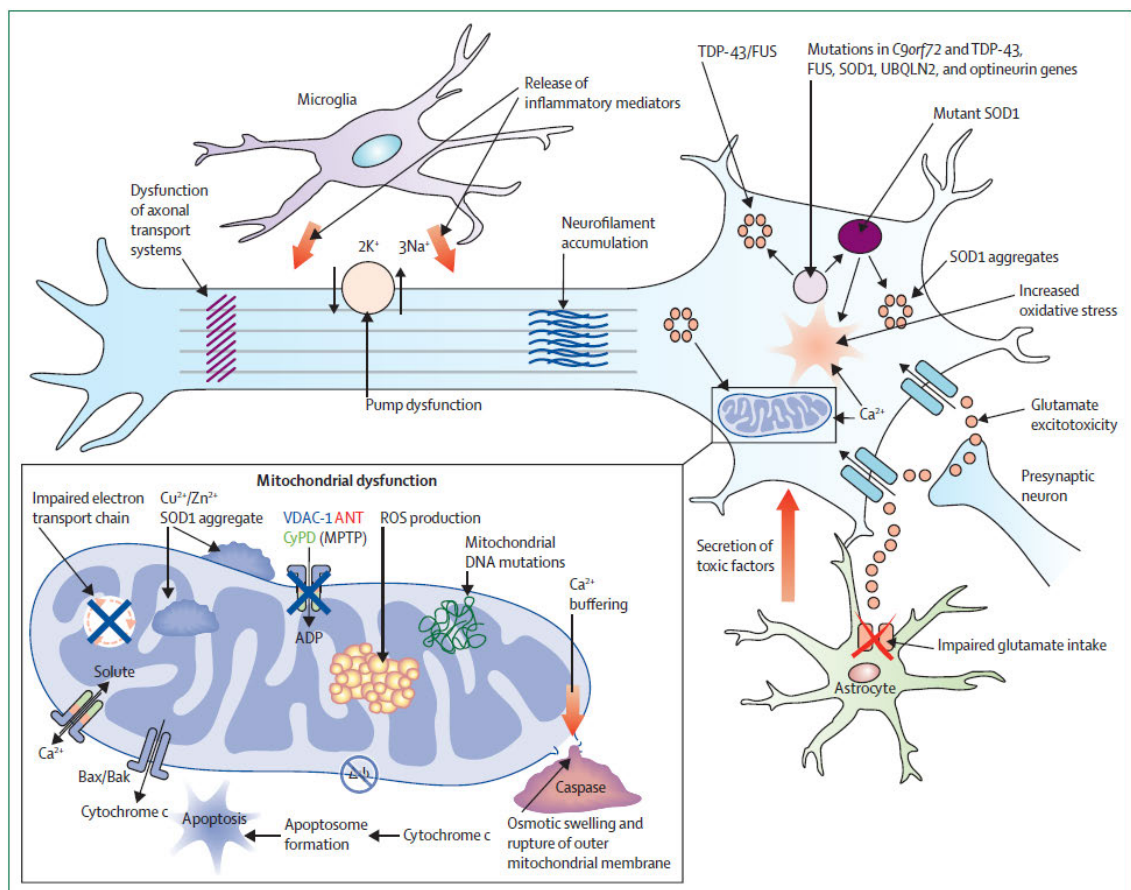
Riluzole, a medication shown to confer a modest survival benefit in patients with ALS, is thought to block glutamatergic neurotransmission as one of its many mechanisms of action.<sup>234</sup>

Transcranial magnetic stimulation (TMS) has been used to study changes in cortical excitability in ALS.<sup>235-237</sup> Studies in early ALS consistently demonstrate lower resting motor threshold, higher motor evoked potentials, and reduced short intra-cortical inhibition, indicating that early ALS is associated with hyper-excitability of the motor cortex.<sup>238-240</sup> A further study using TMS in familial ALS found that cortical hyper-

excitability may be occurring prior to the onset of symptoms in pre-symptomatic SOD-1 mutation carriers.<sup>241</sup> One study using threshold tracking TMS found that riluzole exerts a transient effect on cortical and axonal hyper-excitability.<sup>242</sup>

The phenomenon of hyper-excitability does not appear to be sustained, as in those with more advanced ALS TMS shows a hypo-excitable motor cortex compared to controls.<sup>238</sup> This could be because the changes associated with a hyper-excitable motor cortex constitute an early or compensatory mechanism in the pathogenesis of ALS which is ultimately overcome. Additionally, the mechanism underlying hyper-excitability may require a critical number of motor neurons and is therefore lost when the population becomes too small. The period at which the switch from hyper-excitable to hypo-excitable cortex occurs has not yet been ascertained and how cortical hyper-excitability relates to the biology of ALS is not fully understood.

**Figure 1.6 Neurodegenerative mechanisms proposed in ALS**



A figure to show the possible pathogenic mechanism underlying ALS, used with permission from Turner MR et al., 2013.<sup>31</sup>

### 1.1.8.5 Oxidative stress

Accumulation of free radicals and oxidative stress are likely to be occurring alongside the neurodegenerative process underlying ALS. Post-mortem studies in ALS

demonstrate irreversible free radical damage to macromolecules,<sup>243,244</sup> and CSF examination exhibits abnormal free radical metabolism.<sup>1,245</sup> Furthermore, one study demonstrated increased sensitivity of fibroblasts cultured from ALS patients to oxidative stress.<sup>246</sup>

One of the main enzymes involved in preventing oxidative damage is SOD1, and mutations in the SOD1 gene are associated with an autosomal dominant familial form of ALS.<sup>102</sup> SOD-1 protein scavenges superoxide free radicals generated by mitochondrial ATP production.<sup>102,195,222,223</sup>

#### **1.1.8.6 Mitochondrial dysfunction**

Mitochondrial dysfunction is intimately associated with the generation of free radicals and oxidative stress. Mitochondria are vital cellular organelles, involved in cellular respiration, energy production, and calcium homeostasis. Abnormal SOD-1 protein accumulates within mitochondria and causes disruption of function.<sup>247–249</sup> In addition, altered mitochondrial protein expression, inadequate ATP production, loss of calcium regulation, and altered mitochondrial transport along axons have all been reported in ALS<sup>246-248</sup>.

#### **1.1.8.7 Inflammation and glial cells**

Inflammation is likely to be pivotal in the neurodegenerative process occurring in ALS, where pathological immune changes are associated with both onset and progression. Immune activation may arise as a result of other associated mechanisms or priming events, such as glutamate excitotoxicity, protein aggregation and oxidative stress. The cascade of immunological events may then, once activated, become a catalyst to the pathogenesis of ALS.<sup>249-252</sup>

The immune response involves microglial and dendritic cell activation in the corticospinal tracts and motor cortex, which induces lymphocyte infiltration and inflammatory cytokine release.<sup>250–253</sup>

An increased number of activated microglia are present in the regions of motor neuron loss on post-mortem in people with ALS.<sup>254</sup> In addition, there is a correlation between the number of activated microglia and the rate of disease progression.<sup>255</sup> Moreover, increased levels of pro-inflammatory cytokines are detected in the CSF of patients with ALS.<sup>256</sup> Cerebral microglial activation in ALS has also been detected '*in vivo*' using positron emission tomography.<sup>257,258</sup>

Reactive gliosis is another feature of the degenerative process occurring in ALS.<sup>259–262</sup> Astrocytes play a key role in maintaining neuronal homeostasis and supporting survival. Microglial cells interact with astrocytes and when motor neuron damage becomes

established astrocytes release acute phase reactants, complement, and proteinases, which encourage microglial cells to switch from a neuroprotective to neurotoxic role.<sup>250,253,263,264</sup> This is supported by post mortem studies, where analysis of astrocytes within the affected tissue revealed upregulation of genes encoding pro-inflammatory cytokines, chemokines, and elements of the complement cascade.<sup>253</sup>

Astrocytes are thought to partially provide a neuroprotective role, reducing excitotoxicity by promoting glutamate uptake. However, reactive gliosis may hinder the level of neuroprotection conferred by the astrocytes leading to a more toxic function.<sup>265</sup>

Immunological activation is also evident in the lower motor neurons and muscles in ALS. Muscle biopsies from patients with ALS are positive for antibodies against voltage gated calcium channels neuromuscular junction, cell adhesion molecules and myofibers.<sup>251,265</sup>

The immune profile has been shown to relate to the speed of progression in ALS, where higher levels of circulating regulatory T lymphocytes are associated with slower speed of progression.<sup>250,266</sup> Microglial activation and other pro-inflammatory mechanisms thereby offer potential targets for therapies in ALS.<sup>250</sup>

#### **1.1.8.8 RNA processing**

There are both direct and indirect associations of RNA biogenesis with degeneration of motor neurones in ALS.<sup>267-270</sup> Several genetic mutations linked to ALS encode proteins involved in RNA transport, processing, translation, and metabolism, all of which are fundamental in neuronal homeostasis. TDP-43 and FUS are both RNA binding proteins concerned with RNA metabolism, while Sentaxin is involved in RNA processing, and GLE-1 isoforms are important in nuclear export of mRNA and stress granule function, see tables 1.2 and 1.3.<sup>100,133</sup>

RNA binding proteins, particularly TDP43 but also FUS, are central components of the erroneous protein aggregates that constitute a pathological hallmark in ALS, raising the potential involvement of dysregulated RNA metabolism in ALS progression.<sup>270</sup> Dysregulation of localised RNA metabolism within axons, through defects in RNA transport and/or translation, could be a contributing factor in many of the defective cellular mechanisms implicated in ALS such as proteostasis, mitochondrial dysfunction, oxidative stress, and neuroinflammation.

Micro-RNAs are a subset of tissue specific non-coding RNA molecules, involved in the regulation of gene expression through their association with messenger-RNAs. Micro-RNAs have fundamental roles in motor neurone physiology such as in maintenance of the synapse, neurofilaments, neurogenesis, RNA and protein

metabolism.<sup>271,272</sup> Dysfunction of micro-RNAs has been reported to be associated with motor neurone degeneration in ALS.<sup>267,273</sup>

### **1.1.9 ALS onset and propagation**

Clinically ALS is characterised by focal onset with progression over time in a sequential manner to ultimately affect all body regions. Spread of disease is not random but follows recognisable neuro-anatomical pathways, independent of the underlying genetic component, at both the UMN and LMN level.<sup>13,36</sup> Somatotopic anatomy differs in the brain and spinal cord so that as the disease advances there is increasing diversity of the clinical phenotype.<sup>274,275</sup>

Like other neurodegenerative diseases, ALS is likely to have a pre-clinical phase,<sup>276</sup> with abnormal neuronal function mounting initially at the individual synaptic level but ultimately affecting larger connected neuronal networks. During this latent period the entire cortical motor neuronal system could be partially compensated by intrinsic mechanisms while attempting to abort ongoing pathogenesis. However, at some point the disease process reaches the critical threshold of cellular dysfunction and manifests clinically. Therefore, although focal onset is apparent clinically, it seems plausible that this could represent the random area where the compensatory mechanisms are first overcome by the burden of pathogenic molecular mechanisms, rather than a site specific event in time triggering the disease 'de novo'.<sup>37</sup> This is supported by the observation that a single genetic mutation causes a cluster of differing ALS clinical phenotypes within the same family.<sup>274,277</sup>

There are important considerations regarding the dissemination of pathology underlying the neurodegenerative process in ALS. Proposed mechanisms of pathological propagation include contiguous spread and synaptic network propagation. Contiguous spread describes the regional transmission from one cell to its neighbouring cell through the extracellular matrix.<sup>36</sup> This exchange occurs between neurons and glial cells,<sup>278</sup> which may account for the presence of protein aggregates within astrocytes and oligodendrocytes.<sup>279</sup> One hypothesis is that aggregates of misfolded protein trigger propagation and accumulation of toxic protein structures in a self-perpetuating mechanism similar to that underlying prion disease.<sup>280</sup> Proteins found within the aggregates such as TDP-43 contain prion-like domains, which can act as structural templates to propagate further misfolding of proteins.<sup>281</sup> However, simultaneous corticospinal tract and spinal motor neurone involvement is typically evident clinically in ALS suggesting involvement of the whole corticomotor-neuronal system. Network propagation through axonal pathways with synaptic connections may account for this finding.



The earliest detectable changes in ALS are cortical hyper-excitability using TMS<sup>282</sup> and functional MRI.<sup>17</sup> Resting state functional MRI captures spontaneous neuronal brain activity at rest, which demonstrate resting state networks, a low level of persistent functional activity between brain regions. Altered functional connectivity within the sensorimotor network and default mode network have been detected early in ALS.<sup>17</sup> This raises the possibility that the initial abnormalities are within the cortical motor neurones, which have monosynaptic connections with the anterior horn cells of the spinal cord. Anterograde degeneration or "dying forward," could then transmit insult through to the postsynaptic lower motor neurone.<sup>3,235,236,238</sup> Cortico-fugal axonal spread has been proposed to account for the dissemination of TDP-43 pathology in ALS.<sup>283,284</sup>

Attempts have been made to predict neuropathological staging according to burden and distribution of TDP-43 pathological inclusions. One post mortem study of 76 patients with ALS proposed that the progression of pathology can be divided into four stages according to the sequential dissemination of TDP-43 aggregates.<sup>285</sup> In this model stage 1 describes TDP-43 pathology confined to the Betz pyramidal cells of the motor neocortex, alpha motor neurones of the ventral spinal cord, and cranial motor neurones (XII, XI, X, VII, and V). In stage 2 there is involvement of the middle frontal gyrus, brainstem reticular formation, pre-cerebellar nuclei and red nucleus. Further prefrontal areas (gyrus rectus and orbital gyri) along with the postcentral neocortex and striatum become involved during stage 3. Finally, in stage 4 there is spread of pathology to the anteromedial temporal lobe, including the hippocampus. This staging model supports propagation of TDP-43 pathology along axonal pathways.<sup>284</sup> This study is limited by the extrapolation that the TDP-43 pathology assessed at post mortem in a cross-sectional study correlates with the severity of disease.

Interestingly loss of Betz cells in the motor cortex is often variable<sup>195,198</sup> despite consistent, and often extensive, loss of the large myelinated axons of the corticospinal tract, particularly below the medullary pyramid.<sup>193,194,201</sup> This is more consistent with a retrograde degeneration or "dying back" axonopathy, where the peripheral axon degenerates prior to the cell body due to pathological insult.<sup>286-288</sup> A analogous process could also affect the anterior horn cell and lower motor neurone axon.<sup>289,290</sup>

One final consideration is the contribution of non-synaptic and non-contiguous mechanisms driving the dissemination of pathology in ALS, such as through blood and CSF. In particular immune mediated mechanisms could play important roles in how the disease develops. Studies have demonstrated simultaneous inflammatory component in both muscle and nerve.<sup>285,291,292</sup>

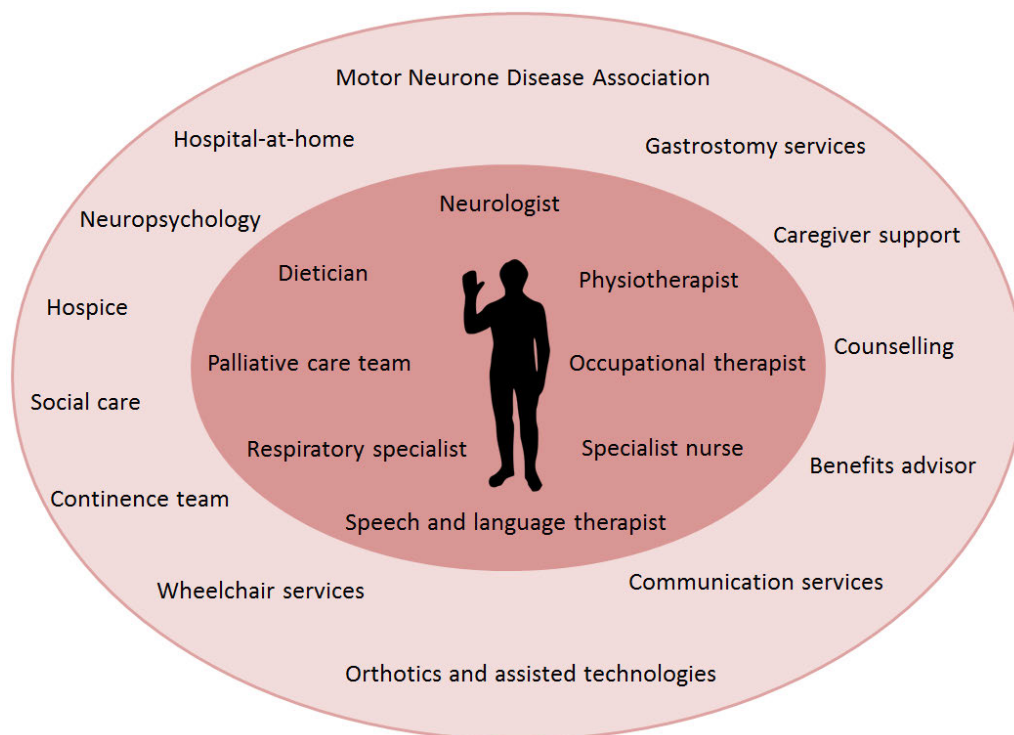
A combination of the different mechanisms described above are likely to work synergistically and catalytically contributing to the inexorable propagation of pathology in ALS and driving the relentless neurodegeneration of the motor neurones. Whatever the

cellular and axonal mechanisms it is evident that by the time muscle weakness presents, there has been substantial degeneration of the whole corticomotor neuronal system. This has important implications in finding effective disease modifying treatments and is one explanation for the multiple clinical trial failures in ALS.

### 1.1.10 Management

Despite the advances in understanding of ALS and numerous clinical trials of potential neuroprotective agents being conducted over the last two decades, no curative treatment is yet available for ALS.<sup>26,293</sup> Supportive and symptomatic care provide the mainstay of management in ALS with the aim of maintaining quality of life and maximizing physical function.<sup>294</sup> The National Institute of Clinical Excellence developed guidelines for the assessment and management of ALS in 2016 ([www.nice.org.uk/guidance/ng42](http://www.nice.org.uk/guidance/ng42)), covering all aspects of holistic multidisciplinary care, see figure 1.7.

**Figure 1.7 Multidisciplinary care in ALS**



A figure to show the range of multidisciplinary care services involved in the supportive care of patients with ALS and their family, adapted from Hobson E and McDermott C., 2016.<sup>292</sup>

#### 1.1.10.1 Supportive and symptomatic management

Supportive care and symptomatic treatments are pivotal in the management of those with ALS. Coordinated multidisciplinary care, in dedicated units, provides the best

environment for comprehensive management of those with ALS and improves patient survival. Integrated ALS care also improves quality of life.<sup>295–297</sup>

The psychological burden of living with this disease should be considered and support in the form of counselling should be offered to both the patient with ALS and their relatives.<sup>292</sup> Issues surrounding respiratory and nutritional interventions, as well as advanced healthcare directives, should be discussed early in the course of the disease. Regular monitoring, in particular of respiratory function and nutritional status, combined with advanced planning can ease the distress caused by progressive symptoms. Additional considerations are the provision of communication aids in those with bulbar symptoms and orthotic devices for those with neck and ankle weakness.<sup>292</sup>

Guidelines for the management of certain symptoms in ALS are becoming more evidence based, for example the use of non-invasive ventilation (NIV) in early respiratory failure has been shown to benefit both survival and quality of life in a randomized control trial.<sup>298,299</sup> A comprehensive overview of the management options for the common symptoms in ALS are given in table 1.8.

#### **1.1.10.2 Disease modifying treatments**

Riluzole was shown to prolong survival by 2-3 months in ALS participants of two large randomized controlled trials.<sup>300,301</sup> Although the mechanism of action of riluzole is complex, the neuroprotective effects are thought to be derived through inhibition of glutamate release and modulation of sodium channels.<sup>1,3,7,233</sup> TMS studies have demonstrated a transient normalization of cortical and axonal hyper-excitability in those with ALS taking riluzole,<sup>242</sup> providing support for glutamate associated excitotoxicity occurring in ALS. Whether the excitotoxicity is causative of neurodegeneration, or occurs as a result of pathophysiological mechanisms remains to be established. Further studies with riluzole suggest that most benefit is derived when functional impairment is moderate.<sup>302–304</sup>

Presumably riluzole exerts other neuroprotective mechanisms as despite only transient normalization of hyper-excitability demonstrated by TMS over two months, studies have shown that the beneficial effects of taking riluzole continue after the time frame.<sup>235</sup> One study in China found that longer term use of riluzole over years was associated with a better prognosis for ALS patients, whereas short-term use had little effect on survival.<sup>305</sup> In the same study higher cumulative dosing of riluzole related to better prognosis. The results of a more recent study suggest that riluzole prolongs survival in the later stages of ALS.<sup>303</sup>

Riluzole is generally well tolerated but may cause fatigue, nausea, and liver transaminase abnormalities.<sup>306</sup> NICE recommend that treatment with riluzole is discussed with all ALS patients at the time of diagnosis.

**Table 1.8: Management of ALS symptoms**

<b>Symptom</b>	<b>Pharmacological Intervention</b>	<b>Nonpharmacological strategies</b>
Cramps	Quinine Levetiracetam Carbamazepine Mexiletine	Physiotherapy Exercise
Spasticity	Baclofen Tizanidine Dantrolene Benzodiazepines	Physiotherapy Hydrotherapy Massage
Weakness and disability	None	Orthotics Adaptive aids Physiotherapy
Pain	Paracetamol NSAIDS Gabapentin Opioids	Physiotherapy Hydrotherapy Regular repositioning Pressure cushions and mattresses
Dysphagia	None	Speech and Language assessment Safe swallow techniques Dietitian Modified diet Gastrostomy
Dysarthria	None	Speech and Language assessment Communication aids Education of family and caregivers
Dyspnoea and poor cough	Morphine Benzodiazepines	Non-invasive ventilation Manually assisted cough techniques Chest physiotherapy Suction
Excess respiratory secretions	Carbocystein Nebulised saline	Humidified NIV Manually assisted cough techniques Chest physiotherapy Suction machine
Sialorrhoea	Botulin toxin Hyoscine patch Amytriptyline Glycopyrrolate Atropine drops	Suction Mouth care products Salivary glands radiotherapy
Dry mouth	Artificial saliva sprays	Mouth care products Humidified NIV
Fatigue	Modafinil	Lifestyle changes
Depression and Anxiety	SSRIs Benzodiazepines	Counselling

Cognitive changes	Antidepressants	Explanation of symptoms to family and caregivers
Sleep disturbance	Benzodiazepine Antidepressants	Respiratory assessment and NIV if indicated
Emotional lability	SSRIs Dextromethorphan-quinidine combination treatment Amitriptyline	Education of patient with ALS, their family and caregivers
Constipation	Lactulose Movicol	Ensure adequate hydration Increase fiber intake

(Abbreviations NSAIDs, Nonsteroidal anti-inflammatory drugs; SSRI, Selective serotonin reuptake inhibitors) Adapted from Hobson E et al., 2016.<sup>294</sup>

One other treatment has more recently shown potential to alter the relentless pathophysiological process driving progression of ALS in some patients. Edavarone was shown to be associated with a slower rate of decline in ALSFRS-R on post-hoc analysis in a subset of patients with early stage ALS.<sup>307</sup>

### 1.1.11 Prognosis

ALS is relentlessly progressive and is inevitable fatal; however, the rate of progression varies considerably.<sup>308</sup> While some with ALS live for only a few months from symptom onset, some (10-20%) survive more than 5 years, and a small proportion (5-10%) live for over 10 years.<sup>309</sup> Nonetheless, the median survival from onset of symptoms is reported as 2-3 years for bulbar onset and 3-5 years in limb onset.<sup>1,3,5,307</sup>

Certain factors have consistently been shown to be important indicators of prognosis in ALS. Limb onset, younger age at onset, diagnostic delay, lack of cognitive impairment, absence of respiratory muscle involvement, and slower rate of progression are all independently associated with longer survival.<sup>1,307,310</sup> Further research is required to evaluate whether exercise is beneficial or harmful in ALS.<sup>311</sup>

Conversely bulbar onset, older age at onset of symptoms, early diagnostic confirmation, presence of respiratory or cognitive impairment at diagnosis, and faster rate of symptoms progression are all associated with a worse prognosis, see table 1.9.<sup>310</sup> Neck weakness was also identified as an independent prognostic factor for both morbidity and mortality in ALS.<sup>312</sup>

ALS centres report longer survival times compared with population-based studies, suggesting that care within specialized centres, where there is access to a multidisciplinary team, confers a survival benefit.<sup>294-296,307</sup>

**Table 1.9: Factors affecting rate of progression**

<b>Factor</b>	<b>Associated with shorter survival</b>	<b>Associated with longer survival</b>
Phenotype	<ul style="list-style-type: none"> <li>• Bulbar onset ALS<sup>313,314</sup></li> <li>• Respiratory onset ALS<sup>298</sup></li> <li>• Cognitive impairment<sup>315,316</sup></li> <li>• Impaired nutritional status<sup>317</sup></li> <li>• Neck flexor weakness<sup>312</sup></li> </ul>	<ul style="list-style-type: none"> <li>• Flail limb variants<sup>318–320</sup></li> <li>• LMN predominant (PMA)<sup>48</sup></li> <li>• UMN predominant<sup>321</sup> (PLS)</li> <li>• Longer time interval between onset and diagnosis<sup>322</sup></li> </ul>
Demographics	<ul style="list-style-type: none"> <li>• Older age at diagnosis<sup>314</sup></li> <li>• Smoking<sup>323</sup></li> <li>• Lower socio-economic status</li> </ul>	<ul style="list-style-type: none"> <li>• Younger age at diagnosis<sup>324</sup></li> </ul>
Genetic influences	<ul style="list-style-type: none"> <li>• A4V SOD 1 mutation<sup>325</sup></li> <li>• FUS mutation with basophilic inclusions<sup>326</sup></li> </ul>	<ul style="list-style-type: none"> <li>• E21G, G37R, D90A, G93C, and I113T SOD1 mutations<sup>327</sup></li> <li>• Reduced KIFAP3 expression<sup>328</sup></li> <li>• Reduced EPHA4 gene expression<sup>329</sup></li> </ul>
Management	<ul style="list-style-type: none"> <li>• Topiramate<sup>330</sup></li> <li>• Diaphragmatic stimulation<sup>331</sup></li> </ul>	<ul style="list-style-type: none"> <li>• Riluzole<sup>1,3,7,233,235</sup></li> <li>• Enteral Feeding (PEG)<sup>332</sup></li> <li>• Non-invasive ventilation<sup>333</sup></li> <li>• Multidisciplinary care centre<sup>294-296</sup></li> </ul>

A table to show factors contributing to rate of progression in ALS.

Abbreviations: EPHA4, ephrine type-A receptor 4; FUS, fused in sarcoma; KIFAP3, kinesin-associated protein 3; SOD, superoxide dismutase.

Genetic factors are also known to contribute to rate of disease progression, see table 1.9.<sup>324-328</sup> As previously mentioned the LMN variant PMA and the UMN variant PLS, also have better prognoses than classical ALS.<sup>48,320</sup>

Riluzole has a positive independent effect on survival in ALS, improving mortality rates at 6 months and 12 months by 23% and 15% respectively.<sup>309</sup> In addition, Riluzole

has been shown to improve morbidity by providing a small beneficial effect on both bulbar and limb function.<sup>334</sup> Evidence from recent studies suggests that Riluzole exerts most effect in the advanced stages of ALS.<sup>304,335</sup>

Additional therapeutic interventions which have been shown to confer a positive benefit in quality of life and survival are gastrostomy insertion in those with suboptimal nutritional status caused by dysphagia,<sup>331</sup> and early non-invasive ventilation (NIV) in those with evidence of respiratory impairment.<sup>332</sup>

The predominant cause of death in ALS is respiratory failure and concurrent respiratory infection, due to respiratory muscle weakness.<sup>336</sup> Many die in their sleep due to hypercapnia.<sup>337</sup>

Once diagnosed with ALS, patients often enquire what length of time they might expect to live. However, given the large number of variables it is difficult to provide an accurate answer to each individual. Attempts have recently been made to create a clinical tool for predicting survival in ALS, by incorporating the prognostic factors discussed.<sup>309</sup> However, not every patient wants such detailed prognostic information and the clinical tool proposed for predicting survival is based on probabilities and may therefore not accurately predict the outcome in every individual.<sup>338</sup>

## 1.2 Imaging in Amyotrophic Lateral Sclerosis

A major challenge for understanding the disease mechanisms underlying ALS is to visualize the pathological changes occurring within the brain '*in vivo*'.

Neuroimaging techniques, particularly the many modalities of magnetic resonance imaging (MRI), have provided some important insights into the localization and the evolution of brain alterations associated with ALS.<sup>17,18,339–341</sup> However, imaging studies focusing on defining the processes accompanying the evolution of the disease are limited and models of progression in ALS have largely been hypothesized using pathological staging.<sup>283</sup>

Significant attention has been applied to developing advanced neuro-imaging techniques which may provide non-invasive diagnostic and staging information in patients with neurodegenerative disorders such as ALS.<sup>342</sup> The main objectives being to facilitate early diagnosis, develop disease stratification models for clinical trials, and to quantify altered microstructure within the brain and spinal cord.<sup>338-341</sup>

There are recognized limitations to using imaging data in ALS relating to the techniques themselves, to the challenges of acquiring longitudinal data in those with ALS, and to the increasingly recognized heterogeneity of the disease.

In these sections I will give an overview of MRI and then go on to describe the techniques that I combined in my research study; structural MRI, diffusion tensor imaging (DTI), neurite orientation dispersion and density imaging (NODDI) and quantitative

magnetization transfer imaging (qMTi). This study provides a multi-parametric assessment of ALS, in order to better characterize the neurodegenerative processes underlying ALS. I used NODDI and qMTi to investigate what further information can be gained when compared directly with the characterized changes already demonstrated using DTI and structural MRI.

### 1.2.1 The basics of magnetic resonance imaging

Magnetic resonance imaging (MRI) uses the phenomenon of nuclear magnetic resonance (NMR) to differentiate between different structures.<sup>343,344</sup> A powerful magnet is used to apply a strong magnetic field, which leads to spin polarization of the protons, see figure 1.8. In this state protons precess around an axis which can be either parallel or anti-parallel to the main field ( $B_0$ ). The precession occurs at a frequency known as the Larmor frequency, which is directly proportional to the strength of the magnetic field ( $B_0$ ), see figure 1.8. The majority of spins align parallel to the magnetic field, which is equivalent to a more favourable energy state. A small proportion of spins also align in an anti-parallel manner, producing a net magnetization under a static magnetic field.<sup>342,343</sup> This net magnetization increases with higher magnetic field strength ( $B_0$ ), see figure 1.8.

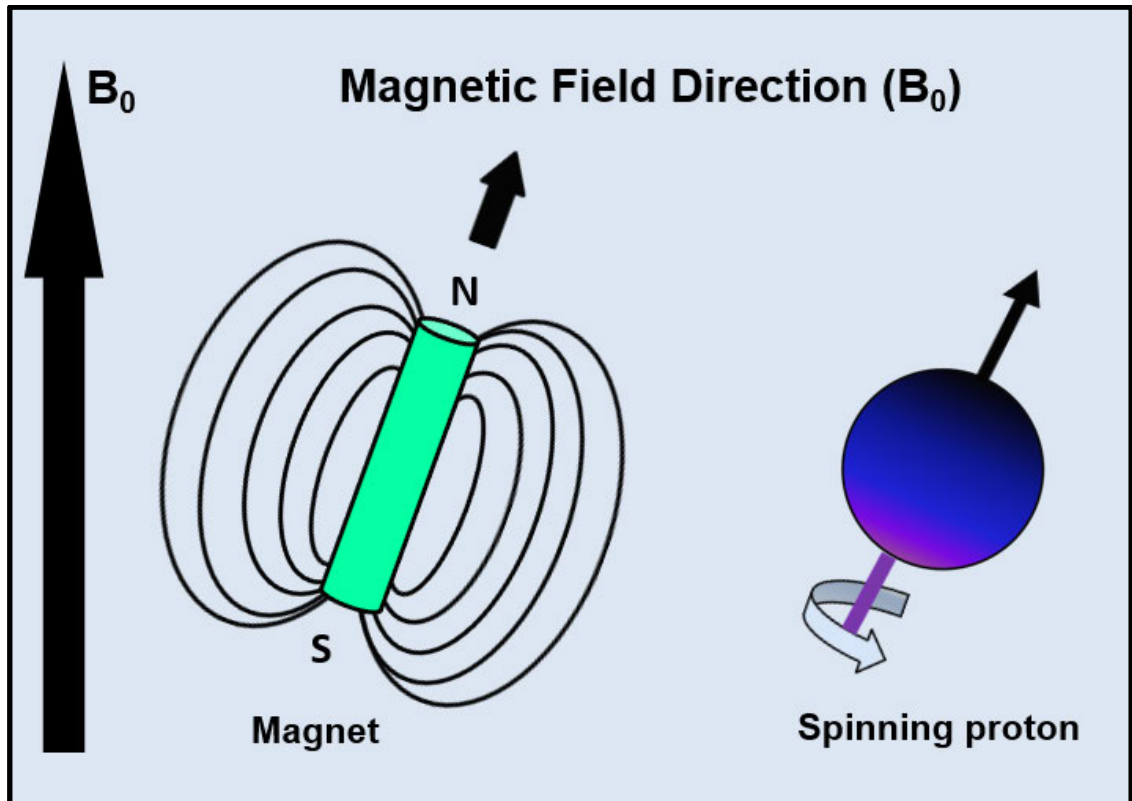
When an additional time-varying magnetic field is applied, by means of a radiofrequency (RF) pulse, the protons absorb energy. When the RF is applied perpendicular to the orientation of  $B_0$ , and at the appropriate radiofrequency, the proton spins tend to align with the new field, thus causing the net magnetization to tilt towards a direction orthogonal to  $B_0$ .

From a quantum physics perspective, applying a radio frequency at the appropriate level can induce a transition in spin states known as a spin flip, which places some of the proton spins in a higher energy state.<sup>345</sup> Switching off the radiofrequency allows for the relaxation of the spins back to their lower state, producing a radiofrequency signal that can be measured associated with the spin flip. The relaxation processes occur at different rates for different tissue (described by the longitudinal relaxation time,  $T_1$ , and the transverse relaxation time  $T_2$ ), depending on factors such as macromolecular content and density.<sup>343-344</sup>

These techniques of manipulating proton behaviour are employed during the MRI brain acquisition in order to acquire structural information regarding the different tissues being studied. As the MR signal is sensitive to a range of biophysical phenomena, different types of MR images can be generated, providing contrasts that reflect differing tissue characteristics. The most commonly used MR contrasts in clinical routine include  $T_1$  and  $T_2$  weighted scans, proton-density (PD) weighted scans and fluid attenuated inversion recovery (FLAIR) – a type of imaging that suppressed the signal from CSF thus enhancing the information from parenchyma.<sup>344</sup>



**Figure 1.8: The effect of magnetic field strength on net magnetization.**



A figure to show how a spinning proton creates a magnetic field similar to a bar magnet, adapted from the basics of nuclear medicine, wikibooks.org (<https://en.wikibooks.org>)

### 1.2.2 MRI in ALS

Despite the devastating clinical features of ALS, changes in signal intensity are rarely observed directly using conventional Magnetic resonance imaging (MRI).<sup>346</sup> There have been reports of T2-weighted hyper-intensity of the corticospinal tract (CST),<sup>347</sup> as well as subcortical white matter foci within the frontal lobes,<sup>348</sup> thought to be related to ALS. Additionally, T2-weighted hypo-intensity at the margin of the precentral gyrus has been reported.<sup>349</sup> Similar findings were demonstrated using fluid attenuated inversion recovery (FLAIR) sequences and proton density MR images.<sup>350</sup> However, these findings were not found to correlate with clinical measures and similar findings have been detected in healthy controls. Moreover, in the majority of ALS patients the MRI brain appearances are normal, all of which raises uncertainty regarding the specificity and pathological relevance of conventional MRI findings in ALS. MRI is therefore widely used in patients presenting with both UMN and LMN signs to exclude more treatable differential diagnoses that mimic ALS, such as cervical myelo-radiculopathy or primary progressive multiple sclerosis, rather than to facilitate the diagnosis of ALS.<sup>351</sup>

A major challenge for understanding disease mechanisms in ALS and neurodegenerative disorders in general is to interrogate pathological mechanisms in life, ideally at an early stage of disease evolution. While providing only limited direct

information, MRI has remained a pillar for developing more advanced techniques of image acquisition. These include structural MRI,<sup>352,353</sup> magnetic resonance spectroscopy (MRS),<sup>354</sup> functional MRI,<sup>355</sup> diffusion tensor imaging (DTI),<sup>356</sup> neurite orientation dispersion and density imaging (NODDI)<sup>357</sup> and magnetization transfer imaging.<sup>358</sup> Many of these have already provided important insights into the localization and the evolution of cellular pathology in ALS but suffer from limitations relating to the techniques themselves, the difficulties of acquiring longitudinal data in this patient group, and to the increasingly recognized heterogeneity of ALS.<sup>28</sup>

### 1.2.3 Structural MRI

Structural MRI techniques are used to quantify the cortical thickness, surface area, and volumes in specific brain regions. Application of different sequences, for example conventional T1-weighted and T2-weighted, allow for good contrast between grey matter, white matter, and cerebrospinal fluid (CSF). High resolution MRI sequences are typically required to optimize tissue identification and segmentation throughout the brain. Tools are available such as Statistical Parametric Mapping (SPM; Welcome Trust Centre for Neuroimaging, London, UK), FMRIB Software Library (FSL; Centre for Functional MRI of the brain, Oxford, UK), and FreeSurfer (Harvard University, Cambridge, USA), which conduct automated segmentation of the cortical and subcortical brain structures. These allow analysis of grey matter and white matter morphometry.<sup>359,360</sup>

Voxel based morphometry (VBM) is a computational MRI technique used mainly to quantify specific GM volumes, using voxel-wise analysis. VBM has been successful in detecting regional brain atrophy patterns using group comparisons of grey matter and white matter.<sup>17,341</sup> VBM studies have consistently demonstrated reduced GM volume within the precentral gyrus in ALS.<sup>342,361</sup> VBM comparing limb-onset with bulbar-onset ALS subgroups shows corresponding differential patterns of atrophy within the motor strip, reflecting focal cortical degeneration.<sup>171,362</sup> Atrophy within the frontotemporal lobes has also been reported in ALS, where subgroups with cognitive impairment demonstrate more widespread atrophy of such extra-motor regions.<sup>363–365</sup>

Surface-based morphometry (SBM) focuses on the reconstruction of GM and WM boundaries to allow the quantification of cortical thickness, volumes, and surface areas in specified brain regions.<sup>17,341,366</sup> SBM has provided additional structural information with respect to cortical thinning of the primary motor regions in ALS.<sup>367,368</sup> Studies focusing on cortical thickness reveal significant thinning of the precentral gyrus.<sup>368–370</sup> Focal reductions in cortical thickness have the greatest sensitivity to disease related changes in ALS.<sup>367–370</sup> They have also been shown to reflect clinical features of ALS and demonstrate specificity for UMN involvement clinically.<sup>172,368</sup> Patients with additional cognitive deficits show more pronounced cortical thinning of the extra-motor

regions.<sup>17,84</sup> Longitudinal studies incorporating SBM techniques have demonstrated a reduction in cortical thickness over time.<sup>17,84</sup> Furthermore, cortical thinning of the precentral gyrus in ALS has been shown to co-localize with increased glial marker uptake using combined MRI-PET assessment.<sup>371</sup>

The involvement of subcortical structures, such as the basal ganglia and hippocampus, have been revealed using VBM and SBM analysis, where reduced volumes were associated with ALS.<sup>17,171,372,373</sup> Finally atrophy within the cerebellum has been demonstrated, particularly in relation to the ALS-FTD continuum.<sup>374</sup>

In the one study comparing 3T MRI data from 45 patients with ALS to 25 controls, surface-based cortical morphometry analyses showed specific thinning of the precentral gyrus, without statistically significant changes in volume or surface area of this region.<sup>368</sup> This is in keeping with previous studies of cortical morphometry, which provide evidence to support thickness and surface area being independent of one another.<sup>375</sup> In contrast regional surface area and volume are more intimately related and changes in volume may therefore be diluted by changes in surface area or vice versa and neither reach statistical threshold for significance as a result.<sup>368</sup>

## **1.2.4 Diffusion Tensor Imaging**

### **1.2.4.1 The Principles of Diffusion Tensor Imaging**

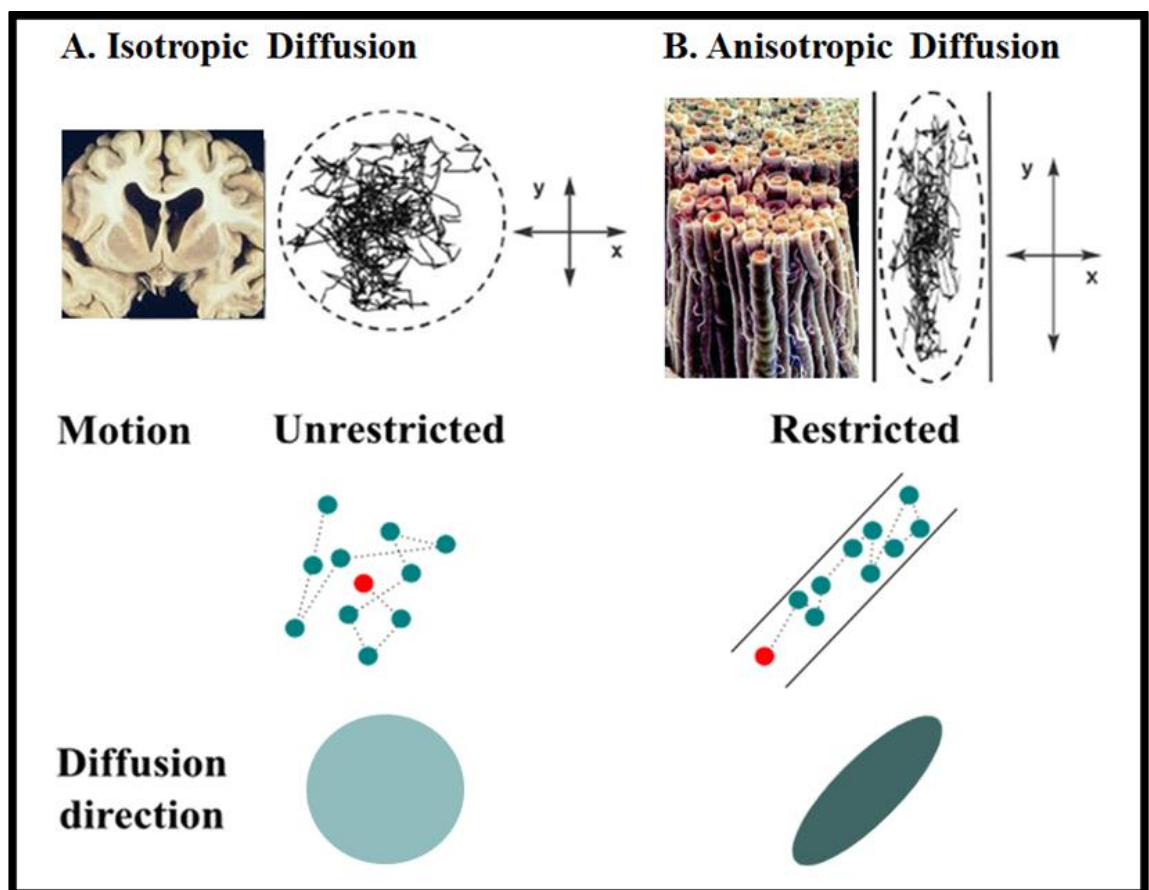
Diffusion tensor imaging (DTI) models the signal measured using diffusion weighted imaging (DWI), and enables the assessment of structural integrity within the brain tissue based on the sensitivity to Brownian motion of water molecules.<sup>376</sup> As the presence of membranes, oriented structures and organelles impacts on this motion, DWI provides indirect information about the tissue in which the water molecules reside, see figure 1.9.<sup>377–380</sup> The enormous potential of DWI was recognized as it provides a means of indirectly evaluating biological tissues '*in vivo*' by focusing on the molecular displacement of water.<sup>17,341,370,381</sup>

Depending on type of tissue, diffusion is typically modelled according to one of 3 models: free diffusion, hindered diffusion, and restricted diffusion.<sup>382</sup> Free and hindered diffusion models both follow a Gaussian displacement distribution and exhibit a linear relationship between mean displacement and diffusion time.<sup>383</sup> Restricted diffusion differs in that it is characterized by a limitation on the maximum rate of diffusion and therefore remains constant over time.<sup>382</sup>

The geometrical representation of the diffusion tensor is an ellipsoid, i.e., a 3D shape resembling a rugby ball, which is used to describe the profile of water molecule displacement within each voxel. The shape and the size of the ellipsoid reflects the diffusion properties of tissue at each location. In the WM, where diffusion is anisotropic,

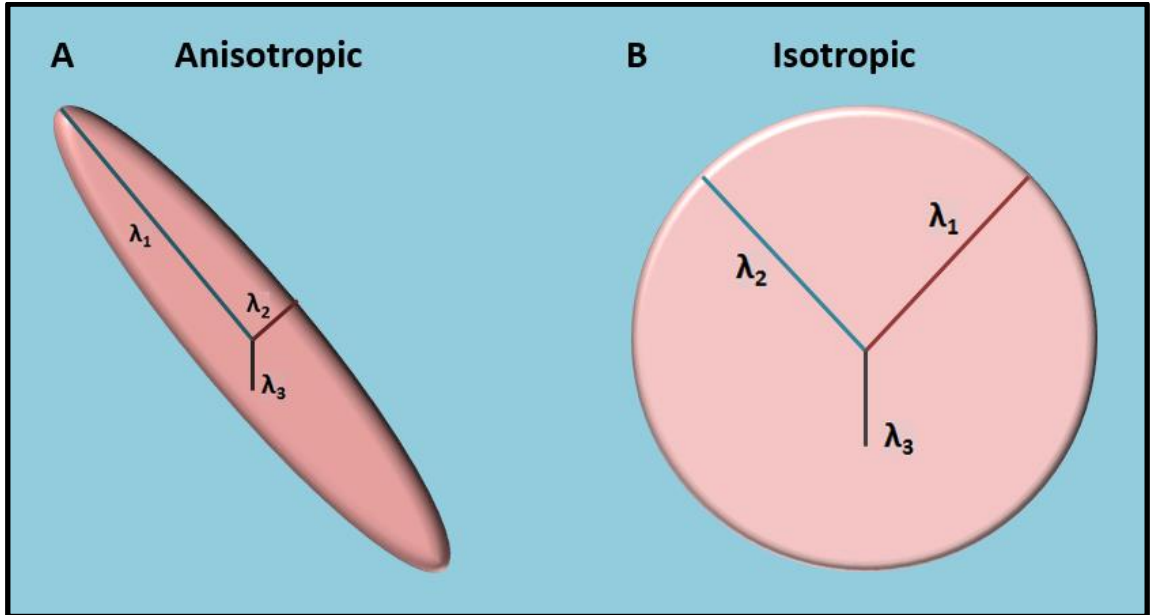
the greatest motion occurs along axons and perpendicular motion is restricted due to the presence of membranes. The profile of diffusion direction in the WM environment is therefore prolate (i.e. an elongated spheroid, which resembles a zeppelin), see figure 1.10A. In contrast within the cerebrospinal fluid, diffusion is fast and occurs at the same rate in all directions (i.e., it is isotropic). In this case, the ellipsoid has a spherical profile with relatively large radius, see figure 1.10B. Anisotropy refers to the property of directional dependence and is the opposite of isotropy which describes uniformity in all directions. When applied to diffusion properties these terms relate to the relative restriction and freedom of movement of the diffusing water molecules respectively. Potential biological sources of anisotropy include the intracellular cytoskeleton, axon membranes, and myelin.<sup>384</sup>

**Figure 1.9: The Diffusion Tensor Model**



A figure to demonstrate the Brownian motion of water molecules in different CNS environments, adapted from Roceanu A et al., 2012.<sup>385</sup>

**Figure 1.10: Diffusion tensor eigenvalues**



A figure to show the geometrical representation of diffusion, with illustrated eigenvalues.

Mathematically, the diffusion tensor is a covariance matrix described by a multivariate normal distribution as follows:-

$$\mathbf{D} = \begin{bmatrix} D_{xx} & D_{xy} & D_{xz} \\ D_{xy} & D_{yy} & D_{yz} \\ D_{xz} & D_{yz} & D_{zz} \end{bmatrix}$$

Although the elements of the tensor vary with the reference frame, it is always possible to find a frame in which the off-diagonal elements are zero. This is achieved through a mathematical operation called “diagonalization”.<sup>376</sup>

The diagonal terms of this particular diffusion tensor provide three eigenvalues ( $\lambda_{1-3}$ ), which describe the magnitude of diffusivity in the principle directions of diffusion or eigenvectors ( $\epsilon_{1-3}$ ). The eigenvalues are specific properties of the tensor “invariants”, thus every quantity computed from the eigenvalues is also an invariant and does not depend on the position of the patient in the scanner. These eigenvalues can then be used to calculate measures of Fractional Anisotropy (FA), Mean Diffusivity (MD), Radial Diffusivity (RD), and Axial Diffusivity (AD) using the following equations :-

$$FA = \sqrt{\frac{1}{2} \frac{\sqrt{(\lambda_1 - \lambda_2)^2 + (\lambda_1 - \lambda_3)^2 + (\lambda_2 - \lambda_3)^2}}{\sqrt{(\lambda_1^2 + \lambda_2^2 + \lambda_3^2)}}}$$

$$MD = \frac{\lambda_1 + \lambda_2 + \lambda_3}{3}$$

$$RD = \frac{\lambda_2 + \lambda_3}{2}$$

$$AD = \lambda_1$$

FA describes the directionality of the diffusion process in each voxel, while MD provides a measure of the bulk diffusion displacement within a given voxel and is independent of orientation. FA is without units and can assume values between 0 (perfect isotropy) and 1 (perfect anisotropy). AD is a measure of diffusion along the principal axis, also referred to as longitudinal or parallel diffusion and is regarded as a marker of axonal integrity. RD is a measure of diffusivity perpendicular to the principle axis. It provides assessment of restriction due to physiological structures such as membranes and is therefore thought to be a marker of myelin composition. All of these DTI derived measures are scalar.<sup>374,384</sup>

#### 1.2.4.2 Diffusion Tensor Imaging in ALS

DTI is the most widely used technique for identification and quantification of changes in WM structure associated with ALS.<sup>16,17,339-342,356,360</sup> Intact WM tracts restrict the diffusion of water molecules, due to the inherent structure of tightly packed myelinated axonal fascicles. In most, but not all cases, tissue damage leads to the diffusing water molecules exhibiting a reduction in the defined directionality of diffusion, and a concurrent increase in the magnitude of water diffusion in all directions, due to the breakdown of barriers to diffusion. In this way DTI indirectly detects microstructural abnormalities associated with damage or disease.<sup>374,384</sup>

The sensitivity of DTI in detecting cerebral changes associated with the neurodegenerative process underlying ALS is undisputable. The first study using DTI in ALS used a relatively small cohort of 22 ALS participants (11 with limb-onset and 11 with bulbar onset), and 20 age-match controls but demonstrated significantly reduced FA and increased MD along the corticospinal tracts, with most marked changes being observed in the bulbar onset group.<sup>169</sup> Ellis et al. also demonstrated correlation between FA and measures of ALS severity, and further correlation between MD and disease duration. This study set the benchmark and over the last two decades there has been an exponential increase in worldwide research using DTI in ALS.<sup>339-342</sup> DTI methods of acquisition, processing, and analysis have also evolved rapidly over recent years, becoming more refined and leading to improved accuracy of the measurements.

The altered DTI diffusivity profile in ALS is now well established, where FA is reduced and MD is increased in the CST.<sup>16,17,339-342,356</sup> AD and RD are increasingly being utilized in ALS as additional measures to comprehend the alterations in tissue microstructure.<sup>340,386,387</sup>

Studies incorporating RD have demonstrated an associated increase within the CST of ALS participants.<sup>16,17</sup> The posterior limb of the internal capsule (PLIC), a region of the CST with densely packed WM fibers, appears to be particularly sensitive to changes in DTI profile, where decreased FA, increased MD, AD, and RD have all been reported.<sup>17</sup>

Within the CST as a whole FA values have been shown to correlate with ALSFRS-R and UMN scores.<sup>388</sup> FA values specifically within the PLIC have also been shown to correlate with measures of ALS severity and disease duration.<sup>389</sup> However, statistically significant correlations between DTI metrics and clinical measures of disease severity are inconsistent across studies in ALS, with some reporting a clinical correlation.<sup>390</sup> Proposed reasons for a correlation gap between imaging and clinical data include the limitations of clinical disease assessments, the biological complexity of ALS, and also the limitations of imaging methodology.<sup>290</sup>

There are longitudinal studies focusing on the CST in ALS, which have demonstrated reduction in FA.<sup>168,391</sup> While other studies did not find significant changes in FA in the CST over time.<sup>173,392,393</sup> However, the diagnostic delay and rapid disease progression pose a challenge for early initial assessment with neuro-imaging in patients with ALS. It is suggested that by this time the core WM neurodegenerative changes are already established, and subsequent scope for evolution of structural changes is limited.<sup>171</sup> This is in keeping with studies on asymptomatic carriers of ALS-associated mutations, where detectable decreases in CST FA are already apparent.<sup>394</sup>

DTI studies providing insight into the spread of neurodegenerative change along the CST and beyond are limited and conflicting. Some have found the largest alterations in diffusivity in the rostral CST,<sup>17,388,395</sup> which may support an anterograde or dying-forward degeneration of the cortico-motor neurones in ALS. Conversely, other studies have demonstrated predominant changes in the caudal CST in ALS,<sup>396</sup> which may suggest retrograde disease progression or dying-back of motor neurones from the anterior horn cells in the spinal cord.

It has also become apparent using DTI that the corpus callosum (CC) is typically involved, where numerous studies have demonstrated reduced FA in the genu, body, and splenium, in ALS participants compared to healthy controls.<sup>17,339,340,395</sup> This is in keeping with earlier post-mortem studies in ALS.<sup>193,194,201</sup> Longitudinal decreases in FA within the genu have been detected in participants with bulbar-onset ALS.<sup>397</sup> FA values in the corpus callosum have been shown to correlate with clinical measures of ALSFRS-

R and UMN scores.<sup>17,339,340</sup> The posterior mid-body of the corpus callosum shows the most consistent decreases in FA, where increases in MD, AD, and RD have also been reported.<sup>17</sup> This callosal region is composed of larger fiber axons, which rapidly convey information between the primary motor, premotor and supplementary motor areas.<sup>398</sup> The changes in DTI metrics within these fibers of the corpus callosum suggest there is a propagation of the disease process along these structural connections.<sup>17</sup>

Variations in DTI metrics are also capable of distinguishing between patterns of microstructural damage in bulbar and limb onset sporadic ALS,<sup>399</sup> as well as demonstrating differences in white matter degeneration between sporadic and familial forms of ALS.<sup>400</sup>

Studies using DTI have demonstrated involvement of extra-motor cortical regions in ALS, where reduced FA values have been found in the prefrontal and temporal WM.<sup>401</sup> The involvement of subcortical structures has also been demonstrated, supporting the notion of ALS being a multi-system neurodegenerative disorder.<sup>339-341</sup>

Changes in FA have been reported in the CST and CC in patients prior to the onset of UMN signs.<sup>17</sup> In addition when applied to pre-symptomatic fALS gene carriers DTI has also been shown to detect abnormalities.<sup>394</sup> This demonstrates the sensitivity of FA in detecting WM tract degeneration in ALS, even in the early stages of disease.

#### **1.2.4.3 Diffusion tensor imaging structural connectivity and tractography**

DTI has the additional capacity to assess structural connectivity and allows the reconstruction of white matter tracts using DTI tractography. DTI-based fiber tracking allows the localization and quantification of WM pathways where anisotropy is used as the basis for determining inter-voxel connectivity. The primary eigenvector of the diffusion tensor predicts the dominant direction of axonal tract in each brain voxel, and this can be followed through each voxel in a process called fiber tracking, which can be combined with high resolution structural information to reconstruct specific neural pathways.<sup>380</sup>

Tractography studies investigating WM tract integrity in ALS have reported damage in the CST, corpus callosum, and uncinate fasciculus. Those specifically using probabilistic fiber tractography have demonstrated a decrease in CST structural connectivity,<sup>380,401,402</sup> and an association between rate of ALS disease progression correlated and severity of CST damage.<sup>401,402</sup> These findings provide important insight into the consequences of ALS within the brain neural networks, however studies relating these alterations to the pathogenesis underlying ALS are limited. In one study where staging based on TDP-43 aggregation was cross referenced with DWI data, a computational model provided evidence that spread of TDP-43 pathology follows the



topographical pattern of neuronal networks.<sup>403</sup> This supports the hypothesis of TDP-43 inclusions spreading along axonal pathways, propagating from the motor cortex.<sup>404</sup>

#### **1.2.4.4 Fractional anisotropy as a potential imaging biomarker in ALS**

There is a pressing unmet need for an accurate biomarker in ALS, to facilitate in diagnosis, stratification and monitoring of progression in clinical trials studying potentially disease modifying interventions. MRI is non-invasive and widely accessible making MRI techniques including DTI attractive candidates for establishing radiological biomarkers. Currently the most promising DTI parameter is FA, which is exquisitely sensitive at detecting changes associated with ALS in group comparison studies despite lacking specificity. FA along the CST has also been shown to progressively fall in linear manner in longitudinal studies.<sup>4,19,20,405</sup> In addition, FA values in the CST correlate with clinical measures of disease severity and disease duration.<sup>405</sup> Finally, FA has been used in a DTI-based fiber tracking study to analyze how the major WM tracts of interest involved in ALS correspond to the proposed spread of TDP-43 pathology.<sup>285</sup> The results demonstrated that the greatest effect size was for alterations in FA were within the CST, and suggested that a DTI-based staging system could serve as a non-invasive surrogate marker of disease progression.<sup>406</sup>

However, despite consistently demonstrating CST involvement when comparing ALS and healthy control groups, the diagnostic sensitivity of FA on the individual basis in ALS is inadequate.<sup>17,339,340</sup> This is likely due to the variable involvement along the CST as illustrated in post mortem studies.<sup>193,194,201</sup>

Discrepancies in the significance of FA alterations within the CST remain in both cross-sectional and longitudinal studies, likely due to a combination of variability of study inclusion criteria with heterogeneity of methodology utilized.<sup>407</sup>

#### **1.2.4.5 Limitations of diffusion tensor imaging**

The changes in diffusion characteristics clearly reflect the neurodegenerative process underlying ALS. However, the alterations in DTI indices associated with ALS are nonspecific in the microstructural changes they reflect and provide no definite information regarding the underlying mechanisms. Structural and environmental changes should both be considered when hypothesizing what is contributing to these alterations in DTI metrics. Intuitively increased molecular diffusivity suggests axonal disorganization, degeneration, or loss, on a potential background of inflammation and gliosis. Neuropathological studies of ALS have demonstrated changes in structural integrity of WM fibers and inflammation associated with microglial activation, both of which could be contributing to the altered DTI metrics observed in ALS.<sup>16,18,339-341</sup>

The assumption of a single compartment and a single diffusing process within each voxel are recognized limitations of the diffusion tensor model. Studies evaluating fiber architecture suggest that it is rare for there to be a unified direction of diffusion and that a high proportion of voxels contain multiple fiber orientations.<sup>408</sup> DTI-derived diffusion indices do not differentiate between a reduction of fiber density and an increase in fiber crossing, which leads to the potential of tensor-derived measures being misleading and inaccurate in regions where there is complex axonal or dendritic architecture.<sup>408</sup> DTI measures do not therefore provide an optimal model for interpretation of tissue integrity in areas such as the WM of the cerebral cortex where there is fanning and crossing of axons, or within the deep GM neuropil where there is arborization of sparse dendrites. Focus has therefore been directed towards developing more advanced techniques for quantification of microstructural changes in ALS, such as NODDI.<sup>409</sup>

Variations in acquisition and analysis pipelines can lead to disparities in the results, making it difficult to directly compare the findings obtained in different studies. This was recognized by the Neuro-imaging Society in ALS (NiSALS), which established the consensus criteria of MRI sequences in the study of ALS and seeks to encourage multicenter collaboration. The methodological techniques used to acquire, handle, process, and analyze DTI data should therefore be carefully considered and follow the current recommendations for optimization.<sup>410</sup>

## **1.2.5 Neurite orientation dispersion and density imaging (NODDI)**

### **1.2.5.1 The Principles of NODDI**

There has been a recent trend in diffusion MRI towards developing more advanced techniques incorporating mathematical models to improve evaluation of microstructural features within the brain tissue.<sup>411,412</sup> One major aim of such techniques is to overcome the main limitation of DTI, which is a one compartment model with low specificity to differentiating microstructural alterations.

Neurite Orientation Dispersion and Density Imaging (NODDI) is a quantitative diffusion MRI technique which applies a geometric model in order to characterize the microstructural features of the tissues. NODDI was introduced by Zhang and colleagues in 2012 as a practical '*in vivo*' diffusion MRI technique for estimating the microstructural complexity of dendrites and axons within a clinically feasible timeframe.<sup>409</sup> The term 'neurite' is used to describe the two main projections of neurons which encompass the axons in the white matter and dendrites in the grey matter. Quantifying alterations in neurite density and orientation dispersion allows the structural integrity of the neurons to be assessed. This provides an opportunity to learn more about the microstructural changes associated with neurodegenerative diseases such as ALS, where plasticity and

changes in neurite architecture have been implicated by alternative imaging techniques and postmortem studies.

Imaging of postmortem baboon brain samples confirmed that diffusion MRI can be used to quantify neurite density and orientation.<sup>413</sup> Neurite morphology determined using diffusion MRI has subsequently been shown to correlate well with histological analysis of neurite distribution ex-vivo using golgi-impregnated brain tissue.<sup>414</sup> NODDI provides a simplified model of diffusion MRI, making ‘*in vivo*’ assessment of microstructural changes associated with neurodegeneration more feasible.<sup>409,415</sup>

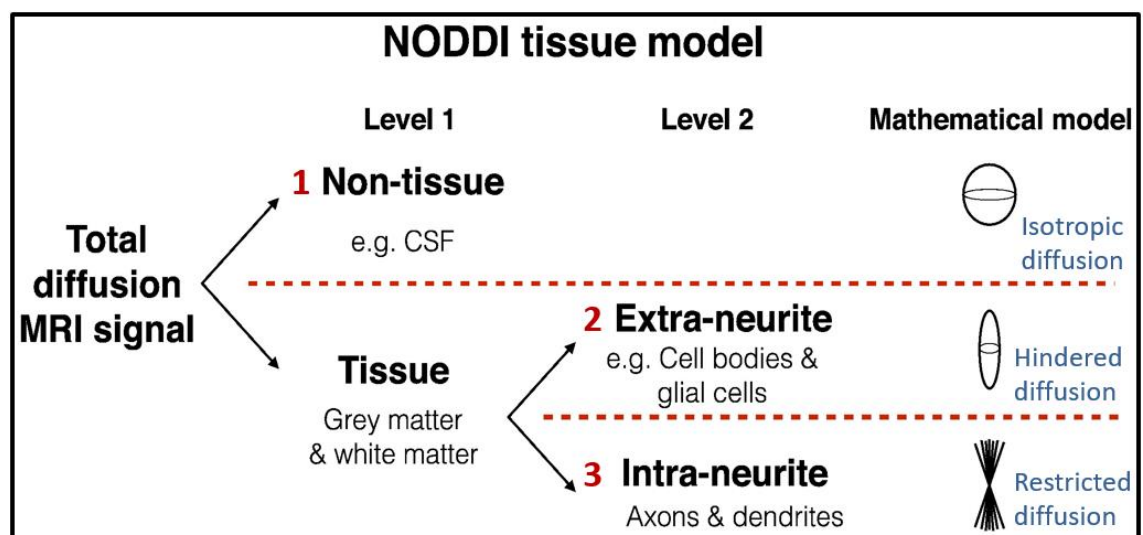
### 1.2.5.2 The NODDI Tissue Model

NODDI separates the MRI signal into three separate microstructural compartments for analysis, the CSF, extra-cellular, and intracellular compartment,<sup>409</sup> see figure 1.11. A geometric model is used to predict the MR signal arising from water diffusion in each tissue compartment. There are unique diffusion properties within each specified environment, which contribute to the normalized magnetic resonance signal (A) as written in the following equation: -

$$A = (1 - V_{iso}) (V_{ic}A_{ic} + (1 - V_{ic})A_{ec}) + V_{iso}A_{iso}$$

Where  $V_{iso}$  and  $A_{iso}$  are the volume fraction and normalised signal of the CSF compartment respectively,  $V_{ic}$  and  $A_{ic}$  are the volume fraction and normalised signal of the intracellular compartment respectively, and  $A_{ec}$  is the normalised signal of the extracellular compartment.<sup>409</sup>

**Figure 1.11: NODDI Tissue Compartment Model**

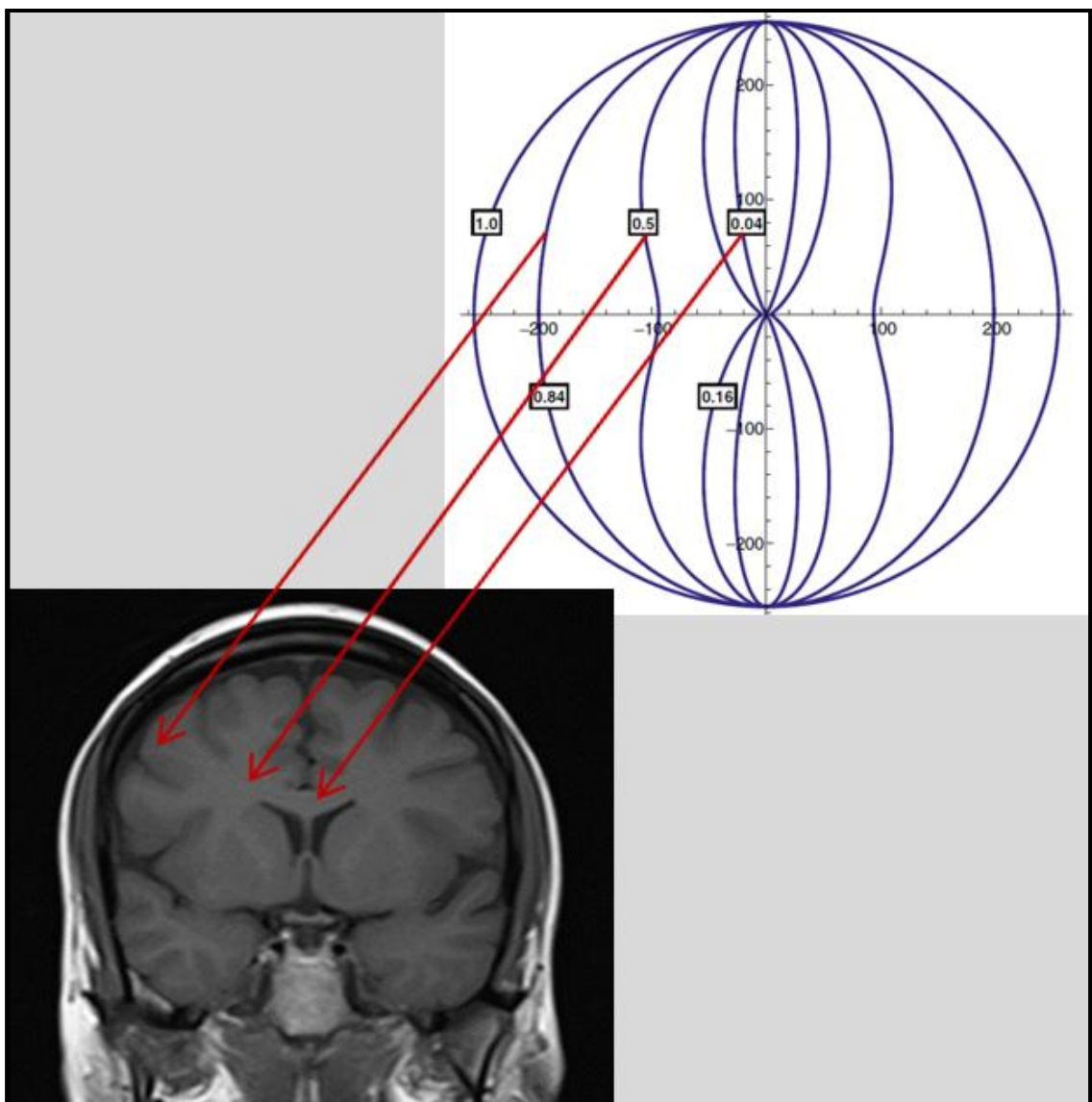


A figure to demonstrate the separation of the NODDI signal in separate tissue compartments, adapted from Tariq M et al., 2016.<sup>415</sup>

The first compartment is outside the brain tissue in the CSF spaces, where diffusion is isotropic, for example within the ventricles and sulci. This CSF compartment is modelled by isotropic Gaussian diffusion with diffusivity  $D_{iso}$ .

The remaining two compartments are within the brain parenchyma of the white matter and grey matter. The second compartment is the extra-neurite compartment, which is the space around the neurites occupied by neuronal cell bodies and glial cells, where diffusion is hindered but not restricted. This extra-neurite compartment is modelled on dispersed cylinders and assumes Gaussian anisotropic diffusion. Parallel and perpendicular diffusivities are coupled using a tortuosity model.<sup>416</sup> The Watson distribution is implemented to capture the effect of orientation dispersion on the apparent diffusivities, see figure 1.12.<sup>409</sup>

**Figure 1.12 Watson distribution for a range of OD values**



A figure to show how the Watson distribution relates to different structural components of the CNS, adapted from Zhang H et al., 2013.

The final compartment is the intracellular compartment, within the axons and dendrites, where diffusion is highly restricted, or anisotropic, due to the presence of neurite membranes. This intra-neurite compartment is modelled using sticks, see figure 1.11, where parallel and perpendicular diffusivities are coupled using the tortuosity model in the same way as the extracellular compartment.<sup>416</sup> The stick composition can range from coherently parallel, reflecting for example the corpus callosum, to highly dispersed, simulating the dendritic arborisation within the cortical neuropil. The orientation dispersion function within this compartment is again modelled by the Watson distribution.

The Watson distribution is used to accommodate variations in architecture across both grey and white matter structures. It allows for parallel assessment of orientation and dispersion of neurites in the extracellular and intracellular compartments. Figure 1.12 illustrates a set of Watson distributions with the same mean orientation but different orientation dispersion indices, 0.04, 0.16, 0.5, 0.84, and 1.0.<sup>409</sup>

One limitation of this model is that it is modelled using isotropic orientation dispersion. In the more recent Bingham NODDI, the Bingham distribution is used to further quantify the orientation distribution of neurites into isotropic and anisotropic dispersion.<sup>415</sup> This limitation needs to be considered when interpreting the results of this research, which uses the original NODDI technique.<sup>409</sup>

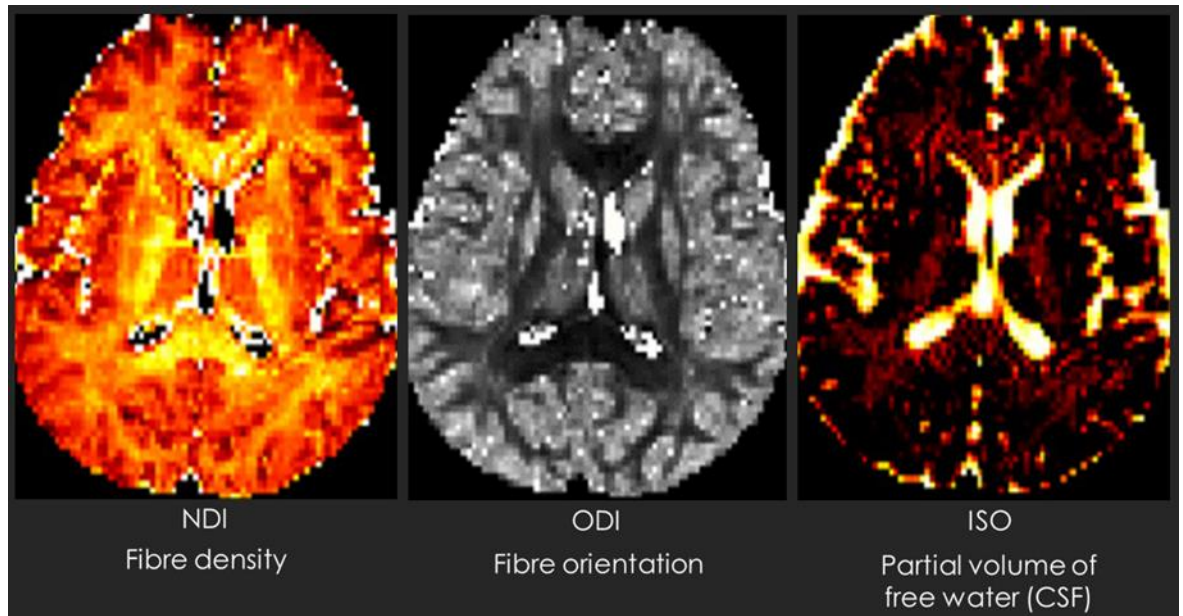
The mathematical modelling behind the compartment models and derivation of the NODDI parameters is beyond the scope of this thesis but is described in detail in the original NODDI publication.<sup>409</sup> In brief  $V_{ic}$  is the intracellular volume fraction and provides a measure of neurite density.  $V_{iso}$  corresponds directly to the isotropic volume fraction. The concentration parameter of the Watson distribution ( $\kappa$ ) is used to calculate ODI using the following equation: -

$$OD = \frac{2}{\pi} \arctan(1/\kappa)$$

### 1.2.5.3 NODDI segmentation model

With NODDI the brain parenchyma is segmented into three partitions. The CSF partition is defined as voxels with a mean diffusivity of less than 80%  $d_{iso}$ , derived from the diffusion tensor. The grey matter partition is defined as all voxels with a linearity of less than 0.2, estimated from fitting the diffusion tensor. The white matter partition constitutes the remaining voxels with a linearity of more than 0.2 according to the diffusion tensor fit. NODDI ultimately yields three parameters; neurite density index or intracellular volume fraction (NDI or ICVF), orientation dispersion index (ODI) and partial volume of free water or isotropic compartment (ISO), see figure 1.13.

**Figure 1.13: The NODDI Parameters**



A figure to show a coloured representation of the NODDI parameters created in FSLview using one healthy control study participant.

As expected, when applying NODDI to the normal brain, NDI was found to be lower in the GM and higher in coherent bundles of WM such as the corpus callosum and internal capsule.<sup>409</sup> Conversely ODI was highest in the GM and lowest in the corpus callosum. ISO showed highest values in the CSF of the ventricles and sulci.

#### **1.2.5.4 Neurological Studies using NODDI**

Since being introduced in 2012, NODDI has been employed in a wide range of imaging studies of the human brain and spinal cord.

NODDI has been used to study normal neonatal brain development,<sup>417–420</sup> childhood maturation,<sup>421</sup> and axonal development in adolescents.<sup>422</sup> Abnormalities associated with infantile metabolic and genetic diseases,<sup>423,424</sup> and changes associated with developmental dyslexia,<sup>425</sup> have also been assessed using NODDI.

NODDI has also been used to assess for variations in adult cortical GM,<sup>426</sup> to understand the normal changes observed with aging,<sup>427,428</sup> as well as alterations associated with neurodegenerative diseases.<sup>429–434</sup>

WM changes associated with hypertension,<sup>435</sup> and WM reorganization following stroke,<sup>436</sup> have been investigated using the NODDI indices.

NODDI was shown to be successful at detecting alterations associated with unilateral temporal lobe epilepsy,<sup>437</sup> and focal cortical dysplasia.<sup>438</sup> In addition cortical and subcortical GM structural abnormalities have been demonstrated using NODDI in patients with MRI negative refractory epilepsy.<sup>439</sup> Furthermore, NODDI has been used in

a brain connectivity study to understand the changes relating to brain networks underlying temporal lobe epilepsy.<sup>440</sup>

NODDI has been used to assess WM abnormalities relating to first episode psychosis,<sup>441</sup> and neurite changes associated with schizophrenia.<sup>442,443</sup>

Characterization of glioma grade as well as differentiation between oedema, tumour, and normal brain tissue has been achieved using NODDI,<sup>444–446</sup> which has implications for improving neurosurgical procedures.

In multiple sclerosis (MS) NODDI has been used to study parenchymal alterations in both the brain<sup>447–449</sup> and the spinal cord.<sup>450,451</sup> NODDI has been shown to characterize intracranial MS lesions, where abnormalities were more marked in secondary progressive MS compared to relapsing-remitting MS.<sup>447–449</sup> Microstructural changes associated with normal-appearing WM have also been consistently demonstrated using the NODDI parameters, even in the early stages of MS.<sup>447–449</sup> In one post-mortem study using NODDI to assess MS pathology within the thoracic spinal cord,<sup>450</sup> the NODDI parameter of NDI was shown to match the histologically derived measure of dispersion, thereby validating this model against histological analysis.

Acute microstructural changes associated with interferon-alpha treatment have been demonstrated using NODDI in a subpopulation of patients with Hepatitis C, where an acute increase in striatal neurite density correlated with side effects of fatigue and mood disturbance.<sup>452</sup>

Further studies using NODDI analysis of the spinal cord have been used to assess recovery after surgical treatment of degenerative cervical myelopathy.<sup>453,454</sup>

Typically, NODDI parameters are estimated within each voxel independently. However, NODDI also has the potential to be incorporated into tractography frameworks.<sup>455</sup> NODDI has been implemented using tract-based special statistics (TBSS) to assess for white matter abnormalities in first episode psychosis,<sup>441</sup> sickle cell anaemia,<sup>456</sup> and traumatic brain injury.<sup>457</sup>

#### **1.2.5.5 Advantages and limitations of NODDI**

NODDI is potentially superior to DTI, in the generated parameters, because it provides an estimate of neurite orientation dispersion as well as neurite density. NODDI can therefore facilitate disentangling the components of FA, but in addition because it analyses at the sub-voxel level NODDI increases the specificity for individual tissue microstructural features. As a three compartment model NODDI also allows better categorization of how microstructural changes contribute to alterations in the arising diffusion MRI signal.<sup>409,458,459</sup> A comparison of NODDI with DTI, showing the similarities and differences, is given in table 1.10.

**Table 1.10: Similarities and differences between NODDI and DTI**

Similarities	Differences
<p>NODDI and DTI techniques can both be applied in clinically feasible time frames.</p>	<p>The imaging acquisition time is higher for NODDI, in order to acquire multi-shell diffusion data.</p> <p>While for DTI, only a single shell of diffusion data is required, which leads to a shorter imaging acquisition time.</p>
<p>NODDI and DTI are quantitative diffusion imaging techniques. The imaging data is acquired using diffusion-weighted MRI, and quantitative methods are used to extract the parameters.</p>	<p>NODDI parameters:-</p> <ul style="list-style-type: none"> <li>• Neurite Density Index (NDI)</li> <li>• Orientation Dispersion Index (ODI)</li> <li>• Isotropic compartment (ISO)</li> </ul> <p>DTI parameters:-</p> <ul style="list-style-type: none"> <li>• Fractional Anisotropy (FA)</li> <li>• Mean Diffusivity (MD)</li> <li>• Axial Diffusivity (AD)</li> <li>• Radial Diffusivity (RD)</li> </ul>
<p>Mathematical models are used to derive the parameters for both NODDI and DTI.</p>	<p>NODDI uses a biophysically informed multi-compartment tissue model. The diffusion signal is separated into three microstructural compartments:</p> <ul style="list-style-type: none"> <li>• Intra-neurite (WM)</li> <li>• Extra- neurite (GM)</li> <li>• CSF</li> </ul> <p>DTI adopts a simplistic model consisting of a single compartment.</p>
<p>The quantitative models for NODDI and DTI are both based on a number of assumptions</p>	<p>NODDI assumptions:-</p> <ul style="list-style-type: none"> <li>• Neurites are modelled as highly anisotropic sticks, with zero perpendicular diffusivity.</li> <li>• The intrinsic parallel diffusivity is fixed (<math>1.7 \mu\text{m}^2 \cdot \text{ms}^{-1}</math>) and is assumed to be constant across the extra- and intra-neurite compartments in both the WM and GM. Fixing of intrinsic parallel</li> </ul>



	<p>diffusivity is necessary for stability of the NODDI parameter estimates.</p> <ul style="list-style-type: none"> <li>• The extra-neurite compartment is modelled using Gaussian anisotropic diffusion.</li> <li>• Orientation dispersion is modelled using the Watson distribution.</li> </ul> <p>DTI assumes anisotropic Gaussian diffusion.</p>
<p>There are criticisms regarding both NODDI and DTI techniques.</p>	<p>A source of criticism for NODDI is the fixed parameters within the model, which could lead to bias in the derivation of the variable parameters (NDI, ODI, ISO). In particular the fixed intrinsic parallel diffusivity, which is optimised for cerebral WM but sub-optimal for analysis of the GM. This causes a parameter bias of NDI towards the WM and limits the capacity if NODDI to detect GM alterations.</p>
<p>NODDI and DTI are both optimised for analysis of the cerebral WM and are limited in their capacity for GM analyses.</p>	<p>The main criticism for DTI is that the parameters do not relate to specific microstructural tissue alterations and can therefore be affected by multiple concurrent biophysical mechanisms. A good example is that FA cannot distinguish between changes in axon density versus axon rearrangements (fanning or crossing).</p>

A table comparing NODDI with DTI, highlighting the similarities and differences of these quantitative diffusion MRI techniques.

The original NODDI technique utilized in this research (NODDI),<sup>409</sup> models orientation dispersion isotropically and is limited in its capacity to model multiple fiber orientations arising from complex axonal architecture such as fanning and bending within white matter structures.<sup>415,460</sup> A high proportion of voxels are estimated to contain multiple fibre orientations from both histological,<sup>461</sup> and imaging data,<sup>408</sup> which NODDI is unlikely to be

capturing in its original form.<sup>460</sup> NODDI has subsequently been developed further to incorporate a quantification of anisotropic orientation dispersion.<sup>415</sup>

There are assumptions underlying the NODDI model which have the potential to result in a parameter bias of NDI, which is derived directly from the intracellular compartment fraction, towards the WM.<sup>460</sup> Within the NODDI model, estimation of the intracellular compartment is related to the mean diffusivity of the tissue. The same model is applied for analysis of the intracellular compartment and subsequent estimation of NDI in both the WM and GM, where the parallel and perpendicular diffusivities are coupled using a tortuosity constraint.<sup>409</sup> This is based on the assumption that mean diffusivity provides a good contrast between GM and WM, however this is not a consistent finding.<sup>460,462</sup> This tortuosity model applied to the intracellular compartment in NODDI potentially increases the sensitivity of the intracellular fraction to alterations in mean diffusivity and creates a dependency of NDI on the diffusivity of the tissue. This facilitates the NODDI model fitting of intracellular compartment, within the highly organized coherent axons of the WM, where diffusivity is relatively consistent. However, estimation of neurite density within the GM, where the intracellular compartment is finely dispersed within the predominantly extracellular compartment, and diffusivity is highly variable, is intuitively more challenging. It is possible that the NODDI analysis emphasizes the contribution of diffusion within WM and thereby increases sensitivity towards detecting changes in this compartment. The assumptions of this model could therefore potentially have limitations in the GM, where the architecture of the neuropil is more complex.<sup>460,462</sup>

## **1.2.6 Quantitative Magnetization Transfer Imaging (QMTi)**

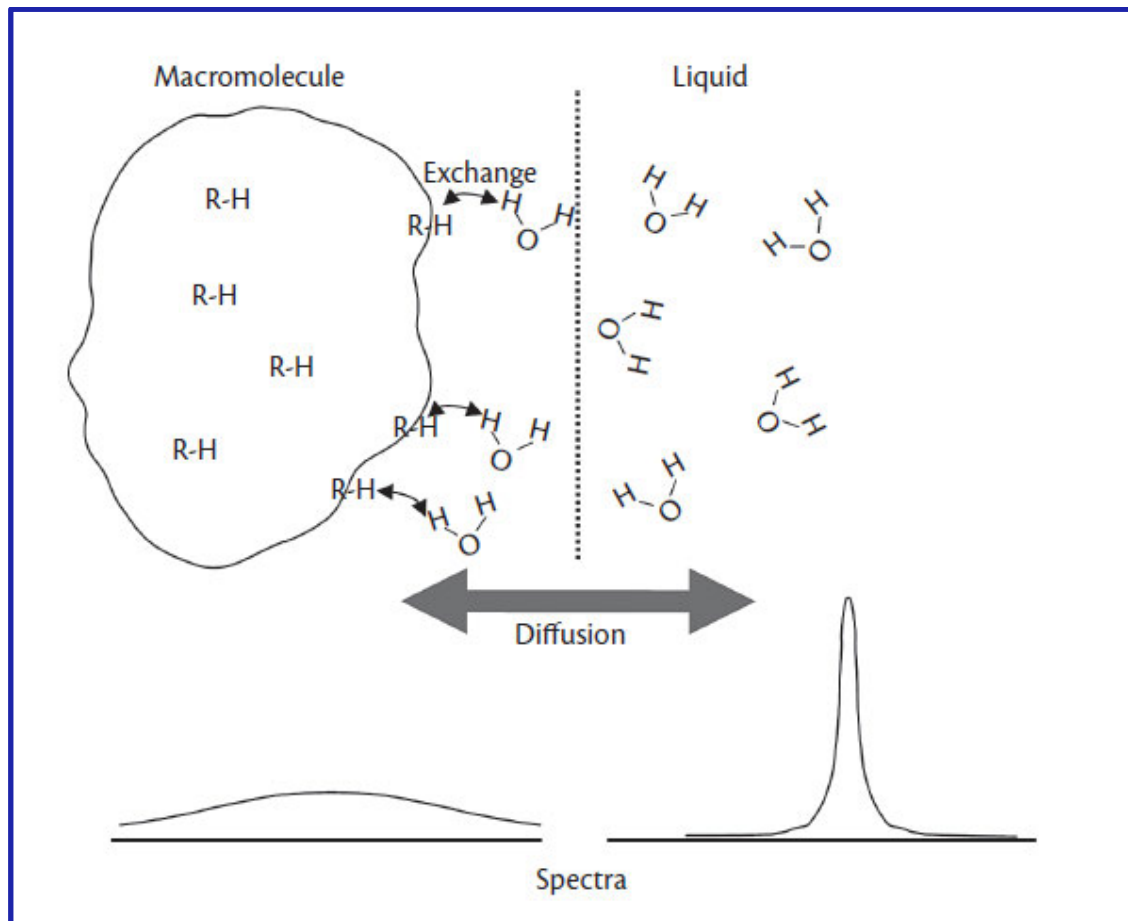
### **1.2.6.1 Magnetization Transfer**

Magnetization Transfer (MT) has been recognized as providing an additional method of contrast in MRI, complementary to T1 and T2, since the late 1980s.<sup>463,464</sup> Conventional MRI detects the signal produced by protons within liquid surroundings, which are therefore unrestricted in their resonance, see chapter 1.2.1. Within this environment the motion of protons becomes synergistic, exhibiting averaging of behaviour and uniformity of resonance (Larmor frequency), leading to longer T<sub>1</sub> and T<sub>2</sub> relaxation times.<sup>465</sup>

Protons bound within macromolecules such cell membranes, myelin, proteins, lipids, and polysaccharides, are restricted in their motion and produce a variable resonance signal which decays too rapidly to be detected by standard MRI. It is therefore not possible to directly measure the signal from these protons with MRI, making the additional properties of these protons and the tissue in which they are embedded undetectable. However, the free protons are in constant motion are free to interact with the macromolecular protons and when this occurs the spin magnetization can be

exchanged between protons in either direction, see figure 1.14.<sup>465</sup> This exchange of magnetization provides the basis for magnetization transfer imaging.

**Figure 1.14: Transfer of magnetization between free and bound protons.**



A figure to show the exchange of magnetization between protons bound in macromolecules and freely mobile protons, taken from Horsfield MA and Cercignani M, 2015.<sup>466</sup>

The dynamics of MT can be manipulated to provide an indirect measure of the activity within the macromolecular protons. When an appropriate off-resonance radiofrequency is applied to preferentially excite the macromolecular protons then their spins will become saturated. Interaction with the free protons rapidly allows transfer of this magnetization, and the effect can be measured in the change of magnetization in the free protons, which results in signal attenuation.<sup>466</sup> Despite MT being accessible for almost three decades MT has had low uptake in the study of neurological diseases.

Traditionally MT effects have been quantified using the MT ratio (MTR), which is a relatively crude parameter.<sup>467,468</sup> MTR is a simple quantification of the difference between the MRI signal measured with and without the off-resonance saturation pulse sequence. MTR also depends heavily on the acquisition parameters such as the repetition time (TR), the excitation flip angle and the saturation pulse characteristics.

MTR does not measure one particular property and is therefore non-specific in the biophysical measures it reflects.<sup>465,469</sup>

Investigations in ALS conducted on 1.5T MRI scanners have demonstrated a decreased MTR in regions already known to be implicated from neuropathological and structural MRI studies including the primary motor cortex, CST, and the fronto-temporal cortex.<sup>470–472</sup> As MTR reflects the tissue capacity to exchange magnetization this reduction is likely to reflect some alteration in tissue, such as loss of structural integrity. In one a recent study using a 7T MRI scanner there was a significant increase in MTR detected in the right CST.<sup>473</sup> The authors argue that this could be due to the accumulation of aggregated proteins contributing to the macromolecular component or an increase in the tissue liquid fraction secondary to neurodegeneration. However, this is contrary to the reported decrease in MTR previously reported in this region.<sup>472</sup> This highlights the challenges in using MTR, which is possibly influenced by too many variables, its quantification should therefore be interpreted with caution.

Quantitative magnetization transfer imaging (qMTi) describes the application of MT to a set of quantitative parameters.<sup>465,466</sup> The underlying basis for derivation of these parameters comes from the two-pool model, a quantitative extension of MT, see figure 1.15. This model identifies the protons in free water as the ‘liquid pool’, and the protons bound within the macromolecules as the ‘macromolecular pool’. In figure 1.15 the grey portions in each box reflect the saturated spins at a specified time and the white areas indicate the proportion of longitudinal spins.  $M_0^A$  and  $M_0^B$  represent the density of spins, while  $R_A$  and  $R_B$  indicate the longitudinal relaxation times within each pool, respectively. The rate of loss of longitudinal magnetization, due to application of off-resonance radiofrequency, is represented by  $R_{RFA}$  in the liquid pool, and  $R_{RFB}$  in the macromolecular pool. The rate of exchange of magnetization ( $R$ ) is assumed to be symmetrical.

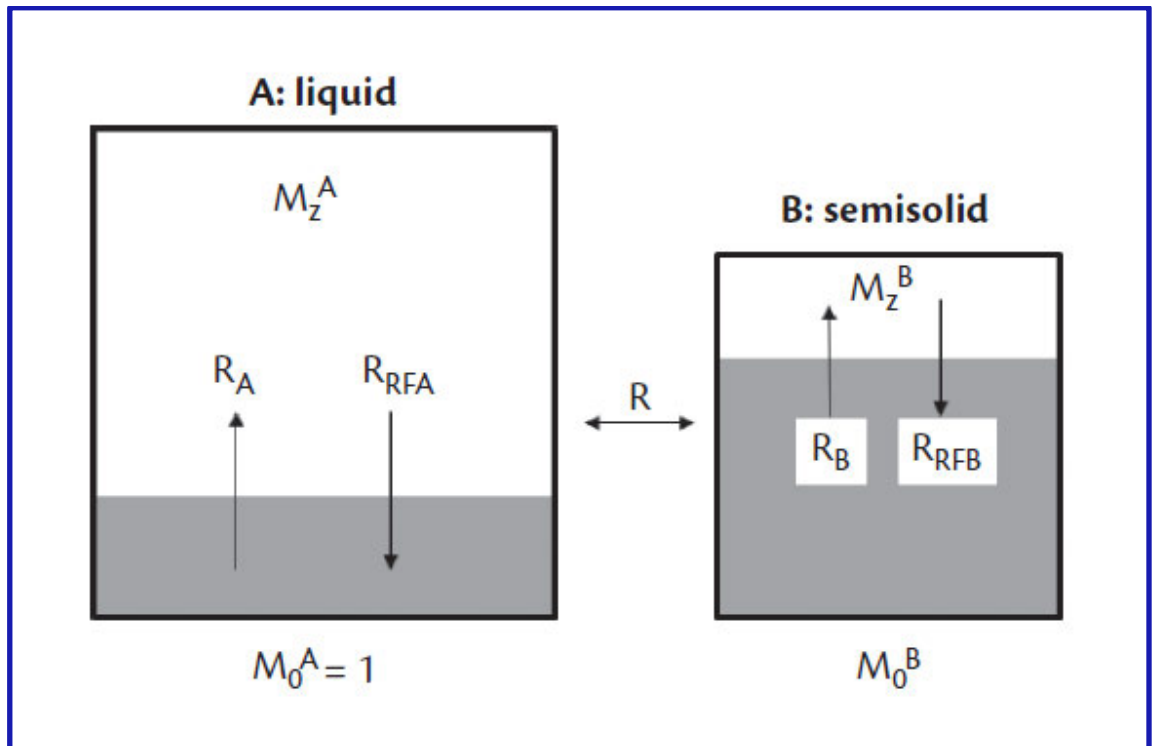
The rate of exchange from A to B,  $RM_0^B$ , also known as  $k_f$ , is described as the forward magnetization exchange rate. The interpretation of  $k_f$  is not yet fully understood but changes in  $k_f$  are thought to reflect alteration in functional integrity within the tissue, for example due to inflammation or metabolic changes.<sup>465,466</sup> Evidence to support this comes from studies in Alzheimer’s disease, where  $k_f$  detected cortical grey matter alterations corresponding to regions of atrophy,<sup>474</sup> and recent investigations on the effects of peripheral inflammation within the CNS.<sup>452,475</sup>

A further parameter can be quantified from the fractional size of the macromolecular pool where  $F = M_0^B / M_0^A$ . Due to the high density of macromolecules within myelin, MT effect is greater in the white matter, which leads to an increase in  $F$ . This parameter is therefore used as a measure of myelin content within the tissue, and is supported by animal models of demyelination.<sup>476</sup>

The final parameter is the transverse relaxation time of the liquid pool  $T_{2f}$ , which provides assessment of water content. Increases in  $T_{2f}$  are likely to reflect atrophy associated with neurological conditions, however  $T_{2f}$  appears to be relatively stable in across different conditions, for example in acute inflammation.<sup>475</sup>

### 1.2.6.2 The Principles of Quantitative Magnetization Transfer Imaging

**Figure 1.15: Two-pool model for quantification of magnetization transfer**

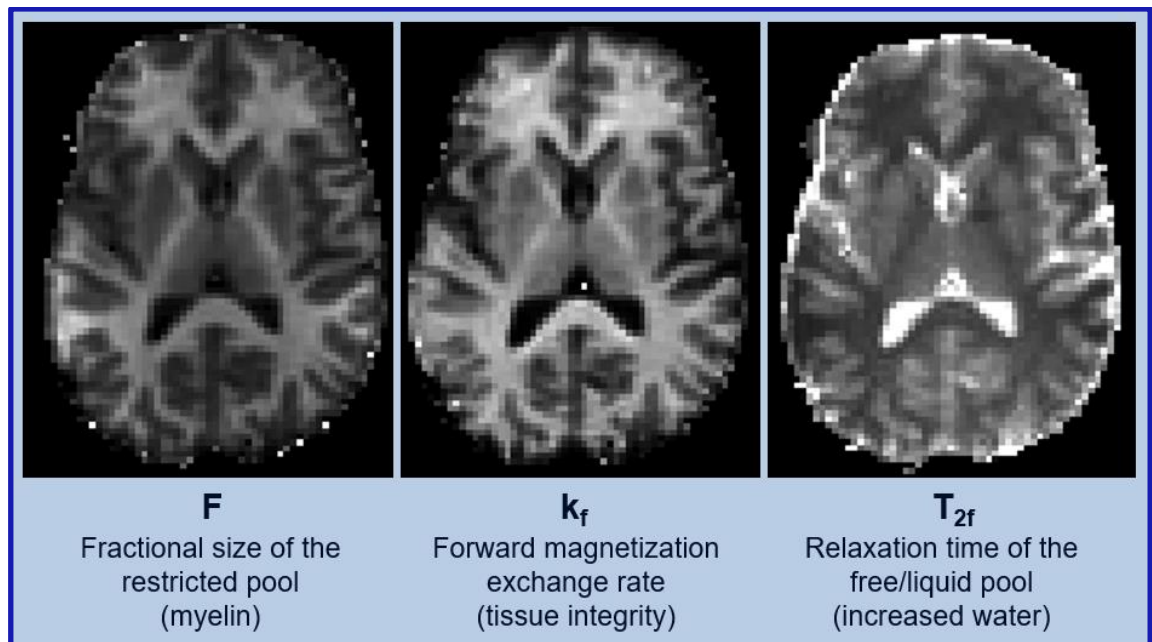


A figure to demonstrate the two-pool model for quantification of magnetization transfer, taken from Horsfield MA and Cercignani M, 2015.<sup>466</sup>

The three quantitative parameters obtained from qMTi;  $F$ ,  $k_f$ , and  $T_{2f}$ , are demonstrated in figure 1.16. These parameters provide the basis for quantitative magnetization transfer (qMTi) imaging, which attempts to model the MRI signal as a function of these biological parameters thus enabling their estimation. The parameters have been shown to demonstrate consistency in healthy subjects making them a feasible option for monitoring changes in neurodegenerative conditions.<sup>477</sup> Biologically the qMTi signal depends on density of protons in macromolecules and thereby the structure of the tissue, qMTi therefore provides nonspecific indicators of the functional integrity of the tissue. Although MTR has been applied alongside VBM studies in ALS,<sup>478</sup> qMTi imaging has not yet been used to study the associated neurodegenerative profile. I am therefore the first to be incorporating this technique into assessing the biophysical changes occurring in ALS. I will be using the balanced steady-state free precession method, which provides

high resolution qMTi parameter maps across the human brain in a clinically feasible time frame.<sup>479</sup>

**Figure 1.16: The qMTi parameters**



A figure to demonstrate the qMTi parameters, created using a healthy control participant imaging data in FSLview.

### 1.2.6.3 Neurological Studies using qMTi

Although there are no previous studies using qMTi in ALS for comparison, important considerations can be gained from what qMTi demonstrates in other degenerative and inflammatory brain conditions and what has previously been demonstrated by studies incorporating basic magnetization transfer concepts.

The majority of the magnetization transfer occurs in within the WM, due to presence of myelin associated lipids. Therefore qMTi, and more specifically F, has been proposed as a potential tool for assessing myelinated axonal regions. With this in regard the technique has gained substantial interest in multiple sclerosis research. In chronic burned out MS plaques, sometimes referred to as black holes, one study showed a reduced F using qMTi imaging.<sup>480</sup> Similarly, a significant reduction in F was demonstrated in the CST of patients with benign MS compared to healthy controls.<sup>481</sup> In one study comparing qMTi parameters in relapsing remitting MS and controls, both F and k<sub>f</sub> were found to be reduced in lesions compared to normal appearing white matter (NAWM).<sup>482</sup> F is therefore consistently reduced in brain tissue affected by multiple sclerosis and is likely to represent a demyelinating process.

In acute MS inflammatory lesions qMTi has demonstrated reduced  $F$  and  $k_f$ , accompanied by an increase in  $T_{2f}$ ,<sup>477</sup> which eventually return to baseline after several months. In addition, NAWM also demonstrates reduced  $F$  and  $k_f$  in MS.<sup>483</sup>

In an experimentally induced state of mild inflammation, a rapid rise in  $k_f$  was demonstrated in the insular cortex, which correlated with FDG-PET, implicating increased glucose metabolism as a contributing factor to the changes observed in  $k_f$ .<sup>475</sup>

Finally, in Alzheimer's disease  $k_f$  was reduced in the hippocampus as well as other regions such as the posterior cingulate and insular cortex, where differences were located predominantly in the GM and surrounding WM.<sup>474</sup> The regions involved are known to be implicated in Alzheimer's disease as demonstrated by previous structural imaging studies,<sup>484</sup> and FDG-PET.<sup>485</sup> One theory is that changes in mitochondrial metabolism, secondary to the accumulation of aggregated protein (e.g.  $\beta$  amyloid) associated with Alzheimer's disease, underlies the changes in  $k_f$ .<sup>474</sup>

As qMTi has detected changes relating to inflammation in MS and neurodegeneration in Alzheimer's disease, it is reasonable to hypothesize that alterations in qMTi parameters may occur in ALS due to the underlying disease mechanisms, particularly as there are likely to be both immune,<sup>253</sup> and degenerative,<sup>341</sup> components to the disease pathogenesis.

In ALS, magnetization transfer contrast (MTC) T1-weighted images have demonstrated CST and corpus callosum hyperintensity in a proportion of patient with ALS, which related to reduced FA from concurrent DTI analysis.<sup>486,487</sup> Voxel wise analyses have reported reduced MTR within the CST and PCG in patients with ALS when compared to healthy controls.<sup>470,472,478</sup>

### **1.3 Research Rationale, Objectives, and Study Design**

#### **1.3.1 Research Rationale**

ALS is a rare but clinically distinctive neurodegenerative disease, which has devastating consequences, causing worldwide morbidity and mortality. In order to tackle the challenge of finding effective treatments further understanding of this complex condition is essential. Despite decades of dedicated research ALS remains incurable and causes relentless demise of the motor system, potentially spreading through network connections to become a multisystem disorder.<sup>3</sup> Progressive disability due to muscle weakness is evident clinically and ultimately death occurs, typically as a result of respiratory failure. There is heterogeneity of ALS at the genetic, phenotypic, and molecular level, all of which complicate attempts at disease stratification and hinders progress in clinical trials.

Multimodal approaches using a combination of advanced imaging techniques are required to facilitate advances in the understanding of the progression of ALS and evaluate responses to therapeutic strategies from the outset of the disease.<sup>4</sup>

One major challenge in research of neurodegenerative diseases such as ALS is the inability to visualise the microstructural abnormalities '*in vivo*'. This limits our knowledge of the processes taking place within the nervous system and leads to hypotheses of progression based on pathological staging.<sup>283</sup> As yet the site of disease onset has not been established and the dynamics of the neurodegenerative process are not fully understood in ALS. Assessing changes associated with ALS during life and in particular early in the course of the disease using advanced MRI techniques such as NODDI provides a means of advancing our understanding of the microstructural disease mechanisms.

Developing and piloting advanced neuro-imaging techniques is crucial in the study of ALS, where the main objectives include being able to quantify altered tissue microstructure, provide non-invasive diagnostic information, develop disease stratification models for clinical trials, and provide a means of assessing response to treatment. Assessing the capacity of potential imaging modalities in their ability to detect changes underlying the neurodegenerative process in ALS therefore has important considerations for the future of ALS. In particular imaging biomarkers could be incorporated into future clinical trials and play an important role in finding effective treatments.

### **1.3.2 Research Objectives**

The mechanisms and dynamics of the neurodegenerative processes underlying ALS require clarification in order to facilitate development of disease modifying treatments. The main objective of my research study was to pioneer the novel quantitative diffusion MRI technique, NODDI, alongside qMTi, in order to scrutinize the neurodegenerative process occurring in ALS and gain insight into the abnormalities in tissue microstructure. Furthermore by comparing the extent of damage in the cortical GM to that of the major WM motor tracts, the hope was to gain evidence to support or refute the dying back, dying forward, and Wallerian degeneration hypotheses of neurodegeneration in ALS.

To my knowledge this study is the first incorporating NODDI and qMTi in a multi-modal, multi-parametric, cross-sectional analysis of brain changes in ALS. The specific hypotheses relating to NODDI and qMTi are given below.



### 1.3.2.1 NODDI Hypotheses

The NODDI parameters offer potential to provide microstructural information regarding changes in both the GM and WM neurites in ALS. The NODDI hypotheses are as follows:-

- Due to the known degeneration of CST motor axons from previous DTI and post-mortem studies,<sup>193-195, 339-342</sup> I hypothesized that NODDI would detect reduced neurite density (NDI) in the CST WM accompanied by increase in free water compartment (ISO)
- I hypothesized that alongside axonal and secondary myelin tract damage in the WM, NODDI would detect reduced arborisation (ODI) and density (NDI) of dendrites within the GM neuropil of the primary motor cortex, in keeping with a process of dendritic pruning relating to the disease process underlying ALS.
- I also hypothesized that the different phenotypes of ALS, such as limb and bulbar onset, could be distinguished by the distribution of microstructural abnormalities demonstrated on imaging using NODDI.
- More widespread clinical involvement, cognitive involvement, and more advanced disease according to the King's Stages of ALS were predicted to relate to more extensive microstructural damage demonstrated by NODDI.
- Conventional DTI was used alongside NODDI to test the hypothesis that NDI from NODDI would detect more axonal damage within the WM tracts than FA, by removing the confounding effect of orientation dispersion.
- As the clinical measures of ALS severity reflect the underlying pathological processes occurring, a correlation between these and the NODDI parameters were predicted. In particular NDI was hypothesised to correlate with ALSFRS-R, MRC score, UMN burden, and disease duration.

### 1.3.2.2 qMTi Hypotheses

An additional contrast method in MRI measuring distinct characteristics and yielding information regarding the biophysical properties of the brain tissue composition can be gained using qMTi. The integrity of WM tracts and an assessment of myelin content can also be gained with qMTi. The qMTi hypotheses are as follows:-

- I hypothesised that qMTi would show reduced relative density of the macromolecular pool (F) in the CST of patients with ALS, reflecting damage to myelinated axons.
- I also hypothesized that  $k_f$  would be reduced in the CST, due to molecular abnormalities associated with the pathological processes underlying ALS.

- A reduction in  $k_f$  was also predicted in the motor cortex, where pathological processes associate with loss of dendritic complexity.
- An increase in  $T_{2f}$  was anticipated in relation to the degenerative process affecting the motor regions.
- I hypothesized that there would be more extensive molecular changes relating to more widespread clinical disease, cognitive involvement and higher King's stage of ALS.
- Finally I hypothesised that molecular changes would correlate with disease duration and other markers of disease severity in ALS (ALSFRS-R, MRC score, UMN burden).

### 1.3.3 Study Design

A cross-sectional study design was used to investigate for differences in quantitative brain imaging parameters derived from NODDI and qMTi techniques, as well as DTI and structural MRI analysis, between ALS and healthy control participants.

#### 1.3.3.1 Sample size calculation

The main quantitative imaging technique used in this study, NODDI, has not previously been studied in ALS. The sample size calculation was therefore based on previous results acquired using the comparable quantitative imaging technique of DTI. The DTI parameter of FA was regarded as relatively equivalent to the NODDI parameter of NDI for the purpose of the sample size calculation. The study published by Blain CR and colleagues<sup>393</sup> was used to provide the mean FA values for the sporadic ALS and control groups, along with the standard deviation (SD). Using these values, the effect size (d), which is required for estimating the sample size in our clinical study, was calculated using the following equation:

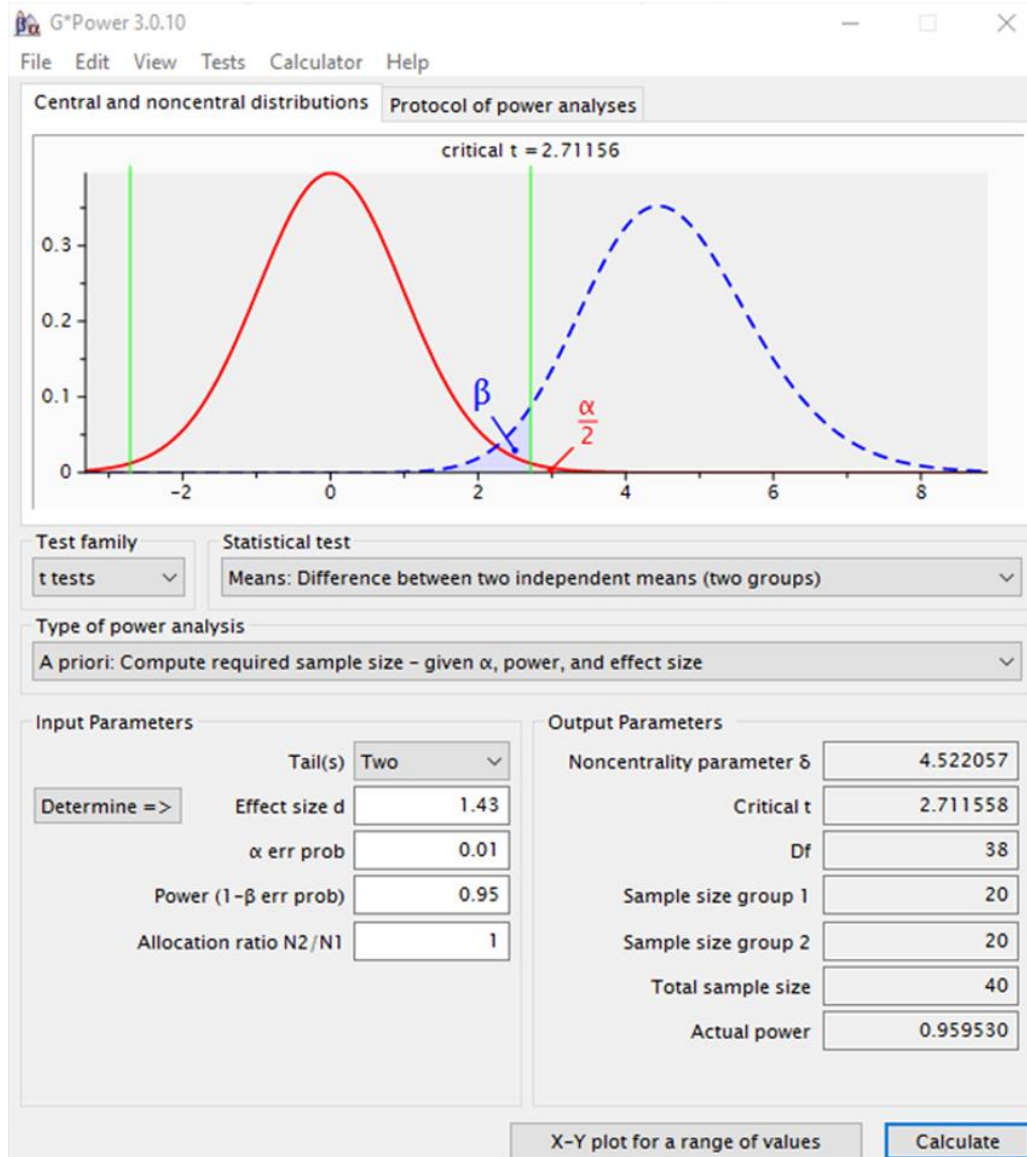
$$d = \text{Mean FA ALS group} - \text{Mean FA control group} / \text{SD}$$

$$d = 0.46 - 0.51 / 0.035 = -1.43$$

Using a statistical software program called G\*power (<http://www.gpower.hhu.de/en.html>),<sup>488</sup> assuming a normal distribution, setting an error probability of 1% (0.01), and setting a power of 95% (0.95), the sample size was estimated at being 20 in each group, see figure 1.17.

However, it should be highlighted that as the power analysis was conducted using FA, which is the strongest DTI parameter, it could lead to some of the NODDI and qMTi parameters being underpowered in this study. Furthermore, it could have an impact on the power of all the subgroup analyses.

**Figure 1.17: Sample Size Calculation using G\*Power Statistical Program**



A figure to show how G\*Power statistical program was used to calculate the sample size required to reach power of 95%, assuming normal distribution, and error probability of 1%.

### 1.3.3.2 Study Approval, and Funding

Prior to the study favourable ethical opinion was obtained from the National Research Ethics (NRES) South-East London Research Ethics Committee (14/LO/0195), see appendix A5. The study was sponsored by Brighton and Sussex Medical School, see appendix A6, and was adopted into the Dementias and Neurodegeneration (DeNDRoN) speciality portfolio of the NIHR Clinical Research Network (UKCRN ID 16861), see appendix A7. The entire research study was funded by a medical research grant from the Motor Neurone Disease Association (Leigh/Apr14/824-791), see appendix A8. All the research related to this study took place at the Clinical Imaging Sciences Centre, Brighton and Sussex Medical School, University of Sussex.

**CHAPTER 2:  
CLINICAL DATA  
ACQUISITION AND  
ANALYSIS**

## **CHAPTER 2 CLINICAL DATA ACQUISITION AND ANALYSIS**

This chapter will focus on the methods used to attain the clinical data of the participants in this study, followed by the exploration of the ALS group clinical characteristics.

### **2.1 Participant Recruitment**

ALS participants (n=twenty three; sixteen male and seven female; median age 67 years, range 45 – 73 years), diagnosed with El Escorial definite, probable, or laboratory supported sporadic ALS were recruited into this research study between June 2014 and February 2016. Recruitment was predominantly from a specialist neurology clinic conducted by Professor PN Leigh at Hurstwood Park Neurosciences Centre, as well as through liaison with consultant colleagues within Brighton and Sussex University Hospitals NHS Trust.

Healthy controls (n= twenty three; fourteen male and nine female; median age 64 years, range 43–76 years) were included in the study for comparison. Healthy participants were recruited largely by participation of family members, friends, and contacts of people diagnosed with ALS.

Those interested in taking part in the study were given a participant information sheet (PIS) and then allowed time to decide if they wished to take part in the study. As the recruitment target was challenging I decided not to be selective for this study. As long as the diagnostic criteria were fulfilled, the inclusion and exclusion criteria were met, and the participants had capacity to consent, they were included in this study.

### **2.2 Participant Consenting and Screening**

All participants gave written informed consent to take part in the research study after reading the PIS and having the opportunity to discuss what taking part in the study would entail, see appendix A9. A screening questionnaire was then used to ensure that all the inclusion and exclusion criteria were met, see appendix A10.

Slow vital capacity assessment (SVC)<sup>489</sup> was performed on participants with ALS to ensure they had sufficient respiratory function (VC >60% predicted) to safely undergo the MRI scanning protocol. Capacity to consent was another requirement, as well as being an adult, and meeting the El Escorial diagnostic criteria for ALS, see table 2.1. Exclusion criteria were any contra-indication to MRI or inability to tolerate lying flat for 1 hour due to either severe illness or respiratory compromise, see table 2.1.

There was no known family history of ALS among any of the participants; however, no genetic testing was performed for ethical reasons.

**Table 2.1: Inclusion and Exclusion Criteria**

Inclusion Criteria	Exclusion Criteria
Sufficient respiratory function (FVC >60% predicted in ALS group) to allow lying flat comfortably for up to one hour	Impaired respiratory function (FVC <60%)
	Inability to lay flat for 1 hour due to underlying cardiac or respiratory compromise
Capacity to give fully informed consent	
No contraindication to MRI	Lack of capacity to consent
	Cardiac pacemaker or implantable cardioverter-defibrillator in situ
	Metal implants (eg: artificial joints, surgical clips, prosthetic heart valve, intra-uterine device, nerve stimulator, cochlea implant, drug pump), or metal fragments in or close to the eyes or blood vessels
Age (18 – 80 years)	
ALS participants required a diagnosis of El Escorial definite, probable, or laboratory supported ALS	Any other contra-indication to either MRI (eg: pregnancy, claustrophobia)

## 2.3 Clinical Data Acquisition

### 2.3.1 Clinical Assessments of ALS participants

Participants with ALS were asked to give an account of the timings and site of onset of disease symptoms. Then they underwent a standardized neurological examination, assessment with the revised ALS functional rating scale (ALSF<sub>RS</sub>-R)<sup>152</sup> and finally the Edinburgh Cognitive and Behavioural ALS screen (ECAS),<sup>78</sup> see appendix A1-A4. Participants were also assigned an upper motor neurone (UMN) score and total Medical Research Council (MRC) muscle strength. This information was used to stratify ALS participants according to site of disease onset, disease distribution at the time of assessment, disease duration, King's stage of ALS, and presence of any cognitive deficits or behavioural changes relating to the ALS-frontotemporal spectrum disorder (ALS-FTSD).

### 2.3.2 The Total Medical Research Council (MRC) Score

During neurological assessment participants with ALS had twenty two pairs of muscles assessed for strength of power using the Medical Research Council (MRC) power score. This scores muscle strength from a minimum of 0, where there is no visible movement,

up to a maximum score of 5 which relates to normal power. When added together this gives a possible maximum total score out of 220, please see appendix A2.

### **2.3.3 The Upper Motor Neurone Score**

ALS participants were assessed for upper motor neurone (UMN) involvement using the UMN score which has previously been described by Turner MR et al., 2004.<sup>185</sup> During the neurological examination reflexes were assessed for pathological briskness bilaterally at the biceps, supinator, triceps, finger, knee, ankle, and plantar, where a score of 1 was given according to the presence of pathologically brisk reflexes. The facial and jaw jerk reflexes were also assessed giving a total maximum possible score out of 16, see appendix A3.

### **2.3.4 The revised ALS Functional Rating Scale (ALSFRS-R)**

The ALSFRS-R was used to assess the functional ability of ALS participants in carrying out common daily activities across four domains of bulbar function, gross motor function, fine motor function, and respiratory function.<sup>152</sup> Each domain was assessed with a series of three questions and allocated a score on the scale of 0 – 4, giving a maximum possible score of 48, see appendix A1.

### **2.3.5 The rate of change in ALSFRS-R**

No longitudinal data was acquired on this cohort and therefore the ALSFRS-R was not serially measured. The monthly rate of change of ALSFRS-R ( $\Delta$ ALSFRS-R) was instead calculated as the reduction in ALSFRS-R score, from 48 at baseline (symptom onset) to the score at the time of assessment, divided by the number of months between the two scores (disease duration). The calculated monthly rate of decline in ALSFRS-R score is widely accepted as a useful estimate of the rate of disease progression as described by Menke RA., et al 2018.<sup>168</sup>

### **2.3.6 The Edinburgh Cognitive and Behavioural Screen in ALS (ECAS)**

I assessed all the ALS participants using the ECAS, to detect the presence of any cognitive deficits and behavioural changes relating to ALS-FTSD, see appendix A4 for the ECAS tool used during the clinical assessment, and Table 1.5 in chapter 1 for the scoring of ECAS. The ECAS cut off scores for detecting cognitive impairments are summarized in Table 2.2. The presence of behavioural abnormalities across the six domains of disinhibition, apathy or inertia, loss of sympathy or empathy, perseverative, stereotypes, compulsive or ritualistic behaviour, hyper-orality or altered food preferences, and psychosis were recorded.<sup>78</sup>

Due to the recognised cognitive and behavioural profile of ALS, wherever possible the behavioural assessment questions were conducted with the ALS participant’s carers and relatives. There were three ALS participants who did not have a relative or carer available to answer these questions, these were participants 2, 19, and 23.

**Table 2.2: ECAS cut off scores for detecting cognitive impairments.**

<b>Cut off scores for abnormality using the ECAS<sup>78</sup></b>		
ECAS Total Score		105
ALS Specific Scores	Total	77
	Language	26
	Verbal Fluency	14
	Executive	33
ALS Non-specific Scores	Total	24
	Memory	13
	Visuospatial	10

The cognitive and behavioural scores derived from the ECAS were used for the assessment of ALS-FTSD, as described in section 1.1.6.4 and shown in Table 1.6. The Rascovsky criteria<sup>490</sup> were used for the consideration of the diagnosis of behavioural variant FTD relating to ALS.

### **2.3.7 King’s Staging Allocation**

The information gathered in the clinical assessment was used to allocate all ALS participants with a stage of ALS disease according to the King’s Staging System,<sup>187</sup> where stages 1 to 3 reflect the number of regions affected by ALS (e.g. upper limb, lower limb, bulbar regions), stage 4 represents nutritional or respiratory failure, and stage 5 indicates death, see table 1.7.

## **2.4 Clinical Data Statistical analysis**

### **2.4.1 Participant demographics and clinical characteristics**

The age and sex of all participants in the ALS and the control groups were tabulated in Microsoft Excel. The mean and standard deviations for age were calculated in Excel. T-test and chi-squared statistical tests were performed in SPSS (IBM SPSS version 22 for Windows) to assess for significant differences between ALS and control group mean ages and ratio of male to female participants, respectively.



The site of onset, time from onset to diagnosis, total MRC score, UMN score, disease duration, ALSFRS-R,  $\Delta$ ALSFRS-R, and King's ALS stage for all ALS participants were also tabulated in Microsoft Excel. The mean, standard deviation, mode and median were calculated for each variable using the statistical analysis feature of excel.

To assess the distribution of rates of progression within the ALS group, the frequency of  $\Delta$ ALSFRS-R scores were tabulated and a histogram constructed using excel.

#### 2.4.2 ECAS cognitive scores and behavioural changes

ALS participant total ECAS scores as well as the sub-scores for language, verbal fluency, executive, memory, and visuospatial were all tabulated in Microsoft Excel. The Mean and standard deviation were calculated using the appropriate Excel function. In addition, any behavioural abnormalities of disinhibition, apathy or inertia, loss of sympathy or empathy, perseverative, stereotypes, compulsive or ritualistic behaviour, hyper-orality or altered food preferences, and psychosis were recorded. Bar charts were then constructed using Excel graph function to demonstrate the frequency of the abnormal cognitive scores and behavioural changes across these domains.

#### 2.4.3 Clinical Data Correlations

SPSS was used to assess for Pearson correlation between all clinical variables and to construct scatter plots to demonstrate correlations. Results were accepted as statistical significance where  $P < 0.05$ .

### 2.5 Clinical Data Analysis

**Table 2.3: Demographics of ALS and healthy control groups.**

	ALS n = 23	Controls n = 23	P values (Statistical Test)
Gender (Male: female)	16: 7	14: 9	$\chi^2 = 0.38$ $P = 0.53$
Age (years)			
mean (SD)	64.3 (7.99)	61.5 (9.27)	t-test = 1.11
median (range)	67 (45 – 73)	64 (43 - 76)	$P = 0.27$
Handedness (right: left)	22: 1	20: 3	$\chi^2 = 1.09$ $P = 0.29$

A table to show the gender, age, and handedness of the ALS and healthy control groups.

### **2.5.1 Participant Demographics**

In total, forty six participants were recruited into this study, twenty three participants with ALS and twenty three healthy controls of similar age and gender distribution.

The mean age for the ALS group was 64.3 years (SD 7.99), while that for the control group was 61.5 years (SD 9.27), the demographics of all participants are summarized in table 2.3. The two groups were well matched in terms of gender ( $\chi^2 = 0.38$ ,  $P=0.53$ ) and age ( $t = 1.11$ ,  $P=0.27$ ). Over two thirds of the participants with ALS were male (70%), reflecting the expected epidemiology of the disease within the general population.

### **2.5.2 Clinical Characteristics of the ALS group**

Clinically the ALS group was phenotypically heterogeneous with a wide breadth of weakness, spasticity, functional disability, rate of progression, and cognitive deficit, see table 2.4. All had capacity to give fully informed consent and vital capacity (VC) values of over 60% predicted. Individual participant data is given in table 2.5. All ALS participants except one were taking Riluzole at the time of clinical assessment.

Bulbar onset occurred in three participants (13.0%), truncal onset occurred in one participant (4.3%) while the remaining nineteen participants had limb onset (82.6%) of disease symptoms, see table 2.4. Two of the bulbar onset participants were female and the remaining participant was male. Within the limb onset subgroup ten participants experienced initial symptoms in the upper limbs and nine participants in the lower limbs.

The median delay from symptom onset to diagnosis for the whole group was 8.5 months with a range of 2 months to 27 months. Bulbar onset was associated with the longest median delay to diagnosis of 12 months. The lower limb onset group had one of the lower median diagnostic delays of 8 months. However, one of the lower limb onset participants had the longest individual delay between symptom onset and diagnosis of 27 months. The mean diagnostic delay for the upper limb group was 9.5 months and the shortest individual delay occurred in this group, where one participant was diagnosed with ALS 2 months after symptom onset in the dominant right hand.

The disease duration amongst ALS participants at the time of assessment varied considerably, with a range from 9 months to 39 months, and a median of 17.5 months.

The MRC score, used as a proxy for assessment of overall strength, varied between 91 and 220, with a median of 189.5. Two ALS participants scored the maximum of 220 on MRC muscle power assessment suggesting normal muscle strength. One of these was a 51-year-old male with lower limb onset of a predominantly UMN form of ALS, and the other was a 72-year-old female with progressive bulbar palsy, see table 2.5. The lowest MRC score was found in a 64-year-old male with right hand onset who was classified as having King's stage three ALS.

UMN score ranged from 2 to 16, out of a maximum of 16, with a median of 8 within the group. The majority of ALS participants recruited had typical ALS with a mixture of upper and lower motor neurone involvement. However, four ALS participants were recruited with LMN-predominant ALS (two flail arm, two flail leg), and one participant with UMN-predominant phenotype. To demonstrate the spread of phenotypes please see Table 2.6.

**Table 2.4: Clinical characteristics of the ALS group.**

Site of onset (no. of participants)	Bulbar	3
	Upper Limb	10
	Lower limb	9
	Trunk	1
Time to diagnosis (months)	Whole group, median (range)	8.5 (2 – 27)
	Bulbar subgroup, median (range)	12 (8 – 15)
	Upper limb subgroup, median (range)	9.5 (2 – 17)
	Lower limb subgroup, median (range)	8 (4 – 27)
	Participant with truncal onset	6
Disease duration, median Range (months)		17.5 9 - 39
Total MRC power score, median Range (out of total maximum 220)		189.5 91 – 220
UMN score, median Range (out of total maximum 16)		8 2 - 16
ALSFRS-R median Range (out of total maximum 48)		40 25 – 46
$\Delta$ ALSFRS-R, median Range (continuous variable)		0.36 0.09 - 1.33
ECAS scores	ALS specific score, median Range (out of total maximum 100)	87 65 - 100
	ALS non-specific score, median Range (out of total maximum 36)	28 13 - 36
	Total score, median Range (out of total maximum 136 )	113 88 - 135
Slow Vital Capacity (%) median Range		79 61-127

Abbreviations: ALSFRS-R, ALS revised functional rating scale;  $\Delta$  ALSFRS-R, Change in ALS revised functional rating scale over time; ECAS, Edinburgh Cognitive and behavioural screen ALS screen; MRC, Medical Research Council; UMN, Upper Motor Neurone Score.

The median ALSFRS-R was 40 with a range from 25 to 45, out of a possible total of 48, demonstrating the breadth of functional disability within the group. Similarly rate of change in ALSFRS-R illustrated a large variation in the group ranging from 0.09 to 1.33, with a median of 0.36.

**Table 2.5: Individual participant with sporadic ALS clinical data.**

Pt HD	Age Sex	Site of onset	Time from onset to diagnosis	Total MRC Score	UMN Score	Disease Duration	ALSFRS -R	$\Delta$ ALSFRS -R	King's Stage
1 Rt	46 M	Bulbar	12	193	12	38	34	0.37	2
2 Rt	65 M	Limb Rt H	3	180	5	39	37	0.28	2
3 Rt	62 M	Limb Rt H	15	163	8	27	36	0.44	3
4 Rt	71 M	Limb Rt H	2	184	8	17	39	0.53	1
5 Lt	58 F	Bulbar	8	209	12	21	40	0.38	1
6 Rt	66 M	Limb Rt F	5	178	10	12	44	0.33	1
7 Rt	51 M	Limb Rt L	4	220	12	21	46	0.09	2
8 Rt	67 M	Limb Lt H	10	153	4	34	35	0.38	3
9 Rt	64 M	Limb Rt H	9	91	12	22	25	1.04	3
10 Rt	67 F	Limb Lt H	11	184	8	13	40	0.61	2
11 Rt	69 M	Limb Rt H	13	203	10	14	44	0.28	1
12 Rt	71 M	Limb Lt F	8	170	10	18	39	0.5	2
13 Rt	69 M	Limb Lt H	4	124	16	10	40	0.8	3
14 Rt	68 M	Limb Rt L	5	197	4	16	43	0.31	2
15 Rt	72 F	Bulbar	15	220	3	17	44	0.23	1
16 Rt	73 M	Limb Rt L	12	193	5	20	41	0.35	1
17 Rt	73 M	Limb Lt L	27	162	5	28	32	0.57	3
18 Rt	67 F	Limb Lt F	6	187	6	15	44	0.27	1
19 Rt	65 M	Trunk	6	213	4	9	46	0.22	1
20 Rt	69 M	Limb Lt H	17	207	2	22	45	0.14	1
21 Rt	56 F	Limb Lt F	8	208	12	10	44	0.4	2
22 Rt	66 F	Limb Rt H	6	188	12	9	36	1.33	2
23 Rt	45 F	Limb Lt F	10	191	5	11	45	0.27	1
Med	67	-	8.5	189.5	8	17.5	40	0.36	-
Mean	64.3	-	10.0	184.1	8	19.2	40	0.43	-
SD	7.8	-	6.25	29.9	3.7	9.2	5.2	0.28	-
Mode	67	-	8.0	193	12	21	44	0.38	-

Abbreviations: Pt, participant; HD, hand dominance; M, male; F, female; Rt, right; Lt, left; H, hand; F, foot; L, leg; MRC, Medical Research Council; UMN, Upper Motor Neurone Score; ALSFRS-R, revised ALS rating scale;  $\Delta$ ALSFRS-R, rate of change in ALSFRS-R; ECAS, Edinburgh Cognitive and behavioural screen ALS screen; SD, standard deviation; Med, median.

When looking at the spread of  $\Delta$ ALSFRS-R, there appeared to be two subgroups in this cohort of participants with ALS. Using a histogram to demonstrate, the majority of

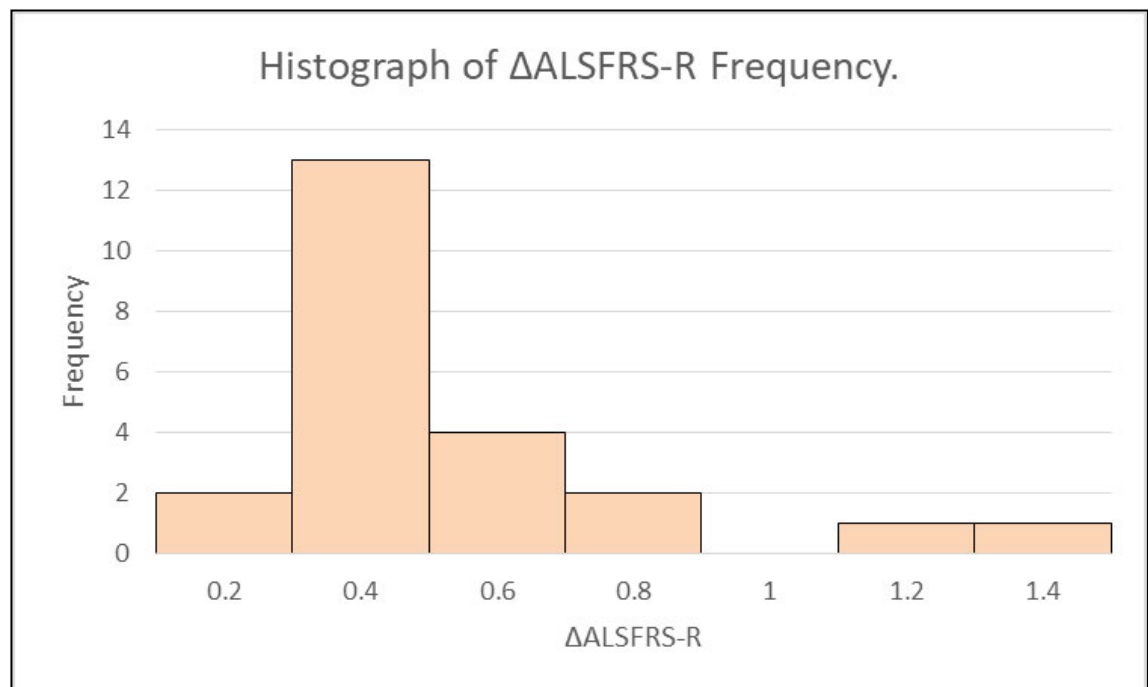
participants fall into the first component distribution of rates up to 0.80. Then there is another group of fewer participants who have rates of more than 1.0. This is suggestive of a bimodal distribution of  $\Delta$ ALSFRS-R scores, see figure 2.1.

**Table 2.6: Phenotypes within the ALS group**

Typical ALS		LMN Predominance		UMN Predominance	Bulbar Onset ALS
UL onset	LL onset	Flail Arm	Flail Leg		
8	7	2	2	1	3

In terms of stage of ALS, using the King's staging system, ten participants were classified as having stage 1 ALS, eight participants with stage 2 and only five participants were classified as having stage 3 ALS. No participants had nutritional or respiratory failure, therefore no participants were allocated stage 4. All participants remained alive for the duration of the study.

**Figure 2.1: Bimodal distribution of  $\Delta$ ALSFRS-R**



A figure to demonstrate the frequency of ALSFRS-R scores across the ALS group, showing a bimodal distribution.

### 2.5.3 Cognitive Impairment and Behavioural Changes

ECAS total scores ranged from 88 to 135 within the ALS group, with a median of 113 out of a possible maximum of 136. A breakdown of the participant's scores within the ECAS

five cognitive domains of language, verbal fluency, executive, memory and visuospatial, as well as the behavioural changes are given in table 2.7.

At the time of assessment none of the ALS participants fulfilled the revised diagnostic criteria for ALS frontotemporal dementia (ALS-FTD),<sup>77,187</sup> and none complained of progressive, symptomatic, cognitive issues.

However, twelve participants (52%) fell on or below the cut off for normal cognitive performance in at least one of the cognitive sub-domains, see table 2.7. Five of these participants met the criteria for ALS-FTSD. One of these participants was classified as having ALS cognitive and behavioural impairment (ALS<sub>cbi</sub>; 17) and four were classified as having ALS cognitive impairment (ALS<sub>ci</sub>; 8, 11, 12, and 14).

Six of the ALS participants had abnormal cognitive sub-scores but did not meet the criteria for ALS<sub>ci</sub> (5, 7, 10, 13, 16, 22), and of these four had normal ECAS total scores. Finally, one patient had an isolated borderline language sub-score (18), see table 2.7.

In terms of spread of deficits across the ALS specific (language, verbal fluency, and executive) and ALS non-specific (memory, and visuospatial) domains, five participants had abnormal performance spread across both the ALS specific and ALS non-specific cognitive domains to varying extents (5, 11, 12, 14, 17). Only three participants demonstrated abnormal scores selectively in the ALS specific domains (7, 8, 18). While four ALS participants had abnormal scores confined to ALS non-specific domains. Figure 2.2 illustrates the frequency of abnormal performance within each cognitive domain within the ALS group. Memory deficit was the most frequent domain in which deficit was apparent, while none of the participants had impairment in visuospatial scores.

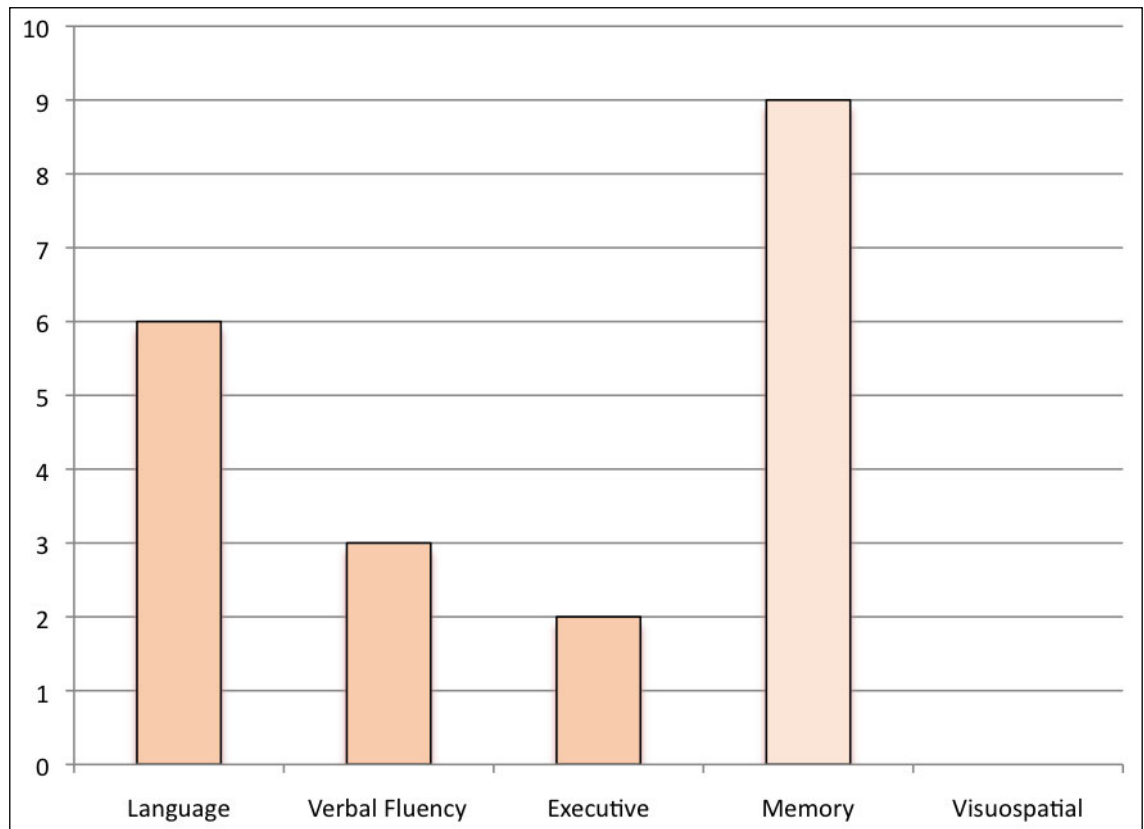
Behavioural changes were evident in two participants with ALS (8.6%), both of which had additional cognitive impairment in at least one domain, see table 2.7. One of these participants had suboptimal scores selectively in the ALS specific domains. This participant had considerable impairment in verbal fluency as well as borderline impairment in language cognition but normal executive function. ALS non-specific scores were also normal. This participant was classified as having ALS<sub>ci</sub> because although he exhibited stereotyped behaviour during the assessment no other behavioural abnormalities were described or observed, therefore did not meet the criteria for ALS<sub>cbi</sub>, see table 2.7, participant 8. In the other participant with behavioural changes, disinhibition, compulsivity, and loss of sympathy were apparent during clinical assessment. This participant demonstrated impairment in all of the ALS specific cognitive domains as well as considerable impairment in memory, bringing their ALS specific score, ALS non-specific score, and total ECAS score below the cut off for normal, see table 2.6; participant 17, such that he met the criteria for ALS<sub>cbi</sub>.

**Table 2.7: ECAS scores and behavioural changes in the ALS group.**

Pt	ECAS								Behavioural Change (six domains)	ALS-FTSD
	Total	ALS specific scores				ALS non-specific scores				
		L	VF	E	Total	M	VS	Total		
1	131	28	24	43	95	22	12	36	X	X
2	124	28	22	41	91	21	12	33	X	X
3	123	27	24	44	95	16	12	28	X	X
4	116	27	20	40	87	17	12	29	X	X
5	111	25	20	40	85	10	12	22	X	Abnormal sub-scores
6	129	28	24	44	96	21	12	33	X	X
7	107	28	20	31	79	15	12	28	X	Abnormal sub-score
8	93	26	0	39	65	17	11	28	One domain	ALSci
9	119	27	16	43	86	21	12	33	X	X
10	110	27	20	38	85	13	12	25	X	Abnormal sub-score
11	105	28	14	42	84	9	12	21	X	ALSci
12	99	24	16	37	77	9	12	22	X	ALSci
13	105	27	20	38	85	8	12	20	X	Abnormal sub-scores
14	88	25	16	34	75	1	12	13	X	ALSci
15	121	28	22	43	93	16	12	28	X	X
16	113	28	18	43	89	12	12	24	X	Abnormal sub-scores
17	83	26	10	32	68	3	12	15	Three domains	ALSci
18	108	26	18	38	82	14	12	26	X	Borderline sub-score
19	129	28	24	45	97	21	12	32	X	X
20	115	27	20	42	89	14	12	26	X	X
21	135	28	24	48	100	23	12	35	X	X
22	105	28	20	39	87	6	12	18	X	Abnormal sub-scores
23	120	27	20	42	89	19	12	31	X	X
Med	113	27	20	41	87	15	12	28	-	-
Mean	112.5	27	18.7	40.2	86.0	14.2	11.9	26.3	-	-
SD	13.6	1.1	5.4	4.1	8.8	6.2	0.2	6.2	-	-
Mode	105	28	20	43	85	21	12	28	-	-

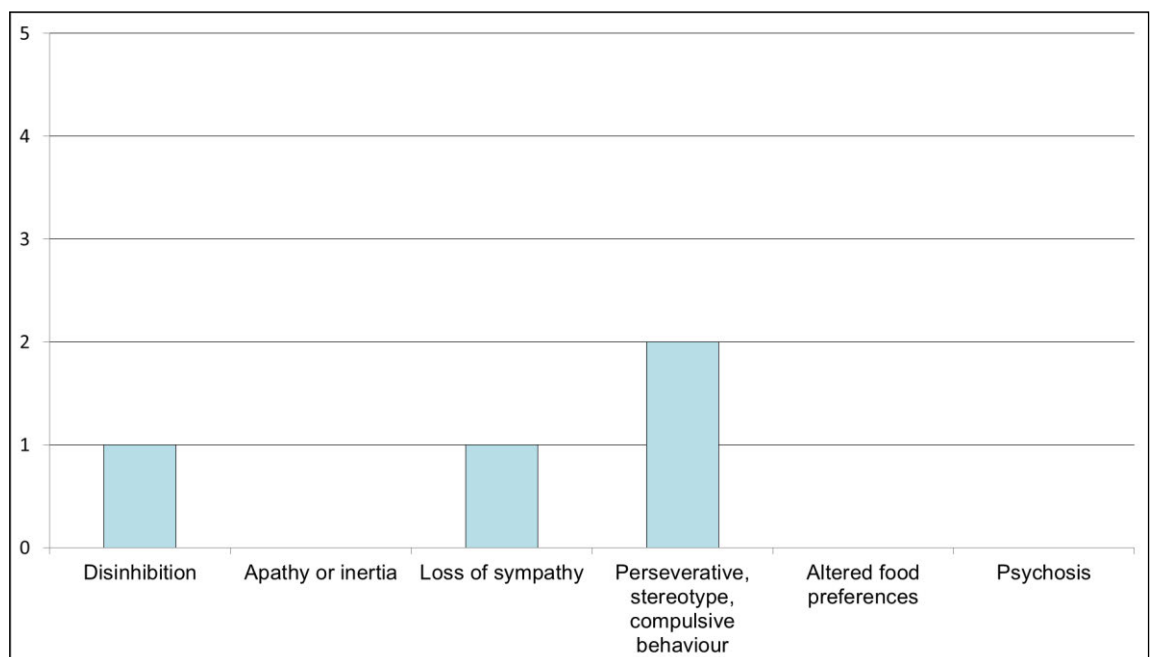
Those highlighted in blue fell below the normal cut off within at least one cognitive domain.  
 Abbreviations: Pt, participant; L, language; VF, verbal fluency; E, executive; M, memory; VS, visuospatial; SD, standard deviation.

**Figure 2.2: Frequency of abnormal performance in the ALS group within each of the cognitive domains assessed using the ECAS.**



A figure to show the cognitive impairments found in the ALS participants. ALS specific domains are shown using darker pink. ALS non-specific domains are represented by lighter pink.

**Figure 2.3: Frequency of altered behaviour in the six behavioural domains.**



A figure to demonstrate the behavioural alterations observed in the ALS participants.



Figure 2.3 illustrates the frequency of behavioural changes observed within the ALS group across the six domains. There were no behavioural changes observed or reported in the remaining participants with ALS.

## 2.6 Clinical Data Correlations

There were several correlations within the clinical variables of the ALS group, please see table 2.8 and figure 2.4. Age correlated with total ECAS cognitive score, where older age was associated with lower total ECAS scores and younger age was associated with higher ECAS total score, see figure 2.4A.

Duration of ALS correlated with ALSFRS-R, where, as to be expected longer disease duration was associated with lower ALSFRS-R scores, see figure 2.4B. This reflects the nature of the disease where over time the disease starts to affect more muscles and the functional ability declines.

**Table 2.8: Correlations between clinical variables within the ALS group.**

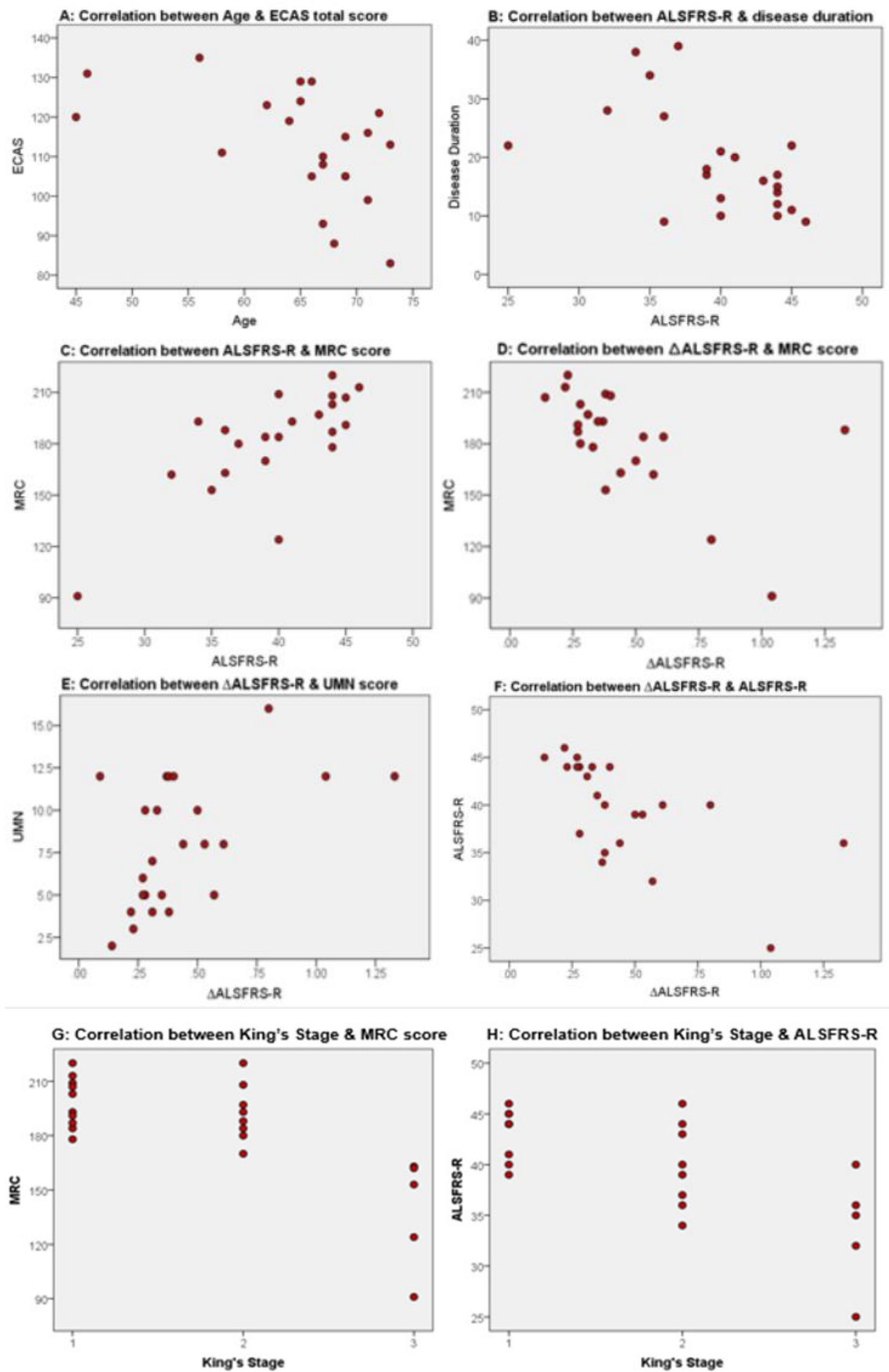
	Age	Duration	UMN	MRC	ALSFRS-R	$\Delta$ ALSFRS-R	ECAS total	King's Stage
<b>Age</b> PCC Sig. (2-tailed)	1	-0.13 0.56	-0.32 0.14	-0.20 0.35	-0.83 0.71	0.19 0.39	-0.44* 0.04	0.012 0.955
<b>Duration</b> PCC Sig. (2-tailed)	-0.13 0.56	1	-0.19 0.38	-0.18 0.42	-0.53** 0.01	-0.19 0.38	-0.05 0.80	0.383 0.072
<b>UMN</b> PCC Sig. (2-tailed)	-0.32 0.14	-0.19 0.38	1	-0.31 0.15	-0.35 0.54	0.50* 0.01	0.13 0.54	0.303 0.161
<b>MRC</b> PCC Sig. (2-tailed)	-0.20 0.35	-0.18 0.42	-0.31 0.15	1	0.76** 0.000	-0.62** 0.002	0.20 0.37	-0.706** 0.000
<b>ALSFRS-R</b> PCC Sig. (2-tailed)	-0.83 0.71	-0.53** 0.01	-0.35 0.54	0.76** 0.00	1	-0.65** 0.001	0.17 0.43	-0.700** 0.000
<b><math>\Delta</math>ALSFRS-R</b> PCC Sig. (2-tailed)	0.19 0.39	-0.19 0.38	0.50* 0.01	-0.62** 0.002	-0.65** 0.001	1	-0.17 0.42	.485* 0.019
<b>ECAS total</b> PCC Sig. (2-tailed)	-0.44* 0.04	-0.05 0.80	0.13 0.54	0.20 0.37	0.17 0.43	-0.17 0.42	1	-0.340 0.112
<b>King's Stage</b> PCC Sig. (2-tailed)	0.012 0.955	0.383 0.072	0.303 0.161	-0.706** 0.000	-0.700** 0.000	.485* 0.019	-0.340 0.112	1

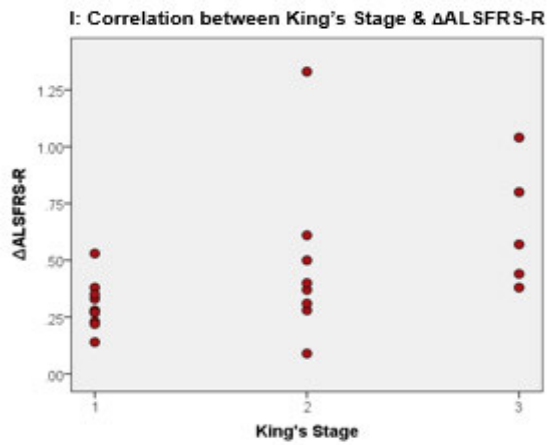
\*Correlation is significant at the  $P < 0.05$  level (2-tailed).

\*\*Correlation is significant at the  $P < 0.01$  level (2-tailed).

Abbreviation: PCC, Pearson's Correlation Coefficient

Figure 2.4: A figure to show the parameter correlations within the clinical data.





Scatter plots demonstrating significant correlation between clinical parameters of the ALS participant group. A, Age and ECAS; B, ALS duration and ALSFRS; C, MRC score and ALSFRS-R; D, UMN score and  $\Delta$ ALSFRS-R; E, MRC score and  $\Delta$ ALSFRS-R; F, ALSFRS-R and  $\Delta$ ALSFRS-R; G, King's Stage and MRC score; H, King's Stage and ALSFRS-R; I, King's stage and  $\Delta$ ALSFRS-R.

The total MRC score correlated with both ALSFRS-R and  $\Delta$ ALSFRS-R, see figure 2.4C and 2.4D. Higher MRC scores were associated with higher ALSFRS-R scores and slower rates of disease progression, as measured by the  $\Delta$ ALSFRS-R. While lower MRC scores, typically reflecting more severe and widespread disease, were associated with lower ALSFRS-R scores and higher rates of disease progression. However, one participant with a relatively high MRC score of 188 exhibited the fastest rate of progression with a  $\Delta$ ALSFRS-R of 1.33 and can be seen as an outlier in figure 2.4D. This participant had one of the shortest disease durations of nine months, with onset in the right hand, please see table 2.5 participant 22.

There was correlation between the total UMN score and  $\Delta$ ALSFRS-R, with an apparent association between lower UMN scores and slower rate of progression, particularly in those with UMN scores of less than 5 where rates of progression were less than 0.25, see table 2.5 and figure 2.4E. Three participants with UMN scores over 12 out of a possible total of 16 had progression rates of over 0.75. However, another participant with an UMN score of 12 had the lowest progression rate within the group (0.09) and appears to be another outlier, see participant 7, table 2.5.

ALSFRS-R correlated with  $\Delta$ ALSFRS-R, see table 2.8 and figure 2.4F, where higher ALSFRS-R scores related to slower rates of disease progression and lower ALSFRS-R scores were associated with faster rates of progression. These two variables are related by definition and therefore such a correlation is to be anticipated.

Finally, King's Stage significantly correlated with MRC score, ALSFRS-R, and  $\Delta$ ALSFRS-R, see figure 2.4 G, H, and I respectively.

## 2.7 Clinical Results Discussion

This chapter reports the overall demographics of all recruited participants as well as the results obtained from clinical assessment of participants with ALS. The results

demonstrate that the participants with ALS recruited into this study formed a heterogeneous group in all measures of ALS disease characteristics.

Demographically the ALS group was similar to the general population of those living with ALS in terms of gender, with over two thirds recruited being male and less than one third being female.<sup>1,3,5,491–493</sup> However, the mean age of the ALS group was relatively high at almost 65 years, which is older than that reported in many clinical research studies. Nonetheless the control group was well matched to the ALS group for both gender and age, see table 2.3.

The majority of ALS patients recruited into this study had typical ALS with a mixture of upper and lower motor neuron involvement. However, there were a wide range of clinical presentations including four with LMN predominance and one with UMN predominance. To demonstrate the spread of phenotypes please see table 2.6. Overall the ALS group reflected a typical spread in terms of ALS phenotype, with limb being the predominant site of onset and bulbar onset accounting for less than a quarter.<sup>1,3,5</sup> Two thirds of the bulbar onset participants were female, which is in keeping with the literature where higher prevalence of progressive bulbar palsy is reported in women.<sup>1,3,5,494</sup> One participant presented with truncal weakness, which is the least reported site of onset. There were insufficient numbers to allow for meaningful statistical analysis based on these ALS phenotypes.

The participants with ALS all differed in the evolution of disease, as reflected by the wide variation in terms of disease duration, MRC score, ALSFRS-R, and King's Stage of ALS. There was also a wide variation in rate of disease progression, as measured by the  $\Delta$ ALSFRS-R. This demonstrates that every individual was following a different disease projection in terms of areas affected by spread of disease, severity of weakness, and subsequent decline in ability to perform activities of daily living over time. This is reinforced by the broad range of timescales between symptom onset and diagnosis, where subtle differences in the underlying neurobiology may account for such variation. This heterogeneity is typical and recognised in ALS.<sup>9</sup>

Looking at how site of symptom onset relates to disease characteristics within the ALS group, not surprisingly bulbar onset was associated with longest median duration before diagnosis, which is consistently reported in the literature.<sup>147,495</sup> This highlights the challenges often experienced in reaching a diagnosis of ALS in those who present with early bulbar features, where often assessments used to facilitate diagnosis such as electromyography can remain normal in the limbs for many months.

The upper limb onset sub-group had a longer median time from onset of ALS symptoms to diagnosis than the lower limb onset subgroup. However, the shortest time to diagnosis, of just 2 months, in the whole ALS group was in a participant with onset of ALS symptoms in the right hand, see participant 4, table 2.5. While the overall longest duration from

onset to diagnosis of 27 months was in a participant with lower limb onset, see participant 17, table 2.5. The rationale behind this pattern of presentation is that the shortest time to diagnosis was in a participant with onset in the dominant hand, which would likely have a noticeable impact on functional ability in daily life from a very early stage and may prompt a person to seek medical attention earlier. Symptom onset in the left leg could have less of an impact in the early stages than hand involvement and may therefore lead to a longer period of time before someone seeks expert advice. Interestingly both of these participants had similar trajectories in terms of rate of progression, with  $\Delta$ ALSFRS-R scores of 0.53 and 0.57 respectively.

The overall mean  $\Delta$ ALSFRS-R for the group was 0.43, see table 2.5. However, this, like all other measures varied considerably amongst the participants with ALS. It was beyond the scope of this research study to obtain longitudinal clinical data and therefore the ALSFRS-R was not serially measured to determine the rate of progression. Instead, the  $\Delta$ ALSFRS-R was calculated as the decline in ALSFRS-R over the disease duration. Although not ideal, this calculated monthly rate of decline in ALSFRS-R score is widely accepted as a useful estimate of the rate of disease progression. A recent paper looking at trajectories of impairment in ALS has shown that the slope calculated from baseline ALSFRS-R score, is strongly correlated with slope calculated during follow-up assessment.<sup>496</sup>

When looking at the spread of  $\Delta$ ALSFRS-R in this cohort using a histogram, the majority of ALS participants fall into a distribution component with rate of change in ALSFRS-R of up to 0.8 per month, see figure 2.1. There is then a second group, consisting of fewer participants, where the rate of change is greater than 1.0 per month. It is therefore possible to envisage a bimodal distribution of  $\Delta$ ALSFRS-R scores, which suggests the ALS participants can be grouped into faster and slower groups according to rate of progression. This method of assessing progressive physical impairment in ALS, whether using the questionnaire-based ALSFRS-R or other scores such as the examination-based Appel ALS (AALS) score<sup>266</sup> have been widely used as a means of dividing faster from slower progressing patients with ALS.

The ECAS results demonstrate that cognitive impairment was detected in just over half the group (52%), indicating that this cohort of ALS participants is similar to the ALS population as a whole, where cognitive changes can be present in up to 50%.<sup>71,91,500</sup> However; the pattern of cognitive and behavioural deficits did not follow the pattern typically described in ALS.<sup>92,497</sup> Language, verbal fluency, and executive function are thought to be most frequently affected in ALS, while memory and visuospatial skills are often preserved. However, the most frequent domain for detecting impairment in this cohort of participants with ALS was memory, see figure 2.2. This was without any participant exhibiting impairment on visuospatial assessment, and is therefore

suggestive of age-related decline in memory.<sup>498</sup> This is supported by the observed correlation between the age and the ECAS scores, see figure 2.4A. As previously mentioned the mean age of the ALS group, 64.5 years, was older than many groups previously studied in the literature. It was older than the group in which the ECAS was originally assessed, where the mean age was 59.9 years.<sup>78</sup> The age of those affected by cognitive changes within the group ranged from 51 to 73 years with a median of 68 years. The five participants with selective impairment in memory and normal scores for the remaining cognitive domains were aged between 66 and 73 years.

Three participants exhibited cognitive impairment within only the ALS specific domains. Two of these had isolated impairment in only one ALS specific domain (one in executive function and one in language), while the remaining participant demonstrated impairment in two ALS specific domains (language and verbal fluency) but attained a normal score for executive function. The remaining five participants with cognitive impairment demonstrated impairment in both ALS specific cognitive domains and memory, see table 2.6 and figure 2.2.

Language was the ALS specific cognitive domain with the highest frequency of abnormal performance, see figure 2.2. This finding is consistent with previous studies using ECAS in ALS.<sup>78,499</sup>

One participant had impairment in all the cognitive domains except visuospatial skills, and in addition exhibited disinhibition, see table 2.6 participant 17, suggesting cortical spread of disease. In this participant alterations in attention may have had an impact on memory processing.

At the time of assessment none of the ALS participants met the criteria for ALS-FTD. However, using the revised diagnostic criteria to assess for ALS-FTSD,<sup>77</sup> one of the ALS participants was classified as having ALS cognitive and behavioural impairment (ALS<sub>cbi</sub>; 17) and four were classified as having ALS cognitive impairment (ALS<sub>ci</sub>; 8,11,12,14). Six of the ALS participants had abnormal sub-scores but did not meet the criteria for ALS<sub>ci</sub>. Finally one patient had an isolated borderline language sub-score, see table 2.7. An important factor, which was overlooked in this study, is the participant education. This may have had some effect on the cognitive scores obtained, as those with higher education typically have increased propensity to compensate for any deficits.

Behavioural changes can occur alongside cognitive alterations, or in isolation.<sup>77,91,501</sup> Alterations in the prefrontal cortical regions are thought to be responsible for the cognitive and behavioural profile of ALS,<sup>83,84,502</sup> which demonstrates both clinical and pathological overlap with FTD.<sup>62,71-75,83,84,503-505</sup> While compromise of the dorsolateral prefrontal cortex has been associated with cognitive decline,<sup>83,84</sup> changes within the ventromedial prefrontal cortex are thought to contribute to behavioural changes.<sup>501</sup>

Apathy is the most common behavioural alteration reported in ALS and is associated with caregiver burden, as well as worse prognosis.<sup>88-93</sup> However, in this study none of the ALS participants or their accompanying family member reported apathy, see figure 2.3. This could be related to selection bias, because it is typically motivated patients with ALS who get involved with research. In addition behavioural changes were evident in only two of the ALS participants, one with isolated stereotyped behaviour and another with a combination of disinhibition, loss of sympathy, and compulsivity. These findings suggest that the cohort of ALS participants in this study were not entirely representative of the behavioural changes typically associated with ALS.<sup>88-93</sup>

Interestingly none of the participants reported any changes in their thinking capacity, despite cognitive impairment being detected on formal assessment using the ECAS. Similarly, no participant reported behavioural changes and in those with evident behavioural changes this was confirmed by the spouse or carer. This suggests lack of insight, or anosognosia, which is a recognised feature in ALS.<sup>91</sup> Overall, these findings highlight the subtleness of the cognitive and behavioural changes associated with ALS and reinforces the importance of screening in all those diagnosed with ALS, as these have important considerations for those ALS as well as their families.

As well as correlation between age and ECAS total score, there were further predictable correlations within the clinical data, see figure 2.4. ALSFRS-R correlated with both disease duration and MRC score, see figure 2.4B and 2.4C respectively. Longer duration of disease is typically associated with a decline in ALSFRS-R due to a decline in limb, bulbar, and respiratory function over time.<sup>506</sup> Correlation between MRC and ALSFRS-R is to be expected because muscle power has a direct effect on functional ability, where reduced muscle strength will lead to a reduction in the ability of that muscle to function and will therefore reduce the ALSFRS-R score. There was additional correlation between MRC score and  $\Delta$  ALSFRS-R, where higher MRC scores correlated with lower rates of ALS progression, which can be attributed to the likelihood that those with lower  $\Delta$ ALSFRS-R are maintaining higher muscle strength for longer duration than those with faster rates of progression, reflected by higher  $\Delta$ ALSFRS-R.

There was a correlation between UMN score and progression rate, where higher UMN scores were associated with faster rates of change in the ALSFRS-R. This result provides support for lower UMN scores being associated with slower rates of progression and higher UMN scores relating to faster rates of disease progression, see table 2.7 and figure 2.4E. This has previously been described in ALS and may relate to the different rates of spread between the pyramidal neurones in the cortex versus the anterior horn cells in the spinal cord.<sup>309</sup>

ALSFRS-R correlated with  $\Delta$ ALSFRS-R, see figure 2.4F, where higher ALSFRS-R scores were associated with lower  $\Delta$ ALSFRS-R. This suggests that when the

functional rating scale score remains higher, which for most people would be in the earlier stages of disease onset, the rate of disease progression is slower. Conversely, when the ALSFRS-R falls to lower values such as below 40, the associated rate of progression in this cohort of participants is faster. However, the values of  $\Delta$  ALSFRS-R calculated for the purpose of this study were based on only one ALSFRS-R assessment score, whereas ideally at least two measures of ALSFRS-R should be performed longitudinally. Nonetheless these results suggest that the rate of change in ALSFRS-R was not consistent throughout, within this cohort, and that as the disease progressed there was an increase in momentum with respect to acquisition of disability. Variability of decline in ALSFRS-R is reported in ALS patients during the disease.<sup>507</sup> Furthermore, plateaus and even reversals in ALSFRS-R score have been reported to occur in a small proportion.<sup>166</sup> This may reflect a limitation in the ALSFRS-R as an overall measure of disease severity and progression. Instead the ALSFRS-R constitutes domain scores (i.e; bulbar, respiratory, fine motor and gross motor) reflecting the profile of disease magnitude in ALS.<sup>508</sup>

MRC score, ALSFRS-R, and  $\Delta$ ALSFRS-R all correlated significantly with King's Stage of ALS, see figure 2.4 G, H, and I respectively. King's stage 1 was associated with the highest MRC scores while the lowest MRC scores were in those who had reached King's stage 3. This is to be anticipated because the King's stage reflects the number of regions affected by ALS, which typically causes weakness to some degree and thereby reduces the MRC score.

The disease duration did not correlate with the King's stage of ALS, which is interesting as this suggests that individuals are reaching the different King's stage at different time points in the course of their disease. There was however correlation between King's stage and ALSFRS-R, where higher King's stage was associated with reduced ALSFRS-R scores, indicating that those in the higher stages have less functional capacity. The highest rates of progression, as measured by the  $\Delta$ ALSFRS-R, were associated with higher King's stage of ALS. This suggests that the rate of progression may increase towards the later stages of the disease and lends support for the notion that the rate of progression is dynamic and may alter during the course of the disease process.<sup>507</sup>

Extremes of UMN involvement are typically observed in the ALS variants PLS and PMA, see chapter 1, table 1.1, which are associated clinically with pure UMN and pure LMN involvement respectively. Slower disease course is typically observed in both PLS and PMA.<sup>56,58,61</sup> With this in mind slower rates of progression may have been expected to be associated with both the lowest and the highest UMN scores, but in this cohort the highest UMN scores were associated with the faster rates of progression suggesting more aggressive disease and worse prognosis in those with larger UMN



burden. The participant with the lowest rate of progression, however, had one of the highest UMN scores, demonstrating the variable nature of ALS.

There are a number of predictable limitations relating to the clinical data obtained during this study. The inclusion and exclusion criteria were designed to ensure the safety of potential participants but may have also indirectly mitigated against those with more advanced disease taking part and as result the ALS-cohort may appear somewhat preselected. It is difficult to avoid this unintentional selection bias, except by having very large samples and only few exclusion criteria. In reality as reaching the recruitment target was going to be a challenge, no one who wanted to be in the study was rejected. As long as potential participants fulfilled the chosen diagnostic criteria for ALS (therefore not 'PMA', and in practical terms not respiratory onset), met the inclusion/exclusion criteria, and were judged to have capacity to consent, they were included. Nonetheless, a large number of participants were early in the progression of their disease these were the ones who were more likely to want to participate in research. This is further demonstrated by the King's staging system where 78% ALS participants were in stages 1 or 2, only 22% were in stage 3, and none were in stage 4 ALS. The ALS group being heterogeneous is also recognised to be a limitation, as this can make finding statistically significant differences between ALS and control groups more challenging. The final limitation is that there were insufficient numbers to allow for meaningful statistical analysis based on ALS phenotype.

In conclusion this chapter demonstrates how the participants with ALS recruited into this cross-sectional study represent a heterogeneous group in relation to demographics, clinical characteristics, and manifestation of cognitive impairment or behavioural changes. It also highlights that ALS is not entirely predictable in the course of disease progression. These phenotypic features of the ALS group will be an important consideration when analysing the imaging data in subsequent chapters.

**CHAPTER 3:  
QUANTITATIVE  
DIFFUSION WEIGHTED  
MRI IN ALS**

## CHAPTER 3 QUANTITATIVE DIFFUSION MRI IN ALS

This chapter includes data from the research article published in the Journal of Neurology, Neurosurgery, and Psychiatry in 2019, for which I was the first and corresponding author.<sup>357</sup>

### 3.1 Background

ALS is phenotypically and genetically heterogeneous;<sup>1,3,5,6,9,13,15,30,491</sup> nonetheless, consistent intracranial neuropathological features of amyotrophic lateral sclerosis (ALS) are degeneration of the corticospinal tract (CST) and cortical atrophy.<sup>193,194,201</sup> However, the mechanisms underlying neurodegeneration are not well understood. It is unclear whether degeneration of corticospinal neurons represents a ‘dying back’, ‘dying forward’, or wallerian-like degeneration.<sup>3,235,236,238,286-288</sup> Furthermore, the relevance of such categories proposed from histological (i.e. end stage) analyses to the dynamics of cell damage ‘*in vivo*’ remains uncertain.

Neuroimaging has the potential to interrogate neuronal changes early in the course of ALS disease evolution. In this regard diffusion tensor imaging (DTI), a quantitative diffusion weighted MRI technique, has provided important insights into the localization and extent of cellular pathology in ALS,<sup>17,18,138,339-341,360,401,410,509</sup> however; DTI is limited by having relatively non-specific indices.<sup>17,339-341,460,469,510,511</sup> Furthermore, the interpretation in areas of complex axonal or dendritic architecture is not straightforward with DTI.<sup>512,513</sup> Although newer indices such as the mode of anisotropy can provide some useful information in regions of crossing or fanning a quantification of neurite density in such areas is challenging with DTI.<sup>408</sup>

Recent developments in modelling diffusion-weighted (DW) MRI have addressed some of the limitations of standard DTI and advanced capacity to illustrate tissue microstructure. Neurite orientation dispersion and density imaging (NODDI), a multi-compartment model of diffusion MRI, estimates the density and fanning of neurites, as well as the partial volume contamination from CSF, using standard MRI scanners within a clinically feasible time frame. NODDI facilitates the analysis of neurite morphology and focuses on quantifying the altered architecture of these multifaceted structures.<sup>409</sup>

I applied NODDI, alongside DTI, in a cross-sectional study using whole brain analyses, to explore the altered density and complexity of neurites in ALS. Analyzing these characteristics, and how they relate to the disease process ‘*in vivo*’, provides an exciting opportunity to advance the understanding of ALS pathogenesis.

### 3.2 Hypotheses

The principal aim of this study was to use NODDI in a whole brain analysis study of ALS, to test the hypothesis that cortical pathology, such as loss or altered complexity of dendrites in the neuropil of the precentral gyrus (PCG), is occurring alongside axonal degeneration of the CST in ALS. Specifically, within the PCG, I hypothesized that NODDI would detect reduced neurite density (NDI) and orientation dispersion (ODI), accompanied by an increase in free water compartment (ISO).

An additional aim was to clarify the microstructural changes within the WM, where I hypothesized that axonal degeneration within the CST would be detected as a reduction in NDI using NODDI.

NODDI was used in parallel with conventional DTI to test the hypothesis that, by removing the confounding effect of orientation dispersion, NODDI would detect more axonal damage within the WM tracts than conventional DTI. NODDI was also used to facilitate interpretation of the changes in fractional anisotropy (FA), mean diffusivity (MD), radial diffusivity (RD) and axial diffusivity (AD) frequently reported ALS.

I was keen to interrogate whether the NODDI parameters could differentiate subgroups of ALS based on disease distribution, stage of ALS, and cognitive status. The NODDI parameters were used to assess whether a combination of bulbar and limb involvement clinically would reveal radiological differences when compared with limb-confined disease, to test the hypothesis that more widespread clinical involvement would relate to more extensive microstructural damage. The King's staging subgroups of ALS were also compared using NODDI. I hypothesized that the King's stage 3 ALS subgroup, with the most advanced disease, would demonstrate the most significant changes in the NODDI parameters. The NODDI parameters were also used to assess for differences in those with normal ECAS scores compared to those with abnormal ECAS scores, to test the hypothesis that cognitive impairment would relate to more significant brain atrophy and would therefore demonstrate reduced NDI and ODI together with increased ISO within the frontal and temporal cortices.

Finally, correlation of each of the NODDI parameters with the clinical variables of ALS were explored. The anticipation was that because clinical measures of ALS severity reflect the underlying pathological processes, there would be correlation between these and the NODDI parameters.

Whole brain analysis is recognised as being less statistically powerful than region of interest analysis. However, the rationale for using whole brain analysis in this study was that NODDI was being applied to ALS for the first time and in an exploratory nature. Using a region of interest approach could have reduced the possibility of finding something novel.

### 3.3 Diffusion weighted MRI Acquisition

Participants completed an MRI safety questionnaire and provided additional consent to undergo an MRI scan, see appendix A11. MRI acquisition was performed using a dedicated 1.5 T Siemens AVANTO scanner in the clinical imaging sciences centre (CISC) at the University of Sussex. All scanning sequences were acquired along the anterior commissure (AC) - posterior commissure (PC) line, with the exception of NODDI and multi-echo resting state functional MRI, which was acquired with a 30 degree tilt to minimize susceptibility. During the scan participants were asked to lie still without performing any task. All but one of the participants were taking Riluzole at the time of MRI.

The whole protocol lasted approximately 1 hour and included T2-weighted fast attenuated inversion recovery (FLAIR), high-resolution T1 volume, DW-MRI, qMTi, and resting-state functional MRI. In this chapter I will focus on the analysis of DW-MRI. Details of the sequences used for this analysis are as follows:

- i) Dual-echo turbo spin-echo  
Acquisition time 2 minutes  
Echo time (TE) = 11 and 86 ms  
Repetition time (TR) = 3040 ms  
Echo-train length=6  
FoV = 240 x 210mm<sup>2</sup>  
Matrix = 256 x 224  
Slice thickness = 5mm  
22 slices
- ii) T2-weighted fast fluid-attenuated inversion recovery (FLAIR)  
Acquisition time 2 minutes  
TE 89ms  
TR 9720ms  
TI 2578ms  
Echo-train length = 16  
FoV = 240 x 210mm<sup>2</sup>  
Matrix = 256 x 224  
Slice thickness 5mm  
22 slices
- iii) T1-weighted volumetric high-resolution magnetization prepared rapid gradient - echo (MPRAGE)  
Acquisition time 6 minutes  
TE 3.57ms

TR 2730ms  
TI=100ms  
Flip angle =70  
FoV=256x240mm<sup>2</sup>  
Matrix=254x240  
Slice thickness 1mm  
Voxel size 1x1x1mm, 1 excitation, flip angle 7 degrees, 192 slices

- iv) Multi-shell DW-MRI optimised for NODDI<sup>409</sup>  
Acquired with single-shot, twice-refocused pulse-gradient spin-echo<sup>514</sup> (echo planar imaging; (<https://www.ncbi.nlm.nih.gov/pmc/articles/PMC4831788>))  
Acquisition time 17 minutes  
Three b-values were used  
(a) B300  $\text{mm}^2$ , 9 directions  
(b) B800  $\text{mm}^2$ , 30 directions  
(c) B2400  $\text{mm}^2$ , 60 directions  
TE 99ms  
TR 8400ms  
Slice thickness 2.5mm  
60 slices  
FoV = 240 x 240mm<sup>2</sup>  
Matrix = 96 x 96  
Ten non-diffusion-weighted (b=0) volumes were also acquired

### 3.4 Quantitative Diffusion Weighted MRI Data Processing

The diffusion-weighted (DW) images were first corrected for eddy-current distortions and for involuntary movement, using the following pipeline. A “within-b-value” co-registration was performed, and average b=0, b=300, b=800, and b=2400 images were created. Each of these averages was co-registered to the mean b=0 image to obtain the transformation matching them. Each DW volume was realigned to the mean DW image with the same b-value, and the final transformation matching each DW volume with the b = 0 image was obtained by combining the matrices from either step. The b-matrices were rotated accordingly.<sup>515</sup>

The resulting images were skull-stripped using the FMRIB Software Library (FSL) brain extraction tool (<http://fsl.fmrib.ox.ac.uk/fslwiki>). Data were analysed using software distributed by the developers of NODDI ([http://www.nitrc.org/projects/noddi\\_toolbox](http://www.nitrc.org/projects/noddi_toolbox)), implemented in Matlab (version 2012b), which yielded maps of the neurite density (NDI), orientation dispersion (ODI), and free water volume fraction for each participant (isotropic

compartment; ISO.<sup>409</sup> Camino (camino.org.uk) was used to fit the diffusion tensor to the same data using weighted least squares regression and to compute maps of FA, MD, RD and AD.

The FA images were warped to common space to create a group-specific template, using advanced normalization tools (ANTs) V2.1.0 (<http://stnava.github.io/ANTs>). The resulting template was co-registered with the Montreal Neurological Institute (MNI) template from FSL. The combination of these two transformations was applied to each NODDI and DTI parametric maps. Three-dimensional Gaussian smoothing with full-width at half maximum of 6mm was performed in SPM12 (<http://www.fil.ion.ucl.ac.uk/spm/>).

### **3.5 Statistical Analysis**

#### **3.5.1 Whole Brain Voxel-Wise Analysis of NODDI and DTI Parameters**

Statistical Package for the Social Sciences (SPSS IBM version 22 for Windows) was used for statistical analysis of the demographic data. Voxel-wise comparisons of whole brain NDI, ODI, ISO, FA, MD, RD, and AD maps between ALS and control groups were performed within the framework of the general linear model of SPM12. The results were accepted as significant where  $P < 0.05$  after family-wise error (FWE) correction at cluster level, where clusters were formed using  $P < 0.001$ . Participant age was used as a covariate.

#### **3.5.2 Subgroup Analysis using NODDI parameters**

ALS subgroups were created with three sets of categorical clinical data. Firstly, the ALS group was divided into two subgroups based on the distribution of ALS clinically, more specifically the presence or absence of bulbar symptoms (11 bulbar plus limb versus 12 limb alone). These groups were compared with one another and the control group, using whole brain analyses to investigate for differences in each of the NODDI parameters, NDI, ODI, and ISO.

Secondly, the allocated King's stage was used to create three ALS subgroups for comparison; 10 participants in stage 1, 8 in stage 2, and 5 in stage 3. As the stage 3 group was particularly small this was combined with the participants in stage 2, to create a group of 13 ALS participants for further comparison. These subgroups were also compared with each other and the control group, to assess for significant differences in NDI, ODI and ISO on whole brain analyses.

Lastly, the ECAS data was used to create two ALS groups, one with normal ECAS scores and the other with abnormal scores in more than one domain. The latter group included all the ALS participants classified as ALS-FTSD. These groups were

compared with one another and the control group, using whole brain analyses to assess for differences in NDI, ODI, and ISO.

Voxel-wise whole brain analysis of NDI, ODI and ISO maps between the control and ALS subgroups was performed using the general linear model framework within SPM12. The results were accepted as significant where  $P < 0.05$  after family-wise error (FWE) correction at cluster level, where clusters were formed using  $P < 0.001$ . Participant age was used as a covariate.

The rationale for performing subgroup analyses are given in the quantitative diffusion MRI in ALS hypotheses, section 3.2.

### **3.5.3 Correlation Analysis of NODDI parameters with clinical measures of ALS**

I analysed the NODDI parameters of the ALS group for correlation with the continuous clinical measures of disease severity. As with the image data analysis described above, I used SPM12, with age included as a covariate, and accepted correlations as significant if  $P < 0.05$  after FWE correction at cluster level, clusters formed with  $P < 0.001$ .

The clinical measures used to assess for correlation with the NODDI parameters were the disease duration, MRC (medical research council) composite muscle power score, upper motor neurone (UMN) composite score, the revised ALS functional rating scale (ALSFRS-R) score, the rate of change in ALSFRS-R, and the ECAS score.

I also looked for any correlation between NODDI parameters and age in order to assess for the magnitude of effect age could have on the results if not accounted for as a covariant in the analysis.

### **3.6 NODDI parameters within the Precentral Gyrus**

To further investigate the changes of NODDI parameters within the PCG a further analyses was carried out to compare the mean parameter values.

NODDI parameter values were extracted from the high resolution MPRAGE images using the automated processing stream within FreeSurfer (<http://surfer.nmr.mgh.harvard.edu>). This segments the cortex of each participant into a set of parcellated regions in a process that involves skull stripping, registration to Talairach space, intensity normalization, tissue segmentation to determine the grey-white matter boundary, followed by tessellation and deformation of this boundary, and finally surface parcellation.

The transformation matching DWI and MPRAGE was computed using FreeSurfer's diffusion tensor processing pipeline and applied to the resulting parcellation.



The mean values for NDI, ODI and ISO within the PCG were extracted for both the right and left hemispheres and tabulated for all participants in excel. SPSS was then used to compare means between the control and ALS group, using age as a covariate, to assess for patterns of change within the NODDI parameters relating to ALS.

### **3.7 Whole Brain Voxel-Wise analysis comparing ALS and control groups**

#### **3.7.1 NODDI Parameters**

In the whole brain analysis of NODDI parameters, NDI was reduced in the ALS group bilaterally within a large continuous region of the (CST) extending from the posterior limb of the internal capsule rostrally through the corona radiata into the subcortical WM of the PCG ( $P<0.001$ ) (Figure 3.1; Table 3.1). The area of decreased NDI also extended into the transcallosal connection fibres between the primary motor cortices.

A region within the right anterior internal capsule was detected where ODI was reduced in the ALS group ( $P=0.014$ ). This contiguous cluster extended into the right PCG (Figure 3.1B; Table 3.1).

Finally, ISO was increased within the region of the right lateral ventricle ( $P=0.006$ ) (Figure 3.1C; Table 3.1).

#### **3.7.2 Diffusion tensor imaging parameters**

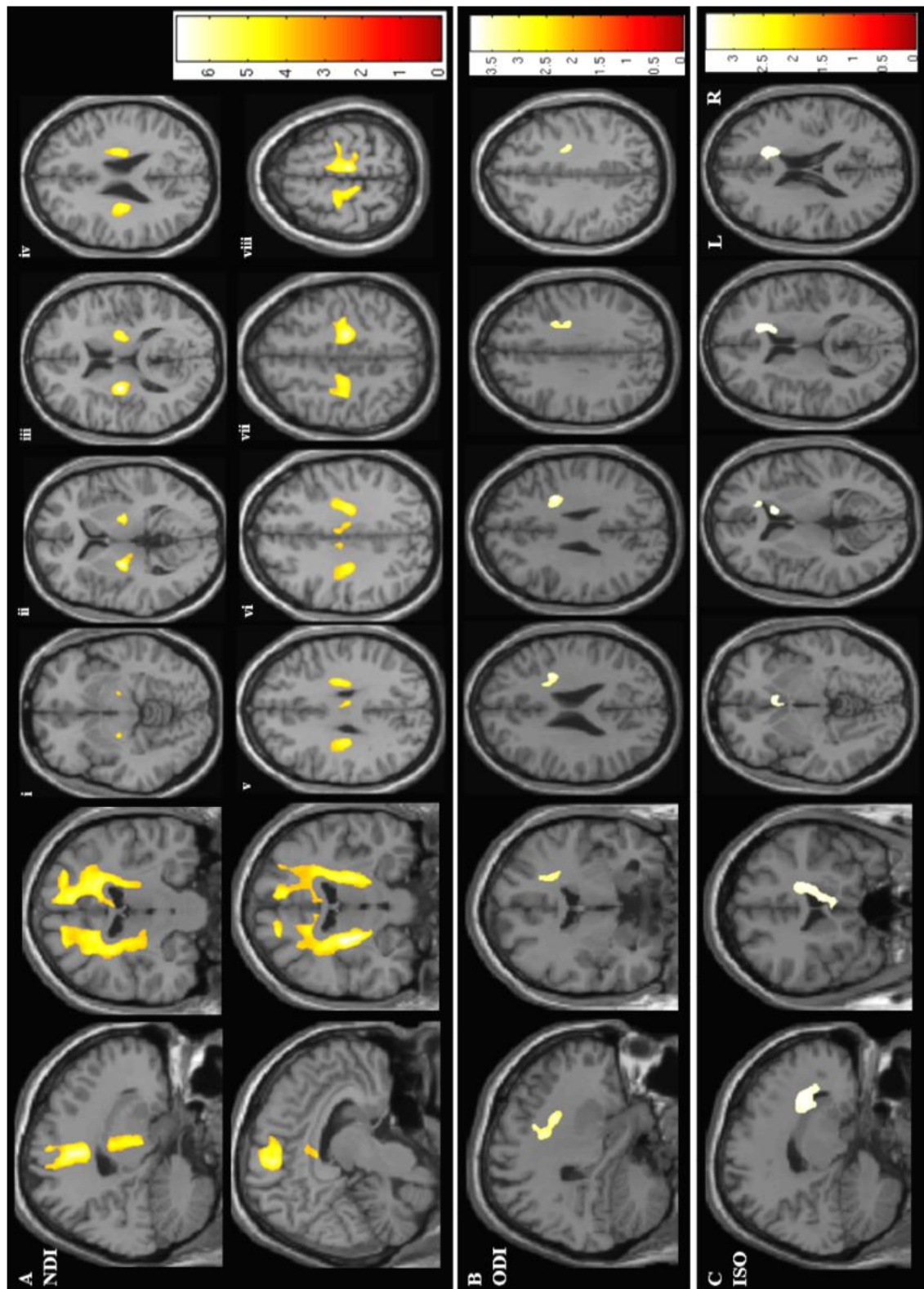
Fractional anisotropy (FA) was reduced in the ALS group bilaterally within two regions of the corticospinal tracts (CST), firstly in the pontine CST ( $P=0.006$ ) and secondly within the superior corona radiata and subcortical white matter of the precentral gyrus (right  $P<0.001$ , left  $P=0.002$ ) (Table 3.1; Figure 3.2A). At the statistical threshold utilized FA in the ALS group was not reduced in the internal capsule in either cerebral hemisphere or within the corpus callosum.

MD was significantly increased in the ALS group within the internal capsule of the left CST ( $P=0.048$ ) (Table 3.1; Figure 3.2B). No significant changes in MD of the ALS group were detected in the brainstem portion of the CST or the corpus callosum.

RD was significantly increased bilaterally within the cerebral WM, in contiguous clusters extending from the internal capsule caudally up to the subcortical WM on the left and the PCG on the right. The region of lower RD on the right side also extended into the corpus callosum (Table 3.1 and Figure 3.2C).

Changes in AD did not reach statistical threshold on whole brain comparison between ALS and control groups.

Figure 3.1: Figure demonstrating the areas of significant difference between the ALS and control groups on whole brain analysis of the NODDI parameters.



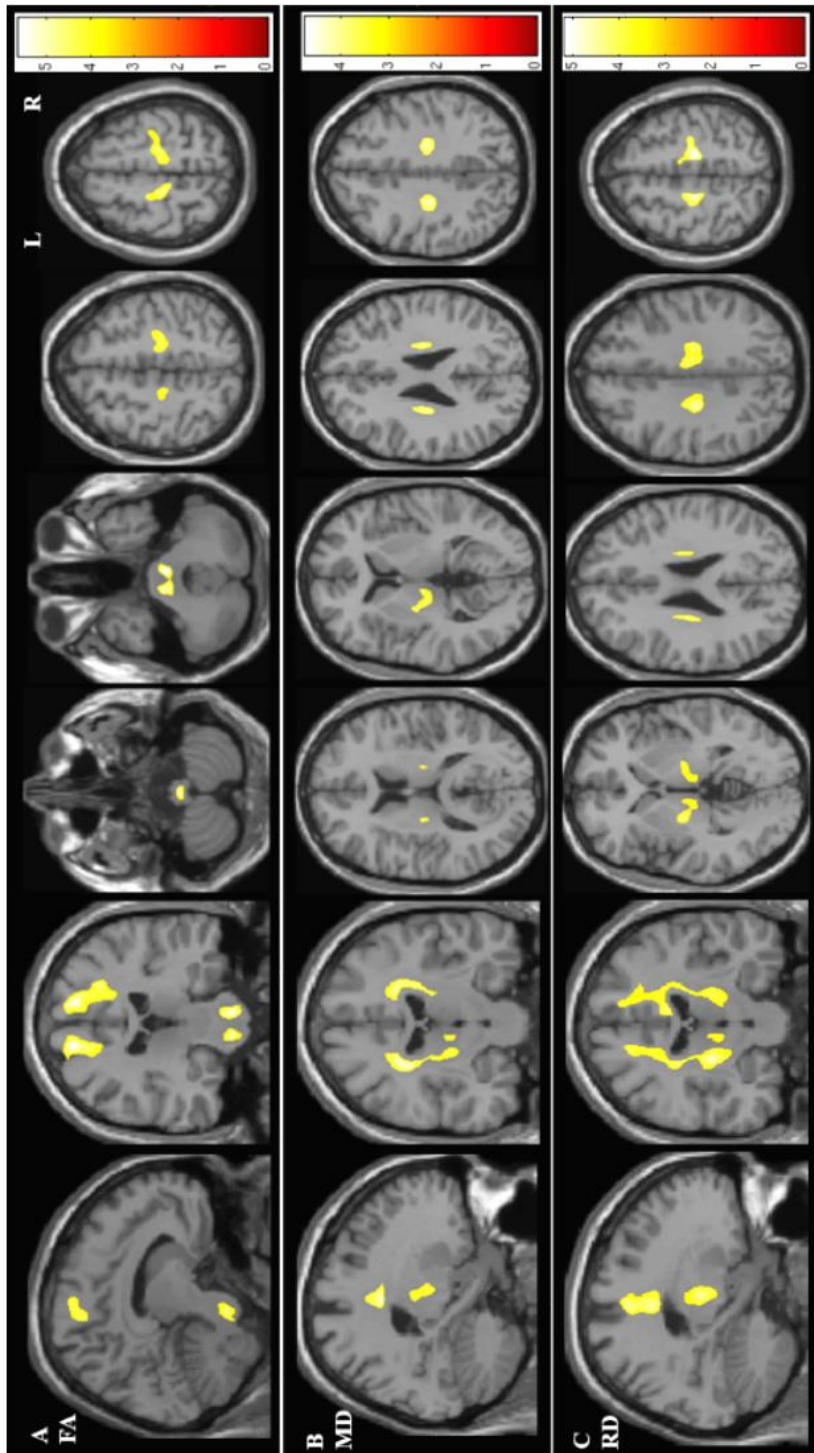
(A) Neurite density index (NDI), (B) orientation dispersion index (ODI) and (C) isotropic compartment (ISO). The results are shown using a statistical significance of  $P < 0.05$  after family-wise error correction at the cluster level, clusters formed using  $P < 0.001$ . Figures Ai - Aviii demonstrate the areas of significant difference in NDI on axial sections from the posterior limb of the internal capsule (vi) extending rostrally up into the subcortical WM of the PCG (viii).

**Table 3.1: Regions of significant differences in quantitative diffusion imaging parameters between ALS and control groups.**

	Contiguous anatomical regions within cluster	MNI co-ordinate (x, y, z)	t-value	K (size)	$P_{\text{cluster level FWE-corr}}$
NDI ALS<CTL	Right cerebral cortex, PCG	11 -25 60	5.85	15344	<0.001
	Right coronal radiata	22 -22 46	5.69		
	Right PLIC	23 -12 7	5.21		
	Left PLIC	-24 -11 12	6.23	14005	<0.001
	Left cerebral CST	-13 -28 58	5.32		
	Left superior corona radiata	-20 -20 41	4.91		
ODI ALS<CTL	Right PCG	32 5 27	3.89	1847	0.014
	Right PCG	25 -1 44	3.60		
	Right internal capsule	21 9 21	3.59		
ISO ALS>CTL	Right caudate, lateral ventricle	11 18 4	3.45	2960	0.006
	Right anterior corona radiata	20 23 19	3.39		
	Right genu of corpus callosum	8 25 8	3.30		
FA ALS<CTL	Right PCG	15 -23 66	5.10	4097	<0.001
	Right cerebral CST	26 -23 49	4.36		
	Right superior corona radiata	18 -21 42	4.19		
	Left cerebral CST	-15 -23 67	5.25	2877	0.002
	Left cerebral cortex, PCG	-21 -18 70	4.32		
		-18 -15 59	4.08		
	Right pons, CST	7 -26 -37	5.11	2309	0.006
	Right brainstem, CST	3 -34 -47	5.10		
	Left pons, CST	-7 -23 -36	4.69		
MD ALS>CTL	Left superior corona radiata	-24 -19 35	4.78	3315	0.048
	Left PLIC	-18 -15 3	3.55		
		-20 -17 14	3.43		
RD ALS>CTL	Right cerebral CST	19 -22 52	5.18	6727	0.008
	Right superior corona radiata	20 -21 42	5.13		
	Right PCG	29 -18 55	4.23		
	Left cerebral CST	-16 -21 56	4.74	6708	0.008
	Left PLIC	-22 -13 5	4.69		
	Left cerebral WM, corona radiata and corpus callosum	-21 -21 36	4.58		

A table to show the anatomical regions where significant changes were demonstrated on whole brain analysis in neurite density index (NDI), fractional anisotropy (FA), mean diffusivity (MD), orientation dispersion index (ODI), and isotropic compartment (ISO). A statistical significance threshold of  $P<0.05$  family-wise error (FWE) correction at cluster level ( $P_{\text{cluster}}$ ) was used, after clusters were formed with an uncorrected  $P<0.001$ . Montreal Neurological Institute (MNI) co-ordinates were used to define the anatomical location of each cluster of voxels within the MRI volume. The MNI coordinates refer to the peak t-value. Local maxima that are more than 8mm apart are shown for each cluster. K indicates the size of the cluster in voxels. Abbreviations: ALS, amyotrophic lateral sclerosis; CTL, control; NDI, neurite density index; ODI, orientation dispersion index; ISO, isotropic diffusion; FA, fractional anisotropy; MD, mean diffusivity; RD, radial diffusivity; CST, corticospinal tract; PCG, precentral gyrus; PLIC, posterior limb of the internal capsule; MNI, Montreal Neurological Institute; FWE, family-wise error.

**Figure 3.2: Areas of significant difference between ALS and control groups on whole brain analysis of the DTI parameters.**



Areas of significant difference between ALS and control groups in DTI parameters.

Results are shown using a statistical significance of  $P < 0.05$  after FWE correction at cluster level, clusters formed with  $P < 0.001$ .

(A) Fractional anisotropy (FA)

(B) Mean diffusivity (MD)

(C) Radial diffusivity (RD)

### 3.8 Analysis of NODDI parameters within the Precentral Gyrus

In the ALS group the mean NDI of the PCG was reduced in both the right and left hemispheres of the ALS group, which when combined gave a statistical difference of  $P = 0.04$ , see table 3.2 and figure 3.3.

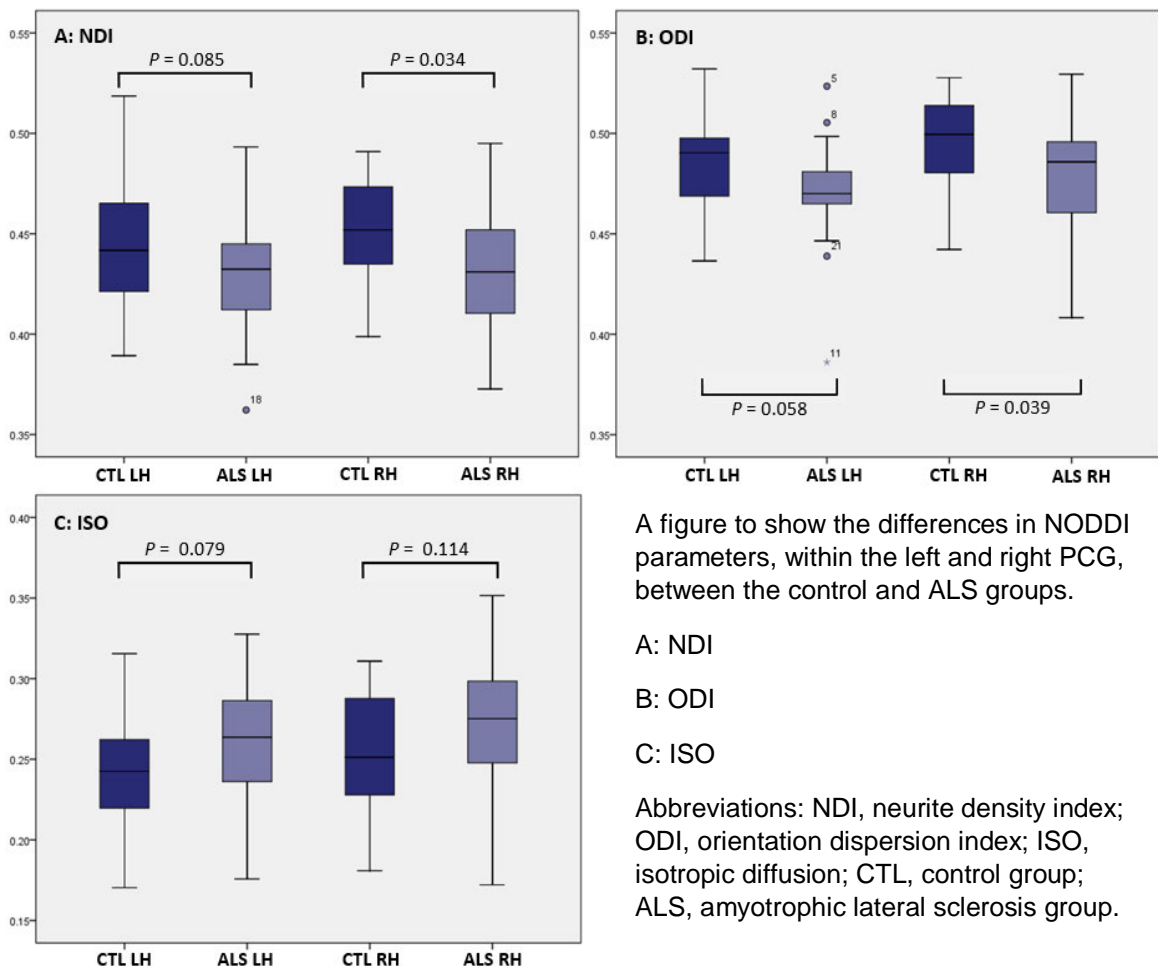
The mean ODI was likewise reduced in both the right and left PCG, with a combined statistical difference of  $P = 0.036$ , see table 3.2 and figure 3.3.

**Table 3.2 NODDI parameters within the PCG**

PCG NODDI Parameter		Control group (mean)	ALS group (mean)	P value
<b>NDI</b>	RH	0.452622	0.432783	<b>0.034</b>
	LH	0.444887	0.429591	0.085
	RH + LH	0.4487543	0.431187	<b>0.04</b>
<b>ODI</b>	RH	0.494709	0.477296	<b>0.039</b>
	LH	0.485865	0.470909	0.058
	RH + LH	0.490287	0.4741022	<b>0.036</b>
<b>ISO</b>	RH	0.252152	0.272009	0.114
	LH	0.238535	0.258739	0.079
	RH + LH	0.2453435	0.2653739	0.08

A table to show the differences in the mean NODDI parameter values for the PCG between the control and ALS groups. Abbreviations: PCG, precentral gyrus; NDI, neurite density index; ODI, orientation dispersion index; ISO, isotropic diffusion; RH, right hemisphere; LH, left hemisphere.

**Figure 3.3 Box plots to show the changes in PCG NODDI parameters in ALS.**



ISO was less significantly increased in the right and left PCG, with a combined statistical difference of  $P=0.08$ , see table 3.2 and figure 3.3.

Therefore, NDI and ODI were the only NODDI parameters to show statistically significant difference, at the threshold of  $P<0.05$ , in the right hemisphere and when the right and left PCG values were combined. None of the NODDI parameters reached the stringent statistical significance for multiple comparisons, such as the Bonferroni correction.<sup>516</sup> Nonetheless, these results still suggest that parameters are altered within the PCG, in the expected manner, in the ALS group.

### 3.9 Subgroup analysis using the NODDI parameters

#### 3.9.1 Distribution of ALS

Whole brain analysis for differences between subgroups revealed that there was a statistical trend of a reduction in NDI ( $P=0.054$ ) in the corona radiata and subcortical WM of the right cerebral hemisphere in the subgroup with both bulbar and limb involvement compared with the limb-only involvement subgroup, see table 3.3 and figure 3.4A.

There were no significant differences in ODI or ISO when comparing the bulbar and limb ALS subgroup with the limb-only ALS subgroup.

**Table 3.3: Regions of significant differences in NODDI parameters comparing bulbar-limb, limb-confined, and the control groups.**

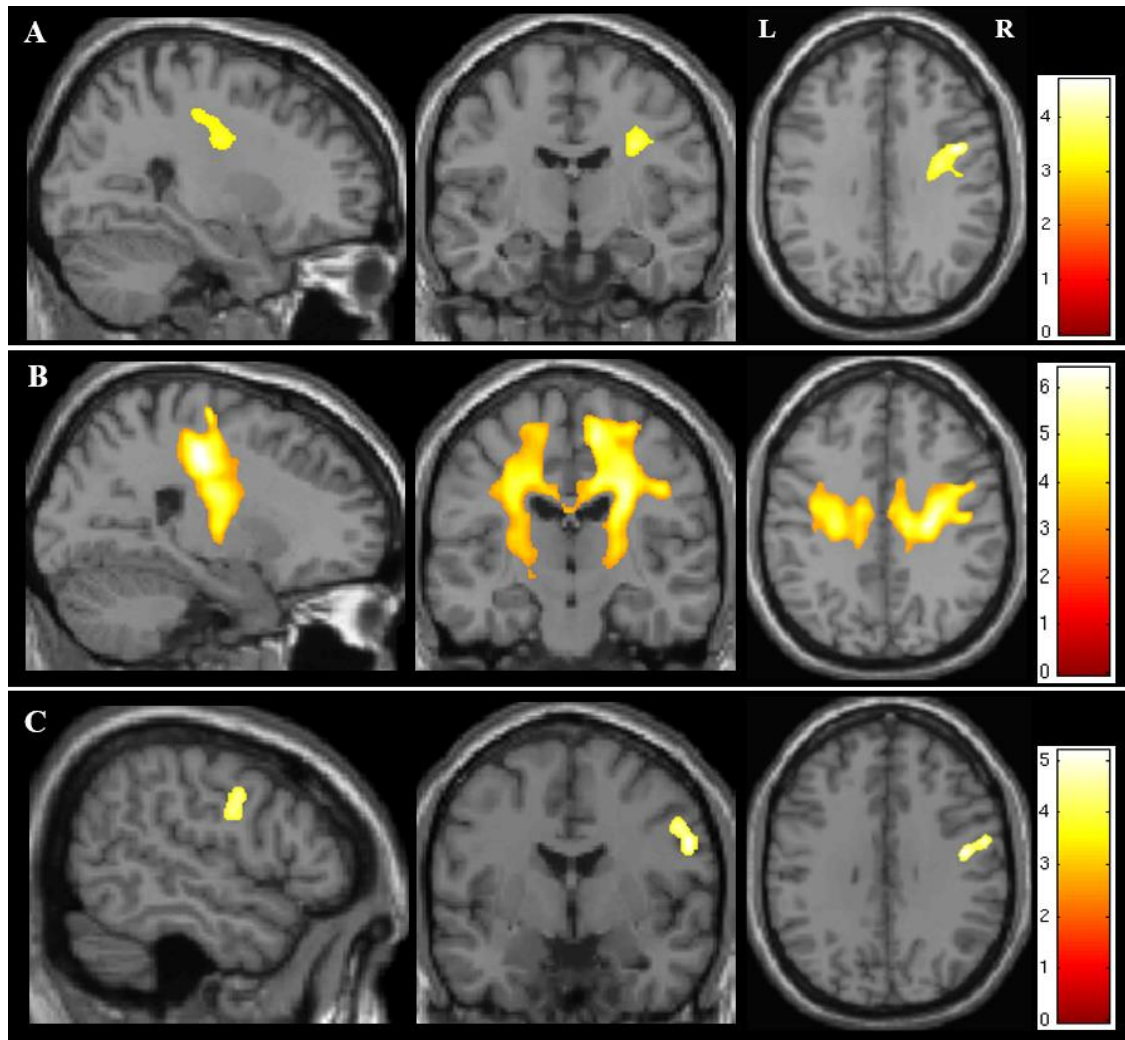
	Contiguous anatomical regions within cluster	MNI co-ordinate (x, y, z)	t-value	K (size)	$P_{\text{cluster level FWE-corr}}$
NDI Limb > Bulbar and limb	Right cerebral cortex and cerebral WM, PCG	43 2 32	4.19	2745	0.054
NDI Control > Bulbar and limb	Right cerebral WM, corticospinal tract, corpus callosum, PCG	24 -21 42	6.40	24296	<0.001
	Left cerebral WM, corticospinal tract, corpus callosum,	-25 -10 14	4.75	15280	<0.001
ODI Control > Bulbar and limb	Right cerebral cortex, PCG	57 -1 -29	4.80	1672	0.043

A table to show the regions where significant differences were demonstrated on whole brain analysis comparing ALS distribution subgroups and the control group. The MNI coordinates refer to the peak t-value and were used to define the anatomical location of each cluster of voxels.

Abbreviations: NDI, neurite density index; ODI, orientation dispersion index; ISO, isotropic diffusion; PCG, precentral gyrus; WM, white matter; MNI, Montreal Neurological Institute; K, cluster size; FWE, family-wise error.



**Figure 3.4: Regions of difference in NODDI parameters on whole brain analysis comparing bulbar and limb ALS, limb confined ALS, and control subgroups.**



A figure to show where differences were detected on subgroup analysis using the NODDI parameters. Results are shown for  $P < 0.05$  after FWE correction at cluster level, clusters formed using  $P < 0.001$ . (A) NDI, Limb > Bulbar and limb; (B) NDI: Control > Bulbar and limb; (C) ODI: Control > Bulbar and limb.

When comparing the bulbar and limb subgroup with the control group there was significantly reduced NDI bilaterally within large regions of the CST ( $P < 0.001$ ), see figure table 3.3 and 3.4B. These results were similar to those identified when comparing the whole ALS group with the control group, but even more extensive with larger cluster sizes, see table 3.2. The differences in NDI when comparing the limb only ALS subgroup with the control group did not reach statistical threshold, suggesting that the differences in NDI are derived largely from those with more extensive disease.

There was also significantly reduced ODI within the right PCG ( $P = 0.043$ ), in the cortical region responsible for bulbar function, see table 3.3 and figure 3.4C.

## **3.9.2 Kings Stages of ALS**

### **3.9.2.1 NDI**

Whole brain analysis for differences in NDI between the control group and the King's stage 2 ALS subgroup showed significant reduction in NDI ( $P < 0.001$ ) throughout the CST bilaterally, from the PMC superiorly down to the PLIC inferiorly, see table 3.4 and figure 3.5Ai and 3.5Aii respectively. The contiguous region of reduced NDI of the right CST also extended into the right transcallosal fibres.

There was patchy reduction in NDI limited to the right CST when comparing the control group to the King's stage 3 ALS subgroup ( $P = 0.004$ ), in a region of the corona radiata superiorly (figure 3.5Bi) and the PLIC inferiorly (figure 3.5Bii).

Finally, the most statistically significant results were seen when comparing NDI of the control group with King's Stages 2 and 3 combined ( $p < 0.001$ ). Large, contiguous, clusters of reduced NDI are demonstrated throughout the CST bilaterally with extension through the transcallosal fibres. These clusters encompass regions of the PMC superiorly and descend to the pontine CST inferiorly, see table 3.4 and figure 3.5C. There were no other statistically significant differences in NDI between King's stages of ALS and control groups.

### **3.9.2.2 ODI**

Comparing the King's stages of ALS and control groups using whole brain analysis for differences in ODI revealed several statistically significant results. ODI was significantly reduced in the cerebral cortex of the right superior temporal gyrus and middle temporal gyrus ( $P = 0.006$ ), of the King's stage 3 ALS group compared to stage 2, see table 3.4 and figure 3.6A. Similar areas of reduced ODI were demonstrated when the King's stage 3 ALS group was compared to King's stage 1 ( $P = 0.019$ ), see figure 3.6B.

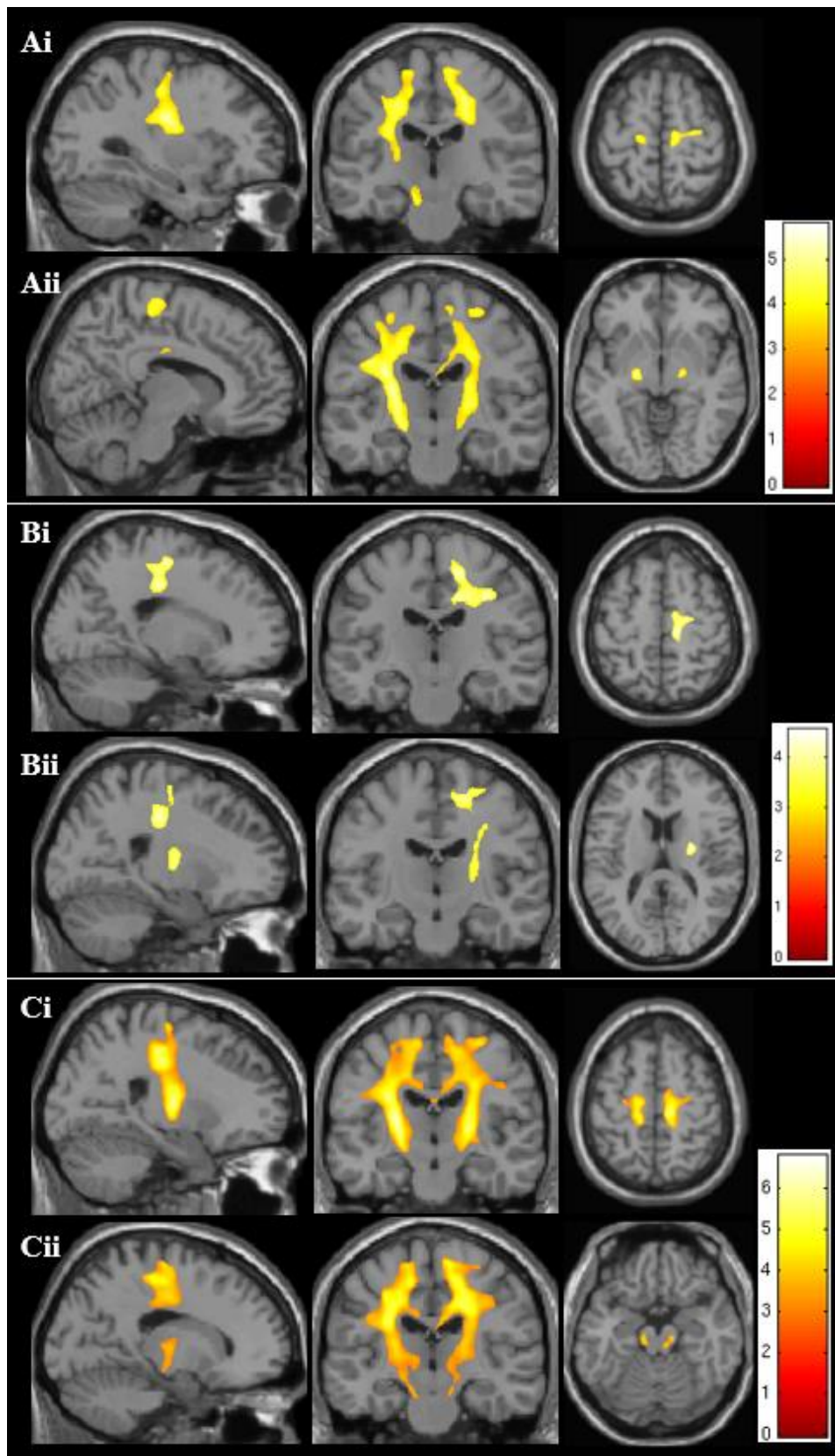
When comparing the control group with King's stage 3 ALS group a reduction in cortical ODI was again seen in the right superior temporal gyrus and middle temporal gyrus ( $P = 0.017$ ), see table 3.4 and figure 3.6Cii. However, an additional cluster of significantly reduced ODI was demonstrated in the right middle frontal gyrus in the region of the dorsolateral prefrontal cortex ( $P = 0.024$ ), see figure 3.6Ci.

A region of significantly increased ODI ( $P = 0.053$ ) in the cerebral WM of the left temporal lobe, including the left hippocampus, was demonstrated in the King's stage 3 ALS group when compared with King's stage 1 group, see table 3.4 and figure 3.6D.

When comparing King's stage 3 group with the control group, a similar more statistically significant region of increased ODI ( $P = 0.021$ ) was seen in the WM of the left temporal lobe. A second region of increased ODI, approaching significance, was revealed in the WM of the right temporal lobe ( $P = 0.052$ ), see table 3.4 and figure 3.5E.



Figure 3.5: Regions of difference on whole brain analysis if NDI comparing King's stages of ALS and control subgroups.



A figure to show where differences were detected on subgroup analysis using the NDI parameter. Results are shown for  $P < 0.05$  after FWE correction at cluster level, clusters formed using  $P < 0.001$ . (A) Control > Stage 2, (i) superior, (ii) inferior; (B) Control > Stage 3, (i) superior, (ii) inferior; (C) Control > Stages 2 and 3 combined (i) superior, (ii) inferior.

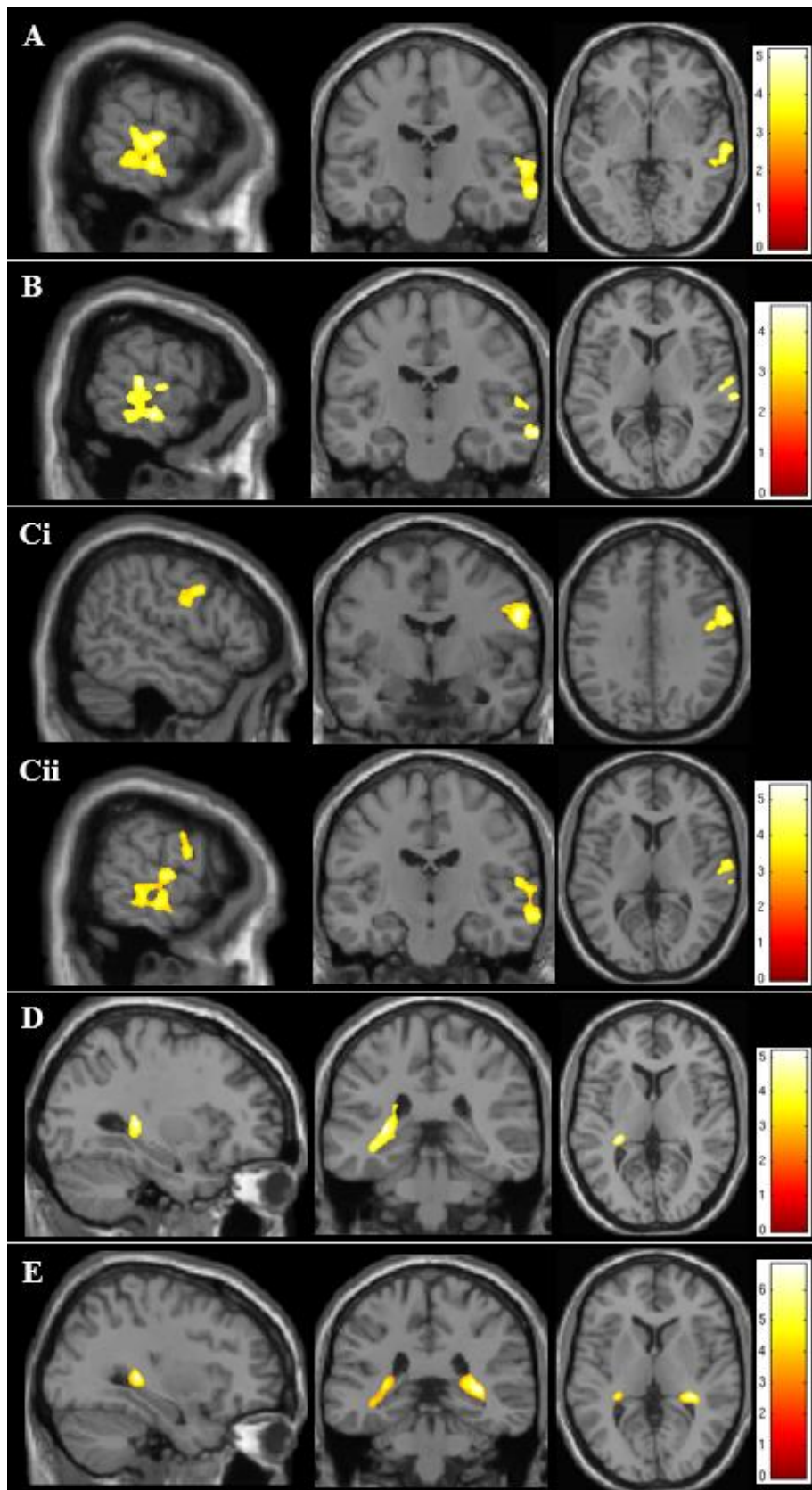
**Table 3.4: Regions of significant differences in NODDI parameters comparing King's Stages of ALS subgroups and the control group.**

	Contiguous anatomical regions within cluster	MNI co-ordinate (x, y, z)	t-value	K (size)	$P_{\text{cluster level FWE-corr}}$
NDI Control > Stage 2	Left cerebral WM, PCG, corona radiata, internal capsule	-24 -13 13	5.78	12269	<0.001
	Right cerebral WM, PCG, corona radiata, corpus callosum, internal capsule	23 -13 5	5.39	8311	<0.001
NDI Control > Stage 3	Right corona radiata, internal capsule	26 -10 13	4.42	5622	0.004
NDI Control > Stage 2 and stage 3 combined	Right cerebral WM, PCG, corona radiata, corpus callosum, internal capsule	24 12 13	5.76	20572	<0.001
	Left cerebral WM, PCG, corona radiata, internal capsule	-24 -12 7	6.77	20316	<0.001
ODI Stage 2 > Stage 3	Right cerebral cortex, superior temporal gyrus, middle temporal gyrus	64 -14 4	5.18	4138	0.006
ODI Stage 1 > Stage 3	Right cerebral cortex, middle temporal gyrus	68 -18 -13	4.64	3285	0.019
ODI CTL > Stage 3	Right cerebral cortex, superior temporal gyrus, middle temporal gyrus	68 -19 -13	4.77	3362	0.017
	Right cerebral cortex, middle frontal gyrus, right cerebral WM	57 -3 29	5.41	3133	0.024
ODI Stage 3 > Stage 1	Left temporal WM, hippocampus	-30 -33 6	5.06	2635	0.053
ODI Stage 3 > CTL	Left temporal WM, hippocampus	-37 -30 -6	5.25	2302	0.021
	Right temporal WM	33 -34 4	6.81	1856	0.052
ISO Stage 3 > CTL	Right lateral ventricle	31 -30 4	5.48	10797	<0.001
ISO Stage 3 > Stage 1	Lateral ventricles	31 -30 3	4.8	5445	0.006

A table to show the anatomical regions where significant differences were demonstrated on whole brain analysis comparing subgroups of ALS according the King's staging system and the control group. The MNI coordinates refer to the peak t-value and were used to define the anatomical location of each cluster of voxels.

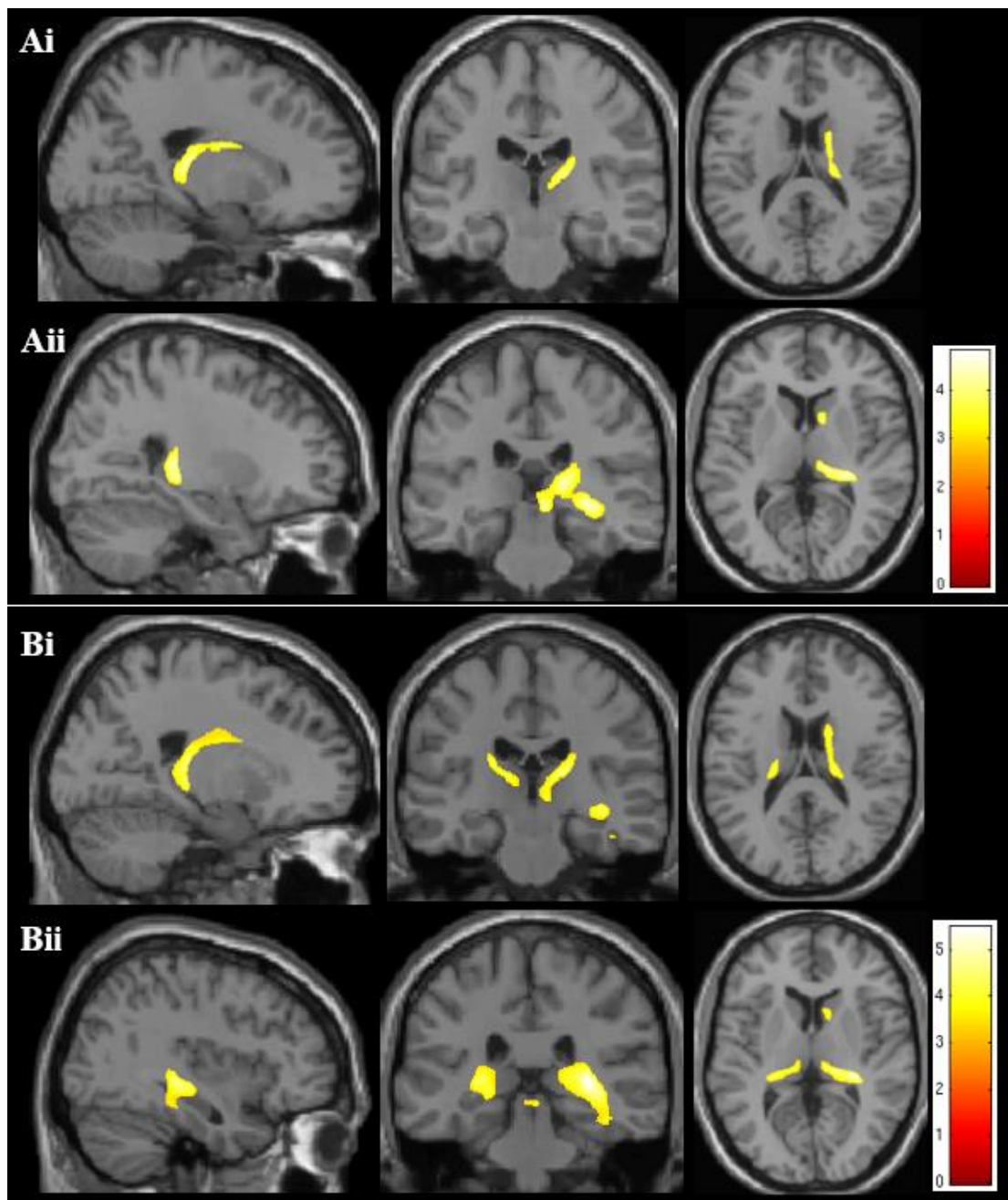
Abbreviations: NDI, neurite density index; ODI, orientation dispersion index; ISO, isotropic diffusion; PCG, precentral gyrus; WM, white matter; MNI, Montreal Neurological Institute; K, cluster size; FWE, family-wise error.

Figure 3.6: Regions of difference on whole brain analysis of ODI comparing King's stages of ALS and control subgroups.



A figure to show the differences detected on subgroup analysis using ODI. Results are shown for  $p < 0.05$  after FWE correction at cluster level, clusters formed using  $p < 0.001$ . (A) Stage 2 > Stage 3; (B) Stage 1 > Stage 3; (C) Control > Stage 3 (i) superior, (ii) inferior; (D) Stage 3 > Stage 1; (E) Stage 3 > Control.

**Figure 3.7: Regions of difference on whole brain analysis of ISO comparing King's stages of ALS and control subgroups.**



A figure to show where differences were detected on subgroup analysis using the ISO parameter. Results are shown for  $P < 0.05$  after FWE correction at cluster level, clusters formed using  $P < 0.001$ . (A) Stage 3 > Stage 1, (i) superior, (ii) inferior; (B) Stage 3 > Control, (i) superior, (ii) inferior.

### 3.9.2.3 ISO

Whole brain analysis for differences in ISO between the King's stage 3 ALS subgroup and King's stage 1 subgroup showed significant increase in ISO ( $P = 0.006$ ), in a region of the right cerebral WM of structures encompassing the right lateral ventricle, from the caudate nucleus and thalamus superiorly, see table 3.4 and figure 3.7Ai, reaching down into the right temporal lobe inferiorly, see figure 3.7Aii.

When comparing the King's stage 3 ALS group with the control group a similar but more significant contiguous region of increased ISO was demonstrated in the right cerebral hemisphere ( $P<0.001$ ) extending into the left cerebral hemisphere at the level of the midbrain (figure 3.7B), in a shape resembling the lateral ventricles.

### **3.9.3: Cognitive Involvement**

Whole brain comparison analysis for differences between ALS cognitive subgroups and the control group also revealed significant differences affecting all of the NODDI parameters.

When the ALS subgroup with normal ECAS was compared to the control group, NDI was significantly reduced within the CST bilaterally ( $P<0.001$ ). These large symmetrical clusters extend from the PMC, down through the corona radiata, and into the internal capsule (see table 3.5 and figure 3.8A).

Comparison of the abnormal ECAS ALS subgroup with the control group also showed significantly reduced NDI in regions of the CST. A large region of significantly reduced NDI ( $P<0.001$ ) was demonstrated superiorly within the right medial PCG, extending down into the corona radiata, see figure 3.5Bi.

In addition, there was reduced NDI bilaterally within the posterior limb of the internal capsule ( $P=0.002$ ), see table 3.5 and figure 3.8Bii.

ODI was only significantly reduced in the ALS group with abnormal ECAS when compared with the control group ( $P=0.004$ ), in a region of the right frontal corona radiata extending into the prefrontal area, see figure 3.8C. There was also an area of increased ODI in the abnormal ECAS ALS group when compared to the control group ( $P=0.004$ ), in a symmetrical cluster of the thalamus bilaterally, see table 3.5 and figure 3.5D.

When comparing the ALS group with abnormal ECAS to the control group, ISO was significantly increased in the in a few regions, see figure 3.8E. These comprise an area in the right anterior cingulate cortex extending around the genu of the corpus calosum into the right head of the caudate nucleus ( $P<0.001$ ), the thalami ( $P<0.001$ ), the left insular cortex and adjacent WM of the left frontal cortex ( $P=0.002$ ), and the right insular cortex ( $P=0.015$ ), see table 3.5.

Finally, ISO was increased in the abnormal ECAS ALS group when compared to the normal ECAS ALS group ( $P=0.026$ ), in a region of the right temporal fusiform gyrus, see table 3.5 and figure 3.8F.

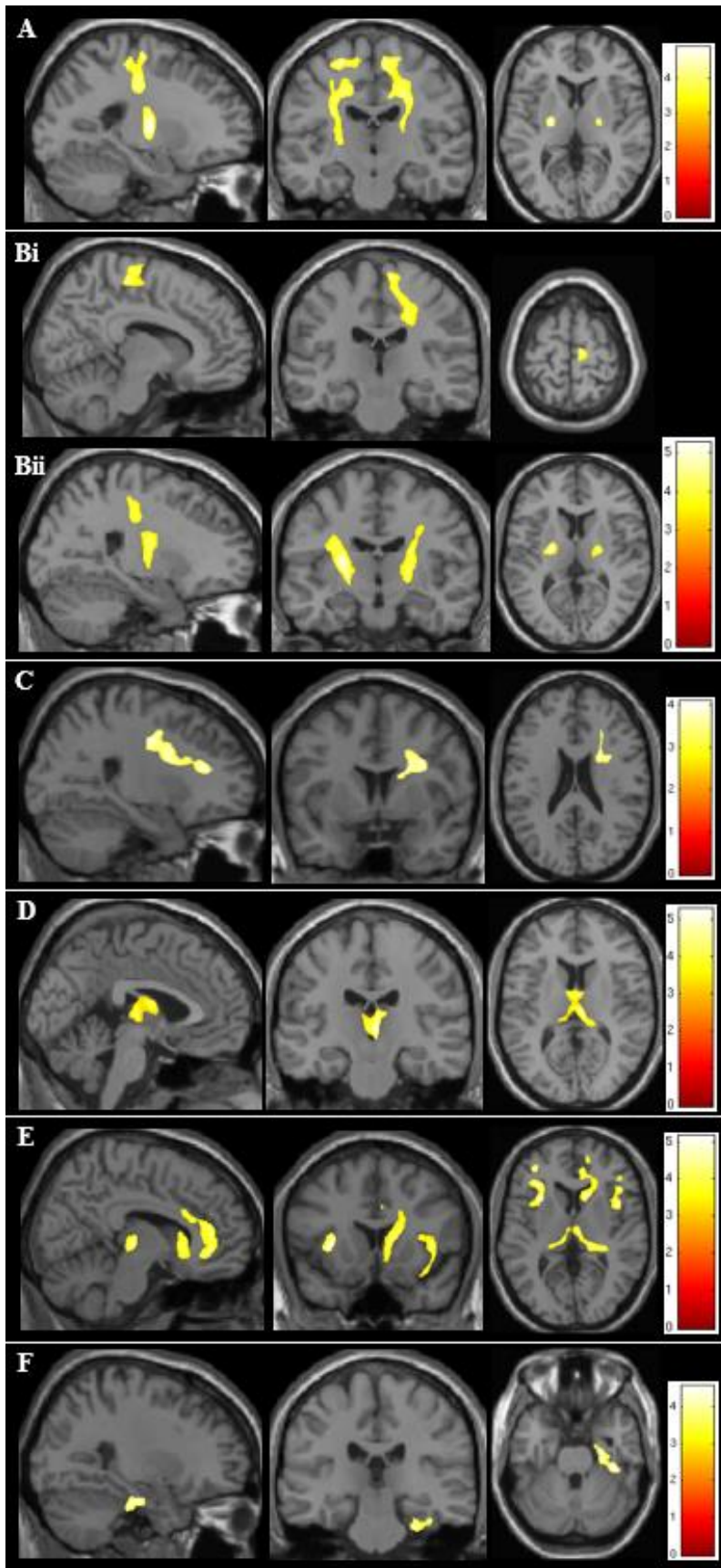


**Table 3.5: Regions of significant differences in NODDI parameters comparing cognitive subgroups of ALS and the control group.**

	Contiguous anatomical regions within cluster	MNI co-ordinate (x, y, z)	t-value	K (size)	$P_{\text{cluster level FWE-corr}}$
NDI Control > Normal ECAS	Left cerebral WM, PCG, corona radiata, internal capsule	-23 -12 5	4.90	7916	<0.001
	Right cerebral WM, PCG, corona radiata, internal capsule	11 -25 59	4.81	7127	<0.001
NDI Control > Abnormal ECAS	Right PCG and cerebral WM	10 -20 69	4.44	5664	<0.001
	Left cerebral WM, PLIC	-24 -11 12	5.26	3880	0.002
ODI Control > Abnormal ECAS	Right cerebral WM, corona radiata	27 30 16	4.09	3632	0.004
ODI Abnormal ECAS > Control	Thalamus	4 -20 3	5.29	4691	0.001
ISO Abnormal ECAS > Control	Right cerebral cortex, right cerebral WM, cingulate gyrus	8 37 -6	4.44	9815	<0.001
	Right thalamus	7 -18 3	4.66	5490	<0.001
	Left cerebral WM, left cerebral cortex, insular cortex	-31 15 4	5.15	4076	0.002
	Right insular cortex	43 -20 -39	4.56	2768	0.015
ISO Abnormal ECAS > Normal ECAS	Right cerebral WM and cortex, temporal fusiform gyrus	40 -30 -27	4.55	2452	0.026

A table to show regions where significant differences were detected on whole brain analysis comparing cognitive ALS subgroups and the control group. The MNI coordinates refer to the peak t-value and were used to define the anatomical location of each cluster of voxels. Abbreviations: ECAS, Edinburgh cognitive and behavioural ALS screen; NDI, neurite density index; ODI, orientation dispersion index; ISO, isotropic diffusion; PCG, precentral gyrus; PLIC, posterior limb of the internal capsule, WM, white matter; MNI, Montreal Neurological Institute; K, cluster size; FWE, family-wise error.

**Figure 3.8: Regions of difference on whole brain analysis of NODDI parameters comparing normal ECAS, abnormal ECAS, and control subgroups.**



A figure to show where differences were detected on subgroup analysis of cognitive groups using the NODDI parameters.

Results are shown for  $P < 0.05$  after FWE correction at cluster level, clusters formed using  $P < 0.001$ .

(A) NDI: Control > Normal ECAS

(B) NDI: Control > Abnormal ECAS; (i) Superior, (ii) Inferior

(C) ODI: Control > Abnormal ECAS

(D) ODI: Abnormal ECAS > Control

(E) ISO: Abnormal ECAS > Control

(F) ISO: Abnormal ECAS > Normal ECAS

### 3.10: Correlation of the NODDI parameters with clinical measures of ALS.

Using whole brain analysis to investigate for correlation between NODDI parameters and clinical measures of disease severity in ALS showed several correlations.

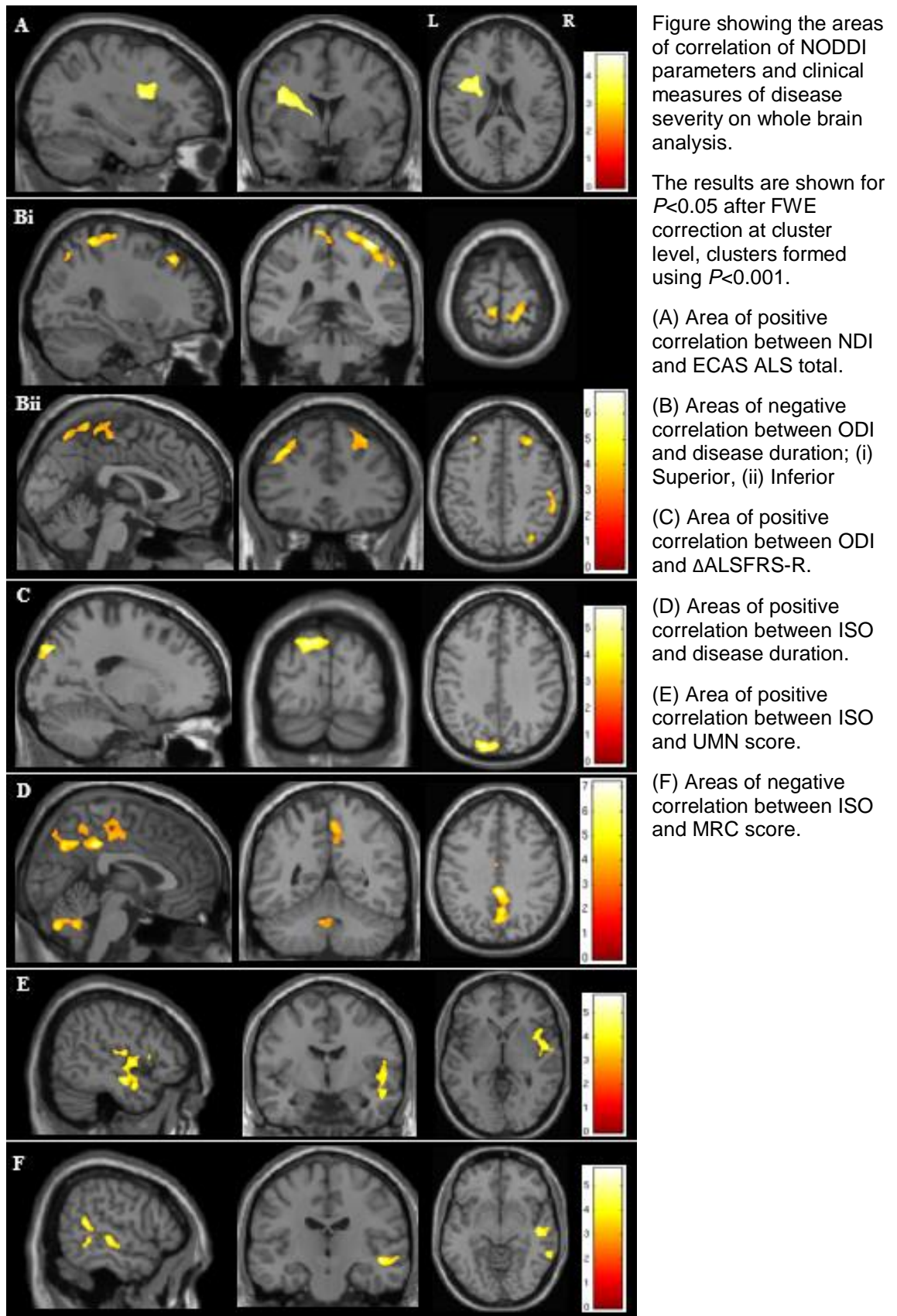
**Table 3.6: Regions of significant correlation between NODDI parameters and clinical measures of ALS severity.**

	Contiguous anatomical regions within cluster	MNI co-ordinate (x, y, z)	t-value	K (size)	$P_{\text{cluster level FWE-corr}}$
NDI positive correlation with ECAS ALS Total	Left cerebral WM, internal capsule, and corona radiata	-38 5 24	4.78	4661	0.002
ODI negative correlation with disease duration	Right cerebral cortex, PCG	36 -35 61	6.84	6481	<0.001
	Left cerebral cortex, PCG, precuneus	-3 -48 69	5.01	3343	<0.001
	Left cerebral cortex, cerebral WM, middle frontal gyrus	-29 39 33	5.94	2197	0.002
	Right cerebral cortex, right cerebral WM, precuneus	23 -67 50	5.98	1352	0.033
	Right cerebral cortex, cerebral WM, middle frontal gyrus	30 28 46	5.35	1220	0.052
ODI positive correlation with ALSFRS-R	Left cerebral cortex, cerebral WM, precuneus	-15 -85 36	5.75	1969	0.051
ISO positive correlation with disease duration	Interhemispheric fissure, paracentral lobule, precuneus, cingulate gyrus	1 -38 38	7.20	5845	<0.001
	4 <sup>th</sup> Ventricle	0 -55 -36	5.84	4132	0.001
	Left cerebral cortex, cerebral WM, paracentral lobule, precuneus, cingulate gyrus	-2 -6 35	4.10	2042	0.028
ISO positive correlation with UMN score	Right cerebral cortex, insula, central opercular cortex	48 -18 12	5.72	5048	<0.001
ISO negative correlation with MRC score	Right cerebral cortex, cerebral WM, middle temporal gyrus	61 -43 10	5.79	2258	0.019
	Right cerebral cortex, cerebral WM, superior temporal gyrus	48 -18 -8	4.83	2197	0.021

A table to show regions where significant correlation between NODDI parameters and clinical measures of ALS severity was detected on whole brain analysis. The MNI coordinates refer to the peak t-value and were used to define the anatomical location of each cluster of voxels. Abbreviations: NDI, neurite density index; ODI, orientation dispersion index; ISO, isotropic diffusion; PCG, precentral gyrus; WM, white matter; MNI, Montreal Neurological Institute; K, cluster size; FWE, family-wise error.



**Figure 3.9: NODDI parameter correlation with measures of ALS disease severity.**



NDI correlated significantly with the ECAS ALS total score, within the left frontal WM ( $P=0.002$ ), in a region extending from the left internal capsule into the corona radiata,

see table 3.6 and figure 3.9A. There was no significant correlation detected between NDI and the overall ECAS score or the non-ALS ECAS total.

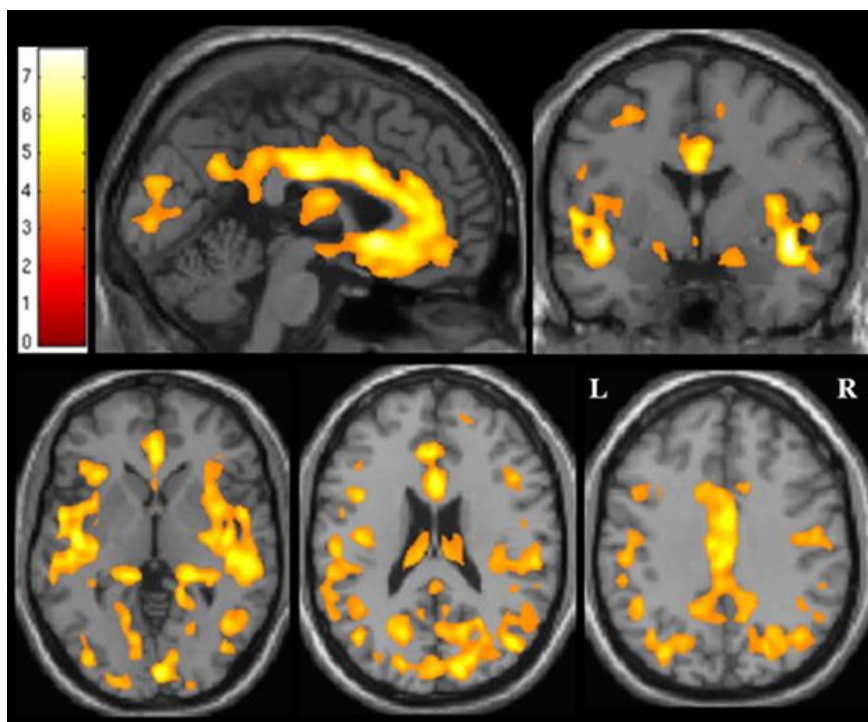
There was significant correlation between ODI and disease duration within the right PCG ( $P<0.001$ ), and the medial left PCG ( $P<0.001$ ), see table 3.6 and figure 3.9Bi. There were additional regions of correlation with the left middle frontal gyrus ( $P=0.002$ ), right precuneus ( $p\ 0.033$ ), and the right middle frontal gyrus ( $P=0.052$ ), see figure 3.9Bii. An area of positive correlation, approaching significance between ODI and  $\Delta$ ALSFRS-R, was detected within the left precuneus ( $P=0.051$ ), see figure 3.9C.

ISO correlated positively with disease duration within the interhemispheric fissure, in a cluster with close proximity to the paracentral lobule, precuneus, and posterior cingulate (right  $P<0.001$ , left  $P=0.028$ ), as well as the fourth ventricle ( $P=0.001$ ), see table 3.6 and figure 3.9D. ISO also correlated positively with UMN score within the right insular cortex ( $P<0.001$ ), see figure 3.9E. Finally, ISO demonstrated negative correlation with MRC score within the right middle temporal gyrus ( $P=0.019$ ) and right superior temporal gyrus ( $P=0.021$ ), see figure 3.9F.

No further significant correlations were found between the NODDI parameters and measures of disease severity; ALSFRS-R,  $\Delta$ ALSFRS-R, UMN score, and MRC power score.

Across the whole cohort of control participants and those with ALS, there was a significant positive correlation between ISO and participant age ( $P<0.001$ ), within large areas of the cortex, the ventricles, and sulci (see figure 3.10).

**Figure 3.10: Correlation between ISO and age across all participants.**



A figure to show the areas of correlation between ISO and age, where results are shown for  $P<0.05$  after FWE correction at cluster level, clusters formed with  $P<0.001$ .

### 3.11 Quantitative diffusion weighted MRI parameters in ALS discussion

The main findings in the application of NODDI to ALS, relate firstly to significant reduction of NDI and ODI within the PCG, where these changes are compatible with loss of both dendrite density and complexity occurring in ALS. Secondly, in relation to white matter, NODDI shows a significant reduction of NDI in the CST and corpus callosum, suggesting loss of axonal density in these pathways accompanying ALS. These results are consistent with previous DTI findings; however, the changes detected using NDI were greater than those detected with FA. Furthermore, NODDI provides a more definitive interpretation of the microstructural changes underlying ALS by separating neurite density from orientation dispersion. Thirdly subgroup analysis revealed significant differences in the NODDI parameters according to disease distribution, King's stage of ALS, and cognitive involvement. Finally, the most striking correlation was between ODI in the PCG and disease duration, which suggests a relationship between cortical pathology and the severity of the ALS disease process.

ALS is a devastating neurodegenerative disease, which is currently incurable despite substantial worldwide research taking place.<sup>517</sup> The ALS syndrome can be recognised clinically due to the typical manifestations of the various phenotypes.<sup>1</sup> However objective neuroimaging biomarkers sufficiently sensitive to detect the different patterns of tissue degeneration at the subject level are lacking. Interrogation of new advanced imaging techniques, such as NODDI, is therefore vital to assess the potential for distinguishing the biological characteristics of disease '*in vivo*'.

In this cross-sectional study using NODDI to investigate a heterogeneous group of patients diagnosed with ALS, together with a control group matched in terms of age and gender, there are several interesting findings which facilitate the understanding of the neurodegenerative process occurring in ALS. In essence NODDI detects both cortical and corticospinal tract degeneration in ALS.<sup>357</sup>

#### 3.11.1 NODDI demonstrates microstructural changes associated with ALS

Whole brain voxel wise analysis of the NODDI parameters in ALS demonstrated statistically significant reduction in NDI and ODI in a region of the right PCG (figure 3.1B). In addition, the NODDI parameter means extracted from the PCG showed reduced NDI and ODI in both cerebral hemispheres, accompanied by increased ISO (figure 3.3). Despite not reaching statistical significance when controlling for multiple comparisons these changes provide the basis for a pattern of changes in the PCG related to ALS, a NODDI signature. These detected alterations are compatible with loss of dendritic density and reduced dendritic arborisation within the GM of the motor cortex, as suggested by recent histopathological analyses in humans and animal models.<sup>518–520</sup>

More extensive changes in ODI and NDI were anticipated throughout the GM of the motor cortex, to reflect altered dendritic complexity and reduced numbers of pyramidal cells, as previously described in post-mortem studies.<sup>195</sup> However, relatively little is known about structural changes occurring within the cortical neuropil in ALS. Some neuropathological studies,<sup>199</sup> have found loss of both large pyramidal neurones and GABAergic interneurons in the primary motor cortex associated with ALS. However, another study failed to detect a reduction in total number of neurones within the primary motor cortex using stereological quantification.<sup>198</sup> As there is typically UMN involvement clinically in ALS, this suggests that within the brain the disease process is involving the Betz pyramidal cells. These giant neurones are named after the Ukrainian anatomist and histologist Vladimir Alekseyevich Betz (1834-94), who first recognised the cyto-architecture of the motor cortex and described the Betz cells in 1974.<sup>521</sup> The Betz cell soma reside in layer V of the primary motor cortex and project their long axons caudally down into the corona radiata, where they descend and converge to form the PLIC.<sup>522</sup> The dendrites of the Betz cells branch out from the soma to form an elaborate arborisation within the cortical neuropil. These dendrites are themselves covered with thousands of dendritic spines, small membranous protrusions that integrate information and facilitate the communication between neurones.

It is likely that disease heterogeneity, recognised clinically by the diversity of ALS phenotype, reflects the variation in neuroanatomical spread of pathology within the Betz cells, which themselves are dispersed throughout the cortex.<sup>195</sup> This could therefore conceivably be an explanation for the difficulties in detecting consistent changes in the PCG using NODDI for whole brain comparisons.

In addition, it is possible that loss of cortical dendrites is a relatively late phenomenon in the evolution of cerebral pathology in ALS with the earlier stages of ALS reflecting a 'dying back' mode of degeneration of corticospinal and other projection fibres,<sup>284,286</sup> although changes in cortical dendrites are observed at early stages of disease evolution in animal models of ALS.<sup>518,519</sup>

Furthermore, NODDI may not separate the effects of orientation dispersion and neurite density effectively within the GM, particularly with the b-values used for this study, and may therefore not distinguish intra-cortical neuropil pathology in ALS.<sup>462</sup> More recently developed quantitative diffusion MRI techniques incorporating microscopic anisotropy mapping may separate different signal components better and highlight differences more effectively.<sup>523</sup> The NODDI technique used in this study<sup>409</sup> models orientation dispersion isotropically and may therefore be limited in its capacity to model multiple fiber orientations arising from complex dendritic structures.<sup>511</sup> NODDI has subsequently been developed further to incorporate a quantification of anisotropic orientation dispersion, and analysis using this more sophisticated modelling system is

warranted in future studies in ALS.<sup>415</sup> Nonetheless, these findings indicate that NODDI can reveal new aspects of the cellular pathology of diseases such as ALS, in keeping with the recent demonstration that changes in NODDI parameters closely reflect complex histological changes in grey and white matter of the spinal cord in multiple sclerosis.<sup>450</sup>

In relation to the WM, whole brain analysis using NODDI revealed striking changes in axonal density associated with ALS. The area of significantly reduced NDI extends from the posterior limb of the internal capsule and continues rostrally into the subcortical WM of the PCG, as well as across the corpus callosum (figure 3.1A). This supports the notion that loss of motor neuron axon density within the cerebral WM is a core feature of the neurodegenerative process associated with ALS, consistent with many pathological studies.<sup>193,194</sup> It is possible that alterations in glial cells and myelin may also contribute somewhat to these changes in NDI. However, as the density of axons per voxel is much higher than that of glial cells, and loss of motor neuron axons is a key feature of ALS, the changes are likely to be explained largely by axonal loss.

A direct comparison of the NDI and FA whole brain findings in this study shows that NDI detected larger areas of neurodegeneration than FA at the same statistical threshold, where the combined cluster sizes for the areas of significantly reduced NDI (29 349) were greater than those for areas of significantly reduced FA (9283) (see table 3.1). This suggests that NDI may have a higher sensitivity than FA for detecting ALS-related WM pathology and also indicates that the primary pathology identified by the diffusion MRI signal is alteration in axon density.

In this study FA was reduced into two separate regions of the CST in the ALS group, one within the pons and another within the corona radiata extending into the subcortical WM of the PCG (figure 3.2A). The CST has previously been implicated in DTI studies demonstrating reduced FA in the ALS group.<sup>396,524,525</sup> Typically, studies report reduced FA in one or several isolated regions, including the pons, cerebral peduncles, posterior limb of the internal capsule, corona radiata and the subcortical WM of the PCG.<sup>169,369,525–527</sup> Low FA within the corpus callosum is also typically demonstrated in ALS<sup>395</sup> but not always.<sup>526</sup> In any case rarely are such extensive, contiguous changes demonstrated throughout the CST and corpus callosum, as evident with our findings of reduced NDI using NODDI.<sup>357</sup>

MD was increased in the ALS group within the left internal capsule (figure 3.2B), which is consistent with previous studies.<sup>169,528</sup> Reports of increased MD have been less consistent than FA findings in ALS, which may be explained by the known dependency of MD on the specific b-value used for the acquisition.<sup>515</sup> In this study, we used a maximum b-value of 2400  $\text{mm}^{-2}$ , which is higher than typical DTI protocols and may account for our findings. We could have restricted our DTI analysis to the inner shell (b=800) data to make it more compatible with other DTI studies. However, this would

have made the comparison with NODDI (fitted with the full data set) unfair. In general the extent of WM changes we found using DTI is somewhat reduced compared with other studies. This might be the consequence of specific methodological differences, the relatively small sample size or the clinical heterogeneity of the cohort.

A significant increase in RD (figure 3.2C) was also demonstrated on whole brain analysis, within the cerebral WM of the CST bilaterally as well as into the right corpus callosum. This is consistent with previous published studies demonstrating an increase in RD within the CST and corpus callosum of ALS participants.<sup>529,530</sup>

NODDI facilitates the interpretation of the altered diffusivity profile in ALS observed using DTI where axonal loss, demonstrated by reduced NDI in the CST and corpus callosum, is likely to be the main contributing factor for the reduced FA accompanied by an increased MD and RD.

We detected reduced ODI in the right internal capsule, a region where there is crossing of WM pathways. This could be explained by the predominant degeneration of axonal fibres in one direction, thereby reducing crossing of fibres in this region. Furthermore, this may contribute to the lack of changes in FA detected in this region as the corresponding FA may not change due to the remaining fibres becoming more coherent, despite axonal degeneration.

On whole brain analysis increased ISO was detected within the right lateral ventricle, likely representing atrophy in ALS leading to increased CSF space (figure 3.1C). However, further changes in ISO relating to the motor regions of the frontal cortex did not reach statistical threshold. Previous studies with positron emission tomography (PET) imaging suggest that widespread cerebral microglial activation is evident in ALS.<sup>185,371</sup> One explanation could therefore be that isotropic fraction does not fully differentiate between brain tissue and the presence of increased inflammatory infiltrates in these regions.

In summary the whole brain analysis of NODDI parameter changes in ALS highlighted extensive axonal degeneration, associated with more inconspicuous loss of dendrite complexity in the motor cortex and atrophy.

### **3.11.2 NODDI parameter subgroup analysis discussion**

There is a pressing need for non-invasive neuroimaging biomarkers that can differentiate between the various phenotypes within the ALS syndrome. The ultimate aim would be to develop an imaging biomarker that is sufficiently sensitive to explore neurodegenerative biological mechanisms, offer accurate prognostication, and provide monitoring of response to therapeutic intervention. Subgroup analysis was performed to explore whether NODDI has the potential to distinguish different biological

characteristics related to the dynamics of disease pathology underlying different subgroups based on clinical features.

The ALS subgroup with both bulbar and limb involvement showed significantly greater loss of right CST axon density than the group with limb-confined ALS, as well as more extensive changes in CST NDI bilaterally when compared to the control group (figure 3.4A and 3.4B). This may indicate that those with bulbar involvement have more cortical pathology than those with limb-confined ALS, where the disease process could be confined to the anterior horn cell.<sup>531</sup> When comparing the bulbar and limb ALS group with the control group, there was also reduced ODI, in the right motor cortex adjacent to the WM changes detected in NDI (figure 3.4C). This cortical region is responsible for bulbar motor function, which therefore indicates that NODDI has the potential to detect cortical alterations relevant to ALS disease distribution. Unfortunately, there were insufficient numbers to statistically assess those with bulbar symptoms as a single ALS group.

NDI was more significantly reduced in the King's stage 2 and stage 3 ALS groups compared to the control group (figure 3.5A and 3.5B). Interestingly it was King's stage 2 ALS group which showed the most significant loss of motor axon density throughout the CST bilaterally and within the right corpus callosum. In the King's stage 3 group the significant reduction in NDI was limited to the right hemisphere centrum semiovale, corona radiata, and rostral PLIC. This highlights the important point that despite King's stage 3 group having more regions affected by ALS symptoms clinically, this does not equate to more cortical involvement pathologically or radiology. Instead this finding suggests that largely spinal or LMN neurodegenerative processes are occurring in this particular subgroup. Nonetheless, the most significant loss of motor axon density was seen when King's stages 2 and 3 were combined and compared with the control group (figure 3.5C), likely in part due to an increase in the subgroup size, but compatible with the notion that more widespread clinical disease relates to more extensive microstructural damage. There were no significant differences detected in NDI when comparing the King's stage 1 ALS group with King's stage 2, King's stage 3, or the control group. This may suggest that in the early stages of ALS the neuropathological changes within the brain have yet to cause significant degeneration. In addition, no significant differences were detected between these subgroups. However, small subgroup sizes may have also made finding statistically significant differences on whole brain analysis challenging.

King's stage 3 ALS showed significantly greater loss of ODI in the cortex of the right temporal lobe when compared to King's stage 2, and King's stage 1, and control group (figure 3.6A, 3.6B, 3.6Cii). The region of cortex with relative loss of neurite complexity is within the superior and middle temporal gyri of the right temporal lobe.

These structures are involved in auditory processing, language recognition, short term memory, and social perception. Loss of dendritic integrity in this region, related to the King's stage 3 ALS subgroup, suggests that in the later stages of disease there are neurodegenerative changes occurring in areas distant to the premotor and primary motor cortex. In addition, there was a relative increase in ODI in the WM of the temporal lobes, on the left when comparing stage 3 with stage 1, and bilaterally when comparing stage 3 with the control group (figure 3.6D and 3.6E). As part of the stem to the temporal lobe, this region likely contains fibres from a number of white matter tracts including the temporo-pontine, amygdalothalamic, parahippocampal bundle and inferior longitudinal fasciculus, as well as the auditory and optic radiations. A compensatory mechanism may account for this apparent increase in ODI related to the highest King's stage of ALS in this region. However, if plasticity was the cause then an increase in NDI may be anticipated in the same region and this was not detected. It is therefore more likely that the neurodegenerative mechanisms underlying ALS have reached such an extent that they are causing degeneration of tracts through the temporal lobes, where predominant loss of large coherent pathways could lead to an increase in neurite dispersion being detected in this region due to loss of axonal integrity. It also indicates that ALS, although clinically manifest mainly as a syndrome of motor dysfunction, is a multisystem neurodegenerative disease pathologically.<sup>532</sup> This is supported by studies mapping the spread of TDP-43 neuropathological inclusions.<sup>533</sup>

Finally, there was a region of significantly reduced ODI in the bulbar region of the right primary motor cortex, when comparing the King's stage 3 ALS group with the control group (figure 3.6Ci). This is a similar finding as demonstrated when comparing the bulbar and limb ALS group with the control group, which would be anticipated as by definition those classified as King's stage 3 have bulbar symptoms as well as the involvement of both upper and lower limb. This indicates that NODDI is consistently detecting cortical pathology related to bulbar symptoms in ALS.

There was significantly more atrophy associated with King's stage 3 of ALS, as indicated by an increase in ISO. Significantly increased ISO was detected in the right hemisphere adjacent to the lateral ventricle when comparing King's stage 3 with stage 1 ALS (figure 3.7A), with similar but bilaterally findings demonstrated when comparing King's stage 3 with the control group (3.7B). The region of increased ISO extends into the temporal horns of the lateral ventricles, suggesting atrophy in this area is occurring in the later stages of ALS. This supports the suggestion that the increase in ODI detected in the temporal lobes described above is related to neurodegeneration rather than neuro-regeneration. This finding indicates that in the cohort of ALS participants involved in this study there were neurodegenerative changes occurring within the temporal lobes, which is a recognised feature of ALS in some cases.<sup>534,535</sup>



Frontotemporal dementia (FTD), a neurodegenerative disorder accompanied by atrophy of the frontal and temporal lobes,<sup>536</sup> is recognised to occur alongside ALS, when it is called the ALS-FTD syndrome. ALS and FTD are linked by common genetic and molecular bases, as well as an overlapping spectrum of clinical features.<sup>63-69,195,374</sup> The presence of frontotemporal dysfunction, which occurs in approximately 50% of patients with ALS, is a negative prognostic indicator.<sup>71-77</sup> Studies suggest that up to 15% of patients with ALS have cognitive and behavioural changes sufficient for a diagnosis of FTD, while a further 35% have milder deficits that meet the criteria for the ALS frontotemporal spectrum disorder (ALS-FTSD).<sup>1-77,536</sup> In the cohort of ALS participant used in this study 22% had sufficient impairment to be classified as ALS-FTSD, with a further 30% exhibiting abnormal ECAS scores but not meeting the diagnostic criteria for ALS-FTSD.<sup>77</sup>

The most exciting finding when assessing subgroups of ALS according to cognitive involvement, was that the ALS subgroup with cognitive impairment was distinguished from the ALS subgroup with normal ECAS scores by a region of increased atrophy within the right temporal fusiform gyrus (figure 3.8F). This finding suggests that temporal atrophy is related to cognitive deficit in the ALS participants studied in this research. In addition, there was more widespread increase in ISO within the frontal lobes when comparing with the control group indicating that the ALS group with cognitive decline exhibits more cortical atrophy (figure 3.8E). The regions involved include the insular cortex bilaterally, the left DLPFC, and the right anterior cingulate cortex, all of which have been implicated in FTD.<sup>365,537,538</sup>

Although there were no significant differences in NDI or ODI when comparing the ALS subgroups based on cognitive involvement, findings were apparent in both these NODDI parameters when comparing the ALS subgroups with the control group. Significantly decreased NDI was found in both ALS subgroups (figure 3.8A and 3.8B), lending further support that loss of CST axons is a core feature of ALS. However, significant changes in neurite architecture were only found in the ALS group with cognitive impairment (figure 3.8C), where an area of reduced ODI was demonstrated in the right frontal corona radiata, with extension into the right DLPFC. This supports previous fMRI findings of fronto-temporal alterations, as part of the default mode network, occurring in ALS.<sup>539-542</sup>

A region of relative increase in ODI was detected in the dorsomedial thalamus bilaterally (figure 3.8D) in the ALS subgroup with cognitive deficit. This is likely due to selective loss of coherent myelinated axons in this area, supported by the increased marker of atrophy in this location (figure 3.8E).

Overall the cognitive subgroup results of this study indicate that altered dendritic complexity and frontotemporal cortical atrophy relate to cognitive impairment in ALS.

In summary for the subgroup analysis NODDI identifies regional loss of axons, reflected by reduced NDI, associated with bulbar involvement. Altered neurite integrity and atrophy, as demonstrated by changes in ODI and ISO, can distinguish between King's stages of ALS. Finally, ISO can detect appropriate changes in the temporal lobe related to cognitive impairment when comparing ALS subgroups. Overall the subgroup analysis results are in keeping with the hypothesis that more widespread clinical involvement in ALS relates to more extensive microstructural damage.

### **3.11.3 NODDI parameter correlation with clinical measures of ALS discussion**

A significant correlation was found between NDI in the left frontal WM and the ECAS ALS total score (figure 3.9A). Interestingly no other NODDI parameter correlated with the ECAS ALS total score and no correlation was found between NDI and the overall ECAS score. This finding was specific to a relationship between CST NDI and cognitive function in the ALS specific domains. This finding is likely to be due to those with relevant cognitive deficit having a higher burden of intracranial ALS pathology, the consistent feature of which is CST degeneration.<sup>17,18,339-341,509,543</sup> Nonetheless it shows that NODDI is detecting pathology related to relevant manifestation in the cognitive profile of ALS.

Despite NDI detecting the most extensive changes on whole brain analysis, this parameter did not correlate with any of the other clinical measures of ALS. Correlation was anticipated particularly with UMN score and disease duration. A correlation gap between imaging and clinical data has previously been reported for DTI studies and may reflect the subjectivity of clinical assessment, the biological complexity of ALS, and also limitations of the imaging methodology utilized.<sup>390</sup>

Regression analysis revealed that both ODI and ISO correlated with disease duration, where regions of both the right and left PCG, and interhemispheric fissure were involved, respectively (figure 3.9B and 3.9D). The correlation of ODI in the PCG with disease duration provides support for the rationale that loss of complex neuropil architecture within the motor cortex is occurring in ALS over time. A further area of ODI correlation with symptom duration was found in the right precuneus adjacent to the region of correlation with ISO. This indicates that loss of cortical dendrites and related cerebral atrophy are occurring alongside axonal degeneration. Regions within the right and left DLPFC also exhibited correlation between ODI and duration of ALS. As previously mentioned the DLPFC has been implicated in the cognitive impairment profile in ALS.<sup>365,537,538</sup> Furthermore, previous studies have shown decreased neurite synaptic density in this region in a cohort of ALS patients using transmission electron microscopy.<sup>74</sup> It is therefore possible that the NODDI parameter of ODI is detecting alterations in dendritic architecture relating to progression of ALS pathology.

Despite the association between frontal cortex ODI and duration of ALS symptoms, the significant changes in ODI detected on whole brain analysis were confined to a small area of the PCG. It is possible that dendritic architectural changes occur later in the disease course of ALS or are more variable in ALS. Therefore, finding significant changes of cortical architecture in ALS would necessitate larger studies with homogenous ALS phenotype, in order to reach statistical significance on whole brain analysis of ODI.

A further association was found between ODI and  $\Delta$ ALSFRS-R, where increased dendritic fanning within the cortex of the left precuneus correlated with increased rate of disease progression. This finding is difficult to explain satisfactorily but one possibility is that a compensatory mechanism is occurring in cortical regions outside the motor systems, as demonstrated by increased functional connectivity in the extra motor regions.<sup>539-542</sup> Another consideration relates to the biological differences in the disease process occurring in those who fall into the faster progressing group. It is recognised that depending on the individual's pathophysiological mechanisms associated with the disease process in ALS, they can fall into two broad groups of either fast or slow progressors.<sup>266,544,545</sup> Indeed, a bimodal distribution of  $\Delta$ ALSFRS-R was found in the cohort of ALS participants of this study, see figure 2.1. Fast progressors are likely to have more widespread neurodegeneration of the motor systems but it is possible that they exhibit relatively less cortical changes in the extra-motor systems compared to slow progressors.<sup>265,309</sup>

Regression analysis showed further associations of right cerebral cortex ISO with UMN and MRC scores. Increased atrophy within the right insular cortex and central opercular cortex correlated with higher UMN score. While increased atrophy in the right middle gyrus and superior temporal gyrus correlated with lower MRC score. These results support increased cerebral atrophy relating to more advanced severity of disease symptoms in ALS.<sup>16-18,171,339-342</sup>

Interestingly there was a significant correlation of ISO with age across the whole cohort (figure 3.10), which indicates that ISO is particularly sensitive to age related atrophy and justifies the inclusion of age as a covariate in the analyses. This also supports previous histopathological and imaging findings that the neurodegenerative process in ALS is unique from the dendritic alterations associated with natural aging.<sup>195,427,428,546</sup>

In summary for the correlation analysis as hypothesised there were relationships detected between the NODDI parameters and some of the clinical measure of ALS severity. The most noteworthy of which being the correlation between dendritic complexity within the PCG and duration of ALS, which suggests NODDI is sensitive to the underlying pathological process occurring in ALS.

### 3.11.4 NODDI in ALS limitations and conclusions

There are undoubtedly limitations to this study. In relation to the technique utilised, NODDI may not separate the effects of orientation dispersion and neurite density effectively within the grey matter and may therefore not fully distinguish intra-cortical neuropil pathology in ALS.<sup>462</sup> More recently developed quantitative diffusion MRI techniques, incorporating microscopic anisotropy mapping, may separate different signal components better and highlight differences more effectively but would require additional imaging sequences that are not yet clinically available.<sup>523,547–549</sup> The NODDI technique used in this study models orientation dispersion isotropically and may therefore be limited in its capacity to model multiple fiber orientations arising from complex dendritic structures. NODDI has subsequently been developed further to incorporate a quantification of anisotropic orientation dispersion, and analysis using this more sophisticated modelling system is warranted in future studies in ALS.<sup>415</sup>

Whole brain voxel-wise analysis was used for this study, which does not require any a priori hypotheses and provides information about changes in both WM and GM. Although whole brain analysis is prone to potential biases due to inter-individual anatomical variation and partial volume effects, NODDI has the advantage over DTI of explicitly modelling the free water (isotropic) component and should therefore be less susceptible to the partial volume contamination of CSF. Alternative processing approaches to whole brain analysis, such as tract-based spatial statistics,<sup>369</sup> and GM special statistics,<sup>427</sup> have been optimised to minimise the potential sources of error and to detect changes in WM and GM, respectively. Tractometry, which maps quantitative indices (such as those derived from NODDI) to points of streamlines reconstructed by diffusion tractography, is a powerful visualisation tool and can potentially give insight into the regions of degeneration but suffers from well-known limitations.<sup>550</sup>

It should also be highlighted that while the imaging data for this study was obtained using a 1.5T MRI scanner, many studies using NODDI were performed at 3T.<sup>428,439</sup> The field strength has obvious implication for the signal to noise ratio (SNR). However, the reduced signal intensity at 1.5T is partially compensated by the longer T2 relaxation time at this field strength. We used a voxel size of 2.5 mm<sup>3</sup>, which is almost twice as large as that used in the original NODDI paper at 3T,<sup>409</sup> and should ensure a comparable SNR at the price of reduced spatial resolution.

Another limitation to this study is the sample size, which precluded viable subgroup analyses related to phenotype. This is particularly relevant given emerging insights into disease heterogeneity in ALS.<sup>1</sup> How the recognised clinical and genetic heterogeneity relates to the nature, severity, and evolution of cortical neuronal and neuropil damage remains unknown. Nonetheless, the findings of this pilot study using NODDI in ALS illustrate the potential for this technique to interrogate mechanisms of

cellular pathology of ALS in life, and paves the way for more extensive analyses of NODDI in ALS.

Clinical heterogeneity of the ALS participants in this study was considerable, which could explain why significant differences in more regions of the PCG were not detected. The topographical spread of disease pathology within the PCG in ALS is likely to have a more dispersed pattern of involvement, with higher variability between patients, when compared with the converging coherently bundled axons of the CST, the common output pathway of all cortical motor fibres. This makes it harder to reach statistical threshold on whole brain analysis, which may therefore only become apparent in much larger cohorts. Although statistically significant cortical GM changes in ODI and NDI were limited to a region within the right PCG, these abnormalities could be more relevant to the site and severity of disease. This notion is supported by the correlation between PCG ODI and disease duration which suggests an intimate link between PCG ALS pathology and progression over time. NODDI also detected discrete parameter alterations associated with bulbar involvement, King's stage of ALS, and cognitive impairment. Larger studies using more homogeneous ALS phenotypes would have the potential to detect statistically significant differences within the PCG on whole brain analysis and relate these with the clinical features of the disease.

In conclusion NODDI reveals evidence compatible with dendritic structural damage in the neuropil of the motor cortex in ALS, provides new insights into the cellular pathology of axonal damage, and demonstrates that reduced density of corticospinal axons is the main contributing factor underlying the altered diffusivity profile detected by DTI. Although the GM results were not as strong as those obtained in the WM, they nevertheless support the hypothesis that dendritic abnormalities parallel disease progression in ALS. More extensive longitudinal studies in larger phenotypically and genetically defined cohorts will be needed to refine our understanding of cortical microstructure alterations in ALS using NODDI and more sophisticated future developments of this technique.

**CHAPTER 4:  
QUANTITATIVE  
MAGNETIZATION  
TRANSFER IMAGING  
(QMTI) IN ALS**

## CHAPTER 4: QUANTITATIVE MAGNETIZATION TRANSFER IMAGING IN ALS

### 4.1 Background

The biological mechanisms underlying the instigation and sequential propagation of pathology within the motor system in ALS remains unknown and the exact pattern of disease spread remains subject to ongoing debate.<sup>13,34,36,201,283,284,289,551,552</sup> Nonetheless, imaging studies indicate consistent involvement of the CST and corpus callosum.<sup>16-18,339-342</sup> Post-mortem pathological studies of the brain and spinal cord in ALS patients often describe variable degrees of myelin damage.<sup>193,194,201</sup> Myelin loss in ALS is believed to be a secondary phenomenon to axonal loss, though rare reports of severe demyelination in the absence axon loss do exist.<sup>289</sup> Recent evidence suggests that myelin damage may have more of a central role in the pathogenesis of ALS, as oligodendrocyte dysfunction and subsequent demyelination could play an important role in the early stages of the degenerative process and accelerate disease progression.<sup>255,553-555</sup> Consequently, there has been a growing interest in exploring the degree and pattern of demyelination in ALS, and how this relates to axonal loss.<sup>555</sup>

Imaging techniques have emerged, which focus on quantifying myelin to allow for further exploration into this relationship. Magnetisation Transfer (MT) exploits the exchange of magnetization occurring between hydrogen protons in free water (liquid pool) and those bound to larger lipid-proteins such as myelin (semi-solid, solid, or macromolecular pool).<sup>556</sup> This system can be manipulated in order to indirectly measure the activity in the macromolecular pool of protons, within the tissue. In quantitative magnetisation transfer imaging (qMTi) a mathematical model is applied to describe the MT signal in relation to the off-resonance radiofrequency pulses that saturate the spins of the macromolecular proton pool. This enables specific assessment of myelin integrity and also detects changes in function related to molecular structure.<sup>465,466,479</sup>

QMTi has proved capable of producing parameters that are stable to sequence modification and specific to biological processes. These parameters are firstly, the restricted to free pool size ratio ( $F$ ), which has been shown to be a sensitive measure of myelin content in brain white matter.<sup>476</sup> Secondly, the forward exchange rate ( $k_f$ ) which is an estimate of magnetization transfer rate between free and bound pools and has been shown to correlate with inflammation and metabolic disturbance.<sup>556-558</sup> Thirdly, the transverse relaxation time of the free/liquid pool ( $T_{2f}$ ), which provides an assessment of water content and is a surrogate marker of atrophy. Whole brain analysis of the qMTi parameters was performed to assess for intracerebral molecular alterations, evaluate how these relate to the clinical features of the ALS group, and to explore for correlation with the NODDI parameters.

## 4.2 Hypotheses

As yet there are no studies of qMTi in ALS, however previous studies in Multiple Sclerosis (MS) have shown that acute, inflammatory, demyelinating, lesions demonstrate reduced  $F$  and  $k_f$ , accompanied by an increase in  $T_{2f}$ .<sup>477</sup> These parameter alterations return to normal over several months as the lesion evolves, suggesting qMTi is sensitive to the biological mechanisms underlying MS.

ALS and MS are clearly very different disease entities; however, both involve WM pathology and both have an immune component.<sup>253,559</sup> Therefore, although the mechanisms underlying these diseases are likely to be very different, it is conceivable that some insight can be gained into the molecular mechanisms underlying ALS by using qMTi.

Cerebral myelin loss within the CST, albeit by varying degrees, has been described in post-mortem studies of ALS.<sup>193,194,201,289</sup> This along with the known changes that occur within the WM '*in vivo*', as demonstrated by quantitative diffusion techniques such as DTI,<sup>16-18,339-342</sup> and NODDI,<sup>357</sup> make some degree of myelin changes likely in ALS. However, demyelination is not thought to be a central process and the pathogenesis of ALS is thought to focus on the axons.<sup>560</sup> I therefore hypothesized that within the WM tracts implicated in ALS, in particular the CST and CC, there would be a reduction in  $F$  to reflect loss of myelin. However, the extent of this was difficult to postulate.

I was keen to explore the molecular characteristics underlying the changes detected within both the WM and GM, demonstrated using NODDI.<sup>357</sup> The parameter of  $k_f$  was used to assess for biological changes within these areas, where a reduction was hypothesized to reflect the neurodegenerative changes occurring. In particular I hypothesized that reduced  $k_f$  would be detected in the CST, where reduced axon density was detected using NODDI,<sup>357</sup> reflecting molecular abnormalities associated with the underlying process driving pathological changes in ALS. I was also interested to see if reduced  $k_f$  would be detected in the motor cortex where the findings with NODDI were consistent with loss of dendritic complexity.

Lastly, in relation to the whole brain analysis of the qMTI parameters, as atrophy is a consistent feature of ALS I expected to detect an increase in  $T_{2f}$  in relation to the degenerative process affecting the motor regions.

The molecular basis of disease pathogenesis in ALS remains unknown and qMTi, which harnesses the behaviour of protons, may provide a more effective biological marker of pathology than quantitative diffusion imaging techniques. In particular qMTi parameters have been shown to be sensitive to the plasticity occurring in an MS lesion over time. This provides some hope that qMTi may be able to monitor the biological changes occurring in ALS and potentially be capable of differentiating between different



subtypes of ALS. I therefore used qMTi in the same way as NODDI and conducted whole brain comparison analyses of ALS subgroups, to assess for differences related to disease distribution, stage of ALS, and cognitive status. Based on the NODDI findings I hypothesized that there would be more extensive molecular changes in the group with both limb and bulbar involvement, in the higher King's stages of ALS, and in the group with cognitive impairment.

I performed a regression analysis, also repeating the same whole brain analyses used with NODDI, to explore whether the qMTi parameters relate to ALS disease duration, as well as the MRC, UMN, ALSFRS-R and ECAS scores. The hypothesis being that molecular changes found using qMTi would correlate particularly with disease duration, but possibly also the other markers of disease severity in ALS.

Finally, I conducted a further regression analysis to investigate whether changes in qMTi parameters would correlate with those detected using the NODDI indices. I hypothesised that the qMTi parameter of F would correlate with NDI from NODDI, which showed significant axonal loss in the CST, a region where associated myelin loss would also be anticipated. As a unique biological marker it was difficult to predict how  $k_f$  would relate to the NODDI parameters, but as NDI was most sensitive to the degenerative changes occurring in the ALS group, I hypothesised that  $k_f$  from qMTi might correlate with the NODDI parameter of NDI. Finally as both are surrogate markers of atrophy I hypothesised that the qMTi parameter of T2f would correlate with ISO from NODDI.

### **4.3 Magnetization Transfer Magnetic Resonance Imaging Acquisition**

Magnetization transfer imaging was incorporated into the same MRI sequence protocol as the diffusion weighted MRI, using the 1.5 tesla Siemens AVANTO scanner, see chapter 3.3. The balanced steady state free precession (bSSFP) method was used [Gloor et al]. The MRI sequence acquisitions relating to magnetization transfer comprised the following:

i) Quantitative (MT) sequence

Acquisition time 9 minutes

FoV = 240 x 180

Matrix = 256 x 96

32 slices

Slice thickness 5 mm

22 volumes (acquired by varying either the flip angle or the TR and pulse duration)

Flip angle varied between 5° and 40° and pulse duration between 0.2 and 2.5 ms, resulting in a range of TR from 3.66ms to 5.96ms.

- (ii) T1-weighted Map
  - Acquisition time 3 minutes
  - T1 mapping was performed by acquiring three 3D gradient echo volumes
  - Excitation flip angles 5°, 15°, and 25°
  - TE 5 ms, TR 30 ms
  - Slice thickness 5mm, 32 slices per slab
  - FoV = 240 x 240
  - Matrix = 256 x 96

#### **4.4 Quantitative Magnetization Transfer Imaging (qMTi) Processing**

The balanced steady-state free precession (bSSFP) method was used to extract qMTi data.<sup>479</sup> This approach involves varying TR, pulse duration and flip angle between 24 volumes and performing the Levenberg-Marquardt, voxel-wise, non-linear, least squares fitting approach to the binary spin bath model. It provides estimates of the fractional size of the restricted proton pool ( $F$ ), the forward magnetization transfer exchange rate ( $k_f$ ), and the relaxation time of the free proton pool ( $T_{2f}$ ).

T1 and qMTi parameter maps were generated using customized software written by the CISC physics team in the computer language C. A within-subject comparison was made for each qMTi parameter map using SPM12 running in Matlab 2012a.

Using SPM12, all parametric maps were normalised then three-dimensional Gaussian smoothing with full-width at half maximum of 6mm was performed.

When performing image quality checks in FSL, abnormalities were detected in the imaging data sets of six participants. This was possibly due to these participants moving their head in between the NODDI and the qMTi sequence acquisition, too much for registration to compensate. The imaging data of these six participants were therefore excluded, leaving 21 participants with ALS and 19 controls included in the subsequent qMTi analysis.

#### **4.5 Statistical analysis of the qMTi data**

##### **4.5.1 Whole brain voxel-wise analysis of qMTi Parameters**

Statistical analysis of the demographic data was performed using Statistical Package for the Social Sciences (SPSS IBM version 24 for Windows).

Voxel-wise comparisons of whole brain  $F$ ,  $k_f$ , and  $T_{2f}$  maps between ALS and control groups were performed using SPM12 within the framework of the general linear model. The results were accepted as significant where  $P < 0.05$  after family-wise error (FWE) correction at cluster level, where clusters were formed using  $P < 0.001$ . Participant age was used as a covariate. When no significant differences were detected a lower

statistical threshold of  $P < 0.005$  uncorrected was utilised to see if there were any changes almost reaching statistical significance. The rationale for performing whole brain qMTi parameter comparison is described in the qMTi hypotheses, section 4.2.

#### **4.5.2 Subgroup analysis using qMTi parameters**

Three sets of categorical clinical data were used to create ALS subgroups. Firstly, the clinical distribution of ALS was used to divide the ALS group into two subgroups; bulbar plus limb (11 participants) and limb confined (12 participants). These groups were compared with each other and the control group.

Secondly, the King's stage of ALS was used to create three subgroups for comparison; stage 1 (10 participants), stage 2 (8 participants), and stage 3 (five participants). Due to the stage 3 group being small this was additionally combined with the participants in stage 2, to create a group of 13 ALS participants with more than one region involved for further comparison. These groups were also compared with the control group.

Thirdly, two ALS groups were created using the ECAS; one with normal ECAS scores (11 participants) and the other with abnormal scores in more than one domain (10 participants). The latter group included all the ALS participants classified as ALS-FTSD. These groups were compared with one another and the control group.

Voxel-wise whole brain analysis of  $F$ ,  $k_f$  and  $T_{2f}$  maps between the control and ALS subgroups were performed using the SPM12 general linear model. The results were accepted as significant where  $P < 0.05$  after family-wise error (FWE) correction at cluster level, where clusters were formed using  $P < 0.001$ . Participant age was used as a covariate. The rationale for conducting whole brain qMTi parameter subgroup comparison is given in the qMTi hypotheses, section 4.2.

#### **4.5.3 Correlation analysis of qMTi parameters with clinical measures of ALS**

The qMTi parameters of the ALS group were analysed for correlation with the continuous clinical variables of disease severity including disease duration, MRC composite muscle power score, UMN composite score, the ALSFRS-R score, the rate of change in ALSFRS-R, and the ECAS score. I used the linear model framework within SPM12, with age included as a covariate, and accepted correlations as significant if  $P < 0.05$  after FWE correction at cluster level, clusters formed with  $P < 0.001$ . I provided the rationale for performing whole brain qMTi parameter correlation with the ALS clinical variables in the qMTi hypotheses, section 4.2.

#### 4.5.4 Correlation of qMTi parameters with NODDI indices

The qMTi parameters of the ALS group were also analysed for correlation with the NODDI parameters. I used the linear model framework within SPM12, including age as a covariate, with the statistical significance threshold of  $P < 0.05$  after FWE correction at cluster level, clusters formed with  $P < 0.001$ . The rationale for conducting regression analysis between the qMTi and NODDI parameters is given in the qMTi hypotheses, section 4.2.

#### 4.6 QMTi parameter whole brain comparison of ALS and control groups

The ALS group demonstrated areas of significantly reduced  $k_f$ , compared to the control group. These regions were detected in cerebral white matter of the corona radiata on the left ( $P < 0.001$ ) and to a lesser extent on the right ( $P = 0.015$ ). A third cluster of significantly reduced  $k_f$  was demonstrated in the left cingulate gyrus ( $P = 0.007$ ), see figure 4.1 and table 4.1.

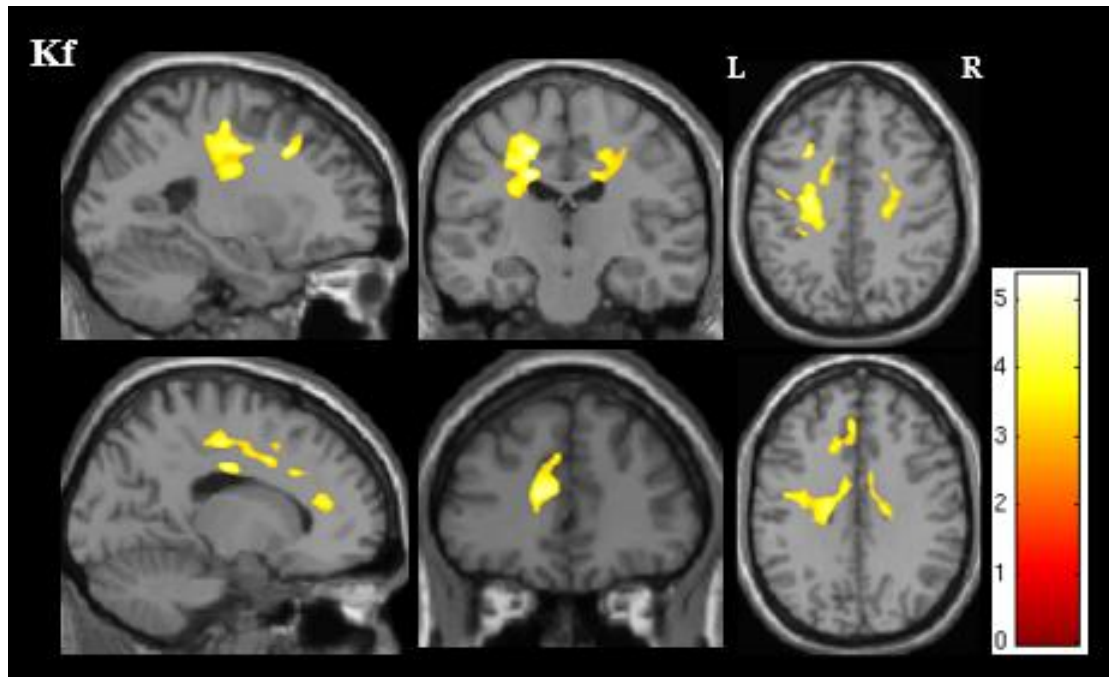
Whole brain voxel-wise analysis for differences in  $F$  and  $T_{2f}$  failed to reach the stated statistical threshold. Differences in these parameters only became apparent at less stringent statistical threshold. A reduction in the parameter reflecting myelin content,  $F$ , was detected in the right medulla of the ALS group ( $P = 0.002$  uncorrected). While an increase in  $T_{2f}$  was detected bilaterally on the frontal cortex and within the right lateral ventricle (all  $P = 0.001$  uncorrected), see figure 4.2 and table 4.2.

**Table 4.1: Regions of significant differences in qMTi parameter  $k_f$  between ALS and control groups.**

	Contiguous anatomical regions within cluster	MNI co-ordinate (x, y, z)	t-value	K (size)	$P_{\text{cluster level FWE-corr}}$
$k_f$ ALS < CTL	Left cerebral white matter, corona radiata Left superior frontal gyrus	-18 -19 47	5.44	10192	<0.001
		-18 -17 34	5.37		
		-25 18 38	4.96		
	Left cerebral white matter Left cerebral cortex, cingulate gyrus, paracingulate gyrus	-12 37 16	4.89	2445	0.007
		-6 23 36	4.15		
		-4 53 19	4.13		
	Right cerebral white matter, corona radiata Right cerebral cortex, PCG	20 -20 44	4.15	2110	0.015
		17 -18 34	3.99		
		15 27 50	3.66		

A table to show the anatomical regions where significant changes were demonstrated on whole brain analysis in forward magnetization exchange rate ( $k_f$ ). A statistical threshold of  $P < 0.05$  family-wise error (FWE) correction at cluster level ( $P_{\text{cluster}}$ ) was used, after clusters were formed with an uncorrected  $P < 0.001$ . Montreal Neurological Institute (MNI) co-ordinates were used to define the anatomical location of each cluster. The MNI coordinates refer to the peak t-value. Local maxima that are more than 8mm apart are shown for each cluster. K indicates the size of the cluster in voxels. Abbreviations:  $k_f$ , forward magnetization exchange rate; MNI, Montreal Neurological Institute; FWE, family-wise error.

**Figure 4.1: Areas of significant difference between the ALS and control groups on whole brain analysis of forward magnetization exchange rate ( $k_f$ ).**



Areas of significant difference between ALS and control groups in the qMTi parameter of  $k_f$ . Results are shown using a statistical significance of  $P < 0.05$  after FWE correction at cluster level, clusters formed with  $P < 0.001$ .

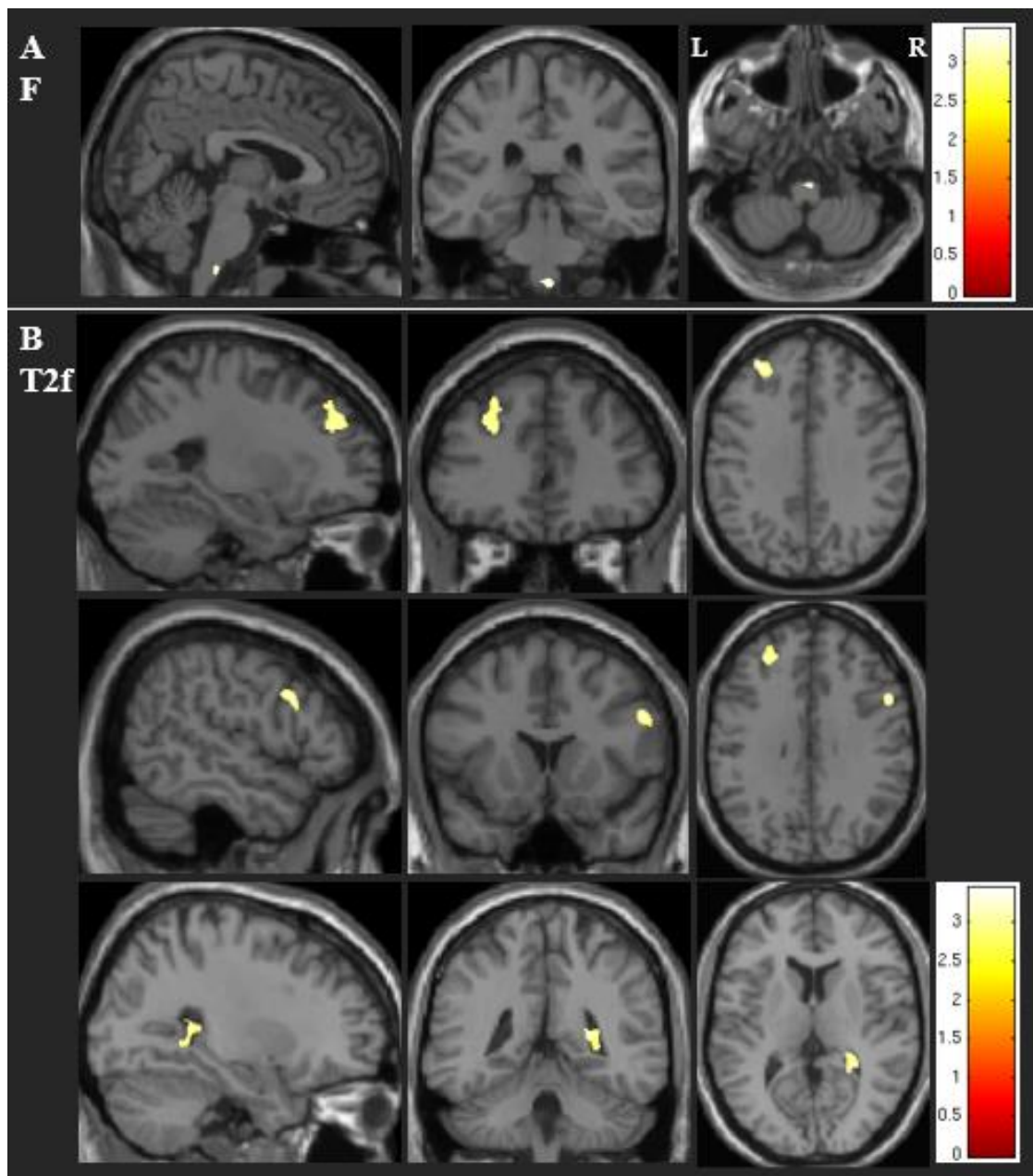
**Table 4.2: Regions of differences in qMTi parameters F and  $T_{2f}$  between ALS and control groups at a less stringent statistical threshold.**

	Contiguous anatomical regions within cluster	MNI co-ordinate (x, y, z)	t-value	K (size)	$P_{\text{uncorr}}$
F ALS<CTL	Right brainstem, medulla	5 -51 -35	3.05	106	0.002
$T_{2f}$ ALS>CTL	Left cerebral cortex frontal lobe, superior frontal gyrus, middle frontal gyrus	-31 45 35	3.18	1006	0.001
		-23 40 29	3.15		
		-24 38 42	3.10		
	Right lateral ventricle	33 -48 0	3.44	812	0.001
		27 -43 10	3.23		
		18 -35 12	2.93		
	Right cerebral cortex, inferior frontal gyrus, precentral gyrus	55 18 25	3.25	366	0.001
		53 13 31	3.18		

A table to show the anatomical regions where changes were demonstrated on whole brain analysis in fractional size of the restricted pool (F) and relaxation time of the free pool ( $T_{2f}$ ). A statistical significance threshold of  $P < 0.005$  uncorrected at cluster level was used. Montreal Neurological Institute (MNI) co-ordinates were used to define the anatomical location of each cluster of voxels within the MRI volume. The MNI coordinates refer to the peak t-value. Local maxima that are more than 8mm apart are shown for each cluster. K indicates the size of the cluster in voxels.

Abbreviations: F, fractional size of the restricted pool;  $T_{2f}$ , relaxation time of the free pool; MNI, Montreal Neurological Institute; Uncorr, uncorrected.

**Figure 4.2: Whole brain analysis showing reduced F and increased  $T_{2f}$  in the ALS group at a less stringent statistical threshold.**



Areas of difference between ALS and control groups in the qMTi parameters at a less stringent statistical threshold of  $P < 0.005$  uncorrected.

(A) Fractional size of the restricted pool (F)

(B) Relaxation time of the free pool ( $T_{2f}$ )

## 4.7 QMTi parameter subgroup analysis results

### 4.7.1 Distribution of ALS

The only qMTi parameter to detect any differences relating to the distribution of ALS was  $k_f$ , see figure 4.3A and table 4.3. However, the significant difference was only detected when comparing the bulbar plus limb group with the control group ( $P < 0.001$ ). No differences in  $k_f$  were detected when comparing the limb only ALS group with the bulbar

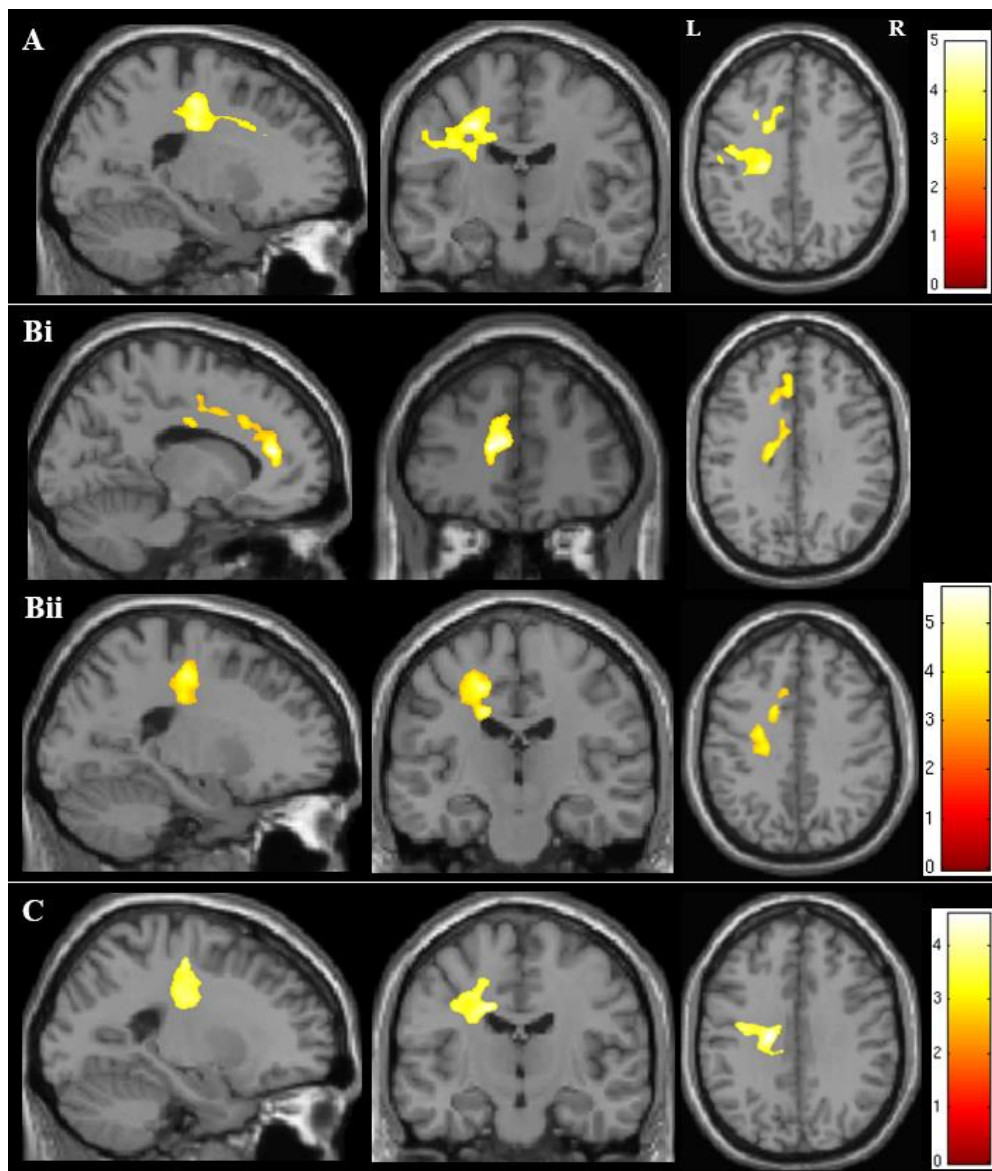
and limb subgroup or the control group. No significant differences were found in  $F$  or  $T_{2f}$  when comparing these groups.

**Table 4.3: Regions of significantly reduced  $k_f$  on subgroup comparison using whole brain analysis.**

	Contiguous anatomical regions within cluster	MNI co-ordinate (x, y, z)	t-value	K (size)	$P_{\text{cluster level FWE-corr}}$
Control > Bulbar and limb ALS group	Left cerebral white matter, corona radiata	-25 -10 40	4.98	9636	<0.001
		-18 -19 35	4.73		
	Left cerebral cortex, precentral gyrus	-45 -7 30	4.73		
Control > Kings Stage 2+3 ALS group	Left cerebral white matter, corona radiata	-12 38 16	5.71	4373	0.011
	Left cerebral cortex, cingulate gyrus and paracingulate gyrus	-9 39 26 -6 23 36	4.25 4.11		
	Left cerebral white matter, corona radiata, posterior cingulate gyrus	-18 -18 47 -17 -17 34 -25 -13 32	5.01 4.94 4.32	4289	0.015
Control > Normal ECAS	Left cerebral white matter, corona radiata	-18 -17 34	4.57	4957	0.005
		-18 -19 48	4.33		
		-36 -12 35	3.74		

A table to show the anatomical regions where significant changes were demonstrated, on whole brain analysis of the subgroups, in forward magnetization exchange rate ( $k_f$ ). A statistical significance threshold of  $P < 0.05$  family-wise error (FWE) correction at cluster level ( $P_{\text{cluster}}$ ) was used, after clusters were formed with an uncorrected  $P < 0.001$ . Montreal Neurological Institute (MNI) co-ordinates were used to define the anatomical location of each cluster of voxels within the MRI volume. The MNI coordinates refer to the peak t-value. Local maxima that are more than 8mm apart are shown for each cluster. K indicates the size of the cluster in voxels. Abbreviations: MNI, Montreal Neurological Institute; FWE, family-wise error.

**Figure 4.3: Whole brain analysis demonstrates regions of significantly reduced  $k_f$  on subgroup comparison.**



A figure to show the regions of significantly reduced  $k_f$  demonstrated on subgroup analysis of qMTi parameters. Results are shown using a statistical significance of  $P < 0.05$  after FWE correction at cluster level, clusters formed with  $P < 0.001$ .

(A)  $k_f$ : Control > Bulbar plus limb ALS group

(B)  $k_f$ : Control > Kings Stage 2+3 ALS group

(C)  $k_f$ : Control > Normal ECAS

#### 4.7.2 Kings Stages of ALS

When comparing the King's stages of ALS subgroups with each other and the control group, the only statistically significant difference found on whole brain analysis was between the combined King's stage 2 and 3 subgroup and the control group. This showed two areas of significantly reduced  $k_f$ . The more anterior area within the left cerebral white matter, involving the cingulate gyrus ( $P = 0.011$ ), see figure 4.3Bi and table



4.3. The other more posterior within the left cerebral white matter of the corona radiate ( $P=0.015$ ), see table 4.3 and figure 4.3Bii.

No other significant differences in  $k_f$  were detected between ALS subgroups based on King's stage. No significant differences were found in  $F$  or  $T_{2f}$  when comparing King's stages of ALS subgroups with each other or the control group.

#### 4.7.3 Cognitive Involvement

Whole brain analysis demonstrated significantly reduced  $k_f$  in the left corona radiate when comparing the normal ECAS ALS subgroup with the control group ( $P=0.005$ ), see figure 4.3C and table 4.3. There were no significant differences detected in  $k_f$  between the normal ECAS and abnormal ECAS subgroups.

No significant differences were detected in  $F$  or  $T_{2f}$  when comparing the ECAS subgroups with one another and the control group.

#### 4.8 Correlation between QMTi data and clinical parameter results

Despite not finding any significant differences in  $F$  between ALS and control groups, two significant correlations were detected between  $F$  and clinical measures of ALS severity, see table 4.4 and figure 4.4.

**Table 4.4 Regions of significant correlation between qMTi parameters and clinical measures of ALS severity.**

	Contiguous anatomical regions within cluster	MNI co-ordinate (x, y, z)	t-value	K (size)	$P_{\text{cluster level FWE-corr}}$
F negative correlation with ALSFRS-R	Ventromedial prefrontal cortex	9 48 -20 1 44 -19 -7 42 -15	7.33 6.86 6.51	6943	<0.001
F negative correlation with MRC power score	Ventromedial prefrontal cortex	8 44 -17 3 28 -8 -4 45 15	5.66 5.08 4.83	4116	0.013
$k_f$ positive correlation with ALSFRS-R	Right corona radiata, cingulate cortex, and precentral gyrus	22 -10 45 15 -34 53 24 -16 52	4.85 4.40 4.27	4113	0.007

A table to show the anatomical regions where significant correlation was demonstrated, on whole brain analysis of the ALS group with clinical measures of disease severity. A statistical significance threshold of  $P<0.05$  family-wise error (FWE) correction at cluster level ( $P_{\text{cluster}}$ ) was used, after clusters were formed with an uncorrected  $P<0.001$ . Montreal Neurological Institute (MNI) co-ordinates were used to define the anatomical location of each cluster of voxels within the MRI volume. The MNI coordinates refer to the peak t-value. Local maxima that are more than 8mm apart are shown for each cluster. K indicates the size of the cluster in voxels.

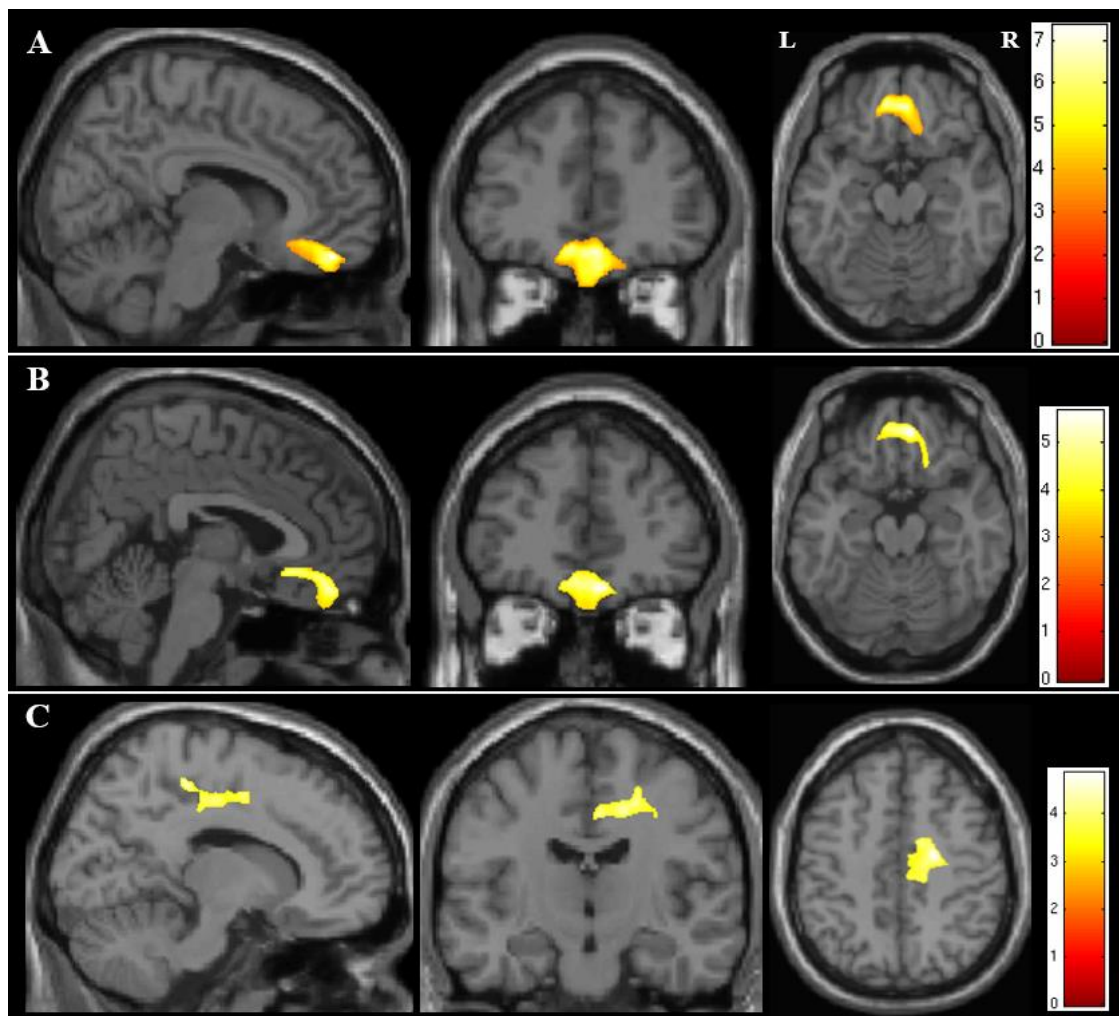
Abbreviations:  $F$ , fractional size of the restricted pool;  $k_f$ , forward magnetization exchange rate; MNI, Montreal Neurological Institute; FWE, family-wise error; corr, corrected.

A negative correlation was found between F and ALSFRS-R within the orbitofrontal cortex ( $P < 0.001$ ), see figure 4.4A and table 4.4. A further negative correlation was also found between F and MRC score, also within the orbitofrontal cortex ( $P = 0.013$ ), see figure 4.4B and table 4.4.

An area of positive correlation was also found in the right cerebral white matter of the corona radiata and cingulate gyrus, between  $k_f$  and ALSFRS-R ( $P = 0.007$ ), see figure 4.4C and table 4.4.

No further correlations were found between the qMTi parameters and the clinical measures of ALS disease severity.

**Figure 4.4: Correlation between qMTi data and clinical parameters on whole brain analysis of the ALS group.**



Areas of significant correlation between the qMTi parameters and clinical measures of ALS disease severity. Results are shown using a statistical significance of  $P < 0.05$  after FWE correction at cluster level, clusters formed with  $P < 0.001$ .

(A) Area of negative correlation between F and ALSFRS-R.

(B) Area of negative correlation between F and MRC power score.

(C) Area of positive correlation between  $k_f$  and ALSFRS-R.

**Table 4.5: Regions of correlation between qMTi and NODDI parameters on whole brain analysis of the ALS group.**

	Contiguous anatomical regions within cluster	MNI co-ordinate (x, y, z)	t-value	K (size)	$P_{\text{uncorr}}$
$k_f$ positive correlation with mean NDI of the cerebral white matter	Left cerebral white matter, corpus callosum, corona radiata	-16 28 10 -18 13 23 -19 20 17	4.46	1864	0.003
	Right cerebral white matter, corpus callosum, corona radiata	15 9 26 15 20 21 19 24 15	5.21	1603	0.005
$T_{2f}$ positive correlation with mean ISO of the corpus callosum	Right cerebral cortex, post central gyrus	30 -38 61 33 -28 65 36 -37 54	5.30	3142	0.001
	Left cerebral cortex, post central gyrus	-51 -28 47 -45 -30 41 -44 -51 50	5.27	3028	0.001
$T_{2f}$ positive correlation with mean ISO of the ventricles	Left lateral ventricle	-21 -43 17 -12 -33 17 -26 -53 9	4.81	2788	0.002

A table to show the anatomical regions where correlation was demonstrated on whole brain analysis between qMTi and NODDI parameters. A statistical significance threshold of  $P < 0.005$  uncorrected at cluster level was used. Montreal Neurological Institute (MNI) co-ordinates were used to define the anatomical location of each cluster of voxels within the MRI volume. The MNI coordinates refer to the peak t-value. Local maxima that are more than 8mm apart are shown for each cluster. K indicates the size of the cluster in voxels.

Abbreviations: F, fractional size of the restricted pool;  $k_f$ , forward magnetization exchange rate;  $T_{2f}$ , relaxation time of the free pool; NDI, Neurite Density Index; ISO, isotropic compartment; MNI, Montreal Neurological Institute; Uncorr, uncorrected.

#### 4.9 Correlation between NODDI and qMTi parameter results

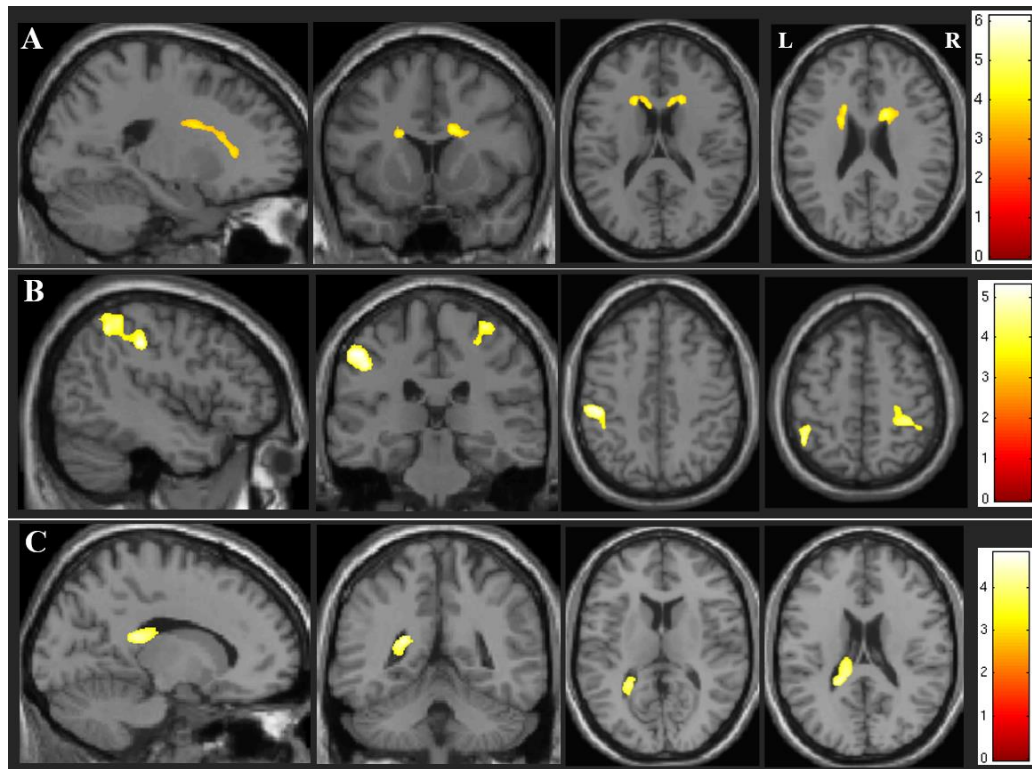
There were no statistically significant correlations between the qMTi and NODDI parameters at the stringent statistical threshold of  $P < 0.05$ , when corrected for family-wise error. At a threshold of  $P < 0.005$  uncorrected three correlations became apparent.

A positive correlation was found between  $k_f$  and the mean cerebral white matter NDI, within the white matter of the callosal genu and adjacent corona radiata on the left ( $P = 0.003$ ) and right ( $P = 0.005$ ), see figure 4.5A and table 4.5.

A positive correlation was detected between  $T_{2f}$  and mean ISO of the corpus callosum, within the cortical white matter of the post-central gyrus bilaterally ( $P = 0.001$ ), see figure 4.5B and table 4.5.

Finally, a positive correlation was found between  $T_{2f}$  and mean ISO of the ventricles, within the left lateral ventricle ( $P = 0.002$ ), see figure 4.5C and table 4.5.

**Figure 4.5 Correlation between qMTi and NODDI in the ALS group at a less stringent statistical threshold.**



A figure to show the regions where correlation was detected on whole brain analysis between qMTi and NODDI parameters at a less stringent statistical threshold of  $p < 0.005$  uncorrected. (A) Areas of positive correlation between  $k_f$  and mean NDI of the cerebral white matter. (B) Area of positive correlation between  $T_{2f}$  and mean ISO of the corpus callosum. (C) Area of positive correlation between  $T_{2f}$  and mean ISO of the ventricles.

#### 4.10: QMTi in ALS discussion

QMTi is an emerging MRI modality that has the potential to broaden our understanding of the processes underlying neurological disorders such as ALS, by providing distinct parameters that reflect biologically relevant tissue alterations within the brain.

It was applied to ALS in this study in order to gain insight into the contribution of specific biological processes, such as myelin loss and inflammatory processes, to the neurodegenerative process occurring in ALS '*in vivo*'.

The main discovery using qMTi in ALS is that there is relative preservation of myelin, which suggests that demyelination is likely to be a secondary process following axonal degeneration. Another interesting finding was a significant reduction in  $k_f$  within the white matter of the CST and corpus callosum, which is consistent with a change in the molecular integrity and supports axonal dysfunction in these regions occurring in ALS, possibly as a result of neuro-inflammation. The same parameter,  $k_f$ , was the only qMTi parameter to demonstrate any statistically significant differences between control and ALS subgroups according to disease distribution, King's stage, and cognitive profile. In addition,  $k_f$  correlated with ALSFRS-R on regression analysis. This suggests that  $k_f$  is

the qMTi parameter with the highest propensity to detect biological alterations occurring in ALS, and therefore offers the most potential to provide insight into the mechanisms underlying neurodegeneration.

#### **4.10.1: Axonal dysfunction in ALS**

Previous studies using quantitative MRI techniques, in particular DTI, have consistently shown degeneration of motor tracts comprising the CST and corpus callosum.<sup>339-342</sup> The altered diffusivity pattern demonstrated using DTI has recently been confirmed as axonal loss by NODDI, an emerging imaging technique which estimates the density and fanning of neurites.<sup>357</sup>

In this study using qMTI the parameter of  $k_f$  was used to explore whether molecular changes relate to the neurodegenerative process underlying ALS. Whole brain comparison analysis demonstrated regions within the cerebral WM bilaterally where statistically significant reduction in the magnetization exchanged rate ( $k_f$ ) was detected. In the left cerebral hemisphere these included the corona radiata ( $P<0.001$ ), and a region of the cingulate gyrus extending into the corpus callosum ( $P=0.007$ ). While a smaller region was detected in the right corona radiata ( $P=0.015$ ) extending into the subcortical WM of the right precentral gyrus, see figure 4.1.

These findings are in keeping with my hypothesis that the molecular integrity within the rostral CST axons is compromised in ALS, which suggests that axonal dysfunction is occurring in this region alongside neurodegeneration. This detected alteration in molecular composition is likely to reflect a change in the normal biological processes within these axonal regions or in the local cellular environment. It is difficult to determine the exact nature of this alteration but possibilities include neuro-inflammatory processes and the pathological accumulation of intra-axonal aggregated protein such as ubiquitin and the RNA-binding protein TDP-43.<sup>561,562</sup>

Neuroinflammation in ALS has been the focus of many studies using a variety of different approaches.<sup>563</sup> Studies using PET have demonstrated activation of microglia within the cerebral motor and frontal regions.<sup>185,258</sup> Microglial cells are typically in a dormant state within the cerebral GM. They become activated in response to tissue damage, transform into brain macrophages, and mediate inflammatory responses such as production of cytokines.<sup>563,564</sup> Interestingly high cytokine levels can be detected in the CSF and peripheral blood of patients with ALS, likely reflecting a systemic pro-inflammatory state.<sup>565-569</sup> Persistent microglial activation can become pathological and contribute to neurodegeneration, which is a logical reason why microglial activation is implicated in the pathogenesis of ALS<sup>254,570</sup> In addition, activated microglia can contribute to reactive astrocytosis.<sup>571</sup> Astrocytes are abundant cells of the CNS and perform important homeostatic functions such as promoting neuronal survival and

synaptogenesis.<sup>572</sup> Activated astrocytes release acute phase reactants, complement, and proteinases, leading to neurotoxicity.<sup>264,573–575</sup> Pathological studies have demonstrated reactive astrocytosis in the brain,<sup>254,576,577</sup> and spinal cord,<sup>254,578</sup> of patients with ALS. In addition, reactive astrocytes have been shown to increase axonal and cytoplasmic inclusions of aggregated proteins characteristic of ALS in a culture model of human motor neurones.<sup>579</sup> The relentless propagation of aggregated insoluble proteins, in a prion-like manner,<sup>216,217</sup> manner, forms the basis for one of the postulated spreading mechanisms of pathogenesis in ALS.

The role of oligodendroglia, which myelinate and provide metabolic support to CNS axons, has also been postulated in the pathogenesis of ALS.<sup>580–582</sup> Oligodendrocyte abnormalities have been reported in several post mortem studies in both human and animal models of ALS.<sup>582–585</sup> Furthermore, aberrant cytoplasmic TDP-43 has been demonstrated in oligodendrocytes.<sup>582</sup> Increased turnover of oligodendrocytes has been demonstrated in ALS, which is associated with oligodendrocyte dysfunction, dysmorphism, and premature apoptosis.<sup>582</sup> The loss of supportive role played by oligodendrocytes is likely to contribute to the loss of vulnerable motor neurones. This so-called non-cell autonomous toxicity is likely to play a role in most neurodegenerative diseases.<sup>586</sup>

Gliosis is the term used to describe the activation of the glial cell lines, microglia, astrocytes, and oligodendrocytes, and is likely to contribute to the disease pathogenesis in ALS as well as other neurodegenerative diseases.<sup>260,262</sup> Once triggered, gliosis leads to altered cellular and molecular function and has the potential to cause widespread detrimental effects, either by loss of normal cellular function or gain of toxic function.<sup>261</sup> Therefore, it is likely that glial cells are not innocent bystanders but actively participate in the pathological disease process underlying ALS. The causes of ALS are likely to be multifactorial and the biological mechanism complex. Nonetheless glial cells provide a rational therapeutic target for impeding CNS damage in ALS.

A further characterizing feature of the neuroinflammatory process associated with ALS is the infiltration of lymphocytes, which have been demonstrated in pathological studies of the brain and spinal cord in ALS patients<sup>254,570,587–589</sup> Regulatory CD4<sup>+</sup>-T lymphocytes (Tregs) play a vital role in modulating the immunological response, enhancing the neuroprotective effects and limiting the detrimental capacity of microglia and astrocytes.<sup>250,263,590</sup> A reduction in Tregs, in the blood of patients has been associated with rapidly progressive ALS<sup>591</sup> and numbers of Tregs have been shown to inversely correlate with both rate of progression and severity of disease in ALS.<sup>591–593</sup> When compared to healthy controls, Tregs from patients with ALS were shown to be dysfunctional with reduced suppressive capacity.<sup>593</sup> Interestingly in the same study they found that the dysfunctional Tregs from ALS patients could regain normal function when

removed from their environment and expanded in vitro. As a result, a phase 1 study was conducted using an infusion of expanded autologous Tregs in patients with ALS, which reportedly lead to slowing of progression rates and was deemed safe.<sup>594</sup> IL-2 upregulates Tregs and thereby plays an important role in the regulation of neuroinflammation. A further phase II clinical trial, MIROCALS (Modifying Immune Response and Outcomes in ALS), is currently taking place in the UK and France to assess the safety and efficacy of IL-2 in ALS.

Finally, an important component of the innate immune system, the complement cascade, is likely to augment the immune response from resident glial cells and thereby potentially contribute to chronic inflammation in ALS neurodegeneration.<sup>595,596</sup> Increased levels of C1q, C3, C4, C5a, C5b, and the MAC (membrane attack complex) have been demonstrated in the blood, CSF, brain and muscle tissue of ALS participants compared to controls.<sup>597-600</sup>

To my knowledge, this is the first study investigating qMTi changes associated with ALS. However, the transfer of magnetization can be used to gain two less sophisticated parameters: MTC and MTR.<sup>467-473,486,487</sup> MTC is a qualitative measure used in contrast-enhanced T1-weighted MRI sequences, and has previously shown hyperintensity within the CST<sup>487</sup> and CC<sup>486</sup> in a proportion of patients with ALS. These findings are similar but more extensive when compared to the changes detected in  $k_f$ , and support tissue alteration in these regions that can be detected as T1 MTC shortening using magnetization transfer. The MTR quantifies the difference between the MRI signal measured with and without the off-resonance saturation pulse. A reduced MTR has previously been reported not only in the CST,<sup>772</sup> but also in the PCG and extra-motors regions,<sup>470</sup> in patients with ALS compared with healthy controls. These are likely to reflect an alteration in tissue such as loss of structural integrity.

I did not find any statistically significant changes in  $k_f$  within the motor cortex on whole brain analysis. This could indicate that the most significant changes in molecular integrity are occurring in the rostral CST and subcortical WM of the motor axons, which may also therefore be the most consistent focus of inflammation. The lack of statistically significant results in the motor cortex may also be due to the anatomical differences between the GM and WM, where changes in the GM are more difficult to detect due to heterogeneity of disease pathology.

I performed the same set of comparisons and correlations with qMTi that I did using NODDI, to see if there were any differences related to disease distribution, stage of ALS, and cognitive status. Based on the NODDI findings I hypothesized that there would be more extensive molecular changes in the group with both limb and bulbar involvement, in the higher King's stages of ALS, and in the group with cognitive impairment. However, the qMTi parameter of  $k_f$  did not differentiate between these

subgroups and only demonstrated significant difference when comparing certain subgroups to the control group. This confirms that the NODDI and qMTi techniques are indeed measuring different components within the tissue alterations, but also suggests that the NODDI parameter of NDI is more sensitive at detecting microstructural changes associated with ALS.

Interestingly when evaluating the subgroup analysis of qMTi, the significant difference between the control group and the ALS subgroup with both limb and bulbar involvement was detected only in the left corona radiata, see figure 4.3A, while the difference comparing the whole ALS group with the control group was similar but bilateral (figure 4.1). This suggests that the bilateral changes detected in  $k_f$  have a contribution from those with earlier more localized disease pathology. A notion supported by similar findings when comparing the control group with the Kings stages 2 and 3 combined, whereby again the significant reduction in  $k_f$  was unilateral, see figure 4.3B. This again raises the possibility that a significant contribution to the  $k_f$  changes, particularly in the right hemisphere is coming from the ALS subgroup in the earliest stage of the disease's clinical manifestation, King's stage 1. Finally, significantly reduced  $k_f$  within the left corona radiata was only seen when comparing the control group with the ALS subgroup with normal ECAS. No significant difference was demonstrated between the normal ECAS subgroup and the subgroup with ALS-FTSD or the control group and the ALS-FTSD subgroup, suggesting that the changes being detected by  $k_f$  do not relate to cognitive decline in ALS. Overall the subgroup analysis of the qMTi findings suggest that  $k_f$  is detecting something that does not equate to the most advanced disease state clinically and may instead be distinguishing between different biological profiles underlying the clinical phenotypes of ALS.

In the regression analysis of the qMTi parameters with clinical measures of ALS severity,  $k_f$  correlated with ALSFRS-R in the right cerebral WM, in a region involving the right centrum semiovale as well as the right cingulate cortex, figure 4.4C. This reinforces the finding that there are changes relating to  $k_f$  in the right hemisphere in the ALS cohort, as seen on whole brain comparison with the control groups, and also suggests these changes are more intimately linked to disease status. It also raises the possibility that  $k_f$  is the qMTi parameter with the highest propensity to detect biological alterations occurring in ALS, and therefore offers the most potential to provide insight into the mechanisms underlying the neurodegenerative process accompanying ALS. However,  $k_f$  did not correlate with disease duration or rate of progression, possibly because the ALS cohort was too small and heterogeneous.

When assessing for correlation between qMTI and NODDI parameters, no correlations were strong enough to reach the statistical significance at  $P < 0.05$  with FWE correction. However, at a lower, uncorrected, statistical threshold there was a positive



correlation between  $k_f$ , within the corpus callosum and corona radiata bilaterally, and mean NDI of the cerebral white matter. This suggests that the changes identified using  $k_f$  relate to the axonal degeneration detected using the NODDI parameter of NDI, which supports the hypothesis that the changes detected by these different imaging modalities would correlate. Furthermore, it raises the possibility that inflammation within the rostral corona radiata contributes to the axonal dysfunction and degeneration occurring in ALS.

It is likely that the inflammatory responses occurring within the brain contribute to the neurodegenerative process underlying ALS, and may be a factor in governing the rate at which the disease progresses. It is well known that the rate of disease progression, measured clinically by the change in ALSFRS-R over time, varies considerably between individuals and that the duration of disease ranges from months to years.<sup>1-9,601</sup> Those with faster decline, the so-called fast progressors, may have a more cytotoxic immune response, which drives more cells through the apoptotic pathway. While slow progressors may have more of a protective immune response to the pathophysiological process occurring in ALS.<sup>570-578</sup>

The ALS participants in this study varied considerably in all markers of ALS disease severity, including rate of progression, and were likely a heterogeneous group with respect to the underlying molecular and biological profiles. It is possible that there was a subset within the cohort of ALS participants who had higher levels of inflammation occurring, predominantly in the corona radiata, leading to the demonstrated difference in  $k_f$  between the ALS and control groups. This subset of ALS are most likely to benefit from treatments that control the immune response. Although the development and progression of ALS is likely to be multifactorial and unique to the individual, pharmacological treatments and stem cells therapies targeted at manipulating the immunological environment have potential to promote survival of motor neurons in the ALS.<sup>602</sup>

#### **4.10.2: Demyelination in ALS**

A significant reduction in myelin was expected to be found within the major motor axonal pathways of the brain known to be involved in ALS, namely the CST and corpus callosum. This expectation was based on the findings from post mortem studies in ALS, where there is typically pyramidal tract demyelination<sup>193,197</sup> However, whole brain voxel wise comparison analysis using  $P < 0.05$  after family-wise error correction at cluster level failed to detect a statistically significant reduction in F, the qMTi parameter reflecting myelin content, within the cohort of ALS participants compared with healthy controls.

A reduction in F was only detected with a less stringent statistical threshold of  $P < 0.005$  uncorrected, and was restricted to the right medulla, see figure 4.2A. This finding could suggest that in the ALS cohort there was a statistical trend towards loss of

myelin in this region of the brainstem, accompanied by a relative sparing of myelin elsewhere within the cerebral motor axons. However, it is important to consider the validity of this finding, as the cluster is small and the medulla is particularly susceptible to registration errors during automated data processing. Demyelination is consistently reported in post-mortem studies of ALS.<sup>193-196</sup> However, these findings represent an end stage of the disease, observed in fixed tissue preparations, and may not be truly illustrative of the changes occurring in the living brain of patients with ALS.

Imaging studies focused on assessing myelin in ALS are sparse. One study using an MRI sequence called multi-component Driven Equilibrium Single Observation of T1 and T2 (mcDESPOT) used to measure myelin content, similarly found no difference between ALS and control groups.<sup>603</sup> However, patients with PLS showed widespread cerebral myelin loss compared to the control group. Furthermore, in the same study a significant correlation was shown between ALS myelin content within frontal lobe regions and cognitive performance. These findings suggest that myelin loss is occurring in ALS to some extent, and that cerebral demyelination is more likely to be detected in those with cognitive decline and upper motor neuron predominant disease.

However, my results suggest that demyelination is not a core feature of ALS '*in vivo*' and could instead be a secondary phenomenon occurring later in the degenerative process. This raises the possibility of axonal degeneration occurring in ALS without concurrent myelin loss, as well as the potential for independent pathological mechanisms affecting the motor axon and the associated myelin. Axonal degeneration leaving a myelin sheath scaffold is a novel concept in ALS and is purely speculative. Axonal loss occurring without demyelination is possible as it has been shown to occur in multiple sclerosis, particularly in normal appearing white matter lesions.<sup>605,606</sup> Although they form a symbiotic unit with the axon, the myelinating oligodendrocytes properties are largely driven intrinsically and are only modulated by axonal electrical activity and signalling molecules. It is therefore conceivable for myelin to remain for some time despite a degenerative axonopathy.

A lack of statistically significant demyelination being detected in my ALS cohort may be due to pathological heterogeneity within the dispersed cerebral CST axons. Furthermore, this could explain why, albeit at a lower statistical threshold, myelin loss was only detected in the convergent motor axons of the medullary pyramids. However, another important consideration is the difference in the sensitivity of the MRI techniques used in this study. NODDI appears to have a relatively high sensitivity, while qMTi appears to be a less sensitive technique, which could be a contributing factor in not detecting significant changes in F at the specified statistical threshold.

Alternatively, this finding may indicate that the caudal corticospinal fibers are at a more advanced stage of degeneration than those within the rostral component. This

could be interpreted as consistent with the 'dying back' hypothesis of ALS, which proposes that neurodegeneration emerges in the spinal cord motor axons and subsequently spreads rostrally.<sup>286-288</sup> However, in reality it is more conceivable that the focus of ALS pathology onset in the individual is anatomically and biologically unique, and therefore highly inconsistent within large populations of people with ALS. This is in keeping with post-mortem studies in ALS, where myelin damage is variable,<sup>194-197,201</sup> and with imaging studies where quantitative applications to diffusion weighted sequences are typically required to find statistically significant differences in a group of ALS participants compared with healthy controls.<sup>339-342</sup> Larger studies using qMTi in more homogenous groups of ALS participants, to assess for changes in myelin from the origin of the CST in the PCG down into the cervical spinal cord, would be required to further investigate these hypotheses.

No differences were detected in myelin content between subgroups based on disease distribution, King's stage, or cognitive profile in ALS. Once again this could be due to heterogeneity within the ALS group as well as relatively small subgroup sizes making it challenging to reach statistical significance.

Interestingly two negative correlations with clinical variables were detected. The first was between F and ALSFRS-R and the second between F and MRC power score, both within the orbitofrontal cortex ( $P < 0.001$ , see figure 4,4A). This suggests that as ALS progresses and these clinical scores are deteriorating, there is an increase in orbitofrontal myelin content, which is difficult to explain. It is possibly caused by a compensatory increase in myelin at this site in response to the neurodegeneration of the motor systems.

No correlation was detected between the qMTi parameter of F and any of the NODDI parameters. In particular no relationship was found between F and mean NDI of either the corpus callosum or cerebral WM. This provides further support that axonal degeneration is not intimately related to loss of myelin and suggests that demyelination is not a key feature in the neurodegenerative process occurring in the cerebral WM in ALS.

Not surprisingly the findings using qMTi in ALS are in stark contrast to the findings in the archetypal demyelinating CNS disease multiple sclerosis (MS),<sup>604-607</sup> where loss of myelin is a consistent feature. This highlights the potential for qMTi to distinguish neurological diseases according to their signature cerebral alterations in the parameters.

Overall the qMTi results relating to myelin content support ALS being primarily a disorder of motor axons, with Wallerian degeneration leading to secondary demyelination.

### 4.10.3: Atrophy in ALS

Cortical atrophy has consistently been reported using imaging studies in ALS.<sup>608–613</sup> In addition, increased ISO and a correlation with disease duration was demonstrated using NODDI,<sup>357</sup> supporting progressive atrophy occurring over time as a result of the ALS disease process. The qMTi parameter of  $T_{2f}$  is not a direct measure of atrophy. However, it is sensitive to increased water content, which tends to occur alongside atrophy. I was therefore expecting to detect an increase in  $T_{2f}$  using qMTi, particularly in relation to the motor regions and the CST. However, differences detected in  $T_{2f}$  did not reach the statistical threshold of FWE corrected  $P < 0.05$ . Increased  $T_{2f}$  was only detected at a less stringent statistical threshold ( $P = 0.001$  uncorrected), in the left frontal cortex and right lateral ventricle (figure 4.2B). In addition, there was no significant difference in  $T_{2f}$  found on the subgroup analyses. This was unexpected as I predicted more atrophy to be evident in the ALS groups with more advanced disease or in the later stages, and in the ALS group with cognitive impairment. One possibility is that the small sample size of the subgroups could have made it more challenging to reach statistical threshold.

The difference in  $T_{2f}$  in the right lateral ventricle seen at a less stringent statistical threshold is in the same location as the increase in ISO demonstrated using NODDI (figure 3.1), but is a much smaller cluster. This indicates that they are measuring subtly different alterations within the tissue and demonstrates that ISO from NODDI is more sensitive at detecting atrophy in ALS than  $T_{2f}$  from qMTi. This is supported by the fact that ISO correlated with disease duration, while  $T_{2f}$  did not show any correlation with the clinical measures of ALS severity on regression analysis.

Interestingly,  $T_{2f}$  of the left lateral ventricle did correlate positively with mean ISO of the ventricles derived from NODDI (figure 4.5C), supporting some overlap in the parameter measurements. A further positive correlation was detected between  $T_{2f}$  of the motor cortices and mean ISO of the corpus callosum (figure 4.5B). Although these findings did not survive FWE correction, they still suggest some atrophy occurring in the PCG that relates to atrophy of the corpus callosum, both of which are known to be degenerating in ALS.<sup>339-342</sup> It is therefore likely that in this cohort the changes were not quite sufficient to reach statistical significance.

Overall, qMTi did not detect as much atrophy as expected related to the degeneration of the motor pathways in ALS. This is potentially because the ALS cohort were largely in the earlier stages of disease and may indicate that atrophy occurs in more advanced disease. However, another contributing factor could be the small sample size.

#### 4.10.4: Limitations and conclusions

In this study I used qMTi to assess for changes in myelin and the presence of molecular (metabolic or inflammatory) alterations within the regions known to degenerate in ALS. The qMTi technique provides greater specificity than the qualitative techniques based on MT ratios,<sup>467-473</sup> and has gained considerable interest over the last decade in various neurological diseases, especially for quantification of myelin in MS.<sup>604-607</sup> The main limitation of qMTi is that data acquisition can be time consuming, but recent optimization techniques have made qMTi more clinically applicable.<sup>479,614-617</sup>

The power of this study was restricted due to the relatively small sample size of both the ALS and control groups. Unfortunately, it was necessary to exclude the data, for two participants with ALS and four control participants, from the analysis due to abnormalities noted within the data sets. This is likely to have further compromised the chance of detecting significant differences between ALS and control groups as well as between ALS subgroups.

Clinical, radiological, and biological heterogeneity within the ALS group is also likely to have contributed to the statistical significance of the qMTi results. Nonetheless this study demonstrates that insights into molecular abnormalities occurring '*in vivo*' can be achieved using qMTi and that qMTi parameters might be capable of improving our understanding of the complex pathogenesis underlying ALS.

The main findings using whole brain, voxel wise analysis of the qMTi parameters were relatively preserved myelin content, as assessed by F, accompanied by reduced magnetization exchange rate ( $k_f$ ) within the rostral CST.

Although the biological correlates of  $k_f$  are not fully understood there is evidence to suggest that this parameter reflects metabolic changes or altered functional integrity, potentially associated with molecular changes and inflammation.<sup>475</sup> The results therefore implicate axonal dysfunction, potentially induced by inflammation in the cerebral WM of the motor tracts, contributing to the pathophysiological processes driving motor neurone degeneration in ALS.

The findings relating to myelin suggest that demyelination occurs in the cerebral WM later in the disease process. The emergence of myelin loss in distal regions of the motor system, albeit at less stringent statistical threshold, would be consistent with the "dying back" hypothesis.<sup>286-288</sup> However, a larger study incorporating evaluation of F in the cervical spinal cord would be needed to further investigate this possibility.

Taken together the qMTi findings are compatible with a process involving predominantly axonal dysfunction and degeneration with secondary myelin damage occurring within the major motor pathways. The apparent dissociation between myelin and axonal injury in ALS suggests novel pathological mechanisms, which are not yet fully understood, and warrant further larger scale studies using qMTi in ALS.

# **CHAPTER 5: STRUCTURAL MRI IN ALS.**

## CHAPTER 5: STRUCTURAL MRI IN ALS

### 5.1: Background

ALS is an incurable disease characterized by progressive motor neuron degeneration,<sup>1-6,29</sup> associated with recognized cognitive and behavioural deficits and thereby forming a spectrum with frontotemporal disorders (ALS-FTSD).<sup>72,123,214,364,618,619</sup>

Macroscopically at post mortem the brain can appear ordinary in ALS, including the motor cortices, which is surprising given the demise of the motor system that causes severe disability leading up to death.<sup>1-6</sup> However, microscopic evaluation of ALS cohorts has demonstrated universal motor pathway degeneration to varying extents, likely relating to phenotype heterogeneity.<sup>193,194,197,201</sup>

Pathologically, cytoplasmic inclusions of ubiquitinated TDP-43 are a recognized feature of ALS and can be visualized in the motor cortices, frontotemporal cortices, CST, brainstem nuclei, anterior horns of the spinal cord and lower motor neurones. Histopathological staging, according to the extent of cerebral TDP-43 pathology, has been proposed.<sup>285</sup> However, this staging system was based on a study of post-mortem brains, which raises important limitations when relating to pathological process occurring in those living with ALS.

The application of neuroimaging to ALS, particularly MRI techniques, allow for '*in vivo*' assessment of atrophy and microstructural alterations. CST hyper-intensities on T2-weighted MRI sequences were initially thought to be a feature of ALS,<sup>381</sup> until similar MRI findings were demonstrated in healthy controls.<sup>350</sup> Conventional MRI is therefore used clinically in order to exclude alternative treatable diagnoses in patients with suspected ALS, rather than to diagnose ALS.

Advanced quantitative MRI modalities, such as DTI and more recently NODDI, have been used extensively in research but have yet to become clinically incorporated into the assessment of those with possible ALS. Nonetheless, DTI and NODDI have demonstrated a radiological signature of ALS, with the descending motor tracts and callosal degeneration being the core features.<sup>339-342,357</sup>

Structural MRI, an alternative technique that provides quantitative volumetric measures, is the method of choice for GM analysis in ALS.<sup>359-373</sup> It can be performed using conventional T1-weighted, high resolution, MRI sequences and can therefore be applied to most clinically derived MRI.<sup>620</sup> Two different techniques have successfully been applied to study the shape and dimensions of cerebral structures, known to be important in ALS. These are called Voxel-based morphometry (VBM) and surface-based morphometry (SBM), both of which have shown structural changes in motor and non-motor regions, consistent with multi-system degeneration in ALS.<sup>17,341,362,367,621</sup>

In this study SBM was used to evaluate for morphological changes in cerebral regions of interest and to assess for correlation with NODDI parameters in order to facilitate the interpretation of the NODDI findings.

## 5.2: Hypotheses

SBM delivers morphometric analysis of specified brain region morphology by providing measures of cortical thickness, volume and surface area. The aim of performing concurrent SBM analysis in this study was to investigate the structural alterations in regions of interest relating to ALS, and to evaluate for any topographical relationship between SBM and NODDI parameters.

I selected the following SBM regions of interest as these were predicted to show changes in ALS, based on the findings from previous studies,<sup>361-369</sup> and were also anticipated to be most informative when relating to the NODDI findings:-

- PCG - As the primary motor area this was the main region of interest in this study, and was evaluated for atrophy related to both the clinical features of the ALS group and the NODDI parameter of ODI, which showed subtle PCG dendritic alterations in this region.
- GM (total and cortical) - To assess for patterns of GM atrophy related to ALS and to investigate for correlation with the NODDI parameter of ODI.
- Cerebral WM - To evaluate for WM atrophy in the ALS group and assess how this relates to the NODDI parameter of NDI, which showed significant CST axonal degeneration.
- Brainstem - To assess for more caudal atrophy relating to ALS, and ascertain how this relates to the NODDI parameter of NDI.
- Middle frontal gyrus - To assess for atrophy related to cognitive features of ALS, and evaluate for correlation with the NODDI parameter of ISO.
- Temporal lobe - To investigate for atrophy related to cognitive impairment in the ALS group, and assess for correlation with the NODDI parameter of ISO.
- Ventricular system - To evaluate for increased size relating to atrophic changes in the ALS group, and to evaluate how this relates to the NODDI parameter of ISO.
- Total cerebral cortex - To assess for global cortical atrophy in ALS and ascertain how this relates to the NODDI parameters of ODI and ISO.

Previous studies using SBM in ALS have demonstrated reduced cortical thickness of the PCG.<sup>366-369</sup> Furthermore, focal reduction in PCG cortical thickness has been shown to reflect clinical features of ALS.<sup>172,366-369</sup> I therefore hypothesized that the main finding using SBM would be significant cortical thinning of the PCG in the ALS group compared



to the control group, and that this may correlate with clinical features such as UMN burden. VBM<sup>362</sup> and SBM<sup>622</sup> studies comparing limb and bulbar onset ALS subgroups have shown differential patterns of focal atrophy within the PCG. I was therefore interested to ascertain whether there would be ALS subgroup differences in PCG morphometry based on disease distribution and stage of ALS. Longitudinal SBM studies have demonstrated decreased cortical thickness over time in ALS.<sup>17,84,392</sup> I therefore hypothesized that cortical thickness of the PCG would correlate with disease duration.

Changes relating to regional brain volumes and surface areas derived from SBM studies in the literature are less consistent and have been reported as failing to reach statistical significance.<sup>368</sup> However, VBM studies have reliably demonstrated regional GM volume reduction of the PCG in ALS.<sup>17,341,361,621</sup> An additional hypothesis was therefore that regional cortical volumes, particularly of the PCG would be reduced in the ALS group. NODDI demonstrated reduced dendritic arborisation in the right PCG, I was therefore keen to assess for correlation between PCG atrophy detected by SBM and the NODDI parameters of ODI and NDI.

Total and cortical GM volumes were also included in this study, where previous studies have shown involvement,<sup>362,372,373</sup> to assess for patterns of GM atrophy in the ALS group. Furthermore as altered neurite morphology would be predicted in the GM, I hypothesised that the NODDI parameter of ODI would correlate with cortical GM volume.

As NODDI demonstrated striking CST axonal loss,<sup>357</sup> reduced WM volume was predicted to accompany ALS on SBM analysis, and was hypothesised to correlate with the NODDI parameter of NDI. Similarly the brainstem SBM volume was included for more caudal analysis, where atrophy was predicted secondary to CST degeneration and a correlation was hypothesized with NDI from NODDI.

SBM and VBM studies have consistently shown atrophy not just confined to the PCG but also in other regions such as frontal and temporal lobes, particularly in relation to cognitive impairment.<sup>17,84,339-341,363-365</sup> I therefore included SBM analysis of the frontal and temporal regions to test the hypothesis that atrophy would be evident. I was particularly interested to see if these SBM measures would relate to cognitive impairment or behavioural changes within the ALS group.

The SBM volume of the ventricular system was included in this analysis as ventricular enlargement is a recognised feature of ALS, related to cerebral atrophy.<sup>193,339-341,373</sup> As NODDI demonstrated an increase in the isotropic compartment of the right lateral ventricle, SBM derived ventricle volume was predicted to correlate with the NODDI parameter of ISO.

Lastly in relation to the SBM region of interests, as ALS is thought to cause multisystem degeneration within the brain,<sup>339-341</sup> total cortical atrophy was anticipated.

Therefore the total cortical SBM volume was included for analysis. I hypothesised that this would relate to the NODDI parameters of ODI and ISO.

Subgroup analyses of SBM derived region of interest volumes, cortical thicknesses, and surface areas were included to assess for patterns of atrophy related to the ALS clinical features of disease distribution, King's stage of ALS, and cognitive involvement. The hypothesis was that more widespread clinical disease, higher King's stage of ALS, and cognitive or behavioural impairment would relate to more significant atrophy.

Finally, in order to gain a complete picture of how brain morphology in the ALS group related to clinical features, regression analyses was performed to examine the relationship between SBM region of interest volumes, cortical thicknesses, and surface areas with ALS clinical measures of ALSFRS-R,  $\Delta$ ALSFRS-R, MRC score, UMN score, disease duration, and total ECAS score. SBM volumes of the PCG, WM, and brain stem were hypothesised to correlate with UMN score and disease duration. Increasing ventricular volume was also anticipated to correlate with disease duration, while total cerebral, cerebral GM, middle frontal gyrus, and temporal lobe volumes were predicted to correlate with total ECAS score.

### **5.3: Structural imaging data acquisition**

The structural imaging was attained during the same MRI protocol as the diffusion weighted and quantitative magnetization MRI sequences, using the 1.5 tesla Siemens AVANTO scanner, see chapter 3.3 and 4.3. The MRI sequence acquisition relating to structural imaging lasted approximately 6 minutes and comprised the following:

T1-weighted volumetric high-resolution magnetization prepared rapid gradient - echo (MPRAGE)

Acquisition time 6 minutes

TE 3.57 ms

TR 2730 ms

TI = 100 ms

Flip angle = 70

FoV = 256 x 240 mm<sup>2</sup>

Matrix = 254 x 240

Slice thickness 1 mm

Voxel size 1 x 1 x 1 mm, 1 excitation, flip angle 7 degrees, 192 slices

#### **5.4: Structural imaging data processing**

SBM was used to quantify the volume, cortical thickness, and surface areas in the regions of interest predicted to show evidence of degeneration in ALS, as listed below and described in the SBM hypotheses, section 5.2. The automated processing stream within FreeSurfer (<http://surfer.nmr.mgh.harvard.edu>) was applied to the high resolution MPRAGE images for SBM data processing. This process involved skull stripping, registration to Talairach space, intensity normalisation, tissue segmentation to determine the WM/GM boundary, followed by tessellation and deformation of this boundary, then finally surface parcellation. The following regional cerebral volumes were extracted for analyses:-

- Total cerebral cortex
- Cerebral WM
- Total cerebral GM and cortical GM
- PCG
- Middle frontal gyrus
- Temporal lobe
- Ventricular system
- Brainstem

In addition, left and right hemisphere volumes were measured for the cerebral cortex, WM, precentral gyrus, middle frontal gyrus, and temporal lobe in order to assess for hemispheric differences. All regional volumes for each participant were normalised using the total intra-cranial brain volume.

The regions available for cortical thickness and surface areas were more limited than those for cerebral volume, therefore the regions of interest, chosen for the same rationale, were as follows:-

- Total cerebral cortex
- Precentral gyrus
- Middle frontal gyrus
- Temporal lobe

Left and right hemisphere measures were obtained, again to assess for hemispheric variation in cortical thickness and surface areas. Cortical thickness data was normalised for each participant using mean cortical thickness, while surface area data was normalised using total surface area.

## **5.5 Surface-based morphometry statistical analysis**

### **5.5.1 SBM analysis comparing ALS and control groups**

IBM SPSS (International Business Machines Corporation, Statistical Package for the Social Sciences, version 24) was used to assess for significant differences between the ALS and control groups in all of the SBM measures. Independent sample t-tests were performed within SPSS and  $P < 0.05$  was considered as statistically significant. As the SBM data was exploratory, and obtained for comparison with the NODDI data, no correction for multiple comparison was applied. The rationale for performing SBM analysis are described in the SBM hypotheses, section 5.2.

### **5.5.2 Subgroup analysis using SBM measures**

The same ALS subgroups used in the NODDI and qMTi analyses, were used to assess for significant differences using the SBM measures of cerebral volume, cortical thickness and surface area, see chapter 3.5.2 and 4.5.2.

The three sets of subgroups were based on clinical distribution of ALS (12 limb only subgroup versus 11 bulbar plus limb), King's stage of ALS (10 stage 1 subgroup, 8 stage 2, 5 stage 3, and 13 combined stage 2 and 3 subgroups), and finally cognitive function (11 normal ECAS versus 12 abnormal ECAS). All subgroups were compared with one another as well as with the control group. SPSS was used to perform independent sample t-tests and assess for significant differences between subgroups in the means of all SBM measures. Statistical significance was set at  $P < 0.05$ . The rationale for conducting subgroup analysis are given in the SBM hypotheses, section 5.2.

### **5.5.3 Correlation analysis of SBM metrics with clinical measures of ALS**

The SBM data for the ALS group was assessed for correlation with the clinical variables of ALSFRS-R,  $\Delta$ ALSFRS-R, MRC score, UMN score, disease duration and ECAS total. SPSS was used to assess for Pearson correlation between all SBM measures and clinical variables, where  $P < 0.05$  was accepted as statistically significant. As these correlations were performed on an exploratory basis no correction for multiple comparison was applied. Rationale for performing regression analysis between SBM metrics and clinical variables of the ALS group are described in the SBM hypotheses, section 5.2.

### **5.5.4 Correlation analysis of NODDI parameters with SBM metrics**

The region of interest SBM measures derived from the ALS group were analysed for correlation with the NODDI parameters. The linear model framework within SPM12 was

used, with age included as a covariate and results were accepted as significant where  $P < 0.05$  after family-wise error (FWE) correction at cluster level, clusters formed with  $P < 0.001$ . FLS view was used to confirm the anatomical locations using the MNI coordinates (<https://fsl.fmrib.ox.ac.uk/fsl/fslwiki/FslView>). I provided the rationale for performing correlation between NODDI and SBM parameters in the SBM hypothesis, section 5.2.

## **5.6 SBM results comparing ALS and control groups**

### **5.6.1 Cerebral volumes**

There was no significant difference in the mean total intracranial volume between the healthy control and ALS groups. Despite this, significant differences were found between control and ALS groups in all of the region of interest normalised cerebral volume measures apart from the middle frontal gyrus and temporal lobe, see table 5.1.

When including the whole brain the cerebral cortex ( $P=0.018$ ), cerebral WM ( $P=0.037$ ), cerebral GM ( $P=0.022$ ), PCG ( $P=0.037$ ), brainstem ( $P=0.027$ ) and corpus callosum ( $P=0.021$ ) all showed significantly lower mean volumes in the ALS group, see figures 5.1 – 5.5 respectively. The mean total ventricular system volume was significantly larger in the ALS group ( $P < 0.001$ ), see figure 5.5.

When analysing the cerebral hemispheres separately, the left ( $P=0.015$ ) and right ( $P=0.021$ ) cerebral cortex as well as the left cerebral WM ( $P=0.024$ ), and the right PCG ( $P=0.020$ ) volumes were all significantly reduced in the ALS group, see table 5.1 and figures 5.1, 5.2, and 5.4.

In addition, cortical GM volume was significantly reduced in the ALS group ( $P=0.034$ ), see table 5.1 and figure 5.3.

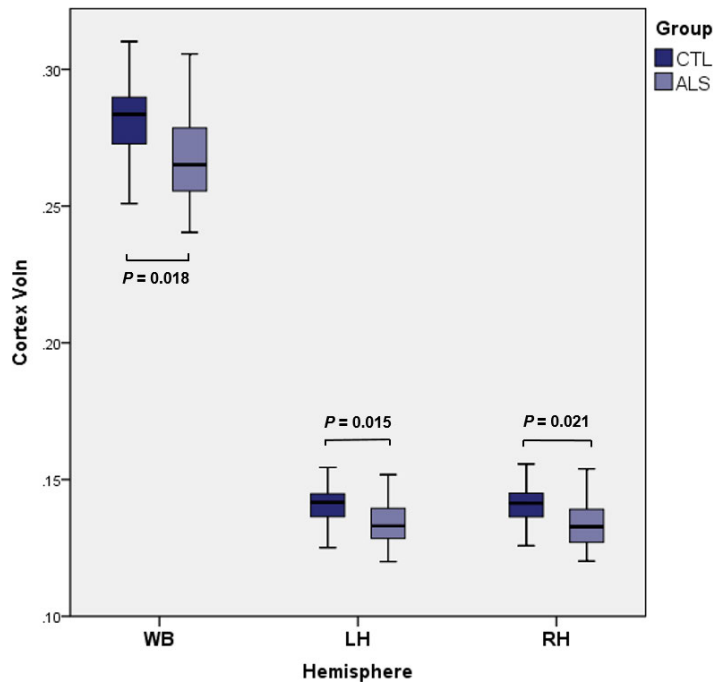
**Table 5.1: Region of interest SBM measures comparing control and ALS groups.**

<b>SBM measure</b>	<b>Region of interest</b>		<b>Healthy control group (mean)</b>	<b>ALS group (mean)</b>	<b>P value</b>
<b>Volume (mm<sup>3</sup>)</b>	Total intracranial volume		1561688	1556345	0.114
<b>Volume (mm<sup>3</sup>) Normalised by total intracranial volume</b>	Cerebral cortex	WB	0.2817	0.2695	<b>0.018</b>
		LH	0.1406	0.1346	<b>0.015</b>
		RH	0.1411	0.1350	<b>0.021</b>
	Cerebral WM	WB	0.3040	0.2926	<b>0.037</b>
		LH	0.1514	0.1447	<b>0.024</b>
		RH	0.1526	0.1470	0.058
	Cerebral GM	Total	0.3785	0.3629	<b>0.022</b>
		Cortical	0.3432	0.3301	<b>0.034</b>
	Precentral gyrus	WB	0.0159	0.0150	<b>0.037</b>
		LH	0.0080	0.0076	0.125
		RH	0.0079	0.0079	<b>0.020</b>
	Middle frontal gyrus	WB	0.0255	0.0250	0.614
		LH	0.0127	0.0125	0.454
		RH	0.0129	0.0126	0.551
	Temporal lobe	WB	0.0452	0.0434	0.188
		LH	0.0228	0.0217	0.110
		RH	0.0224	0.0216	0.161
Ventricles			0.0148	0.0242	<b>0.000</b>
Brainstem			0.0140	0.0138	<b>0.027</b>
Corpus callosum			0.0020	0.0018	<b>0.021</b>
<b>Cortical thickness (mm)</b>	Cerebral cortex	WB	2.3320	2.2750	<b>0.024</b>
		LH	2.3370	2.2796	<b>0.027</b>
		RH	2.3320	2.2747	<b>0.024</b>
<b>Cortical thickness (mm) normalised by mean cortical thickness</b>	Precentral gyrus	WB	1.0266	1.0127	0.236
		LH	1.0306	1.0215	0.427
		RH	1.0225	1.0039	0.075
	Middle frontal gyrus	WB	0.9947	0.9985	0.558
		LH	1.0010	1.0024	0.221
		RH	0.9885	0.9945	0.178
	Temporal lobe	WB	1.1339	1.1404	0.261
		LH	1.1287	1.1419	0.518
		RH	1.1339	1.1405	0.787
<b>Surface Area (mm<sup>2</sup>)</b>	Cerebral cortex	WB	170273	166102	0.103
		LH	84854	82779	0.134
		RH	85419	83323	0.092
<b>Surface Area (mm<sup>2</sup>) Normalised by total surface area</b>	Precentral gyrus	WB	0.0567	0.0563	0.754
		LH	0.0567	0.0573	0.134
		RH	0.0568	0.0553	0.338
	Middle frontal gyrus	WB	0.0923	0.0945	0.194
		LH	0.0914	0.0936	0.250
		RH	0.0931	0.0953	0.245
	Temporal lobe	WB	0.1199	0.1187	0.300
		LH	0.1216	0.1192	0.119
		RH	0.1183	0.1183	0.974

This table summarizes the statistically significant results obtained when comparing the SBM parameters in regions of interest between control and ALS groups. Statistical significance was set at  $P < 0.05$  for all comparisons.

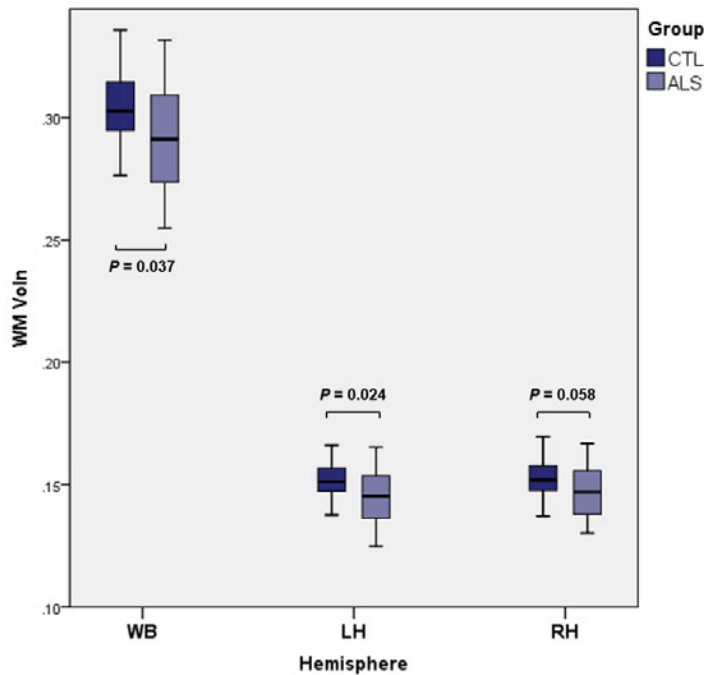
Abbreviations: ALS, amyotrophic lateral sclerosis; WB, whole brain; LH, left hemisphere; RH, right hemisphere.

**Figure 5.1: Comparison of the mean normalized cerebral cortex volumes between control and ALS groups.**



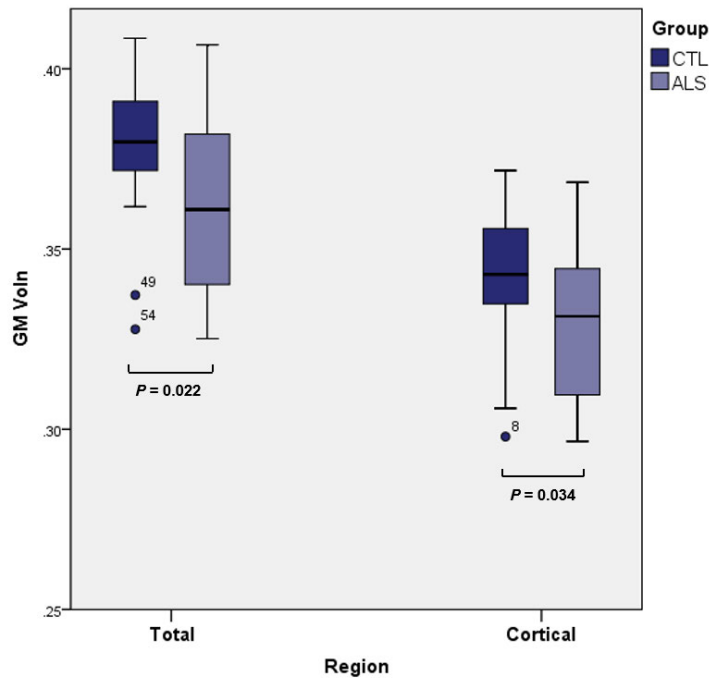
A figure to show the difference between control and ALS groups in cerebral cortex volume including whole brain, left hemisphere, and right hemisphere analysis. Volumes were normalized by total intracranial volume. Abbreviations: CTL, control group; ALS, amyotrophic lateral sclerosis group; Voln, normalized volume; WB, whole brain; LH, left hemisphere; RH, right hemisphere.

**Figure 5.2: Comparison of the mean normalized cerebral white matter volumes between control and ALS groups.**



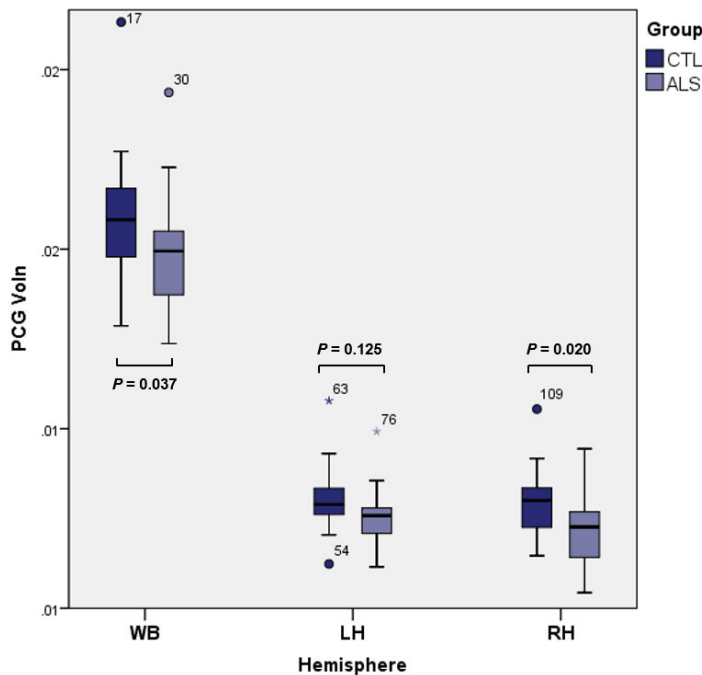
A figure to show the difference between control and ALS groups in cerebral white matter volume including whole brain, left hemisphere, and right hemisphere analysis. Volumes were normalized by total intracranial volume. Abbreviations: CTL, control group; ALS, amyotrophic lateral sclerosis group; WM, white matter; Voln, normalized volume; WB, whole brain; LH, left hemisphere; RH, right hemisphere.

**Figure 5.3: Comparison of the mean normalized grey matter volumes between control and ALS groups.**



A figure to show the difference between control and ALS groups in cerebral volumes of total grey matter and cortical grey matter. Volumes were normalized by total intracranial volume. Abbreviations: CTL, control group; ALS, amyotrophic lateral sclerosis group; GM, grey matter; Voln, normalized volume.

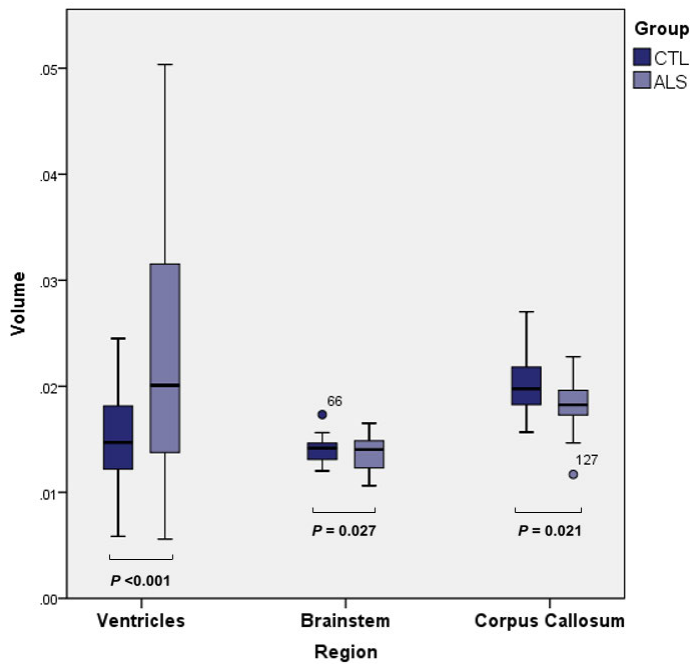
**Figure 5.4: Comparison of the mean normalized precentral gyrus volumes between control and ALS groups.**



A figure to show the difference between control and ALS groups in precentral gyrus volume including whole brain, left hemisphere, and right hemisphere analysis. Volumes were normalized by total intracranial volume. Abbreviations: CTL, control group; ALS, amyotrophic lateral sclerosis group; PCG, precentral gyrus; Voln, normalized volume; WB, whole brain; LH, left hemisphere; RH, right hemisphere.

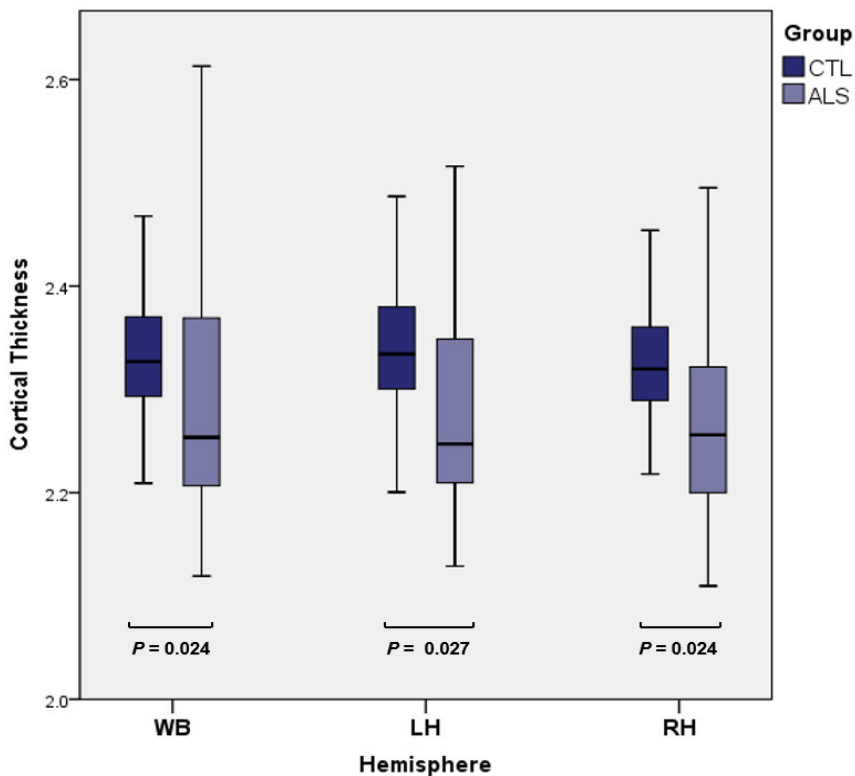


**Figure 5.5: Comparison of the mean normalized volumes between control and ALS groups of the ventricular system, brainstem, and corpus callosum.**



A figure to show the difference between control and ALS groups in cerebral volumes of the ventricular system, brainstem and corpus callosum. Volumes were normalized by total intracranial volume. Abbreviations: CTL, control group; ALS, amyotrophic lateral sclerosis group.

**Figure 5.6: Comparison of the mean cortical thickness between control and ALS groups.**



A figure to show the difference between control and ALS groups in mean cortical thickness of the whole brain, left hemisphere, and right hemisphere. Abbreviations: CTL, control group; ALS, amyotrophic lateral sclerosis group; LH, left hemisphere; RH, right hemisphere.

### **5.6.2: Cortical thickness**

Normalized mean cerebral cortical thickness was significantly reduced in the ALS group ( $P=0.024$ ) compared to the control group. Similarly, the mean cortical thickness in the left hemisphere ( $P=0.027$ ) and right hemisphere ( $P=0.024$ ) were significantly lower in the ALS group, see table 5.1 and figure 5.6. However, the differences in cortical thickness of the precentral gyrus, middle frontal gyrus, and temporal lobe did not reach statistical significance for either hemisphere when analysing separately or when analysing the left and right hemisphere together, see table 5.1.

### **5.6.3: Surface area**

No significant differences in mean surface area were demonstrated between the control and ALS groups when analysing the whole cerebrum, the left hemisphere, or the right hemisphere, see table 5.1. Similarly, no significant reduction was found in the normalised surface areas between healthy controls and the ALS group of the precentral gyrus, middle frontal gyrus, and temporal lobe when analysing the whole brain, left hemisphere, or right hemisphere, see table 5.1.

## **5.7 SBM parameter subgroup analysis results**

### **5.7.1 Distribution of ALS**

#### **5.7.1.1 Cerebral volumes**

There was no significant difference in total intracranial volume between limb-only and bulbar-plus-limb ALS subgroups, or between these ALS subgroups and the control group, see table 5.2.

Whole brain normalized cerebral volume was significantly reduced in the bulbar plus limb subgroup compared to the control group ( $P=0.027$ ). Similarly, the bulbar plus limb involvement ALS subgroup showed significantly reduced cortical volume in both the left ( $P=0.017$ ) and right ( $P=0.042$ ) hemisphere. The difference between limb only ALS subgroup and the control group did not quite reach statistical significance on whole brain ( $P=0.064$ ), left hemisphere ( $P=0.076$ ), or right hemisphere ( $P=0.056$ ).

Whole brain cerebral WM volume was significantly reduced when comparing both the limb only ALS subgroup ( $P=0.007$ ) and the bulbar plus limb ALS subgroup ( $P=0.046$ ) with the control group. Similarly, LH cerebral WM volume was significantly reduced in both the limb only ( $P=0.007$ ) and bulbar plus limb ( $P=0.046$ ) subgroup when comparing with the control group. Cerebral WM volume of the RH was significantly reduced in the limb only ALS subgroup compared with the control group ( $P=0.012$ ). However, the comparison of the bulbar and limb subgroup with the control group did not quite reach statistical significance ( $P=0.056$ ).

**Table 5.2: Subgroup analysis comparing cerebral volumes in regions of interest between control and ALS subgroups based on disease distribution.**

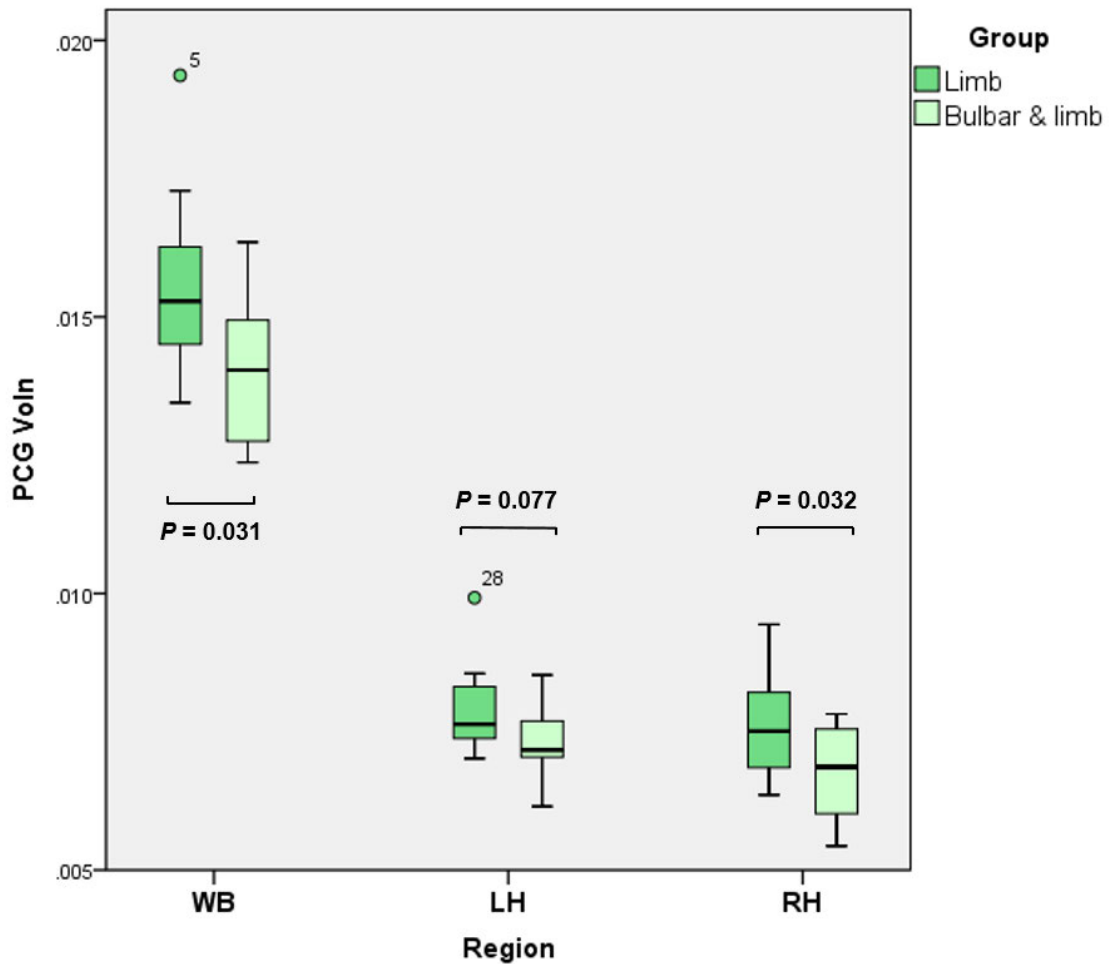
Region of interest volume (mm <sup>3</sup> )		Control (mean)	ALS (mean)			P value
			Whole group	Limb only (12)	Bulbar and limb (11)	
Total intracranial volume		1561688	1556345	1532497	1582359	-
		*	*			0.114
		*		*		0.292
		*			*	0.183
				*	*	0.379
Cortical volume (normalized)	WB	0.2817	0.2695	0.2708	0.2681	-
		*	*			<b>0.018</b>
		*		*		0.064
		*			*	<b>0.027</b>
				*	*	0.730
	LH	0.1406	0.1346	0.1355	0.1335	-
		*	*			<b>0.015</b>
		*		*		0.076
		*			*	<b>0.017</b>
				*	*	0.604
	RH	0.1411	0.1350	0.1353	0.1346	-
		*	*			<b>0.021</b>
		*		*		0.056
		*			*	<b>0.042</b>
				*	*	0.767
	Cerebral white matter volume (normalized)	WB	0.3040	0.2916	0.2858	0.2980
*			*			<b>0.037</b>
*				*		<b>0.007</b>
*					*	<b>0.046</b>
				*	*	0.201
LH		0.1514	0.1447	0.1416	0.1480	-
		*	*			<b>0.024</b>
		*		*		<b>0.005</b>
		*			*	<b>0.037</b>
				*	*	0.188
RH		0.1526	0.1470	0.1441	0.1499	-
		*	*			0.058
		*		*		<b>0.012</b>
	*			*	0.056	
			*	*	0.221	
Cerebral grey matter volume (normalized)	Total	0.3785	0.3629	0.3634	0.3623	-
		*	*			<b>0.022</b>
		*		*		0.057
		*			*	<b>0.046</b>
				*	*	0.816
	Cortical	0.3432	0.3301	0.3310	0.3292	-
		*	*			<b>0.034</b>
		*		*		0.089
		*			*	0.059
				*	*	0.819
Precentral gyrus volume (normalized)	WB	0.0159	0.0150	0.0155	0.0141	-
		*	*			<b>0.037</b>
		*		*		0.530
		*			*	<b>0.004</b>
				*	*	<b>0.031</b>
	LH	0.0080	0.0076	0.0079	0.0073	-
		*	*			0.125
		*		*		0.701

		*			*	<b>0.017</b>
				*	*	0.077
	RH	0.0079	0.0079	0.0076	0.0067	-
		*	*			<b>0.020</b>
		*		*		0.440
		*			*	<b>0.001</b>
				*	*	<b>0.032</b>
Middle frontal gyrus volume (normalized)	WB	0.0255	0.0250	0.0250	0.0250	-
		*	*			0.614
		*		*		0.620
		*			*	0.545
				*	*	0.744
	LH	0.0127	0.0125	0.0127	0.0123	-
		*	*			0.454
		*		*		0.401
		*			*	0.435
				*	*	0.318
	RH	0.0129	0.0126	0.0126	0.0127	-
		*	*			0.551
		*		*		0.525
		*			*	0.562
				*	*	0.672
	Temporal lobe volume (normalized)	WB	0.0452	0.0434	0.0435	0.0433
*			*			0.188
*				*		0.128
*					*	0.116
				*	*	0.921
LH		0.0228	0.0217	0.0218	0.0216	-
		*	*			0.110
		*		*		0.181
		*			*	0.054
				*	*	0.830
RH		0.0224	0.0216	0.0216	0.0216	-
		*	*			0.161
		*		*		0.076
		*			*	0.279
				*	*	0.981
Ventricles volume (normalized)		0.0148	0.0242	0.0233	0.0253	-
	*	*			<b>0.000</b>	
	*		*		<b>0.000</b>	
	*			*	<b>0.000</b>	
			*	*	0.582	
Brainstem volume (normalized)	0.0140	0.0138	0.0134	0.0142	-	
	*	*			<b>0.027</b>	
	*		*		<b>0.017</b>	
	*			*	0.385	
			*	*	0.204	
Corpus callosum volume (normalized)	0.0020	0.0018	0.0018	0.0019	-	
	*	*			<b>0.021</b>	
	*		*		<b>0.026</b>	
	*			*	0.127	
			*	*	0.477	

A table to show the differences in ROI volumes between the control group and the ALS whole group, as well as ALS subgroups of limb-only and bulbar-plus-limb. ROI volumes were normalised by the total intracranial volume (mm<sup>3</sup>). The two \* are used to indicate which subgroups are being compared and statistical significance was set at  $P < 0.05$  for all comparisons. Statistically significant differences are highlighted in bold.

Abbreviations: LH, left hemisphere; RH, right hemisphere; WB, whole brain; ROI, region of interest

**Figure 5.7: Comparison of precentral gyrus volumes between limb only and bulbar limb ALS subgroups.**



A figure to show the difference in normalised precentral gyrus volume in the whole brain, left hemisphere, and right hemisphere between limb only and bulbar limb ALS subgroups. Abbreviations: WB, whole brain; LH, left hemisphere; RH, right hemisphere.

In the cerebral GM comparisons, the total GM volume was significantly reduced only in the bulbar plus limb subgroup ( $P=0.046$ ) compared to the control group, while the reduction in cortical GM volume between these groups almost reached statistical significance ( $P=0.059$ ).

When comparing the bulbar plus limb ALS subgroup with the control group, normalized PCG volumes were significantly reduced on whole brain analysis ( $P=0.004$ ), as well as in the left ( $P=0.017$ ) and right ( $P=0.001$ ) hemispheres. In addition, the PCG volume was significantly reduced in the bulbar plus limb subgroup when compared with the limb only ALS subgroup in the whole brain ( $P=0.031$ ) as well as the right hemisphere ( $P=0.032$ ). This was the only cerebral volume measure to demonstrate significant difference between the ALS subgroups, see figure 5.7.

There were no significant differences between subgroups in the normalized MFG and temporal lobe volumes when analysing the whole brain, left or right hemisphere.

The normalized volume of the ventricles was significantly increased in both the ALS subgroups compared to the control group ( $P<0.001$ ). However, the increased mean ventricular size of the bulbar plus limb subgroup compared to the limb only subgroup did not reach statistical significance.

In the brainstem, only the limb only ALS subgroup showed significantly reduced volume when compared to the control group ( $P=0.017$ ).

Finally, in the corpus callosum it was the limb only ALS subgroup again that showed significantly reduced volume when compared to the control group ( $P=0.026$ ).

### 5.7.1.2 Cortical thickness

In none of the region of interest cortical thickness measures was a significant difference detected between the limb only and bulbar plus limb ALS subgroups. Statistical significance was only achieved when comparing the bulbar plus limb ALS subgroup with the control group, see table 5.3.

**Table 5.3: Subgroup analysis comparing cortical thickness in regions of interest between control and ALS subgroups based on disease distribution.**

Region of interest cortical thickness (mm)		Control (mean)	ALS (mean)			P value
			Whole group (23)	Limb only (12)	Bulbar and limb (11)	
Cortical thickness	WB	2.3320	2.2750	2.2971	2.2502	-
		*	*			<b>0.024</b>
		*		*		0.185
		*			*	<b>0.010</b>
	LH			*	*	0.262
		2.3370	2.2796	2.3040	2.2529	-
		*	*			<b>0.027</b>
		*		*		0.220
	RH			*	*	<b>0.011</b>
				*	*	0.218
		2.3320	2.2747	2.2902	2.2476	-
		*	*			<b>0.024</b>
Precentral gyrus thickness (normalized)	WB			*	*	0.162
				*	*	<b>0.010</b>
				*	*	0.318
		1.0266	1.0127	1.0226	1.0020	-
	LH			*	*	0.236
				*	*	0.603
				*	*	<b>0.029</b>
				*	*	0.123
	RH	1.0306	1.0215	1.0306	1.0116	-
		*	*			0.427
		*		*		0.602
		*		*	*	0.412
RH			*	*	0.289	
	1.0225	1.0039	1.0145	0.9924	-	
	*	*			0.075	

		*		*		0.451	
		*			*	0.451	
				*	*	0.274	
Middle frontal gyrus thickness (normalized)	WB	<b>0.9947</b>	<b>0.9985</b>	<b>0.9999</b>	<b>0.9969</b>	-	
		*	*			0.558	
		*		*		0.514	
					*	*	0.585
					*	*	0.667
	LH	<b>1.0010</b>	<b>1.0024</b>	<b>1.0043</b>	<b>1.0004</b>	-	
		*	*			0.221	
		*		*		0.278	
		*			*	0.412	
					*	*	0.750
	RH	<b>0.9885</b>	<b>0.9945</b>	<b>0.9954</b>	<b>0.9935</b>	-	
		*	*			0.178	
*			*		0.173		
*				*	0.451		
			*	*	0.582		
Temporal thickness (normalized)	WB	<b>1.1339</b>	<b>1.1405</b>	<b>1.1339</b>	<b>1.1416</b>	-	
		*	*			0.443	
		*		*		0.570	
		*			*	0.451	
				*	*	0.881	
	LH	<b>1.1287</b>	<b>1.1419</b>	<b>1.1243</b>	<b>1.1609</b>	-	
		*	*			0.518	
		*		*		0.833	
		*			*	0.144	
				*	*	0.343	
	RH	<b>1.1339</b>	<b>1.1405</b>	<b>1.1485</b>	<b>1.1398</b>	-	
		*	*			0.787	
		*		*		0.549	
		*			*	0.977	
				*	*	0.821	

A table to show the differences in ROI CT between the control group and the ALS whole group, as well as the ALS subgroups of limb-only and bulbar-plus-limb. ROI CT values were normalised by the mean CT (mm). The two \* indicate which subgroups are being compared and statistical significance was set at  $P < 0.05$  for each comparison. Statistically significant differences are highlighted in bold.

Abbreviations: CT, cortical thickness, LH, left hemisphere; RH, right hemisphere; WB, whole brain; ROI, region of interest

Cortical thickness of the whole brain was significantly reduced in the ALS subgroup with bulbar and limb involvement compared to the control group in the whole brain ( $P=0.010$ ), left hemisphere ( $P=0.011$ ), and right hemisphere ( $P=0.010$ ).

Normalized whole brain cortical thickness of the PCG was significantly reduced in the bulbar plus limb ALS subgroup compared to the control group ( $P=0.029$ ). However, the loss of thickness did not reach statistical significance when analysing the left and right hemispheres separately.

No significant difference was found between the ALS subgroups and the control group when analysing the normalized cortical thickness measures of the MFG or temporal lobes in the whole brain, left hemisphere or right hemisphere.

### 5.7.1.3 Surface area

No significant differences were found in any of the region of interest surface area measures when comparing the ALS subgroups with each other or with the control group, see table 5.4.

**Table 5.4: Subgroup analysis comparing surface area in regions of interest between control and ALS subgroups based on disease distribution.**

Region of interest surface area (mm <sup>2</sup> )		Control (mean)	ALS (mean)			P value
			Whole group	Limb only (12)	Bulbar and limb (11)	
Surface area	WB	170273	166102	162517	170013	-
		*	*			0.103
		*		*		0.113
		*			*	0.144
		*		*	*	0.127
	LH	84854	82779	81002	84718	-
		*	*			0.134
		*		*		0.117
		*			*	0.160
		*		*	*	0.131
	RH	85419	83323	81515	85295	-
		*	*			0.092
		*		*		0.110
		*			*	0.152
		*		*	*	0.127
	Precentral gyrus surface area (normalized)	WB	0.0567	0.0563	0.0576	0.055
*			*			0.754
*				*		0.464
*					*	0.265
*				*	*	0.586
LH		0.0567	0.0573	0.0579	0.0568	-
		*	*			0.134
		*		*		0.445
		*			*	0.400
		*		*	*	0.110
RH		0.0568	0.0553	0.0573	0.0532	-
		*	*			0.338
		*		*		0.530
		*			*	0.052
		*		*	*	0.586
Middle frontal gyrus surface area (normalized)		WB	0.0923	0.0945	0.0943	0.0945
	*		*			0.194
	*			*		0.267
	*				*	0.289
	*			*	*	0.275
	LH	0.0914	0.0936	0.0943	0.0928	-
		*	*			0.250
		*		*		0.064
		*			*	0.587
		*		*	*	0.108
	RH	0.0931	0.0953	0.0945	0.0963	-
		*	*			0.245
		*		*		0.555
		*			*	0.171
		*		*	*	0.472



Temporal surface area (normalized)	WB	0.1199	0.1187	0.1182	0.1193	-
		*	*			0.300
		*		*		0.246
		*			*	0.582
				*	*	0.454
	LH	0.1216	0.1192	0.1190	0.1192	-
		*	*			0.119
		*		*		0.202
		*			*	0.158
				*	*	0.812
	RH	0.1183	0.1183	0.1175	0.1191	-
		*	*			0.974
		*		*		0.604
		*			*	0.575
				*	*	0.273

A table to show the differences in ROI SA between the control group and the whole ALS group, as well as the ALS subgroups of limb-only and bulbar-plus-limb. The ROI SA values were normalised by the mean SA (mm<sup>2</sup>). The two \* indicate which subgroups are being compared and statistical significance was set at  $P < 0.05$  for all comparisons. Statistically significant differences are highlighted in bold.

Abbreviations: LH, left hemisphere; RH, right hemisphere; WB, whole brain; ROI, region of interest; SA, surface area.

## 5.7.2 King's Stage of ALS

### 5.7.2.1 Cerebral volumes

There was no significant difference in total intracranial volume amongst any of the King's stage of ALS subgroups or between the ALS subgroups and the control group, see table 5.5.

There was a significant reduction in normalized cortical volume of the King's stage 3 ALS group compared to the control group on analysis of the whole brain ( $P=0.032$ ), left hemisphere ( $P=0.028$ ) and right hemisphere ( $P=0.038$ ). Similarly, cortical volume was significantly reduced in the ALS subgroup combining King's Stage 2 and 3 in the whole brain ( $P=0.036$ ), left hemisphere ( $P=0.030$ ) and right hemisphere ( $P=0.043$ ), when compared with the control group. The difference between the control group and the King's stage 1 ALS subgroup almost reached statistical significance in the whole brain ( $P=0.054$ ), left hemisphere ( $P=0.052$ ), and right hemisphere ( $P=0.057$ ).

Cerebral WM volume was reduced in King's stage 2 subgroup compared to the control group on analysis of the whole brain ( $P=0.018$ ), left hemisphere ( $P=0.006$ ) and the right hemisphere ( $P=0.050$ ). Similarly, King's stage 3 WM volume of the whole brain ( $P=0.001$ ), left hemisphere ( $P=0.001$ ) and the right hemisphere ( $P=0.002$ ) were significantly reduced compared to the control group. Not surprisingly the combined King's stage 2 and 3 subgroup also showed significantly reduced WM volume compared to the control group in the whole brain ( $P=0.030$ ), left hemisphere ( $P=0.017$ ) and the right hemisphere ( $P=0.043$ ). In addition, WM volume was significantly reduced in the King's stage 3 subgroup ( $P=0.042$ ) compared to King's stage 1 on whole brain analysis. In the

left hemisphere there were significant differences between King's stage 1 and 2 ( $P=0.013$ ), King's stages 1 and 3 ( $P=0.044$ ), and between King's stages 2 and 3 ( $P=0.013$ ). While in the right hemisphere there were also significant differences between King's stage 1 and 2 ( $P=0.015$ ), King's stages 1 and 3 ( $P=0.045$ ), and between King's stages 2 and 3 ( $P=0.039$ ), see table 5.5 and figure 5.8.

**Table 5.5: Subgroup analysis comparing region of interest cerebral volumes between control and ALS subgroups based on King's stage of ALS.**

Region of interest volume (mm <sup>3</sup> )		Control (mean)	ALS (mean)					P value	
			Whole group	Stage 1 (10)	Stage 2 (8)	Stage 3 (5)	Stages 2 + 3 (13)		
Total intracranial Volume		1561688	1556344	1520796	1583594	1583842	1583689	-	
		*	*					0.114	
		*		*					0.140
		*			*				0.475
		*				*			0.219
		*					*		0.230
				*	*				0.356
				*		*			0.319
				*			*	*	0.251
				*	*			0.616	
Cort voln	WB	0.2817	0.2695	0.2699	0.2725	0.2642	0.2693	-	
		*	*					<b>0.018</b>	
		*		*				0.054	
		*			*			0.152	
		*				*		<b>0.032</b>	
		*					*	<b>0.036</b>	
				*	*			0.777	
				*		*		0.620	
				*			*	0.775	
					*	*		0.495	
	LH	0.1407	0.1346	0.1348	0.1359	0.1320	0.1344	-	
		*	*					<b>0.015</b>	
		*		*				0.052	
		*			*			0.138	
		*				*		<b>0.028</b>	
		*					*	<b>0.030</b>	
				*	*			0.800	
				*		*		0.599	
				*			*	0.808	
					*	*		0.490	
	RH	0.1411	0.1350	0.1351	0.1365	0.1323	0.1349	-	
		*	*					<b>0.021</b>	
		*		*				0.057	
		*			*			0.168	
		*				*		<b>0.038</b>	
		*					*	<b>0.043</b>	
				*	*			0.756	
			*		*		0.642		
			*			*	0.801		
				*	*		0.501		
WM voln	WB	0.3040	0.2916	0.2950	0.2970	0.2761	0.2890	-	
		*	*					<b>0.037</b>	

		*		*				0.189
		*			*			<b>0.018</b>
		*				*		<b>0.001</b>
		*					*	<b>0.030</b>
				*	*			0.273
				*		*		<b>0.042</b>
				*			*	0.449
					*	*		0.080
	LH	0.1515	0.1447	0.1467	0.1468	0.1374	0.1432	-
		*	*					<b>0.020</b>
		*		*				0.168
		*			*			<b>0.006</b>
		*				*		<b>0.001</b>
		*					*	<b>0.017</b>
				*	*			<b>0.013</b>
				*		*		<b>0.044</b>
				*			*	0.479
					*	*		<b>0.013</b>
	RH	0.1526	0.1469	0.1484	0.1502	0.1387	0.1458	-
		*	*					<b>0.058</b>
		*		*				0.228
		*			*			<b>0.050</b>
		*				*		<b>0.002</b>
		*					*	<b>0.043</b>
				*	*			<b>0.015</b>
				*		*		<b>0.045</b>
				*			*	0.537
					*	*		<b>0.039</b>
GM voln	Total	0.3780	0.3629	0.3654	0.3656	0.3536	0.3610	-
		*	*					<b>0.022</b>
		*		*				0.105
		*			*			0.143
		*				*		<b>0.022</b>
		*					*	<b>0.027</b>
				*	*			0.845
				*		*		0.420
				*			*	0.686
					*	*		0.447
	Cort	0.3432	0.3301	0.3322	0.3320	0.3229	0.3285	-
		*	*					<b>0.034</b>
		*		*				0.138
		*			*			0.163
		*				*		<b>0.042</b>
		*					*	<b>0.041</b>
				*	*			0.864
				*		*		0.481
				*			*	0.691
					*	*		0.523
PCG voln	WB	0.0159	0.0148	0.0154	0.0145	0.0142	0.0144	-
		*	*					<b>0.037</b>
		*		*				0.457
		*			*			<b>0.014</b>
		*				*		0.057
		*					*	<b>0.005</b>
				*	*			0.226
				*		*		0.254
				*			*	0.158
					*	*		0.171
	LH	0.0080	0.0076	0.0078	0.0075	0.0076	0.0075	-
		*	*					0.125

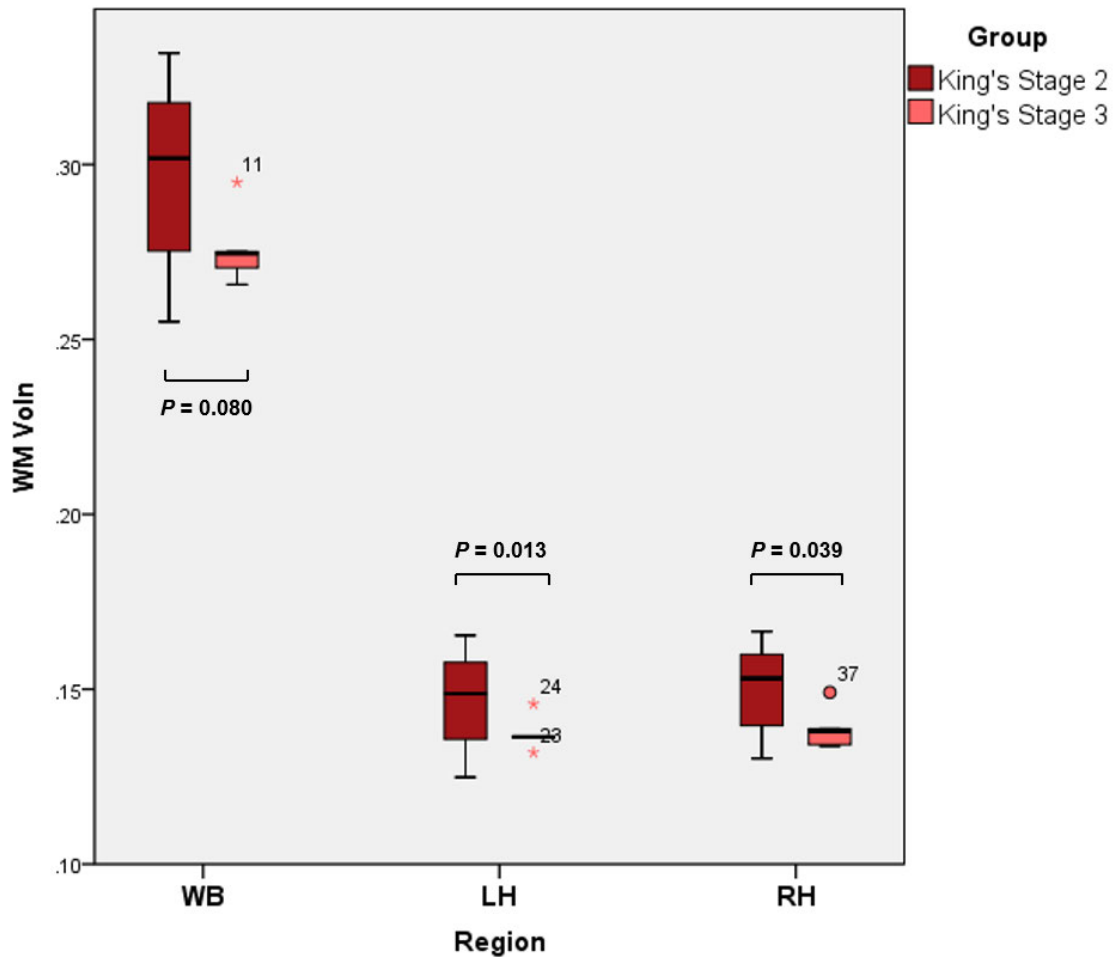
		*		*				0.508
		*			*			<b>0.045</b>
		*				*		0.240
		*					*	<b>0.043</b>
				*	*			0.269
				*		*		0.416
				*			*	0.188
					*	*		0.695
	RH	0.0079	0.0072	0.0076	0.0070	0.0066	0.0069	-
		*	*					<b>0.020</b>
		*		*				0.373
		*			*			<b>0.011</b>
		*				*		<b>0.012</b>
		*					*	<b>0.002</b>
				*	*			0.148
				*		*		0.137
				*			*	0.092
					*	*		0.090
MFG voln	WB	0.2553	0.0252	0.0249	0.0260	0.2430	0.0253	-
		*	*					0.529
		*		*				0.519
		*			*			0.531
		*				*		0.342
		*					*	0.834
				*	*			0.309
				*		*		0.658
				*			*	0.667
					*	*		0.210
	LH	0.0127	0.0125	0.0126	0.0129	0.0118	0.0125	-
		*	*					0.454
		*		*				0.508
		*			*			0.649
		*				*		0.184
		*					*	0.555
				*	*			0.609
				*		*		0.239
				*			*	0.795
					*	*		0.114
	RH	0.0129	0.0126	0.0123	0.0131	0.0125	0.0129	-
		*	*					0.551
		*		*				0.282
		*			*			0.264
		*				*		0.570
		*					*	0.608
				*	*			0.161
				*		*		0.632
				*			*	0.321
					*	*		0.316
Temp voln	WB	0.0452	0.0434	0.0428	0.0448	0.0422	0.0438	-
		*	*					0.188
		*		*				0.097
		*			*			0.758
		*				*		0.073
		*					*	0.158
				*	*			0.259
				*		*		0.805
				*			*	0.551
					*	*		0.287
	LH	0.0228	0.0217	0.0214	0.0222	0.0215	0.0219	-
		*	*					0.110

		*		*				0.083
		*			*			0.317
		*				*		0.067
		*					*	0.091
				*	*			0.439
				*		*		0.625
				*			*	0.587
					*	*		0.487
	RH	0.0224	0.0216	0.0213	0.0226	0.0207	0.0218	-
		*	*					0.161
		*		*				0.136
		*			*			0.728
		*				*		0.069
		*					*	0.317
				*	*			0.177
				*		*		0.609
				*			*	0.561
					*	*		0.126
Ventricles voln		0.0150	0.0242	0.0218	0.0217	0.0332	0.0262	-
		*	*					<b>0.000</b>
		*		*				<b>0.000</b>
		*			*			<b>0.005</b>
		*				*		<b>0.000</b>
		*					*	<b>0.001</b>
				*	*			0.844
				*		*		0.085
				*			*	0.425
					*	*		0.103
Brainstem voln		0.0140	0.0138	0.0141	0.0137	0.0132	0.0135	-
		*	*					<b>0.027</b>
		*		*				0.157
		*			*			0.186
		*				*		0.198
		*					*	0.214
				*	*			0.523
				*		*		0.240
				*			*	0.297
					*	*		0.502
Corpus callosum voln		0.0020	0.0018	0.0019	0.0019	0.0018	0.0018	-
		*	*					<b>0.021</b>
		*		*				0.116
		*			*			0.131
		*				*		<b>0.046</b>
		*					*	<b>0.026</b>
				*	*			0.533
				*		*		0.552
				*			*	0.479
					*	*		0.466

A table to show the differences in ROI volumes between the control group and the ALS whole group, as well as ALS subgroups based on King's stage of ALS. Volumes were normalised by the total intracranial volume (mm<sup>3</sup>). The two \* indicate which subgroups are being compared and statistical significance was set at  $P < 0.05$  for each comparison. Statistically significant differences are highlighted in bold.

Abbreviations: Cort, cortical; Voln, normalized volume; WB, whole brain; LH, left hemisphere; RH, right hemisphere, WM, white matter; GM, grey matter; PCG, precentral gyrus, MFG, middle frontal gyrus; ROI, region of interest.

**Figure 5.8: Comparison of cerebral white matter volume between King's stage 2 and King's stage 3 ALS subgroups.**



A figure to show the difference in cerebral white matter volume between King's stage 2 and King's stage 3 ALS subgroups in the whole brain, left hemisphere, and right hemisphere. Abbreviations: WB, whole brain; LH, left hemisphere; RH, right hemisphere.

The normalized cerebral GM volume was significantly reduced in the King's stage 3 ALS subgroup compared with the control group in both the total ( $P=0.022$ ) and cortical ( $P=0.042$ ) analysis. Similarly, the ALS subgroup combining stage 2 and 3 showed reduced total GM ( $P=0.027$ ) and cortical GM ( $P=0.041$ ) volumes compared with the control group.

The King's stage 2 ALS subgroup showed significantly reduced normalized PCG volume on analysis of the whole brain ( $P=0.014$ ), left hemisphere ( $P=0.045$ ), and right hemisphere ( $P=0.011$ ). The combined King's stages 2 and 3 ALS subgroup also showed significantly reduced PCG volume in the whole brain ( $P=0.005$ ), left hemisphere ( $P=0.043$ ), and right hemisphere ( $P=0.002$ ). While the King's stage 3 ALS PCG volume was significantly reduced in only the right hemisphere ( $P=0.012$ ).

Normalized volume of the ventricles was significantly increased in the King's stage 1 ( $P<0.001$ ), King's stage 2 ( $P=0.005$ ), King's stage 3 ( $P<0.001$ ), and the

combined King's stage 2 and 3 ( $P=0.001$ ) ALS subgroups. However, no significant difference was found between these subgroups.

In the corpus callosum both the King's stage 3 ALS subgroup ( $P=0.046$ ) and the combined King's stage 2 and 3 ALS subgroup ( $P=0.026$ ) showed significantly reduced volume compared to the control group.

There were no significant differences found in the volumes of the MFG, temporal lobe, and brainstem amongst any of the King's stage of ALS subgroups or between the ALS subgroups and the control group on either whole brain or hemispheric analysis.

### 5.7.2.2 Cortical thickness

Mean cortical thickness was significantly reduced in the King's stage 3 ALS subgroup on analysis of the whole brain ( $P=0.010$ ), left hemisphere ( $P=0.013$ ), and right hemisphere ( $P=0.009$ ). Similarly, the ALS subgroup combining King's stages 2 and 3 also showed significant reduction in mean cortical thickness compared to the control group in the whole brain ( $P=0.030$ ), left hemisphere ( $P=0.038$ ), and right hemisphere ( $P=0.024$ ).

The only other statistically significant finding on King's stage of ALS subgroup analysis of cortical thickness measures was a significant reduction in normalized temporal lobe volume of the King's stage 2 ALS subgroup when compared with the control group.

No significant differences were found on analysis of MFG cortical thickness.

**Table 5.6: Subgroup analysis comparing region of interest cortical thickness between control and ALS subgroups based on King's stage of ALS.**

Region of interest cortical thickness (mm)		Control (mean)	ALS (mean)					P value
			Whole group	Stage 1 (10)	Stage 2 (8)	Stage 3 (5)	Stages 2 + 3 (13)	
Cortical thickness	WB	2.3320	2.2747	2.2833	2.2905	2.2323	2.2681	-
		*	*					<b>0.024</b>
		*		*				0.082
		*			*			0.194
		*				*		<b>0.010</b>
		*					*	<b>0.030</b>
				*	*			0.860
				*		*		0.362
				*			*	0.720
				*	*		0.349	
	LH	2.3370	2.2796	2.2864	2.2976	2.2371	2.2743	-
		*	*					<b>0.027</b>
		*		*				0.096
		*			*			0.238
*					*		<b>0.013</b>	
*						*	<b>0.038</b>	
			*	*			0.814	

				*		*		0.369	
				*			*	0.773	
					*	*		0.328	
	RH	2.3270	2.2698	2.2801	2.2835	2.2275	2.2620	-	
		*	*					<b>0.024</b>	
		*		*				0.063	
		*			*			0.157	
		*				*		<b>0.009</b>	
		*					*	<b>0.024</b>	
				*	*			0.853	
				*		*		0.364	
				*			*	0.675	
					*	*		0.371	
PCG thickness (normalized)	WB	1.0266	1.0128	1.0164	1.0042	1.0192	1.0099	-	
		*	*					0.236	
		*		*				0.242	
		*			*			0.146	
		*				*		0.491	
		*					*	0.217	
				*	*			0.422	
				*		*		0.901	
				*			*	0.594	
						*	*	0.556	
		LH	1.0306	1.0215	1.0290	1.0102	1.0246	1.0157	-
			*	*					0.427
			*		*				0.471
			*			*			0.168
			*				*		0.604
			*					*	0.249
				*	*				0.344
				*		*			0.862
				*			*	*	0.463
						*	*		0.550
		RH	1.0225	1.0039	1.0036	0.9982	1.0138	1.0042	-
			*	*					0.075
			*		*				0.149
			*			*			0.173
			*				*		0.545
			*					*	0.176
				*	*				0.821
				*		*		*	0.708
				*			*	*	0.884
						*	*		0.606
MFG thickness (normalized)	WB	0.9947	0.9985	1.0038	0.9953	0.9928	0.9943	-	
		*	*					0.558	
		*		*				0.230	
		*			*			0.811	
		*				*		0.869	
		*					*	0.947	
				*	*			0.366	
				*		*		0.363	
				*			*	0.274	
						*	*	0.817	
		LH	1.0009	1.0024	1.0135	0.9958	0.9910	0.9939	-
			*	*					0.221
			*		*				0.186
			*			*			0.415
			*				*		0.390
			*					*	0.407
				*	*				0.202



				*		*		0.139
				*			*	0.096
					*	*		0.505
	RH	0.9885	0.9945	0.9941	0.9948	0.9949	0.9948	-
		*	*					0.178
		*		*				0.149
		*			*			0.372
		*				*		0.662
		*					*	0.484
				*	*			0.482
				*		*		0.345
				*			*	0.360
					*	*		0.559
Temporal thickness (normalized)	WB	1.1339	1.1405	1.1329	1.1156	1.1301	1.1463	-
		*	*					0.443
		*		*				0.919
		*			*			<b>0.036</b>
		*				*		0.786
		*					*	0.228
				*	*			0.101
				*		*		0.883
				*			*	0.337
					*	*		0.230
	LH	1.1287	1.1418	1.1477	1.1278	1.1525	1.1373	-
		*	*					0.518
		*		*				0.461
		*			*			0.963
		*				*		0.286
		*					*	0.633
				*	*			0.657
				*		*		0.928
				*			*	0.790
					*	*		0.577
	RH	1.1390	1.1443	1.1527	1.1256	1.1446	1.1329	-
		*	*					0.787
		*		*				0.336
		*			*			0.501
		*				*		0.814
		*					*	0.755
				*	*			0.436
			*		*		0.782	
			*			*	0.494	
				*	*		0.724	

A table to show the differences in ROI CT between the control group and the ALS whole group, as well as the ALS subgroups based on King's stage of ALS. The CT values were normalised by the mean CT (mm). The two \* indicate which subgroups are being compared and statistical significance was set at  $P < 0.05$  for all comparisons. Statistically significant differences are highlighted in bold. Abbreviations: CT, cortical thickness; LH, left hemisphere; RH, right hemisphere; WB, whole brain; ROI, region of interest; PCG, precentral gyrus; MFG, middle frontal gyrus

### 5.7.2.3 Surface area

There were no significant differences in mean surface area between King's stages of ALS subgroups or when compared with the control group, see table 5.7.

When analysing the King's stages of ALS subgroups for differences in normalized surface areas only two significant differences were found. The PCG surface area was

significantly reduced in the combined King's stage 2 and 3 ALS subgroup when compared with King's stage 1 ALS subgroup ( $P=0.030$ ), and the temporal lobe surface area was significantly reduced in the King's stage 3 ALS subgroup compared with King's stage 2 ALS ( $P=0.018$ ), both within the right hemisphere.

No other differences in region of interest surface areas reached statistical threshold.

**Table 5.7: Subgroup analysis comparing region of interest surface area between control and ALS subgroups based on King's stage of ALS.**

Region of interest surface area (mm <sup>2</sup> )		Control (mean)	ALS (mean)					P value
			Whole group	Stage 1 (10)	Stage 2 (8)	Stage 3 (5)	Stages 2 + 3 (13)	
Surface area	WB	170273	166102	162463	169534	167888	168901	-
		*	*					0.103
		*		*				0.122
		*			*			0.375
		*				*		0.180
		*					*	0.147
				*	*			0.237
				*		*		0.374
				*			*	0.196
				*	*		0.530	
	LH	84854	82779	80959	84356	83895	84178	-
		*	*					0.134
		*		*				0.126
		*			*			0.333
		*				*		0.248
		*					*	0.160
				*	*			0.253
				*		*		0.356
				*			*	0.199
				*	*		0.718	
	RH	85419	83323	81504	85178	83993	84722	-
		*	*					0.092
		*		*				0.121
		*			*			0.422
		*				*		0.130
		*					*	0.149
				*	*			0.226
			*		*		0.398	
			*			*	0.198	
			*	*		0.382		
PCG surface area (normalized)	WB	0.0568	0.0563	0.0575	0.0553	0.0557	0.0555	-
		*	*					0.754
		*		*				0.547
		*			*			0.427
		*				*		0.610
		*					*	0.384
				*	*			0.252
				*		*		0.375
		*			*	0.204		

					*	*		0.486
	LH	0.0567	0.0574	0.0572	0.0567	0.0587	0.0574	-
		*	*					0.369
		*		*				0.454
		*			*			0.104
		*				*		0.248
				*	*		*	0.478
				*		*		0.395
				*		*		0.284
				*		*	*	0.928
					*	*		0.065
	RH	0.0568	0.0554	0.0578	0.0539	0.0528	0.0535	-
		*	*					0.338
		*		*				0.522
		*			*			0.116
		*				*		0.134
		*					*	0.052
				*	*			0.063
				*		*		0.080
				*		*	*	<b>0.030</b>
					*	*		0.123
MFG surface area (normalized)	WB	0.0923	0.0945	0.0930	0.0972	0.0930	0.0956	-
		*	*					0.194
		*		*				0.160
		*			*			0.269
		*				*		0.611
		*					*	0.099
				*	*			0.074
				*		*		0.468
			*			*	0.205	
					*	*		0.173
	LH	0.0914	0.0936	0.0929	0.0962	0.0907	0.0941	-
		*	*					0.250
		*		*				0.510
		*			*			0.187
		*				*		0.335
		*					*	0.219
				*	*			0.202
				*		*		0.463
			*			*	0.605	
					*	*		0.088
	RH	0.0931	0.0953	0.0931	0.0981	0.0954	0.0971	-
		*	*					0.245
		*		*				0.192
		*			*			0.449
		*				*		0.521
		*					*	0.092
				*	*			0.053
				*		*		0.075
		*			*	0.091		
				*	*		0.304	
Temporal surface area (normalized)	WB	0.1199	0.1187	0.1180	0.1200	0.1181	0.1193	-
		*	*					0.946
		*		*				0.251
		*			*			0.076
		*				*		0.377
		*					*	0.562
				*	*			0.226
				*		*		0.953
		*			*	0.339		

					*	*		0.070
	LH	0.1216	0.1192	0.1186	0.1199	0.1190	0.1196	-
		*	*					0.119
		*		*				0.186
		*			*			0.387
		*				*		0.325
				*	*		*	0.185
				*		*		0.585
				*		*		0.857
				*			*	0.629
					*	*		0.178
	RH	0.1183	0.1183	0.1174	0.1201	0.1171	0.1189	-
		*	*					0.974
		*		*				0.429
		*			*			0.226
		*				*		0.307
		*					*	0.608
				*	*			0.118
				*		*		0.899
				*			*	0.271
					*	*		<b>0.018</b>

A table to show the differences in ROI SA between the control group and the whole ALS group, as well as the ALS subgroups based on King's stage of ALS. SA values were normalised by the mean SA (mm<sup>2</sup>). The two \* indicate which subgroups are being compared and statistical significance was set at  $P < 0.05$  for each comparison. Statistically significant differences are highlighted in bold.

Abbreviations: WB, whole brain; LH, left hemisphere; RH, right hemisphere; ROI, region of interest; SA, surface area; PCG, precentral gyrus; MFG, middle frontal gyrus.

### 5.7.3 Cognitive involvement

#### 5.7.3.1 Cerebral volumes

Total intracranial volume was not significantly difference when comparing the ALS cognitive subgroups with one another or with the control group, see table 5.8.

No significant differences were detected in any of the region of interest normalized cerebral volumes when comparing the normal ECAS subgroup with abnormal ECAS subgroup. Statistically significant results were only achieved on comparison of ALS cognitive subgroups with the control group.

The abnormal ECAS ALS subgroup showed significantly reduced normalised cortical volume in the whole brain ( $P=0.015$ ), left hemisphere ( $P=0.017$ ), and right hemisphere ( $P=0.013$ ), when compared with the control group.

The cerebral WM volume of the left hemisphere was significantly reduced in both the normal ECAS ( $P=0.035$ ), and abnormal ECAS ( $P=0.038$ ) ALS subgroups, when compared with the control group.

The abnormal ECAS ALS subgroup showed significantly reduced GM volume in both total GM ( $P=0.033$ ) and cortical GM ( $P=0.048$ ) measures when compared to the control group.

**Table 5.8: Subgroup analysis comparing region of interest volume between control and ALS cognitive subgroups.**

Region of interest volume (mm <sup>3</sup> )		Control (mean)	ALS (mean)			P value	
			Whole group (23)	Normal ECAS (11)	Abnormal ECAS (12)		
Total intracranial Volume		1561688	1556345	1574270	1539912	-	
		*	*			0.114	
		*		*		0.176	
		*			*	0.279	
				*	*	0.546	
Cortical volume (normalized)	WB	0.2817	0.2695	0.2717	0.2676	-	
		*	*			<b>0.018</b>	
		*		*		0.095	
		*			*	<b>0.015</b>	
				*	*	0.481	
	LH	0.1407	0.1346	0.1353	0.1339	-	
		*	*			<b>0.015</b>	
		*		*		0.078	
		*			*	<b>0.017</b>	
	RH			*	*	0.399	
		0.1411	0.1350	0.1364	0.1336	-	
		*	*			<b>0.021</b>	
		*		*		0.102	
	Cerebral white matter volume (normalized)	WB			*	*	<b>0.013</b>
					*	*	0.514
			0.3040	0.2916	0.2922	0.2911	-
*			*			<b>0.037</b>	
LH		*		*		0.073	
		*			*	0.072	
				*	*	0.691	
		0.1514	0.1447	0.1445	0.1449	-	
RH		*	*			<b>0.024</b>	
		*		*		<b>0.035</b>	
		*			*	<b>0.038</b>	
				*	*	0.640	
Cerebral grey matter volume (normalized)	Total	0.1526	0.1470	0.1477	0.1462	-	
		*	*			<b>0.058</b>	
		*		*		0.146	
		*			*	0.081	
	Cortical			*	*	0.559	
		0.3785	0.3629	0.3642	0.3617	-	
		*	*			<b>0.022</b>	
		*		*		0.079	
Precentral gyrus volume (normalized)	WB	*		*		<b>0.033</b>	
				*	*	0.656	
		0.3432	0.3301	0.3312	0.3292	-	
		*	*			<b>0.034</b>	
Precentral gyrus volume (normalized)	LH	*		*		0.099	
		*			*	<b>0.048</b>	
				*	*	0.571	
		0.0159	0.0148	0.0152	0.0144	-	
Precentral gyrus volume (normalized)	WB	*	*			<b>0.037</b>	
		*		*		0.301	
		*			*	<b>0.018</b>	
				*	*	0.294	
Precentral gyrus volume (normalized)	LH	0.0080	0.0076	0.0079	0.0073	-	
		*	*			0.125	

		*		*		0.778
		*			*	<b>0.010</b>
				*	*	0.068
	RH	0.0079	0.0072	0.0072	0.0071	-
		*	*			<b>0.020</b>
		*		*		0.098
		*			*	<b>0.029</b>
				*	*	0.711
Middle frontal gyrus volume (normalized)	WB	0.0255	0.0252	0.0254	0.0249	-
		*	*			0.529
		*		*		0.840
		*			*	0.368
				*	*	0.570
	LH	0.0127	0.0125	0.0127	0.0123	-
		*	*			0.454
		*		*		0.491
		*			*	0.525
				*	*	0.511
	RH	0.0129	0.0126	0.0128	0.0125	-
		*	*			0.551
		*		*		0.816
		*			*	0.331
				*	*	0.397
	Temporal lobe volume (normalized)	WB	0.0452	0.0434	0.0437	0.0431
*			*			0.188
*				*		0.181
*					*	0.513
				*	*	0.644
LH		0.0228	0.0217	0.0215	0.0219	-
		*	*			0.110
		*		*		0.052
		*			*	0.105
				*	*	0.402
RH		0.0224	0.0216	0.0222	0.0211	-
		*	*			0.161
	*		*		0.518	
	*			*	0.073	
			*	*	0.251	
Ventricles volume (normalized)	0.0148	0.0242	0.0210	0.0273	-	
	*	*			<b>0.000</b>	
	*		*		<b>0.005</b>	
	*			*	<b>0.000</b>	
			*	*	0.189	
Brainstem volume (normalized)	0.0140	0.0138	0.0141	0.0135	-	
	*	*			<b>0.027</b>	
	*		*		0.160	
	*			*	<b>0.029</b>	
			*	*	0.426	
Corpus callosum volume (normalized)	0.0020	0.0018	0.0018	0.0018	-	
	*	*			<b>0.021</b>	
	*		*		0.065	
	*			*	<b>0.048</b>	
			*	*	0.347	

A table to show the difference in ROI volumes between the control group and the whole ALS group, as well as the ALS cognitive subgroups. The volumes were normalised by the mean the total intracranial volume (mm<sup>3</sup>). The two \* indicate which subgroups are being compared and statistical significance was set at  $P < 0.05$  for all comparisons. Statistically significant differences are highlighted in bold.

Abbreviations: WB, whole brain; LH, left hemisphere; RH, right hemisphere; ROI, region of interest.

In the PCG the abnormal ECAS ALS subgroup showed significantly reduced volume in the whole brain ( $P=0.018$ ), left hemisphere ( $P=0.010$ ) and right hemisphere ( $P=0.029$ ).

No significant differences were found in the normalised MFG or temporal lobe volumes.

The ventricle volume was significantly increased in both the normal ECAS ALS subgroup ( $P=0.005$ ) and the abnormal ECAS ALS subgroup ( $P<0.001$ ), compared to the control group.

The abnormal ECAS ALS subgroup showed significantly reduced normalized volumes of the brainstem ( $P=0.029$ ) and the corpus callosum ( $P=0.048$ ), on comparison with the control group.

### 5.7.3.2 Cortical thickness

Mean cortical thickness was significantly reduced in the abnormal ECAS ALS subgroup compared to the control group in the whole brain ( $P=0.011$ ), left hemisphere ( $P=0.018$ ), and right hemisphere ( $P=0.007$ ).

There were no significant differences in normalized regional brain cortical thickness values of the PCG, MFG or temporal lobe when comparing the cognitive ALS subgroups with each other, or between either of the cognitive ALS subgroups and the control group.

**Table 5.9: Subgroup analysis comparing region of interest cortical thickness between control and ALS cognitive subgroups.**

Region of interest cortical thickness (mm)		Control (mean)	ALS (mean)			P value
			Whole group (23)	Normal ECAS (11)	Abnormal ECAS (12)	
Cortical Thickness	WB	2.3320	2.2747	2.2957	2.2555	-
		*	*			<b>0.024</b>
		*		*		0.084
		*			*	<b>0.011</b>
	LH			*	*	0.336
		2.3370	2.2796	2.2968	2.2639	-
		*	*			<b>0.027</b>
		*		*		0.099
	RH			*	*	<b>0.018</b>
		2.3270	2.2698	2.2947	2.2471	-
		*	*			<b>0.024</b>
		*		*		0.075
Precentral gyrus thickness (normalized)			*	*	<b>0.007</b>	
			*	*	0.261	
	1.0266	1.0127	1.0101	1.0152	-	
	*	*			0.236	
Precentral gyrus thickness (normalized)			*		0.275	
	*		*		0.396	
	*		*	*	0.518	

	LH	1.0306	1.0215	1.0271	1.0164	-
		*	*			0.427
		*		*		0.428
		*			*	0.266
				*	*	0.556
	RH	1.0225	1.0039	0.9930	1.0140	-
		*	*			0.075
		*		*		0.073
		*			*	0.584
				*	*	0.309
Middle frontal gyrus thickness (normalized)	WB	0.9948	0.9985	0.9959	1.0008	-
		*	*			0.558
		*		*		0.593
		*			*	0.449
				*	*	0.480
	LH	1.0009	1.0024	1.0028	1.0022	-
		*	*			0.221
		*		*		0.239
		*			*	0.398
				*	*	0.730
	RH	0.9885	0.9945	0.9891	0.9995	-
		*	*			0.178
		*		*		0.181
		*			*	0.235
				*	*	0.237
	Temporal cortex thickness	WB	1.1339	1.1405	1.1487	1.1325
*			*			0.443
*				*		0.132
*					*	0.267
				*	*	0.923
LH		1.1287	1.1418	1.1401	1.1329	-
		*	*			0.518
		*		*		0.597
		*			*	0.502
				*	*	0.931
RH		1.1390	1.1444	1.1372	1.1509	-
		*	*			0.787
		*		*		0.932
		*			*	0.513
				*	*	0.720

A table to show the difference in ROI CT between the control group and the ALS group as a whole, as well as the ALS cognitive subgroups. The CT values were normalised by the mean CT (mm). The two \* indicate which subgroups are being compared and statistical significance was set at  $P < 0.05$  for each comparison. Statistically significant differences are highlighted in bold.

Abbreviations: CT, cortical thickness; WB, whole brain; LH, left hemisphere; RH, right hemisphere; ROI, region of interest.

### 5.7.3.3 Surface area

No significant difference in mean surface area or normalized surface area measurements of the PCG, MFG, and temporal lobe were found when comparing the ALS cognitive subgroups with each other or with the control group, see table 5.10.



**Table 5.10: Subgroup analysis comparing region of interest cerebral surface area between control and ALS cognitive subgroups.**

Region of interest surface area (mm <sup>2</sup> )		Control (mean)	ALS (mean)			P value	
			Whole group (23)	Normal ECAS (11)	Abnormal ECAS (12)		
Surface area	WB	170273	166102	167872	164479	-	
		*	*			0.103	
		*		*		0.413	
		*			*	0.114	
	LH	84854	82779	83382	82227	-	
		*	*			0.134	
		*		*		0.491	
		*			*	0.135	
	RH	85419	83323	84491	82252	-	
		*	*			0.092	
		*		*		0.346	
		*			*	0.101	
	Precentral gyrus surface area (normalized)	WB	0.0568	0.0564	0.0578	0.0550	-
			*	*			0.754
			*		*		0.428
			*			*	0.271
LH		0.0567	0.0574	0.0592	0.0557	-	
		*	*			0.369	
		*		*		0.092	
		*			*	0.208	
RH		0.0568	0.0554	0.0564	0.0544	-	
		*	*			0.338	
		*		*		0.739	
		*			*	0.205	
Middle frontal gyrus surface area (normalized)		WB	0.0923	0.0945	0.0948	0.0942	-
			*	*			0.194
			*		*		0.233
			*			*	0.326
	LH	0.0914	0.0936	0.0944	0.0928	-	
		*	*			0.250	
		*		*		0.189	
		*			*	0.487	
	RH	0.0931	0.0953	0.0951	0.0956	-	
		*	*			0.245	
		*		*		0.422	
		*			*	0.265	
	Temporal surface area (normalized)	WB	0.1199	0.1187	0.1183	0.1191	-
			*	*			0.300
			*		*		0.306
			*			*	0.476
LH		0.1216	0.1192	0.1178	0.1204	-	
		*	*			0.526	
						0.119	

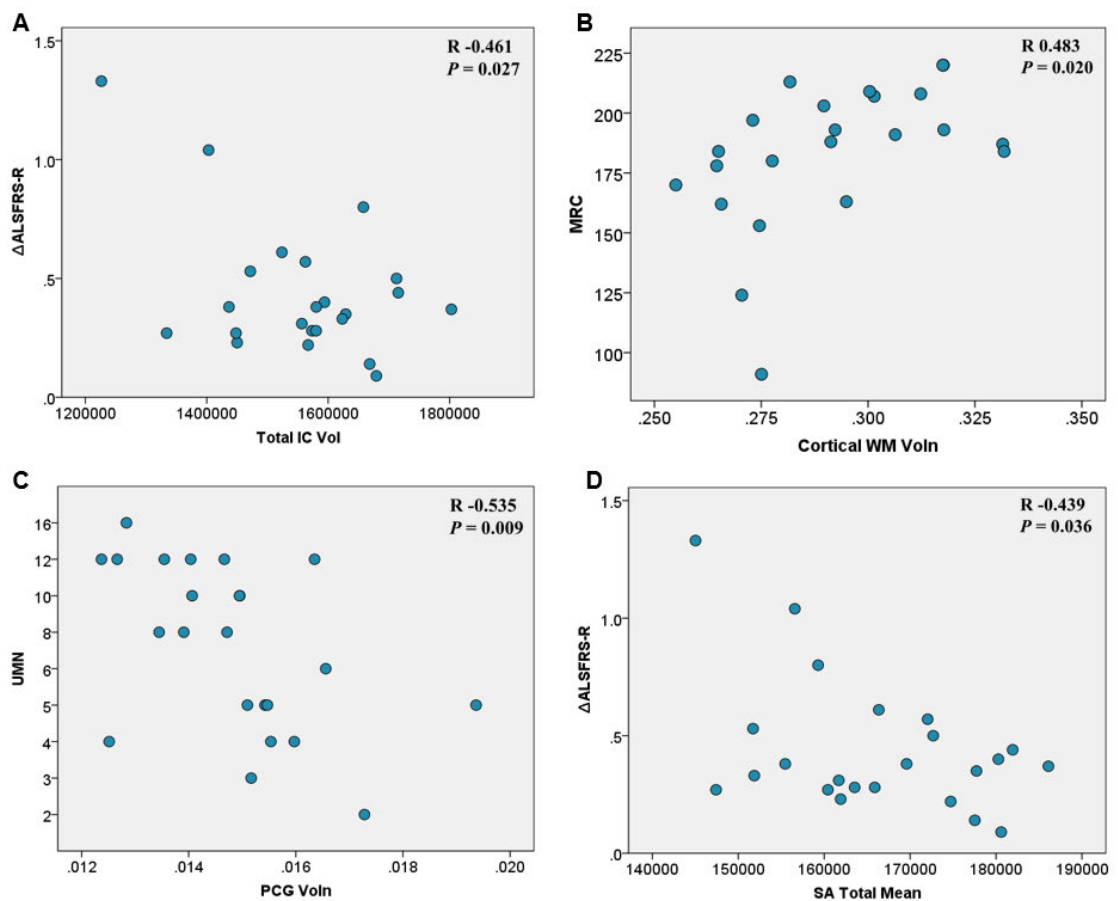
		*		*		0.051
		*			*	0.336
				*	*	0.191
	RH	<b>0.1183</b>	<b>0.1183</b>	<b>0.1187</b>	<b>0.1179</b>	-
		*	*			0.974
		*		*		0.825
		*			*	0.752
				*	*	0.592

A table to show the difference in ROI SA between the control group and the whole ALS group, as well as the ALS cognitive subgroups. The SA values were normalised by the mean SA (mm<sup>2</sup>). The two \* indicate which subgroups are being compared and statistical significance was set at  $P < 0.05$  for all comparisons. Statistically significant differences are highlighted in bold. Abbreviations: WB, whole brain; LH, left hemisphere; RH, right hemisphere; ROI, region of interest; SA, surface area.

## 5.8 Correlation between SBM data and clinical parameter results

There were four statistically significant correlations found on regression analysis, see figure 5.9 and table 5.11,

**Figure 5.9 Correlation between SBM parameters and clinical measures of ALS**



Scatterplots to show the significant correlations between SBM parameters and clinical measures of ALS severity. A,  $\Delta$ ALSFRS-R and total intracranial volume; B, MRC and cortical WM volume (normalized); C, UMN score and PCG volume (normalized); D,  $\Delta$ ALSFRS-R and mean surface area, Statistical significance was set at  $P < 0.05$ .

Abbreviations: R, Pearson's regression coefficient;  $\Delta$  ALSFRS-R, change in ALS revised functional rating scale over time; MRC, Medical Research Council power score; UMN, upper motor neurone score.

**Table 5.11: Correlation of SBM parameters with clinical measures of ALS**

	Disease duration	UMN	MRC	ALSFRS -R	$\Delta$ ALSFRS -R	ECAS total
<b>Total intracranial volume (mm<sup>3</sup>)</b>						
PCC	<b>0.394</b>	0.065	0.037	0.085	<b>-0.461</b>	0.131
Sig. (2-tailed)	<b>0.063</b>	0.768	0.868	0.699	<b>0.027</b>	0.551
<b>Cortical volume, normalized (mm<sup>3</sup>)</b>						
PCC	-0.230	-0.129	0.172	0.100	0.048	0.085
Sig. (2-tailed)	0.291	0.558	0.433	0.651	0.829	0.138
<b>WM volume, normalized (mm<sup>3</sup>)</b>						
PCC	-0.072	-0.029	<b>0.483</b>	0.335	-0.266	0.319
Sig. (2-tailed)	0.743	0.896	<b>0.020</b>	0.118	0.219	0.138
<b>Total GM volume, normalized (mm<sup>3</sup>)</b>						
PCC	-0.284	-0.110	0.248	0.164	0.007	0.054
Sig. (2-tailed)	0.189	0.618	0.255	0.454	0.973	0.805
<b>Cortical GM volume, normalized (mm<sup>3</sup>)</b>						
PCC	-0.284	-0.121	0.219	0.145	0.025	0.028
Sig. (2-tailed)	0.190	0.583	0.315	0.509	0.911	0.897
<b>PCG volume, normalized (mm<sup>3</sup>)</b>						
PCC	-0.206	<b>-0.535</b>	0.082	0.259	-0.260	0.012
Sig. (2-tailed)	0.346	<b>0.009</b>	0.710	0.232	0.230	0.958
<b>MFG volume, normalized (mm<sup>3</sup>)</b>						
PCC	-0.262	0.147	0.082	0.035	0.193	0.194
Sig. (2-tailed)	0.227	0.504	0.710	0.873	0.379	0.376
<b>Temporal volume, normalized (mm<sup>3</sup>)</b>						
PCC	-0.021	-0.167	0.198	-0.023	0.063	0.044
Sig. (2-tailed)	0.924	0.447	0.366	0.916	0.774	0.841
<b>Ventricle volume, normalized (mm<sup>3</sup>)</b>						
PCC	0.199	0.269	<b>-0.398</b>	-0.267	0.141	-0.296
Sig. (2-tailed)	0.363	0.215	<b>0.060</b>	0.219	0.522	0.170
<b>Brainstem volume, normalized (mm<sup>3</sup>)</b>						
PCC	-0.153	-0.011	0.358	0.199	-0.224	0.224
Sig. (2-tailed)	0.487	0.962	0.093	0.362	0.305	0.303
<b>Corpus callosum volume, normalized (mm<sup>3</sup>)</b>						
PCC	-0.300	0.166	0.140	0.263	-0.081	0.241
Sig. (2-tailed)	0.164	0.448	0.524	0.225	0.714	0.268
<b>Cortical thickness, mean (mm)</b>						
PCC	-0.192	-0.208	-0.017	0.298	-0.183	-0.186
Sig. (2-tailed)	0.379	0.340	0.937	0.167	0.403	0.396
<b>PCG thickness, normalized (mm)</b>						
PCC	-0.123	0.089	0.070	0.098	-0.071	-0.148
Sig. (2-tailed)	0.576	0.686	0.752	0.658	0.747	0.500
<b>MFG thickness, normalized (mm)</b>						
PCC	-0.121	0.220	-0.032	0.058	0.116	0.118
Sig. (2-tailed)	0.583	0.313	0.884	0.792	0.597	0.592
<b>Temporal thickness, normalized (mm)</b>						
PCC	0.279	-0.174	0.111	-0.285	0.134	0.167
Sig. (2-tailed)	0.197	0.428	0.613	0.188	0.542	0.448
<b>Surface area, mean (mm<sup>2</sup>)</b>						
PCC	<b>0.397</b>	-0.111	0.221	0.050	<b>-0.439</b>	0.166
Sig. (2-tailed)	<b>0.060</b>	0.613	0.312	0.821	<b>0.036</b>	0.449
<b>PCG surface area, normalized (mm<sup>2</sup>)</b>						
PCC	0.074	-0.490	-0.209	-0.079	-0.171	0.087
Sig. (2-tailed)	0.736	0.018	0.340	0.721	0.435	0.693
<b>MFG surface area, normalized (mm<sup>2</sup>)</b>						
PCC	-0.030	0.294	0.018	-0.047	0.123	0.202
Sig. (2-tailed)	0.892	0.173	0.936	0.830	0.575	0.355
<b>Temporal surface area, normalized (mm<sup>2</sup>)</b>						
PCC	0.285	0.030	0.246	-0.005	-0.111	-0.007
Sig. (2-tailed)	0.187	0.891	0.258	0.982	0.615	0.976

A table to show the statistically significant correlations between SBM parameters and clinical measures of ALS severity. **Correlation is significant at the  $P < 0.05$  level.**

Abbreviation: PCC, Pearson's Correlation Coefficient

Total intracranial volume showed negative correlation with  $\Delta$ ALSFRS-R ( $P=0.027$ ), figure 5.9A. Normalized WM volume showed positive correlation with MRC score ( $P=0.020$ ), see figure 5.9B. Normalized PCG volume showed negative correlation with UMN score ( $P=0.009$ ), see figure 5.9C. Finally mean surface area showed negative correlation with  $\Delta$ ALSFRS-R ( $P=0.036$ ), figure 5.9D.

## 5.9 Correlation between NODDI and SBM parameter results

All of the NODDI parameters showed correlation with some of the SBM volume and cortical thickness measures but none showed correlation with surface area measures.

### 5.9.1 Correlation between NDI and SBM measures

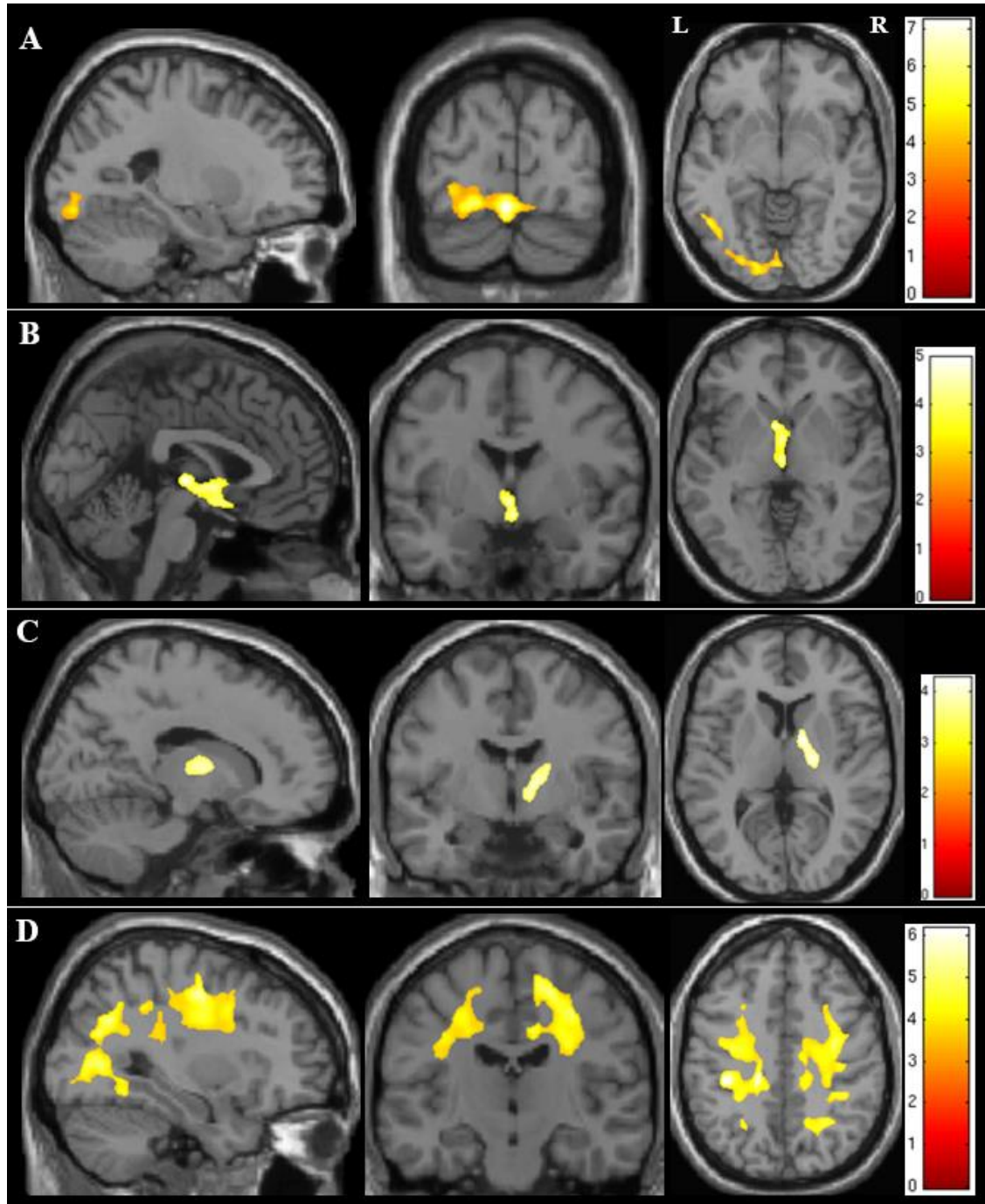
The NODDI parameter of NDI correlated with four SBM measures on regression analysis, see table 5.12. There was positive correlation with normalized WM volume in the left occipital and temporal cortex ( $P<0.001$ ), see figure 5.10A.

**Table 5.12 Regions of significant correlation between NDI and SBM parameters**

NDI correlation	Contiguous anatomical regions within cluster	MNI co-ordinate (x, y, z)	t-value	K (size)	$P_{\text{cluster level FWE-corr}}$
Positive correlation with WM volume	Left cerebral cortex, lingual gyrus, occipital fusiform, and middle temporal gyrus	-2 -85 -11	7.23	5933	<0.001
		-16 -88 -10	6.46		
		-48 -60 -4	5.62		
Positive correlation with total GM volume	Left caudate and internal capsule, left thalamus and right thalamus	-5 9 1	4.96	2432	0.053
		0 -17 1	4.84		
		3 3 -9	4.65		
Positive correlation with brainstem volume	Right thalamus and right cerebral white matter, posterior limb of the internal capsule	13 -1 6	4.27	2680	0.033
		21 -15 9	4.05		
		10 -16 -4	3.68		
Positive correlation with PCG cortical thickness	Right occipital fusiform gyrus	25 -65 -1	5.61	31560	<0.001
	Right postcentral gyrus	19 -53 53	5.59		
	Right precentral gyrus	33 -9 46	5.55		
	Left precentral gyrus	-15 -29 39	6.18	16953	<0.001
	Left postcentral gyrus	-36 -30 40	6.15		
	Left corona radiata	-42 -32 35	6.11		
	Left occipital fusiform gyrus	-28 -63 27	4.93	1917	0.028
	Left cerebral WM	-25 -59 39	4.28		
	Left lateral occipital cortex	-37 -60 18	4.09		
	Left occipital fusiform gyrus	-29 -69 -3	4.64	1687	0.047
Left lateral occipital cortex	-33 -76 15	4.52			
Left temporal fusiform gyrus	-32 -57 -2	4.18			

A table to show the anatomical regions where significant correlation was demonstrated, on whole brain analysis of the NODDI parameter NDI with SBM measures. A statistical significance threshold of  $P<0.05$  family-wise error (FWE) correction at cluster level ( $P_{\text{cluster}}$ ) was used, after clusters were formed with an uncorrected  $P<0.001$ . Montreal Neurological Institute (MNI) co-ordinates were used to define the anatomical location of each cluster of voxels within the MRI volume. The MNI coordinates refer to the peak t-value. Local maxima that are more than 8mm apart are shown for each cluster. K indicates the size of the cluster in voxels. Abbreviations: WM, white matter; GM, grey matter; PCG, precentral gyrus; MNI, Montreal Neurological Institute; FWE, family-wise error; corr, corrected.

**Figure 5.10 Correlation between NDI and SBM parameters**



A figure to show the areas of significant correlation between NDI and SBM parameters on regression analysis, where results are shown using statistical significance of  $P < 0.05$  FWE correction at cluster level, clusters formed with  $P < 0.001$ .

(A) Positive correlation between NDI and normalized WM volume.

(B) Positive correlation between NDI and normalized total GM volume.

(C) Positive correlation between NDI and normalized brainstem volume.

(D) Positive correlation between NDI and normalized PCG cortical thickness.

Positive correlation was also found between NDI and normalized total GM volume in the thalamus, which was very close to statistical significance ( $P = 0.053$ ), see figure 5.10B.

NDI showed positive correlation with normalized brainstem volume in the right posterior limb of the internal capsule and thalamus ( $P = 0.033$ ), see figure 5.10C.

Finally, there was positive correlation between NDI and normalized PCG cortical thickness within the cerebral WM and cortical regions bilaterally, including the corona radiata and the PCG ( $P < 0.001$ ), see figure 5.10D. NDI within the left occipital WM ( $P = 0.028$ ) and left occipital fusiform gyrus ( $P = 0.047$ ) also showed significant correlation with normalized PCG cortical thickness, see figure 5.10D and table 5.12.

### 5.9.2 Correlation between ODI and SBM measures

Regression analysis demonstrated a dozen significant correlations between the NODDI parameter of ODI and SBM measures, see Table 5.13.

**Table 5.13 Regions of significant correlation between ODI and SBM parameters**

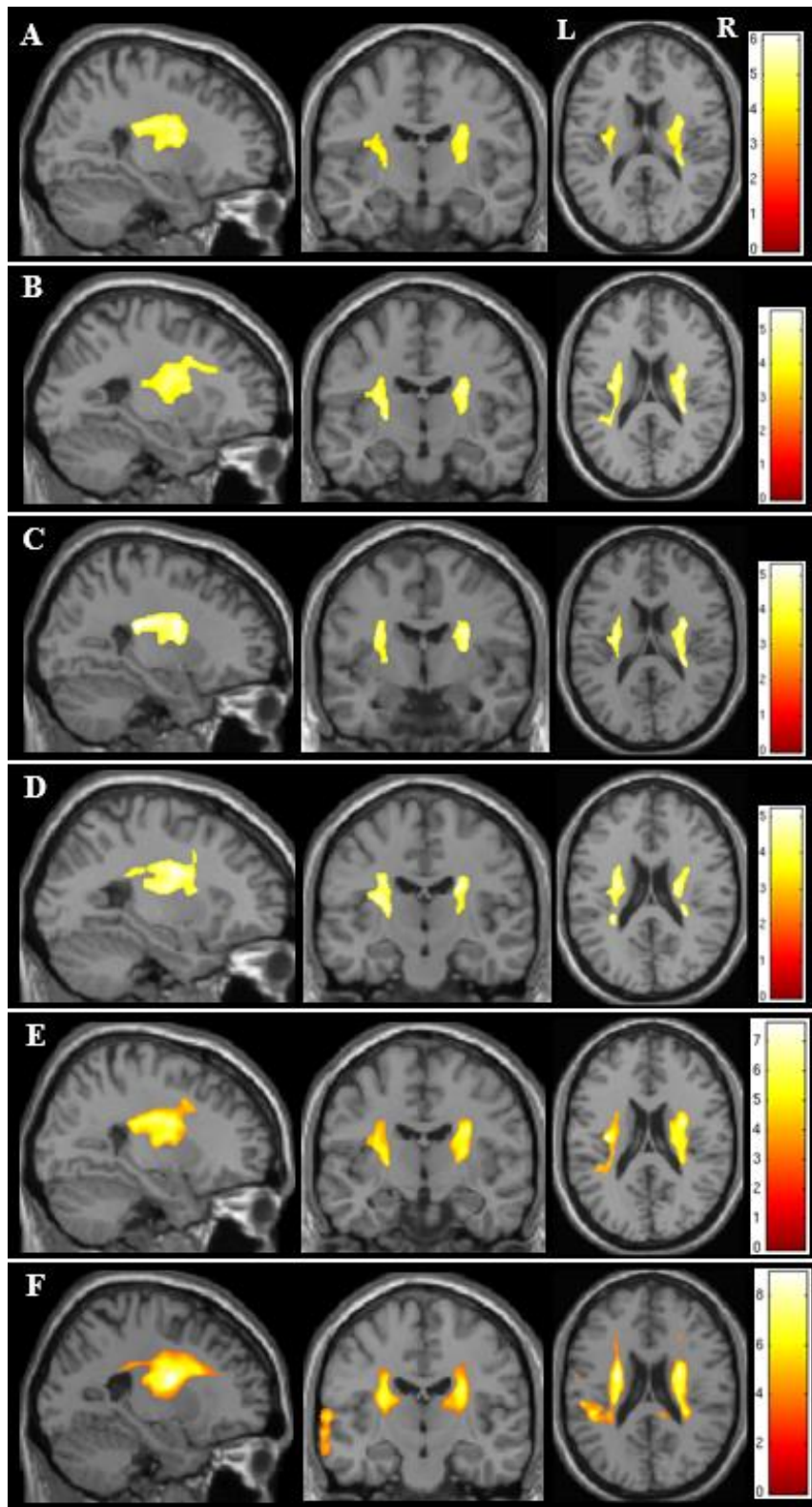
ODI correlation	Contiguous anatomical regions within cluster	MNI co-ordinate (x, y, z)	t-value	K (size)	$P_{\text{cluster level FWE-corr}}$
Positive correlation with cerebral cortex volume	Right cerebral WM, internal capsule, corona radiata and opercular cortex	30 -1 21 28 -30 21 25 -17 24	5.89 5.47 5.26	5584	<0.001
	Left insular cortex Left pallidum, internal capsule, and putamen	-35 -15 19 -23 -9 5 -27 5 12	6.12 4.66 4.63	2514	0.002
Positive correlation with total GM volume	Left pallidum Left cerebral WM, internal capsule and left putamen	-23 -9 4 -30 -15 20 -27 5 13	5.53 5.02 4.98	5107	<0.001
	Right cerebral WM, internal capsule and corona radiata	26 -18 23 29 -2 22 28 -26 23	5.56 5.53 5.42	4894	<0.001
Positive correlation with cortical GM volume	Right cerebral WM, internal capsule and corona radiata	28 -28 22 29 -2 22 26 -18 23	5.30 5.29 5.22	4391	<0.001
	Left pallidum Left cerebral WM, internal capsule and left putamen	-23 -9 4 -31 -15 20 -27 5 13	5.26 4.83 4.75	3734	<0.001
Positive correlation with MFG volume	Left cerebral WM, internal capsule and corona radiata	-35 -44 18 -27 -7 26 -30 -37 21	5.13 4.95 4.85	5620	<0.001
	Right cerebral WM, internal capsule and corona radiata	23 -14 24 29 -33 20 30 3 19	5.22 4.75 3.97	2775	0.001
Positive correlation with temporal lobe volume	Right cerebral WM, internal capsule and corona radiata	29 -2 22 25 -17 24 29 -10 27	7.30 6.42 6.30	9553	<0.001
	Left cerebral WM and insular cortex, temporal operculum, and left putamen	-34 -15 20 -39 -27 13 -27 5 12	7.59 6.01 5.62	7044	<0.001
Negative correlation with ventricle volume	Right cerebral WM, internal capsule and corona radiata	26 -3 24 31 -35 18 26 -16 23	8.75 7.90 7.38	12915	<0.001
	Left cerebral WM, internal capsule and corona radiata Left parietal opercular cortex	-24 -4 19 -27 14 28 -44 -35 20	8.96 7.34 7.21	12119	<0.001
	Left cerebral cortex, planum temporale, superior	-63 -16 5 -65 -13 -5 -64 -11 -15	6.33 5.32 5.20	3938	<0.001

	temporal, and middle temporal gyrus				
	Right cerebral WM, frontal pole	10 57 -13 8 50 14	5.56 5.28	3521	<0.001
	Right paracingulate cortex	-4 58 14	5.24		
	Left frontal pole				
Positive correlation with total WM volume	Right cerebral cortex, precentral gyrus and postcentral gyrus	48 -16 58 35 -27 63 58 -11 45	6.78 6.28 5.46	4464	<0.001
	Right cerebral cortex, middle frontal gyrus and inferior frontal gyrus	50 27 32 52 28 17 53 24 9	6.02 5.47 4.63	2607	0.002
	Right paracingulate gyrus, cingulate gyrus, and supplementary motor cortex	5 19 38 0 -6 39 5 8 51	7.70 5.79 5.02	2432	0.002
	Right superior frontal gyrus	4 36 46	5.52	1950	0.009
	Left superior frontal gyrus	-2 20 63 -2 31 56	5.10 4.70		
	Right cerebral cortex, frontal pole	33 55 8 34 51 25 33 58 0	6.01 4.88 4.61	1620	0.023
	Right cerebral cortex, middle frontal gyrus	32 19 57 47 22 44 39 16 43	4.72 4.68 3.91	1586	0.025
Positive correlation with corpus callosum volume	Right cerebral cortex, frontal pole, superior frontal gyrus	31 48 29 18 33 54 25 37 48	6.76 6.24 5.24	4124	<0.001
	Right cerebral cortex, angular gyrus, supramarginal and postcentral gyrus	47 -46 55 55 -28 51 58 -18 36	5.29 4.81 3.92	2104	0.005
	Right cerebral cortex, middle frontal gyrus,	40 26 42 46 21 44 32 23 54	5.76 4.80 4.46	1862	0.010
Negative correlation with PCG volume	Left thalamus	-1 -19 0	5.34	1469	0.037
	Right thalamus	2 -2 -4	4.47		
	Left thalamus	-4 -2 -11	4.22		
Positive correlation with ventricle volume	Left thalamus	-5 -5 11	10.0	7696	<0.001
	Right thalamus	1 -15 10	8.98		
	Right thalamus	1 2 -1	7.36		
Positive correlation with PCG cortical thickness	Right cerebral cortex, supramarginal gyrus, and postcentral gyrus	55 -33 50 46 -44 48 47 -36 49	4.71 4.62 4.17	2015	0.007
Positive correlation with temporal lobe cortical thickness	Right cerebral WM, internal capsule, corona radiata, and corpus callosum	33 -25 37 11 -37 22 29 -24 26	6.14 5.75 5.28	7608	<0.001
	Left cerebral WM, internal capsule	-35 -40 18 -31 -14 22 -29 -25 26	5.24 4.89 4.42	2618	0.002
	Right cerebral cortex, inferior temporal gyrus, fusiform cortex,	43 -16 -25 41 -35 -14 38 -23 -33	6.88 5.20 3.83	1501	0.031

A table to show the anatomical regions where significant correlation was demonstrated, on whole brain analysis of the NODDI parameter ODI with SBM measures. A statistical significance threshold of  $P < 0.05$  family-wise error (FWE) correction at cluster level ( $P_{cluster}$ ) was used, after clusters were formed with an uncorrected  $P < 0.001$ . Montreal Neurological Institute (MNI) coordinates were used to define the anatomical location of each cluster of voxels within the MRI volume. The MNI coordinates refer to the peak t-value. Local maxima that are more than 8mm apart are shown for each cluster. K indicates the size of the cluster in voxels. Abbreviations: WM, white matter; GM, grey matter; PCG, precentral gyrus; MFG, middle frontal gyrus; MNI, Montreal Neurological Institute; FWE, family-wise error; corr, corrected.



Figure 5.11 Correlation between ODI and SBM volume measures.



A figure to show the significant correlation between ODI and SBM volume measures. The results shown have statistical significance of  $P < 0.05$  FWE correction at cluster level, clusters formed with  $P < 0.001$ .

- (A) Positive correlation between ODI and normalized cerebral cortex volume.
- (B) Positive correlation between ODI and normalized total GM volume.
- (C) Positive correlation between ODI and normalized cortical GM volume.
- (D) Positive correlation between ODI and normalized MFG volume.
- (E) Positive correlation between ODI and normalized temporal lobe volume.
- (F) Negative correlation between ODI and normalized volume of the ventricles.

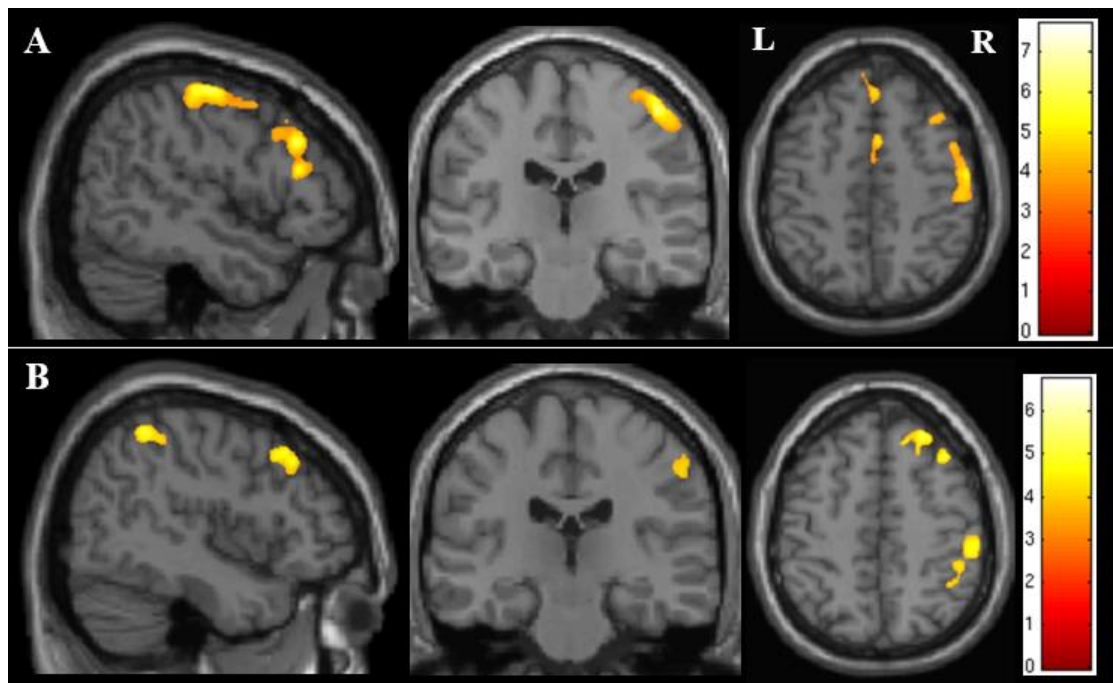


Positive correlation of ODI bilaterally within the internal capsule, in some places extending into the corona radiata, was found with normalized SBM measures of cerebral cortex volume ( $P<0.001$ ; Figure 5.11A), total GM volume ( $P<0.001$ ; Figure 5.11B), cortical GM ( $P<0.001$ ; Figure 5.11C), MFG volume ( $P<0.001$ ; Figure 5.11D), and temporal lobe volume ( $P<0.001$ ; Figure 5.11E). In addition, negative correlation was found between ODI and normalized volume of the ventricles within the internal capsule and corona radiata bilaterally ( $P<0.001$ ) as well as regions in the left temporal cortex ( $P<0.001$ ), see figure 5.11F. These results were all included the same figure due to the similarity of regions where significant correlation was demonstrated (figure 5.11).

Positive correlation was found between ODI and normalized total WM volume, in regions involving the right PCG and postcentral gyrus ( $P<0.001$ ), right MFG ( $P=0.002$ ), right supplementary motor cortex ( $P=0.002$ ), right superior frontal gyrus ( $P=0.009$ ), and right frontal pole ( $P=0.023$ ), see table 5.13 and figure 5.12A.

Similar regions showed significant positive correlation between ODI and normalized volume of the corpus callosum, see table 5.13 and figure 5.12B. These regions include the right frontal pole ( $P<0.001$ ), the right postcentral gyrus ( $P=0.005$ ), and the right MFG ( $P=0.010$ ).

**Figure 5.12 Correlation of ODI with WM and corpus callosum volumes**



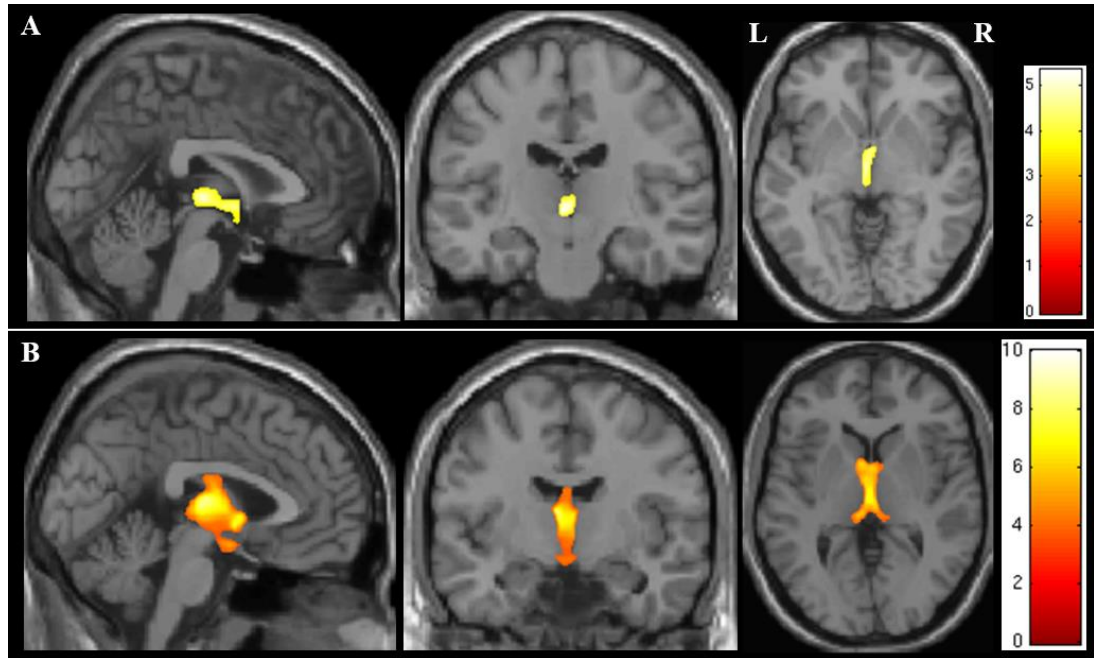
A figure to show the correlation of ODI with normalized volumes of the WM and corpus callosum, where results are shown using statistical significance of  $P<0.05$  FWE correction at cluster level, clusters formed with  $P<0.001$ .

(A) ODI positive correlation with normalized total WM volume.

(B) ODI positive correlation with normalized CC volume.

The thalamus was a region that demonstrated significant correlation of ODI with two further SBM measures, see table 5.13 and figure 5.13. Negative correlation between ODI and normalized PCG volume was found in the thalamus ( $P=0.037$ ), see figure 5.13A. While positive correlation was demonstrated between ODI and normalized ventricular system volume in the thalamus ( $P<0.001$ ), see figure 5.13B.

**Figure 5.13 Correlation of ODI with PCG and ventricle volumes**



A figure to show the correlation in SBM measures with ODI of the thalamus, where results are shown using statistical significance of  $P<0.05$  FWE correction at cluster level, clusters formed with  $P<0.001$ .

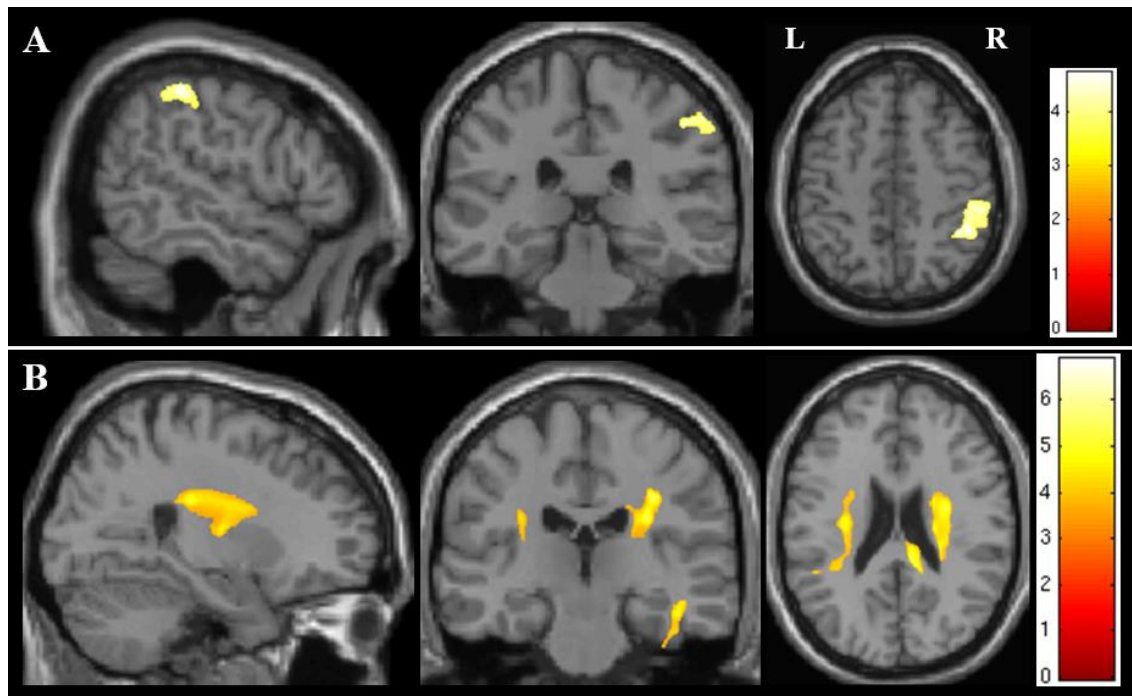
(A) ODI negative correlation with normalized PCG volume.

(B) ODI positive correlation with normalized ventricular system volume.

ODI showed positive correlation with two SBM measures of normalized cortical thickness measures, see table 5.13 and figure 5.13. There was positive correlation between ODI and PCG cortical thickness in the right postcentral gyrus ( $P=0.007$ ), see figure 5.13A. Finally, positive correlation between ODI and temporal lobe cortical thickness was demonstrated within the cerebral WM of the right internal capsule, corona radiata and corpus callsum ( $P<0.001$ ), right interior temporal gyrus ( $P=0.031$ ), and left internal capsule ( $P=0.002$ ), see figure 5.13B.

Finally, ODI correlated with PCG and temporal lobe cortical thickness, see figure 5.14 and table 5.13. There was a positive correlation between PCG cortical thickness and ODI within the right postcentral gyrus ( $P=0.007$ ), see figure 5.14A. Positive correlation was found between the temporal lobe cortical thickness and ODI within a region of the right internal capsule extending into the corpus callosum ( $P<0.001$ ), and with a further region within the left internal capsule ( $P=0.002$ ), and a further area within the right inferior temporal gyrus ( $P=0.031$ ), see figure 5.14B.

**Figure 5.14 Correlation between ODI and Cortical Thickness**



A figure to show the correlation between ODI and cortical thickness measures derived from SBM. Statistical significance was accepted where  $P < 0.05$  FWE correction at cluster level, clusters formed with  $P < 0.001$ .

(A) ODI positive correlation with normalized PCG cortical thickness.

(B) ODI positive correlation with normalized temporal lobe cortical thickness.

### 5.9.3 Correlation between ISO and SBM measures

The NODDI parameter of ISO correlated with a number of SBM volume and cortical thickness measures, see table 5.14.

ISO showed negative correlation with normalized cerebral cortex volume in the right subcallosal cortex and frontal pole ( $P < 0.001$ ), left internal capsule and subcallosal cortex ( $P < 0.001$ ), right cingulate gyrus ( $P = 0.008$ ), left insular cortex ( $P = 0.010$ ), right insular cortex ( $P = 0.022$ ), and right operculum ( $P = 0.027$ ), see figure 5.15A.

There was also negative correlation between ISO and normalized WM volume in the right lateral ventricle ( $P < 0.001$ ), left temporal lobe ( $P < 0.001$ ), and calcarine sulcus ( $P < 0.001$ ), see figure 5.15B.

Negative correlation was evident between ISO and normalized total GM volume in the right frontal pole and left internal capsule ( $P < 0.001$ ), left superior temporal gyrus ( $P < 0.001$ ), left operculum and insular cortex ( $P = 0.011$ ), and right frontal operculum ( $P = 0.014$ ) figure 5.15C.

Similar regions of negative correlation were found between ISO and cortical GM volume including the right frontal pole and left internal capsule ( $P < 0.001$ ), left central and frontal operculum cortex ( $P < 0.001$ ), and right insular cortex ( $P = 0.020$ ) figure 5.15D.

**Table 5.14 Regions of significant correlation between ISO and SBM parameters**

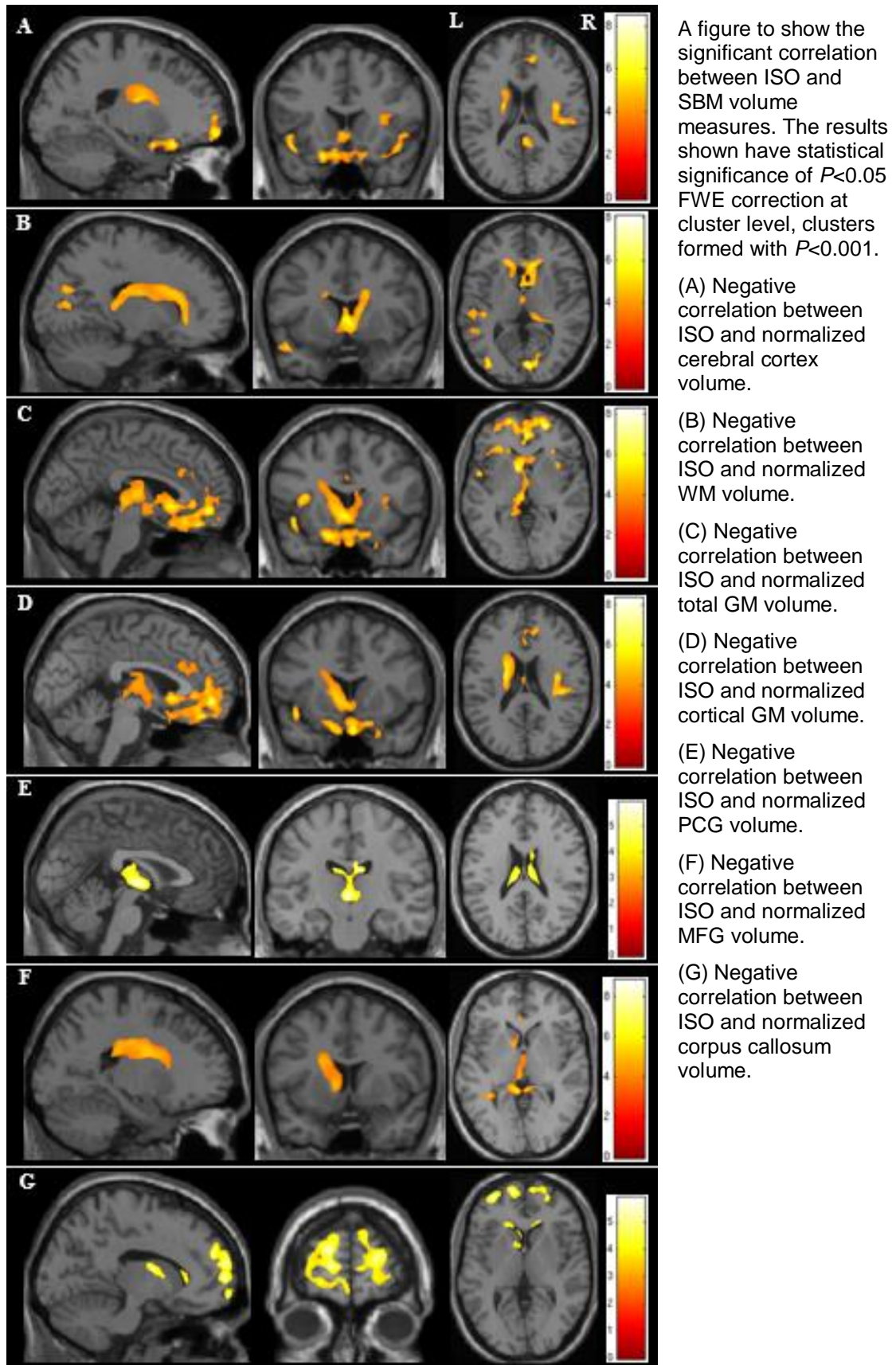
ISO correlation	Contiguous anatomical regions within cluster	MNI co-ordinate (x, y, z)	t-value	K (size)	$P_{\text{cluster level FWE-corr}}$	
Negative correlation with cerebral cortex volume	Right subcallosal cortex	5 13 -24	8.47	21195	<0.001	
	Right frontal pole,	23 56 -3	8.28			
	Left frontal orbital cortex	-19 23 -19	6.42			
	Left cerebral WM, internal capsule	Right subcallosal cortex	-11 7 5	5.44	5704	<0.001
			-21 -6 21	5.36		
	Right cerebral WM, cingulate gyrus, and precuneus	Right subcallosal cortex	0 18 -5	4.88	2850	0.008
			8 -40 11	6.42		
Left cingulate gyrus		10 -49 15	5.10	2746	0.010	
		-4 -43 29	4.77			
Left insular cortex		-44 17 -7	6.15	2294	0.022	
	Left opercular cortex	-52 2 0	5.64			
	Left superior temporal gyrus	-49 -9 -14	5.33			
Right insular cortex		36 -7 13	6.63	2202	0.027	
	Right parietal opercular cortex	43 -25 19	4.85			
		55 -24 18	4.29			
Right frontal opercular cortex		35 23 10	5.41			
	Right central opercular cortex	37 10 9	5.03			
	Right frontal opercular cortex	41 23 3	4.19			
Negative correlation with WM volume	Right lateral ventricle	3 6 3	7.00	23231	<0.001	
	Right corpus callosum	9 27 -3	6.38			
	Right lateral ventricle	1 -2 17	5.93			
Left middle temporal gyrus		-60 -27 -6	5.64	13201	<0.001	
	Left occipital WM	-39 -76 9	5.61			
	Left superior temporal gyrus	-51 -27 1	5.55			
Right cerebral cortex, and calcarine sulcus		6 -83 10	8.10	5075	<0.001	
		5 -72 21	6.03			
		14 -81 11	5.28			
Negative correlation with total GM volume	Right frontal pole	22 56 -1	8.28	62420	<0.001	
	Left caudate and internal capsule	-11 8 4	7.30			
		-21 -3 23	7.14			
	Left cerebral cortex, superior temporal gyrus, frontal operculum, and insular cortex	-49 -9 -13	6.22			
Left central operculum cortex, parietal operculum cortex and insular cortex		-41 24 -2	5.75	6222	<0.001	
		-53 -9 -20	5.64			
		36 -8 13	7.27			
Left central operculum cortex		41 -26 20	5.70	2610	0.011	
	Right frontal operculum	34 -19 19	4.68			
Negative correlation with cortical GM volume		-46 -1 13	6.68	2474	0.014	
		35 18 11	5.92			
		-40 7 11	4.99			
Right cortex, frontal pole		22 56 -2	8.33	46677	<0.001	
	Left caudate, internal capsule	-11 8 4	6.96			
	Paracingulate gyrus	-1 52 -6	6.64			
Left central operculum cortex		-49 -9 -14	5.90	4816	<0.001	
	Left planum polare	-52 2 -1	5.62			
	Left frontal operculum cortex	-41 24 -2	5.41			
Right insular cortex and right parietal operculum cortex		36 -8 13	6.96	2336	0.020	
		41 -26 20	5.29			
		34 -18 19	4.42			
Negative correlation with PCG volume	Right lateral ventricle	9 -17 24	5.92	8485	<0.001	
	Right thalamus	0 -13 0	5.73			
	Left lateral ventricle	-6 -36 7	5.48			
Negative correlation	Left cerebral WM, corona radiata and internal capsule	-21 -3 24	5.19	9241	<0.001	
		-10 6 4	5.17			
		-23 -29 29	4.98			

with MFG volume	Left cingulate gyrus	-8 -39 8	8.81	5631	<0.001
	Third ventricle	-4 -40 1	5.70		
	Right lateral ventricle	8 -38 6	5.57		
	Left transverse temporal gyrus	-44 -22 -12	6.07	3088	0.006
	Left lateral ventricle	-37 -44 -1	4.93		
	Left temporal stem WM	-35 -16 -13	4.38		
Negative correlation with corpus callosum volume	Left frontal pole and Left superior frontal gyrus	-14 61 17 -10 52 26 -32 56 2	5.76 5.75 5.56	8065	<0.001
	Right frontal pole	23 60 13 23 51 25 13 56 31	5.92 5.36 5.24	5759	<0.001
	Left lateral ventricle	-12 -2 12	5.34	2880	0.008
	Subcallosal cortex	-2 20 -1	4.83		
	Left caudate	-16 29 5	4.19		
Positive correlation with ventricle volume	Lateral ventricles	16 12 13 19 6 24 20 -3 28	10.9 10.7 10.4	1659160	<0.001
	Left cingulate sulcus	-9 -55 30	10.3	13576	<0.001
	Right cingulate sulcus	10 -62 16	6.98		
	Left calcarine sulcus	-12 -65 20	6.81		
	Right sylvian fissure	40 -13 18 43 -29 20 37 9 8	10.8 7.22 7.11	13140	<0.001
Negative correlation with temporal lobe volume	Right subcallosal cortex	4 13 -24	8.14	25014	<0.001
	Left temporal pole	-23 6 -22	6.29		
	Left corona radiata	-22 -3 23	6.16		
	Left cerebral WM, middle temporal gyrus and planum polare	-49 -10 -17 -43 -17 -11 -41 -23 -4	6.08 5.69 5.17	4164	0.001
	Right cingulate gyrus	5 -43 16	6.63	3734	0.002
	Left cingulate gyrus	-13 -41 36 -6 -41 30	5.57 5.46		
Negative correlation with temporal lobe cortical thickness	Right frontal pole and frontal medial cortex	22 55 -3 22 56 5 0 55 -16	7.86 6.29 5.28	3518	0.003
	Right insular cortex and right parietal WM	36 -8 14 43 -20 24 33 -19 20	6.09 4.58 4.54	2548	0.014
	Left subcallosal cortex	-3 20 -11	5.94	3863	0.002
	Right cingulate gyrus	3 43 4	4.46		
	Right subcallosal cortex	6 15 -17	4.44		
	Right cerebral WM inferior frontal gyrus and insular cortex	38 33 11 30 14 11 28 19 -3	5.15 5.07 4.66	2206	0.030

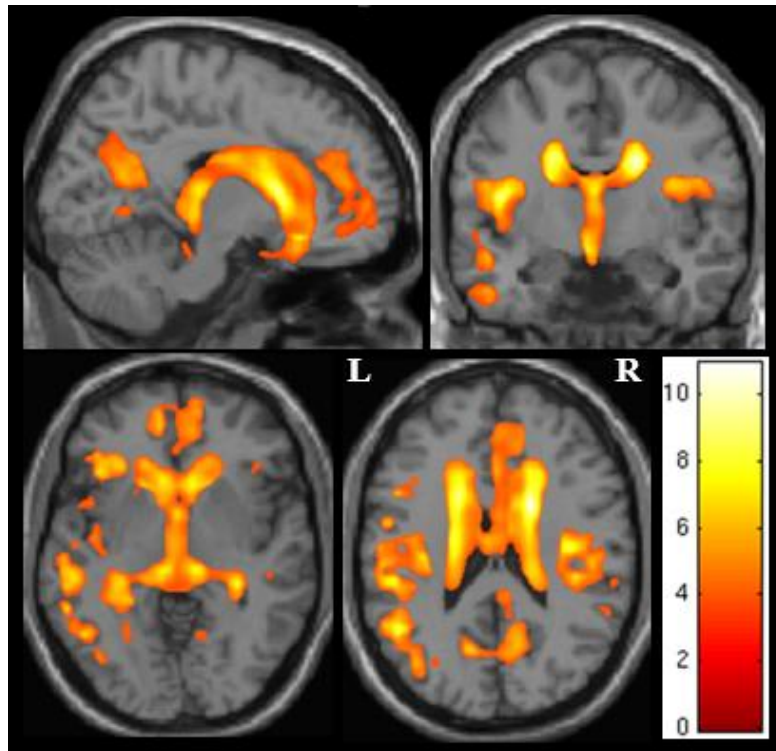
A table to show the anatomical regions where significant correlation was demonstrated, on whole brain analysis of the NODDI parameter ISO with SBM measures. A statistical significance threshold of  $P < 0.05$  family-wise error (FWE) correction at cluster level ( $P_{\text{cluster}}$ ) was used, after clusters were formed with an uncorrected  $P < 0.001$ . Montreal Neurological Institute (MNI) coordinates were used to define the anatomical location of each cluster of voxels within the MRI volume. The MNI coordinates refer to the peak t-value. Local maxima that are more than 8mm apart are shown for each cluster. K indicates the size of the cluster in voxels. Abbreviations: WM, white matter; GM, grey matter; PCG, precentral gyrus; MFG, middle frontal gyrus; MNI, Montreal Neurological Institute; FWE, family-wise error; corr, corrected.



**Figure 5.15 Correlation between ISO and SBM volume measures**

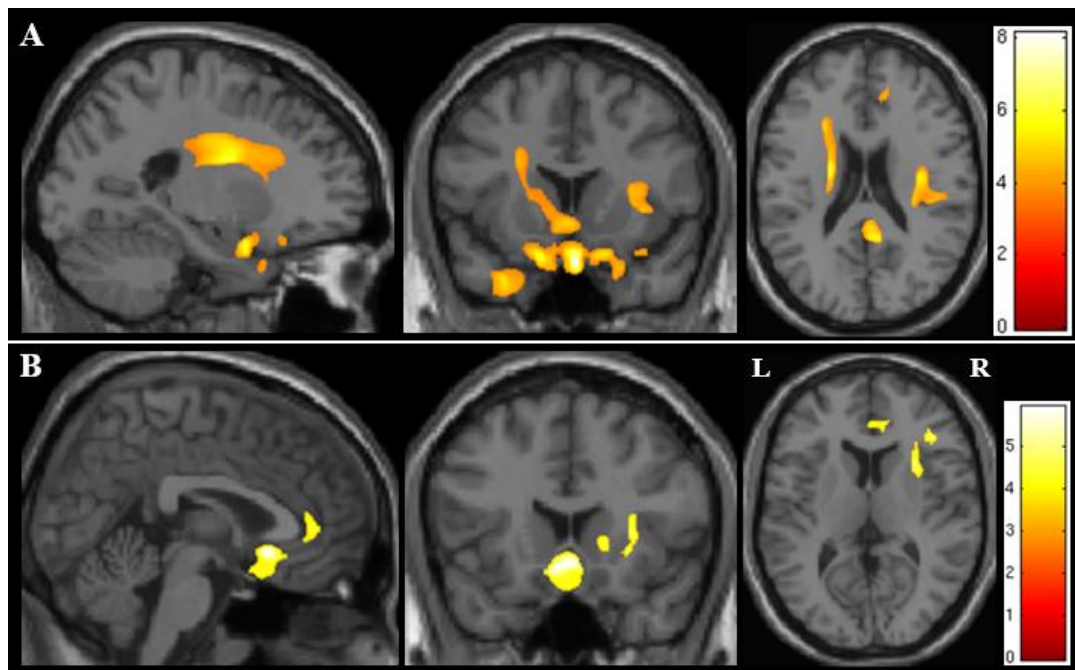


**Figure 5.16 Correlation between ISO and ventricle volume**



A figure to show the positive correlation between ISO and SBM measure of ventricle volume, where  $P < 0.05$  FWE correction at cluster level, clusters formed with  $P < 0.001$ , was accepted as statistically significant.

**Figure 5.17 Correlation between ISO and temporal lobe SBM measures**



A figure to show the areas of significant correlation between ISO and the SBM parameters, where results are shown using statistical significance of  $P < 0.05$  FWE correction at cluster level, clusters formed with  $P < 0.001$ .

(A) Negative correlation between ISO and normalized temporal lobe volume.

(B) Negative correlation between ISO and normalized temporal lobe cortical thickness.

ISO showed negative correlation with normalized PCG volume in the lateral ventricles and thalamus bilaterally ( $P < 0.001$ ), see figure 5.15E.

ISO also showed negative correlation with normalized MFG volume in the left internal capsule ( $P<0.001$ ), third ventricle ( $P<0.001$ ), and left lateral ventricle ( $P=0.006$ ), see figure 5.15F.

Negative correlation was found between ISO and normalized corpus callosum volume in the left frontal pole ( $P<0.001$ ), right frontal pole ( $P<0.001$ ), and anterior horn of the left lateral ventricle ( $P=0.008$ ), see figure 5.15G.

A positive correlation was found between ISO and the volume of the ventricular system in the lateral ventricles ( $P<0.001$ ), left cingulate and calcarine sulci ( $P<0.001$ ), and right sylvian fissure ( $P<0.001$ ), see figure 5.16 and table 5.14.

Negative correlation was demonstrated between ISO and SBM normalized measures of temporal lobe volume and cortical thickness, see table 5.14 and figure 5.16. Temporal lobe volume correlated with ISO in a region extending from the right subcallosal cortex into the left corona radiata ( $P<0.001$ ), middle temporal gyrus ( $P=0.001$ ), right and left cingulate gyrus ( $P=0.002$ ), right frontal pole ( $P=0.003$ ), and right insular cortex ( $P=0.014$ ), see figure 5.16A.

Finally, temporal lobe cortical thickness showed correlation with ISO in the left and right subcallosal cortex ( $P=0.002$ ), as well as the right cingulate gyrus and insular cortex ( $P=0.030$ ), see figure 5.16B.

## 5.10 SBM in ALS discussion

ALS is associated with relentlessly progressive multisystem degeneration of the brain, where uniform loss of central motor pathways is accompanied by varying degrees of extra-motor involvement. In particular frontotemporal demise, which correlates with cognitive impairment and is also associated with worse prognosis.<sup>71,72,500,502</sup>

Structural MRI techniques have successfully been used to evaluate the neurodegenerative morphological alterations occurring in ALS, where both VBM<sup>362-365</sup> and SBM<sup>366-371</sup> have demonstrated significant thinning of the PCG in ALS. In this study I used SBM not only to investigate for patterns of GM atrophy associated with ALS, but also to quantify WM volumes and assess for differences between ALS and control groups. I also exploited the capacity of SBM to measure additional volumes such as the corpus callosum and the ventricular system. I used volume measures alongside cortical thickness and surface area of the PCG, MFG, and temporal lobe to assess for differences based on disease distribution, King's stage of ALS, and cognitive involvement. I also looked for correlation between SBM data and clinical measures of ALS. Finally, I used SBM to scrutinize the findings obtained using NODDI, in order to assess how the microstructural changes demonstrated using NODDI relate to morphological alterations detected using structural MRI.



The main finding using SBM in this study of ALS was that cerebral volumes were significantly reduced in the PCG as well as the WM, GM, corpus callosum, and brainstem, accompanied by an increase in the size of the ventricles. These findings are consistent with the recognised cerebral atrophy occurring in ALS.<sup>17,18,339-341</sup>

Cortical thickness of the PCG was not significantly reduced in the ALS group, however, there was significant correlation of PCG cortical thickness with NDI of the CST, indicating a relevant association between these motor regions in the pathological processes occurring in ALS.

The most striking correlation was between the ventricle volume, measured using SBM, and ISO of the ventricles, quantified using NODDI. This finding reinforces the basis that atrophy, related to neurodegeneration, is a consistent finding in ALS. A further correlation was evident between cortical ODI and volumes of the WM and corpus callosum, which highlights the relationship between reduced dendritic complexity in the GM and loss of motor axons in the WM.

#### **5.10.1 SBM volumes detect widespread atrophy associated with ALS**

SBM studies have previously revealed significant cortical thinning of the precentral gyrus in ALS.<sup>368,369,623</sup> In this study, it was SBM-derived cortical volumes that detected the most statistically significant differences between the ALS and control groups, see table 5.1. All normalized region of interest volumes, apart from the MFG and temporal lobe, showed significant reduction consistent with generalised atrophy.

The normalised mean cortex volume was significantly reduced in the ALS group when analysing the whole brain ( $P=0.037$ ), as well as the left ( $P=0.015$ ) and right ( $P=0.021$ ) hemispheres separately, see figure 5.1. The normalised mean cortical thickness was similarly significantly reduced in the ALS group on whole brain ( $P=0.024$ ), left ( $P=0.027$ ), and right ( $P=0.024$ ) hemispheres, see table 5.3. This indicates that neurodegeneration in ALS is not confined to the motor cortices, and is consistent with previous SBM studies that have shown more widespread cortical thinning particularly associated with cognitive or behavioural impairment but also in those with only motor features.<sup>84,369</sup> Subgroup analysis showed that the significant reduction in both of these morphometric measures in this study was driven by bulbar involvement (table 5.2, 5.3), King's stage 3 ALS (table 5.5, 5.6), and the abnormal ECAS subgroups (table 5.8, 5.9). These findings are in keeping with previous imaging and histopathological studies, where more extensive cortical atrophy has been related to bulbar-onset ALS,<sup>624,625</sup> more advanced clinical stage of ALS,<sup>186</sup> and cognitive impairment in ALS,<sup>84</sup> all of which are associated with worse prognosis. The limb confined ALS, King's Stages 1 and 2 ALS, and normal ECAS ALS subgroups did not show significant reduction in cortical volume

or thickness compared with the control group, indicating less generalized cortical atrophy related to these phenotypes of ALS.

The most statistically significant change in the ALS group was increased volume in the ventricles compared with healthy controls ( $P < 0.001$ , see figure 5.5). An increase in volume of the ventricular system is expected to coincide with the loss of volume of on brain regions described, related to the neurodegeneration occurring in ALS. The normalized total ventricle volume showed correlation with MRC power score, which almost reached statistical significance ( $P = 0.060$ ), see table 5.11, indicating a possible relationship between muscle weakness and ventricle size in ALS. When compared with healthy controls the ventricles were universally enlarged in all the ALS subgroups based on clinical distribution of disease, King's stage of ALS, and ECAS scoring, see tables 5.2, 5.5, and 5.8 respectively. However, there was no difference between ALS subgroups. Ventricle size was significantly increased from Stage 1 ALS onwards, where only one region is affected by the disease. This suggests it is an early feature of ALS, and that significant atrophy may have already occurred by the time of clinical presentation and subsequent diagnosis.

MRI studies including assessment of the ventricles in ALS are limited, but have shown ventricular enlargement which progresses over time and correlates with shorter survival.<sup>626</sup> Similarly, ventricle size in ALS has not been a specific focus for post-mortem assessment. However, subjective dilatation of the ventricles was reported in two out of forty-five ALS patients in an early pathological study,<sup>193</sup> associated with extensive bilateral degeneration of the pyramidal tracts.

The normalized brain stem volume was also significantly reduced in the ALS group ( $P = 0.027$ ), see figure 5.5. Involvement of the brainstem has been demonstrated in histopathological studies of ALS,<sup>193</sup> where degeneration of the corticospinal tracts as well as the motor cranial nerve nuclei and their associated lower motor neurones have been documented. Furthermore, cytoplasmic inclusions of ubiquitinated TDP-43 within the brainstem are defined histo-pathologically as stage 2 according to the large post-mortem study of ALS conducted by Brettschnieder and colleagues.<sup>285</sup> The brainstem has also shown increased metabolic activity on FDG-PET studies of ALS.<sup>627</sup> Quantitative MRI studies reporting significant findings in the brainstem are limited, however, one MRI study found atrophy of the medulla oblongata associated with ALS.<sup>628</sup> Despite progressive reduction in the normalized brainstem volume with each King's stage of ALS, see table 5.5, none of these subgroups showed significant atrophy in the brainstem when independently compared with the control group. The brainstem atrophy appeared to be driven mainly by the limb-confined ALS subgroup ( $P = 0.017$ ) and the abnormal ECAS subgroup ( $P = 0.029$ ), see tables 5.2 and 5.5 respectively. This could indicate that brainstem involvement may be a unique feature limited to a subset of ALS participants,

however further studies with larger numbers of ALS participants would be needed to substantiate this possibility.

Total intracranial volume was not significantly lower in the ALS group compared to healthy controls, see table 5.1. However, TICV within the ALS group correlated with  $\Delta$ ALSFRS-R on regression analysis ( $P=0.027$ ), see figure 5.9A, supporting a relationship between the overall brain volume and progression of disease pathology in ALS. TICV has been used as a proxy for premorbid brain volume, but the method used for TICV estimation can introduce bias.<sup>629–631</sup> The freesurfer technique used in this study has previously been shown to overestimate TICV in patients with atrophy related to dementia.<sup>630</sup> It is therefore plausible that TICV values in the ALS group may have had a somewhat upward bias relating to such limitations in the methodological technique. Structural MRI values derived using SBM were normalized using TICV to compensate for the effect of age and gender, which is recommended due to significant variation in head size.<sup>629</sup> However, this could potentially increase the statistical power relating to changes in regions of interest.

No differences were detected in the total cerebral surface area between ALS and control groups, or in any of the normalized region of interest surface areas, in particular the PCG, see table 5.1. This is consistent with previous studies assessing for changes in cortical surface area.<sup>368</sup> Like TICV, total cerebral surface area correlated with  $\Delta$ ALSFRS-R on regression analysis ( $P=0.036$ ), see figure 5.9D. This supports the notion that cerebral atrophy is more extensive in those with faster rate of progression. Volume and surface area are intimately linked measures, where changes in volume can be driven by altered surface area,<sup>368</sup> which could explain the similar relationship with  $\Delta$ ALSFRS-R.

### **5.10.2 SBM demonstrates PCG Atrophy in ALS**

The PCG was the main region of interest for SBM assessment in this structural MRI analysis, as the region where the primary cortex resides. Normalized PCG volume of the whole brain was significantly reduced in the ALS group ( $P=0.037$ ), in keeping with previous studies showing PCG atrophy<sup>362,367,621</sup> and related pathologically to loss of Betz cells.<sup>195</sup>

There was asymmetry of PCG atrophy, where only the right PCG showed significant atrophy ( $P=0.020$ ) when assessing the cerebral hemispheres separately, see table 5.1 and figure 5.4. This finding coincides with the NODDI results, where more significant decreases in both NDI and ODI were found in the right PCG, see figure 3.1 and 3.3. This provides further support that loss of dendrite density and complexity contribute to PCG atrophy in ALS. The apparent lateralization of pathology to the right hemisphere is a frequent finding in imaging studies of ALS.<sup>609,632</sup> The underlying cause for which is not fully understood but it may suggest vulnerability of the non-dominant

hemisphere to the pathophysiological process underlying ALS.<sup>609</sup> It may also to some extent be related to the right PCG being naturally smaller in comparison to the dominant left PCG, leading to smaller changes in volume being more significant statistically.

The significant atrophy of PCG volume detected in the whole ALS group was evidently driven by the ALS subgroup with bulbar involvement ( $P=0.004$ ). There was no significant difference in PCG volume between the control group and limb-only ALS subgroup, see table 5.2. The PCG cerebral volume also distinguished between the limb-confined and bulbar-plus-limb ALS subgroups ( $P=0.031$ ), see figure 5.7, and once again the atrophy was most significant in the right hemisphere ( $P=0.032$ ).

PCG volume showed negative correlation with UMN score ( $P=0.009$ ), see figure 5.9C. This is consistent with previous SBM studies, where progressive cortical thinning was more significant in UMN predominant ALS.<sup>367</sup> In addition, PCG thickness has been proposed as an early imaging biomarker of UMN dysfunction in ALS.<sup>172,609,633</sup>

Cortical thickness in the PCG was reduced in the ALS group compared to controls in both hemispheres, and it was the right PCG that was closest to statistical significance ( $P=0.075$ ), see table 5.1, again supporting lateralization of ALS pathophysiology to the non-dominant hemisphere.<sup>609,632</sup> However, the differences between whole ALS group and control group failed to reach statistical significance. It was only the bulbar involvement ALS subgroup that demonstrated significant reduction in PCG cortical thickness compared to healthy controls ( $P=0.029$ ), see table 5.3. These results are consistent with previous VBM studies showing more extensive atrophy of the motor cortex relating to bulbar ALS.<sup>362,621,625,634</sup> In addition, bulbar symptoms have been related to a unique cortical signature with topographical atrophy of the PCG bulbar region.<sup>625</sup> The small number of bulbar onset ALS participants in this study was a limitation, which lead to the necessity of having a group made up of those with bulbar only as well as bulbar plus limb features clinically. Nonetheless, the SBM results of this study suggest that bulbar involvement related to more significant atrophy of the motor cortex.

In order to understand why significant cortical thinning of the PCG was not demonstrated in this study I analysed the cortical thickness values of both the ALS and control groups more carefully. The mean PCG thickness in the ALS group was 2.29mm, which falls below the diagnostic cut off value of <2.48mm for ALS.<sup>339</sup> However, the control group mean PCG thickness was 2.39mm, which is not the expected healthy value of 2.6mm. It therefore seems that the control group, despite being of similar mean age as the ALS group, had a higher level of atrophy than the healthy population and it is likely that this was a contributing factor to the lack of statistically significant difference in PCG cortical thickness between the ALS and control groups in this study. In addition the apparent atrophy of the control group could be due to a methodological limitation in the

SBM data acquisition, for example the parameters of the sequence used for MPRAGE and the fact that the magnet field strength was 1.5T.

In the King's stages of ALS subgroup analysis, the right hemisphere showed the most significant decrease in normalized PCG volume compared to the control group. There was progressive reduction in PCG volume from stage 1 onwards in the whole brain and right hemisphere but this only became statistically significant from stage 2 onwards ( $P=0.011$ ), see table 5.5, suggesting that there is increasing atrophy of the PCG volume as ALS progresses. However, no significant difference was detected in PCG volume between the King's stages of ALS subgroups. Furthermore, the normalized PCG volume in the left hemisphere increased slightly between stage 2 and stage 3, see table 5.5. This finding is similar to a previous imaging<sup>186,363,368</sup> and neuropathological<sup>284,635</sup> studies assessing atrophy across subgroups based on King's Stage of ALS. Proposed explanations for this finding of more apparent PCG atrophy related to earlier clinical stages of disease in ALS include the possibility of non-linear progression of tissue loss and the presence of reactive gliosis within the motor cortex that could mask degeneration. However, these notions are likely to be too simplified as biological mechanisms underlying ALS are heterogeneous and complex, therefore the King's Stage of ALS may not necessarily relate to stage of intracranial pathology.

No significant decrease in PCG cortical thickness was evident between the Kings stage of ALS subgroups and the control group, see table 5.6, or between ALS subgroups. The normalized PCG surface area was significantly reduced in the combined King's stage 2 and 3 ALS subgroup when compared with King's stage 1 subgroup ( $P=0.030$ ), see table 5.7, suggesting that more atrophy occurs from Stage 2 onwards. Overall, these results suggest that the King's stage of ALS has less impact than clinically evident distribution of disease, where bulbar involvement is more consistently related to PCG atrophy.

Normalized PCG volume was significantly reduced in the abnormal ECAS ALS subgroup compared to controls in the whole brain ( $P=0.018$ ), left hemisphere ( $P=0.010$ ) and right hemisphere ( $P=0.029$ ), see table 5.8. This relates cognitive impairment and behavioural changes to more extensive cortical atrophy, including the PCG, which is compatible with previous imaging studies in ALS.<sup>362,367,621</sup>

### **5.10.3 SBM demonstrates GM Atrophy in ALS**

Volumes in the total GM ( $P=0.022$ ) and cortical GM ( $P=0.034$ ) were significantly reduced in the ALS group, see figure 5.3, indicating that the neurodegenerative processes underlying ALS involves the GM, and suggesting that widespread cortical and subcortical loss of neuronal cell bodies and dendrites is occurring in ALS. The total GM volume includes the subcortical GM structures such as the basal ganglia, where regional spread

of TDP-43 deposition has been demonstrated and is a characteristic feature of stage 3 ALS, when defined neuropathologically.<sup>285</sup> Furthermore, VBM and SBM studies have shown volume loss in subcortical structures such as the caudate and thalamus, where basal ganglia involvement has been related to worse prognosis.<sup>362,626,636</sup> ALS associated with the C9orf72 mutation has been shown to exhibit more severe GM atrophy of the brain than sporadic ALS in MRI studies,<sup>636,637</sup> including basal ganglia involvement, which has been confirmed by histopathological studies.<sup>638</sup>

Atrophy of the GM was more significant in the ALS subgroup with bulbar involvement, King's stage 3 ALS, and cognitive impairment, see tables 5.2, 5.5, and 5.8 respectively. These findings are in keeping with previous VBM studies, where those with cognitive impairment and those in later stages of the disease have shown more pronounced atrophy extending to extra-motor regions.<sup>364,365</sup> Widespread basal ganglia degeneration is thought to contribute to the neuropsychological profile of ALS.<sup>372</sup> In addition, progressive GM degeneration has been demonstrated in a longitudinal structural MRI study of ALS.<sup>171</sup> The relationship between bulbar involvement and more significant GM atrophy is a less consistent finding but potentially related to different cerebral signatures according to clinical profile in ALS.

In previous structural MRI studies GM atrophy has been reported to extend beyond the primary motor cortex into the frontal, parietal, and temporal cortices. It was for this reason that I included the MFG and temporal lobe as regions of interest. However, there was no cortical thinning or volume loss found in the ALS group of this study to support atrophy. In fact, the mean normalized cortical thickness values the MFG and temporal lobe were slightly increased in the ALS group compared to healthy controls, see table 5.1. This is surprising given that approximately half the ALS participants (52%) fell on or below the cut off for normal cognitive performance in at least one of the cognitive sub-domains, see table 2 in chapter 2. Five participants met the criteria for ALS-FTSD, with one being classified as having ALS cognitive and behavioural impairment (ALS<sub>cbi</sub>) and four being classified as having isolated ALS cognitive impairment (ALS<sub>ci</sub>). Nonetheless none of the ALS participants had sufficient deficits to be diagnosed with FTD at the time of assessment.

GM changes detected with SBM were more statistically significant than those identified using NODDI. This finding suggests that while NDI appears to be particularly good at detecting alterations in coherent bundles of axons in the WM, this parameter is not as sensitive at identifying ALS-related density changes within the sparsely configured GM dendrites. This could be due to a limitation of the NODDI model. The same model is applied for analysis of the intracellular compartment and subsequent estimation of NDI in both the WM and GM, where the parallel and perpendicular diffusivities are coupled using a tortuosity constraint. The tortuosity component increases the sensitivity of the

intracellular compartment to alterations in diffusivity.<sup>409</sup> The assumptions of this model could therefore potentially have limitations in the GM, where the architecture of the neuropil is more complex.<sup>462</sup> It is also plausible that the discrepancy between SBM and NODDI findings are methodological in nature. SBM analysis could be more suitable for GM than voxel-based analyses such as NODDI. GM-based special statistics (GBSS) has been used to derive NODDI parameters of NDI and ODI in a study successfully demonstrating GM microstructural deficits in schizophrenia and bipolar disorder.<sup>442</sup> It is also possible that the maximum b value used for this study ( $b=2400 \text{ smm}^{-2}$ ) is insufficient to capture GM properties. Other studies that have focused on GM microstructure have indeed used b-values of up to 3000 or 4500  $\text{mm}^{-2}$ .<sup>426,428</sup>

#### **5.10.4 SBM demonstrates WM atrophy in ALS**

ALS was associated with significantly reduced normalized cerebral WM volume compared with healthy controls ( $P=0.037$ ), see figure 5.2. This is in keeping with the NODDI finding of significantly reduced axonal density in the corticospinal tracts<sup>357</sup> and is a consistent finding in DTI studies,<sup>473</sup> suggesting loss of WM fibres underlies the cerebral WM atrophy detected using SBM and that this is an integral consequence of the ALS disease process.

In contrast to PCG volume, WM volume was more significantly decreased in the left hemisphere ( $P=0.024$ ), compared to the right hemisphere ( $P=0.058$ ). This finding can be related to the NODDI results, where the cluster of reduced NDI appeared to be confined to the cerebral WM on the left, while the cluster of reduced NDI on the right was more rostral and extended into the right PCG, see figure 3.1 and 3.3.

In DTI studies analysing differences between ALS phenotypes the findings have been inconsistent. Some have shown more significant WM degeneration in UMN predominant ALS,<sup>639</sup> while others have shown greater changes associated with the classic ALS phenotype.<sup>397</sup> In parallel to GM atrophy, WM loss has also been shown to extend beyond the motor system into frontal and occipital regions particularly in association with bulbar onset ALS and cognitive impairment.<sup>538</sup>

In this study, when compared with the control group, WM atrophy was more significant in the limb-confined ALS subgroup ( $P=0.007$ ), rather than the bulbar-limb subgroup ( $P=0.046$ ), see table 5.2. This is in contrast to previous DTI studies showing more significant WM degeneration in bulbar-onset patients when compared with limb-onset patients.<sup>169,538</sup> However, there were insufficient bulbar-onset ALS participants to analyse as a separate group in my study, which is a limitation and makes this finding questionable.

Comparison of King's Stages of ALS with the healthy control group showed that significant WM atrophy was evident from Stage 2 ALS onwards ( $P=0.018$ ), with the most

significant difference seen in Kings stage 3 ALS ( $P=0.001$ ), see table 5.5. There was also significant atrophy detected in whole brain WM volume between King's Stage 1 and 3 ( $P=0.042$ ). These results suggest that WM atrophy occurs during or after Kings stage 1 ALS and that it worsens as the disease progresses. Studies relating King's stage of ALS to WM pathology are lacking and longitudinal studies in ALS have shown variable results. Most DTI studies have found progressive damage of the CST,<sup>391,397,640</sup> while others did not detect significant longitudinal CST degeneration.<sup>392,641</sup> These inconsistencies have been attributed to the recognised heterogeneity of ALS.

Cerebral WM volume loss was only significant in the left hemisphere when comparing normal ECAS ALS ( $P=0.035$ ) and abnormal ECAS ( $P=0.038$ ) subgroups with the control groups, see table 5.8. There was no significant difference in WM atrophy based on the presence of cognitive impairment, suggesting that the cerebral signature of cognitively impaired ALS may relate more to cortical and GM atrophy. However, previous DTI studies have found more significant atrophy of frontal WM, alongside GM changes, particularly in the dorsolateral prefrontal cortex.<sup>364,537,538</sup>

WM volume correlated with the clinical measure of MRC power score, see figure 5.9, suggesting atrophy of the cerebral WM corresponds to worsening muscle weakness in this cohort of participants with ALS. This is in keeping with previous studies where degeneration of the WM motor tracts has been associated with worsening disability.<sup>391,640</sup>

The corpus callosum, another major WM structure, was significantly reduced in volume when comparing the ALS group to healthy controls ( $P=0.021$ ), see figure 5.5. This is in keeping with the reduction of axon density detected in the corpus callosum using NODDI.<sup>357</sup> Furthermore, the altered diffusivity profile demonstrated in the corpus callosum using DTI is an established feature of ALS.<sup>395,642</sup>

The atrophy of the corpus callosum in different ALS subgroups mirrored that of the total cerebral WM volume, with more significant volume loss related to limb-only ALS ( $P=0.026$ ), Kings Stage 3 ALS ( $P=0.046$ ) and the cognitively impaired ( $P=0.048$ ) ALS subgroups, see tables 5.2, 5.5, and 5.8 respectively. Studies specifically relating corpus callosum atrophy to ALS phenotypes are lacking. However, consistent corpus callosum involvement was demonstrated across a heterogeneous group of ALS participants in one study.<sup>395</sup> It has been proposed that involvement of the corpus callosum may relate to interhemispheric spread of ALS pathology or to reflect damage secondary to independent bilateral cortical processes.

The findings from this study indicate that cerebral WM atrophy is linked by the disease process underlying ALS and is a core feature of ALS, which alongside the GM changes support the notion of a cerebral component to the pathogenic process underlying ALS.



### 5.10.5 SBM measures correlate with NODDI parameters

Many correlations were detected between the SBM measures derived from structural MRI and the NODDI parameters extracted using diffusion MRI, supporting a relationship between gross pathological changes and microstructural abnormalities underlying ALS “*in vivo*”.

#### 5.10.5.1 Correlations with NDI

There was a positive correlation between cerebral WM volume and NDI in the left occipital lobe, see figure 5.12A ( $P < 0.001$ ), which was different to the positive correlation between total GM volume and NDI of the thalami, figure 5.10B ( $P = 0.053$ ). This raises the possibility that WM and GM atrophy are occurring as distinct processes, although both are clearly integral parts of the degenerative process in ALS.<sup>535,610</sup> There was also positive correlation of brainstem volume and NDI within the right posterior limb of the internal capsule ( $P = 0.033$ ), see figure 5.10C, suggesting loss of CST motor axon density also relates to brainstem atrophy.

Finally, the most relevant correlation was seen between cortical thickness of the PCG and NDI ( $P < 0.001$ ) involving extensive regions within the corona radiata as well as the tran-callosal fibres in the right hemisphere where see figure 5.12D. This indicates that, as predicted, atrophy of the motor cortex is intimately related to degeneration of the rostral motor pathways. These large clusters also projected posteriorly into the parieto-occipital WM, supporting the notion of ALS pathology becoming widespread and extending into non-motor regions.<sup>84,363,365,369</sup>

#### 5.10.5.2 Correlations with ODI

The NODDI parameter of ODI showed the most correlations with SBM measures, suggesting that this parameter may contribute most to the degenerative changes measured using structural MRI.

Normalized cerebral cortex volume ( $P < 0.001$ ), total GM ( $P < 0.001$ ), cortical GM ( $P < 0.001$ ), MFG ( $P < 0.001$ ), and temporal lobe volume ( $P < 0.001$ ), all showed positive correlation with ODI in the cerebral WM, including the internal capsule and corona radiata bilaterally, see figures 5.11A - E and table 5.13. This suggests that the rostral CST is potentially a site of convergence for altered dendrite architecture and associated atrophy in ALS, which is supported by the NODDI results where the significant reduction in ODI was apparent between the right internal capsule and PCG, see chapter 3 figure 3.1.<sup>357</sup> Similar regions were also involved in a significant negative correlation between the normalized volume of the ventricles and ODI, with the cluster in the left hemisphere extending into the left temporal lobe cortex ( $P < 0.001$ ), see figure 5.11F and table 5.13.

This reinforces the link between cerebral atrophy and loss of dendritic complexity in ALS. It also indicates that the structural abnormalities previously shown in post-mortem studies of ALS patients and mouse models, such as retraction of the dendritic arborisation and decrease in dendritic spine density<sup>195,200,643,644</sup> are being appreciated with advanced MRI techniques.

A different pattern of correlation was seen between ODI and SBM volumes of WM structures see figure 5.12. Normalized total cerebral WM volume ( $P<0.001$ ) and corpus callosum volume ( $P<0.001$ ) both showed positive correlation with ODI of right cortical structures including the right PCG. Additional regions of correlation between the cerebral WM and ODI were the supplementary motor area ( $P=0.002$ ), and middle frontal gyrus ( $P=0.002$ ), see figure 5.12A. While the corpus callosum volume also correlation with ODI in the postcentral gyrus ( $P=0.005$ ) and middle frontal gyrus ( $P=0.010$ ), see figure 5.12B. This reinforces the relationship between altered dendritic complexity in the cortical GM of both motor and non-motor areas and degeneration of the WM tracts in ALS, both of which have been demonstrated in previous imaging studies.<sup>17,341,339-342</sup>

A further pattern of correlation was seen when correlating ODI with the volume of the PCG and the ventricles, see figure 5.13 and table 5.13. A negative correlation with PCG volume ( $P=0.037$ ) and a positive correlation ( $P<0.001$ ) with ventricle volume was seen with ODI in the thalamus bilaterally, see figure 5.13A and 5.13B respectively. The thalamus has been implicated in ALS, showing progressive atrophy over time in previous VBM imaging<sup>171</sup> as well as post-mortem<sup>532</sup> studies. In addition, microglial infiltration has also been demonstrated within the thalamus.

Finally, ODI correlated with two SBM measures of cortical thickness, the PCG and temporal lobe, see figure 5.14 and table 5.13. The positive correlation between PCG cortical thickness and ODI resided in the right postcentral gyrus ( $P=0.007$ ), see figure 5.14A. While the areas of positive correlation between the temporal lobe cortical thickness and ODI involved a region of the right internal capsule extending into the corpus callosum ( $P<0.001$ ), a smaller region of the left internal capsule ( $P=0.002$ ), and a further area within the right inferior temporal gyrus ( $P=0.031$ ), see figure 5.14B. These findings further support the connection between GM atrophy and WM degeneration in ALS.

### 5.10.5.3 Correlations with ISO

Volumetric data from all SBM regions of interest correlated with ISO within the ventricles and additional regions cortical sulci, see figure 5.15 and table 5.14. This indicates that atrophy detected using SBM relates to the increase in CSF component measured using NODDI.

Negative correlation was evident between normalized cortical volume, WM volume, total GM volume, cortical GM volume, and ISO in the lateral ventricles and additional fronto-temporal cortical structures (all  $P < 0.001$  in the most statistically significant clusters), see figures 5.15A, 5.15B, 5.15C, 5.15D respectively. This supports both WM and GM degeneration being related to the overall brain atrophy in ALS, which manifests as increase in size of the ventricles predominantly but also the cortical sulci.

Normalized PCG volume and MFG volume both showed negative correlation with ISO in regions confined to the lateral ventricles (both  $P < 0.001$ ), see figure 5.15E and 5.15F respectively. This suggests that PCG and MFG atrophy are the most intimately linked with WM degeneration of the CST leading to corresponding lateral ventricle enlargement.

Negative correlation was also detected between normalized corpus callosum volume and ISO in the sulci of the frontal lobes and the frontal horns of the lateral ventricles bilaterally ( $P < 0.001$ ), see figure 5.15G. This finding lends further support to the proposed relationship between WM and GM atrophy occurring in ALS.<sup>357</sup>

The most significant correlation was between normalized ventricle volume and ISO, where the most extensive regions of the ventricles ( $P < 0.001$ ), cingulate sulci ( $P < 0.001$ ), and sylvian fissure ( $P < 0.001$ ) were involved, see figure 5.16 and table 5.14. As ISO is a proxy measure of the CSF component, this correlation with increasing volume of the ventricles is as anticipated, and supports enlargement of the ventricles occurring as a result of atrophy in ALS.

Finally, there was negative correlation of SBM measures of normalized temporal lobe volume and temporal lobe cortical thickness with ISO. Temporal lobe volume correlation with ISO in the left CST ( $P < 0.001$ ), left middle temporal gyrus ( $P = 0.001$ ), cingulate gyrus bilaterally ( $P = 0.002$ ), right frontal pole ( $P = 0.003$ ), and right insular cortex ( $P = 0.014$ ), see figure 5.17A, While temporal lobe cortex correlated with ISO in the left subcallosal cortex ( $P = 0.002$ ), and right insular cortex ( $P = 0.030$ ), see figure 5.17B. These results are similar to those seen with SBM volume measures and further supports a relationship between GM and WM atrophy, as well as widespread cerebral atrophy in ALS.

Overall these results support the previous findings of widespread atrophy occurring in ALS in both imaging<sup>17,84,339-341,363-365,608</sup> and histopathological<sup>195-197,201</sup> studies, which is not confined to the motor systems.

#### **5.10.6 SBM in ALS limitations and conclusions**

SBM focuses on the reconstruction of the GM and WM boundaries to allow the quantification of cortical thickness, volumes, and surface areas in specified brain

regions.<sup>645</sup> In this study SBM was used to assess for cerebral morphometric changes and scrutinize how these relate to the NODDI findings.

As previously stated this study was limited by the small sample size, particularly the small number of participants with bulbar onset ALS. Heterogeneity of the ALS group should also be considered as a limitation.

There were also potential methodological limitations including the possibility of TICV overestimation in patients with atrophy using the freesurfer technique. Therefore, when normalizing cerebral volumes to account for age and gender, using TICV, there can potentially be an increase statistical power of the results. Finally, the healthy control group had much lower than expected cortical thickness, which could be a further methodological limitation related to the SBM processing technique.

The results presented in this chapter were not corrected for multiple comparisons, as they were used in an exploratory nature to assess for morphometric changes previously reported to occur in ALS, the statistical validity is therefore questionable.

Despite these limitations many of the results from this study support previous findings in ALS and there are a number of conclusions that can be drawn.

Widespread cerebral atrophy was demonstrated in the ALS group using SBM analysis, consistent with ALS being a multisystem disorder involving the frontal, temporal, and parietal regions as well as the motor systems.<sup>609,632,646</sup> More extensive cerebral atrophy was related to bulbar involvement, later King's stage of ALS, and cognitive impairment, which is consistent with previous imaging studies in ALS.<sup>84,186</sup>

Significant cerebral atrophy by the time of ALS diagnosis was supported by my findings, as significantly increased size of the ventricles was evident from King's stage 1 of ALS. This has implications for future treatment, where diagnosing ALS as early as possible is likely to be needed in order to minimize established irreversible damage.

Brainstem atrophy in the ALS group was related to limb-only involvement, while PCG atrophy was driven by bulbar involvement, raising the possibility of distinct disease processes underlying different phenotypes of ALS and supporting the idea of biological heterogeneity in ALS.

As expected significant PCG atrophy was evident with SBM analysis, which correlated with UMN score, distinguished between limb-only and bulbar-limb subgroups and related to cognitive impairment. This highlights PCG involvement are a core feature of ALS, consistent with degeneration of Betz cells seen in post-mortem studies. Furthermore, atrophy within the PCG was related to loss of axonal density within the CST, as quantified using NODDI. This indicates a biological relationship between the pathological processes occurring within the GM and the WM.

These findings provide some optimism that imaging techniques will become useful tools in future approaches for diagnosis and monitoring of this devastating neurological disease.

**CHAPTER 6:  
MULTIMODAL IMAGING  
ANALYSIS OF  
NEURODEGENERATIVE  
CHANGES IN ALS.**

## **CHAPTER 6: MULTIMODAL IMAGING ANALYSIS OF NEURODEGENERATIVE CHANGES IN ALS**

In this chapter I will provide an overview of the imaging features revealed using NODDI, a technique newly applied to ALS to explore the altered density and complexity of neurites. I will also discuss how the results obtained using NODDI relate to both the qMTi findings and the morphometric changes detected using structural MRI SBM analysis, with the aim of advancing the understanding of ALS pathogenesis.

### **6.1 Discussion**

The mechanisms and dynamics of the neurodegenerative processes underlying ALS require clarification, in order to facilitate development of disease modifying treatments. A multimodal imaging approach, incorporating a novel quantitative MRI technique such as NODDI, provides an opportunity to scrutinize the changes occurring in ALS.

This study has shown that NODDI reveals new aspects of the cerebral neurodegenerative process underlying ALS, which is characterized by decreased CST axon density and reduced dendritic arborisation in the motor cortex neuropil. The relationship between PCG ODI and ALS disease duration, coupled with reduced ODI in the PCG bulbar region relating to bulbar involvement, indicates that the NODDI parameter of ODI has the potential to detect relevant biological alterations associated with ALS such as changes in dendritic architecture relating to site and progression of ALS pathology.

QMTi is a more physiological technique used for assessing myelin content and molecular alterations, which has also provided new insights regarding a possible inflammatory process occurring in the rostral CST in a subset of those with ALS. SBM has been applied to ALS before and is known to be particularly useful for assessing GM degeneration. Therefore combining NODDI with qMTi and SBM in a multimodal approach, allows a thorough interrogation of the structural and functional alterations occurring in ALS 'in vivo'.

#### **6.1.1 Multimodal analysis of WM changes in ALS**

NODDI highlighted extensive axonal degeneration of the CST as a core feature of ALS, with additional axonal loss within the corpus callosum.<sup>357</sup> The reduction in corticofugal axon density was found to be the main factor underlying the altered diffusivity profile detected using concurrent DTI. Although CST degeneration has previously been demonstrated using DTI, the NODDI result is more specific in demonstrating the underlying microstructural alteration is a reduction in axon density.

Despite the different modalities being very distinct the NODDI findings concurred with the SBM result showing significant atrophy within the cerebral WM and

the corpus callosum, when analysed independently. While NODDI demonstrates microstructural alterations within the WM cellular environment, SBM detects larger scale morphometric changes of the WM structures. Taken together these results signify that the pathophysiological processes occurring in ALS undoubtedly involves the WM tracts, particularly those encompassing the motor axons, causing loss of axonal density at the microscopic level and WM atrophy on a larger scale.

Using qMTi, altered molecular composition was demonstrated within the rostral CST. This provides evidence of axonal dysfunction within the region of axonal loss and WM atrophy shown using NODDI and SBM respectively. The axonal dysfunction could potentially indicate inflammation in the cerebral WM of the motor tracts as a contributing factor to the pathogenic processes underlying degeneration in ALS. This is supported by the finding that protein aggregates associated with ALS are found in astrocytes and oligodendrocytes alongside motor neurones.<sup>279</sup> Inflammation within the rostral CST could be acting as a focus, driving the dissemination of the pathological processes underlying ALS, contributing to contiguous spread of pathology within the local environment, as well as synaptic network propagation to more distant sites such as the spinal motor neurones.

Although only evident at an uncorrected statistical threshold of  $P < 0.005$ ,  $k_f$  from qMTi correlated with NDI from NODDI in the corona radiata and corpus callosum bilaterally. This indicates that the process driving the alteration in  $k_f$  in this region, such as inflammation, is contributing to the axonal degeneration detected by NODDI. It also provides support for the process occurring within the rostral CST to be intimately related to the pathophysiological mechanisms underlying ALS. Furthermore, the correlation between  $k_f$  and ALSFRS-R in the right CST suggest that the alterations being detected by  $k_f$  are closely associated with disability caused by ALS. The apparent axonal dysfunction was not related to more advanced disease as anticipated. It is therefore possible that  $k_f$  is a marker for something occurring in a subset of the ALS participants, and could be distinguishing between different biological profiles underlying ALS. One possibility is that the degree of inflammatory changes occurring within the motor pathways is higher in a proportion of participants with ALS. The substrate for these mechanisms and how it relates to clinical phenotype remains to be established. Nonetheless, one would predict that if this is the case then a subset of patients with ALS would be more likely to benefit from immunological therapy.

Myelin content was preserved within the rostral CST and demyelination was only apparent in the medulla at a less stringent statistical threshold. These qMTi results suggest that cerebral demyelination is not a primary feature of the neurodegenerative process underlying ALS but could instead occur secondary to axonal degeneration, and possibly later in the disease process. Loss of myelin confined to the brainstem



CST could also support a dying back process, where the motor neurone axon degenerates from its most caudal location in a retrograde manner, back towards the cell soma within the cortex.

Taken together the relevant NODDI, SBM, and qMTi findings support a pathological process occurring within the cerebral WM, causing motor axon dysfunction and degeneration, or axonopathy, in ALS. Myelin loss did not correspond with the degree of axonal degeneration suggesting novel pathological mechanisms occurring in ALS, which are not fully understood and warrant further investigation.

### **6.1.2 Multimodal analysis of GM changes in ALS**

NODDI revealed reduced neurite density and complexity within the PCG, indicating that changes in dendritic architecture are occurring alongside the apparent central axonopathy in ALS. This is consistent with previous post-mortem studies showing reduced dendrites, and loss of dendritic spines associated with ALS.<sup>195</sup> Although the changes in the GM were more modest, there was significant correlation between loss of dendritic complexity and disease duration, suggesting dendritic abnormalities parallel disease progression in ALS. In addition reduced dendrite complexity was apparent in the bulbar region of the motor cortex in the ALS group with bulbar involvement, indicating that NODDI can detect clinically relevant microstructural alterations relevant to disease pathology.

The NODDI findings within the PCG were supported by the SBM findings, where significant PCG atrophy was evident. This is consistent with post-mortem studies in ALS, where loss of PCG Betz cells is a recognized feature.<sup>195,197</sup> However, the GM atrophy detected using SBM was more extensive than the subtle, localised, changes in dendritic complexity detected using NODDI. SBM is recognised as being suitable for GM analysis,<sup>339</sup> while assumptions of the NODDI model potentially cause limitations of the analysis in the GM neuropil, where the microstructural architecture is more complex.<sup>462</sup> It is also possible that the reactive gliosis, thought to accompany the degenerating Betz cells,<sup>195</sup> could affect the capacity of the NODDI parameters to detect loss of dendrites. Nonetheless, the two techniques are measuring different components of degeneration, so it is possible that atrophy of the GM is occurring independently to the loss of Betz cell dendrites, which could indicate that more than one pathophysiological mechanism is occurring in ALS.

PCG atrophy detected using SBM correlated with UMN score and was more significant in the ALS subgroups with bulbar involvement and cognitive impairment. This provides further support for the motor cortex degeneration occurring in ALS having consequences relevant to the clinical manifestations.

The most striking correlation between the NODDI and SBM was the evident relationship between PCG cortical thickness and CST axon density. Although it is not possible to infer causality, this indicates a link between the pathological process occurring within the GM and WM in ALS.

Despite the reported reactive gliosis affecting the Betz cells in post-mortem studies,<sup>195</sup> there were no significant qMTi results within the PCG to suggest active inflammation within the neuropil. This could be due to the dispersion of cortical pathophysiology in ALS, making it more difficult to reach statistical threshold in a heterogeneous group of ALS participants. However, it could suggest that inflammatory changes within the GM are not a major component of the neurodegenerative process underlying ALS.

Overall, the degenerative changes within the PCG GM appear to have more of a biological relationship with the pathophysiology of ALS, than the changes occurring within the WM. It is therefore possible that while WM degeneration is a consistent feature of ALS, it is the GM changes that predict the clinical phenotype of ALS.

### **6.1.3 Multimodal analysis of atrophy in ALS**

Despite the significant axonal degeneration, NODDI demonstrated increased ISO only within the region of the right lateral ventricle, suggesting that microstructural atrophy was not a widespread feature of the ALS group of this study. Nonetheless, atrophy detected by NODDI related to later King's stage of ALS and cognitive impairment, supporting cerebral atrophy being relevant to the pathogenic mechanisms occurring in ALS.

Interestingly ISO was highly sensitive to age related atrophy in this study, so when accounting for age as a covariate the statistically significant changes in ISO became scarce. This finding provides support that the mechanism underlying age related atrophy is independent from the pathological neurodegenerative processes occurring in ALS.

The qMTi parameter of  $T_{2f}$  is a surrogate marker of atrophy, and similar to the NODDI result detected changes in the right lateral ventricle. However, this was only seen at a less stringent statistical threshold and occurred in a much small cluster. Nonetheless, it supports this region being most affected by atrophy secondary to ALS, likely related to the axonal degeneration within the right CST.

SBM detected more widespread cerebral atrophy in the ALS group and, similar to the NODDI results, more extensive atrophy was related to bulbar involvement, later King's stage of ALS, and cognitive impairment. The SBM results also suggested that significant atrophy had occurred by the time of ALS diagnosis.

The correlation of SBM derived ventricle volume with ISO of the ventricles highlights the relationship between these two different measures from different techniques, and reinforces that atrophy causing increased ventricle size is occurring in ALS.

These findings confirm that the different imaging modalities are detecting different alterations within the brain parenchyma relating to atrophy, and that although SBM appears to be more sensitive at detecting changes, the NODDI and qMTi parameters are likely to be more relevant to the pathophysiological atrophy occurring in ALS.

## **6.2 Conclusions**

Insights into abnormal microstructure and altered biological mechanisms occurring 'in vivo' can be achieved using NODDI alongside qMTi and SBM in ALS. The multimodal analysis provides more robust evidence to suggest that there is a degenerative process focused mainly on the motor axons where there is compromise of both the function and microstructure, accompanied by loss of dendritic arborisation within the motor cortex. In addition there is altered morphometry due to atrophy. All the imaging techniques used in this study were able to differentiate between different ALS subgroups and correlate with clinical measures of ALS severity to some extent. This suggests that they are measuring pathogenic biological alterations relevant to the clinical manifestations of the disease.

### **6.2.1 NODDI conclusions**

This was the first study applying NODDI to a cross-sectional cohort of participants with sporadic ALS compared with healthy controls. Incorporating a geometric, multi-compartment model, improves the characterization of microstructural alterations associated with neurodegeneration.<sup>409</sup> The NODDI parameters, particularly NDI and ODI appear to be sensitive to the pathophysiological processes underlying ALS.

The NODDI data obtained in this study indicates that the main pathological alteration occurring within the corticospinal tract in ALS is loss of axonal density and that this underlies the altered diffusivity profile demonstrated with DTI. There is an accompanying reduction in dendritic complexity within the primary motor cortex, which appears to be more discreet but occurring alongside axonal degeneration. NODDI also demonstrated that more widespread clinical disease relates to more extensive microstructural damage within the WM, as well as spread of cerebral pathology into non-motor regions, which support ALS ultimately being a multisystem neurodegenerative disease.

In this study NODDI showed that NDI detected more widespread changes than FA from DTI. Furthermore the NODDI model, allows the parameter of NDI to provide a more biologically specific measure of neurite density. NODDI thereby advances the understanding of what microstructural changes are occurring in ALS. It is the loss of CST axonal density, demonstrated using NODDI, which is the main contributing factor to the altered diffusivity profile detected by DTI. Similarly, a recent study using NODDI in pre-symptomatic C9orf72 disease has recently shown that NODDI provides higher sensitivity and specificity than conventional DTI for identifying WM abnormalities,<sup>647</sup> which along with the findings of this study,<sup>357</sup> lend support for the NODDI parameters being candidate biomarkers in ALS.

### **6.2.2 qMTi conclusions**

Although the qMTi data were less statistically significant than the NODDI results, they still offer the potential of advancing the understanding of the complex biological mechanisms occurring in ALS. The main finding was that there was a relative lack of demyelination despite the extensive axonal degeneration demonstrated using NODDI. This is an interesting finding as it suggests that degeneration of myelin potentially occurs independently to loss of axons, rather than occurring simultaneously, and raises the possibility of distinct biological mechanisms that are not fully understood. The other interesting result was the suggestion of altered molecular function within the rostral CST axons, in the region of degenerating axons, possibly due to inflammatory processes occurring within a subset of participants with ALS. The qMTI parameter of  $K_f$  demonstrated the highest capacity to detect biological alterations occurring in ALS.

### **6.2.3 SBM conclusions**

Studies using SBM for GM analysis in ALS have previously been reported in the literature.<sup>609,632,646</sup> The SBM results from this study were consistent with ALS being a multisystem disorder with atrophy occurring in the motor systems as well as extra-motor frontal, temporal, and parietal regions. Just like the NODDI results, more extensive cerebral atrophy was related to bulbar involvement, later King's stage of ALS, and cognitive impairment. Additional conclusions can be drawn from the SBM results in this study. Firstly, atrophy involves both the GM and the WM simultaneously. Secondly, atrophy is evident by the time of ALS diagnosis and that the earliest feature on structural MRI is likely to be enlarged ventricles, which is an important consideration as structural MRI is often incorporated into clinical MRI scan protocols. Finally PCG atrophy was highlighted as a core feature of ALS using SBM analysis, relating to clinical measures of UMN score, bulbar involvement, and cognitive decline.

### 6.3 Study limitations

NODDI is a relatively novel technique which has not yet been used to extensively study ALS. Like any model-based approach, the NODDI technique is founded on a number of assumptions and therefore has limitations. The NODDI technique used in this study,<sup>409</sup> models orientation dispersion isotropically, which could limit the capacity to model multiple fiber orientations shown to be arising from complex dendritic structures within the GM.<sup>408</sup> This could have contributed to the more inconspicuous results within the GM obtained in this study. A newer version of NODDI has already been adapted to overcome this limitation. Bingham-NODDI was developed to incorporate a quantification of anisotropic orientation dispersion.<sup>415</sup> However, despite these limitation NODDI demonstrates potential to provide valuable insight into the neurodegenerative process accompanying ALS. In addition NODDI may not separate the effects of orientation dispersion and neurite density effectively within the GM.<sup>462</sup> Techniques incorporating microscopic anisotropy mapping may separate different signal components better and highlight differences more effectively.<sup>523</sup>

Whole brain analysis was performed, which is unbiased, does not require any *a priori* assumptions, and yielded some very interesting results. However, more statistically robust results could have been ascertained by incorporating tract-based spatial statistics and grey matter spatial statistics.

Aspects of the study were statistically underpowered, such as the qMTi parameters and all of the subgroup analyses. This was likely due to using the strongest DTI parameter, FA, in the power calculation, see section 1.3.3.1. The technique of qMTi appeared to be less sensitive at detecting changes associated with ALS than NODDI, and would likely need a larger sample size in order to reach statistical significance.

The imaging data for this study was obtained using a 1.5T MRI scanner, and although the reduced signal intensity was compensated by longer T2 relaxation and larger voxel size, the signal-to-noise ratio may not have been optimum.

Finally, this study was limited by the small sample size and the heterogeneity of the ALS participant group. Heterogeneity in ALS is well recognized at the genetic, molecular, clinical, and radiological levels<sup>1,5,8-15,28,43,137,165,193-195,197,201,585</sup> In this study pathological heterogeneity likely contributed to the modest GM changes being detected using NODDI and qMTi. It is possible that changes in cortical dendrites occur later in the course of ALS, but it is more likely that the loss of dendritic complexity occurs in a neuro-anatomically discreet manner, with more significant variation in cortical pathology across the cohort of participants with ALS in this study.

## 6.4 Future directions

At present the treatment options for ALS are limited and the prognosis for most of those diagnosed is bleak. Clinical trials assessing the effectiveness of various drugs in halting progression of disease has been disappointing. It is becoming evident that, due to the genetic and biological heterogeneity of ALS, personalized medicine is likely to be the way forward for the best hope of effective treatments. The causation and progression of ALS is likely to be multifactorial, with distinct disease entities converging to cause the recognized clinical syndromes. Nonetheless, the qMTi results suggest that pharmacological treatments and stem cell therapy targeted at manipulating the immune responses have potential to promote motor neurone survival in a subset of patients with ALS.

As MRI techniques are evolving and MRI scanners such as the ultra-high-field 7T are being introduced, these increase the possibility of establishing more specific cerebral signatures in ALS related to different phenotypes.<sup>648</sup>

Alternative brain imaging modalities such as positron emission tomography (PET), where specific radioisotope ligands are capable of assessing activation of glial cells as well as GABA-ergic and glutamatergic neurotransmission,<sup>185,627,649</sup> would be interesting to perform concurrently with NODDI and qMTi, to investigate how the microstructural and biological changes occurring in ALS relate to the molecular alterations detected with PET. When additional imaging modalities are used alongside quantitative diffusion MRI and structural MRI techniques, this allows for simultaneous multimodal parameter acquisition and provides improved clarification of biological processes relating to the degenerative changes in ALS.

Future developments of these imaging techniques are likely to become useful assessment tools, used to stratify patients with ALS in order to optimize treatment and yield biomarkers for monitoring of responses to potential disease modifying agents during clinical trials.

NODDI offers greater potential than standard DTI to detect and specify changes in the microstructural integrity of WM and GM associated with ALS.<sup>357</sup> Larger studies using NODDI in phenotypically, genetically, and even biologically defined cohorts of participants with ALS are likely to be required to fully characterize the changes in dendrite architecture within the GM and their relevance. It would also be useful to relate the NODDI changes to the pathophysiology of ALS.<sup>235,236</sup>

Longitudinal studies would be beneficial in order to discern how the NODDI indices and their associated correlations evolve over time in ALS.<sup>171,406</sup> Longitudinal NODDI analyses could be especially informative and allow for a better understanding of the neurobiological mechanisms underlying ALS. In particular GM alterations

detected using NODDI could become more apparent in longitudinal studies, as demonstrated by previous studies using DTI.<sup>171</sup>

Realistically NODDI is likely to be superseded by other more refined and sophisticated techniques for analysing neurite microstructure. However, in the meantime NODDI provides a clinically feasible option to apply to ALS and other neurodegenerative diseases in order to advance understanding of the microstructural correlates underlying cerebral parenchymal changes. Greater potential still comes from combining NODDI, or developments of NODDI,<sup>415,650</sup> into a multimodal approaches to study disease pathogenesis.

## REFERENCES

1. Wijesekera LC, Leigh PN. Amyotrophic lateral sclerosis. *Orphanet J Rare Dis.* 2009;4:3. doi:10.1186/1750-1172-4-3
2. Talbot K. Motor neuron disease: the bare essentials. *Pract Neurol.* 2009;9(5):303-309. doi:10.1136/jnnp.2009.188151
3. Kiernan MC, Vucic S, Cheah BC, et al. Amyotrophic lateral sclerosis. *Lancet.* 2011;377(9769):942-955. doi:10.1016/S0140-6736(10)61156-7
4. Turner MR, Bowser R, Bruijn L, et al. Mechanisms, models and biomarkers in amyotrophic lateral sclerosis. *Amyotroph Lateral Scler Front Degener.* 2013;14(sup1):19-32. doi:10.3109/21678421.2013.778554
5. van Es MA, Hardiman O, Chio A, et al. Amyotrophic lateral sclerosis. *Lancet (London, England).* May 2017. doi:10.1016/S0140-6736(17)31287-4
6. Dharmadasa T, Henderson RD, Talman PS, et al. Motor neurone disease: progress and challenges. *Med J Aust.* 2017;206(8):357-362. doi:10.5694/mja16.01063
7. Dharmadasa T, Matamala JM, Kiernan MC. Treatment approaches in motor neurone disease. *Curr Opin Neurol.* 2016;29(5):581-591. doi:10.1097/WCO.0000000000000369
8. Bäumer D, Talbot K, Turner MR. Advances in motor neurone disease. *J R Soc Med.* 2014;107(1):14-21. doi:10.1177/0141076813511451
9. Beghi E, Mennini T, Bendotti C, et al. The Heterogeneity of Amyotrophic Lateral Sclerosis: A Possible Explanation of Treatment Failure. *Curr Med Chem.* 2007;14(30):3185-3200. doi:10.2174/092986707782793862
10. Goutman SA, Chen KS, Paez-Colasante X, Feldman EL. Emerging understanding of the genotype–phenotype relationship in amyotrophic lateral sclerosis. In: *Handbook of Clinical Neurology.* Vol 148. ; 2018:603-623. doi:10.1016/B978-0-444-64076-5.00039-9
11. Ilieva H, Maragakis NJ. Motoneuron Disease: Clinical. In: *Advances in Neurobiology.* Vol 15. ; 2017:191-210. doi:10.1007/978-3-319-57193-5\_7
12. McCombe PA, Wray NR, Henderson RD. Extra-motor abnormalities in amyotrophic lateral sclerosis: another layer of heterogeneity. *Expert Rev Neurother.* 2017;17(6):561-577. doi:10.1080/14737175.2017.1273772
13. Ravits JM, La Spada AR. ALS motor phenotype heterogeneity, focality, and spread: deconstructing motor neuron degeneration. *Neurology.* 2009;73(10):805-811. doi:10.1212/WNL.0b013e3181b6bbbd
14. Sabatelli M, Conte A, Zollino M. Clinical and genetic heterogeneity of amyotrophic lateral sclerosis. *Clin Genet.* 2013;83(5):408-416. doi:10.1111/cge.12117
15. Su XW, Broach JR, Connor JR, Gerhard GS, Simmons Z. Genetic heterogeneity of amyotrophic lateral sclerosis: Implications for clinical practice and research. *Muscle Nerve.* 2014;49(6):786-803. doi:10.1002/mus.24198
16. Bede P, Hardiman O. Lessons of ALS imaging: Pitfalls and future directions — A critical review. *NeuroImage Clin.* 2014;4:436-443. doi:10.1016/j.nicl.2014.02.011
17. Foerster BR, Welsh RC, Feldman EL. 25 years of neuroimaging in amyotrophic lateral sclerosis. *Nat Rev Neurol.* 2013;9(9):513-524. doi:10.1038/nrneurol.2013.153
18. Menke RAL, Agosta F, Grosskreutz J, Filippi M, Turner MR. Neuroimaging Endpoints in Amyotrophic Lateral Sclerosis. *Neurotherapeutics.* 2017;14(1):11-23. doi:10.1007/s13311-016-0484-9
19. Turner MR, Kiernan MC, Leigh PN, Talbot K. Biomarkers in amyotrophic lateral



- sclerosis. *Lancet Neurol.* 2009;8(1):94-109. doi:10.1016/S1474-4422(08)70293-X
20. Verber NS, Shephard SR, Sassani M, et al. Biomarkers in Motor Neuron Disease: A State of the Art Review. *Front Neurol.* 2019;10:291. doi:10.3389/fneur.2019.00291
  21. Goetz CG. Chapter 15 Jean-Martin Charcot and the anatomo-clinical method of neurology. In: *Handbook of Clinical Neurology.* Vol 95. ; 2009:203-212. doi:10.1016/S0072-9752(08)02115-5
  22. Koehler PJ. Neurology: Past achievements and future developments. *J Hist Neurosci.* 1993;2(4):323-327. doi:10.1080/09647049309525580
  23. Kumar DR, Aslinia F, Yale SH, Mazza JJ. Jean-Martin Charcot: the father of neurology. *Clin Med Res.* 2011;9(1):46-49. doi:10.3121/cm.2009.883
  24. Rowland LP. How Amyotrophic Lateral Sclerosis Got Its Name. *Arch Neurol.* 2001;58(3):512-515. doi:10.1001/archneur.58.3.512
  25. Thorburn AL. Jean Martin Charcot, 1825-1893. An appreciation. *Sex Transm Infect.* 1967;43(2):77-80. doi:10.1136/sti.43.2.77
  26. Hardiman O, Al-Chalabi A, Chio A, et al. Amyotrophic lateral sclerosis. *Nat Rev Dis Prim.* 2017;3:17071. doi:10.1038/nrdp.2017.71
  27. Ellis JR. Lord Brain: an appreciation. *Br J Med Educ.* 1967;1(2):78-79. <http://www.ncbi.nlm.nih.gov/pubmed/4866082>. Accessed September 29, 2019.
  28. Grad LI, Rouleau GA, Ravits J, Cashman NR. Clinical Spectrum of Amyotrophic Lateral Sclerosis (ALS). *Cold Spring Harb Perspect Med.* 2017;7(8):a024117. doi:10.1101/cshperspect.a024117
  29. Hardiman O, Al-Chalabi A, Chio A, et al. Amyotrophic lateral sclerosis. *Nat Rev Dis Prim.* 2017;3(1):17071. doi:10.1038/nrdp.2017.71
  30. Norris F, Shepherd R, Denys E, et al. Onset, natural history and outcome in idiopathic adult motor neuron disease. *J Neurol Sci.* 1993;118(1):48-55. doi:10.1016/0022-510x(93)90245-t
  31. Turner MR, Hardiman O, Benatar M, et al. Controversies and priorities in amyotrophic lateral sclerosis. *Lancet Neurol.* 2013;12(3):310-322. doi:10.1016/S1474-4422(13)70036-X
  32. van Es MA, Hardiman O, Chio A, et al. Amyotrophic lateral sclerosis. *Lancet.* May 2017. doi:10.1016/S0140-6736(17)31287-4
  33. Pradat P-F, Kabashi E, Desnuelle C. Deciphering spreading mechanisms in amyotrophic lateral sclerosis. *Curr Opin Neurol.* 2015;28(5):455-461. doi:10.1097/WCO.0000000000000239
  34. Sekiguchi T, Kanouchi T, Shibuya K, et al. Spreading of amyotrophic lateral sclerosis lesions--multifocal hits and local propagation? *J Neurol Neurosurg Psychiatry.* 2014;85(1):85-91. doi:10.1136/jnnp-2013-305617
  35. Hu F, Jin J, Jia R, et al. Spread Direction and Prognostic Factors in Limb-Onset Sporadic Amyotrophic Lateral Sclerosis. *Eur Neurol.* 2016;75(5-6):244-250. doi:10.1159/000446365
  36. Ravits J. Focality, stochasticity and neuroanatomic propagation in ALS pathogenesis. *Exp Neurol.* 2014;262:121-126. doi:10.1016/j.expneurol.2014.07.021
  37. Talbot K. Amyotrophic lateral sclerosis: cell vulnerability or system vulnerability? *J Anat.* 2014;224(1):45-51. doi:10.1111/joa.12107
  38. Rivara C-B, Sherwood CC, Bouras C, Hof PR. Stereologic characterization and spatial distribution patterns of Betz cells in the human primary motor cortex. *Anat Rec.* 2003;270A(2):137-151. doi:10.1002/ar.a.10015
  39. Lemon RN. Descending Pathways in Motor Control. *Annu Rev Neurosci.* 2008;31(1):195-218. doi:10.1146/annurev.neuro.31.060407.125547

40. Welniarz Q, Dusart I, Roze E. The corticospinal tract: Evolution, development, and human disorders. *Dev Neurobiol.* 2017;77(7):810-829. doi:10.1002/dneu.22455
41. Wijesekera LC, Leigh PN. Amyotrophic lateral sclerosis. *Orphanet J Rare Dis.* 2009;4(1):3. doi:10.1186/1750-1172-4-3
42. Stifani N. Motor neurons and the generation of spinal motor neuron diversity. *Front Cell Neurosci.* 2014;8:293. doi:10.3389/fncel.2014.00293
43. Sabatelli M, Conte A, Zollino M. Clinical and genetic heterogeneity of amyotrophic lateral sclerosis. *Clin Genet.* 2013;83(5):408-416. doi:10.1111/cge.12117
44. Jawdat O, Statland JM, Barohn RJ, Katz JS, Dimachkie MM. Amyotrophic Lateral Sclerosis Regional Variants (Brachial Amyotrophic Diplegia, Leg Amyotrophic Diplegia, and Isolated Bulbar Amyotrophic Lateral Sclerosis). *Neurol Clin.* 2015;33(4):775-785. doi:10.1016/j.ncl.2015.07.003
45. Morris HR, Al-Sarraj S, Schwab C, et al. A clinical and pathological study of motor neurone disease on Guam. *Brain.* 2001;124(Pt 11):2215-2222. <http://www.ncbi.nlm.nih.gov/pubmed/11673323>. Accessed May 10, 2017.
46. Geser F, Winton MJ, Kwong LK, et al. Pathological TDP-43 in parkinsonism–dementia complex and amyotrophic lateral sclerosis of Guam. *Acta Neuropathol.* 2007;115(1):133-145. doi:10.1007/s00401-007-0257-y
47. Shankar SK, Gourie-Devi M, Shankar L, Yasha TC, Santosh V, Das S. Pathology of Madras type of motor neuron disease (MMND)--a histological and immunohistochemical study. *Acta Neuropathol.* 2000;99(4):428-434. <http://www.ncbi.nlm.nih.gov/pubmed/10787043>. Accessed May 10, 2017.
48. Talbot K. Motor neuron disease: the bare essentials. *Pract Neurol.* 2009;9(5):303-309. doi:10.1136/jnnp.2009.188151
49. Sarikcioglu L, Arican RY. Wilhelm Heinrich Erb (1840-1921) and his contributions to neuroscience. *J Neurol Neurosurg Psychiatry.* 2007;78(7):732. doi:10.1136/jnnp.2007.115956
50. Gordon PH, Cheng B, Katz IB, Mitsumoto H, Rowland LP. Clinical features that distinguish PLS, upper motor neuron-dominant ALS, and typical ALS. *Neurology.* 2009;72(22):1948-1952. doi:10.1212/WNL.0b013e3181a8269b
51. Pringle CE, Hudson AJ, Munoz DG, Kiernan JA, Brown WF, Ebers GC. Primary lateral sclerosis. Clinical features, neuropathology and diagnostic criteria. *Brain.* 1992;115 ( Pt 2)(2):495-520. doi:10.1093/brain/115.2.495
52. Singer MA, Kojan S, Barohn RJ, et al. Primary Lateral Sclerosis. *J Clin Neuromuscul Dis.* 2005;7(1):1-9. doi:10.1097/01.cnd.0000176974.61136.45
53. Singer MA, Statland JM, Wolfe GI, Barohn RJ. Primary lateral sclerosis. *Muscle Nerve.* 2007;35(3):291-302. doi:10.1002/mus.20728
54. Statland JM, Barohn RJ, Dimachkie MM, Floeter MK, Mitsumoto H. Primary Lateral Sclerosis. *Neurol Clin.* 2015;33(4):749-760. doi:10.1016/j.ncl.2015.07.007
55. Brown WF, Ebers GC, Hudson AJ, Pringle CE, Veitch J. Motor-evoked responses in primary lateral sclerosis. *Muscle Nerve.* 1992;15(5):626-629. doi:10.1002/mus.880150515
56. Gordon PH, Cheng B, Katz IB, et al. The natural history of primary lateral sclerosis. *Neurology.* 2006;66(5):647-653. doi:10.1212/01.wnl.0000200962.94777.71
57. Kuipers-Upmeijer J, de Jager AE, Hew JM, Snoek JW, van Weerden TW. Primary lateral sclerosis: clinical, neurophysiological, and magnetic resonance findings. *J Neurol Neurosurg Psychiatry.* 2001;71(5):615-620. doi:10.1136/jnnp.71.5.615

58. Liewluck T, Saperstein DS. Progressive Muscular Atrophy. *Neurol Clin*. 2015;33(4):761-773. doi:10.1016/j.ncl.2015.07.005
59. de Carvalho M, Scotto M, Swash M. Clinical patterns in progressive muscular atrophy (PMA): A prospective study. *Amyotroph Lateral Scler*. 2007;8(5):296-299. doi:10.1080/17482960701452902
60. Visser J, de Jong JMBV, Visser M d. The history of progressive muscular atrophy: Syndrome or disease? *Neurology*. 2008;70(9):723-727. doi:10.1212/01.wnl.0000302187.20239.93
61. Yedavalli VS, Patil A, Shah P. Amyotrophic Lateral Sclerosis and its Mimics/Variants: A Comprehensive Review. *J Clin Imaging Sci*. 2018;8:53. doi:10.4103/jcis.JCIS\_40\_18
62. Ling S-C, Polymenidou M, Cleveland DW. Converging Mechanisms in ALS and FTD: Disrupted RNA and Protein Homeostasis. *Neuron*. 2013;79(3):416-438. doi:10.1016/j.neuron.2013.07.033
63. Burrell JR, Halliday GM, Kril JJ, et al. The frontotemporal dementia-motor neuron disease continuum. *Lancet (London, England)*. March 2016. doi:10.1016/S0140-6736(16)00737-6
64. Bang J, Spina S, Miller BL. Frontotemporal dementia. *Lancet (London, England)*. 2015;386(10004):1672-1682. doi:10.1016/S0140-6736(15)00461-4
65. Bott NT, Radke A, Stephens ML, Kramer JH. Frontotemporal dementia: diagnosis, deficits and management. *Neurodegener Dis Manag*. 2014;4(6):439-454. doi:10.2217/nmt.14.34
66. Olney NT, Spina S, Miller BL. Frontotemporal Dementia. *Neurol Clin*. 2017;35(2):339-374. doi:10.1016/j.ncl.2017.01.008
67. Bak TH. The importance of looking in dark places. *Amyotroph Lateral Scler Front Degener*. 2013;14(1):1-2. doi:10.3109/21678421.2013.760150
68. Boxer AL, Mackenzie IR, Boeve BF, et al. Clinical, neuroimaging and neuropathological features of a new chromosome 9p-linked FTD-ALS family. *J Neurol Neurosurg Psychiatry*. 2011;82(2):196-203. doi:10.1136/jnnp.2009.204081
69. Byrne S, Elamin M, Bede P, et al. Cognitive and clinical characteristics of patients with amyotrophic lateral sclerosis carrying a C9orf72 repeat expansion: a population-based cohort study. *Lancet Neurol*. 2012;11(3):232-240. doi:10.1016/S1474-4422(12)70014-5
70. Neary D, Snowden J. Frontal lobe dementia, motor neuron disease, and clinical and neuropathological criteria. *J Neurol Neurosurg Psychiatry*. 2013;84(7):713-714. doi:10.1136/jnnp-2012-304549
71. Phukan J, Pender NP, Hardiman O. Cognitive impairment in amyotrophic lateral sclerosis. *Lancet Neurol*. 2007;6(11):994-1003. doi:10.1016/S1474-4422(07)70265-X
72. Phukan J, Elamin M, Bede P, et al. The syndrome of cognitive impairment in amyotrophic lateral sclerosis: a population-based study. *J Neurol Neurosurg Psychiatry*. 2012;83(1):102-108. doi:10.1136/jnnp-2011-300188
73. Crockford C, Newton J, Lonergan K, et al. ALS-specific cognitive and behavior changes associated with advancing disease stage in ALS. *Neurology*. September 2018;10.1212/WNL.0000000000006317. doi:10.1212/WNL.0000000000006317
74. Henstridge CM, Sideris DI, Carroll E, et al. Synapse loss in the prefrontal cortex is associated with cognitive decline in amyotrophic lateral sclerosis. *Acta Neuropathol*. 2018;135(2):213-226. doi:10.1007/s00401-017-1797-4
75. Woolley SC, Strong MJ. Frontotemporal Dysfunction and Dementia in Amyotrophic Lateral Sclerosis. *Neurol Clin*. 2015;33(4):787-805. doi:10.1016/j.ncl.2015.07.011

76. Strong MJ, Grace GM, Freedman M, et al. Consensus criteria for the diagnosis of frontotemporal cognitive and behavioural syndromes in amyotrophic lateral sclerosis. *Amyotroph Lateral Scler*. 2009;10(3):131-146. <http://www.ncbi.nlm.nih.gov/pubmed/19462523>. Accessed September 24, 2018.
77. Strong MJ, Abrahams S, Goldstein LH, et al. Amyotrophic lateral sclerosis - frontotemporal spectrum disorder (ALS-FTSD): Revised diagnostic criteria. *Amyotroph Lateral Scler Front Degener*. 2017;18(3-4):153-174. doi:10.1080/21678421.2016.1267768
78. Abrahams S, Newton J, Niven E, Foley J, Bak TH. Screening for cognition and behaviour changes in ALS. *Amyotroph Lateral Scler Front Degener*. 2014;15(1-2):9-14. doi:10.3109/21678421.2013.805784
79. Niven E, Newton J, Foley J, et al. Validation of the Edinburgh Cognitive and Behavioural Amyotrophic Lateral Sclerosis Screen (ECAS): A cognitive tool for motor disorders. *Amyotroph Lateral Scler Frontotemporal Degener*. 2015;16(3-4):172-179. doi:10.3109/21678421.2015.1030430
80. Abrahams S, Leigh PN, Harvey a, Vythelingum GN, Gris  D, Goldstein LH. Verbal fluency and executive dysfunction in amyotrophic lateral sclerosis (ALS). *Neuropsychologia*. 2000;38(6):734-747. <http://www.ncbi.nlm.nih.gov/pubmed/10689049>.
81. Abrahams S, Goldstein LH, Simmons A, et al. Word retrieval in amyotrophic lateral sclerosis: a functional magnetic resonance imaging study. *Brain*. 2004;127(Pt 7):1507-1517. doi:10.1093/brain/awh170
82. Abrahams S, Goldstein LH, Suckling J, et al. Frontotemporal white matter changes in amyotrophic lateral sclerosis. *J Neurol*. 2005;252(3):321-331. doi:10.1007/s00415-005-0646-x
83. Canosa A, Pagani M, Cistaro A, et al. <sup>18</sup>F-FDG-PET correlates of cognitive impairment in ALS. *Neurology*. 2016;86(1):44-49. doi:10.1212/WNL.0000000000002242
84. Schuster C, Kasper E, Dyrba M, et al. Cortical thinning and its relation to cognition in amyotrophic lateral sclerosis. *Neurobiol Aging*. 2014;35(1):240-246. doi:10.1016/j.neurobiolaging.2013.07.020
85. Gibbons ZC, Richardson A, Neary D, Snowden JS. Behaviour in amyotrophic lateral sclerosis. *Amyotroph Lateral Scler*. 2008;9(2):67-74. doi:10.1080/17482960701642437
86. Taylor LJ, Brown RG, Tsermentseli S, et al. Is language impairment more common than executive dysfunction in amyotrophic lateral sclerosis? *J Neurol Neurosurg Psychiatry*. 2013;84(5):494-498. doi:10.1136/jnnp-2012-303526
87. Witgert M, Salamone AR, Strutt AM, et al. Frontal-lobe mediated behavioral dysfunction in amyotrophic lateral sclerosis. *Eur J Neurol*. 2010;17(1):103-110. doi:10.1111/j.1468-1331.2009.02801.x
88. Girardi A, MacPherson SE, Abrahams S. Deficits in emotional and social cognition in amyotrophic lateral sclerosis. *Neuropsychology*. 2011;25(1):53-65. doi:10.1037/a0020357
89. Tsujimoto M, Senda J, Ishihara T, et al. Behavioral changes in early ALS correlate with voxel-based morphometry and diffusion tensor imaging. *J Neurol Sci*. 2011;307(1-2):34-40. doi:10.1016/j.jns.2011.05.025
90. Woolley SC, Zhang Y, Schuff N, Weiner MW, Katz JS. Neuroanatomical correlates of apathy in ALS using 4 Tesla diffusion tensor MRI. *Amyotroph Lateral Scler*. 2011;12(1):52-58. doi:10.3109/17482968.2010.521842
91. Goldstein LH, Abrahams S. Changes in cognition and behaviour in amyotrophic lateral sclerosis: nature of impairment and implications for assessment. *Lancet Neurol*. 2013;12(4):368-380. doi:10.1016/S1474-4422(13)70026-7

92. Beeldman E, Raaphorst J, Klein Twennaar M, de Visser M, Schmand BA, de Haan RJ. The cognitive profile of ALS: a systematic review and meta-analysis update. *J Neurol Neurosurg Psychiatry*. 2016;87(6):611-619. doi:10.1136/jnnp-2015-310734
93. Bora E. Meta-analysis of social cognition in amyotrophic lateral sclerosis. *Cortex*. 2017;88:1-7. doi:10.1016/j.cortex.2016.11.012
94. Sterling LE, Jawaid A, Salamone AR, et al. Association between dysarthria and cognitive impairment in ALS: A prospective study. *Amyotroph Lateral Scler*. 2010;11(1-2):46-51. doi:10.3109/17482960903207997
95. Zucchi E, Ticozzi N, Mandrioli J. Psychiatric Symptoms in Amyotrophic Lateral Sclerosis: Beyond a Motor Neuron Disorder. *Front Neurosci*. 2019;13:175. doi:10.3389/fnins.2019.00175
96. Snowden JS, Rollinson S, Thompson JC, et al. Distinct clinical and pathological characteristics of frontotemporal dementia associated with C9ORF72 mutations. *Brain*. 2012;135(3):693-708. doi:10.1093/brain/awr355
97. Hayashi Y, Homma K, Ichijo H. SOD1 in neurotoxicity and its controversial roles in SOD1 mutation-negative ALS. *Adv Biol Regul*. 2016;60:95-104. doi:10.1016/j.jbior.2015.10.006
98. Boylan K. Familial Amyotrophic Lateral Sclerosis. *Neurol Clin*. 2015;33(4):807-830. doi:10.1016/j.ncl.2015.07.001
99. Kirby J, Al Sultan A, Waller R, Heath P. The genetics of amyotrophic lateral sclerosis: current insights. *Degener Neurol Neuromuscul Dis*. May 2016:49. doi:10.2147/DNND.S84956
100. Ryan M, Heverin M, McLaughlin RL, Hardiman O. Lifetime Risk and Heritability of Amyotrophic Lateral Sclerosis. *JAMA Neurol*. July 2019. doi:10.1001/jamaneurol.2019.2044
101. Alsultan AA, Waller R, Heath PR, Kirby J. The genetics of amyotrophic lateral sclerosis: current insights. *Degener Neurol Neuromuscul Dis*. 2016;6:49-64. doi:10.2147/DNND.S84956
102. Chia R, Chiò A, Traynor BJ. Novel genes associated with amyotrophic lateral sclerosis: diagnostic and clinical implications. *Lancet Neurol*. 2018;17(1):94-102. doi:10.1016/S1474-4422(17)30401-5
103. Rosen DR, Siddique T, Patterson D, et al. Mutations in Cu/Zn superoxide dismutase gene are associated with familial amyotrophic lateral sclerosis. *Nature*. 1993;362(6415):59-62. doi:10.1038/362059a0
104. Yang Y, Hentati A, Deng HX, et al. The gene encoding alsin, a protein with three guanine-nucleotide exchange factor domains, is mutated in a form of recessive amyotrophic lateral sclerosis. *Nat Genet*. 2001;29(2):160-165. doi:10.1038/ng1001-160
105. Hand CK, Khoris J, Salachas F, et al. A novel locus for familial amyotrophic lateral sclerosis, on chromosome 18q. *Am J Hum Genet*. 2002;70(1):251-256. doi:10.1086/337945
106. Chen Y-Z, Bennett CL, Huynh HM, et al. DNA/RNA helicase gene mutations in a form of juvenile amyotrophic lateral sclerosis (ALS4). *Am J Hum Genet*. 2004;74(6):1128-1135. doi:10.1086/421054
107. Orlacchio A, Babalini C, Borreca A, et al. SPATACSIN mutations cause autosomal recessive juvenile amyotrophic lateral sclerosis. *Brain*. 2010;133(2):591-598. doi:10.1093/brain/awp325
108. Kwiatkowski TJ, Bosco DA, LeClerc AL, et al. Mutations in the FUS/TLS Gene on Chromosome 16 Cause Familial Amyotrophic Lateral Sclerosis. *Science (80-)*. 2009;323(5918):1205-1208. doi:10.1126/science.1166066
109. Sapp PC, Hosler BA, McKenna-Yasek D, et al. Identification of two novel loci

- for dominantly inherited familial amyotrophic lateral sclerosis. *Am J Hum Genet.* 2003;73(2):397-403. doi:10.1086/377158
110. Nishimura AL, Mitne-Neto M, Silva HCA, et al. A mutation in the vesicle-trafficking protein VAPB causes late-onset spinal muscular atrophy and amyotrophic lateral sclerosis. *Am J Hum Genet.* 2004;75(5):822-831. doi:10.1086/425287
  111. Greenway MJ, Andersen PM, Russ C, et al. ANG mutations segregate with familial and “sporadic” amyotrophic lateral sclerosis. *Nat Genet.* 2006;38(4):411-413. doi:10.1038/ng1742
  112. Sreedharan J, Blair IP, Tripathi VB, et al. TDP-43 Mutations in Familial and Sporadic Amyotrophic Lateral Sclerosis. *Science (80- )*. 2008;319(5870):1668-1672. doi:10.1126/science.1154584
  113. Chow CY, Landers JE, Bergren SK, et al. Deleterious Variants of FIG4, a Phosphoinositide Phosphatase, in Patients with ALS. *Am J Hum Genet.* 2009;84(1):85-88. doi:10.1016/j.ajhg.2008.12.010
  114. Maruyama H, Morino H, Ito H, et al. Mutations of optineurin in amyotrophic lateral sclerosis. *Nature.* 2010;465(7295):223-226. doi:10.1038/nature08971
  115. Elden AC, Kim H-J, Hart MP, et al. Ataxin-2 intermediate-length polyglutamine expansions are associated with increased risk for ALS. *Nature.* 2010;466(7310):1069-1075. doi:10.1038/nature09320
  116. Johnson JO, Mandrioli J, Benatar M, et al. Exome sequencing reveals VCP mutations as a cause of familial ALS. *Neuron.* 2010;68(5):857-864. doi:10.1016/j.neuron.2010.11.036
  117. Deng H-X, Chen W, Hong S-T, et al. Mutations in UBQLN2 cause dominant X-linked juvenile and adult-onset ALS and ALS/dementia. *Nature.* 2011;477(7363):211-215. doi:10.1038/nature10353
  118. Al-Saif A, Al-Mohanna F, Bohlega S. A mutation in sigma-1 receptor causes juvenile amyotrophic lateral sclerosis. *Ann Neurol.* 2011;70(6):913-919. doi:10.1002/ana.22534
  119. Cox LE, Ferraiuolo L, Goodall EF, et al. Mutations in CHMP2B in Lower Motor Neuron Predominant Amyotrophic Lateral Sclerosis (ALS). Cookson MR, ed. *PLoS One.* 2010;5(3):e9872. doi:10.1371/journal.pone.0009872
  120. Wu C-H, Fallini C, Ticozzi N, et al. Mutations in the profilin 1 gene cause familial amyotrophic lateral sclerosis. *Nature.* 2012;488(7412):499-503. doi:10.1038/nature11280
  121. Takahashi Y, Fukuda Y, Yoshimura J, et al. ERBB4 mutations that disrupt the neuregulin-ErbB4 pathway cause amyotrophic lateral sclerosis type 19. *Am J Hum Genet.* 2013;93(5):900-905. doi:10.1016/j.ajhg.2013.09.008
  122. Kim HJ, Kim NC, Wang Y-D, et al. Mutations in prion-like domains in hnRNPA2B1 and hnRNPA1 cause multisystem proteinopathy and ALS. *Nature.* 2013;495(7442):467-473. doi:10.1038/nature11922
  123. Renton AE, Majounie E, Waite A, et al. A Hexanucleotide Repeat Expansion in C9ORF72 Is the Cause of Chromosome 9p21-Linked ALS-FTD. *Neuron.* 2011;72(2):257-268. doi:10.1016/j.neuron.2011.09.010
  124. Freischmidt A, Wieland T, Richter B, et al. Haploinsufficiency of TBK1 causes familial ALS and fronto-temporal dementia. *Nat Neurosci.* 2015;18(5):631-636. doi:10.1038/nn.4000
  125. Williams KL, Topp S, Yang S, et al. CCFN mutations in amyotrophic lateral sclerosis and frontotemporal dementia. *Nat Commun.* 2016;7(1):11253. doi:10.1038/ncomms11253
  126. Kaneb HM, Folkmann AW, Belzil V V, et al. Deleterious mutations in the essential mRNA metabolism factor, hGle1, in amyotrophic lateral sclerosis. *Hum*

- Mol Genet.* 2015;24(5):1363-1373. doi:10.1093/hmg/ddu545
127. Smith BN, Ticozzi N, Fallini C, et al. Exome-wide Rare Variant Analysis Identifies TUBA4A Mutations Associated with Familial ALS. *Neuron.* 2014;84(2):324-331. doi:10.1016/j.neuron.2014.09.027
  128. Johnson JO, Pioro EP, Boehringer A, et al. Mutations in the Matrin 3 gene cause familial amyotrophic lateral sclerosis. *Nat Neurosci.* 2014;17(5):664-666. doi:10.1038/nn.3688
  129. Kenna KP, van Doornaal PTC, Dekker AM, et al. NEK1 variants confer susceptibility to amyotrophic lateral sclerosis. *Nat Genet.* 2016;48(9):1037-1042. doi:10.1038/ng.3626
  130. Mackenzie IR, Nicholson AM, Sarkar M, et al. TIA1 Mutations in Amyotrophic Lateral Sclerosis and Frontotemporal Dementia Promote Phase Separation and Alter Stress Granule Dynamics. *Neuron.* 2017;95(4):808-816.e9. doi:10.1016/j.neuron.2017.07.025
  131. Cooper-Knock J, Moll T, Ramesh T, et al. Mutations in the Glycosyltransferase Domain of GLT8D1 Are Associated with Familial Amyotrophic Lateral Sclerosis. *Cell Rep.* 2019;26(9):2298-2306.e5. doi:10.1016/j.celrep.2019.02.006
  132. Smith BN, Topp SD, Fallini C, et al. Mutations in the vesicular trafficking protein annexin A11 are associated with amyotrophic lateral sclerosis. *Sci Transl Med.* 2017;9(388):eaad9157. doi:10.1126/scitranslmed.aad9157
  133. Nicolas A, Kenna KP, Renton AE, et al. Genome-wide Analyses Identify KIF5A as a Novel ALS Gene. *Neuron.* 2018;97(6):1268-1283.e6. doi:10.1016/j.neuron.2018.02.027
  134. White MA, Sreedharan J. Amyotrophic lateral sclerosis. *Curr Opin Neurol.* 2016;29(5):557-564. doi:10.1097/WCO.0000000000000367
  135. Dolinar A, Ravnik-Glavač M, Glavač D. Epigenetic mechanisms in amyotrophic lateral sclerosis: A short review. *Mech Ageing Dev.* 2018;174:103-110. doi:10.1016/j.mad.2018.03.005
  136. Leblond CS, Kaneb HM, Dion PA, Rouleau GA. Dissection of genetic factors associated with amyotrophic lateral sclerosis. *Exp Neurol.* 2014;262:91-101. doi:10.1016/j.expneurol.2014.04.013
  137. Su XW, Broach JR, Connor JR, Gerhard GS, Simmons Z. Genetic heterogeneity of amyotrophic lateral sclerosis: implications for clinical practice and research. *Muscle Nerve.* 2014;49(6):786-803. doi:10.1002/mus.24198
  138. Riva N, Agosta F, Lunetta C, Filippi M, Quattrini A. Recent advances in amyotrophic lateral sclerosis. *J Neurol.* 2016;263(6):1241-1254. doi:10.1007/s00415-016-8091-6
  139. Brooks BR, Miller RG, Swash M, Munsat TL, World Federation of Neurology Research Group on Motor Neuron Diseases. El Escorial revisited: revised criteria for the diagnosis of amyotrophic lateral sclerosis. *Amyotroph Lateral Scler Other Motor Neuron Disord.* 2000;1(5):293-299. <http://www.ncbi.nlm.nih.gov/pubmed/11464847>. Accessed October 2, 2019.
  140. Traynor BJ, Codd MB, Corr B, Forde C, Frost E, Hardiman OM. Clinical Features of Amyotrophic Lateral Sclerosis According to the El Escorial and Airlie House Diagnostic Criteria. *Arch Neurol.* 2000;57(8):1171. doi:10.1001/archneur.57.8.1171
  141. Costa J, Swash M, de Carvalho M. Awaji Criteria for the Diagnosis of Amyotrophic Lateral Sclerosis. *Arch Neurol.* 2012;69(11):1410. doi:10.1001/archneurol.2012.254
  142. Geevasinga N, Loy CT, Menon P, et al. Awaji criteria improves the diagnostic sensitivity in amyotrophic lateral sclerosis: A systematic review using individual patient data. *Clin Neurophysiol.* 2016;127(7):2684-2691.

- doi:10.1016/j.clinph.2016.04.005
143. Belsh JM. ALS diagnostic criteria of El Escorial Revisited: do they meet the needs of clinicians as well as researchers? *Amyotroph Lateral Scler Other Motor Neuron Disord.* 2000;1 Suppl 1:S57-60.  
<http://www.ncbi.nlm.nih.gov/pubmed/11464928>. Accessed October 2, 2019.
  144. Agosta F, Al-Chalabi A, Filippi M, et al. The El Escorial criteria: Strengths and weaknesses. *Amyotroph Lateral Scler Frontotemporal Degener.* 2014;8421(March):1-7. doi:10.3109/21678421.2014.964258
  145. Ludolph A, Drory V, Hardiman O, et al. A revision of the El Escorial criteria - 2015. *Amyotroph Lateral Scler Frontotemporal Degener.* 2015;16(5-6):291-292. doi:10.3109/21678421.2015.1049183
  146. Nzwalo H, de Abreu D, Swash M, Pinto S, de Carvalho M. Delayed diagnosis in ALS: The problem continues. *J Neurol Sci.* 2014;343(1-2):173-175. doi:10.1016/j.jns.2014.06.003
  147. Paganoni S, Macklin EA, Lee A, et al. Diagnostic timelines and delays in diagnosing amyotrophic lateral sclerosis (ALS). *Amyotroph Lateral Scler Front Degener.* 2014;15(5-6):453-456. doi:10.3109/21678421.2014.903974
  148. Chiò A, Logroscino G, Traynor BJ, et al. Global Epidemiology of Amyotrophic Lateral Sclerosis: A Systematic Review of the Published Literature. *Neuroepidemiology.* 2013;41(2):118-130. doi:10.1159/000351153
  149. Logroscino G, Traynor BJ, Hardiman O, et al. Incidence of amyotrophic lateral sclerosis in Europe. *J Neurol Neurosurg Psychiatry.* 2010;81(4):385-390. doi:10.1136/jnnp.2009.183525
  150. Ingre C, Roos PM, Piehl F, Kamel F, Fang F. Risk factors for amyotrophic lateral sclerosis. *Clin Epidemiol.* 2015;7:181-193. doi:10.2147/CLEP.S37505
  151. Oskarsson B, Horton DK, Mitsumoto H. Potential Environmental Factors in Amyotrophic Lateral Sclerosis. *Neurol Clin.* 2015;33(4):877-888. doi:10.1016/j.ncl.2015.07.009
  152. Cedarbaum JM, Stambler N, Malta E, et al. The ALSFRS-R: a revised ALS functional rating scale that incorporates assessments of respiratory function. BDNF ALS Study Group (Phase III). *J Neurol Sci.* 1999;169(1-2):13-21.  
<http://www.ncbi.nlm.nih.gov/pubmed/10540002>. Accessed December 8, 2015.
  153. The Amyotrophic Lateral Sclerosis Functional Rating Scale. Assessment of activities of daily living in patients with amyotrophic lateral sclerosis. The ALS CNTF treatment study (ACTS) phase I-II Study Group. *Arch Neurol.* 1996;53(2):141-147. <http://www.ncbi.nlm.nih.gov/pubmed/8639063>. Accessed September 29, 2018.
  154. Cedarbaum JM, Stambler N. Performance of the Amyotrophic Lateral Sclerosis Functional Rating Scale (ALSFRS) in multicenter clinical trials. *J Neurol Sci.* 1997;152 Suppl 1:S1-9. <http://www.ncbi.nlm.nih.gov/pubmed/9419047>. Accessed September 29, 2018.
  155. Bakker LA, Schröder CD, van Es MA, Westers P, Visser-Meily JMA, van den Berg LH. Assessment of the factorial validity and reliability of the ALSFRS-R: a revision of its measurement model. *J Neurol.* 2017;264(7):1413-1420. doi:10.1007/s00415-017-8538-4
  156. Franchignoni F, Mora G, Giordano A, Volanti P, Chiò A. Evidence of multidimensionality in the ALSFRS-R Scale: a critical appraisal on its measurement properties using Rasch analysis. *J Neurol Neurosurg Psychiatry.* 2013;84(12):1340-1345. doi:10.1136/jnnp-2012-304701
  157. Rooney J, Burke T, Vajda A, Heverin M, Hardiman O. What does the ALSFRS-R really measure? A longitudinal and survival analysis of functional dimension subscores in amyotrophic lateral sclerosis. *J Neurol Neurosurg Psychiatry.*



- November 2016:jnnp-2016-314661. doi:10.1136/jnnp-2016-314661
158. Gomeni R, Fava M, Pooled Resource Open-Access ALS Clinical Trials Consortium. Amyotrophic lateral sclerosis disease progression model. *Amyotroph Lateral Scler Front Degener.* 2014;15(1-2):119-129. doi:10.3109/21678421.2013.838970
  159. Marin B, Couratier P, Arcuti S, et al. Stratification of ALS patients' survival: a population-based study. *J Neurol.* 2016;263(1):100-111. doi:10.1007/s00415-015-7940-z
  160. Pfohl SR, Kim RB, Coan GS, Mitchell CS. Unraveling the Complexity of Amyotrophic Lateral Sclerosis Survival Prediction. *Front Neuroinform.* 2018;12:36. doi:10.3389/fninf.2018.00036
  161. Kollwe K, Mauss U, Krampf K, Petri S, Dengler R, Mohammadi B. ALSFRS-R score and its ratio: A useful predictor for ALS-progression. *J Neurol Sci.* 2008;275(1-2):69-73. doi:10.1016/j.jns.2008.07.016
  162. Watanabe H, Atsuta N, Nakamura R, et al. Factors affecting longitudinal functional decline and survival in amyotrophic lateral sclerosis patients. *Amyotroph Lateral Scler Front Degener.* 2015;16(3-4):230-236. doi:10.3109/21678421.2014.990036
  163. Elamin M, Bede P, Montuschi A, Pender N, Chio A, Hardiman O. Predicting prognosis in amyotrophic lateral sclerosis: a simple algorithm. *J Neurol.* 2015;262(6):1447-1454. doi:10.1007/s00415-015-7731-6
  164. Schuster C, Hardiman O, Bede P. Survival prediction in Amyotrophic lateral sclerosis based on MRI measures and clinical characteristics. *BMC Neurol.* 2017;17(1):73. doi:10.1186/s12883-017-0854-x
  165. Mandrioli J, Biguzzi S, Guidi C, et al. Heterogeneity in ALSFRS-R decline and survival: a population-based study in Italy. *Neurol Sci.* 2015;36(12):2243-2252. doi:10.1007/s10072-015-2343-6
  166. Bedlack RS, Vaughan T, Wicks P, et al. How common are ALS plateaus and reversals? *Neurology.* 2016;86(9):808-812. doi:10.1212/WNL.0000000000002251
  167. Cardenas-Blanco A, Machts J, Acosta-Cabronero J, et al. Structural and diffusion imaging versus clinical assessment to monitor amyotrophic lateral sclerosis. *NeuroImage Clin.* 2016;11:408-414. doi:10.1016/j.nicl.2016.03.011
  168. Menke RAL, Proudfoot M, Talbot K, Turner MR. The two-year progression of structural and functional cerebral MRI in amyotrophic lateral sclerosis. *NeuroImage Clin.* 2018;17:953-961. doi:10.1016/j.nicl.2017.12.025
  169. Ellis CM, Simmons A, Jones DK, et al. Diffusion tensor MRI assesses corticospinal tract damage in ALS. *Neurology.* 1999;53(5):1051-1058. <http://www.ncbi.nlm.nih.gov/pubmed/10496265>. Accessed February 12, 2016.
  170. Stoppel CM, Vielhaber S, Eckart C, et al. Structural and functional hallmarks of amyotrophic lateral sclerosis progression in motor- and memory-related brain regions. *NeuroImage Clin.* 2014;5:277-290. doi:10.1016/j.nicl.2014.07.007
  171. Menke RAL, Körner S, Filippini N, et al. Widespread grey matter pathology dominates the longitudinal cerebral MRI and clinical landscape of amyotrophic lateral sclerosis. *Brain.* 2014;137(9):2546-2555. doi:10.1093/brain/awu162
  172. Walhout R, Westeneng H-J, Verstraete E, et al. Cortical thickness in ALS: towards a marker for upper motor neuron involvement. *J Neurol Neurosurg Psychiatry.* 2015;86(3):288-294. doi:10.1136/jnnp-2013-306839
  173. Menke RAL, Abraham I, Thiel CS, et al. Fractional anisotropy in the posterior limb of the internal capsule and prognosis in amyotrophic lateral sclerosis. *Arch Neurol.* 2012;69(11):1493-1499. doi:10.1001/archneurol.2012.1122
  174. Matthews WB. Aids to the examination of the peripheral nervous system. *J*

- Neurol Sci.* 1977;33(1-2):299. doi:10.1016/0022-510X(77)90205-2
175. John J. Grading of muscle power: comparison of MRC and analogue scales by physiotherapists. Medical Research Council. *Int J Rehabil Res.* 1984;7(2):173-181. <http://www.ncbi.nlm.nih.gov/pubmed/6490272>. Accessed October 4, 2018.
  176. Swash M. MUNIX in the clinic in ALS: MUNE comes of age. *Clin Neurophysiol.* 2017;128(3):482-483. doi:10.1016/j.clinph.2016.12.021
  177. Great Lakes ALS Study Group. A comparison of muscle strength testing techniques in amyotrophic lateral sclerosis. *Neurology.* 2003;61(11):1503-1507. <http://www.ncbi.nlm.nih.gov/pubmed/14663032>. Accessed October 4, 2018.
  178. Kaufmann P, Pullman SL, Shungu DC, et al. Objective tests for upper motor neuron involvement in amyotrophic lateral sclerosis (ALS). *Neurology.* 2004;62(10):1753-1757. <http://www.ncbi.nlm.nih.gov/pubmed/15159473>. Accessed October 1, 2018.
  179. Swash M. Why are upper motor neuron signs difficult to elicit in amyotrophic lateral sclerosis? *J Neurol Neurosurg Psychiatry.* 2012;83(6):659-662. doi:10.1136/jnnp-2012-302315
  180. Huynh W, Simon NG, Grosskreutz J, Turner MR, Vucic S, Kiernan MC. Assessment of the upper motor neuron in amyotrophic lateral sclerosis. *Clin Neurophysiol.* 2016;127(7):2643-2660. doi:10.1016/j.clinph.2016.04.025
  181. Ince PG, Evans J, Knopp M, et al. Corticospinal tract degeneration in the progressive muscular atrophy variant of ALS. *Neurology.* 2003;60(8):1252-1258. doi:10.1212/01.WNL.0000058901.75728.4E
  182. Huynh W, Dharmadasa T, Vucic S, Kiernan MC. Functional Biomarkers for Amyotrophic Lateral Sclerosis. *Front Neurol.* 2019;9:1141. doi:10.3389/fneur.2018.01141
  183. Wang S, Melhem ER, Poptani H, Woo JH. Neuroimaging in Amyotrophic Lateral Sclerosis. *Neurotherapeutics.* 2011;8(1):63-71. doi:10.1007/s13311-010-0011-3
  184. Geevasinga N, Menon P, Yiannikas C, Kiernan MC, Vucic S. Diagnostic utility of cortical excitability studies in amyotrophic lateral sclerosis. *Eur J Neurol.* 2014;21(12):1451-1457. doi:10.1111/ene.12422
  185. Turner M, Cagnin A, Turkheimer F., et al. Evidence of widespread cerebral microglial activation in amyotrophic lateral sclerosis: an [11C](R)-PK11195 positron emission tomography study. *Neurobiol Dis.* 2004;15(3):601-609. doi:10.1016/j.nbd.2003.12.012
  186. Trojsi F, Caiazzo G, Corbo D, et al. Microstructural Changes across Different Clinical Milestones of Disease in Amyotrophic Lateral Sclerosis. Kassubek J, ed. *PLoS One.* 2015;10(3):e0119045. doi:10.1371/journal.pone.0119045
  187. Roche JC, Rojas-Garcia R, Scott KM, et al. A proposed staging system for amyotrophic lateral sclerosis. *Brain.* 2012;135(3):847-852. doi:10.1093/brain/awr351
  188. Chiò A, Hammond ER, Mora G, Bonito V, Filippini G. Development and evaluation of a clinical staging system for amyotrophic lateral sclerosis. *J Neurol Neurosurg Psychiatry.* 2015;86(1):38-44. doi:10.1136/jnnp-2013-306589
  189. Hardiman O, Al-Chalabi A, Chio A, et al. Amyotrophic lateral sclerosis. *Nat Rev Dis Prim.* 2017;3:17071. doi:10.1038/nrdp.2017.71
  190. Fang T, Al Khleifat A, Stahl DR, et al. Comparison of the King's and MiToS staging systems for ALS. *Amyotroph Lateral Scler Front Degener.* 2017;18(3-4):227-232. doi:10.1080/21678421.2016.1265565
  191. Ferraro D, Consonni D, Fini N, et al. Amyotrophic lateral sclerosis: a comparison of two staging systems in a population-based study. *Eur J Neurol.* 2016;23(9):1426-1432. doi:10.1111/ene.13053

192. Thakore NJ, Lapin BR, Kinzy TG, Piore EP. Deconstructing progression of amyotrophic lateral sclerosis in stages: a Markov modeling approach. *Amyotroph Lateral Scler Frontotemporal Degener.* 2018;19(7-8):483-494. doi:10.1080/21678421.2018.1484925
193. Brownell B, Oppenheimer DR, Hughes JT. The central nervous system in motor neurone disease. *J Neurol Neurosurg Psychiatry.* 1970;33(3):338-357. doi:10.1136/jnnp.33.3.338
194. Smith MC. Nerve Fibre Degeneration in the Brain in Amyotrophic Lateral Sclerosis. *J Neurol Neurosurg Psychiatry.* 1960;23(4):269-282. doi:10.1136/jnnp.23.4.269
195. Hammer RP, Tomiyasu U, Scheibel AB. Degeneration of the human Betz cell due to amyotrophic lateral sclerosis. *Exp Neurol.* 1979;63(2):336-346.
196. Saberi S, Stauffer JE, Schulte DJ, Ravits J. Neuropathology of Amyotrophic Lateral Sclerosis and Its Variants. *Neurol Clin.* 2015;33(4):855-876. doi:10.1016/j.ncl.2015.07.012
197. LAWYER T, NETSKY MG. Amyotrophic lateral sclerosis. *AMA Arch Neurol Psychiatry.* 1953;69(2):171-192. <http://www.ncbi.nlm.nih.gov/pubmed/13007227>. Accessed October 2, 2019.
198. Gredal O, Pakkenberg H, Karlsborg M, Pakkenberg B. Unchanged total number of neurons in motor cortex and neocortex in amyotrophic lateral sclerosis: a stereological study. *J Neurosci Methods.* 2000;95(2):171-176. <http://www.ncbi.nlm.nih.gov/pubmed/10752488>. Accessed April 21, 2017.
199. Maekawa S, Al-Sarraj S, Kibble M, et al. Cortical selective vulnerability in motor neuron disease: A morphometric study. *Brain.* 2004;127(6):1237-1251. doi:10.1093/brain/awh132
200. Udaka F, Kameyama M, Tomonaga M. Degeneration of betz cells in motor neuron disease. A Golgi study. *Acta Neuropathol.* 1986;70(3-4):289-295. doi:10.1007/BF00686086
201. DAVISON C. AMYOTROPHIC LATERAL SCLEROSIS. *Arch Neurol Psychiatry.* 1941;46(6):1039. doi:10.1001/archneurpsyc.1941.02280240094006
202. Iwata M, Hirano A. Sparing of the Onufrowicz nucleus in sacral anterior horn lesions. *Ann Neurol.* 1978;4(3):245-249. doi:10.1002/ana.410040309
203. Blokhuis AM, Groen EJM, Koppers M, van den Berg LH, Pasterkamp RJ. Protein aggregation in amyotrophic lateral sclerosis. *Acta Neuropathol.* 2013;125(6):777-794. doi:10.1007/s00401-013-1125-6
204. Julien JP. Amyotrophic lateral sclerosis. unfolding the toxicity of the misfolded. *Cell.* 2001;104(4):581-591. doi:10.1016/s0092-8674(01)00244-6
205. Bonafede R, Mariotti R. ALS Pathogenesis and Therapeutic Approaches: The Role of Mesenchymal Stem Cells and Extracellular Vesicles. *Front Cell Neurosci.* 2017;11:80. doi:10.3389/FNCEL.2017.00080
206. Mackenzie IRA, Rademakers R. The role of transactive response DNA-binding protein-43 in amyotrophic lateral sclerosis and frontotemporal dementia. *Curr Opin Neurol.* 2008;21(6):693-700. doi:10.1097/WCO.0b013e3283168d1d
207. Rohn TT. Cytoplasmic inclusions of TDP-43 in neurodegenerative diseases: a potential role for caspases. *Histol Histopathol.* 2009;24(8):1081-1086. doi:10.14670/HH-24.1081
208. Hergesheimer RC, Chami AA, de Assis DR, et al. The debated toxic role of aggregated TDP-43 in amyotrophic lateral sclerosis: a resolution in sight? *Brain.* 2019;142(5):1176-1194. doi:10.1093/brain/awz078
209. Prasad A, Bharathi V, Sivalingam V, Girdhar A, Patel BK. Molecular Mechanisms of TDP-43 Misfolding and Pathology in Amyotrophic Lateral Sclerosis. *Front Mol Neurosci.* 2019;12:25. doi:10.3389/fnmol.2019.00025

210. Scotter EL, Chen H-J, Shaw CE. TDP-43 Proteinopathy and ALS: Insights into Disease Mechanisms and Therapeutic Targets. *Neurotherapeutics*. 2015;12(2):352-363. doi:10.1007/s13311-015-0338-x
211. Hill SJ, Mordes DA, Cameron LA, et al. Two familial ALS proteins function in prevention/repair of transcription-associated DNA damage. *Proc Natl Acad Sci*. 2016;113(48):E7701-E7709. doi:10.1073/pnas.1611673113
212. Coan G, Mitchell CS. An Assessment of Possible Neuropathology and Clinical Relationships in 46 Sporadic Amyotrophic Lateral Sclerosis Patient Autopsies. *Neurodegener Dis*. 2015;15(5):301-312. doi:10.1159/000433581
213. Dormann D, Haass C. TDP-43 and FUS: a nuclear affair. *Trends Neurosci*. 2011;34(7):339-348. doi:10.1016/j.tins.2011.05.002
214. Neumann M, Sampathu DM, Kwong LK, et al. Ubiquitinated TDP-43 in Frontotemporal Lobar Degeneration and Amyotrophic Lateral Sclerosis. *Science* (80- ). 2006;314(5796):130-133. doi:10.1126/science.1134108
215. Da Cruz S, Bui A, Saberi S, et al. Misfolded SOD1 is not a primary component of sporadic ALS. *Acta Neuropathol*. February 2017. doi:10.1007/s00401-017-1688-8
216. Ludolph AC, Brettschneider J. TDP-43 in amyotrophic lateral sclerosis - is it a prion disease? *Eur J Neurol*. 2015;22(5):753-761. doi:10.1111/ene.12706
217. Smethurst P, Newcombe J, Troakes C, et al. In vitro prion-like behaviour of TDP-43 in ALS. *Neurobiol Dis*. 2016;96:236-247. doi:10.1016/j.nbd.2016.08.007
218. Corbo M, Hays AP. Peripherin and neurofilament protein coexist in spinal spheroids of motor neuron disease. *J Neuropathol Exp Neurol*. 1992;51(5):531-537. doi:10.1097/00005072-199209000-00008
219. De Vos KJ, Hafezparast M. Neurobiology of axonal transport defects in motor neuron diseases: Opportunities for translational research? *Neurobiol Dis*. February 2017. doi:10.1016/j.nbd.2017.02.004
220. Duncan JE, Goldstein LSB. The Genetics of Axonal Transport and Axonal Transport Disorders. *PLoS Genet*. 2006;2(9):e124. doi:10.1371/journal.pgen.0020124
221. Ikenaka K, Katsuno M, Kawai K, Ishigaki S, Tanaka F, Sobue G. Disruption of Axonal Transport in Motor Neuron Diseases. *Int J Mol Sci*. 2012;13(1):1225. doi:10.3390/IJMS13011225
222. Morfini GA, Burns M, Binder LI, et al. Axonal transport defects in neurodegenerative diseases. *J Neurosci*. 2009;29(41):12776-12786. doi:10.1523/JNEUROSCI.3463-09.2009
223. Borchelt DR, Wong PC, Becher MW, et al. Axonal transport of mutant superoxide dismutase 1 and focal axonal abnormalities in the proximal axons of transgenic mice. *Neurobiol Dis*. 1998;5(1):27-35. doi:10.1006/nbdi.1998.0178
224. Williamson TL, Cleveland DW. Slowing of axonal transport is a very early event in the toxicity of ALS-linked SOD1 mutants to motor neurons. *Nat Neurosci*. 1999;2(1):50-56. doi:10.1038/4553
225. Rothstein JD, Tsai G, Kuncl RW, et al. Abnormal excitatory amino acid metabolism in amyotrophic lateral sclerosis. *Ann Neurol*. 1990;28(1):18-25. doi:10.1002/ana.410280106
226. Shaw PJ, Forrest V, Ince PG, Richardson JP, Wastell HJ. CSF and plasma amino acid levels in motor neuron disease: elevation of CSF glutamate in a subset of patients. *Neurodegeneration*. 1995;4(2):209-216. <http://www.ncbi.nlm.nih.gov/pubmed/7583686>. Accessed October 2, 2019.
227. Rothstein JD. Excitotoxicity hypothesis. *Neurology*. 1996;47(Issue 4, Supplement 2):19S-26S. doi:10.1212/WNL.47.4\_Suppl\_2.19S

228. Rothstein JD, Dykes-Hoberg M, Pardo CA, et al. Knockout of Glutamate Transporters Reveals a Major Role for Astroglial Transport in Excitotoxicity and Clearance of Glutamate. *Neuron*. 1996;16(3):675-686. doi:10.1016/S0896-6273(00)80086-0
229. Kim K, Lee S-G, Kegelmann TP, et al. Role of Excitatory Amino Acid Transporter-2 (EAAT2) and glutamate in neurodegeneration: Opportunities for developing novel therapeutics. *J Cell Physiol*. 2011;226(10):2484-2493. doi:10.1002/jcp.22609
230. Shaw PJ, Ince PG. Glutamate, excitotoxicity and amyotrophic lateral sclerosis. *J Neurol*. 1997;244(S2):S3-S14. doi:10.1007/BF03160574
231. Corona JC, Tovar-y-Romo LB, Tapia R. Glutamate excitotoxicity and therapeutic targets for amyotrophic lateral sclerosis. *Expert Opin Ther Targets*. 2007;11(11):1415-1428. doi:10.1517/14728222.11.11.1415
232. Howells J, Matamala JM, Park SB, et al. *In vivo* evidence for reduced ion channel expression in motor axons of patients with amyotrophic lateral sclerosis. *J Physiol*. 2018;596(22):5379-5396. doi:10.1113/JP276624
233. Do-Ha D, Buskila Y, Ooi L. Impairments in Motor Neurons, Interneurons and Astrocytes Contribute to Hyperexcitability in ALS: Underlying Mechanisms and Paths to Therapy. *Mol Neurobiol*. February 2017. doi:10.1007/s12035-017-0392-y
234. Bellingham MC. A review of the neural mechanisms of action and clinical efficiency of riluzole in treating amyotrophic lateral sclerosis: what have we learned in the last decade? *CNS Neurosci Ther*. 2011;17(1):4-31. doi:10.1111/j.1755-5949.2009.00116.x
235. Vucic S, Kiernan MC. Transcranial Magnetic Stimulation for the Assessment of Neurodegenerative Disease. *Neurotherapeutics*. 2017;14(1):91-106. doi:10.1007/s13311-016-0487-6
236. Vucic S, Ziemann U, Eisen A, Hallett M, Kiernan MC. Transcranial magnetic stimulation and amyotrophic lateral sclerosis: pathophysiological insights. *J Neurol Neurosurg Psychiatry*. 2013;84(10):1161-1170. doi:10.1136/jnnp-2012-304019
237. van den Bos MAJ, Geevasinga N, Higashihara M, Menon P, Vucic S. Pathophysiology and Diagnosis of ALS: Insights from Advances in Neurophysiological Techniques. *Int J Mol Sci*. 2019;20(11):2818. doi:10.3390/ijms20112818
238. Vucic S, Kiernan MC. Novel threshold tracking techniques suggest that cortical hyperexcitability is an early feature of motor neuron disease. *Brain*. 2006;129(Pt 9):2436-2446. doi:10.1093/brain/awl172
239. Menon P, Kiernan MC, Vucic S. Cortical hyperexcitability precedes lower motor neuron dysfunction in ALS. *Clin Neurophysiol*. 2015;126(4):803-809. doi:10.1016/j.clinph.2014.04.023
240. Do-Ha D, Buskila Y, Ooi L. Impairments in Motor Neurons, Interneurons and Astrocytes Contribute to Hyperexcitability in ALS: Underlying Mechanisms and Paths to Therapy. *Mol Neurobiol*. 2018;55(2):1410-1418. doi:10.1007/s12035-017-0392-y
241. Vucic S, Nicholson GA, Kiernan MC. Cortical hyperexcitability may precede the onset of familial amyotrophic lateral sclerosis. *Brain*. 2008;131(6):1540-1550. doi:10.1093/brain/awn071
242. Geevasinga N, Menon P, Ng K, et al. Riluzole exerts transient modulating effects on cortical and axonal hyperexcitability in ALS. *Amyotroph Lateral Scler Front Degener*. 2016;17(7-8):580-588. doi:10.1080/21678421.2016.1188961
243. Shaw PJ, Ince PG, Falkous G, Mantle D. Oxidative damage to protein in sporadic

- motor neuron disease spinal cord. *Ann Neurol.* 1995;38(4):691-695.  
doi:10.1002/ana.410380424
244. Ferrante RJ, Browne SE, Shinobu LA, et al. Evidence of Increased Oxidative Damage in Both Sporadic and Familial Amyotrophic Lateral Sclerosis. *J Neurochem.* 2002;69(5):2064-2074. doi:10.1046/j.1471-4159.1997.69052064.x
  245. Tefera TW, Borges K. Metabolic Dysfunctions in Amyotrophic Lateral Sclerosis Pathogenesis and Potential Metabolic Treatments. *Front Neurosci.* 2017;10:611. doi:10.3389/fnins.2016.00611
  246. Aguirre T, van Den Bosch L, Goetschalckx K, et al. Increased sensitivity of fibroblasts from amyotrophic lateral sclerosis patients to oxidative stress. *Ann Neurol.* 1998;43(4):452-457. doi:10.1002/ana.410430407
  247. Magrané J, Hervias I, Henning MS, Damiano M, Kawamata H, Manfredi G. Mutant SOD1 in neuronal mitochondria causes toxicity and mitochondrial dynamics abnormalities. *Hum Mol Genet.* 2009;18(23):4552-4564. doi:10.1093/hmg/ddp421
  248. Tafuri F, Ronchi D, Magri F, Comi GP, Corti S. SOD1 misplacing and mitochondrial dysfunction in amyotrophic lateral sclerosis pathogenesis. *Front Cell Neurosci.* 2015;9:336. doi:10.3389/fncel.2015.00336
  249. Vehviläinen P, Koistinaho J, Gundars G. Mechanisms of mutant SOD1 induced mitochondrial toxicity in amyotrophic lateral sclerosis. *Front Cell Neurosci.* 2014;8:126. doi:10.3389/fncel.2014.00126
  250. Hooten KG, Beers DR, Zhao W, Appel SH. Protective and Toxic Neuroinflammation in Amyotrophic Lateral Sclerosis. *Neurotherapeutics.* 2015;12(2):364-375. doi:10.1007/s13311-014-0329-3
  251. A. McCombe P, D. Henderson R. The Role of Immune and Inflammatory Mechanisms in ALS. *Curr Mol Med.* 2011;11(3):246-254. doi:10.2174/156652411795243450
  252. Molteni M, Rossetti C. Neurodegenerative diseases: The immunological perspective. *J Neuroimmunol.* 2017;313:109-115. doi:10.1016/j.jneuroim.2017.11.002
  253. Zhao W, Beers DR, Appel SH. Immune-mediated Mechanisms in the Pathoprosession of Amyotrophic Lateral Sclerosis. *J Neuroimmune Pharmacol.* 2013;8(4):888-899. doi:10.1007/s11481-013-9489-x
  254. Kawamata T, Akiyama H, Yamada T, McGeer PL. Immunologic reactions in amyotrophic lateral sclerosis brain and spinal cord tissue. *Am J Pathol.* 1992;140(3):691-707. <http://www.ncbi.nlm.nih.gov/pubmed/1347673>. Accessed October 2, 2019.
  255. Bretschneider J, Toledo JB, Van Deerlin VM, et al. Microglial Activation Correlates with Disease Progression and Upper Motor Neuron Clinical Symptoms in Amyotrophic Lateral Sclerosis. Petrucelli L, ed. *PLoS One.* 2012;7(6):e39216. doi:10.1371/journal.pone.0039216
  256. Rentzos M, Rombos A, Nikolaou C, et al. Interleukin-15 and Interleukin-12 Are Elevated in Serum and Cerebrospinal Fluid of Patients with Amyotrophic Lateral Sclerosis. *Eur Neurol.* 2010;63(5):285-290. doi:10.1159/000287582
  257. Turner MR, Cagnin a, Turkheimer FE, et al. Evidence of widespread cerebral microglial activation in amyotrophic lateral sclerosis: an [11C](R)-PK11195 positron emission tomography study. *Neurobiol Dis.* 2004;15(3):601-609. doi:10.1016/j.nbd.2003.12.012
  258. Corcia P, Tauber C, Vercoullie J, et al. Molecular Imaging of Microglial Activation in Amyotrophic Lateral Sclerosis. Guillemin GJ, ed. *PLoS One.* 2012;7(12):e52941. doi:10.1371/journal.pone.0052941
  259. Brites D, Vaz AR. Microglia centered pathogenesis in ALS: insights in cell

- interconnectivity. *Front Cell Neurosci.* 2014;8:117.  
doi:10.3389/fncel.2014.00117
260. Lasiene J, Yamanaka K. Glial cells in amyotrophic lateral sclerosis. *Neurol Res Int.* 2011;2011:718987. doi:10.1155/2011/718987
  261. Philips T, Rothstein JD. Glial cells in amyotrophic lateral sclerosis. *Exp Neurol.* 2014;262 Pt B:111-120. doi:10.1016/j.expneurol.2014.05.015
  262. Pekny M, Pekna M. Reactive gliosis in the pathogenesis of CNS diseases. *Biochim Biophys Acta - Mol Basis Dis.* 2016;1862(3):483-491. doi:10.1016/J.BBADIS.2015.11.014
  263. Thonhoff JR, Simpson EP, Appel SH. Neuroinflammatory mechanisms in amyotrophic lateral sclerosis pathogenesis. *Curr Opin Neurol.* 2018;31(5):1. doi:10.1097/WCO.0000000000000599
  264. Gendelman HE, Appel SH. Neuroprotective activities of regulatory T cells. *Trends Mol Med.* 2011;17(12):687-688. doi:10.1016/j.molmed.2011.08.005
  265. Malaspina A, Puentes F, Amor S. Disease origin and progression in amyotrophic lateral sclerosis: an immunology perspective. *Int Immunol.* 2015;27(3):117-129. doi:10.1093/intimm/dxu099
  266. Henkel JS, Beers DR, Wen S, et al. Regulatory T-lymphocytes mediate amyotrophic lateral sclerosis progression and survival. *EMBO Mol Med.* 2013;5(1):64-79. doi:10.1002/emmm.201201544
  267. Barmada SJ. Linking RNA Dysfunction and Neurodegeneration in Amyotrophic Lateral Sclerosis. *Neurotherapeutics.* 2015;12(2):340-351. doi:10.1007/s13311-015-0340-3
  268. Butti Z, Patten SA. RNA Dysregulation in Amyotrophic Lateral Sclerosis. *Front Genet.* 2019;9:712. doi:10.3389/fgene.2018.00712
  269. Mathis S, Couratier P, Julian A, Corcia P, Le Masson G. Current view and perspectives in amyotrophic lateral sclerosis. *Neural Regen Res.* 2017;12(2):181. doi:10.4103/1673-5374.200794
  270. Yasuda K, Mili S. Dysregulated axonal RNA translation in amyotrophic lateral sclerosis. *Wiley Interdiscip Rev RNA.* 2016;7(5):589-603. doi:10.1002/wrna.1352
  271. Brites D, Fernandes A. Neuroinflammation and Depression: Microglia Activation, Extracellular Microvesicles and microRNA Dysregulation. *Front Cell Neurosci.* 2015;9:476. doi:10.3389/fncel.2015.00476
  272. Rinchetti P, Rizzuti M, Faravelli I, Corti S. MicroRNA Metabolism and Dysregulation in Amyotrophic Lateral Sclerosis. *Mol Neurobiol.* 2018;55(3):2617-2630. doi:10.1007/s12035-017-0537-z
  273. Emde A, Eitan C, Liou L, et al. Dysregulated mi RNA biogenesis downstream of cellular stress and ALS -causing mutations: a new mechanism for ALS. *EMBO J.* 2015;34(21):2633-2651. doi:10.15252/embj.201490493
  274. Ravits J, Appel S, Baloh RH, et al. Deciphering amyotrophic lateral sclerosis: what phenotype, neuropathology and genetics are telling us about pathogenesis. *Amyotroph Lateral Scler Frontotemporal Degener.* 2013;14 Suppl 1:5-18. doi:10.3109/21678421.2013.778548
  275. Grad LI, Rouleau GA, Ravits J, Cashman NR. Clinical Spectrum of Amyotrophic Lateral Sclerosis (ALS). *Cold Spring Harb Perspect Med.* 2017;7(8):a024117. doi:10.1101/cshperspect.a024117
  276. Eisen A, Kiernan M, Mitsumoto H, Swash M. Amyotrophic lateral sclerosis: a long preclinical period? *J Neurol Neurosurg Psychiatry.* 2014;85(11):1232-1238. doi:10.1136/jnnp-2013-307135
  277. Yamashita S, Ando Y. Genotype-phenotype relationship in hereditary amyotrophic lateral sclerosis. *Transl Neurodegener.* 2015;4(1):13. doi:10.1186/s40035-015-0036-y

278. Polymenidou M, Cleveland D. The Seeds of Neurodegeneration: Prion-like Spreading in ALS. *Cell*. 2011;147(3):498-508. doi:10.1016/j.cell.2011.10.011
279. Kang SH, Li Y, Fukaya M, et al. Degeneration and impaired regeneration of gray matter oligodendrocytes in amyotrophic lateral sclerosis. *Nat Neurosci*. 2013;16(5):571-579. doi:10.1038/nn.3357
280. Polymenidou M, Cleveland DW. Prion-like spread of protein aggregates in neurodegeneration. *J Exp Med*. 2012;209(5):889-893. doi:10.1084/jem.20120741
281. Maniecka Z, Polymenidou M. From nucleation to widespread propagation: A prion-like concept for ALS. *Virus Res*. 2015;207:94-105. doi:10.1016/J.VIRUSRES.2014.12.032
282. Vucic S, Ziemann U, Eisen A, Hallett M, Kiernan MC. Transcranial magnetic stimulation and amyotrophic lateral sclerosis: pathophysiological insights. *J Neurol Neurosurg Psychiatry*. 2013;84(10):1161-1170. doi:10.1136/jnnp-2012-304019
283. Braak H, Brettschneider J, Ludolph AC, Lee VM, Trojanowski JQ, Tredici K Del. Amyotrophic lateral sclerosis? a model of corticofugal axonal spread. *Nat Rev Neurol*. 2013;9(12):708-714. doi:10.1038/nrneurol.2013.221
284. Eisen A, Weber M. The motor cortex and amyotrophic lateral sclerosis. *Muscle Nerve*. 2001;24(4):564-573. <http://www.ncbi.nlm.nih.gov/pubmed/11268031>. Accessed April 21, 2017.
285. Brettschneider J, Del Tredici K, Toledo JB, et al. Stages of pTDP-43 pathology in amyotrophic lateral sclerosis. *Ann Neurol*. 2013;74(1):20-38. doi:10.1002/ana.23937
286. Dadon-Nachum M, Melamed E, Offen D. The “Dying-Back” Phenomenon of Motor Neurons in ALS. *J Mol Neurosci*. 2011;43(3):470-477. doi:10.1007/s12031-010-9467-1
287. Fischer LR, Culver DG, Tennant P, et al. Amyotrophic lateral sclerosis is a distal axonopathy: evidence in mice and man. *Exp Neurol*. 2004;185(2):232-240. <http://www.ncbi.nlm.nih.gov/pubmed/14736504>. Accessed March 29, 2017.
288. Eisen A, Weber M. The motor cortex and amyotrophic lateral sclerosis. *Muscle Nerve*. 2001;24(4):564-573.
289. Chou SM, Norris FH. Issues & Opinions: Amyotrophic lateral sclerosis: Lower motor neuron disease spreading to upper motor neurons. *Muscle Nerve*. 1993;16(8):864-869. doi:10.1002/mus.880160810
290. Piotrkiewicz M, Hausmanowa-Petrusewicz I. Amyotrophic lateral sclerosis: a dying motor unit? *Front Aging Neurosci*. 2013;5:7. doi:10.3389/fnagi.2013.00007
291. Aguzzi A, Rajendran L. The Transcellular Spread of Cytosolic Amyloids, Prions, and Prionoids. *Neuron*. 2009;64(6):783-790. doi:10.1016/J.NEURON.2009.12.016
292. Steiner JA, Angot E, Brundin P. A deadly spread: cellular mechanisms of  $\alpha$ -synuclein transfer. *Cell Death Differ*. 2011;18(9):1425-1433. doi:10.1038/cdd.2011.53
293. Petrov D, Mansfield C, Moussy A, Hermine O. ALS Clinical Trials Review: 20 Years of Failure. Are We Any Closer to Registering a New Treatment? *Front Aging Neurosci*. 2017;9. doi:10.3389/fnagi.2017.00068
294. Hobson E V., McDermott CJ. Supportive and symptomatic management of amyotrophic lateral sclerosis. *Nat Rev Neurol*. 2016;12(9):526-538. doi:10.1038/nrneurol.2016.111
295. Hogden A, Foley G, Henderson RD, James N, Aoun SM. Amyotrophic lateral sclerosis: improving care with a multidisciplinary approach. *J Multidiscip Healthc*. 2017;10:205-215. doi:10.2147/JMDH.S134992



296. Mitsumoto H, Del Bene M. Improving the quality of life for people with ALS: the challenge ahead. *Amyotroph Lateral Scler Other Motor Neuron Disord*. 2000;1(5):329-336. <http://www.ncbi.nlm.nih.gov/pubmed/11464851>. Accessed October 3, 2019.
297. Van den Berg JP, Kalmijn S, Lindeman E, et al. Multidisciplinary ALS care improves quality of life in patients with ALS. *Neurology*. 2005;65(8):1264-1267. doi:10.1212/01.wnl.0000180717.29273.12
298. Bourke SC, Tomlinson M, Williams TL, Bullock RE, Shaw PJ, Gibson GJ. Effects of non-invasive ventilation on survival and quality of life in patients with amyotrophic lateral sclerosis: a randomised controlled trial. *Lancet Neurol*. 2006;5(2):140-147. doi:10.1016/S1474-4422(05)70326-4
299. Heiman-Patterson TD, Cudkovicz ME, De Carvalho M, et al. Understanding the use of NIV in ALS: results of an international ALS specialist survey. *Amyotroph Lateral Scler Front Degener*. 2018;19(5-6):331-341. doi:10.1080/21678421.2018.1457058
300. Bensimon G, Lacomblez L, Meininger V. A Controlled Trial of Riluzole in Amyotrophic Lateral Sclerosis. *N Engl J Med*. 1994;330(9):585-591. doi:10.1056/NEJM199403033300901
301. Lacomblez L, Bensimon G, Leigh PN, Guillet P, Meininger V. Dose-ranging study of riluzole in amyotrophic lateral sclerosis. Amyotrophic Lateral Sclerosis/Riluzole Study Group II. *Lancet (London, England)*. 1996;347(9013):1425-1431. <http://www.ncbi.nlm.nih.gov/pubmed/8676624>. Accessed April 5, 2017.
302. Bensimon G, Lacomblez L, Delumeau JC, et al. A study of riluzole in the treatment of advanced stage or elderly patients with amyotrophic lateral sclerosis. *J Neurol*. 2002;249(5):609-615. doi:10.1007/s004150200071
303. Dharmadasa T, Kiernan MC. Riluzole, disease stage and survival in ALS. *Lancet Neurol*. 2018;17(5):385-386. doi:10.1016/S1474-4422(18)30091-7
304. Fang T, Al Khleifat A, Meurgey J-H, et al. Stage at which riluzole treatment prolongs survival in patients with amyotrophic lateral sclerosis: a retrospective analysis of data from a dose-ranging study. *Lancet Neurol*. 2018;17(5):416-422. doi:10.1016/S1474-4422(18)30054-1
305. Chen L, Liu X, Tang L, Zhang N, Fan D. Long-Term Use of Riluzole Could Improve the Prognosis of Sporadic Amyotrophic Lateral Sclerosis Patients: A Real-World Cohort Study in China. *Front Aging Neurosci*. 2016;8:246. doi:10.3389/fnagi.2016.00246
306. Bensimon G, Doble A. The tolerability of riluzole in the treatment of patients with amyotrophic lateral sclerosis. *Expert Opin Drug Saf*. 2004;3(6):525-534. <http://www.ncbi.nlm.nih.gov/pubmed/15500412>. Accessed October 3, 2019.
307. WRITING GROUP ON BEHALF OF THE EDARAVONE (MCI-186) ALS 19 STUDY GROUP. Open-label 24-week extension study of edaravone (MCI-186) in amyotrophic lateral sclerosis. *Amyotroph Lateral Scler Front Degener*. 2017;18(sup1):55-63. doi:10.1080/21678421.2017.1364269
308. Simon NG, Turner MR, Vucic S, et al. Quantifying disease progression in amyotrophic lateral sclerosis. *Ann Neurol*. 2014;76(5):643-657. doi:10.1002/ana.24273
309. Chiò A, Logroscino G, Hardiman O, et al. Prognostic factors in ALS: A critical review. *Amyotroph Lateral Scler*. 2009;10(5-6):310-323. doi:10.3109/17482960802566824
310. Knibb JA, Keren N, Kulka A, et al. A clinical tool for predicting survival in ALS. *J Neurol Neurosurg Psychiatry*. 2016;87(12):1361-1367. doi:10.1136/jnnp-2015-312908

311. Dal Bello-Haas V, Florence JM. Therapeutic exercise for people with amyotrophic lateral sclerosis or motor neuron disease. *Cochrane Database Syst Rev.* 2013;(5):CD005229. doi:10.1002/14651858.CD005229.pub3
312. Nakamura R, Atsuta N, Watanabe H, et al. Neck weakness is a potent prognostic factor in sporadic amyotrophic lateral sclerosis patients. *J Neurol Neurosurg Psychiatry.* 2013;84(12):1365-1371. doi:10.1136/jnnp-2013-306020
313. Scotton WJ, Scott KM, Moore DH, et al. Prognostic categories for amyotrophic lateral sclerosis. *Amyotroph Lateral Scler.* 2012;13(6):502-508. doi:10.3109/17482968.2012.679281
314. Georgouloupoulou E, Fini N, Vinceti M, et al. The impact of clinical factors, riluzole and therapeutic interventions on ALS survival: A population based study in Modena, Italy. *Amyotroph Lateral Scler Front Degener.* 2013;14(5-6):338-345. doi:10.3109/21678421.2013.763281
315. Elamin M, Phukan J, Bede P, et al. Executive dysfunction is a negative prognostic indicator in patients with ALS without dementia. *Neurology.* 2011;76(14):1263-1269. doi:10.1212/WNL.0b013e318214359f
316. Hu WT, Shelnett M, Wilson A, et al. Behavior matters--cognitive predictors of survival in amyotrophic lateral sclerosis. Le W, ed. *PLoS One.* 2013;8(2):e57584. doi:10.1371/journal.pone.0057584
317. Desport JC, Preux PM, Truong TC, Vallat JM, Sautereau D, Couratier P. Nutritional status is a prognostic factor for survival in ALS patients. *Neurology.* 1999;53(5):1059-1063. doi:10.1212/wnl.53.5.1059
318. Katz JS, Wolfe GI, Andersson PB, et al. Brachial amyotrophic diplegia: a slowly progressive motor neuron disorder. *Neurology.* 1999;53(5):1071-1076. doi:10.1212/wnl.53.5.1071
319. Hu MT, Ellis CM, Al-Chalabi A, Leigh PN, Shaw CE. Flail arm syndrome: a distinctive variant of amyotrophic lateral sclerosis. *J Neurol Neurosurg Psychiatry.* 1998;65(6):950-951. doi:10.1136/jnnp.65.6.950
320. Vucic S, Kiernan MC. Abnormalities in cortical and peripheral excitability in flail arm variant amyotrophic lateral sclerosis. *J Neurol Neurosurg Psychiatry.* 2007;78(8):849-852. doi:10.1136/jnnp.2006.105056
321. Sabatelli M, Zollino M, Luigetti M, et al. Uncovering amyotrophic lateral sclerosis phenotypes: clinical features and long-term follow-up of upper motor neuron-dominant ALS. *Amyotroph Lateral Scler.* 2011;12(4):278-282. doi:10.3109/17482968.2011.580849
322. Haverkamp LJ, Appel V, Appel SH. Natural history of amyotrophic lateral sclerosis in a database population Validation of a scoring system and a model for survival prediction. *Brain.* 1995;118(3):707-719. doi:10.1093/brain/118.3.707
323. de Jong SW, Huisman MHB, Sutedja NA, et al. Smoking, Alcohol Consumption, and the Risk of Amyotrophic Lateral Sclerosis: A Population-based Study. *Am J Epidemiol.* 2012;176(3):233-239. doi:10.1093/aje/kws015
324. Georgouloupoulou E, Fini N, Vinceti M, et al. The impact of clinical factors, riluzole and therapeutic interventions on ALS survival: a population based study in Modena, Italy. *Amyotroph Lateral Scler Frontotemporal Degener.* 2013;14(5-6):338-345. doi:10.3109/21678421.2013.763281
325. Juneja T, Pericak-Vance MA, Laing NG, Dave S, Siddique T. Prognosis in familial amyotrophic lateral sclerosis: progression and survival in patients with glu100gly and ala4val mutations in Cu,Zn superoxide dismutase. *Neurology.* 1997;48(1):55-57. doi:10.1212/wnl.48.1.55
326. Bäumer D, Hilton D, Paine SML, et al. Juvenile ALS with basophilic inclusions is a FUS proteinopathy with FUS mutations. *Neurology.* 2010;75(7):611-618. doi:10.1212/WNL.0b013e3181ed9cde

327. Cudkowicz ME, McKenna-Yasek D, Sapp PE, et al. Epidemiology of mutations in superoxide dismutase in amyotrophic lateral sclerosis. *Ann Neurol*. 1997;41(2):210-221. doi:10.1002/ana.410410212
328. Landers JE, Melki J, Meininger V, et al. Reduced expression of the Kinesin-Associated Protein 3 (KIFAP3) gene increases survival in sporadic amyotrophic lateral sclerosis. *Proc Natl Acad Sci U S A*. 2009;106(22):9004-9009. doi:10.1073/pnas.0812937106
329. Van Hoecke A, Schoonaert L, Lemmens R, et al. EPHA4 is a disease modifier of amyotrophic lateral sclerosis in animal models and in humans. *Nat Med*. 2012;18(9):1418-1422. doi:10.1038/nm.2901
330. Cudkowicz ME, Shefner JM, Schoenfeld DA, et al. A randomized, placebo-controlled trial of topiramate in amyotrophic lateral sclerosis. *Neurology*. 2003;61(4):456-464. doi:10.1212/wnl.61.4.456
331. McDermott CJ, Bradburn MJ, Maguire C, et al. DiPALS: Diaphragm Pacing in patients with Amyotrophic Lateral Sclerosis – a randomised controlled trial. *Health Technol Assess (Rockv)*. 2016;20(45):1-186. doi:10.3310/hta20450
332. Cui F, Sun L, Xiong J, Li J, Zhao Y, Huang X. Therapeutic effects of percutaneous endoscopic gastrostomy on survival in patients with amyotrophic lateral sclerosis: A meta-analysis. Green J, ed. *PLoS One*. 2018;13(2):e0192243. doi:10.1371/journal.pone.0192243
333. Dorst J, Ludolph AC. Non-invasive ventilation in amyotrophic lateral sclerosis. *Ther Adv Neurol Disord*. 2019;12:175628641985704. doi:10.1177/1756286419857040
334. Miller RG, Mitchell JD, Moore DH. Riluzole for amyotrophic lateral sclerosis (ALS)/motor neuron disease (MND). *Cochrane Database Syst Rev*. 2012;(3):CD001447. doi:10.1002/14651858.CD001447.pub3
335. Brooks BR, Bravver EK, Langford VL, Bockenek WL, Lindblom SS. Stage of prolonged survival in ALS. *Lancet Neurol*. 2018;17(7):579. doi:10.1016/S1474-4422(18)30207-2
336. Pinto S, De Carvalho M. Seasons and ALS time of death. *Amyotroph Lateral Scler Front Degener*. 2017;18(3-4):291-295. doi:10.1080/21678421.2017.1293112
337. Neudert C, Oliver D, Wasner M, Borasio GD. The course of the terminal phase in patients with amyotrophic lateral sclerosis. *J Neurol*. 2001;248(7):612-616. doi:10.1007/s004150170140
338. Talbot K. Clinical tool for predicting survival in ALS: do we need one? *J Neurol Neurosurg Psychiatry*. 2016;87(12):1275-1275. doi:10.1136/jnnp-2016-313683
339. Dharmadasa T, Huynh W, Tsugawa J, Shimatani Y, Ma Y, Kiernan MC. Implications of structural and functional brain changes in amyotrophic lateral sclerosis. *Expert Rev Neurother*. 2018;18(5):407-419. doi:10.1080/14737175.2018.1464912
340. Agosta F, Spinelli EG, Filippi M. Neuroimaging in amyotrophic lateral sclerosis: current and emerging uses. *Expert Rev Neurother*. 2018;18(5):395-406. doi:10.1080/14737175.2018.1463160
341. Turner MR, Verstraete E. What Does Imaging Reveal About the Pathology of Amyotrophic Lateral Sclerosis? *Curr Neurol Neurosci Rep*. 2015;15(7):45. doi:10.1007/s11910-015-0569-6
342. Kassubek J, Ludolph AC, Müller H-P. Neuroimaging of motor neuron diseases. *Ther Adv Neurol Disord*. 2012;5(2):119-127. doi:10.1177/1756285612437562
343. Berger A. Magnetic resonance imaging. *BMJ*. 2002;324(7328):35. doi:10.1136/bmj.324.7328.35
344. Mlynárik V. Introduction to nuclear magnetic resonance. *Anal Biochem*.

- 2017;529:4-9. doi:10.1016/j.ab.2016.05.006
345. Grover VPB, Tognarelli JM, Crossey MME, Cox IJ, Taylor-Robinson SD, McPhail MJW. Magnetic Resonance Imaging: Principles and Techniques: Lessons for Clinicians. *J Clin Exp Hepatol*. 2015;5(3):246-255. doi:10.1016/j.jceh.2015.08.001
  346. Gupta A, Nguyen TB, Chakraborty S, Bourque PR. Accuracy of Conventional MRI in ALS. *Can J Neurol Sci*. 2014;41(1):53-57. doi:10.1017/s0317167100016267
  347. Carrara G, Carapelli C, Venturi F, et al. A Distinct MR Imaging Phenotype in Amyotrophic Lateral Sclerosis: Correlation between T1 Magnetization Transfer Contrast Hyperintensity along the Corticospinal Tract and Diffusion Tensor Imaging Analysis. *Am J Neuroradiol*. 2012;33(4):733-739. doi:10.3174/ajnr.A2855
  348. Andreadou E, Sgouropoulos P, Varelas P, Gouliamos A, Papageorgiou C. Subcortical frontal lesions on MRI in patients with motor neurone disease. *Neuroradiology*. 1998;40(5):298-302. doi:10.1007/s002340050588
  349. Hecht MJ, Fellner F, Fellner C, Hilz MJ, Neundörfer B, Heuss D. Hyperintense and hypointense MRI signals of the precentral gyrus and corticospinal tract in ALS: a follow-up examination including FLAIR images. *J Neurol Sci*. 2002;199(1-2):59-65. doi:10.1016/s0022-510x(02)00104-1
  350. Ngai S, Tang YM, Du L, Stuckey S. Hyperintensity of the precentral gyral subcortical white matter and hypointensity of the precentral gyrus on fluid-attenuated inversion recovery: variation with age and implications for the diagnosis of amyotrophic lateral sclerosis. *AJNR Am J Neuroradiol*. 2007;28(2):250-254. <http://www.ncbi.nlm.nih.gov/pubmed/17296988>. Accessed October 3, 2019.
  351. Turner MR, Talbot K. Mimics and chameleons in motor neurone disease. *Pract Neurol*. 2013;13(3):153-164. doi:10.1136/practneurol-2013-000557
  352. Senda J, Atsuta N, Watanabe H, et al. Structural MRI correlates of amyotrophic lateral sclerosis progression. *J Neurol Neurosurg Psychiatry*. 2017;88(11):901-907. doi:10.1136/jnnp-2016-314337
  353. Ferraro PM, Agosta F, Riva N, et al. Multimodal structural MRI in the diagnosis of motor neuron diseases. *NeuroImage Clin*. 2017;16:240-247. doi:10.1016/j.nicl.2017.08.002
  354. Kalra S. Magnetic Resonance Spectroscopy in ALS. *Front Neurol*. 2019;10:482. doi:10.3389/fneur.2019.00482
  355. Lulé D, Ludolph AC, Kassubek J. MRI-based functional neuroimaging in ALS: An update. *Amyotroph Lateral Scler*. 2009;10(5-6):258-268. doi:10.3109/17482960802353504
  356. Li J, Pan P, Song W, Huang R, Chen K, Shang H. A meta-analysis of diffusion tensor imaging studies in amyotrophic lateral sclerosis. *Neurobiol Aging*. 2012;33(8):1833-1838. doi:10.1016/j.neurobiolaging.2011.04.007
  357. Broad RJ, Gabel MC, Dowell NG, et al. Neurite orientation and dispersion density imaging (NODDI) detects cortical and corticospinal tract degeneration in ALS. *J Neurol Neurosurg Psychiatry*. 2019;90(4):404-411. doi:10.1136/jnnp-2018-318830
  358. Cosottini M, Pesaresi I, Piazza S, et al. Magnetization Transfer Imaging Demonstrates a Distributed Pattern of Microstructural Changes of the Cerebral Cortex in Amyotrophic Lateral Sclerosis. *Am J Neuroradiol*. 2011;32(4):704-708. doi:10.3174/ajnr.A2356
  359. Helms G. Segmentation of human brain using structural MRI. *Magn Reson Mater Physics, Biol Med*. 2016;29(2):111-124. doi:10.1007/s10334-015-0518-z

360. Verstraete E, Foerster BR. Neuroimaging as a New Diagnostic Modality in Amyotrophic Lateral Sclerosis. *Neurotherapeutics*. 2015;12(2):403-416. doi:10.1007/s13311-015-0347-9
361. Agosta F, Pagani E, Rocca MA, et al. Voxel-based morphometry study of brain volumetry and diffusivity in amyotrophic lateral sclerosis patients with mild disability. *Hum Brain Mapp*. 2007;28(12):1430-1438. doi:10.1002/hbm.20364
362. Bede P, Bokde A, Elamin M, et al. Grey matter correlates of clinical variables in amyotrophic lateral sclerosis (ALS): a neuroimaging study of ALS motor phenotype heterogeneity and cortical focality. *J Neurol Neurosurg Psychiatry*. 2013;84(7):766-773. doi:10.1136/jnnp-2012-302674
363. Mezzapesa DM, Ceccarelli A, Dicuonzo F, et al. Whole-brain and regional brain atrophy in amyotrophic lateral sclerosis. *AJNR Am J Neuroradiol*. 2007;28(2):255-259. <http://www.ncbi.nlm.nih.gov/pubmed/17296989>. Accessed June 19, 2019.
364. Lillo P, Mioshi E, Burrell JR, Kiernan MC, Hodges JR, Hornberger M. Grey and White Matter Changes across the Amyotrophic Lateral Sclerosis-Frontotemporal Dementia Continuum. Stamatakis EA, ed. *PLoS One*. 2012;7(8):e43993. doi:10.1371/journal.pone.0043993
365. Rajagopalan V, Pioro EP. Distinct patterns of cortical atrophy in ALS patients with or without dementia: An MRI VBM study. *Amyotroph Lateral Scler Front Degener*. 2014;15(3-4):216-225. doi:10.3109/21678421.2014.880179
366. Das SR, Avants BB, Grossman M, Gee JC. Registration based cortical thickness measurement. *Neuroimage*. 2009;45(3):867-879. doi:10.1016/j.neuroimage.2008.12.016
367. Schuster C, Kasper E, Machts J, et al. Focal thinning of the motor cortex mirrors clinical features of amyotrophic lateral sclerosis and their phenotypes: a neuroimaging study. *J Neurol*. 2013;260(11):2856-2864. doi:10.1007/s00415-013-7083-z
368. Verstraete E, Veldink JH, Hendrikse J, Schelhaas HJ, van den Heuvel MP, van den Berg LH. Structural MRI reveals cortical thinning in amyotrophic lateral sclerosis. *J Neurol Neurosurg Psychiatry*. 2012;83(4):383-388. doi:10.1136/jnnp-2011-300909
369. Agosta F, Valsasina P, Riva N, et al. The Cortical Signature of Amyotrophic Lateral Sclerosis. Le W, ed. *PLoS One*. 2012;7(8):e42816. doi:10.1371/journal.pone.0042816
370. Verstraete E, Foerster BR. Neuroimaging as a New Diagnostic Modality in Amyotrophic Lateral Sclerosis. *Neurotherapeutics*. 2015;12(2):403-416. doi:10.1007/s13311-015-0347-9
371. Alshikho MJ, Zürcher NR, Loggia ML, et al. Glial activation colocalizes with structural abnormalities in amyotrophic lateral sclerosis. *Neurology*. 2016;87(24):2554-2561. doi:10.1212/WNL.0000000000003427
372. Bede P, Elamin M, Byrne S, et al. Basal ganglia involvement in amyotrophic lateral sclerosis. *Neurology*. 2013;81(24):2107-2115. doi:10.1212/01.wnl.0000437313.80913.2c
373. Westeneng H-J, Verstraete E, Walhout R, et al. Subcortical structures in amyotrophic lateral sclerosis. *Neurobiol Aging*. 2015;36(2):1075-1082. doi:10.1016/j.neurobiolaging.2014.09.002
374. Tan RH, Devenney E, Dobson-Stone C, et al. Cerebellar Integrity in the Amyotrophic Lateral Sclerosis - Frontotemporal Dementia Continuum. Kassubek J, ed. *PLoS One*. 2014;9(8):e105632. doi:10.1371/journal.pone.0105632
375. Winkler AM, Kochunov P, Blangero J, et al. Cortical thickness or grey matter volume? The importance of selecting the phenotype for imaging genetics studies.

- Neuroimage*. 2010;53(3):1135-1146. doi:10.1016/j.neuroimage.2009.12.028
376. Soares JM, Marques P, Alves V, Sousa N. A hitchhiker's guide to diffusion tensor imaging. *Front Neurosci*. 2013;7:31. doi:10.3389/fnins.2013.00031
  377. Dong Q, Welsh RC, Chenevert TL, et al. Clinical applications of diffusion tensor imaging. *J Magn Reson Imaging*. 2004;19(1):6-18. doi:10.1002/jmri.10424
  378. Chenevert TL, Brunberg JA, Pipe JG. Anisotropic diffusion in human white matter: demonstration with MR techniques in vivo. *Radiology*. 1990;177(2):401-405. doi:10.1148/radiology.177.2.2217776
  379. Beaulieu C. The basis of anisotropic water diffusion in the nervous system - a technical review. *NMR Biomed*. 2002;15(7-8):435-455. doi:10.1002/nbm.782
  380. Ciccarelli O, Catani M, Johansen-Berg H, Clark C, Thompson A. Diffusion-based tractography in neurological disorders: concepts, applications, and future developments. *Lancet Neurol*. 2008;7(8):715-727. doi:10.1016/S1474-4422(08)70163-7
  381. Comi G, Rovaris M, Leocani L. Review neuroimaging in amyotrophic lateral sclerosis. *Eur J Neurol*. 1999;6(6):629-637. <http://www.ncbi.nlm.nih.gov/pubmed/10529749>. Accessed March 2, 2017.
  382. Le Bihan D, Iima M. Diffusion Magnetic Resonance Imaging: What Water Tells Us about Biological Tissues. *PLOS Biol*. 2015;13(7):e1002203. doi:10.1371/journal.pbio.1002203
  383. Assaf Y, Freidlin RZ, Rohde GK, Basser PJ. New modeling and experimental framework to characterize hindered and restricted water diffusion in brain white matter. *Magn Reson Med*. 2004;52(5):965-978. doi:10.1002/mrm.20274
  384. Winston GP. The physical and biological basis of quantitative parameters derived from diffusion MRI. *Quant Imaging Med Surg*. 2012;2(4):254-265. doi:10.3978/j.issn.2223-4292.2012.12.05
  385. Roceanu A, Onu M, Antochi F, Bajenaru O. Diffusion Tensor Imaging (DTI) - A New Imaging Technique Applied in Multiple Sclerosis. *Maedica (Buchar)*. 2012;7(4):355-357. <http://www.ncbi.nlm.nih.gov/pubmed/23482844>. Accessed October 3, 2019.
  386. Metwalli NS, Benatar M, Nair G, Usher S, Hu X, Carew JD. Utility of axial and radial diffusivity from diffusion tensor MRI as markers of neurodegeneration in amyotrophic lateral sclerosis. *Brain Res*. 2010;1348:156-164. doi:10.1016/j.brainres.2010.05.067
  387. Geraldo AF, Pereira J, Nunes P, et al. Beyond fractional anisotropy in amyotrophic lateral sclerosis: the value of mean, axial, and radial diffusivity and its correlation with electrophysiological conductivity changes. *Neuroradiology*. 2018;60(5):505-515. doi:10.1007/s00234-018-2012-6
  388. Sage CA, Peeters RR, Görner A, Robberecht W, Sunaert S. Quantitative diffusion tensor imaging in amyotrophic lateral sclerosis. *Neuroimage*. 2007;34(2):486-499. doi:10.1016/j.neuroimage.2006.09.025
  389. Graham JM, Papadakis N, Evans J, et al. Diffusion tensor imaging for the assessment of upper motor neuron integrity in ALS. *Neurology*. 2004;63(11):2111-2119. doi:10.1212/01.WNL.0000145766.03057.E7
  390. Verstraete E, Turner MR, Grosskreutz J, Filippi M, Benatar M. Mind the gap: The mismatch between clinical and imaging metrics in ALS. *Amyotroph Lateral Scler Frontotemporal Degener*. 2015;16(7-8):524-529. doi:10.3109/21678421.2015.1051989
  391. Keil C, Prell T, Peschel T, Hartung V, Dengler R, Grosskreutz J. Longitudinal diffusion tensor imaging in amyotrophic lateral sclerosis. *BMC Neurosci*. 2012;13:141. doi:10.1186/1471-2202-13-141
  392. Agosta F, Rocca MA, Valsasina P, et al. A longitudinal diffusion tensor MRI

- study of the cervical cord and brain in amyotrophic lateral sclerosis patients. *J Neurol Neurosurg Psychiatry*. 2009;80(1):53-55. doi:10.1136/jnnp.2008.154252
393. Blain CR V, Williams VC, Johnston C, et al. A longitudinal study of diffusion tensor MRI in ALS. 2007;(February):348-355. doi:10.1080/17482960701548139
394. Benatar M, Wu J. Presymptomatic studies in ALS: rationale, challenges, and approach. *Neurology*. 2012;79(16):1732-1739. doi:10.1212/WNL.0b013e31826e9b1d
395. Filippini N, Douaud G, Mackay CE, Knight S, Talbot K, Turner MR. Corpus callosum involvement is a consistent feature of amyotrophic lateral sclerosis. *Neurology*. 2010;75(18):1645-1652. doi:10.1212/WNL.0b013e3181fb84d1
396. Iwata NK, Kwan JY, Danielian LE, et al. White matter alterations differ in primary lateral sclerosis and amyotrophic lateral sclerosis. *Brain*. 2011;134(9):2642-2655. doi:10.1093/brain/awr178
397. van der Graaff MM, Sage CA, Caan MWA, et al. Upper and extra-motoneuron involvement in early motoneuron disease: a diffusion tensor imaging study. *Brain*. 2011;134(Pt 4):1211-1228. doi:10.1093/brain/awr016
398. Fabri M, Pierpaoli C, Barbaresi P, Polonara G. Functional topography of the corpus callosum investigated by DTI and fMRI. *World J Radiol*. 2014;6(12):895-906. doi:10.4329/wjr.v6.i12.895
399. Prell T, Peschel T, Hartung V, et al. Diffusion tensor imaging patterns differ in bulbar and limb onset amyotrophic lateral sclerosis. *Clin Neurol Neurosurg*. 2013;115(8):1281-1287. doi:10.1016/j.clineuro.2012.11.031
400. Stanton BR, Shinhmar D, Turner MR, et al. Diffusion tensor imaging in sporadic and familial (D90A SOD1) forms of amyotrophic lateral sclerosis. *Arch Neurol*. 2009;66(1):109-115. doi:10.1001/archneurol.2008.527
401. Agosta F, Pagani E, Petrolini M, et al. Assessment of white matter tract damage in patients with amyotrophic lateral sclerosis: a diffusion tensor MR imaging tractography study. *AJNR Am J Neuroradiol*. 2010;31(8):1457-1461. doi:10.3174/ajnr.A2105
402. Bastin ME, Pettit LD, Bak TH, Gillingwater TH, Smith C, Abrahams S. Quantitative tractography and tract shape modeling in amyotrophic lateral sclerosis. *J Magn Reson Imaging*. 2013;38(5):1140-1145. doi:10.1002/jmri.24073
403. Schmidt R, de Reus MA, Scholtens LH, van den Berg LH, van den Heuvel MP. Simulating disease propagation across white matter connectome reveals anatomical substrate for neuropathology staging in amyotrophic lateral sclerosis. *Neuroimage*. 2016;124(Pt A):762-769. doi:10.1016/j.neuroimage.2015.04.005
404. Schmidt R, Verstraete E, de Reus MA, Veldink JH, van den Berg LH, van den Heuvel MP. Correlation between structural and functional connectivity impairment in amyotrophic lateral sclerosis. *Hum Brain Mapp*. 2014;35(9):4386-4395. doi:10.1002/hbm.22481
405. Grolez G, Moreau C, Danel-Brunaud V, et al. The value of magnetic resonance imaging as a biomarker for amyotrophic lateral sclerosis: a systematic review. *BMC Neurol*. 2016;16(1):155. doi:10.1186/s12883-016-0672-6
406. Kassubek J, Müller H-P, Del Tredici K, et al. Diffusion tensor imaging analysis of sequential spreading of disease in amyotrophic lateral sclerosis confirms patterns of TDP-43 pathology. *Brain*. 2014;137(Pt 6):1733-1740. doi:10.1093/brain/awu090
407. Hornberger M, Kiernan MC. Emergence of an imaging biomarker for amyotrophic lateral sclerosis: is the end point near? *J Neurol Neurosurg Psychiatry*. 2016;87(6):569. doi:10.1136/jnnp-2015-312882
408. Jeurissen B, Leemans A, Tournier J-D, Jones DK, Sijbers J. Investigating the

- prevalence of complex fiber configurations in white matter tissue with diffusion magnetic resonance imaging. *Hum Brain Mapp.* 2013;34(11):2747-2766. doi:10.1002/hbm.22099
409. Zhang H, Schneider T, Wheeler-Kingshott C a, Alexander DC. NODDI: practical in vivo neurite orientation dispersion and density imaging of the human brain. *Neuroimage.* 2012;61(4):1000-1016. doi:10.1016/j.neuroimage.2012.03.072
  410. Müller H-P, Turner MR, Grosskreutz J, et al. A large-scale multicentre cerebral diffusion tensor imaging study in amyotrophic lateral sclerosis. *J Neurol Neurosurg Psychiatry.* January 2016. doi:10.1136/jnnp-2015-311952
  411. Abhinav K, Yeh F-C, Pathak S, et al. Advanced diffusion MRI fiber tracking in neurosurgical and neurodegenerative disorders and neuroanatomical studies: A review. *Biochim Biophys Acta - Mol Basis Dis.* 2014;1842(11):2286-2297. doi:10.1016/j.bbadis.2014.08.002
  412. Basser PJ, Pierpaoli C. Microstructural and Physiological Features of Tissues Elucidated by Quantitative-Diffusion-Tensor MRI. *J Magn Reson Ser B.* 1996;111(3):209-219. doi:10.1006/JMRB.1996.0086
  413. Jespersen SN, Kroenke CD, Østergaard L, Ackerman JJH, Yablonskiy DA. Modeling dendrite density from magnetic resonance diffusion measurements. *Neuroimage.* 2007;34(4):1473-1486. doi:10.1016/j.neuroimage.2006.10.037
  414. Jespersen SN, Leigland LA, Cornea A, Kroenke CD. Determination of Axonal and Dendritic Orientation Distributions Within the Developing Cerebral Cortex by Diffusion Tensor Imaging. *IEEE Trans Med Imaging.* 2012;31(1):16-32. doi:10.1109/TMI.2011.2162099
  415. Tariq M, Schneider T, Alexander DC, Wheeler-Kingshott CAG, Zhang H. Bingham-NODDI: Mapping anisotropic orientation dispersion of neurites using diffusion MRI. *Neuroimage.* January 2016. doi:10.1016/j.neuroimage.2016.01.046
  416. Szafer A, Zhong J, Gore JC. Theoretical Model for Water Diffusion in Tissues. *Magn Reson Med.* 1995;33(5):697-712. doi:10.1002/mrm.1910330516
  417. Batalle D, O’Muircheartaigh J, Makropoulos A, et al. Different patterns of cortical maturation before and after 38 weeks gestational age demonstrated by diffusion MRI in vivo. *Neuroimage.* May 2018. doi:10.1016/j.neuroimage.2018.05.046
  418. Kunz N, Zhang H, Vasung L, et al. Assessing white matter microstructure of the newborn with multi-shell diffusion MRI and biophysical compartment models. *Neuroimage.* 2014;96:288-299. doi:10.1016/j.neuroimage.2014.03.057
  419. Karmacharya S, Gagoski B, Ning L, et al. Advanced diffusion imaging for assessing normal white matter development in neonates and characterizing aberrant development in congenital heart disease. *NeuroImage Clin.* 2018;19:360-373. doi:10.1016/j.nicl.2018.04.032
  420. Pecheva D, Kelly C, Kimpton J, et al. Recent advances in diffusion neuroimaging: applications in the developing preterm brain. *F1000Research.* 2018;7:1326. doi:10.12688/f1000research.15073.1
  421. Mah A, Geeraert B, Lebel C. Detailing neuroanatomical development in late childhood and early adolescence using NODDI. Leemans A, ed. *PLoS One.* 2017;12(8):e0182340. doi:10.1371/journal.pone.0182340
  422. Genc S, Malpas CB, Ball G, Silk TJ, Seal ML. Age, sex, and puberty related development of the corpus callosum: a multi-technique diffusion MRI study. *Brain Struct Funct.* 2018;223(6):2753-2765. doi:10.1007/s00429-018-1658-5
  423. Timmers I, Zhang H, Bastiani M, Jansma BM, Roebroek A, Rubio-Gozalbo ME. White matter microstructure pathology in classic galactosemia revealed by neurite orientation dispersion and density imaging. *J Inherit Metab Dis.*



- 2014;38(2):295-304. doi:10.1007/s10545-014-9780-x
424. Owen JP, Chang YS, Pojman NJ, et al. Aberrant White Matter Microstructure in Children with 16p11.2 Deletions. *J Neurosci*. 2014;34(18):6214-6223. doi:10.1523/JNEUROSCI.4495-13.2014
425. Caverzasi E, Mandelli ML, Hoeft F, et al. Abnormal age-related cortical folding and neurite morphology in children with developmental dyslexia. *NeuroImage Clin*. 2018;18:814-821. doi:10.1016/j.nicl.2018.03.012
426. Fukutomi H, Glasser MF, Zhang H, et al. Neurite imaging reveals microstructural variations in human cerebral cortical gray matter. *Neuroimage*. 2018;182:488-499. doi:10.1016/j.neuroimage.2018.02.017
427. Chang YS, Owen JP, Pojman NJ, et al. White Matter Changes of Neurite Density and Fiber Orientation Dispersion during Human Brain Maturation. Gong G, ed. *PLoS One*. 2015;10(6):e0123656. doi:10.1371/journal.pone.0123656
428. Nazeri A, Chakravarty MM, Rotenberg DJ, et al. Functional consequences of neurite orientation dispersion and density in humans across the adult lifespan. *J Neurosci*. 2015;35(4):1753-1762. doi:10.1523/JNEUROSCI.3979-14.2015
429. Slattery CF, Zhang J, Paterson RW, et al. ApoE influences regional white-matter axonal density loss in Alzheimer's disease. *Neurobiol Aging*. 2017;57:8-17. doi:10.1016/j.neurobiolaging.2017.04.021
430. Kamagata K, Hatano T, Okuzumi A, et al. Neurite orientation dispersion and density imaging in the substantia nigra in idiopathic Parkinson disease. *Eur Radiol*. October 2015. doi:10.1007/s00330-015-4066-8
431. Bruggen T Van, Zhang H, Pasternak O, Meinzer H, Stieltjes B, Fritzsche KH. Free-water elimination for assessing microstructural gray matter pathology - with application to Alzheimer's Disease. 2013;21:2013.
432. Parker TD, Slattery CF, Zhang J, et al. Cortical microstructure in young onset Alzheimer's disease using neurite orientation dispersion and density imaging. *Hum Brain Mapp*. 2018;39(7):3005-3017. doi:10.1002/hbm.24056
433. Andica C, Kamagata K, Hatano T, et al. Neurite orientation dispersion and density imaging of the nigrostriatal pathway in Parkinson's disease: Retrograde degeneration observed by tract-profile analysis. *Parkinsonism Relat Disord*. 2018;51:55-60. doi:10.1016/j.parkreldis.2018.02.046
434. Colgan N, Siow B, O'Callaghan JM, et al. Application of neurite orientation dispersion and density imaging (NODDI) to a tau pathology model of Alzheimer's disease. *Neuroimage*. 2016;125:739-744. doi:10.1016/j.neuroimage.2015.10.043
435. Suzuki H, Gao H, Bai W, et al. Abnormal brain white matter microstructure is associated with both pre-hypertension and hypertension. Lenglet C, ed. *PLoS One*. 2017;12(11):e0187600. doi:10.1371/journal.pone.0187600
436. Adluru G, Gur Y, Anderson JS, Richards LG, Adluru N, DiBella EVR. Assessment of white matter microstructure in stroke patients using NODDI. *Conf Proc . Annu Int Conf IEEE Eng Med Biol Soc IEEE Eng Med Biol Soc Annu Conf*. 2014;2014:742-745. doi:10.1109/EMBC.2014.6943697
437. Sone D, Sato N, Ota M, Maikusa N, Kimura Y, Matsuda H. Abnormal neurite density and orientation dispersion in unilateral temporal lobe epilepsy detected by advanced diffusion imaging. *NeuroImage Clin*. 2018;20:772-782. doi:10.1016/j.nicl.2018.09.017
438. Winston GP, Micallef C, Symms MR, Alexander DC, Duncan JS, Zhang H. Advanced diffusion imaging sequences could aid assessing patients with focal cortical dysplasia and epilepsy. *Epilepsy Res*. 2014;108(2):336-339. doi:10.1016/j.eplepsyres.2013.11.004
439. Rostampour M, Hashemi H, Najibi SM, Oghabian MA. Detection of structural

- abnormalities of cortical and subcortical gray matter in patients with MRI-negative refractory epilepsy using neurite orientation dispersion and density imaging. *Phys Medica*. 2018;48:47-54. doi:10.1016/j.ejmp.2018.03.005
440. Lemkaddem A, Daducci A, Kunz N, et al. Connectivity and tissue microstructural alterations in right and left temporal lobe epilepsy revealed by diffusion spectrum imaging. *NeuroImage Clin*. 2014;5:349-358. doi:10.1016/j.nicl.2014.07.013
  441. Rae CL, Davies G, Garfinkel SN, et al. Deficits in Neurite Density Underlie White Matter Structure Abnormalities in First-Episode Psychosis. *Biol Psychiatry*. February 2017. doi:10.1016/j.biopsych.2017.02.008
  442. Nazeri A, Mulsant BH, Rajji TK, et al. Gray Matter Neuritic Microstructure Deficits in Schizophrenia and Bipolar Disorder. *Biol Psychiatry*. 2017;82(10):726-736. doi:10.1016/j.biopsych.2016.12.005
  443. Kraguljac NV, Anthony T, Monroe WS, et al. A longitudinal neurite and free water imaging study in patients with a schizophrenia spectrum disorder. *Neuropsychopharmacology*. 2019;44(11):1932-1939. doi:10.1038/s41386-019-0427-3
  444. Masjoodi S, Hashemi H, Oghabian MA, Sharifi G. Differentiation of Edematous, Tumoral and Normal Areas of Brain Using Diffusion Tensor and Neurite Orientation Dispersion and Density Imaging. *J Biomed Phys Eng*. 2018;8(3):251-260. <http://www.ncbi.nlm.nih.gov/pubmed/30320029>. Accessed October 22, 2018.
  445. Zhao J, Li J, Wang J, et al. Quantitative analysis of neurite orientation dispersion and density imaging in grading gliomas and detecting IDH-1 gene mutation status. *NeuroImage Clin*. 2018;19:174-181. doi:10.1016/j.nicl.2018.04.011
  446. Maximov II, Tonoyan AS, Pronin IN. Differentiation of glioma malignancy grade using diffusion MRI. *Phys Medica*. 2017;40:24-32. doi:10.1016/j.ejmp.2017.07.002
  447. Granberg T, Fan Q, Treaba CA, et al. In vivo characterization of cortical and white matter neuroaxonal pathology in early multiple sclerosis. *Brain*. 2017;140(11):2912-2926. doi:10.1093/brain/awx247
  448. Schneider T, Brownlee W, Zhang H, Ciccarelli O, Miller DH, Wheeler-Kingshott CG. Sensitivity of multi-shell NODDI to multiple sclerosis white matter changes: a pilot study. *Funct Neurol*. 32(2):97-101. <http://www.ncbi.nlm.nih.gov/pubmed/28676143>. Accessed November 5, 2018.
  449. Spanò B, Giulietti G, Pisani V, et al. Disruption of neurite morphology parallels MS progression. *Neurol - Neuroimmunol Neuroinflammation*. 2018;5(6):e502. doi:10.1212/NXI.0000000000000502
  450. Grussu F, Schneider T, Tur C, et al. Neurite dispersion: a new marker of multiple sclerosis spinal cord pathology? *Ann Clin Transl Neurol*. 2017;4(9):663-679. doi:10.1002/acn3.445
  451. By S, Xu J, Box BA, Bagnato FR, Smith SA. Application and evaluation of NODDI in the cervical spinal cord of multiple sclerosis patients. *NeuroImage Clin*. 2017;15:333-342. doi:10.1016/j.nicl.2017.05.010
  452. Dowell NG, Bouyagoub S, Tibble J, Voon V, Cercignani M, Harrison NA. Interferon-alpha induced changes in NODDI predispose to the development of fatigue. *Neuroscience*. December 2017. doi:10.1016/j.neuroscience.2017.12.040
  453. Okita G, Ohba T, Takamura T, et al. Application of neurite orientation dispersion and density imaging or diffusion tensor imaging to quantify the severity of cervical spondylotic myelopathy and to assess postoperative neurologic recovery. *Spine J*. 2018;18(2):268-275. doi:10.1016/j.spinee.2017.07.007
  454. Ma X, Han X, Jiang W, et al. A Follow-up Study of Postoperative DCM Patients

- Using Diffusion MRI with DTI and NODDI. *Spine (Phila Pa 1976)*. 2018;43(15):1. doi:10.1097/BRS.0000000000002541
455. Reddy CP, Rathi Y. Joint Multi-Fiber NODDI Parameter Estimation and Tractography Using the Unscented Information Filter. *Front Neurosci*. 2016;10:166. doi:10.3389/fnins.2016.00166
  456. Stotesbury H, Kirkham FJ, Kölbel M, et al. White matter integrity and processing speed in sickle cell anemia. *Neurology*. 2018;90(23):e2042-e2050. doi:10.1212/WNL.0000000000005644
  457. Wu Y-C, Mustafi SM, Harezlak J, Kodiweera C, Flashman LA, McAllister TW. Hybrid Diffusion Imaging in Mild Traumatic Brain Injury. *J Neurotrauma*. 2018;35(20):2377-2390. doi:10.1089/neu.2017.5566
  458. Farooq H, Xu J, Nam JW, et al. Microstructure Imaging of Crossing (MIX) White Matter Fibers from diffusion MRI. *Sci Rep*. 2016;6:38927. doi:10.1038/srep38927
  459. Ferizi U, Schneider T, Panagiotaki E, et al. A ranking of diffusion MRI compartment models with in vivo human brain data. *Magn Reson Med*. 2014;72(6):1785-1792. doi:10.1002/mrm.25080
  460. Jelescu IO, Budde MD. Design and validation of diffusion MRI models of white matter. *Front Phys*. 2017;28. doi:10.3389/fphy.2017.00061
  461. Schilling KG, Janve V, Gao Y, Stepniewska I, Landman BA, Anderson AW. Histological validation of diffusion MRI fiber orientation distributions and dispersion. *Neuroimage*. 2018;165:200-221. doi:10.1016/j.neuroimage.2017.10.046
  462. Lampinen B, Szczepankiewicz F, Mårtensson J, van Westen D, Sundgren PC, Nilsson M. Neurite density imaging versus imaging of microscopic anisotropy in diffusion MRI: A model comparison using spherical tensor encoding. *Neuroimage*. 2017;147:517-531. doi:10.1016/j.neuroimage.2016.11.053
  463. Wolff SD, Balaban RS. Magnetization transfer contrast (MTC) and tissue water proton relaxation in vivo. *Magn Reson Med*. 1989;10(1):135-144. doi:10.1002/mrm.1910100113
  464. van Buchem MA. Magnetization Transfer: Applications in Neuroradiology. *J Comput Assist Tomogr*. 1999;23:S9-S18. doi:10.1097/00004728-199911001-00003
  465. Deichmann R, Gracien R-M. *Quantitative MRI of the Brain. Principles of Physical Measurement.*; 2018. doi:10.1201/B21837-6
  466. Mark A, Horsfield and Mara Cercignani. Chapter 5, Magnetization transfer imaging. Filippi M, ed. *Oxford Textbook of Neuroimaging*. Oxford University Press; 2015. doi:10.1093/med/9780199664092.001.0001
  467. Dousset V, Grossman RI, Ramer KN, et al. Experimental allergic encephalomyelitis and multiple sclerosis: lesion characterization with magnetization transfer imaging. *Radiology*. 1992;182(2):483-491. doi:10.1148/radiology.182.2.1732968
  468. Cercignani M, Bozzali M, Iannucci G, Comi G, Filippi M. Magnetisation transfer ratio and mean diffusivity of normal appearing white and grey matter from patients with multiple sclerosis. *J Neurol Neurosurg Psychiatry*. 2001;70(3):311-317. doi:10.1136/jnnp.70.3.311
  469. Barritt AW, Gabel MC, Cercignani M, Leigh PN. Emerging Magnetic Resonance Imaging Techniques and Analysis Methods in Amyotrophic Lateral Sclerosis. *Front Neurol*. 2018;9:1065. doi:10.3389/fneur.2018.01065
  470. Cosottini M, Pesaresi I, Piazza S, et al. Magnetization transfer imaging demonstrates a distributed pattern of microstructural changes of the cerebral cortex in amyotrophic lateral sclerosis. *AJNR Am J Neuroradiol*. 2011;32(4):704-

708. doi:10.3174/ajnr.A2356
471. Cosottini M, Cecchi P, Piazza S, et al. Mapping Cortical Degeneration in ALS with Magnetization Transfer Ratio and Voxel-Based Morphometry. Jones KE, ed. *PLoS One*. 2013;8(7):e68279. doi:10.1371/journal.pone.0068279
  472. Tanabe JL, Vermathen M, Miller R, Gelinas D, Weiner MW, Rooney WD. Reduced MTR in the corticospinal tract and normal T2 in amyotrophic lateral sclerosis. *Magn Reson Imaging*. 1998;16(10):1163-1169. <http://www.pubmedcentral.nih.gov/articlerender.fcgi?artid=2735261&tool=pmcentrez&rendertype=abstract>. Accessed August 7, 2016.
  473. Verstraete E, Polders DL, Mandl RCW, et al. Multimodal tract-based analysis in ALS patients at 7T: A specific white matter profile? *Amyotroph Lateral Scler Front Degener*. 2014;15(1-2):84-92. doi:10.3109/21678421.2013.844168
  474. Giulietti G, Bozzali M, Figura V, et al. Quantitative magnetization transfer provides information complementary to grey matter atrophy in Alzheimer's disease brains. *Neuroimage*. 2012;59(2):1114-1122. doi:10.1016/j.neuroimage.2011.09.043
  475. Harrison NA, Cooper E, Dowell NG, et al. Quantitative Magnetization Transfer Imaging as a Biomarker for Effects of Systemic Inflammation on the Brain. *Biol Psychiatry*. 2015;78(1):49-57. doi:10.1016/j.biopsych.2014.09.023
  476. Turati L, Moscatelli M, Mastropietro A, et al. In vivo quantitative magnetization transfer imaging correlates with histology during de- and remyelination in cuprizone-treated mice. *NMR Biomed*. 2015;28(3):327-337. doi:10.1002/nbm.3253
  477. Levesque IR, Giacomini PS, Narayanan S, et al. Quantitative magnetization transfer and myelin water imaging of the evolution of acute multiple sclerosis lesions. *Magn Reson Med*. 2010;63(3):633-640. doi:10.1002/mrm.22244
  478. Cosottini M, Cecchi P, Piazza S, et al. Mapping cortical degeneration in ALS with magnetization transfer ratio and voxel-based morphometry. *PLoS One*. 2013;8(7):e68279. doi:10.1371/journal.pone.0068279
  479. Gloor M, Scheffler K, Bieri O. Quantitative magnetization transfer imaging using balanced SSFP. *Magn Reson Med*. 2008;60(3):691-700. doi:10.1002/mrm.21705
  480. Levesque I, Sled JG, Narayanan S, et al. The role of edema and demyelination in chronic T1 black holes: A quantitative magnetization transfer study. *J Magn Reson Imaging*. 2005;21(2):103-110. doi:10.1002/jmri.20231
  481. Spanò B, Cercignani M, Basile B, et al. Multiparametric MR investigation of the motor pyramidal system in patients with "truly benign" multiple sclerosis. *Mult Scler*. 2010;16(2):178-188. doi:10.1177/1352458509356010
  482. Cercignani M, Basile B, Spanò B, et al. Investigation of quantitative magnetisation transfer parameters of lesions and normal appearing white matter in multiple sclerosis. *NMR Biomed*. 2009;22(6):646-653. doi:10.1002/nbm.1379
  483. Liu Z, Pardini M, Yaldizli Ö, et al. Magnetization transfer ratio measures in normal-appearing white matter show periventricular gradient abnormalities in multiple sclerosis. *Brain*. 2015;138(5):1239-1246. doi:10.1093/brain/awv065
  484. Bozzali M, Serra L, Cercignani M. Quantitative MRI to understand Alzheimer's disease pathophysiology. *Curr Opin Neurol*. 2016;29(4):437-444. doi:10.1097/WCO.0000000000000345
  485. Rice L, Bisdas S. The diagnostic value of FDG and amyloid PET in Alzheimer's disease—A systematic review. *Eur J Radiol*. 2017;94:16-24. doi:10.1016/j.ejrad.2017.07.014
  486. Carrara G, Carapelli C, Venturi F, et al. A distinct MR imaging phenotype in amyotrophic lateral sclerosis: correlation between T1 magnetization transfer contrast hyperintensity along the corticospinal tract and diffusion tensor imaging

- analysis. *AJNR Am J Neuroradiol*. 2012;33(4):733-739. doi:10.3174/ajnr.A2855
487. da Rocha AJ, Oliveira ASB, Fonseca RB, Maia ACM, Buainain RP, Lederman HM. Detection of corticospinal tract compromise in amyotrophic lateral sclerosis with brain MR imaging: relevance of the T1-weighted spin-echo magnetization transfer contrast sequence. *AJNR Am J Neuroradiol*. 2004;25(9):1509-1515. <http://www.ncbi.nlm.nih.gov/pubmed/15502129>. Accessed March 2, 2017.
  488. Faul F, Erdfelder E, Lang A-G, Buchner A. G\*Power 3: a flexible statistical power analysis program for the social, behavioral, and biomedical sciences. *Behav Res Methods*. 2007;39(2):175-191. <http://www.ncbi.nlm.nih.gov/pubmed/17695343>. Accessed October 4, 2019.
  489. Lechtzin N, Cudkowicz ME, de Carvalho M, et al. Respiratory measures in amyotrophic lateral sclerosis. *Amyotroph Lateral Scler Frontotemporal Degener*. 2018;19(5-6):321-330. doi:10.1080/21678421.2018.1452945
  490. Rascovsky K, Hodges JR, Knopman D, et al. Sensitivity of revised diagnostic criteria for the behavioural variant of frontotemporal dementia. *Brain*. 2011;134(Pt 9):2456-2477. doi:10.1093/brain/awr179
  491. Al-Chalabi A, Hardiman O. The epidemiology of ALS: a conspiracy of genes, environment and time. *Nat Rev Neurol*. 2013;9(11):617-628. doi:10.1038/nrneurol.2013.203
  492. Talbot EO, Malek AM, Lacomis D. The epidemiology of amyotrophic lateral sclerosis. In: *Handbook of Clinical Neurology*. Vol 138. ; 2016:225-238. doi:10.1016/B978-0-12-802973-2.00013-6
  493. Chiò A, Logroscino G, Traynor BJ, et al. Global Epidemiology of Amyotrophic Lateral Sclerosis: A Systematic Review of the Published Literature. *Neuroepidemiology*. 2013;41(2):118-130. doi:10.1159/000351153
  494. Alonso A, Logroscino G, Jick SS, Hernán MA. Incidence and lifetime risk of motor neuron disease in the United Kingdom: a population-based study. *Eur J Neurol*. 2009;16(6):745-751. <http://www.ncbi.nlm.nih.gov/pubmed/19475756>. Accessed October 4, 2019.
  495. Palese F, Sartori A, Logroscino G, Pisa FE. Predictors of diagnostic delay in amyotrophic lateral sclerosis: a cohort study based on administrative and electronic medical records data. *Amyotroph Lateral Scler Front Degener*. 2019;20(3-4):176-185. doi:10.1080/21678421.2018.1550517
  496. Thakore NJ, Lapin BR, Pioro EP, Pooled Resource Open-Access ALS Clinical Trials Consortium. Trajectories of impairment in amyotrophic lateral sclerosis: Insights from the Pooled Resource Open-Access ALS Clinical Trials cohort. *Muscle Nerve*. 2018;57(6):937-945. doi:10.1002/mus.26042
  497. Strong MJ, Abrahams S, Goldstein LH, et al. Amyotrophic lateral sclerosis - frontotemporal spectrum disorder (ALS-FTSD): Revised diagnostic criteria. *Amyotroph Lateral Scler Front Degener*. 2017;18(3-4):153-174. doi:10.1080/21678421.2016.1267768
  498. Small SA. Age-Related Memory Decline. *Arch Neurol*. 2001;58(3):360-364. doi:10.1001/archneur.58.3.360
  499. Taylor LJ, Brown RG, Tsermentseli S, et al. Is language impairment more common than executive dysfunction in amyotrophic lateral sclerosis? *J Neurol Neurosurg Psychiatry*. 2013;84(5):494-498. doi:10.1136/jnnp-2012-303526
  500. Ringholz GM, Appel SH, Bradshaw M, Cooke NA, Mosnik DM, Schulz PE. Prevalence and patterns of cognitive impairment in sporadic ALS. *Neurology*. 2005;65(4):586-590. doi:10.1212/01.wnl.0000172911.39167.b6
  501. Waldron EJ, Barrash J, Swenson A, Tranel D. Personality Disturbances in Amyotrophic Lateral Sclerosis: A Case Study Demonstrating Changes in Personality Without Cognitive Deficits. *J Int Neuropsychol Soc*.

- 2014;20(07):764-771. doi:10.1017/S1355617714000459
502. Tsermentseli S, Leigh PN, Goldstein LH. The anatomy of cognitive impairment in amyotrophic lateral sclerosis: more than frontal lobe dysfunction. *Cortex*. 2012;48(2):166-182. doi:10.1016/j.cortex.2011.02.004
  503. Talbot K, Ansorge O. Recent advances in the genetics of amyotrophic lateral sclerosis and frontotemporal dementia: common pathways in neurodegenerative disease. *Hum Mol Genet*. 2006;15(suppl\_2):R182-R187. doi:10.1093/hmg/ddl202
  504. Lomen-Hoerth C. Clinical Phenomenology and Neuroimaging Correlates in ALS-FTD. *J Mol Neurosci*. 2011;45(3):656-662. doi:10.1007/s12031-011-9636-x
  505. Lomen-Hoerth C, Anderson T, Miller B. The overlap of amyotrophic lateral sclerosis and frontotemporal dementia. *Neurology*. 2002;59(7):1077-1079. doi:10.1212/wnl.59.7.1077
  506. Castrillo-Viguera C, Grasso DL, Simpson E, Shefner J, Cudkowicz ME. Clinical significance in the change of decline in ALSFRS-R. *Amyotroph Lateral Scler*. 2010;11(1-2):178-180. doi:10.3109/17482960903093710
  507. Mandrioli J, Biguzzi S, Guidi C, et al. Heterogeneity in ALSFRS-R decline and survival: a population-based study in Italy. *Neurol Sci*. 2015;36(12):2243-2252. doi:10.1007/s10072-015-2343-6
  508. Bakker LA, Schröder CD, van Es MA, Westers P, Visser-Meily JMA, van den Berg LH. Assessment of the factorial validity and reliability of the ALSFRS-R: a revision of its measurement model. *J Neurol*. June 2017. doi:10.1007/s00415-017-8538-4
  509. Chiò A, Pagani M, Agosta F, Calvo A, Cistaro A, Filippi M. Neuroimaging in amyotrophic lateral sclerosis: insights into structural and functional changes. *Lancet Neurol*. 2014;13(12):1228-1240. doi:10.1016/S1474-4422(14)70167-X
  510. Foerster BR, Dwamena BA, Petrou M, Carlos RC, Callaghan BC, Pomper MG. Diagnostic accuracy using diffusion tensor imaging in the diagnosis of ALS: a meta-analysis. *Acad Radiol*. 2012;19(9):1075-1086. doi:10.1016/j.acra.2012.04.012
  511. Jelescu IO, Veraart J, Fieremans E, Novikov DS. Degeneracy in model parameter estimation for multi-compartmental diffusion in neuronal tissue. *NMR Biomed*. 2016;29(1):33-47. doi:10.1002/nbm.3450
  512. Alexander AL, Hasan KM, Lazar M, Tsuruda JS, Parker DL. Analysis of partial volume effects in diffusion-tensor MRI. *Magn Reson Med*. 2001;45(5):770-780.
  513. Vos SB, Jones DK, Jeurissen B, Viergever MA, Leemans A. The influence of complex white matter architecture on the mean diffusivity in diffusion tensor MRI of the human brain. *Neuroimage*. 2012;59(3):2208-2216. doi:10.1016/j.neuroimage.2011.09.086
  514. Reese TG, Heid O, Weisskoff RM, Wedeen VJ. Reduction of eddy-current-induced distortion in diffusion MRI using a twice-refocused spin echo. *Magn Reson Med*. 2003;49(1):177-182. doi:10.1002/mrm.10308
  515. Leemans A, Jones DK. The B-matrix must be rotated when correcting for subject motion in DTI data. *Magn Reson Med*. 2009;61(6):1336-1349. doi:10.1002/mrm.21890
  516. Bland JM, Altman DG. Multiple significance tests: the Bonferroni method. *BMJ*. 1995;310(6973):170. doi:10.1136/bmj.310.6973.170
  517. Petrov D, Mansfield C, Moussy A, Hermine O. ALS Clinical Trials Review: 20 Years of Failure. Are We Any Closer to Registering a New Treatment? *Front Aging Neurosci*. 2017;9:68. doi:10.3389/fnagi.2017.00068
  518. Fogarty MJ, Klenowski PM, Lee JD, et al. Cortical synaptic and dendritic spine

- abnormalities in a presymptomatic TDP-43 model of amyotrophic lateral sclerosis. *Sci Rep.* 2016;6(1):37968. doi:10.1038/srep37968
519. Jara JH, Villa SR, Khan NA, Bohn MC, Ozdinler PH. AAV2 mediated retrograde transduction of corticospinal motor neurons reveals initial and selective apical dendrite degeneration in ALS. *Neurobiol Dis.* 2012;47(2):174-183. doi:10.1016/j.nbd.2012.03.036
  520. Genç B, Jara JH, Lagrimas AKB, et al. Apical dendrite degeneration, a novel cellular pathology for Betz cells in ALS. *Sci Rep.* 2017;7:41765. doi:10.1038/srep41765
  521. Kushchayev S V., Moskalenko VF, Wiener PC, et al. The discovery of the pyramidal neurons: Vladimir Betz and a new era of neuroscience. *Brain.* 2012;135(1):285-300. doi:10.1093/brain/awr276
  522. Chenot Q, Tzourio-Mazoyer N, Rheault F, et al. A population-based atlas of the human pyramidal tract in 410 healthy participants. *Brain Struct Funct.* 2019;224(2):599-612. doi:10.1007/s00429-018-1798-7
  523. Kaden E, Kruggel F, Alexander DC. Quantitative mapping of the per-axon diffusion coefficients in brain white matter. *Magn Reson Med.* 2016;75(4):1752-1763. doi:10.1002/mrm.25734
  524. Agosta F, Valsasina P, Riva N, et al. The Cortical Signature of Amyotrophic Lateral Sclerosis. Le W, ed. *PLoS One.* 2012;7(8):e42816. doi:10.1371/journal.pone.0042816
  525. Zhang Y, Schuff N, Woolley SC, et al. Progression of white matter degeneration in amyotrophic lateral sclerosis: A diffusion tensor imaging study. *Amyotroph Lateral Scler.* 2011;12(6):421-429. doi:10.3109/17482968.2011.593036
  526. Canu E, Agosta F, Riva N, et al. The Topography of Brain Microstructural Damage in Amyotrophic Lateral Sclerosis Assessed Using Diffusion Tensor MR Imaging. *Am J Neuroradiol.* 2011;32(7):1307-1314. doi:10.3174/ajnr.A2469
  527. Keil C, Prell T, Peschel T, Hartung V, Dengler R, Grosskreutz J. Longitudinal diffusion tensor imaging in amyotrophic lateral sclerosis. *BMC Neurosci.* 2012;13(1):141. doi:10.1186/1471-2202-13-141
  528. Toosy AT, Werring DJ, Orrell RW, et al. Diffusion tensor imaging detects corticospinal tract involvement at multiple levels in amyotrophic lateral sclerosis. *J Neurol Neurosurg Psychiatry.* 2003;74(9):1250-1257. <http://www.ncbi.nlm.nih.gov/pubmed/12933929>. Accessed April 21, 2017.
  529. Chapman MC, Jelsone-Swain L, Johnson TD, Gruis KL, Welsh RC. Diffusion tensor MRI of the corpus callosum in amyotrophic lateral sclerosis. *J Magn Reson Imaging.* 2014;39(3):641-647. doi:10.1002/jmri.24218
  530. Metwalli NS, Benatar M, Nair G, Usher S, Hu X, Carew JD. Utility of axial and radial diffusivity from diffusion tensor MRI as markers of neurodegeneration in amyotrophic lateral sclerosis. *Brain Res.* 2010;1348:156-164. doi:10.1016/j.brainres.2010.05.067
  531. Shellikeri S, Karthikeyan V, Martino R, et al. The neuropathological signature of bulbar-onset ALS: A systematic review. *Neurosci Biobehav Rev.* 2017;75:378-392. doi:10.1016/j.neubiorev.2017.01.045
  532. Geser F, Brandmeir NJ, Kwong LK, et al. Evidence of Multisystem Disorder in Whole-Brain Map of Pathological TDP-43 in Amyotrophic Lateral Sclerosis. *Arch Neurol.* 2008;65(5):636-641. doi:10.1001/archneur.65.5.636
  533. Brettschneider J, Del Tredici K, Toledo JB, et al. Stages of pTDP-43 pathology in amyotrophic lateral sclerosis. *Ann Neurol.* 2013;74(1):20-38. doi:10.1002/ana.23937
  534. Consonni M, Contarino VE, Catricalà E, et al. Cortical markers of cognitive syndromes in amyotrophic lateral sclerosis. *NeuroImage Clin.* 2018;19:675-682.

- doi:10.1016/j.nicl.2018.05.020
535. Rajagopalan V, Liu Z, Allexandre D, et al. Brain white matter shape changes in amyotrophic lateral sclerosis (ALS): a fractal dimension study. *PLoS One*. 2013;8(9):e73614. doi:10.1371/journal.pone.0073614
  536. Warren JD, Rohrer JD, Rossor MN. Frontotemporal dementia. *BMJ*. 2013;347(aug12 3):f4827-f4827. doi:10.1136/bmj.f4827
  537. Agosta F, Ferraro PM, Riva N, et al. Structural brain correlates of cognitive and behavioral impairment in MND. *Hum Brain Mapp*. February 2016. doi:10.1002/hbm.23124
  538. Trojsi F, Corbo D, Caiazzo G, et al. Motor and extramotor neurodegeneration in amyotrophic lateral sclerosis: A 3T high angular resolution diffusion imaging (HARDI) study. *Amyotroph Lateral Scler Front Degener*. 2013;14(7-8):553-561. doi:10.3109/21678421.2013.785569
  539. Agosta F, Valsasina P, Absinta M, et al. Sensorimotor Functional Connectivity Changes in Amyotrophic Lateral Sclerosis. *Cereb Cortex*. 2011;21(10):2291-2298. doi:10.1093/cercor/bhr002
  540. Agosta F, Canu E, Valsasina P, et al. Divergent brain network connectivity in amyotrophic lateral sclerosis. *Neurobiol Aging*. 2013;34(2):419-427. doi:10.1016/j.neurobiolaging.2012.04.015
  541. Chiò A, Pagani M, Agosta F, Calvo A, Cistaro A, Filippi M. Neuroimaging in amyotrophic lateral sclerosis: insights into structural and functional changes. *Lancet Neurol*. 2014;13(12):1228-1240. doi:10.1016/S1474-4422(14)70167-X
  542. Verstraete E, van den Heuvel MP, Veldink JH, et al. Motor Network Degeneration in Amyotrophic Lateral Sclerosis: A Structural and Functional Connectivity Study. Zhan W, ed. *PLoS One*. 2010;5(10):e13664. doi:10.1371/journal.pone.0013664
  543. Crockford C, Newton J, Lonergan K, et al. ALS-specific cognitive and behavior changes associated with advancing disease stage in ALS. *Neurology*. September 2018;10.1212/WNL.0000000000006317. doi:10.1212/WNL.0000000000006317
  544. Ong M-L, Tan PF, Holbrook JD. Predicting functional decline and survival in amyotrophic lateral sclerosis. Musaro A, ed. *PLoS One*. 2017;12(4):e0174925. doi:10.1371/journal.pone.0174925
  545. Müller H-P, Agosta F, Riva N, et al. Fast progressive lower motor neuron disease is an ALS variant: A two-centre tract of interest-based MRI data analysis. *NeuroImage Clin*. 2018;17:145-152. doi:10.1016/j.nicl.2017.10.008
  546. Dickstein DL, Weaver CM, Luebke JI, Hof PR. Dendritic spine changes associated with normal aging. *Neuroscience*. 2013;251:21-32. doi:10.1016/j.neuroscience.2012.09.077
  547. Jespersen SN, Lundell H, Sønderby CK, Dyrby TB. Orientationally invariant metrics of apparent compartment eccentricity from double pulsed field gradient diffusion experiments. *NMR Biomed*. 2013;26(12):1647-1662. doi:10.1002/nbm.2999
  548. Shemesh N, Cohen Y. Microscopic and compartment shape anisotropies in gray and white matter revealed by angular bipolar double-PFG MR. *Magn Reson Med*. 2011;65(5):1216-1227. doi:10.1002/mrm.22738
  549. Szczepankiewicz F, Lasič S, van Westen D, et al. Quantification of microscopic diffusion anisotropy disentangles effects of orientation dispersion from microstructure: applications in healthy volunteers and in brain tumors. *Neuroimage*. 2015;104:241-252. doi:10.1016/j.neuroimage.2014.09.057
  550. Campbell JSW, Pike GB. Potential and limitations of diffusion MRI tractography for the study of language. *Brain Lang*. 2014;131:65-73. doi:10.1016/j.bandl.2013.06.007



551. Baker MR. ALS--dying forward, backward or outward? *Nat Rev Neurol*. 2014;10(11):660. doi:10.1038/nrneurol.2013.221-c1
552. Kanouchi T, Ohkubo T, Yokota T. Can regional spreading of amyotrophic lateral sclerosis motor symptoms be explained by prion-like propagation? *J Neurol Neurosurg Psychiatry*. 2012;83(7):739-745. doi:10.1136/jnnp-2011-301826
553. Hoch-Kraft P, Trotter J, Gonsior C. Missing in Action: Dysfunctional RNA Metabolism in Oligodendroglial Cells as a Contributor to Neurodegenerative Diseases? *Neurochem Res*. March 2019. doi:10.1007/s11064-019-02763-y
554. Tognatta R, Miller RH. Contribution of the oligodendrocyte lineage to CNS repair and neurodegenerative pathologies. *Neuropharmacology*. 2016;110(Pt B):539-547. doi:10.1016/j.neuropharm.2016.04.026
555. Nonneman A, Robberecht W, Den Bosch L Van. The role of oligodendroglial dysfunction in amyotrophic lateral sclerosis. *Neurodegener Dis Manag*. 2014;4(3):223-239. doi:10.2217/nmt.14.21
556. Cercignani M, Symms MR, Schmierer K, et al. Three-dimensional quantitative magnetisation transfer imaging of the human brain. *Neuroimage*. 2005;27(2):436-441. doi:10.1016/j.neuroimage.2005.04.031
557. Schmierer K, Tozer DJ, Scaravilli F, et al. Quantitative magnetization transfer imaging in postmortem multiple sclerosis brain. *J Magn Reson Imaging*. 2007;26(1):41-51. doi:10.1002/jmri.20984
558. Garcia M, Gloor M, Wetzel SG, Radue E-W, Scheffler K, Bieri O. Characterization of normal appearing brain structures using high-resolution quantitative magnetization transfer steady-state free precession imaging. *Neuroimage*. 2010;52(2):532-537. doi:10.1016/j.neuroimage.2010.04.242
559. Schwartz M, Baruch K. Breaking peripheral immune tolerance to CNS antigens in neurodegenerative diseases: Boosting autoimmunity to fight-off chronic neuroinflammation. *J Autoimmun*. 2014;54:8-14. doi:10.1016/j.jaut.2014.08.002
560. Morgan S, Orrell RW. Pathogenesis of amyotrophic lateral sclerosis. *Br Med Bull*. 2016;119(1):87-98. doi:10.1093/bmb/ldw026
561. Neumann M, Kwong LK, Lee EB, et al. Phosphorylation of S409/410 of TDP-43 is a consistent feature in all sporadic and familial forms of TDP-43 proteinopathies. *Acta Neuropathol*. 2009;117(2):137-149. doi:10.1007/s00401-008-0477-9
562. Kwong LK, Neumann M, Sampathu DM, Lee VM-Y, Trojanowski JQ. TDP-43 proteinopathy: the neuropathology underlying major forms of sporadic and familial frontotemporal lobar degeneration and motor neuron disease. *Acta Neuropathol*. 2007;114(1):63-70. doi:10.1007/s00401-007-0226-5
563. Evans MC, Couch Y, Sibson N, Turner MR. Inflammation and neurovascular changes in amyotrophic lateral sclerosis. *Mol Cell Neurosci*. 2013;53:34-41. doi:10.1016/j.mcn.2012.10.008
564. Block ML, Zecca L, Hong J-S. Microglia-mediated neurotoxicity: uncovering the molecular mechanisms. *Nat Rev Neurosci*. 2007;8(1):57-69. doi:10.1038/nrn2038
565. Blasco H, Garcon G, Patin F, et al. Panel of Oxidative Stress and Inflammatory Biomarkers in ALS: A Pilot Study. *Can J Neurol Sci / J Can des Sci Neurol*. 2017;44(1):90-95. doi:10.1017/cjn.2016.284
566. Ono S, Hu J, Shimizu N, Imai T, Nakagawa H. Increased interleukin-6 of skin and serum in amyotrophic lateral sclerosis. *J Neurol Sci*. 2001;187(1-2):27-34. doi:10.1016/s0022-510x(01)00514-7
567. Lu C-H, Allen K, Oei F, et al. Systemic inflammatory response and neuromuscular involvement in amyotrophic lateral sclerosis. *Neurol Neuroimmunol neuroinflammation*. 2016;3(4):e244. doi:10.1212/NXI.0000000000000244

568. Moreau C, Devos D, Brunaud-Danel V, et al. Elevated IL-6 and TNF- levels in patients with ALS: Inflammation or hypoxia? *Neurology*. 2005;65(12):1958-1960. doi:10.1212/01.wnl.0000188907.97339.76
569. Sekizawa T, Openshaw H, Ohbo K, Sugamura K, Itoyama Y, Niland JC. Cerebrospinal fluid interleukin 6 in amyotrophic lateral sclerosis: immunological parameter and comparison with inflammatory and non-inflammatory central nervous system diseases. *J Neurol Sci*. 1998;154(2):194-199. doi:10.1016/s0022-510x(97)00228-1
570. Philips T, Robberecht W. Neuroinflammation in amyotrophic lateral sclerosis: role of glial activation in motor neuron disease. *Lancet Neurol*. 2011;10(3):253-263. doi:10.1016/S1474-4422(11)70015-1
571. Liddelow SA, Guttenplan KA, Clarke LE, et al. Neurotoxic reactive astrocytes are induced by activated microglia. *Nature*. 2017;541(7638):481-487. doi:10.1038/nature21029
572. Liddelow S, Barres B. SnapShot: Astrocytes in Health and Disease. *Cell*. 2015;162(5):1170-1170.e1. doi:10.1016/j.cell.2015.08.029
573. Appel SH, Zhao W, Beers DR, Henkel JS. The microglial-motoneuron dialogue in ALS. *Acta Myol myopathies cardiomyopathies Off J Mediterr Soc Myol*. 2011;30(1):4-8. <http://www.ncbi.nlm.nih.gov/pubmed/21842586>. Accessed October 6, 2019.
574. Henkel JS, Beers DR, Zhao W, Appel SH. Microglia in ALS: The Good, The Bad, and The Resting. *J Neuroimmune Pharmacol*. 2009;4(4):389-398. doi:10.1007/s11481-009-9171-5
575. Thonhoff JR, Simpson EP, Appel SH. Neuroinflammatory mechanisms in amyotrophic lateral sclerosis pathogenesis. *Curr Opin Neurol*. 2018;31(5):635-639. doi:10.1097/WCO.0000000000000599
576. Kushner PD, Stephenson DT, Wright S. Reactive Astrogliosis is Widespread in the Subcortical White Matter of Amyotrophic Lateral Sclerosis Brain. *J Neuropathol Exp Neurol*. 1991;50(3):263-277. doi:10.1097/00005072-199105000-00008
577. Nagy D, Kato T, Kushner PD. Reactive astrocytes are widespread in the cortical gray matter of amyotrophic lateral sclerosis. *J Neurosci Res*. 1994;38(3):336-347. doi:10.1002/jnr.490380312
578. Schiffer D, Cordera S, Cavalla P, Migheli A. Reactive astrogliosis of the spinal cord in amyotrophic lateral sclerosis. *J Neurol Sci*. 1996;139 Suppl:27-33. doi:10.1016/0022-510x(96)00073-1
579. Tripathi P, Rodriguez-Muela N, Klim JR, et al. Reactive Astrocytes Promote ALS-like Degeneration and Intracellular Protein Aggregation in Human Motor Neurons by Disrupting Autophagy through TGF- $\beta$ 1. *Stem Cell Reports*. 2017;9(2):667-680. doi:10.1016/j.stemcr.2017.06.008
580. Lee Y, Morrison BM, Li Y, et al. Oligodendroglia metabolically support axons and contribute to neurodegeneration. *Nature*. 2012;487(7408):443-448. doi:10.1038/nature11314
581. Nave K-A. Myelination and support of axonal integrity by glia. *Nature*. 2010;468(7321):244-252. doi:10.1038/nature09614
582. Philips T, Bento-Abreu A, Nonneman A, et al. Oligodendrocyte dysfunction in the pathogenesis of amyotrophic lateral sclerosis. *Brain*. 2013;136(2):471-482. doi:10.1093/brain/aws339
583. Niebroj-Dobosz I, Rafałowska J, Fidziańska A, Gadamski R, Grieb P. Myelin composition of spinal cord in a model of amyotrophic lateral sclerosis (ALS) in SOD1G93A transgenic rats. *Folia Neuropathol*. 2007;45(4):236-241. <http://www.ncbi.nlm.nih.gov/pubmed/18176898>. Accessed October 6, 2019.

584. Seilhean D, Cazeneuve C, Thuriès V, et al. Accumulation of TDP-43 and  $\alpha$ -actin in an amyotrophic lateral sclerosis patient with the K17I ANG mutation. *Acta Neuropathol.* 2009;118(4):561-573. doi:10.1007/s00401-009-0545-9
585. Mackenzie IRA, Ansorge O, Strong M, et al. Pathological heterogeneity in amyotrophic lateral sclerosis with FUS mutations: two distinct patterns correlating with disease severity and mutation. *Acta Neuropathol.* 2011;122(1):87-98. doi:10.1007/s00401-011-0838-7
586. Ilieva H, Polymenidou M, Cleveland DW. Non-cell autonomous toxicity in neurodegenerative disorders: ALS and beyond. *J Cell Biol.* 2009;187(6):761-772. doi:10.1083/jcb.200908164
587. Sussmuth S, Brettschneider J, Ludolph A, Tumani H. Biochemical Markers in CSF of ALS Patients. *Curr Med Chem.* 2008;15(18):1788-1801. doi:10.2174/092986708785133031
588. Engelhardt JI, Tajti J, Appel SH. Lymphocytic Infiltrates in the Spinal Cord in Amyotrophic Lateral Sclerosis. *Arch Neurol.* 1993;50(1):30-36. doi:10.1001/archneur.1993.00540010026013
589. Fiala M, Chattopadhyay M, La Cava A, et al. IL-17A is increased in the serum and in spinal cord CD8 and mast cells of ALS patients. *J Neuroinflammation.* 2010;7(1):76. doi:10.1186/1742-2094-7-76
590. Liu J, Wang F. Role of Neuroinflammation in Amyotrophic Lateral Sclerosis: Cellular Mechanisms and Therapeutic Implications. *Front Immunol.* 2017;8:1005. doi:10.3389/fimmu.2017.01005
591. Henkel JS, Beers DR, Wen S, et al. Regulatory T-lymphocytes mediate amyotrophic lateral sclerosis progression and survival. *EMBO Mol Med.* 2013;5(1):64-79. doi:10.1002/emmm.201201544
592. Beers DR, Henkel JS, Zhao W, et al. Endogenous regulatory T lymphocytes ameliorate amyotrophic lateral sclerosis in mice and correlate with disease progression in patients with amyotrophic lateral sclerosis. *Brain.* 2011;134(5):1293-1314. doi:10.1093/brain/awr074
593. Beers DR, Zhao W, Wang J, et al. ALS patients' regulatory T lymphocytes are dysfunctional, and correlate with disease progression rate and severity. *JCI Insight.* 2017;2(5):e89530. doi:10.1172/jci.insight.89530
594. Thonhoff JR, Beers DR, Zhao W, et al. Expanded autologous regulatory T-lymphocyte infusions in ALS. *Neurol - Neuroimmunol Neuroinflammation.* 2018;5(4):e465. doi:10.1212/NXI.0000000000000465
595. Parker SE, Hanton AM, Stefanou SN, Noakes PG, Woodruff TM, Lee JD. Revisiting the role of the innate immune complement system in ALS. *Neurobiol Dis.* 2019;127:223-232. doi:10.1016/j.nbd.2019.03.003
596. Kjældgaard A-L, Pilely K, Olsen KS, et al. Amyotrophic lateral sclerosis: The complement and inflammatory hypothesis. *Mol Immunol.* 2018;102:14-25. doi:10.1016/j.molimm.2018.06.007
597. Ganesalingam J, An J, Shaw CE, Shaw G, Lacomis D, Bowser R. Combination of neurofilament heavy chain and complement C3 as CSF biomarkers for ALS. *J Neurochem.* 2011;117(3):528-537. doi:10.1111/j.1471-4159.2011.07224.x
598. Bahia El Idrissi N, Bosch S, Ramaglia V, Aronica E, Baas F, Troost D. Complement activation at the motor end-plates in amyotrophic lateral sclerosis. *J Neuroinflammation.* 2016;13(1):72. doi:10.1186/s12974-016-0538-2
599. Sta M, Sylva-Steenland RMR, Casula M, et al. Innate and adaptive immunity in amyotrophic lateral sclerosis: Evidence of complement activation. *Neurobiol Dis.* 2011;42(3):211-220. doi:10.1016/j.nbd.2011.01.002
600. Mantovani S, Gordon R, Macmaw JK, et al. Elevation of the terminal complement activation products C5a and C5b-9 in ALS patient blood. *J*

- Neuroimmunol.* 2014;276(1-2):213-218. doi:10.1016/j.jneuroim.2014.09.005
601. Robberecht W, Philips T. The changing scene of amyotrophic lateral sclerosis. *Nat Rev Neurosci.* 2013;14(4):248-264. doi:10.1038/nrn3430
  602. Calvo A, Moglia C, Balma M, Chiò A. Involvement of immune response in the pathogenesis of amyotrophic lateral sclerosis: a therapeutic opportunity? *CNS Neurol Disord Drug Targets.* 2010;9(3):325-330. <http://www.ncbi.nlm.nih.gov/pubmed/20406178>. Accessed October 6, 2019.
  603. Kolind S, Sharma R, Knight S, Johansen-Berg H, Talbot K, Turner MR. Myelin imaging in amyotrophic and primary lateral sclerosis. *Amyotroph Lateral Scler Front Degener.* 2013;14(7-8):562-573. doi:10.3109/21678421.2013.794843
  604. Tozer D, Ramani A, Barker GJ, Davies GR, Miller DH, Tofts PS. Quantitative magnetization transfer mapping of bound protons in multiple sclerosis. *Magn Reson Med.* 2003;50(1):83-91. doi:10.1002/mrm.10514
  605. Narayanan S, Francis SJ, Sled JG, et al. Axonal injury in the cerebral normal-appearing white matter of patients with multiple sclerosis is related to concurrent demyelination in lesions but not to concurrent demyelination in normal-appearing white matter. *Neuroimage.* 2006;29(2):637-642. doi:10.1016/j.neuroimage.2005.07.017
  606. Levesque I, Sled JG, Narayanan S, et al. The role of edema and demyelination in chronic T1 black holes: A quantitative magnetization transfer study. *J Magn Reson Imaging.* 2005;21(2):103-110. doi:10.1002/jmri.20231
  607. Fooladi M, Sharini H, Masjoodi S, Khodamoradi E. A Novel Classification Method using Effective Neural Network and Quantitative Magnetization Transfer Imaging of Brain White Matter in Relapsing Remitting Multiple Sclerosis. *J Biomed Phys Eng.* 2018;8(4):409-422. <http://www.ncbi.nlm.nih.gov/pubmed/30568931>. Accessed October 6, 2019.
  608. Mioshi E, Lillo P, Yew B, et al. Cortical atrophy in ALS is critically associated with neuropsychiatric and cognitive changes. *Neurology.* 2013;80(12):1117-1123. doi:10.1212/WNL.0b013e31828869da
  609. Mezzapesa DM, D'Errico E, Tortelli R, et al. Cortical Thinning and Clinical Heterogeneity in Amyotrophic Lateral Sclerosis. Pirko I, ed. *PLoS One.* 2013;8(11):e80748. doi:10.1371/journal.pone.0080748
  610. Senda J, Kato S, Kaga T, et al. Progressive and widespread brain damage in ALS: MRI voxel-based morphometry and diffusion tensor imaging study. *Amyotroph Lateral Scler.* 2011;12(1):59-69. doi:10.3109/17482968.2010.517850
  611. Kassubek J, Unrath A, Huppertz H, et al. Global brain atrophy and corticospinal tract alterations in ALS, as investigated by voxel-based morphometry of 3-D MRI. *Amyotroph Lateral Scler.* 2005;6(4):213-220. doi:10.1080/14660820510038538
  612. Pagani E, Horsfield MA, Rocca MA, Filippi M. Assessing atrophy of the major white matter fiber bundles of the brain from diffusion tensor MRI data. *Magn Reson Med.* 2007;58(3):527-534. doi:10.1002/mrm.21346
  613. Mezzapesa DM, Ceccarelli A, Dicuonzo F, et al. Whole-brain and regional brain atrophy in amyotrophic lateral sclerosis. *AJNR Am J Neuroradiol.* 2007;28(2):255-259. <http://www.ncbi.nlm.nih.gov/pubmed/17296989>. Accessed October 6, 2019.
  614. Gochberg DF, Gore JC. Quantitative magnetization transfer imaging via selective inversion recovery with short repetition times. *Magn Reson Med.* 2007;57(2):437-441. doi:10.1002/mrm.21143
  615. Bagnato F, Franco G, Ye F, et al. Selective inversion recovery quantitative magnetization transfer imaging: Toward a 3 T clinical application in multiple sclerosis. *Mult Scler J.* March 2019:135245851983301.

- doi:10.1177/1352458519833018
616. Levesque IR, Sled JG, Pike GB. Iterative optimization method for design of quantitative magnetization transfer imaging experiments. *Magn Reson Med*. 2011;66(3):635-643. doi:10.1002/mrm.23071
  617. Ramani A, Dalton C, Miller DH, Tofts PS, Barker GJ. Precise estimate of fundamental in-vivo MT parameters in human brain in clinically feasible times. *Magn Reson Imaging*. 2002;20(10):721-731. doi:10.1016/s0730-725x(02)00598-2
  618. Burrell JR, Halliday GM, Kril JJ, et al. The frontotemporal dementia-motor neuron disease continuum. *Lancet*. 2016;388(10047):919-931. doi:10.1016/S0140-6736(16)00737-6
  619. Turner MR, Swash M. The expanding syndrome of amyotrophic lateral sclerosis: a clinical and molecular odyssey. *J Neurol Neurosurg Psychiatry*. 2015;86(6):667-673. doi:10.1136/jnnp-2014-308946
  620. Deichmann R, Good CD, Josephs O, Ashburner J, Turner R. Optimization of 3-D MP-RAGE Sequences for Structural Brain Imaging. *Neuroimage*. 2000;12(1):112-127. doi:10.1006/nimg.2000.0601
  621. Shen D, Cui L, Fang J, Cui B, Li D, Tai H. Voxel-Wise Meta-Analysis of Gray Matter Changes in Amyotrophic Lateral Sclerosis. *Front Aging Neurosci*. 2016;8:64. doi:10.3389/fnagi.2016.00064
  622. Chen ZY, Liu MQ, Ma L. Cortical Thinning Pattern of Bulbar- and Spinal-onset Amyotrophic Lateral Sclerosis: a Surface-based Morphometry Study. *Chin Med Sci J*. 2018 Jun 30;33(2):100-106 doi:10.24920/11812
  623. Roccatagliata L, Bonzano L, Mancardi G, Canepa C, Caponnetto C. Detection of motor cortex thinning and corticospinal tract involvement by quantitative MRI in amyotrophic lateral sclerosis. *Amyotroph Lateral Scler*. 2009;10(1):47-52. doi:10.1080/17482960802267530
  624. Shellikeri S, Karthikeyan V, Martino R, et al. The neuropathological signature of bulbar-onset ALS: A systematic review. *Neurosci Biobehav Rev*. 2017;75:378-392. doi:10.1016/j.neubiorev.2017.01.045
  625. Kim H-J, de Leon M, Wang X, et al. Relationship between Clinical Parameters and Brain Structure in Sporadic Amyotrophic Lateral Sclerosis Patients According to Onset Type: A Voxel-Based Morphometric Study. Kassubek J, ed. *PLoS One*. 2017;12(1):e0168424. doi:10.1371/journal.pone.0168424
  626. Westeneng H-J, Verstraete E, Walhout R, et al. Subcortical structures in amyotrophic lateral sclerosis. *Neurobiol Aging*. 2015;36(2):1075-1082. doi:10.1016/j.neurobiolaging.2014.09.002
  627. Pagani M, Chio A, Valentini MC, et al. Functional pattern of brain FDG-PET in amyotrophic lateral sclerosis. *Neurology*. 2014;83(12):1067-1074. doi:10.1212/WNL.0000000000000792
  628. Grolez G, Kyheng M, Lopes R, et al. MRI of the cervical spinal cord predicts respiratory dysfunction in ALS. *Sci Rep*. 2018;8(1):1828. doi:10.1038/s41598-018-19938-2
  629. Barnes J, Ridgway GR, Bartlett J, et al. Head size, age and gender adjustment in MRI studies: a necessary nuisance? *Neuroimage*. 2010;53(4):1244-1255. doi:10.1016/j.neuroimage.2010.06.025
  630. Ridgway G, Barnes J, Pepple T, Fox N. Estimation of total intracranial volume; a comparison of methods. *Alzheimer's Dement*. 2011;7(4):S62-S63. doi:10.1016/j.jalz.2011.05.099
  631. Nordenskjöld R, Malmberg F, Larsson E-M, et al. Intracranial volume estimated with commonly used methods could introduce bias in studies including brain volume measurements. *Neuroimage*. 2013;83:355-360.

- doi:10.1016/j.neuroimage.2013.06.068
632. Cosottini M, Pesaresi I, Piazza S, et al. Structural and functional evaluation of cortical motor areas in Amyotrophic Lateral Sclerosis. *Exp Neurol*. 2012;234(1):169-180. doi:10.1016/j.expneurol.2011.12.024
633. Grieve SM, Menon P, Korgaonkar MS, et al. Potential structural and functional biomarkers of upper motor neuron dysfunction in ALS. *Amyotroph Lateral Scler Front Degener*. 2016;17(1-2):85-92. doi:10.3109/21678421.2015.1074707
634. Sheng L, Ma H, Zhong J, Shang H, Shi H, Pan P. Motor and extra-motor gray matter atrophy in amyotrophic lateral sclerosis: quantitative meta-analyses of voxel-based morphometry studies. *Neurobiol Aging*. 2015;36(12):3288-3299. doi:10.1016/j.neurobiolaging.2015.08.018
635. Ince PG, Highley JR, Kirby J, et al. Molecular pathology and genetic advances in amyotrophic lateral sclerosis: an emerging molecular pathway and the significance of glial pathology. *Acta Neuropathol*. 2011;122(6):657-671. doi:10.1007/s00401-011-0913-0
636. Agosta F, Ferraro PM, Riva N, et al. Structural and functional brain signatures of C9orf72 in motor neuron disease. *Neurobiol Aging*. 2017;57:206-219. doi:10.1016/j.neurobiolaging.2017.05.024
637. Bede P, Bokde ALW, Byrne S, et al. Multiparametric MRI study of ALS stratified for the C9orf72 genotype. *Neurology*. 2013;81(4):361-369. doi:10.1212/WNL.0b013e31829c5eee
638. Al-Sarraj S, King A, Troakes C, et al. p62 positive, TDP-43 negative, neuronal cytoplasmic and intranuclear inclusions in the cerebellum and hippocampus define the pathology of C9orf72-linked FTLN and MND/ALS. *Acta Neuropathol*. 2011;122(6):691-702. doi:10.1007/s00401-011-0911-2
639. Agosta F, Galantucci S, Riva N, et al. Intrahemispheric and interhemispheric structural network abnormalities in PLS and ALS. *Hum Brain Mapp*. 2014;35(4):1710-1722. doi:10.1002/hbm.22286
640. Kassubek J, Müller H-P, Del Tredici K, et al. Imaging the pathoanatomy of amyotrophic lateral sclerosis in vivo: targeting a propagation-based biological marker. *J Neurol Neurosurg Psychiatry*. 2018;89(4):374-381. doi:10.1136/jnnp-2017-316365
641. Kwan JY, Meoded A, Danielian LE, Wu T, Floeter MK. Structural imaging differences and longitudinal changes in primary lateral sclerosis and amyotrophic lateral sclerosis. *NeuroImage Clin*. 2012;2:151-160. doi:10.1016/j.nicl.2012.12.003
642. Müller H-P, Turner MR, Grosskreutz J, et al. A large-scale multicentre cerebral diffusion tensor imaging study in amyotrophic lateral sclerosis. *J Neurol Neurosurg Psychiatry*. 2016;87(6):570-579. doi:10.1136/jnnp-2015-311952
643. Fogarty MJ, Noakes PG, Bellingham MC. Motor Cortex Layer V Pyramidal Neurons Exhibit Dendritic Regression, Spine Loss, and Increased Synaptic Excitation in the Presymptomatic hSOD1<sup>G93A</sup> Mouse Model of Amyotrophic Lateral Sclerosis. *J Neurosci*. 2015;35(2):643-647. doi:10.1523/JNEUROSCI.3483-14.2015
644. Horoupian DS, Thal L, Katzman R, et al. Dementia and motor neuron disease: Morphometric, biochemical, and Golgi studies. *Ann Neurol*. 1984;16(3):305-313. doi:10.1002/ana.410160306
645. Fischl B, Dale AM. Measuring the thickness of the human cerebral cortex from magnetic resonance images. *Proc Natl Acad Sci*. 2000;97(20):11050-11055. doi:10.1073/pnas.200033797
646. Grosskreutz J, Kaufmann J, Frädrieh J, Dengler R, Heinze H-J, Peschel T. Widespread sensorimotor and frontal cortical atrophy in Amyotrophic Lateral

- Sclerosis. *BMC Neurol.* 2006;6(1):17. doi:10.1186/1471-2377-6-17
647. Wen J, Zhang H, Alexander DC, et al. Neurite density is reduced in the presymptomatic phase of C9orf72 disease. *J Neurol Neurosurg Psychiatry.* 2019;90(4):387-394. doi:10.1136/jnnp-2018-318994
648. Cardenas AM, Sarlls JE, Kwan JY, et al. Pathology of callosal damage in ALS: An ex-vivo, 7 T diffusion tensor MRI study. *NeuroImage Clin.* 2017;15:200-208. doi:10.1016/j.nicl.2017.04.024
649. Van Laere K, Vanhee A, Verschueren J, et al. Value of <sup>18</sup> Fluorodeoxyglucose–Positron-Emission Tomography in Amyotrophic Lateral Sclerosis. *JAMA Neurol.* 2014;71(5):553. doi:10.1001/jamaneurol.2014.62
650. Koay CG, Yeh P-H, Ollinger JM, et al. Tract Orientation and Angular Dispersion Deviation Indicator (TOADDI): A framework for single-subject analysis in diffusion tensor imaging. *Neuroimage.* 2016;126:151-163. doi:10.1016/j.neuroimage.2015.11.046

## **APPENDIX**

### **A1 ALSFRS-R**

#### **SPEECH**

4. Normal speech processes
3. Detectable speech disturbance
2. Intelligible with repeating
1. speech combined with non-vocal communication
0. loss of useful speech

#### **SALIVATION**

4. Normal
3. slight but definite excess of saliva in mouth, may have night-time drooling
2. moderately excessive saliva, may have minimal drooling
1. marked excess of saliva with some drooling
0. marked drooling, requires constant tissue

#### **SWALLOWING**

4. Normal eating habits
3. early eating problems, occasional choking
2. dietary consistency changes
1. needs supplemental tube feedings
0. NPO (exclusively parental or enteral feedings)

#### **HANDWRITING**

4. Normal
3. slow or sloppy, all words legible
2. not all words legible
1. able to grip pen, unable to write
0. unable to grip pen

#### **CUTTING FOOD AND HANDLING UTENSILS**

(patients without gastrostomy)

4. Normal
3. somewhat slow and clumsy, needs no help
2. can cut most foods, slow of clumsy, some help needed
1. foods cut by someone else, can still feed slowly
0. needs to be fed

#### **CUTTING FOOD AND HANDLING UTENSILS**

(patients with gastrostomy)

4. Normal
3. clumsy, able to perform all manipulations
2. some help needed with closures and fasteners



1. provides minimal assistance to caregiver
0. unable to perform any aspect of task

#### **DRESSING AND HYGEINE**

4. Normal
3. independent self-care with effort of decreased efficiency
2. intermittent assistance or substitute methods
1. needs attendant for self-care
0. total dependence

#### **TURNING IN BED AND ADJUSTING BEDCLOTHES**

4. Normal
3. somewhat slow or clumsy, needs no help
2. can turn alone or adjust sheets with great difficulty
1. can initiate, cannot turn or adjust sheets
0. helpless

#### **WALKING**

4. Normal
3. early ambulation difficulties
2. walks with assistance
1. non-ambulatory functional movement only
0. no purposeful leg movement

#### **CLIMBING STAIRS**

4. Normal
3. slow
2. mild unsteadiness or fatigue
1. needs assistance
0. cannot do

#### **DYSPNOEA**

4. None
3. occurs when walking
2. occurs with one or more: eating, bathing, dressing
1. occurs at rest, either sitting or lying
0. significant difficulty, considering mechanical support

#### **ORTHOPNOEA**

4. None
3. some difficulty sleeping, d/t shortness of breath, does not routinely use >2 pillows
2. needs extra pillows to sleep (>2)
1. can only sleep sitting up

0. unable to sleep

### RESPIRATORY INSUFFICIENCY

4. None

3. intermittent use of BiPAP

2. continuous use of BiPAP at night

1. continuous use of BiPAP day and night

0. invasive mechanical ventilation by intubation/tracheostomy

**Total ALSFRS-R score /48**

## A2 MRC

- Scoring:**
- 0 - No muscle activity
  - 1 - Flicker of Activity
  - 2 - Movement with gravity eliminated
  - 3 - Movement against gravity but not resistance
  - 4 - Movement against resistance but weak
  - 5 - Normal power

Neck Flexion (C1-C4)	<input type="checkbox"/> 0	<input type="checkbox"/> 1	<input type="checkbox"/> 2	<input type="checkbox"/> 3	<input type="checkbox"/> 4	<input type="checkbox"/> 5	<input type="checkbox"/> Not tested
Neck Extension (C1-C4)	<input type="checkbox"/> 0	<input type="checkbox"/> 1	<input type="checkbox"/> 2	<input type="checkbox"/> 3	<input type="checkbox"/> 4	<input type="checkbox"/> 5	<input type="checkbox"/> Not tested
Neck Lateral Flexion (C3)							
Right	<input type="checkbox"/> 0	<input type="checkbox"/> 1	<input type="checkbox"/> 2	<input type="checkbox"/> 3	<input type="checkbox"/> 4	<input type="checkbox"/> 5	<input type="checkbox"/> Not tested
Left	<input type="checkbox"/> 0	<input type="checkbox"/> 1	<input type="checkbox"/> 2	<input type="checkbox"/> 3	<input type="checkbox"/> 4	<input type="checkbox"/> 5	<input type="checkbox"/> Not tested
Shoulder Elevation (C4)							
Right	<input type="checkbox"/> 0	<input type="checkbox"/> 1	<input type="checkbox"/> 2	<input type="checkbox"/> 3	<input type="checkbox"/> 4	<input type="checkbox"/> 5	<input type="checkbox"/> Not tested
Left	<input type="checkbox"/> 0	<input type="checkbox"/> 1	<input type="checkbox"/> 2	<input type="checkbox"/> 3	<input type="checkbox"/> 4	<input type="checkbox"/> 5	<input type="checkbox"/> Not tested
Shoulder Abduction (C5-C6)							
Right	<input type="checkbox"/> 0	<input type="checkbox"/> 1	<input type="checkbox"/> 2	<input type="checkbox"/> 3	<input type="checkbox"/> 4	<input type="checkbox"/> 5	<input type="checkbox"/> Not tested
Left	<input type="checkbox"/> 0	<input type="checkbox"/> 1	<input type="checkbox"/> 2	<input type="checkbox"/> 3	<input type="checkbox"/> 4	<input type="checkbox"/> 5	<input type="checkbox"/> Not tested
Shoulder Adduction (C6-C8)							
Right	<input type="checkbox"/> 0	<input type="checkbox"/> 1	<input type="checkbox"/> 2	<input type="checkbox"/> 3	<input type="checkbox"/> 4	<input type="checkbox"/> 5	<input type="checkbox"/> Not tested
Left	<input type="checkbox"/> 0	<input type="checkbox"/> 1	<input type="checkbox"/> 2	<input type="checkbox"/> 3	<input type="checkbox"/> 4	<input type="checkbox"/> 5	<input type="checkbox"/> Not tested
Elbow Flexion (C6)							
Right	<input type="checkbox"/> 0	<input type="checkbox"/> 1	<input type="checkbox"/> 2	<input type="checkbox"/> 3	<input type="checkbox"/> 4	<input type="checkbox"/> 5	<input type="checkbox"/> Not tested
Left	<input type="checkbox"/> 0	<input type="checkbox"/> 1	<input type="checkbox"/> 2	<input type="checkbox"/> 3	<input type="checkbox"/> 4	<input type="checkbox"/> 5	<input type="checkbox"/> Not tested
Elbow Extension (C7)							
Right	<input type="checkbox"/> 0	<input type="checkbox"/> 1	<input type="checkbox"/> 2	<input type="checkbox"/> 3	<input type="checkbox"/> 4	<input type="checkbox"/> 5	<input type="checkbox"/> Not tested
Left	<input type="checkbox"/> 0	<input type="checkbox"/> 1	<input type="checkbox"/> 2	<input type="checkbox"/> 3	<input type="checkbox"/> 4	<input type="checkbox"/> 5	<input type="checkbox"/> Not tested
Wrist Flexion (C7)							
Right	<input type="checkbox"/> 0	<input type="checkbox"/> 1	<input type="checkbox"/> 2	<input type="checkbox"/> 3	<input type="checkbox"/> 4	<input type="checkbox"/> 5	<input type="checkbox"/> Not tested
Left	<input type="checkbox"/> 0	<input type="checkbox"/> 1	<input type="checkbox"/> 2	<input type="checkbox"/> 3	<input type="checkbox"/> 4	<input type="checkbox"/> 5	<input type="checkbox"/> Not tested
Wrist Extension (C5/C6)							
Right	<input type="checkbox"/> 0	<input type="checkbox"/> 1	<input type="checkbox"/> 2	<input type="checkbox"/> 3	<input type="checkbox"/> 4	<input type="checkbox"/> 5	<input type="checkbox"/> Not tested
Left	<input type="checkbox"/> 0	<input type="checkbox"/> 1	<input type="checkbox"/> 2	<input type="checkbox"/> 3	<input type="checkbox"/> 4	<input type="checkbox"/> 5	<input type="checkbox"/> Not tested

<b>Finger Extension (C7/C8)</b>							
Right	<input type="checkbox"/> 0	<input type="checkbox"/> 1	<input type="checkbox"/> 2	<input type="checkbox"/> 3	<input type="checkbox"/> 4	<input type="checkbox"/> 5	<input type="checkbox"/> Not tested
Left	<input type="checkbox"/> 0	<input type="checkbox"/> 1	<input type="checkbox"/> 2	<input type="checkbox"/> 3	<input type="checkbox"/> 4	<input type="checkbox"/> 5	<input type="checkbox"/> Not tested
<b>Hand Grip (C8/T1)</b>							
Right	<input type="checkbox"/> 0	<input type="checkbox"/> 1	<input type="checkbox"/> 2	<input type="checkbox"/> 3	<input type="checkbox"/> 4	<input type="checkbox"/> 5	<input type="checkbox"/> Not tested
Left	<input type="checkbox"/> 0	<input type="checkbox"/> 1	<input type="checkbox"/> 2	<input type="checkbox"/> 3	<input type="checkbox"/> 4	<input type="checkbox"/> 5	<input type="checkbox"/> Not tested
<b>Distal Phalangeal Flexion (C7/C8)</b>							
Right	<input type="checkbox"/> 0	<input type="checkbox"/> 1	<input type="checkbox"/> 2	<input type="checkbox"/> 3	<input type="checkbox"/> 4	<input type="checkbox"/> 5	<input type="checkbox"/> Not tested
Left	<input type="checkbox"/> 0	<input type="checkbox"/> 1	<input type="checkbox"/> 2	<input type="checkbox"/> 3	<input type="checkbox"/> 4	<input type="checkbox"/> 5	<input type="checkbox"/> Not tested
<b>Finger Abduction (C8/T1)</b>							
Right	<input type="checkbox"/> 0	<input type="checkbox"/> 1	<input type="checkbox"/> 2	<input type="checkbox"/> 3	<input type="checkbox"/> 4	<input type="checkbox"/> 5	<input type="checkbox"/> Not tested
Left	<input type="checkbox"/> 0	<input type="checkbox"/> 1	<input type="checkbox"/> 2	<input type="checkbox"/> 3	<input type="checkbox"/> 4	<input type="checkbox"/> 5	<input type="checkbox"/> Not tested
<b>Thumb Abduction (C7-T1)</b>							
Right	<input type="checkbox"/> 0	<input type="checkbox"/> 1	<input type="checkbox"/> 2	<input type="checkbox"/> 3	<input type="checkbox"/> 4	<input type="checkbox"/> 5	<input type="checkbox"/> Not tested
Left	<input type="checkbox"/> 0	<input type="checkbox"/> 1	<input type="checkbox"/> 2	<input type="checkbox"/> 3	<input type="checkbox"/> 4	<input type="checkbox"/> 5	<input type="checkbox"/> Not tested
<b>Thumb/finger Opposition (C8/T1)</b>							
Right	<input type="checkbox"/> 0	<input type="checkbox"/> 1	<input type="checkbox"/> 2	<input type="checkbox"/> 3	<input type="checkbox"/> 4	<input type="checkbox"/> 5	<input type="checkbox"/> Not tested
Left	<input type="checkbox"/> 0	<input type="checkbox"/> 1	<input type="checkbox"/> 2	<input type="checkbox"/> 3	<input type="checkbox"/> 4	<input type="checkbox"/> 5	<input type="checkbox"/> Not tested
<b>Hip Flexion (L1/L2)</b>							
Right	<input type="checkbox"/> 0	<input type="checkbox"/> 1	<input type="checkbox"/> 2	<input type="checkbox"/> 3	<input type="checkbox"/> 4	<input type="checkbox"/> 5	<input type="checkbox"/> Not tested
Left	<input type="checkbox"/> 0	<input type="checkbox"/> 1	<input type="checkbox"/> 2	<input type="checkbox"/> 3	<input type="checkbox"/> 4	<input type="checkbox"/> 5	<input type="checkbox"/> Not tested
<b>Hip Extension (L5/S1)</b>							
Right	<input type="checkbox"/> 0	<input type="checkbox"/> 1	<input type="checkbox"/> 2	<input type="checkbox"/> 3	<input type="checkbox"/> 4	<input type="checkbox"/> 5	<input type="checkbox"/> Not tested
Left	<input type="checkbox"/> 0	<input type="checkbox"/> 1	<input type="checkbox"/> 2	<input type="checkbox"/> 3	<input type="checkbox"/> 4	<input type="checkbox"/> 5	<input type="checkbox"/> Not tested
<b>Knee Flexion (S1/S2)</b>							
Right	<input type="checkbox"/> 0	<input type="checkbox"/> 1	<input type="checkbox"/> 2	<input type="checkbox"/> 3	<input type="checkbox"/> 4	<input type="checkbox"/> 5	<input type="checkbox"/> Not tested
Left	<input type="checkbox"/> 0	<input type="checkbox"/> 1	<input type="checkbox"/> 2	<input type="checkbox"/> 3	<input type="checkbox"/> 4	<input type="checkbox"/> 5	<input type="checkbox"/> Not tested
<b>Knee Extension (L2-L4)</b>							
Right	<input type="checkbox"/> 0	<input type="checkbox"/> 1	<input type="checkbox"/> 2	<input type="checkbox"/> 3	<input type="checkbox"/> 4	<input type="checkbox"/> 5	<input type="checkbox"/> Not tested
Left	<input type="checkbox"/> 0	<input type="checkbox"/> 1	<input type="checkbox"/> 2	<input type="checkbox"/> 3	<input type="checkbox"/> 4	<input type="checkbox"/> 5	<input type="checkbox"/> Not tested
<b>Ankle Dorsiflexion (L4/L5)</b>							
Right	<input type="checkbox"/> 0	<input type="checkbox"/> 1	<input type="checkbox"/> 2	<input type="checkbox"/> 3	<input type="checkbox"/> 4	<input type="checkbox"/> 5	<input type="checkbox"/> Not tested
Left	<input type="checkbox"/> 0	<input type="checkbox"/> 1	<input type="checkbox"/> 2	<input type="checkbox"/> 3	<input type="checkbox"/> 4	<input type="checkbox"/> 5	<input type="checkbox"/> Not tested
<b>Ankle Plantar Flexion (S1/S2)</b>							
Right	<input type="checkbox"/> 0	<input type="checkbox"/> 1	<input type="checkbox"/> 2	<input type="checkbox"/> 3	<input type="checkbox"/> 4	<input type="checkbox"/> 5	<input type="checkbox"/> Not tested
Left	<input type="checkbox"/> 0	<input type="checkbox"/> 1	<input type="checkbox"/> 2	<input type="checkbox"/> 3	<input type="checkbox"/> 4	<input type="checkbox"/> 5	<input type="checkbox"/> Not tested
<b>Ankle Eversion (L5/S1)</b>							
Right	<input type="checkbox"/> 0	<input type="checkbox"/> 1	<input type="checkbox"/> 2	<input type="checkbox"/> 3	<input type="checkbox"/> 4	<input type="checkbox"/> 5	<input type="checkbox"/> Not tested
Left	<input type="checkbox"/> 0	<input type="checkbox"/> 1	<input type="checkbox"/> 2	<input type="checkbox"/> 3	<input type="checkbox"/> 4	<input type="checkbox"/> 5	<input type="checkbox"/> Not tested

**Total MRC score /220**

**A3 UMN score**




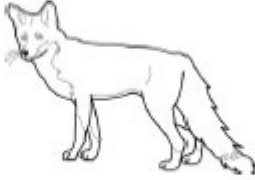




**UMN Score**

Pathologically brisk reflexes at the following sites:

Biceps	Right <input type="checkbox"/>	Left <input type="checkbox"/>	/2
Triceps	Right <input type="checkbox"/>	Left <input type="checkbox"/>	/2
Supinator	Right <input type="checkbox"/>	Left <input type="checkbox"/>	/2
Finger	Right <input type="checkbox"/>	Left <input type="checkbox"/>	/2
Knee	Right <input type="checkbox"/>	Left <input type="checkbox"/>	/2
Ankle	Right <input type="checkbox"/>	Left <input type="checkbox"/>	/2
Plantar	Right <input type="checkbox"/>	Left <input type="checkbox"/>	/2
Facial	<input type="checkbox"/>		/1
Mandibular	<input type="checkbox"/>		/1

**Total UMN score /16**

**A4 Edinburgh cognitive and behavioural screen in ALS (ECAS)**

EDINBURGH COGNITIVE AND BEHAVIOURAL ALS SCREEN – ECAS English Version (2013)	
Date of testing: ..... Age at leaving full-time education: ..... Occupation: ..... Handedness: .....	Name: ..... Date of Birth: ..... Hospital No. or Address: ..... ..... .....
LANGUAGE - Naming	
➤ Ask: Say or write down the names of these pictures:	
 ..... <input type="checkbox"/>	 ..... <input type="checkbox"/>
 ..... <input type="checkbox"/>	 ..... <input type="checkbox"/>
 ..... <input type="checkbox"/>	 ..... <input type="checkbox"/>
 ..... <input type="checkbox"/>	 ..... <input type="checkbox"/>
LANGUAGE - Comprehension	
➤ Ask: point to the one which is:	
1. Something you can fly in ..... 3. An animal that climbs trees ..... 5. A means of transport ..... 7. Something with a sting .....	2. Something with webbed feet ..... 4. Something used for chopping ..... 6. Something with a sharp edge ..... 8. Something with a diet of nuts and seeds .....
Score 0-8 <input style="width: 40px; height: 20px;" type="text"/>	

<b>MEMORY – Immediate recall</b>		Score 0-10																											
<p>⇒ Say: 'I am going to read you a short story. Please listen carefully. When I am finished, say or write as much as you can remember'. Score 1 point for each (either entire or part of) underlined section recalled.</p> <p><i>Last <u>Sunday</u>, the <u>annual litter collection</u> took place in <u>Primrose Woods</u>. <u>Forty two</u> people joined in to remove old <u>bicycles and shopping trolleys</u>. Mr <u>Douglas Watt</u> from the <u>woodland project</u> told local reporters that he was very <u>impressed and especially proud</u> of the <u>17 children</u> who came along.</i></p>	<input style="width: 40px; height: 20px;" type="text"/>	<p>Also use this score to calculate % retention later</p>																											
<b>LANGUAGE - Spelling</b>																													
<p>⇒ Say: 'Spell, either by writing or speaking, the following words.' If the person is using assistive technology, ask them to turn off any predictive text facility.</p> <table style="width: 100%; border: none;"> <tr> <td style="width: 50%;">1. Envelope .....</td> <td style="width: 50%;">2. Skateboard .....</td> </tr> <tr> <td>3. Constructing .....</td> <td>4. Partner .....</td> </tr> <tr> <td>5. Biscuit .....</td> <td>6. Lawnmower .....</td> </tr> <tr> <td>7. Deliver .....</td> <td>8. Recorded .....</td> </tr> <tr> <td>9. Coathanger .....</td> <td>10. Orchestra .....</td> </tr> <tr> <td>11. Screwdriver .....</td> <td>12. Brought .....</td> </tr> </table>	1. Envelope .....	2. Skateboard .....	3. Constructing .....	4. Partner .....	5. Biscuit .....	6. Lawnmower .....	7. Deliver .....	8. Recorded .....	9. Coathanger .....	10. Orchestra .....	11. Screwdriver .....	12. Brought .....	<p>Score 0-12</p> <input style="width: 40px; height: 20px;" type="text"/>																
1. Envelope .....	2. Skateboard .....																												
3. Constructing .....	4. Partner .....																												
5. Biscuit .....	6. Lawnmower .....																												
7. Deliver .....	8. Recorded .....																												
9. Coathanger .....	10. Orchestra .....																												
11. Screwdriver .....	12. Brought .....																												
<b>FLUENCY - Letter S</b>																													
<p>⇒ Say: 'I am going to give you a letter of the alphabet and I would like you to say or write as many different words as you can beginning with that letter, but not names of people or places, or numbers.'</p> <ul style="list-style-type: none"> <li>▪ If writing, say: 'You will have <b>two</b> minutes. The letter is S.'</li> <li>▪ If speaking, say 'You will have <b>one</b> minute. The letter is S.'</li> </ul> <p>⇒ Next the person copies/reads these words aloud.</p> <ul style="list-style-type: none"> <li>▪ If writing, say: 'copy these words as fast as possible. I will time you. Ready? Begin.'</li> </ul> <p>If speaking, say: 'read aloud these words as fast as possible. Before you do this, check that you can read them. I will time you. Ready? Begin.'</p>		<p>No. of correct words =</p> <p>Time to copy/ read aloud =</p>																											
<p><b>Verbal Fluency Index (Vfi) calculation:</b></p> <p>If spoken:  <math display="block">Vfi = \frac{60\text{seconds} - \text{no. of seconds to read aloud words}}{\text{No. of correct words generated}}</math></p> <p>If written:  <math display="block">Vfi = \frac{120\text{seconds} - \text{no. of seconds to copy words}}{\text{No. of correct words generated}}</math></p>	<table border="1" style="margin: auto; border-collapse: collapse; font-size: x-small;"> <thead> <tr> <th colspan="3">VFI conversion to score table</th> </tr> <tr> <th>SPOKEN VFI</th> <th>WRITTEN VFI</th> <th>Score</th> </tr> </thead> <tbody> <tr> <td>≥ 12.00</td> <td>≥ 20.00</td> <td>0</td> </tr> <tr> <td>10.00 to &lt;12.00</td> <td>16.50 to &lt; 20.00</td> <td>2</td> </tr> <tr> <td>8.00 to &lt; 10.00</td> <td>13.00 to &lt; 16.50</td> <td>4</td> </tr> <tr> <td>6.00 to &lt; 8.00</td> <td>9.50 to &lt; 13.00</td> <td>6</td> </tr> <tr> <td>4.00 to &lt; 6.00</td> <td>6.00 to &lt; 9.50</td> <td>8</td> </tr> <tr> <td>2.00 to &lt; 4.00</td> <td>2.50 to &lt; 6.00</td> <td>10</td> </tr> <tr> <td>&lt; 2.00</td> <td>&lt; 2.50</td> <td>12</td> </tr> </tbody> </table>	VFI conversion to score table			SPOKEN VFI	WRITTEN VFI	Score	≥ 12.00	≥ 20.00	0	10.00 to <12.00	16.50 to < 20.00	2	8.00 to < 10.00	13.00 to < 16.50	4	6.00 to < 8.00	9.50 to < 13.00	6	4.00 to < 6.00	6.00 to < 9.50	8	2.00 to < 4.00	2.50 to < 6.00	10	< 2.00	< 2.50	12	<p>Score 0-12</p> <input style="width: 40px; height: 20px;" type="text"/>
VFI conversion to score table																													
SPOKEN VFI	WRITTEN VFI	Score																											
≥ 12.00	≥ 20.00	0																											
10.00 to <12.00	16.50 to < 20.00	2																											
8.00 to < 10.00	13.00 to < 16.50	4																											
6.00 to < 8.00	9.50 to < 13.00	6																											
4.00 to < 6.00	6.00 to < 9.50	8																											
2.00 to < 4.00	2.50 to < 6.00	10																											
< 2.00	< 2.50	12																											

**EXECUTIVE – Reverse Digit Span**

☞ Say: 'I am going to say some numbers and I would like you to say them back to me in reverse order. For example, if I say '2 3 4', you should say '4 3 2'. Let's have a practice. If I say '7 1 9', what would you say?' Stop when person gets both trials of a line wrong. Score total number of trials correct.

Score  
0-12

Trial		Check	Trial		Check
1	2 6		2	5 8	
3	9 3 5		4	4 1 6	
5	7 2 8 4		6	9 5 7 3	
7	6 9 4 2 1		8	8 3 2 5 6	
9	8 1 3 5 7 9		10	3 6 2 7 3 4	
11	1 6 9 3 5 8 6		12	2 3 6 8 4 9 2	

**EXECUTIVE – Alternation**

☞ Say: 'I want you to alternate between numbers and letters, starting with 1-A, then 2-B, 3-C, and so on. Please alternate between numbers and letters, in order, without skipping any until I tell you to stop. Let's begin together: 1A, 2B, 3C...'

Score  
0-12

Trial		Check	Trial		Check	Trial		Check	Trial		Check
1	4-D		2	5-E		3	6-F		4	7-G	
5	8-H		6	9-I		7	10-J		8	11-K	
9	12-L		10	13-M		11	14-N		12	15-O	

**FLUENCY - Letter T**

☞ Say: 'I am going to give you a letter of the alphabet and I would like you to say or write as many different words as you can beginning with that letter, but not names of people or places, or numbers. This time the word must only be four letters long. No more or less than four letters'

- If writing, say: 'You will have **two** minutes. The letter is T.'
- If speaking, say 'You will have **one** minute. The letter is T.'

No. of correct words =  
  
Time to copy/ read aloud =

☞ Next the person copies/reads these words aloud.

- If writing, say: 'copy these words as fast as possible. I will time you. Ready? Begin.'

If speaking, say: 'read aloud these words as fast as possible. Before you do this, check that you can read them. I will time you. Ready? Begin.'

Verbal Fluency Index (Vfi) calculation:	VFI conversion to score table		
	SPOKEN VFI	WRITTEN VFI	Score
If spoken: Vfi = $\frac{60\text{seconds} - \text{no. of seconds to read aloud words}}{\text{No. of correct words generated}}$	≥ 20.00	≥ 27.25	0
	16.75 to < 20.00	23.00 to < 27.25	2
If written: Vfi = $\frac{120\text{seconds} - \text{no. of seconds to copy words}}{\text{No. of correct words generated}}$	13.50 to < 16.75	18.75 to < 23.00	4
	10.25 to < 13.50	14.50 to < 18.75	6
	7.00 to < 10.25	10.25 to < 14.50	8
	3.75 to < 7.00	6.00 to < 10.25	10
	< 3.75	< 6.00	12

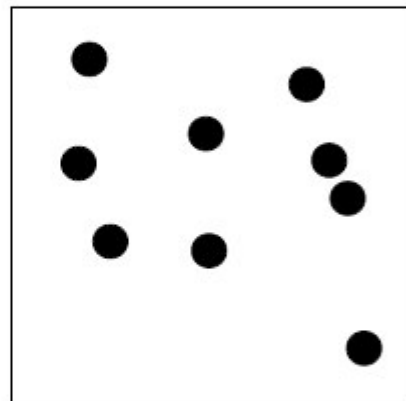
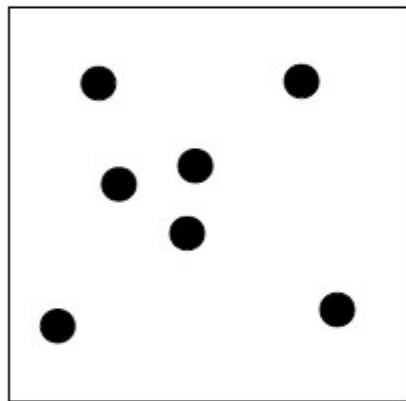
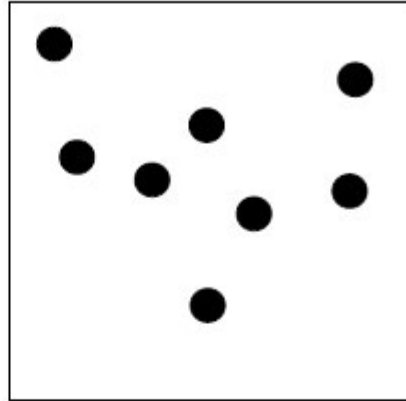
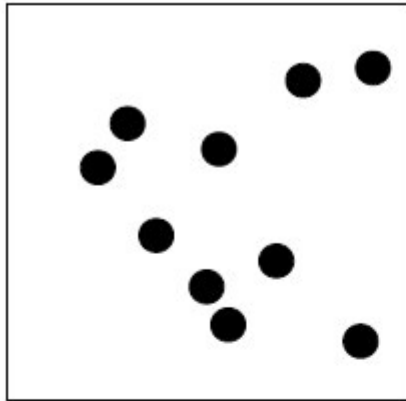
Score  
0-12



**VISUOSPATIAL – Dot Counting**

⇒ Say: 'I would like you to count how many dots are in each box, but without pointing to them.'

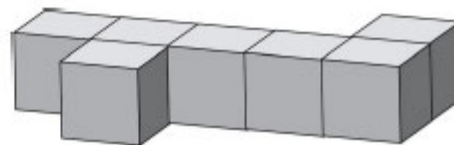
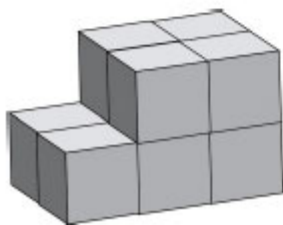
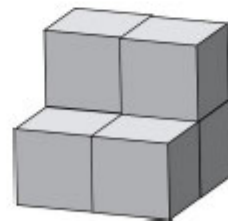
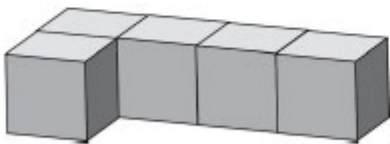
Score  
0-4



**VISUOSPATIAL – Cube Counting**

⇒ Say: 'How many cubes are in each structure, including the ones you may not be able to see?'

Score  
0-4







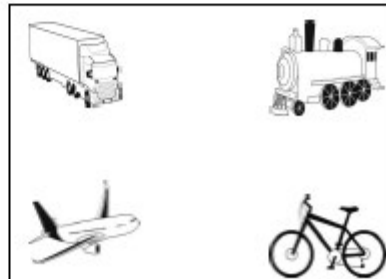
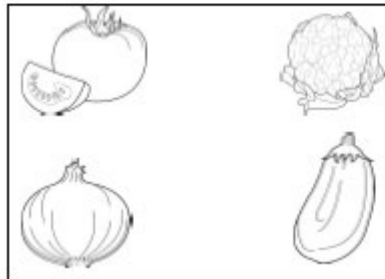
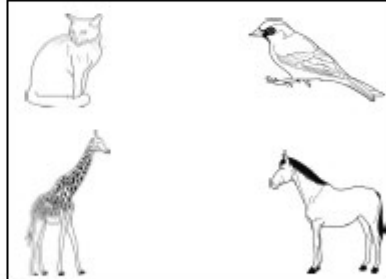
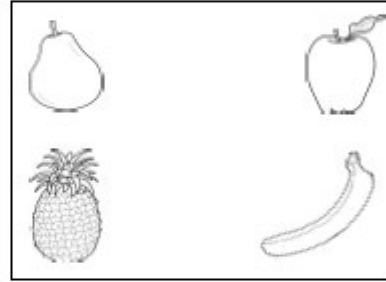
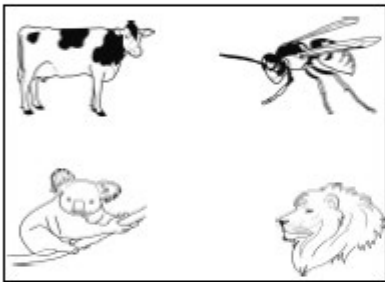
1. The postman knocked on the .....
2. He brought his umbrella with him in case of .....
3. Sally spread her toast with butter and .....
4. John went to the barbers to get his hair .....
5. She dived into the swimming .....
6. They all went to the local café for something to .....

Score  
0-12

Give 2 points for different word, 1 point for related word (e.g. associated or opposite meaning) or 0 points for exact word.

### SOCIAL COGNITION – Part A

☞ Say: 'You are going to see some pictures, one in each corner of a box. You have to choose **which picture you like best**. Either point to or say which picture you like best. Please respond as quickly as possible.' Circle participant's choice.





☞ Say: 'At the beginning of this interview, I read you a short story. Tell me as much as you can remember from that story'. Mark 1 point for each (either entire or part of) underlined section recalled.

*Last Sunday, the annual litter collection took place in Primrose Woods. Forty two people joined in to remove old bicycles and shopping trolleys. Mr Douglas Watt from the woodland project told local reporters that he was very impressed and especially proud of the 17 children who came along.*

Delayed recall =   
 Score (0-10)

**MEMORY – Delayed Recognition**

If all items recalled, skip and score 4. Otherwise ask questions below.

Say: 'Lets see if you can remember anything more about that story. I will ask you some questions, please tell me if they are true or false'.

Circle responses (true or false) and mark 1 point for each item recognised in this section. Use table below to calculate score.

Was the story about an event that occurred last Saturday?	T	F	1
Was the event the annual litter collection?	T	F	1
Did this take place in Primrose Woods?	T	F	1
Did they remove old drink cans and sweet wrappers?	T	F	1
Was the man in the story called Mr Watt?	T	F	1
Was his first name 'Thomas'?	T	F	1
Was he from the local council?	T	F	1
Was he especially proud of the children for coming along?	T	F	1

Score 0-4

Recognition to recognition score table	
Number of correct answers	Score
0-4	0
5	1
6	2
7	3
8	4

SCORES		
<b>Language</b>	Naming, Comprehension, Spelling	/28
<b>Verbal Fluency</b>	Fluency Letter S, Fluency Letter T	/24
<b>Executive</b>	Reverse Digit Span, Alternation, Sentence Completion, Social Cognition	/48
<b>ALS-SPECIFIC:</b>		<b>/100</b>
<b>Memory</b>	Immediate recall, Delayed recall score, Delayed recognition	/24
<b>Visuospatial</b>	Dot Counting, Cube Counting, Number Location	/12
<b>ALS NON-SPECIFIC:</b>		<b>/36</b>
<b>ECAS TOTAL SCORE:</b>		<b>/136</b>

© Copyright, The University Court of the University of Edinburgh, 2009 - 2013. All Rights Reserved. The authors being S. Abrahams & T. H. Bak 8  
 Dot counting is reproduced with kind permission from J. R. Hodges



**EDINBURGH COGNITIVE and BEHAVIOURAL ALS SCREEN – ECAS**  
English Version (2013)

**BEHAVIOUR SCREEN – Carer Interview**

☞ Please ask the carer about the following possible behaviours. Symptoms should have occurred repeatedly and not just on one instance, and may have occurred prior to the development of any motor signs. Tick 'Yes', 'No' or 'Don't Know'. If 'Yes', please provide a brief written description. Give one mark for every 'Yes' response (maximum = 10).

<b>A Behavioural disinhibition</b>			
1	Socially inappropriate behaviour, e.g. <i>inappropriate behaviour with strangers</i> <i>criminal behaviour</i>	Y	N DK
2	Loss of manners or decorum, e.g. <i>crude or sexually explicit remarks, jokes or opinions that may be offensive to others</i> <i>lack of response to social cues</i>	Y	N DK
3	Impulsive, rash or careless actions, e.g. <i>new onset gambling, or buying or selling property without regard for consequences</i> <i>giving out personal information inappropriately, e.g. credit card numbers</i>	Y	N DK
<b>B Apathy or inertia</b>			
4	Loss of interest, drive or motivation, e.g. <i>passivity and lack of spontaneity</i> <i>needs prompting to initiate or continue routine activities</i>	Y	N DK
<b>C Loss of sympathy or empathy</b>			
5	Diminished response to other people's needs and feelings <i>Positive rating on this feature should be based on specific examples that reflect a lack of understanding or indifference to other people's feelings, e.g.</i> <i>hurtful comments</i> <i>disregard for others' pain or distress</i>	Y	N DK
6	Diminished social interest, interrelatedness, personal warmth or general closeness in social engagement, e.g. <i>coldness</i> <i>lack of eye contact</i>	Y	N DK
<b>D Perseverative, stereotyped, compulsive or ritualistic behaviour</b>			
7	Simple repetitive movements, e.g. <i>tapping, clapping</i> <i>scratching, picking skin or clothing</i> <i>repeating words</i>	Y	N DK
8	Complex, compulsive or ritualistic behaviours, e.g. <i>counting, cleaning rituals, checking</i> <i>collecting, hoarding</i>	Y	N DK

BEHAVIOUR

<b>E</b>	<b>Hyperorality and altered food preferences</b>			
9	Altered food preferences, e.g. <i>food fads</i> <i>carbohydrate craving (particularly sweets)</i>	Y	N	DK
10	Binge eating or hyperorality, e.g., <i>cramming or continuing to eat despite satiety</i> <i>oral exploration or consumption of inedible objects</i>	Y	N	DK
<b>SCORE</b>		<b>TOTAL</b>		<b>/10</b>
<b>SYMPTOMS</b>				
☞ Please tick box if at least one of the symptoms was present in each of the following categories.				
<b>A. Behavioural disinhibition</b>				
<b>B. Apathy or inertia</b>				
<b>C. Loss of sympathy or empathy</b>				
<b>D. Perseverative, stereotyped, compulsive or ritualistic behaviour</b>				
<b>E. Hyperorality and altered food preferences</b>				
<b>ALS Psychosis Screen</b>				
☞ Please ask the carer about the following possible symptoms. Tick 'Yes', 'No' or 'Don't Know'. If 'Yes', please provide a brief written description. Give one mark for every 'Yes' response (maximum = 3).				
1	Has strange and/or bizarre beliefs and behaviours	Y	N	DK
2	Hears or sees things that are not there, and/or feels the presence of someone who is not there	Y	N	DK
3	Is overly suspicious, and/or feels persecuted	Y	N	DK
<b>SCORE</b>		<b>TOTAL</b>		<b>/3</b>
<b>ONSET AND DURATION OF SYMPTOMS</b>				
☞ Please tick or complete box to indicate response.				
<b>1. Do these symptoms represent a CHANGE from the patient's previous behaviour?</b>		Y	N	
If yes, did the changes occur:				
a. BEFORE the onset of the disease?		Y	N	
b. at the same time as other symptoms?		Y	N	
c. AFTER the onset of the disease?		Y	N	
<b>2. Do they still persist?</b>		Y	N	
<b>3. If not, how long did they last?</b>				

## A5 Favourable ethical opinion



### NRES Committee London - South East

Bristol Research Ethics Committee Centre  
Level 3, Block B  
Whitefriars,  
Lewins Mead,  
Bristol  
BS1 2NT

Telephone: (0117) 3421382  
Facsimile: (0117) 3420445

24 March 2014

Dr Rebecca Broad  
Clinical Research Fellow Neurology  
Brighton and Sussex Medical School  
Brighton and Sussex University Hospitals NHS Trust.  
Trafford Centre for Medical Research  
University of Sussex  
Falmer BN1 9RY

Dear Dr Broad

**Study title:** Neurite Orientation Dispersion and Density Imaging ('NODDI'): A new approach to understanding cellular pathology in Motor Neurone Disease.  
**REC reference:** 14/LO/0195  
**Protocol number:** 13/180/LEI  
**IRAS project ID:** 140658

Thank you for your letter of 10 March 2014, responding to the Committee's request for further information on the above research and submitting revised documentation.

The further information was considered in correspondence by a sub-committee of the REC A list of the sub-committee members is attached.

We plan to publish your research summary wording for the above study on the HRA website, together with your contact details, unless you expressly withhold permission to do so. Publication will be no earlier than three months from the date of this favourable opinion letter. Should you wish to provide a substitute contact point, require further information, or wish to withhold permission to publish, please contact the REC Assistant Mr Wai Yeung, [nrescommittee.london-southeast@nhs.net](mailto:nrescommittee.london-southeast@nhs.net).

#### Confirmation of ethical opinion

On behalf of the Committee, I am pleased to confirm a favourable ethical opinion for the above research on the basis described in the application form, protocol and supporting documentation as revised, subject to the conditions specified below.

A Research Ethics Committee established by the Health Research Authority



## Ethical review of research sites

### Conditions of the favourable opinion

The favourable opinion is subject to the following conditions being met prior to the start of the study.

Management permission or approval must be obtained from each host organisation prior to the start of the study at the site concerned.

*Management permission ("R&D approval") should be sought from all NHS organisations involved in the study in accordance with NHS research governance arrangements.*

Guidance on applying for NHS permission for research is available in the Integrated Research Application System or at <http://www.rdforum.nhs.uk>.

*Where a NHS organisation's role in the study is limited to identifying and referring potential participants to research sites ("participant identification centre"), guidance should be sought from the R&D office on the information it requires to give permission for this activity.*

*For non-NHS sites, site management permission should be obtained in accordance with the procedures of the relevant host organisation.*

*Sponsors are not required to notify the Committee of approvals from host organisations*

### Registration of Clinical Trials

All clinical trials (defined as the first four categories on the IRAS filter page) must be registered on a publically accessible database within 6 weeks of recruitment of the first participant (for medical device studies, within the timeline determined by the current registration and publication trees).

There is no requirement to separately notify the REC but you should do so at the earliest opportunity e.g when submitting an amendment. We will audit the registration details as part of the annual progress reporting process.

To ensure transparency in research, we strongly recommend that all research is registered but for non clinical trials this is not currently mandatory.

If a sponsor wishes to contest the need for registration they should contact Catherine Blewett ([catherineblewett@nhs.net](mailto:catherineblewett@nhs.net)), the HRA does not, however, expect exceptions to be made. Guidance on where to register is provided within IRAS.

**It is the responsibility of the sponsor to ensure that all the conditions are complied with before the start of the study or its initiation at a particular site (as applicable).**

### Approved documents

The final list of documents reviewed and approved by the Committee is as follows:

**A Research Ethics Committee established by the Health Research Authority**



<i>Document</i>	<i>Version</i>	<i>Date</i>
Advertisement	3	06 January 2014
Covering Letter		14 January 2014
Covering Letter		10 March 2014
Evidence of insurance or indemnity		12 July 2013
GP/Consultant Information Sheets	3	06 January 2014
Investigator CV		14 January 2014
Letter from Sponsor		10 January 2014
Other: Summary CV for Supervisor (student research)		14 January 2014
Other: A13 IRAS Methodology Section	4	03 March 2014
Other: A35 IRAS Loss of capacity	4	03 March 2014
Participant Consent Form: Cosent form MND participants		06 January 2014
Participant Consent Form: Consent form control participants		06 January 2014
Participant Information Sheet: NODDI PIS	3	06 January 2014
Participant Information Sheet: NODDI PIS MND	4	03 March 2014
Participant Information Sheet: NODDI PIS Controls	4	03 March 2014
Protocol	3	06 January 2014
Questionnaire: The ALS Functional Rating Scale - Revised (ALSFRS-R)		
Questionnaire: EDINBURGH COGNITIVE AND BEHAVIOURAL ALS SCREEN – ECAS		
Questionnaire: NODDI Study MRI Safety Questionnaire	3	06 January 2014
Questionnaire: NODDI Study TMS Screening Questionnaire	3	06 January 2014
Questionnaire: NODDI Study Verbal Recognition Memory Test	3	06 January 2014
REC application		14 January 2014
Referees or other scientific critique report		14 January 2014
Response to Request for Further Information	Email	10 March 2014
Summary/Synopsis	3	06 January 2014

### Statement of compliance

The Committee is constituted in accordance with the Governance Arrangements for Research Ethics Committees and complies fully with the Standard Operating Procedures for Research Ethics Committees in the UK.

### After ethical review

#### Reporting requirements

The attached document “*After ethical review – guidance for researchers*” gives detailed guidance on reporting requirements for studies with a favourable opinion, including:

- Notifying substantial amendments
- Adding new sites and investigators

**A Research Ethics Committee established by the Health Research Authority**

- Notification of serious breaches of the protocol
- Progress and safety reports
- Notifying the end of the study

The NRES website also provides guidance on these topics, which is updated in the light of changes in reporting requirements or procedures.

Feedback

You are invited to give your view of the service that you have received from the National Research Ethics Service and the application procedure. If you wish to make your views known please use the feedback form available on the website.

Further information is available at National Research Ethics Service website > After Review

14/LO/0195 Please quote this number on all correspondence

We are pleased to welcome researchers and R & D staff at our NRES committee members' training days – see details at <http://www.hra.nhs.uk/hra-training/>

With the Committee's best wishes for the success of this project.

Yours sincerely



**Mr Wai Yeung**  
Research Ethics Committee (REC) Assistant

pp Professor David Caplin  
Chair

Email: [nrescommittee.london-southeast@nhs.net](mailto:nrescommittee.london-southeast@nhs.net)

*Enclosures: List of names and professions of members who were present at the meeting and those who submitted written comments*

*"After ethical review – guidance for researchers"*

*Copy to: Professor Kevin Davies*

**NRES Committee London - South East**  
**Attendance at Sub-Committee of the REC**

**Committee Members:**

<i>Name</i>	<i>Profession</i>	<i>Present</i>
Professor David Caplin	Physicist	Yes
Professor John Eastwood	Consultant Renal Physician	Yes
Mrs Vera Hughes	Training Consultant	Yes

**Also in attendance:**

<i>Name</i>	<i>Position (or reason for attending)</i>
Mr Rajat Khullar	REC Manager



## A6 BSMS Sponsorship

### BSMS Research Governance & Ethics Committee (RGEC)

Chair: Professor Kevin Davies  
Deputy Chair: Professor Bobbie Farsides

Secretary: Miss Caroline Brooks  
Tel: 01273 696955 ext. 3905 (Monday – Wednesday) Tel: 01273  
872855 (Thursday and Friday) [Caroline.Brooks@bsuh.nhs.uk](mailto:Caroline.Brooks@bsuh.nhs.uk)

Applications and general enquiries: [rgec@bsms.ac.uk](mailto:rgec@bsms.ac.uk)



Brighton and Sussex Medical School  
Medical Teaching Building  
University of Sussex  
Falmer  
Brighton  
BN1 9PX

04/12/2013

Professor Nigel Leigh  
Brighton and Sussex Medical School  
Clinical Imaging Sciences Centre (CISC)  
University of Sussex  
Falmer  
Brighton  
BN1 9RR

Dear Professor Leigh

**Full Study Title:** Neurite Orientation Dispersion and Density Imaging ('NODDI'): A new approach to understanding cellular pathology in MND.

**R&D Ref No. :** 13/180/LEI

I am writing to inform you that the Brighton and Sussex Medical School Research Governance and Ethics Committee (RGEC) (Sub-Panel) which met on **Thursday 28<sup>th</sup> November 2013** has now assessed your application and granted you **Provisional Sponsorship Approval** for the above named project.

The Committee will be pleased to grant full Sponsorship Approval for the study once a number of amendments requested by the Committee have been made. These amendments are outlined below:

- The Committee noted a Consent Form had not been included as part of the submission and advised this was a mandatory requirement. Please can the research team draft a Consent Form for re-submission.
- The Committee identified conflicting messages in relation to anonymisation. In the RGEC Application Form (Section 10) it stated "All the data collected from the study will be kept confidential and will be anonymized for storage." However, in Section 9, and in the Participant Information Sheet, ("What about confidentiality?") it stated: "The data will be anonymised where possible and where this is not possible confidentiality will be maintained." Please could the procedure in relation to anonymisation be clarified?
- The Committee expressed concerns about retaining blood for unknown research purposes. In the RGEC Application Form (page 4) it stated: "Bloods will therefore be taken from all participants for 'banking' for future studies that may provide new insights into the disease mechanisms." Following the end of the NRES approval for the project these samples would fall under the aegis of the HTA License. However, the logistics and governance arrangements for the retention and storing of the blood post project were not specified in the Application Form. Please could Dr Natalie Chaplin be consulted in the first instance and detailed information in relation to the logistical and governance arrangements for these samples be provided in the Application Form.
- It was unclear whether the blood samples being retained would also remain linked to the clinical characteristics and imaging findings (scans). Please could the research team clarify whether blood samples will be linked or un-linked?
- Please remove the 1<sup>st</sup> line of Section 8 of the Participant Information Sheet, which states "There are no disadvantages to taking part in the study." The Committee felt the amount of time invested by participants would be perceived as a disadvantage.
- In the Participant Information Sheet (page 2) it stated: "If you are taking Riluzole you will be asked to stop taking it for one week before the TMS visit as this can affect the results. Stopping Riluzole for one week will not cause and significant change to the overall affect of taking this medication."

Please could the research team clarify the clinical guidance regarding the effect of not taking Riluzole for one week? The Committee felt it was important to make very clear in the protocol, and also explicitly re-assure participants in the Participant Information Sheet, that there are no ill-effects of not taking the drug.

- It was unclear who would be completing the screening questionnaire - please could this be clarified?
- The Committee felt that navigating the campus for some of the patients participating in the study could be quite challenging. The Committee recommended participants were either given the option of receiving a voucher for their lunch (rather than receiving reimbursement for food expenses) or of having their lunch brought to them by the research team.

Please could the research team send a re-submitted application to the Committee in time for its next meeting on 20<sup>th</sup> January (the submission deadline is 18<sup>th</sup> December 2013). Please include as part of your re-submission a covering letter which provides an itemized list of all the changes made in response to each of our recommendations, explaining where these revisions have been made, in addition to enclosing the revised paperwork.

Yours sincerely



Professor Kevin Davies  
Chair of the BSMS Research Governance and Ethics Committee

**Study Title: Application of "NODDI" in Motor Neurone Disease**  
**IRAS: 140658**  
**Portfolio ID: 16861**

Dear Dr Broad

We have been notified that your study now has NHS Permissions at your first site as of **16/06/2014** and therefore we have changed the entry in the NIHR CRN Portfolio to reflect this change. I have also copied this email to our Associate Director for MND, Professor Pamela Shaw, so that she is aware that this study is now released as 'In Set-Up NHS permissions received'. I have also copied staff at Kent, Surrey & Sussex LCRN so they are also aware of the status of this study.

Your study record is  
at: <http://public.ukcrn.org.uk/Search/StudyDetail.aspx?StudyID=16861>

We will contact Dr Rebecca Broad with information and guidance about uploading your recruitment data to the NIHR CRN Portfolio. The NIHR require this upload to be carried out on a monthly basis and we will supply the standard template that is used for this purpose.

It is the aim that all portfolio studies recruit their first participant as soon as possible after NHS Permissions have been received with a target of 30 days which for this study would be **by 15th July**. I would therefore be grateful if you could let me know once you have recruited your first participant. However, if you anticipate any problems with your readiness to recruit, please do not hesitate to contact us and we will support you in any way we can.

**IMPORTANT NOTE:**

Acknowledgement of Network support must be made when publishing study findings. It is your responsibility to ensure that the following standard text is used to acknowledge the support of the Clinical Research Network when publishing your study findings in peer-review journals, or any other form of publication:

**"(Research team or organisation) acknowledges the support of the National Institute for Health Research Clinical Research Network"**

Please let me know if you have any queries or require any further information.

Best Wishes  
Hazel

**Hazel Reynolds**  
Development Portfolio Assistant | [DeNDRoN](http://www.ukcrn.org.uk)

t. 0191 208 1331 | e. [hazel.reynolds@nihr.ac.uk](mailto:hazel.reynolds@nihr.ac.uk)  
a. Institute for Ageing and Health  
Campus for Ageing & Vitality  
Newcastle University  
Newcastle upon Tyne  
NE4 5PL



## A8 MND Funding



Application Number 92 / 443 (Office Use)

Prof Nigel Leigh  
Professor of Neurology  
Clinical Medicine  
Brighton and Sussex Medical School  
Trafford Centre for Biomedical Research  
University of Sussex  
Falmer  
East Sussex  
BN1 9RY

23 May 2014

Dear Prof Leigh

### MND ASSOCIATION RESEARCH GRANT

**Re: Neurite Orientation Dispersion and Density Imaging ('NODDI') - a new approach to understanding cellular pathology in MND.**

I am pleased to advise you that the Board of Trustees of the MND Association has agreed to offer you an award of a research grant to the total value of **£91,778.00** over an **18 month** period, to start **1 June 2014**.

Summary of support offered; (see original application)	1st Year	2nd Year	3rd Year	TOTAL £
(a) Personal support of applicant				
(b) Research Staff no of posts: 1 whole time	34,566	23,325		<b>57,891</b>
(c) Technical assistance no. of posts: whole/part time				
Addition of pension & NI (a) (b) & (c)	8,599	5,803		<b>14,402</b>
(d) (e) (f) expenses	12,049	5,436		<b>17,485</b>
(f) Conference		2,000		<b>2,000</b>
<b>Total support offered</b>	<b>55,214</b>	<b>36,564</b>		<b>91,778</b>

The award is subject to MND Association's conditions for grants and I enclose three copies. One is for your retention; another (together with a copy of this letter) is for the finance department administering the grant from your side (University of Sussex); the third copy is to be signed by you and the appropriate person in your finance department and returned to the Association, within four weeks of receipt of this letter.

continued...

**Royal Patron**  
HRH The Princess Royal

David Niven House  
10-15 Notre Dame Mews  
Northampton NN1 2BG  
Tel 01604 250505  
Fax 01604 624726

enquiries@mndassociation.org  
www.mndassociation.org

MND Connect 08457 626262

**President**  
Prof Colin Blakemore FMedSci HonFRCP FRSc

**Patrons**  
Sir Roger Bannister CBE  
Chris Broad  
Joel Cadbury  
Baroness Iora Finlay of Llandaff  
Baroness Susan Greenfield CBE  
Prof Stephen Hawking CH CBE FRSc FRSA  
James Niven  
Richard Noble OBE  
Sir Chris Woodhead

It is important that:

- Once everything is in place for the project to commence, the **grant activation form** is completed and returned at least one month prior to the agreed start date (grant condition 10.1)
- All correspondence regarding this project is marked for the attention of Natasha Rowe, quoting the reference: **Leigh/Apr14/824-791**
- Invoices are received as soon as possible following the end of each quarter. Reimbursement is made on actual expenditure and it is essential that a **detailed** breakdown of salary and non-pay costs incurred is included with every invoice. Copy invoices for claims of £500.00 or above must be provided. (Please see 'Research Grants Payment & Reporting Guidelines')
- **Annual, interim and final reports** are received as soon as possible during and after the project is completed. (Please see 'Research Grants Payment & Reporting Guidelines')
- **Publications** arising from this award in scientific journals or for public distribution will acknowledge the MND Association as funders

You are mandated to make your peer reviewed papers arising directly from this grant available through open access. These research papers should be available within the Europe PubMed Central repository as soon as possible but within six months of the publication date. (See Grant Condition 17.2 and MND Association Grantee Guide to our Open Access Policy)

- **Reprints/copies of published papers** are received as soon as possible during and after the project is completed

The MND Association logo will be forwarded to you, in due course, for use in publications and when giving talks on this particular aspect of your work. If you would like a copy sooner, please contact [research.grants@mndassociation.org](mailto:research.grants@mndassociation.org) and one of us will be happy to provide one, together with our visual identity guidelines.

With best wishes for a successful and fruitful project,

Yours sincerely



**Natasha Rowe**  
**Research Grants Co-ordinator**

Enc.      Grant Conditions  
            Research Grant Payment Guidelines  
            Grant Activation Form  
            MND Association Guide to our Open Access Policy

cc         Finance Department

## A9 Consent

**Title of Project: Neurite Orientation Dispersion and Density Imaging ('NODDI') - A new approach to understanding cellular pathology in Motor Neurone Disease.**

**Name of Researcher: Dr Rebecca Broad**

Please initial box

I confirm that I have read and understood the participant information sheet, version number 4, dated 03/03/2014, for the study Neurite Orientation Dispersion and Density Imaging ('NODDI'): A new approach to understanding cellular pathology in MND. I have had the chance to read the information and ask questions about the study and I am satisfied with the answers I have been given.

I understand that my participation in this study is voluntary, that I am free to stop at any time, and that I do not have to give a reason for doing so. I understand that if I withdraw from the study my medical care and legal rights will not be affected in any way.

I agree to my GP being informed of my participation in the study.

I understand that relevant sections of my medical notes and data collected during the study, may be looked at by individuals from Brighton and Sussex Medical School, from regulatory authorities, or from the Brighton and East Sussex University Hospitals NHS Trust, where it is relevant to my taking part in this research. I give permission for these individuals to have access to my medical records.

I understand that I will undergo a set of neurological assessments, a Magnetic Resonance Imaging brain scan, Transcranial Magnetic Stimulation with Electroencephalography, and two cognitive tasks during this study. I understand that the data collected from these assessments will be anonymised and will remain confidential.

I understand that if there are any unexpected findings on imaging that need further investigation you will, with my consent, inform my GP who will notify me if further tests are needed.

I appreciate that research data collected during this study may be useful in future studies of MND and I agree that my data being used for this purpose. I understand that my anonymised data will be stored securely for up to 10 years.

I understand that in the unlikely event that I lose my capacity to consent during this research study I will be withdrawn from the study and no further data will be collected. Data already collected will be retained in the anonymised form. It will be used in this research study and may also be used in further research of Motor Neurone Disease.

I consent to taking part in the above study.

\_\_\_\_\_  
Name of Participant

\_\_\_\_\_  
Date

\_\_\_\_\_  
Signature

- 
- I have explained the information in this document and encouraged the participant to ask questions and provided adequate time to answer them.

\_\_\_\_\_  
Name of Researcher  
Seeking Consent

\_\_\_\_\_  
Date

\_\_\_\_\_  
Signature

1 copy for the participant; 1 copy for the researcher site file; 1 copy (original) to be kept in medical notes.

VERSION NUMBER 3  
DATE 06/01/2014



## Consent Form: Control Participants

**Title of Project: Neurite Orientation Dispersion and Density Imaging ('NODDI') - A new approach to understanding cellular pathology in Motor Neurone Disease.**

**Name of Researcher: Dr Rebecca Broad**

Please initial box

I confirm that I have read and understood the participant information sheet, version number 4, dated 03/03/2014, for the study Neurite Orientation Dispersion and Density Imaging ('NODDI'): A new approach to understanding cellular pathology in MND. I have had the chance to read the information and ask questions about the study and I am satisfied with the answers I have been given.

I understand that my participation in this study is voluntary, that I am free to stop at any time, and that I do not have to give a reason for doing so. I understand that if I withdraw from the study my medical care and legal rights will not be affected in any way.

I agree to my GP being informed of my participation in the study.

I understand that relevant sections of my medical notes and data collected during the study, may be looked at by individuals from Brighton and Sussex Medical School, from regulatory authorities, or from the Brighton and East Sussex University Hospitals NHS Trust, where it is relevant to my taking part in this research. I give permission for these individuals to have access to my medical records.

I understand that I will undergo a Magnetic Resonance Imaging brain scan, Transcranial Magnetic Stimulation with Electroencephalography, and two cognitive tasks during this study. I understand that the data collected from these assessments will be anonymised and will remain confidential.

I understand that if there are any unexpected findings on imaging that need further investigation you will, with my consent, inform my GP who will notify me if further tests are needed.

I appreciate that research data collected during this study may be useful in future studies of MND and I agree to my data being used for this purpose. I understand that my anonymised data will be stored securely for up to 10 years.

I understand that in the unlikely event that I lose my capacity to consent during this research study I will be withdrawn from the study and no further data will be collected. Data already collected will be retained in the anonymised form. It will be used in this research study and may also be used in further research of Motor Neurone Disease.

I consent to taking part in the above study.

\_\_\_\_\_  
Name of Participant

\_\_\_\_\_  
Date

\_\_\_\_\_  
Signature

- I have explained the information in this document and encouraged the participant to ask questions and provided adequate time to answer them.

\_\_\_\_\_  
Name of Researcher  
Seeking Consent

\_\_\_\_\_  
Date

\_\_\_\_\_  
Signature

1 copy for the participant; 1 copy for the researcher site file; 1 copy (original) to be kept in medical notes.

VERSION NUMBER 3  
DATE 06/01/2014

## A10 Screening

NODDI Identifier: \_\_\_\_\_

### Inclusion criteria

(Tick each box that applies)

Participants with Motor Neurone Disease (MND) must be El Escorial definite, probable, and possible, or have a laboratory supported diagnosis of MND

All participants must have good respiratory function (Forced Vital Capacity > 60% predicted) and be able to lie flat in comfort for up to one hour

All participants must have no other contraindication to MRI or TMS, see below

All participants must be able to give fully informed consent

### Exclusion criteria

(Cross each box that applies that does not apply)

Lack of capacity to consent

Impaired respiratory function (FVC <60% predicted)

Inability to lay flat for 1 hour due to any underlying cardiac or respiratory compromise

Previous history of epilepsy or seizures

Previous history of migraine

Previous history of tinnitus

Claustrophobia, or the inability to lie still in a confined space

Pregnancy

A pacemaker in situ

An implantable cardioverter-defibrillator (ICD)

A nerve stimulator

A cochlea implant

A drug pump implant

Brain aneurysm clips

Metallic fragments in or near the eyes or blood vessels

Prosthetic metal heart valves

Penile implants

Metal eye implants

An intrauterine device (IUD)

Permanent makeup or tattoos with metallic dyes

Artificial joints (hip replacement or knee replacement)

Tubal ligation clips

Surgical clips or staples

Intracranial metal prosthesis

Any other condition that the investigator believes might put the participant at risk

## A11 MRI safety questionnaire

### MRI Safety Questionnaire

*The MRI scanner uses a powerful magnetic field so we need to make sure that you are safe to enter the scanning room. Please remove all loose metal objects before your scan eg: keys, coins, credit cards, dentures, hearing aids, mobile phones / pagers, watches, hairclips, metallic body piercings and if you are requested change into the clothes provided.*

Name	Date of Birth	Weight (kg)	Contact Number	CISC Number
Address		Name and Address of GP		

Do you have any of the following? If yes please include details & dates:			
	No	Yes	Details / Dates
Cardiac pacemaker/defibrillator?			
Heart surgery / valve replacement?			
Head surgery including that to the eye or ears (including a hydrocephalus shunt)?			
Any other surgery?			
Neurological stimulator or any other implanted medical device?			
Epilepsy?			
Skin patches? (HRT, nicotine, pain relief, contraceptive)			
Tattoos or permanent eye makeup?			
Have you ever worked with metal? eg. Mechanics / metal sheet worker			
Have you EVER had metal fragments in your eyes?			
Shrapnel injury?			
Have you had a previous MRI scan at this centre?			

<b>Women of child bearing age (12-65)</b>		
Is there any chance of you being pregnant?	Yes	No

*Patients / participants with false limbs or callipers please remove them before entering the MRI room. Inform a radiographer if you need assistance*

I confirm that I have answered and understood the above questions and information, and that the information I have provided is correct to the best of my knowledge

Patient / Participant Signature (parent / guardian if under 16)	Date	Radiographer Signature	Date

